Expanding the toolbox of modified nucleobases and click chemistry for investigations on non-coding RNA

Dissertation

zur

Erlangung des Doktorgrades (Dr. rer. nat.)

der

Mathematisch-Naturwissenschaftlichen Fakultät

der

Rheinischen Friedrich-Wilhelms-Universität Bonn

vorgelegt von

Christof Domnick

aus

Siegburg

Bonn 2018

Angefertigt mit Genehmigung der Mathematisch-Naturwissenschaftlichen Fakultät der

Rheinischen Friedrich-Wilhelms-Universität Bonn

1. Gutachter: Prof. Dr. Michael Famulok

2. Gutachter: Priv. Doz. Dr. Marianne Engeser

Erscheinungsjahr: 2019

Tag der Promotion: 07.05.2019

In science, most of the time things aren't working.

<div style="text-align: right">Venkatraman „Venki" Ramakrishnan</div>

Parts of this thesis have been published in:

Pyka, A., Domnick, C., Braun, F., Kath-Schorr, S., Diels-Alder Cycloadditions on Synthetic RNA in Mammalian Cells, *Bioconjugate Chem.*, **2014**, *25*, 1438-1443.

Domnick, C., Eggert, F., Kath-Schorr, S., Site-specific enzymatic introduction of a norbornene modified unnatural base into RNA and application in posttranscriptional labeling, *Chem. Commun.*, **2015**, 51, 8253-8256.

Wilson, T., Liu, Y., Domnick, C., Kath-Schorr, S., Lilley, D. M. J., The Novel Chemical Mechanism of the Twister Ribozyme, *J. Am. Chem. Soc.*, **2016**, *138*, 6151-6162.

Eggert, F., Kulikov, K., Domnick, C., Leifels, P., Kath-Schorr, S., Iluminated by foreign letters – Strategies for site-specific cyclopropene modification of large functional RNAs via *in vitro* transcription, *Methods*, **2017**, *120*, 17-27.

Abstract

Non-coding ribonucleic acid (RNA) consists of highly structured molecules whose arrangement and function can be investigated using different chemical labeling approaches. Contemporary labeling techniques show restrictions either in labeling specificity or oligonucleotide length. Literature describes highly efficient and fast labeling strategies as well as different approaches of unnatural base pairs (*ubp*) specifically recognized by enzymes, but previous work failed to address a combined technique for labeling. In this thesis, an enzymatic template-directed labeling approach is shown based on unnatural ribonucleoside triphosphates either suitable for structural investigations using electron paramagnetic resonance (*EPR*) spectroscopy or modified for subsequent inverse electron demand Diels-Alder (*IEDDA*) click chemistry on non-coding RNA. Chemical synthesis of *ubp* and *IEDDA* click building blocks, successful template-directed T7 *in vitro* transcriptions with subsequent fluorescent labeling or EPR-based distance measurement will be described. This novel approach reveals a site-specific labeling technique of long RNA strands to get a better insight in catalysis and regulation on RNA level.

Zusammenfassung

Nicht-kodierende Ribonukleinsäuren (RNA) bestehen aus hoch strukturierten Molekülen deren Arrangement und Funktion mit Hilfe verschiedener chemischer Markierungen untersucht werden kann. Heutige Markierungsmethoden unterliegen jedoch entweder Restriktionen in der Ortsspezifität oder der Oligonukleotidlänge. In der Literatur sind sowohl hocheffiziente und schnelle Markierungsmethoden beschrieben als auch verschiedene Ansätze unnatürlicher Basenpaare (*ubp*), die von Enzymen spezifisch erkannt werden. Allerdings ist bis dato keine kombinierte dieser Methodiken für Markierungsverfahren bekannt. Diese Arbeit beschreibt einen templatgesteuerte Markierungsmethode, die auf unnatürlichen Ribonukleintriphosphaten basiert, welche entweder für strukturelle Untersuchungen mit Hilfe von Elektronenspinresonanz (*EPR*), oder eine nachträgliche Diels-Alder Reaktion mit inversem Elektroenbedarf (*IEDDA*) an nichtkodierender RNA zulassen. Die chemische Synthese der *ubp* und *IEDDA* Bausteine, erfolgreiche T7 *in vitro* Transkriptionen mit anschließender Fluoreszenzmarkierung respektive EPR-basierten Abstandsmessungen werden beschrieben. Dieser neuartige Ansatz ermöglicht eine ortsspezifische Markierung langer RNA Stränge für ein besseres Verständnis der Katalyse und Regulation auf biomolekularem Niveau.

Content

1 Theoretical background

1.1 Labeling strategies on oligonucleotides

The four canonical nucleobases adenine (A), cytosine (C), guanine (G) and thymine (T; DNA) or uracil (U; RNA) as two-base-pair alphabet encode information in the genomes and define organisms since the origin of life.[1]

After discovering the structure of desoxyribonucleic acid (DNA) in 1953, nobel prize winner Francis Crick enunciated the central dogma of molecular biology: DNA encodes ribonucleic acid (RNA), RNA encodes proteins.[2,3] Nowadays science states, that about 80% of human DNA is non-protein coding and up to 98% of mammalian RNA content comprises of non-coding RNA.[4] By discovering other RNA classes like minor class RNA[5], structural and mechanistic studies on these oligonucleotides have been carried out in scientific research.[6] Minor class RNAs also contain information and catalytic or structural function.[7] The functionality of RNA is determined in most cases by its structural and sequencial properties. Thus, scientific approaches to understand the folding behavior, structural dynamics and intracellular distribution with minimal influence on mentioned characteristics is crucial to understand biological function and cellular activity of minor class RNA.[8–10]
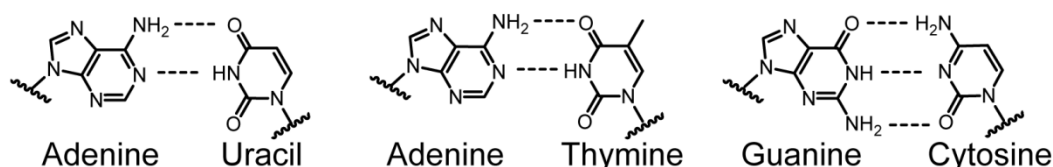
Fig. 1: Canonical nucleobases in oligonucleotides. Shown are pyrimidine based nucleobases adenine (A) and uracil (U) occurring in ribonucleic acid (RNA, left) and adenine thymine (T) pairing occurring in DNA (middle) with its two Watson-Crick hydrogen bonds. Also guanine (G) cytosine (C) pairing is shown (right) found in RNA and DNA with its three Watson-Crick hydrogen bonds. Shown are only nucleobases. Sugar moieties are not depicted.

To study these biomolecules, several strategies and techniques were developed. A well-established method to investigate the structure and folding of oligonucleotides is crystallization of biomolecuels and subsequent X-ray crystal structure determination.[10] In non-denaturing conditions, crystalls of oligonucleotides can be yielded by slow and controlled precipitation from aqueous solution.[10,11] Crystallization can be perfomed either on unmodified or modified oligonucleotides.

Another strategy to investigate biomolecules in view of conformational properties is chemical probing. This superordinate comprises different techniques, in which an oligonucleotide is modified by treatment with a chemical reagent.[12] In general, four types

of informations about oligonucleotides can be obtained using chemical probing of RNA or DNA, respectively.[12] Using base-specific reagents reveal informations about base stacking or hydrogen bonds of adjacent bases in the oligonucleotide of interest. Usage of hydroxyl radicals, cleaving backbone of RNA shows solvent accessibility and leads to structural informations.[12] Informations regarding structural changes can be obtained by another chemical probing technique, namely 2′-hydroxyl acylation analyzed by primer extension (SHAPE), exploiting flexibility of nucleotides.[12] Through-space informations can be obtained by chemical probing techniques using bifunctional reagents suitable for coss-linking experiments.[12,13] Another possibility achieving structural and dynamic properties of RNA is nuclear magnetic resonance (NMR).[14] This powerful tool enables scientists to derive informations about base-pairing pattern as well as structure prediction or conformational equilibria and flexibility.[15,16] Approaches introducing ^{13}C- or ^{15}N-labeled nucleobases for NMR investigations as modification on chemnically synthesized RNA tend to be expensive and difficult.[15] Enzymatic *in vitro* transcription techniques as an alternative pathway gaining labeled RNA deal with restrictions, too. Inhomogenous 3′-transcripts caused by T7 RNA polymerase (RNAP),[17,18] complex template preparation and RNA purification steps make sample preparation suitable for NMR studies sophisticated.[15,19]

Regarding inert nature of nucleobases and backbone residues[20], lacking reactive amino or sulfhydryl groups available at amino acids and therefor suitable for structural investigatins on proteins, synthetic introduction of labels has to be carried out for oligonucleotides.[20] Caused by restrictions in length during solid-phase synthesis, only short DNA and RNA molecules can be labeled during chemical synthesis using modified nucleotides.[20–24] Longer oligonucleotides with labeled nucleotides are prepared by ligation.[25] Thus, for longer RNA post-synthetic labeling is used usually.[20] Post-transcriptional or post-synthetic radioactive labeling using T4 ligase is a common method.[26,27] This method is very sensitive, widely used, and well elaborated. Radiolabeling is possible either at 3′- and 5′-end of oligonucleotides.[28] This technique is useful for experiments in view of interactions or sequencing, respectively.[27] Structural aspects of oligonucleotides in contrast can not be worked out by radiolabeling.RNA. Introducing functionalities to investigate structure and function of RNA or mechanistic characteristics can be carried out using a plethora of different techniques.[20,29–31] Isotope labeling for NMR studies up to post synthetic labeling of oligonucleotides with Palladium catalyzed tin chemistry represents only an excerpt of possibilities.[19,32]

As most desired feature site-specificity can be announced. Introducing a modification to understand structure and function of DNA or RNA has to be very precise. This can be

done by solid phase synthesis or postsynthetically.[20] From a chemical point of view, click chemistry was a milestone in labeling strategies of oligonucleotides.[33,34] Using high yielding and insensitive "cream of the crop" reactions in green solvents[33] gained enormous interest in biomedical applications.[35] Using small and bio-orthogonal functionalities which do not interfer structural and functional properties of biomolecules opened up new opportunities in science.[36] Improved cell-permeability of small molecular probes providing less disturbance of living systems can be named for example.[37]

Despite permanent progress in bio-orthogonal chemistry, several challenges are still prominent. High concentrations of reagents as well as required additives can be listed.[37] Those difficulties can be solved by an increase in reaction efficiency, for example.

Another everpresent subject is mentioned site-specificity of incorporated functionalities. Using a combined approach of enzymatic ligation and solid-phase RNA synthesis was state of the art for a long time and is still used steadily.[37] This work deals with chemical abilities to widen the arsenal of chemically modified nucleosides and corresponding counterparts. Furthermore, this work attemps to show novel strategies for site-specific incorporation of functionalized biomolecules.

1.1.1 Labeling strategies during chemical solid phase oligonucleotide synthesis

Beside the abundance of labeling methods on peptides[34,38–40] or lipids[41,42], labeling on oligonucleotide level can be carried out in different ways, too. Functional groups can be attached at various positions of the nucleotide. Using solid phase synthesis, modified nucleotides can be incorporated site-specifically. 2′-OH modified nucleotides like depicted in Fig. 2 are usually used for target binding or affinity binding experiments respectively and consists of fluoro, amino or methoxy modificatios as shown in Fig. 2.[43,44] Another 2′-ribose modification also shown in Fig. 2 is called locked nucleic acid (LNA).[45,46] LNAs are nucleotides, whose 2′-OH is bridged to 4′-C with a methylene moiety. These modified RNA building blocks affect on hybridization properties of corresponding oligonucleotide.[47] Fluorescent labeled nucleotides at 2′ position are not common.
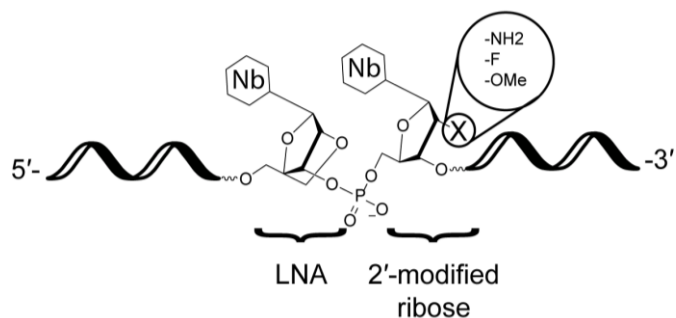
Fig. 2: 2'-modifications on ribose moieties of oligonucleotides.[45–47] Shown are a locked nucleic acid (LNA) and three possible of 2'-position depicted as X. (Nb = nucleobase)

Phosphoramidites suitable for solid phase synthesis modified with fluorescent reporter groups at 2′-position are literature known, but might disturb three dimensional structure of oligonucleotides.[29] Terminal labeling for structured RNA or DNA constructs during synthesis is preffered.[29] A schematic presentation of terminal labeling during synthesis is shown in Fig. 3. Either 3′-end or 5′-end modifications can be introduced. Exemplary shown are a biotin modification (Fig. 3 D) and a fluoresceine label (Fig. 3 E). Variety of modifications and labels expands continuously and can be reread in recent literature.[20,29,48]
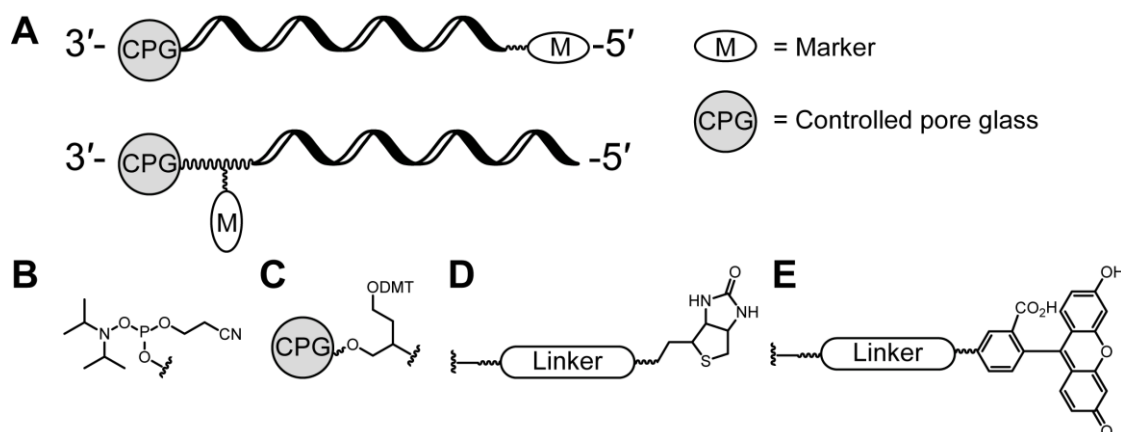
Fig. 3: Terminal labeling during synthesis. Schematic presentation of terminal labeling positions during solid phase synthesis of oligonucleotides (A) using 5′-terminal modifier (B) and 3′-terminal modifier (C) for labeling with either biotin (D) or fluorescent (E) labels during synthesis.[20,29]

Introducing a site-specific functionalization by solid-phase synthesis of oligonucleotides using functionalized and commercially available cyanoethylphosphoramidites (*CEP*) can be carried out at every position. Using solid phase synthesis as technique provides a site-specific incorporation of functionalized nucleotides, but technical circumstances restrict length of oligonucleotides below 100 nucleotides (nt) as stated by suppliers.[21,23,24] DNA or RNA strands consisting of more than 100 nt can be achieved by ligation strategies using T4 ligase.[49] This strategy is known since decades and commonly used

to attach functional handles like biotin or fluorophores at terminal positions of nucleic acids.[50]

1.1.2 Postsynthetic and posttranscriptional labeling of oligonucleotides

Labeling of nucleic aids containing more than 100 nt can be carried out by ligation of shorter fragments synthesized by solid phase synthesis.[25] Several drawbacks for this methology can be mentioned. Chemical synthesis of labeled nucleotides results in low yields caused by synthetic complexity. Solid phase synthesis using modified nucleotides lowers coupling efficiency and labels have to withstand harsh conditions of nucleic acid synthesis.[51] Introduction of small reactive handles and postsynthetic functionalization of fragments or complete oligonucleotides using chemical approaches like on column labeling with Palladium catalyzed cross coupling[32] or other labeling strategies[52] is a versatile alternative. Gaining desired length can be achieved by template directed enzymatic transcription and posttranscriptional ligation.[53]

In 2011 Jäschke and coworkers showed that initiator nucleotides bearing a reactive handle are recognized by T7 RNAP also and 5'-labeled RNA can be directly transcribed *in vitro* (see Fig. 4).[54,55]

1
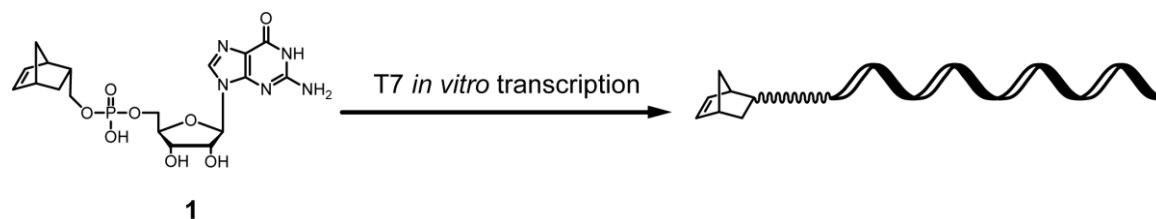
Fig. 4: Terminal enzymatic RNA labeling using a norbornene modified guanosine nucleotide.[54]

Srivatsan showed a fluorescent pyrimidine ribonucleotide, which is recognized and incorporated by T7 RNAP at intrastrand positions.[56] Other examples are given, too.[57,58] Nevertheless, all reactive modifications publiched by Srivatsan are uridine based as shown in Fig. 5 and in addition, used sequences of templates permit only one position for incorporation. Additionally, used sequences are quite short as shown.[56–58]

5'-GCG G*U*G ACA CC-3'
5'-GCG GCG *U*GC-3'
5'-GCG *U*CG CGC A-3'
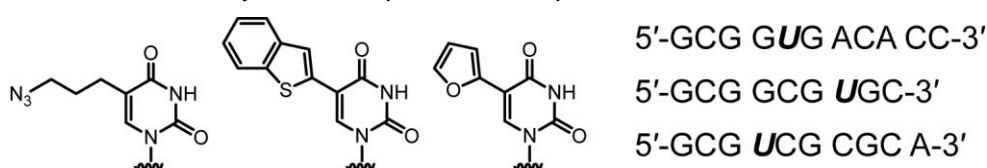
Fig. 5: Uridine derivatives published by Srivatsan and coworkers with used transcript sequences.[57–59]

Enzymes like e.g. T7 RNAP might distinguish between an unmodified and a modified ribonucleotide resulting in different incorporation rates and preferences, as shown by Srivatsan.[56] Recognition of modified nucleotides is possible by usage of specialized polymerases and enzymes.[60–64] Another example for such chemo-enzymatic approaches was published by Rentmeister and coworkers.[65] They used a methyltransferase analog to transfer a terminal azido moiety to a 5′-capped RNA.[65] However, an enzymatic site-specific incorporation of a modified canonical nucleotide within a strand is not possible lacking distinct spatial information in corresponding template. Genetic alphabet consisting of four canonical letters A, C, G and T for DNA or U for RNA respectively is not able to store the required additional information if e.g. T7 RNAP should incorporate modified or unmodified nucleotide. A site-specific enzymatic incorporation would require an "X" and a "Y" as third base pair, accurately recognized by enzymes to communicate additional information.

1.1.3 Inverse electron-demand Diels-Ader (*IEDDA*) click reaction

1.1.3.1 Principles and advantages of this reaction

Chemistry as traditional science of synthesis and structural molecule manipulation also undergoes tasks in biology-oriented synthesis.[66] Using bio-orthogonal click chemistry in the field of biochemical applications enabled a plethora of previously inaccessible modifications.[67] Since definition of click chemistry as chemistry of modular blocks to form C-X-C bonds under well-known conditions by Sharpless as well as Bertozzi defining the term of bio-orthogonal reactions and bio-orthogonality as well as it's elaboration, biological processes can be better understood by probing biomolecules within their native habitats.[68–74] Examples include protein or nucleic acid modifications by incorporating fluorophores, ligands, radioisotopes and tags as molecular labels.[75]

The 1,3-dipolar cycloaddition published by Huisgen in 1967 between an alkyne and an azide yielding a triazole is said to be the archetype of click reactions[76] and often referred to as 'The Click Reaction'.[75] It's applicability towards bioconjugation was first reported by Meldal in 2002 using the Cu(I) catalyzed variant.[77] Carell and coworkers pushed this highly efficient and specific post-synthetic functionalization to a high density functionalization method for DNA.[78] They had to admit strand breaks by applying the method without stabilizers. Cu(I) exhibits considerable cell toxicity and shows hence minor applicability regarding experiments *in vivo*.[75,78] Only Cu(I) stabilizing reagents prevent formation of reactive oxygen species caused by increased copper concentration.[79]
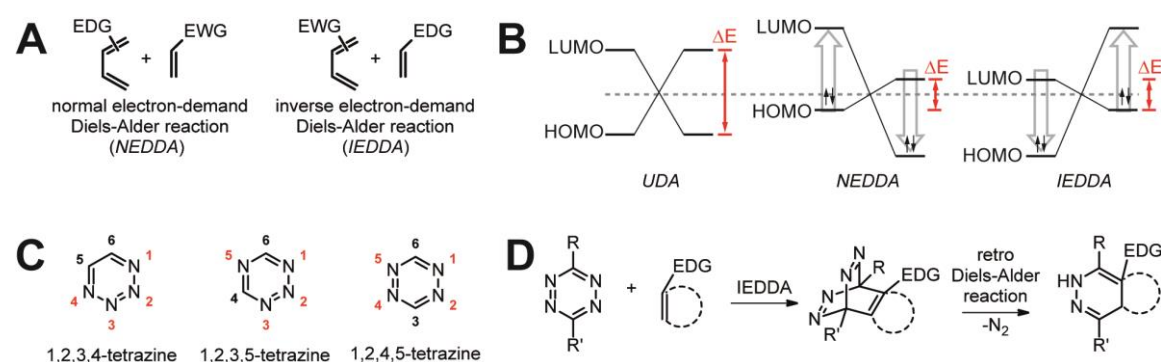
Fig. 6: Outlined *IEDDA* conditions. (A) Diels-Alder reactions are promoted by electron withdrawing groups (*EWGs)* and electron donating groups (*EDGs).* (B) Schematic frontier orbital model of [4+2] Diels-Alder cycloadditions in an unsubstituted Diels-Alder reaction (*UDA*), a substituted normal electron-demand Diels-Alder (*NEDDA*) reaction, and a substituted *IEDDA* reaction. (C) Different nitrogen patterns of tetrazines. (D) Outlined *IEDDA* reaction between a tetrazine and a terminal dienophile.

A more recent kind of click reaction is the inverse electron-demand Diels-Alder (*IEDDA*) cycloaddition between a tetrazine and a strained alkene or alkyne published by two

working groups simultaneously in 2008.[80,81] *IEDDA* reactions are defined as [4+2] cycloaddition between a conjugated electron-deficient dienophile and an electron-rich diene.[82] Usually, Diels-Alder reactions are promoted by electron withdrawing groups (*EWG*s) at the reacting dienophile and electron donating groups (*EDG*s) at the diene as shown in Fig. 6. In contrast, *IEDDA* reactions – as in the name – are promoted by *EWG*s at the reacting diene and *EDG*s at corresponding dienophile (see Fig. 6 A) resulting in other energetic levels of frontier orbitals. The influence of electron withdrawing and donating substituents on the highest occupied molecular orbital (*HOMO*) and the lowest unoccupied molecular orbital (*LUMO*) is shown in in Fig. 6 B. There is a tremendous energetic difference between the frontier orbitals of a [4+2] Diels-Alder cycloaddition without any substitution on reactants (Fig. 6 B, left), a normal electron-demand Diels-Alder (*NEDDA*) reaction as shown in Fig. 6 A on the left-hand side using an *EDG* at the diene and an *EWG* at the dienophile (Fig. 6 B, middle) and an *IEDDA* cycloaddition with an *EWG* attached to the diene and an *EDG* attached to the dienophile as depicted in Fig. 6 A on the right-hand side (Fig. 6 B, right).[41]

Fig. 6 C shows the three different nitrogen patterns of tetrazines. 1,2,3,4-tetrazine (Fig. 6 C, left) known as *v*-tetrazine, 1,2,3,5-tetrazine (Fig. 6 C, middle) known as *as*-tetrazine and 1,2,4,5-tetrazine (Fig. 6 C, right) known as *s*-tetrazine,[83] but only the 1,2,4,5-tetrazine or s-tetrazine (*symmetric* tetrazine) are able to undergo *IEDDA* reactions with subsequent nitrogen extrusion.[84–86] Regarding this, it should be mentioned, that all shown and discussed tetrazine derivatives inherit the 1,2,4,5 nitrogen pattern and belong to *s*-tetrazines. Thus, general term tetrazine(s) describes only *s*-tetrazines in the context of this thesis and will be used in this kind of manner.

After cycloaddition between diene and dienophile, a bicyclic intermediate is formed. A subsequent retro Diels-Alder reaction including nitrogen extrusion results in a 1,4-dihydropyrazine derivative product as formed, like outlined in Fig. 6 D.

The reaction takes place under physiological conditions in a rapid manner and is lacking the need for catalysts or additives in contrast to other candidates the toolbox of click reactions. This is one of the main advantages using *IEDDA* click reactions. Additionally it works efficiently at very low reactant concentrations down to 10 nM.[87,88]

Detailed synthetic and mechanistic considerations regarding tetrazine synthesis will be outlined later. In order to expand the scope of asymmetric substituted tetrazines, several new synthetic techniques and pathways were established and elaborated in the last decade.[89–93] In addition, the field of applications for this click reaction increased in a rapid

manner. *IEDDA* click reactions were carried out on oligonucleotides[94–97], peptides[98–100], proteins[101–103], lipids[104–106], and glycans[107,108].
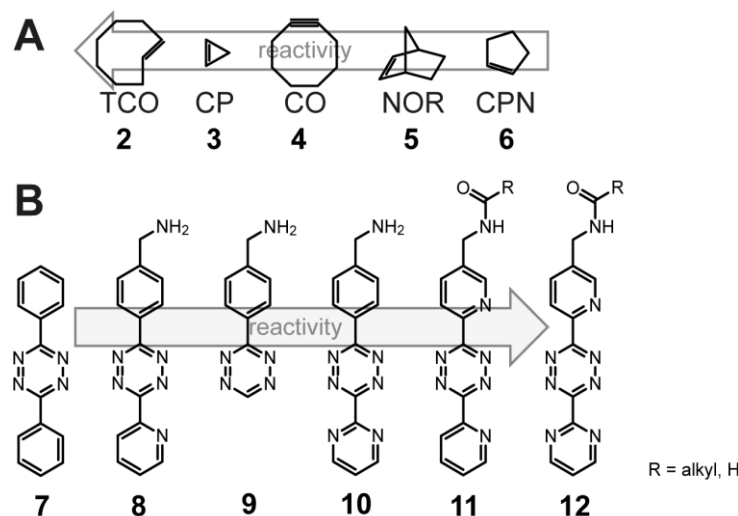

Fig. 7: Relative reactivity of *IEDDA* reaction partners. Dienophiles (TCO: *trans*-cyclooctene, CP: cyclopropene, CO: cyclooctine, NOR: norbornene, CPN: cyclopentene) (A) and substituted tetrazines (B) used in *IEDDA* reactions show different reaction rates. This is caused by ring strain effects on the dienophile as well as EWGs at 3- and 6-positions of the tetrazine.[41,82,87,88,109]

Different reaction rates as depicted in Fig. 7 A do occur in *IEDDA* click reactions related to different alkenes and alkynes as reaction partner. Sauer described a comparing assay using an unsubstituted tetrazine reacted to different alkynes in order to determine reaction rate constants in 1997.[110] Other people also published comparing studies showing reaction rates of different cyclooctyne derivatives.[111] Comparing reactivity of different dienophiles ends up in lacking different reactivities of tetrazine derivatives among themselves. Representing new derivatives with possible applications was done also, but not in a detailed and comparing manner.[87] As a general trend in tetrazine reactivity, *EWG*s substituents in 3- and 6-position of the tetrazine ring accelerate *IEDDA* reactions due to the lowered *LUMO* frontier orbitals as shown in Fig. 6 D. Based on this rule of thumb, a general order in reactivities can be drawn up.[87] An excerpt of tetrazine derivatives according to their reactivity is depicted in Fig. 7 B.

Reaction	Reactant	Rate [$M^{-1}s^{-1}$]
CuAAC	Alkine / azide	$10^{-2} - 10^{-4}$
Staudinger-Bertozzi ligation	Azide / phosphine	10^{-3}
SPAAC	Strained alkine / azide	1
IEDDA	Norbornene / tetrazine	$1 - 10$
	TCO / tetrazine	10^5

Table 1: Averaged reaction rates of click reactions.

The overall reaction rate of an *IEDDA* reaction between a strained alkene and a tetrazine compared to other click-reactions is shown in Table 1. In contrast to the copper-

catalyzed alkyne/azide click (*CuAAC*), mostly reffered as the archetype of click-reactions or the Staudinger-Bertozzi ligation between an azide and a phosphine, *IEDDA* reactions, are a thousand times faster. Strain-promoted alkyne/azide click-reactions (*SPAAC*) are in the same range of reaction rates like a usual *IEDDA* reaction. Using high reactive dienophiles like TCO, *IEDDA*s' reaction rate is increased again about a tenthousand fold. As biggest advantage in *IEDDA* click chemistry regarding mentioned reaction kinetics is the tuning possibility of reaction partners. By using solvent influences and coordinating the nature of diene and corresponding dienophile to one another, a golden mean for desired applications can be chosen.[68,87,96,101,112]

1.1.3.2 Synthesis of asymmetric substituted tetrazines suitable for *IEDDA* click

Tetrazines undergo an *IEDDA* cycloaddition with strained alkenes followed by a subsequent nitrogen extrusion caused by a retro-Diels-Alder reaction resulting in a dihydropyridazine derivative. As already mentioned this reaction is high-yielding and fast at room temperature in aqueous media.[87]

Symmetric and asymmetric substituted tetrazines can be yielded by different reaction pathways. Two main pathways are pointed out in retrosynthetic scheme shown in Fig. 8. In both pathways first retrosynthetic step is a reduction to a dihydrotetrazine as precursor. Following the upper pathway in Fig. 8, hydrolysis is next retrosynthetic step leading to bisaminde derivatives, which can be separated by further hydrolysis into hydrazine and carboxylic acids.[113] Following lower pathway in Fig. 8 shows a direct separation of dihydrotetrazine precursor into nitriles can be achieved using Pinner reaction like conditions. Thus, an *in situ* generated amidine is used as reactive intermediate.[113,114]
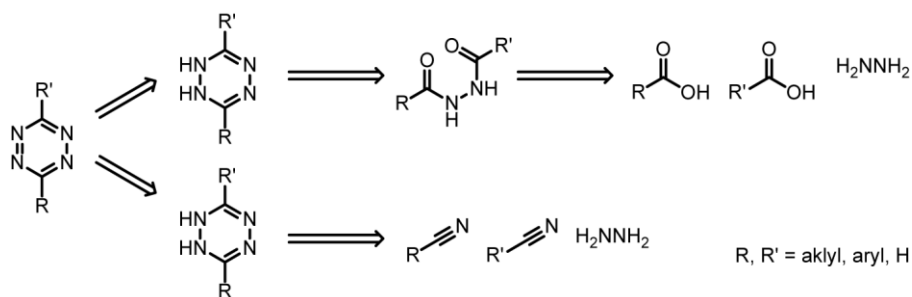

Fig. 8: Retrosynthetic reflection of tetrazine formation.[113]

Pinner reaction was first reported in 1876[114] and describes formation of imidines using nitriles.[115] In general, nitriles are treated with an excess of a strong acid and an alcohol first. Subsequent excess of amines forms desired amidines as shown in Fig. 9. In the

first step, terminal nitrile is protonated and after addition of primary alcohol corresponding imino ether is formed. Amidine formation takes place via a tetrahedral intermediate. After intramolecular rearrangement, double bond between nitrogen and carbon can be formed. After deprotonation, an amidine is formed.[114,115]
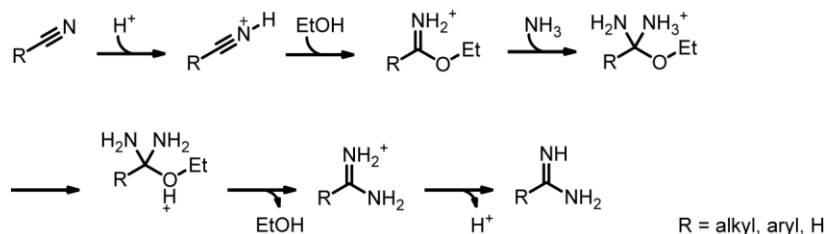

Fig. 9: Mechanism of Pinner reaction.[115]

Transferring Pinner reaction to tetrazine synthesis, the alleged tetrazine intermediate – a 1,2-dihydrotetrazine or 1,4-dihydrotetrazine – which is gained after the Pinner reaction[114] of two nitriles and hydrazine has to be oxidized to the aromatic tetrazine as depicted in Fig. 10 as final step.

As first step of the reaction, a terminal nitrile reacts with hydrazine in an addition to hydrazide. After an analogous addition of a second nitrile, precursor is formed. After intramolecular extrusion of hydrogen 1,2-dihydrotetrazine is formed. Subsequent mild oxidation yields corresponding tetrazine as product.[113–115] The reaction is usually carried out in aqueous hydrazine solution and can be performed with various sterically accessible nitriles.[116] Subsequent oxidation of the 1,2-dihydrotetrazine intermediate[93] can be either performed using sodium nitrite in acetic acid or 2,3-dichloro-5,6-dicyano-1,4-benzoquinone (*DDQ*) in toluene.[80] Oxidation proceeds in both reaction pathways usually in a quantitative manner.[80]
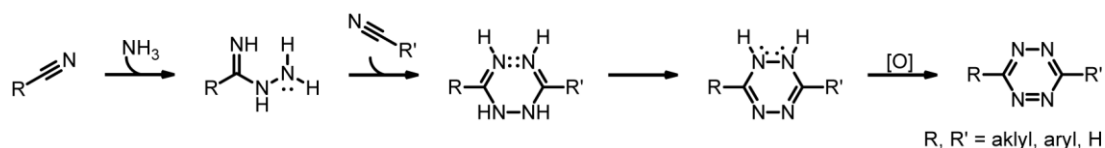
Fig. 10: Tetrazine synthesis via Pinner reaction.

As crucial synthetic impediment in asymmetric substituted 1,2,4,5-tetrazine synthesis according to shown synthetic pathway, probability calculation has to be named. Obtaining asymmetric substituted tetrazines, a statistic yield of 33% is estimated. Lewis-acid promoted synthesis and adapted synthetic pathways raised yields and variety of asymmetric substituted tetrazines suitable for *IEDDA* applications[90,91,93,117–119] as well as elementary sulfur was used[120] to increase yield.
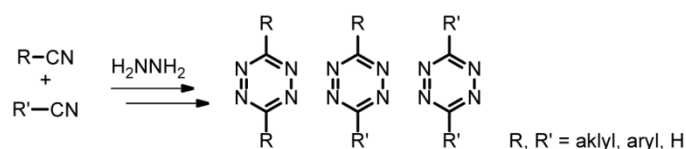
Fig. 11: Statistic distribution of asymmetric tetrazines synthesized via Pinner reaction.

Main goals in synthetic approaches are improvements in yield of asymmetric substituted tetrazines using additives like Lewis-acids[89], sulfur[121], or metal triflates[93] respectively. Harsh reaction conditions of Pinner tetrazine synthesis[116] led to other synthetic pathways far from Pinner type reactions following second retrosynthetic pathway shown in Fig. 8. Alternative pathway was partly published in the late 1970s by Baddar et al.[122] A full synthetic route according to this route was published in 2004[123]. Main advantage of this multistep synthesis is avoidance of unwanted byproducts[124]. Synthetic pathway is shown in Fig. 13 and will be discussed in the following. Synthesis of asymmetric tetrazines via satistic distributed Pinner synthesis as shown in Fig. 11 generates an excess of symmetric tetrazines, which is described in literature, too.[125] In the 1970s Cohen and coworkers showed the diversity of possible byproducts using a Pinner like synthetic pathway.[124] Identified byproducts are shown in Fig. 12. Byproducts can be removed by chromatographic separation.
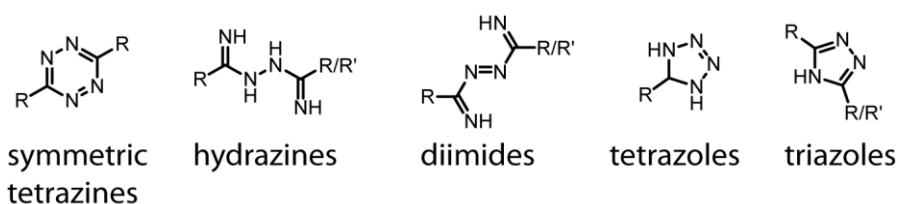

symmetric tetrazines   hydrazines   diimides   tetrazoles   triazoles

Fig. 12: Identified byproducts in tetrazine synthesis using Pinner reaction like conditions.[124]

As already mentioned, statistic distribution can be ceased by synthesizing a preformed tetrazine precursor. Retrosynthesis can be carried out as described in the following (see Fig. 13 A). Before final oxidation of a dihydrotetrazine, the heterocyclic ring can be closed using a hydrazine-mediated cyclocondensation on a dichloroazine. This compound can be easily gained using a substituted hydrazide. Eicher and Hauptmann[123] described the synthetic approach as explained in Fig. 13. A hydrazide and a carboxylic acid chloride are fused in a base mediated way to corresponding coupled hydrazine derivative. Conversion into the dichloroazine is carried out using a suitable chlorination reagent. The cyclocondensation is performed under standard conditions using aqueous hydrazine solution. Subsequent oxidation can be done using NaNO$_2$ in glacial acetic acid or *DDQ* in toluene respectively.
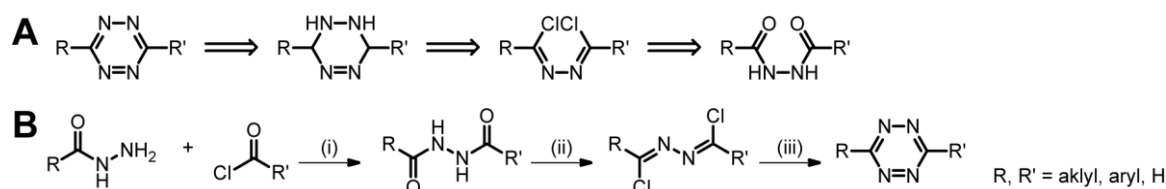
Fig. 13: Tetrazine synthesis using precursors. (A) Retrosynthetic pathway for tetrazine synthesis using a 1,4-dichloroazine precursor. (B) Synthetic pathway for tetrazine synthesis: (i) basemediated hydrazine formation, (ii) chlorination, (iii) cyclocondensation and subsequent oxidation.[123]

In addition to an optimized tetrazine synthesis, a constant tuning of diene and dienophiles occurred. Different dienophiles are shown in Fig. 7. Two examples are depicted in Fig. 14. Norbornene is a moderate reaction partner for *IEDDA* applications, lacking reaction rates like TCO. As advantage in contrast to TCO, norbornene is stable under most conditions.[41,81,87] Same applies for tetrazine derivatives.[81] Striking a balance between stability and reactivity can be considered as highest purpose. In this work, two different dienophiles – norbornene and cyclopropene – will be used.
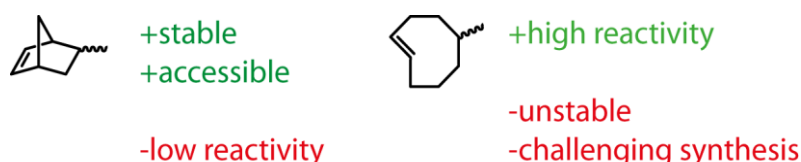

Fig. 14: Comparison of properties between norbornene and TCO as dieneophile.

1.1.3.3 Labeling of biomolecules using *IEDDA* reactions

Using different labeling systems broadens the variety of applications. Thus, *IEDDA* reactions can be used for a plethora of labeling strategies in different biochemical applications like briefly listed before. Ranging from ^{18}F-labeled TCO tracers suitable for *IEDDA* click reactions on tetrazine bearing enzymes[105,126] up to green fluorescent protein (GFP) fused to a tetrazine containing amino acid, which can be clicked with TCO.[112]

As mentioned beforehand, in 2008 two working groups published simultaneously the *IEDDA* reaction between tetrazines and strained alkenes.[80,81] Neither Fox nor Hilderbrand nicknamed it a click reaction. Both only referred to the similarities to other click reactions. Fox described an unusual fast reaction using a system of TCO and tetrazines on proteins, Hilderbrand on the other hand used a tetrazine norbornene system for antibody targeted live cell labeling.[80,81] Hereinafter Hilderbrand's group set a milestone for biorthogonal labeling more or less by accident. As subsequent attempt for intracellular labeling, tetrazine fluorophore conjugates have been synthesized and a

strongly reduction of fluorescence between parent succimidyl esters of fluorophores and synthesized conjugates were measured.[103]
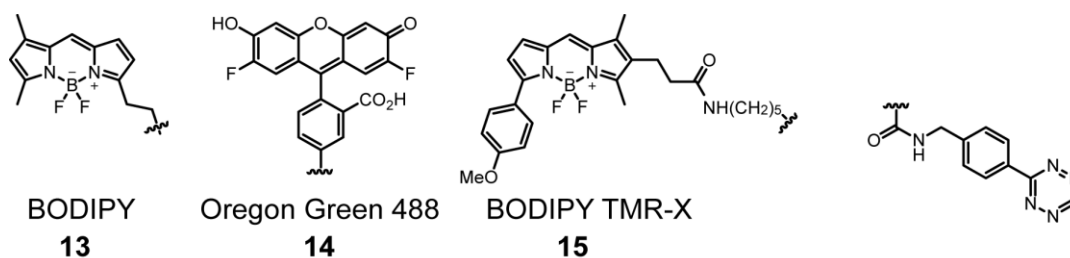
They realized the scope of such activatable turn-on probes and the related benefical signal-to-background ratio, which is essential for *in cell* and *in vivo* imaging.[81,103] The caused avalanche of labeling approaches on nearly all kinds of biomolecules. Labeling via genetic encoding during protein synthesis as well as enzymatic or chemical modification of proteins can be named for example. Furthermore, modified mono- and polysaccharides were synthesized and chemical reporters for lipid labeling are literature known, too. All those methods will not be explained in detail and can be reread in the related literature.[40,82,87–93,95,96,98–103,105–107,111,112,116,118,119,121,126–147]
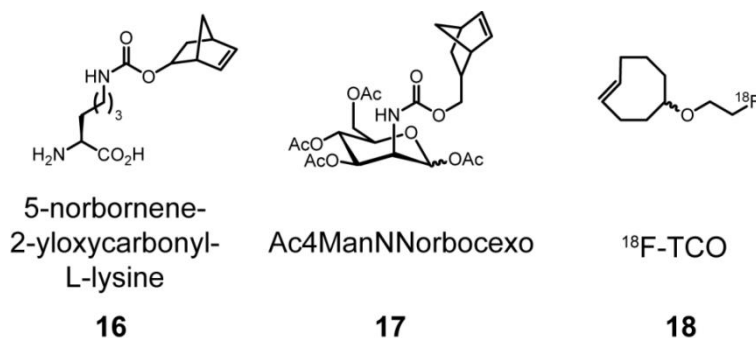

Fig. 16: Norbornene modified amino-acid[99] **(left), a norbornene modified mannose**[148] **(center) and a radiolabelled TCO**[126] **(right) suitable for *IEDDA* click.**

1.1.3.4 Quenching properties of tetrazines suitable for *IEDDA* click reactions

Mentioned GFP quenching by spatially close tetrazines groups[112] as well as discussed tetrazine-fluorophore conjugates[80,81] leads to another aspect of *IEDDA* reaction between tetrazines and strained alkenes or alkynes not yet explained in detail.

Tetrazines possess quenching properties around 500 nm.[149–151] The bright red to purple colored compounds have low-lying π* orbitals and support an n→π* transition of electrons in the visible light range.[152] Substituent pattern in 3- and 6-position have only minor influences on the precise absorption wavelength and the absorption maxima can

be settled between λ = 515 nm (3,6-dichloro-1,2,4,5-tetrazine) and λ = 540 nm (3,6-dipenyl-1,2,4,5-tetrazine). The corresponding fluorescence wavelengths are roughly between λ = 550 nm and λ = 600 nm.[121,149] An excerpt of 3,6-substituted tetrazines and the corresponding absorption and fluorescence maxima are shown in Table 2. A second absorption maximum based on the π→π* transition is in the UV region[121] and therefore not relevant.

Substituent X	Substituent Y	UV/VisAbsorption λ^{abs} [nm]	Fluorescence λ^{em} [nm]
Cl	Cl	515	551
⋮			⋮
OMe	OMe	524	575
⋮			⋮
Phenyl	Phenyl	542	602

Table 2: Absorption and fluorescence maxima of different tetrazine derivatives recorded in dichloromethane (DCM).[149]

Absorption maxima between 520 nm and 565 nm are in the range of visible green light[153], so quenching of suitable fluorophores by tetrazines is a possible application. In the following, exemplary tetrazines and fluorophores will be discussed for *IEDDA* applications.

In 1972, fluorescence and quenching of tetrazines was described by Cassen and coworkers.[150] Energetic levels and wavenumbers of tetrazines showed the ability for quenching and this thesis[150] was confirmed in 2005 by electro- and photochemical investigations of Méallet-Renault and coworkers.[149] After Fox'[80] and Weissleders'[81] publications from 2008, subsequent investigations on quenching properties of tetrazines have been carried out.[117,147,154] First studies showed, that stability of tetrazines under physiological conditions is caused by adjacent benzyleamino modifikations.[155] Additionally, quenching properties of tetrazines are pH-independent.[81] The studies agree with former spectroscopic, electrochemical and theoretical studies carried out by Audebret and coworkers.[149,152,156]

Most commercially available fluorophores can be purchased as N-hydroxysuccinimide or maleimide derivatives, which are highly reactive.[157,158] Fluoresceine- and Rhodaminederivatives are widespread fluorescent tags, caused by their absorption maxima between λ = 510 nm and λ = 615 nm as well as their very high molar extinction coefficient up to ϵ = 80000 M^{-1}cm^{-1}.[153] Boron-dipyrromethene (*BODIPY*) based dyes are also applicable for tetrazine based quenching, but possess a very small Stokes'shift[153] as referred in Table 3.[159]

Fluorophore	Absorption maximum [nm]	Emission maximum [nm]	Δ [nm]
BODIPY	505	513	8
Oregon GreenTM 488	496	524	28
Rhodamin Green	502	527	25

Table 3: Absorption and emission maxima of selected fluorophores.[159]

Furthermore increasing turn-on ratios by variation in fluorophores and corresponding substituent modification were carried out.[89–91,93,118,137,142,146] Discussed quenching properties on fluorogenic dyes suitable for biochemical or biological labeling applications combined with physiologically stable tetrazines is a highly interesting aspect for *in vitro* and *in vivo* applications. Caused by tetrazines' quenching properties, an in-cell application is favored. Unreacted tetrazine-fluorophore conjugates can not be washed out, but will also not affect the measured signal. Based on this idea, several intracellular labeling experiments were carried out.[98,141,160,161] For this study, nontoxic[162] fluorescein-based Oregon Green[TM] 488 was chosen to investigate quenching properties of tetrazines, because it shows a higher quantum yield than other literature-known fluorophores e.g. *BODIPY* or coumarin[155] and therefore better applicable for super-resolution microscopy[163] or other super-resolution applications.

1.1.3.5 Former synthesis of asymmetric substituted tetrazines as fundamentals for improved derivatives

Based on former results during diploma thesis[164] synthesis on amine-bearing asymmetric substituted tetrazine derivatives was continued to improve quenching properties for appropriate fluorophores.

All former synthesized tetrazine derivatives were modified with a *para*-aniline or *para*-benzylamine moiety regarding the 3-position of the 1,2,4,5-tetrazine scaffold. So fluorophores and other molecular probes can be introduced via *N*-hydroxysuccinimide (*NHS*) chemistry. Opposite this functional component, various aromatic systems were attached to investigate influence of different aromatic systems in view of quenching properties towards centered tetrazine. After conjugation of the synthesized tetrazine derivatives to commercially available fluorophore Oregon Green[TM] 488 (*Thermo Fisher Scientific*) an *IEDDA* click reaction was carried out in aqueous media using a norbornene carboxylic acid (**24**, Fig. 17 C) as role model. Explained workflow and the synthesized compounds are shown below in Fig. 17.
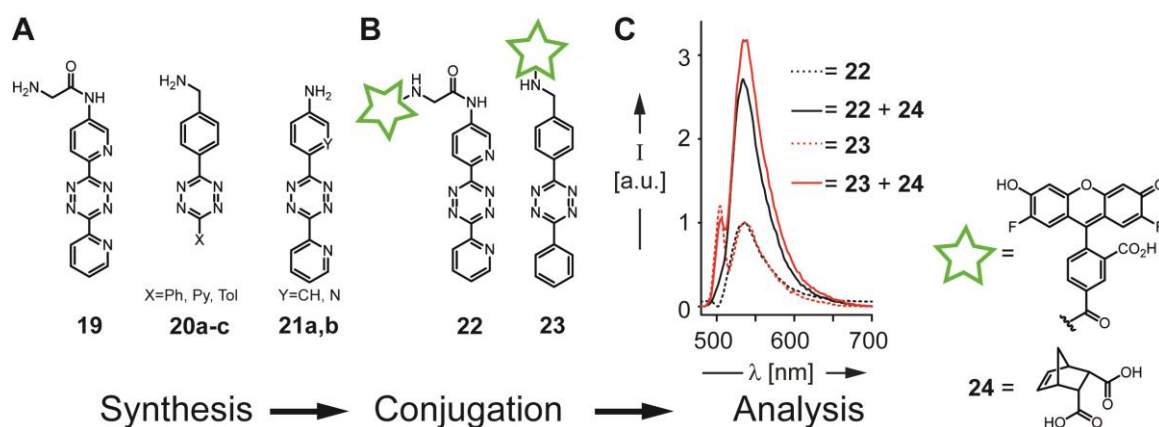
Fig. 17: General workflow during diploma thesis. After synthesis of asymmetric tetrazine derivatives (A), tetrazine-fluorophore conjugates were prepared (B) and analysed in view of turn-on activity (C).[101,164]

An increase in quenching was suggested lacking –CH_2– like between compound **21a** and **21b** (see Fig. 17). Unfortunately no conjugation between aniline moiety of **21a** or **21b** and Oregon Green™ 488 was observed using different reaction conditions. LC-MS analysis of the reactions showed only traces of corresponding tetrazine-fluorophore conjugates. This concludes that the methylamine moieties crucial for a successful amide coupling using base mediated reaction conditions.[164]
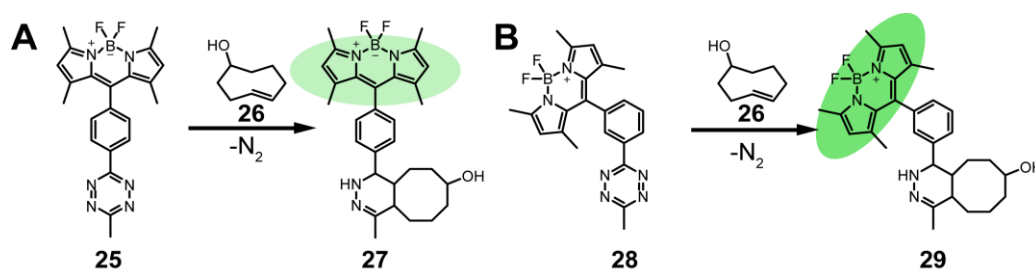

Fig. 18: Weissleder compared turn-on ratios of a para substituted tetrazine-fluorophore conjugate (A) and a meta-substituted one (B).[146]

In 2013 Weissleder and coworkers reported a correlation between the position of an attached fluorophore and quenching properties of tetrazines.[146] By using similar reaction conditions, a meta positioned fluorophore **28**[146] showed a 1.8-fold increase of turn-on ratio in water and a 3.2-fold increase in acetonitrile related to its para positioned analogue **25**[146]. Based on this research meta-placed methylamine functionalized aromatic nitriles are used to generate novel tetrazine derivatives suitable for *IEDDA* click applications.

Based on former research of Burgess and Topp[165] it is also stated, that fluorophore quenching takes place by Förster resonance energy transfer (*FRET)* and through bond energy transfer (*TBET*). *TBET*-related quenching is only possible by using a direct

linkage between the fluorophore and the tetrazine. Desired tetrazine derivatives bear a methylamine linker to attach different functional moieties. The usage of aniline nitriles was rejected based on former negative results in tetrazine-fluorophore conjugation.[164] A *TBET* influence is not possible under available conditions and compounds.

1.2 Non-coding RNA with catalytic properties

1.2.1 Non-coding RNA play major roles in cellular context

Often referenced central tenet of molecular biology that RNA acts as an intermediate between DNA and protein was refuted by many publications, showing a wide repertoire of RNA's biological functions.[7] In the following some of the main non-coding classes of RNA will briefly be presented.

The highest number of RNA molecules per cell inherits transfer RNA (tRNA).[7,166,167] Transfer RNA is involved in the translation of mRNA into protein and its principal function is to transport amino acids to the ribosome.[168,169] The oligonucleotides ranging from 70 nt up to 95 nt are folded in a tertiary structure, which is characteristic for tRNA.[168,170] The formed cloverleaf can be separated in four parts, shown and lettered in Fig. 19. Taking a walk from 5′-end to 3′-end, D-stem and D-loop can be named as first landmark found in all tRNAs. This region is named after common occurrence of uridines reduced form dihydrouridine [D].[168,170] Next, anticodon-region, consisting of anticodon-stem and anticodon-loop is reached, bearing the defined base triplets binding to mRNA's code triplet.[169] Third region is formed by TΨC-stem and TΨC-loop. TΨC signifies thymine (T), pseudouridine (Ψ) and cytidine, the three commonly occurring necleobases in this tRNA region.[168,170] Reaching 3′-end, amino acid attachement site is reached. Bearing the anticodon region and corresponding amino acid at 3′-end, tRNA's function includes initiation and elongation in peptide synthesis transferring mRNAs information into proteins.[168]
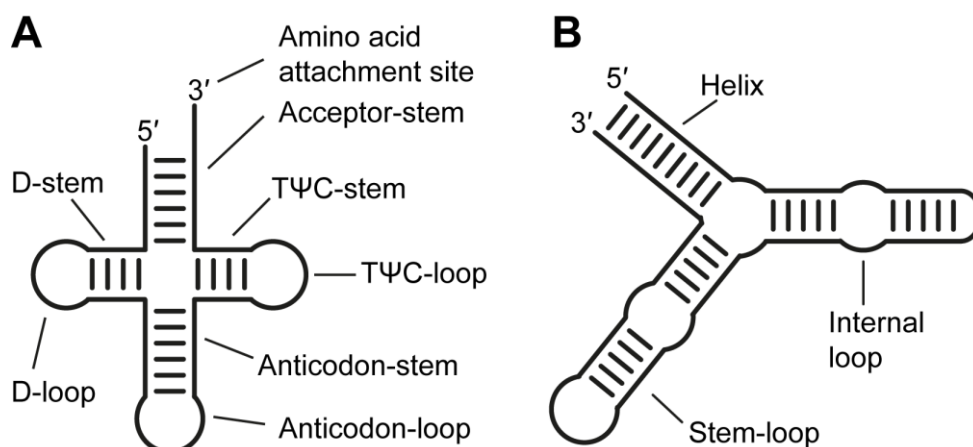

Fig. 19: Characteristic cloverleaf structure of a tRNA[168,171] **(A) and schematic presentation of *E. coli* 5S rRNA**[9,172] **(B).**

Second place in cell's RNA class by number of molecules is taken by ribosomal RNA (rRNA). Caused by its averge size of about 7 kilo bases (kb), rRNA receives more than

80% of cellular RNA by mass. As an integral part of the ribosome, rRNA represents 50% to 60% of the ribonuleoprotein.[172] Regarding structural aspects, rRNA possesses high conservation of primary structures even though rRNAs vary in sizes between 500 nt up to several thousand nucleotides.[172] Secondary structures have been solved by interactions between comparative sequence analysis, crystallographic and computational experiments. Fig. 19 shows a schematic presentation of *E. coli* 5S rRNA. This small oligonucleotide presents the kinds of local features seen in large rRNAs, consisting of helices, internal loops and stem-loops.[9,172] Tertiary structure of this class of non-coding RNA has to be described with its associated proteins,[9,172] but this is beyond the scope of this work.

Another class of RNA present in cells is long non-coding RNA (lncRNA). There is no widely accepted definition of lncRNA, apart from a commonly used threshold lower than 200 nt in RNA length.[173] This definition is arbitrary and does not represent any function or mechanism of RNA. LncRNAs can be found in a variety of species ranging from viruses to animals[173] and they are involved in a plethora of biological processes[174–176], such as splicing[177], translation[178], cellular structure integrity[179], or heat shock response.[180] Caused by the fact, that lncRNAs are commonly expressed on very low levels[173], this class of RNA was regarded as transcriptional noise or dark matter.[167,173] Approaches to classify the masses of identified lncRNAs by the four major characteristics, namely genomic location, exerted effects on DNA, functional and targeting mechanism help to create a scientific valid definition of lncRNA.[167,173,174,181] Modern computational methods deal with exon mapping[182], database screening[183] and connectivity mapping[184] between lncRNAs, small molecues and diseases. If only 10% of the plethora of mapped and validated lncRNAs proven to hold a biologic function, it would represent a wealth of biology.[167] One major disadvantage of mapping techniques is the lack of structural information of large RNA molecules.[185] In 2014 only nine unique RNAs over 200 nt were visualized crystallographically.[185] Expanding robust technologies and methods developed for e.g. ribonucleic enzyme (ribozyme) visualization on other non-coding RNAs[185] seems to be a promising approach to shed light on lncRNAs.

1.2.2 Ribozymes

Ribonucleic acid enzymes or shortened ribozymes are catalytic RNAs found in nature[186] or developed in test tubes.[187,188] They revitalized the "RNA world" theory[189], stating a primordial era when RNA served as genotype and phenotype.[190] Since the discovery of the RNA moiety of Ribonuclease P in the early 1980s[191] interest in this small, site-specific and self-cleaving RNAs of 50 nt to 150 nt nucleotides length was increased up to modern applications like CRISPR technique for genome editing.[192,193]

In general, ribozymes, excluding the ribosome, can be divided into two groups according to their functionality.[194] A differentiation between self-cleaving ribozymes and splicing ribozymes can be made.[194] Splicing ribozymes perform excision of introns and covalent linkage of corresponding exons without assistance of proteins.[194] Those heterogeneous self-splicing introns (group I and group II) are present in many precursors of mRNA, tRNA and rRNA.[194] In Fig. 20 are exemplarily shown the crystal strutures of a self-splicing group I intron including both exons (left)[195] and crystal structure of a self-splicing group II intron (right)[196].
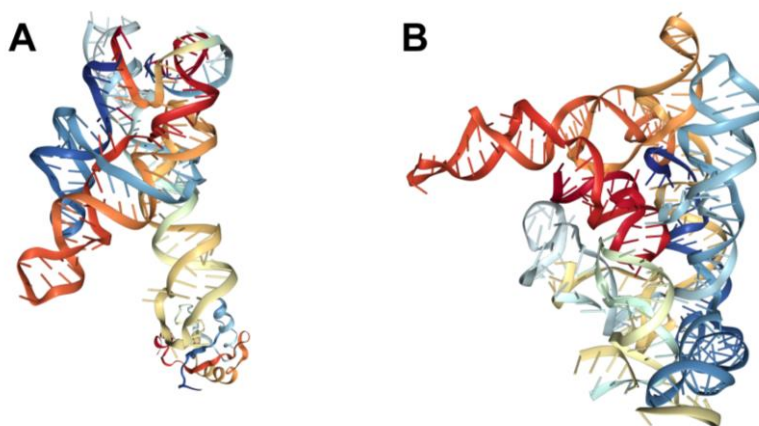

Fig. 20: Crystal structures of a self-splicing group I intron (left; pdb: 1U6B)[195] **and a self-splicing group II intron (right; pdb: 3BWP)**[196]**.**

Regarding small nucleolytic ribozymes in the last decades, fourteen classes were discovered. Most prominent ones like the hammerhead or hairpin ribozyme up to new classes like *twister*, *hatched* or *pistol* ribozymes.[189,197] A schematic presentation of secondary structure of hammerhead, hairpin, Varkud satellite (VS) and hepatitis delta virus (HDV) ribozyme is shown in Fig. 21. A brief overview of this fourcatalytic active RNAs will be given in the following.
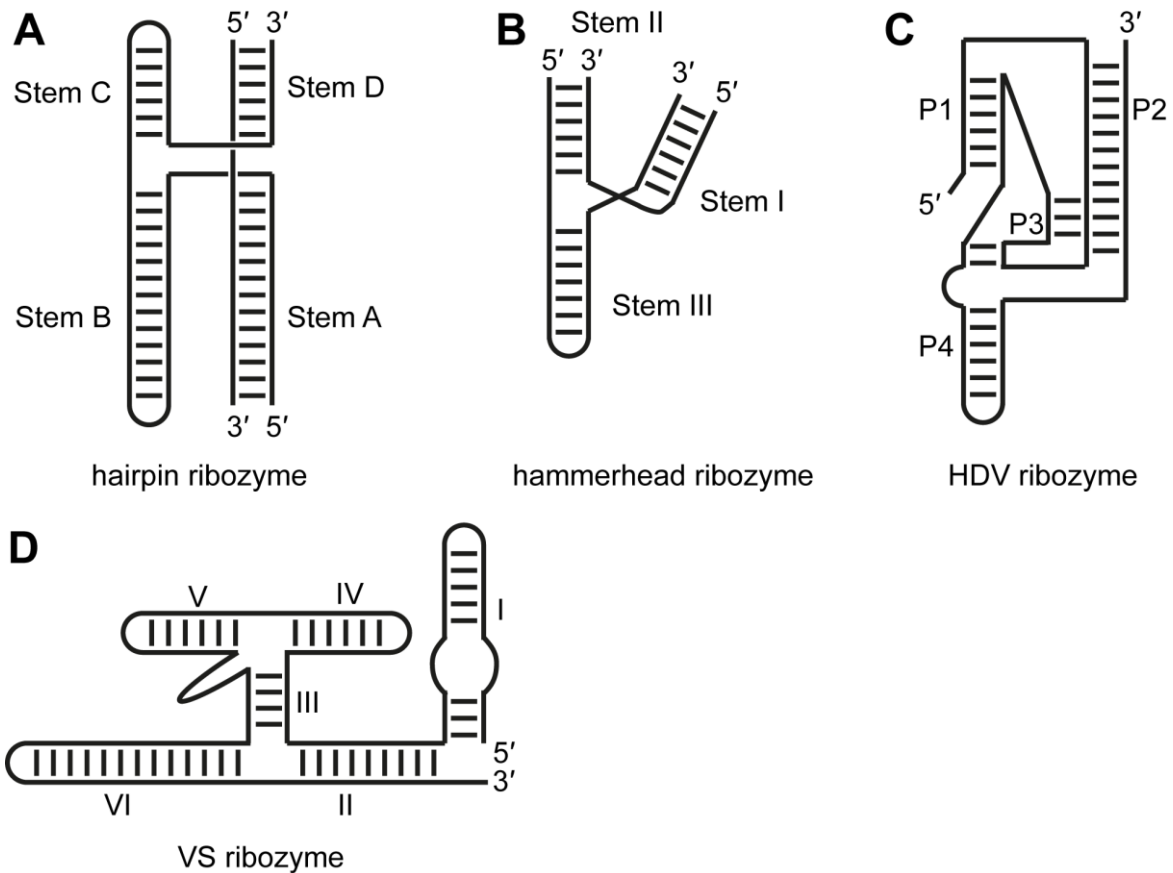
Fig. 21: Schematic presentation of secondary structure of hairpin (A), hammerhead (B), HDV (C) and VS (D) ribozyme.[186,194]

Hairpin ribozyme with its biological role to perform site-specific phosphosdiester bondcleavage in the course of virus replication was first isolated in tobacco ringspot virus.[198] It consists of four helical regions (Fig. 21 A, Stem A to Stem D) interrupted by two internal loops.[199] The hammerhead ribozyme which was originally found in autonomous subviral plant pathogens has also been discovered in the genome of higher organisms like e.g. salamanders.[198] Biological relevance of this self-cleaving RNA is the processing of unit-length viral genomes during rolling circle replication.[198] The three-strand junction composed of three helices is depicted in Fig. 21 B.[198,200] VS ribozyme (Fig. 21 D) was found in the mitochondria of certain *Neurospora* isolates. The VS ribozyme is responsible for monomeric transcript formation for subsequent reverse transcription forming VS ribozyme strand cDNA.[198,201] Unlike for the other shown ribozymes, there is crystal structure for the VS ribozyme so far and general fold (Fig. 21 D) could only be provided by biophysical studies.[201] HDV ribozyme was originally thought to exist only in hepatitits D virus, but other HDV-like ribozymes have been discovered in mammals or fruit flies.[198] The structure consists of five paired domains and two pseudoknots as shown in Fig. 21 C.[198,202]

Mechanistic investigations on this catalytically active RNA constructs pointed out a mechanistic relation to the mechanism of proteins. After a nucleophilic attack on the RNA's phosphate backbone, cleavage results in a 2',3'-cyclic phosphate product and a 5' hydroxyl termini product. Cleavage can occur by general acid-base catalysis or a divalent metal ion mediated way as depicted in Fig. 22.[203]
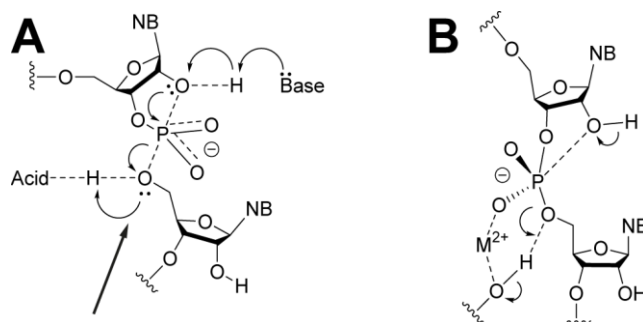

Fig. 22: Cleavage mechanisms of catalytic RNA. General acid-base catalysis (A)[200,202,204] **and metal-ion mediated way (B)**[205–209]**.**

The acid-base mediated pathway recommends an in-line trajectory to follow the S_N2 mechanism with inversion of configuration at the phosphate as shown in Fig. 22 (A). Depicted in Fig. 22 (B) is the metal-ion mediated way assumed for small ribozymes. This reaction pathway is a combination of metal ions and RNA nucleobase contribution. For larger constructs like splicing ribozymes more metal ions are involved in this catalytic pathway, catalyzing several reactions in the act of splicing.[198] Metal-ion mediated catatysis was assumed for several ribozymes listed above.[199,208,210] Indeed, newer studies verify general acid-base catalysis for nucleolytic ribozymes.[200–202,204,211] However, metal-ions influence on catalytic activity and structural contribution is still discussed controversial in some cases.[198]
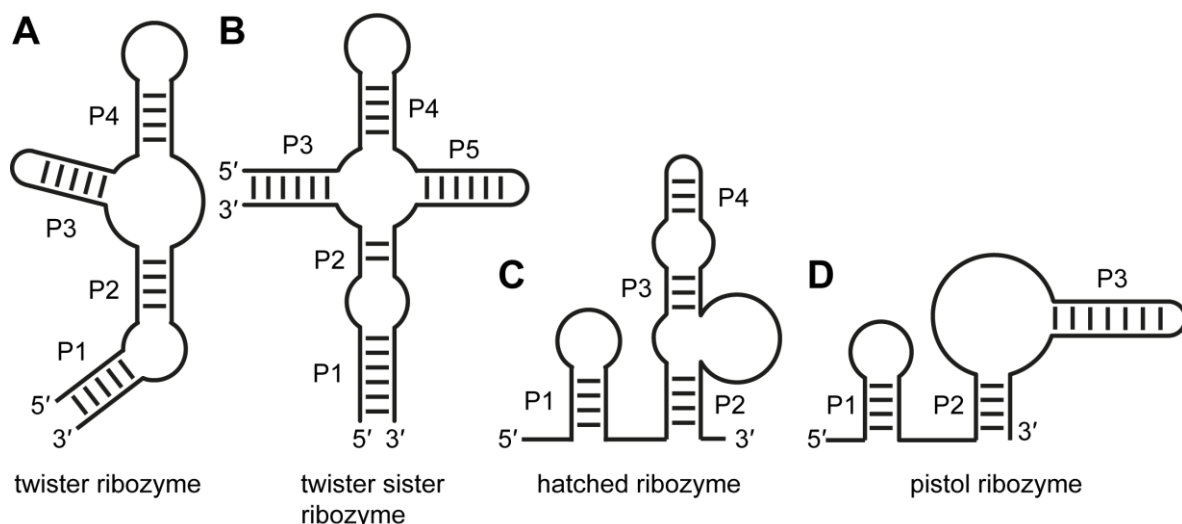
Fig. 23: Secondary structure of recently identified ribozyme motifs: Twister (A)[212–214] and twister sister (B)[215] as well as hatched (C)[216] and pistol ribozyme (D)[216,217].

Recently identified ribozymes and ribozyme motifs shown in Fig. 23 such as twister[212–214,218] or pistol[215,216,219,220] ribozyme still have to be investigated, wether the catalytic mechanism is also based on general acid-base or metal-ion mediated catalysis.

1.2.3 Twister as novel ribozyme motif

In 2013 a widespread RNA motif was identified in bacteria.[218,221] The three-dimensional structure of twister motif resembles an Egyptian hieroglyph 'twisted flax'[222] caused by intrastrand pseudoknots and was named in the same manner. Fig. 24 shows a comparison of the hieroglyph and secondary structure of twister ribozyme.[222,223] First hypothesis about function and classification of identified catalytic active RNA were carried out by Breaker and coworkers,[218] who also proofed *in vitro* and *in vivo* self-cleaving activity.
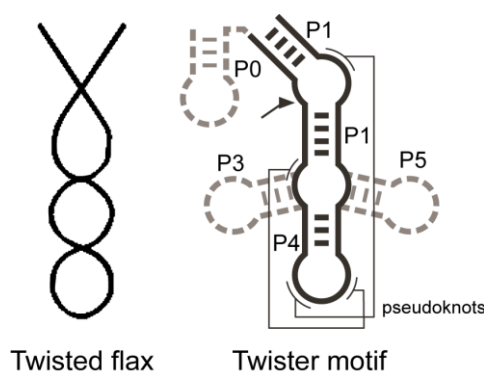

Twisted flax   Twister motif

Fig. 24: Comparison of Egyptian hieroglyph twisted flax[222] and secondary structure of twister RNA motif.[218]

24

In addition, Breakers' lab did first pH and metal ion dependant activity studies.[218] Assuming a rather structural than catalytic role of divalent metal ions in cleavage process, and thus an acid-base mediated cleavage mechanism (see Fig. 22) Breaker was not able to state a definite mechanism for self-cleaving of twister ribozyme validated by obtained data.[218] Structure of this nucleolytic ribozyme class was solved by two independent groups in the following year.[212,213] Two sequencial different variants of twister ribozyme have been used for crystallization experiments. On the one hand crystal structure was solved by a basic form of twister ribozyme from rice (*Oryza sativa*).[212,218] On the other hand genomic context was taken from an environmental sample (*env22*).[213,218] Structural differences of crystallized constructs are shown in Fig. 25.

O. sativa   **env22**
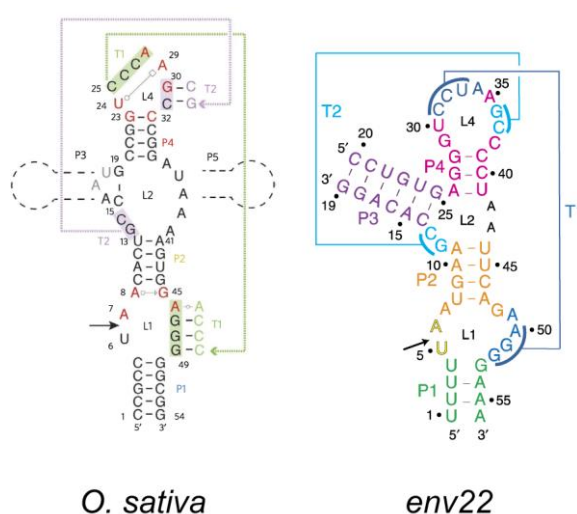
Fig. 25: Sequence and secondary structure of twister ribozyme constructs used for crystalization.[212,213] **Supposed cleavage site is marked with an arrow.**

The highly-conserved secondary pseudoknot structure is preserved either in the twister ribozyme from *O. sativa* or the *env22* sequences. Regarding both ribozymes, global fold is similar, but differ in conformational and sequential features near cleavage site.[212,213,224] Using both variants, a third group crystallized twister ribozymes, too.[214] Similar to Breaker and coworkers, a defined statement about cleavage mechanism could not be done yet.[212–214,218] Tendencially an acid-base mediated catalysis is assumed,[212–214,218] as it occurs in several other catalytic active RNAs, like the hammerhead[200,205], glucosamine-6-phosphate riboswitch (*glmS*)[225], or hepatitis delta virus (*HDV*)[226,227] ribozyme. Breakers presumption of a metal ion independent cleavage mechanism was supported by other working groups in general.[212–214] Major inconclusive points were discussed by Micura and coworkers[213] and by Steitz and coworkers.[214] If divalent metal ions inherit rather structural than catalytic role in cleavage mechanism, twister is still lacking conditions usually required for a general acid-base catalyzed cleavage. As shown in Fig. 26,

missing in-line trajectory (A) and similarities to hairpin ribozyme[199] indicate metal ion mediated cleavage and direct participation of Mg^{2+} ions in cleavage mechanism.[213]
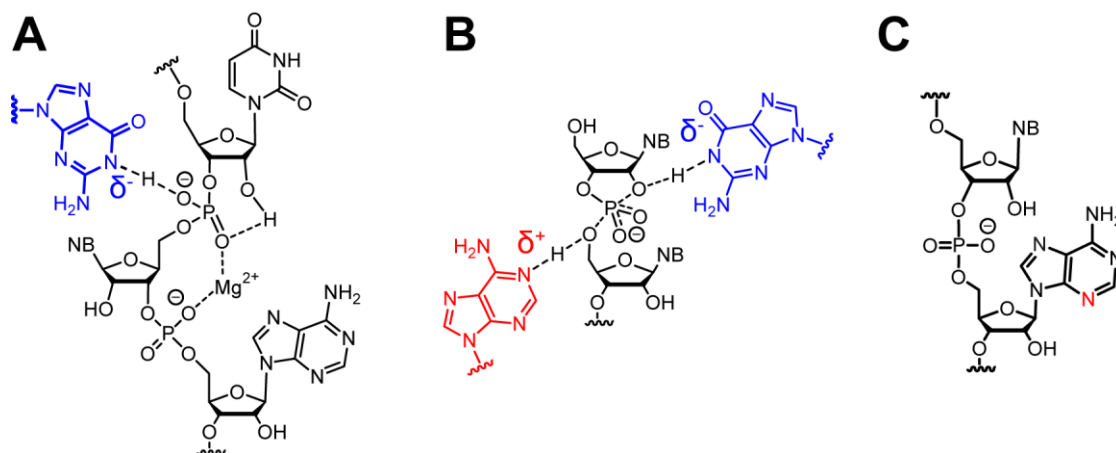

Fig. 26: Assumptions on cleavage mechanism of twister ribozyme. Missing in-line trajectory and therefor metal-ion mediated cleavage (A)[213] in contrast to in-line trajectory suitable for acid-base mediated catalysis (B).[204] N3 highlighted in red of adjacent adenine represents the only nitrogen with reasonable geometry (C).[214]

These assumptions are corroborated partly by other literature sources, stating a missing proton donor with good geometry.[214] A proton donor with reasonable geometric nature would be N3 of adjacent adenine as shown in Fig. 26 C. Refered values of adenosine's acid-base properties are based on datasets measured at nucleosides.[228,229] Kath-Schorr et al. showed in 2012[204] that logarithmic acid dissociation constants (pK_a) differ between the free nucleoside and a nucleotide incorporated in RNA. Values of an incorporated nucleotide are shifted strongly[204] and therefore an experimental verification is recommended.

Fig. 27 shows measured and published pK_a values of nitrogen atoms positioned in adenosine.[228] A detailed mechanistic probing of point mutated twister ribozyme derivatives using modified adenine will be able to enlighten the mechanistic peculiarity.
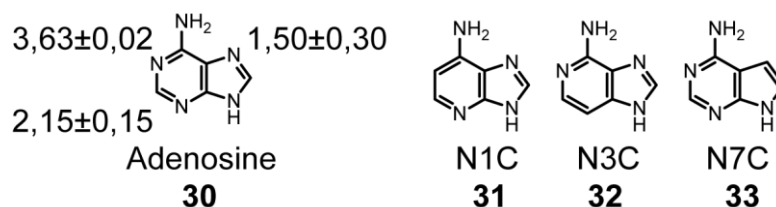

Fig. 27: Adenosine with corresponding pK_a values[228] **and needed derivatives. Only nucleobase moyeties are shown.**

Chemically synthesized RNA strands containing adenosine derivatives depicted in Fig. 27 have to be used in a comparing study regarding a pH dependent cleavage assay with and without divalent ions present.

1.2.4 Synthesis of an Adenosine analogue for probing ribozyme activity

Former discussed experimental setup requires three different adenosine derivatives suitable for chemical RNA synthesis. Derivatives N3C O2′H and N7C (see Fig. 27) are commercially available as diisopropylcyanoethylphosphoramidite (CEP).[230,231] Existing approaches towards N1C synthesis are described in the following section. For a brief overview, Fig. 28 shows general numbering of the bicyclic scaffold.
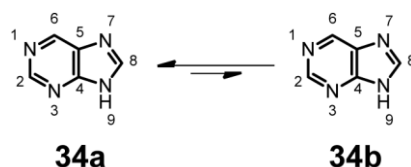

Fig. 28: Purine structure with standard atom numbering attached. Shown is the tautomeric equilibrium between 9*H*-purine (left) and the 7*H*-purine (right). Unequal equilibrium arrows depict the major and minor occuring tautomers.[232]

Literature known pathways can be used to achieve free nucleoside as depicted briefly in Fig. 29. After condensation of **35** and triethyl orthoformate, the bicyclic scaffold is formed. Subsequent nitration at position six forms the precursor of adenosine's primary amine resulting in **37**. Stannic chloride catalyzed formation of N-glycosidic bond yields protected ribonucleoside precursor **38**. Deprotection of peracetylated ribose and final heterogenic reduction of nitrogen leads to N1C adenosine **39**.
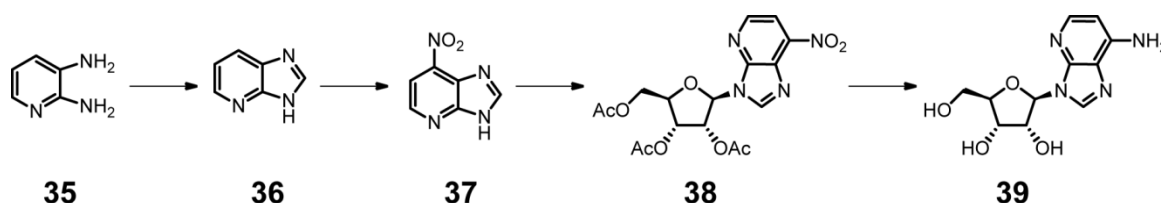

Fig. 29: Schematic overview of 1-Deazaadenosine synthesis.[233,234]

Adapting preparation Beigelman's[235] strategy, required compound **44** should be yielded after a linear five step protection cascade. As depicted in Fig. 30, primary and secondary hydroxyl groups of nucleoside **39** are protected with suitable silyl protection groups yielding **40**. In a second step, primary amine of adenosine is protected as depicted in Fig. 30 yielding **41**. Fluoride mediated deprotection of 3′-OH and 5′-OH yields **42**. Primary 5′-OH can be then protected with dimethoxytrityl chloride yielding **43**, which can be chemically converted into phosphoramidite **44** suitable for solid-phase synthesis. Listed protection groups will be discussed in a more detailed way in sec 3.5.1 regarding chemical and structural properties as well as synthetic characteristics.
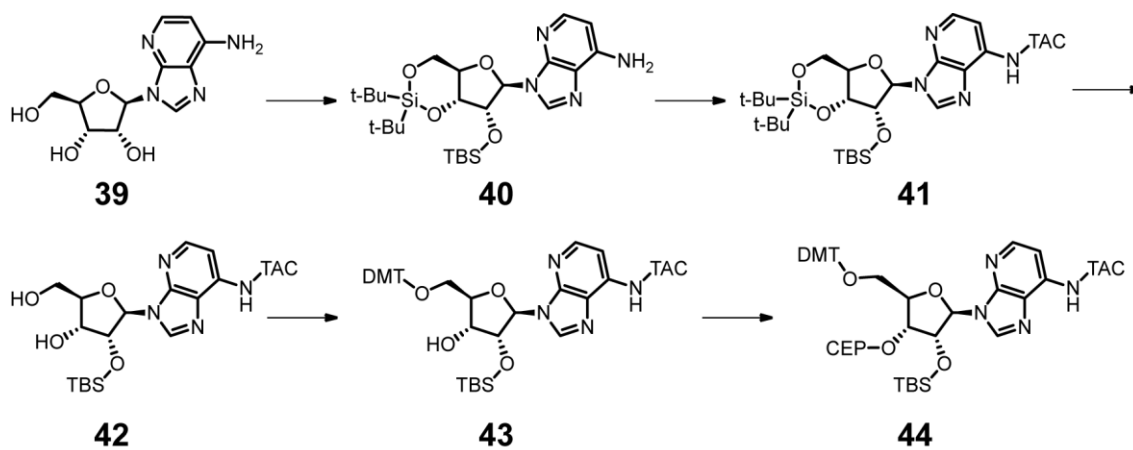
Fig. 30: Protection strategy according to Beigelman and coworkers.[235] (t-Bu = *tert*-butyl; TBS = *tert*-butyldimethylsilyl; TAC = *tert*-butylphenoxyacetyl; DMT = dimethoxytrityl)

1.3 Unnatural base pairs

1.3.1 Recommended properties of nucleobases and the expectation towards a third base pair

The specificity of enzymatic oligonucleotide replication is based on the hydrogen bonding pattern in purine and pyrimidine interactions. The A-T pairing in DNA or A-U pairing in RNA with its two proton donor/acceptor residues and the G-C pairing with its three proton donor/acceptor residues is shown in Fig. 1 before. Already in 1962 Rich discussed the role of DNA and RNA as information carrier of life using a four letter alphabet.[236] He also discussed the possibility of a two letter alphabet like used in Morse code to carry informations as well as an expanded genetic six letter alphabet.[236] He assumed a base pair consisting of isoguanine (**iso-G**) and isocytosine (**iso-C**).[236] This third, unnatural base pair (*ubp*) would comprise the required conditions for a successful application in the central dogma of biochemistry.[236] Mimicing a canonical nucleobase or base pair recommends geometric and dimensional properties.[236,237] The distance between complementary anomeric carbon atoms of corresponding molecules has to be in a certain distance range, according to natural distances in a DNA double strand or an RNA duplex. Spacing should be around 10 Å up to 11 Å and the angle λ defined as angle between paired bases related to an imaginary level has to be around λ = ~55° (see Fig. 31).[237]
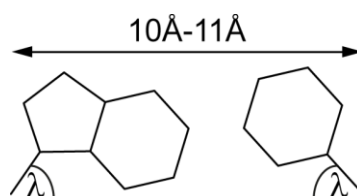

Fig. 31: Schematic presentation of required geometric conditions towards molecules acting as nucleobases suitable for DNA applications.[237] Shown are only nucleobases. Sugar moieties are not depicted.

Furthermore, the artificial nucleobases has to be hydrophobic. This is required by polymerases hydrophobic active site.[238–240] They also have to be recognized in replication in the same specificity as canonical nucleobases.[236]

If an unnatural base or unnatural base pair (*ubp*) accomplishes all recommended properties listed above, this expanded genetic alphabet would enable less biased constructions of oligonucleotides and in parallel expend the biological and chemical potential of DNA and RNA.[241,242] On the one hand, an increased insight into nucleic acids structure and function would be given by the introduction of a nucleobase, not interacting with one of the four canonical ones.[243] On the other hand, an ubp can be transcribed into

into artificial tRNA and subsequently proteins with increased functionality can be translated by introducing unnatural amino acids as depicted in Fig. 32.[244,245]
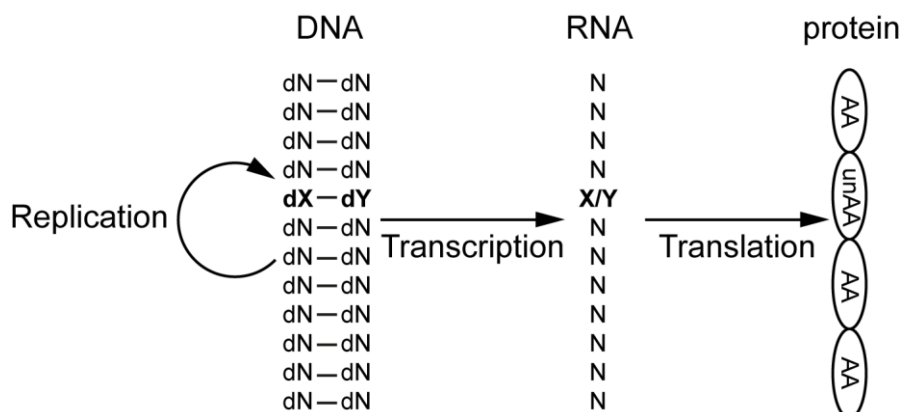

Fig. 32: An expanded genetic alphabet with a six letter alphabet (depicted as (d)X and (d)Y) would enable novel proteins by the introduction of unnatural amino acids (unAA) in contrast to natural amino acids (AA) during translation.

In addition, an artificial expanded genetic system using an extra base pair would provide novel aspects for biopolymers with increased functionality to improve hybridization or replication properties for novel biotechnologies. It could also provide new aspects on the origin of A-T(U) and G-C pairing during the prebiotic era on Earth.[244–248]

1.3.2 Development of unnatural nucleobases and unnatural base pairs

In 1989 Benner and coworker[249] synthesized mentioned **iso-G** and **iso-C** base pair depicted in Fig. 33 and showed successful *in vitro* applications on DNA level, using exonuclease-deficient Klenow fragment of *E. coli* DNA polymerase I. This scientific approach was expanded for RNA applications and other enzymatic incorporation studies.[249,250]
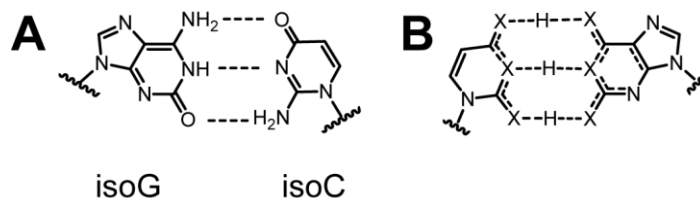
Fig. 33: Benner's isoG-isoC pair[249] **shows Watson-Crick like hydrogen bond pattern (A). These H-bonds are formed between exocyclic functional groups and the heteroatoms (depicted as X) of nucleobases heterocycles (B).**[251] Shown are only nucleobases. Sugar moieties are not depicted.

Several *ubp* systems were published using Watson-Crick like hydrogen bond pattern or reconfigured hydrogen bond pattern.[251] Also *ubp*s with the ability to form four hydrogen bonds synthesized and published.[251,252]

The importance of assumed hydrogen bonding interactions between the purine and pyrimidine nucleobases either in its natural appearance (A-T; A-U; G-C) or in an unnatural manner (**isoG**-**isoC**)[249] was refuted in 1998 by Kool and coworkers.[253]

They showed that an *ubp* consisting of nucleoside analogs with a strongly reduced polarity are enzymatically incorporated too. These nucleobases mimic the shape of a canonical base pair very closely. Compared with the natural A-T or A-U base pair the synthetic nonpolar difluorotoluene (**F**) and 4-methylbenzimidazole (**Z**) pair is closely related in size and shape (see Fig. 33). In this regard, shape selection seems to have a major influence on enzymatic processing rather than long time stated hydrogen bonding.[253,254]

Z: X=CH
Q: X=N   F
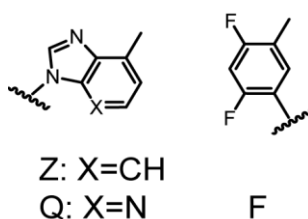
Fig. 34: Kool's Z/Q-F ubp[253–255]**is based on shape, size, and hydrophobibity. Structure is closely related to canonical nucleobases.** Shown are only nucleobases. Sugar moieties are not depicted.

This hypothesis is corroborated by Kool and coworkers by a modified unnatural base also published by this working group.[255] The exchange of a carbon into a nitrogen atom at position three in the purine-like scaffold increased replication efficiency about a 170-fold. It is guessed, that interactions between the amino acids of the polymerase with the oligonucleotide's minor groove are crucial.[255]

In this content other working groups developed also *ubp*s based on shape complementary and hydrophobicity. Exemplarily mentioned are Hirao and coworkers as well as Romesberg and coworkers. Concerning the work of Hirao's lab, only a briefly outlined overview will be given. The focus will be set on work of Romesberg's lab especially on the *ubp* (d)**NaM**:(d)**TPT3** which is part of this thesis.

The group of Hirao and coworkers adapted the work of Benner's concept, combining hydrogen-bond geometry and steric hindrance to synthesize *ubp*s based on purine and pyrimidine geometry.[256,257] Another approach was carried out, based on Kool's hydrophobic **Q**-**F** and **Z**-**F** *ubp*. To improve shape complementary, the pyrimidine analogue was modified to obtain Pa and furthermore the purine analogue was adapted to the unnatural base **Ds**. [257,258] Functionalized and improved derivatives of this *ubp* are also published. Improved **Ds**-**Px** *ubp* was successfully used for polymerase chain

reaction (*PCR*) amplification and *in vitro* selection using systematic evolution of ligands by exponential enrichment (*SELEX*) in 2016.[259,260]
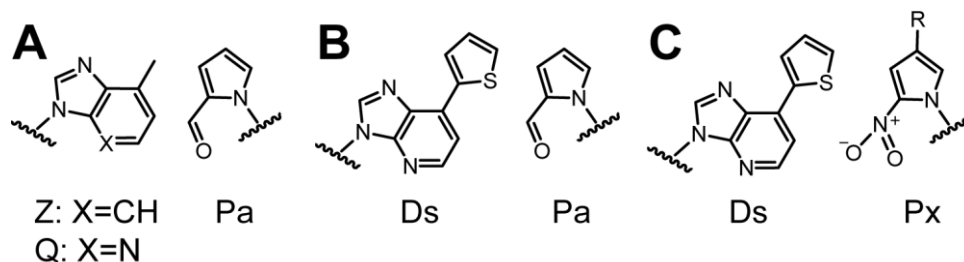

Fig. 35: ***Ubp*s published by Hirao and coworkers.** Only unnatural nucleobases without ribose moieties are shown. Based on Kool's work, *ubp*s **Q-Pa** and **Z-Pa** were published in the early 2000's (A).[246,256–258] Improved *ubp*s published by Hirao and coworkers are **Ds-Pa**[246,261] (B) and functionalized *ubp* **Ds-Px** (C).[259,261,262] Shown are only nucleobases. Ribose moieties are not depicted.

The group of Romesberg and coworkers started on the subject of *ubp* using molecular self-pairing abilities for first developments in 1999.[242] In order to avoid an overload of information not every unnatural base will be reviewed. Only milestones in *ubp* development synthesized by Romesberg and coworkers will be discussed.
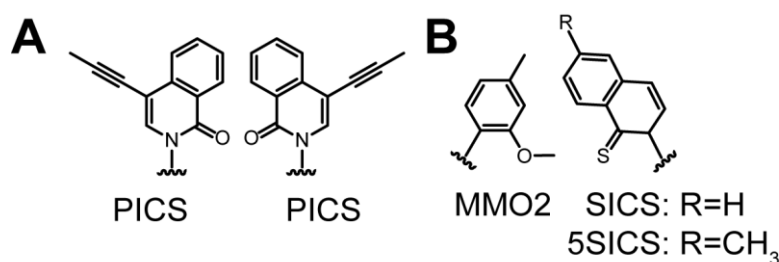
Fig. 36: Summarized overview of *ubp*s, published by Romesberg and coworkers. First successful approaches were carried out using self-pairing isocarbostyril based **PICS** (A, 1999).[242] In screening experiments, methoxymethylbenzene-based nucleotide **MMO2** and sulfonated isocarbostyril derivative **SICS** were identified as *ubp* (B, 2008).[254] Methylated **5SICS** represents an optimized derivative of **SICS**.[263] Shown are only nucleobases. Sugar moieties are not depicted.

First efforts based on hydrophobic stacking of 7-azaindole and isocarbostyril derivatives were tested in DNA. Modifications of the base scaffold were designed to test influences on the minor or major groove in DNA duplex and to increase hydrophobicity or to modify electronic structure of the molecule.[242,264]

In several studies influences of unnatural nucleobase related surface area, ring size, heteroatom- and substituent pattern were investigated. [264–268] Stability tests using thermal denaturation experiments on stacking interactions of benzene-based unnatural nucleobases in DNA positioned between two pyrimidins or two purines showed sequence dependent variations of the melting temperature. This suggests that

positioning hydrophobic nucleobase between pyrimidines is of insufficient size for an efficient packing of the unnatural nucleobase flanked by dC or dT.[269]

In 2008 Romesberg and coworkers published results of two independent screens using 3600 different *ubp*s. In summary, both screens identified d**SICS** and d**MMO2** (see Fig. 36 B) as most promising. Used screening methods are visualized in Fig. 37. Both screening methods will be outlined in a short manner in the following.

First, extension efficiency of the supposed *ubp* regarding the recognition of unnatural nucleotides by exonuclease-deficient Klenow fragment of *E. coli* DNA polymerase I was investigated *via* primer extension with dC-TP. In the second screen misincorporation of canonical NTPs opposite to the unnatural base was evaluated in a fluorescent assay, recognizing the amount of synthesized double strand DNA with and without *ubp* counterpart.[270]
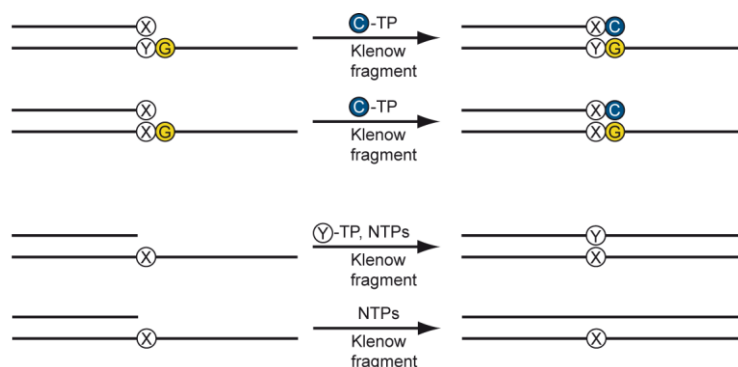
Fig. 37: Screening methods used by Romesberg and coworkers for *ubp* extension efficiency (upper part) and suppression of misincorporation (lower part). Shown are only nucleobases. Sugar moieties are not depicted.

Optimization of d**SICS** was carried out and culminated in d**5SICS** (see Fig. 36 B). The structure is strongly related to d**SICS**, but the methyl group at position five prevents unintended d**5SICS**:d**5SICS** self-pairing, detected as a side effect of the d**SICS**:d**SICS** base pair.[270]

As resulting next step optimization of d**MMO2** was necessary. An increased aromatic surface opposite to the methoxy group or the deoxyribose in the unnatural nucleotide d**NaM** showed the best results as counterpart for d**5SICS**. The overall fidelity of the d**NaM**:d**5SICS** heteropair (see Fig. 38 A) is stated as remarkable.[271]

First experiments using the *ubp*s d**5SICS**:d**MM2** and d**5SICS**:d**NaM** concerning *PCR* amplification rates and modification options of the individual nucleotides at proper positions RNA applications of the mentioned *ubp*s were done similar. Also structural investigations on the behavior of *ubp*s during replication by the KlenTaq DNA polymerase were done. [241,272,273]

33

Ongoing research created a variety of unnatural nucleobases, bearing different substitution pattern and different substituents.[276] As next milestone in progress, discovery of *ubp* d**TPT3**:d**NaM** (see Fig. 38 B) will be mentioned.[277] This *ubp* as "the most promising one"[277] obtained also our interest.
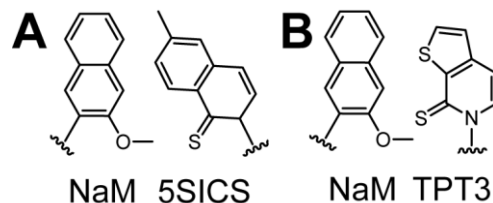

Fig. 38: In 2014, *ubp* 5SICS:NaM was used in the first organism propagating stably with an expanded genetic alphabet (A).[1] NaM based on methoxynaphthalene was also stated to be part of the most promising *ubp* NaM:TPT3 (B, 2014).[274] TPT3, a thieno substituted substituted pyridinethione combined with NaM is the prosperous *ubp* up to date.[275] Shown are only nucleobases. Sugar moieties are not depicted.

1.3.3 Biochemical properties of ubp recommended for replication and transription

As discussed beforehand, unnatural nucleobases have to fulfill recommended properties regarding shape and geometrie that they are able to fit into polymerases active site.[236,237] The major requirement for an unnatural nucleobase is hydrophobicity that it can interact with polymerases active site.[238,239] In addition, an ubp has to be replicated on DNA level and transcribed into RNA with similar efficiency and specificity as canonical base pairs. Several important interactions, such as base stacking among neighbouring nucleobases, hydrogen bonding, dipole moment of pairing bases and of course the interactions between enzyme, DNA and nucleotide can be listed.[245,278] Kool showed with the **Z-F** and **Q-F** ubps (see Fig. 34), that hydrogen bonding is not as important for a replicable base pair assize and shape complementarity is.[245,253,254]

In analogy to protein biochemistry, hydrophobic interactions can be predicted for hydrophobic and heteroaromatic nucleobases in a certain way,[279,280] but discovery of self-pairing (e.g. **PICS**, see Fig. 36) or heteropairing (e.g. **MMO**:**SICS**, Fig. 36) unnatural nucleobases is an assay based research.[245,267,275,280] Possible candidates have to be tested in view of replication and extension fidelity. Selectivities below 99% is not sufficient for replication.[245]

Another main aspect in ubp design was pointed out first by Kool in 1999[255] and elaborated in the following decade by other working groups[268,281,282]: Minor groove interactions are important for DNA and RNA synthesis.

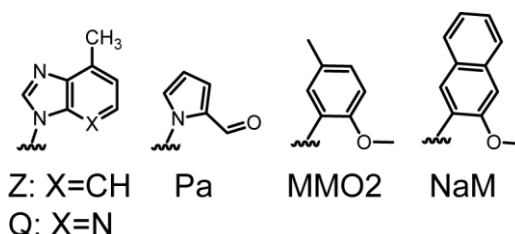Kool's nucleobases **Q** and **Z** are analogues of adenine lacking heteroatoms suitable for hydrogen bonds.[255]

Fig. 39: Unnatural nucleobases bearing heteroatomic functionalities in ortho positions to glycosydic bond. [245,262,277,283]

They still possess nitrogen atoms at position 7 of purine scaffold. Other unnatural nucleobases as depicted in Fig. 39 show heteroatoms in similar positions. Hirao's **Pa** uses aldehyde functionality and Romesberg's **NaM** or **MMO** have methoxy groups in *ortho* position to glycosydic bond to point out some examples.[245,262,277,283] Extension experiments with exonuclease-deficient Klenow fragment of *E. coli* DNA polymerase I showed a massive decrease in primer extension, when dG at primer terminus was subsitituted by 3-deaza-dG.[282,284,285] A similar approach using unnatural nucleosides carried out by Romesberg's and coworkers showed similar results when methoxy groups were substituted by methyl groups.[281] All those functional groups and heteroatoms act as H-bond acceptor interacting with polymerases arginine at position 668 (Arg668) as H-bond donor to align the primer terminus for efficient extension.[281]

Regarding these restrictions, a plethora of *ubp*s were identified, wether they are derivatives of natural purine and pyrimidine scaffold or nucleobase analogs with minor to no homology to canonical nucleobases.[275]

Moreover, crystal structures of KlenTaq DNA polymerase bound to template-primer DNA hybrids revealed the circumstances during enzymatic replication.[273] Structural investigations using d**NaM** and d**5SICS** opposite a primer terminating with ddC revealed conformational changes of polymerases helices. Main conformational change of O-helix during incorporation and extension of an oligonucleotide bearing unnatural nucleobases is similar to the conformational changes using only canonical ones.[273,275] Fig. 40 shows this change in a schematig presenation. Enzymes temporary folding forces the *ubp* to an edge-to-edge structure similar to a Watson-Crick-like. After enzymatic incorporation or subsequent extension step, ubp changes to a cross-strand intercalated structure.[273,275]
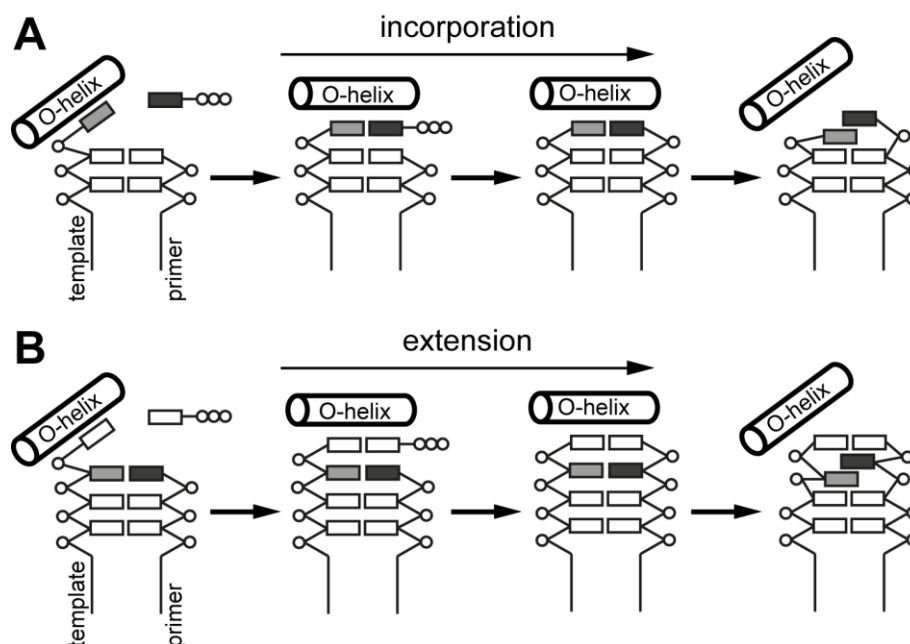
Fig. 40: Schematic presentation of conformational and structural change during incorporaton (A) and extension (B) of DNA bearing an *ubp*. Canonical nucleotides are indicated with open rectangles, unnatural nucleotides are indicaed with gray rectangles.

Using an expanded genetic alphabet in DNA creating a semi-synthetic organism (*sso*) was done recently.[1,286,287] After proof-of-concept by means of nucleotide carrier proteins to make used ubp available in cells' cytoplasm and other restrictions[1] chemical optimization and genetic engineering lead to an *sso* that is able store increased information using a six-letter genetic alphabet.[287] As last step, translation of proteins containing unAAs by *ubp* containing codons in tRNA was carried out too.[286] Semi-synthetic life with an expanded genetic alphabet to store and retrieve information on genome level reveals a plethora of possibilities.

1.3.4 Labeling of oligonucleotides using unnatural nucleotides

Labeling of oligonucleotides can be carried out with a variety of strategies. Most of them were discussed beforehand and are well-established in biochemistry.[19,20,82,288–290,26–29,37,52,73,74] A major disadvantage of most labeling strategies is lacking site-specificity caused by natural four-letter genetic alphabet.[241] Solid-phase synthesis, able to incorporate a modified nucleotide at required position is restricted in technical limitations regarding fidelity and length of DNA or RNA respectively.[21–24] Using mother nature's enzymatic amplification and transcription tools, chemically synthesized and modified nucleotides can be incorporated in longer constructs.[291,292] Expanding genetic alphabet with an ubp fully recognized and amplified by polymerase on DNA level as well as

transcribed to RNA with natural-like efficiency and fidelity,[241,271] required site-specificity would be given and technical restrictions of solid-phase synthesis can be circumvented.

From a chemical point of view, modifications of nucleotides can be achieved by introducing terminal functionalities suitable for subsequent Palladium catalyzed cross-coupling reactions.[241] This strategy was carried out and revealed unnatural nucleotides suitable for site-specific labeling approaches.
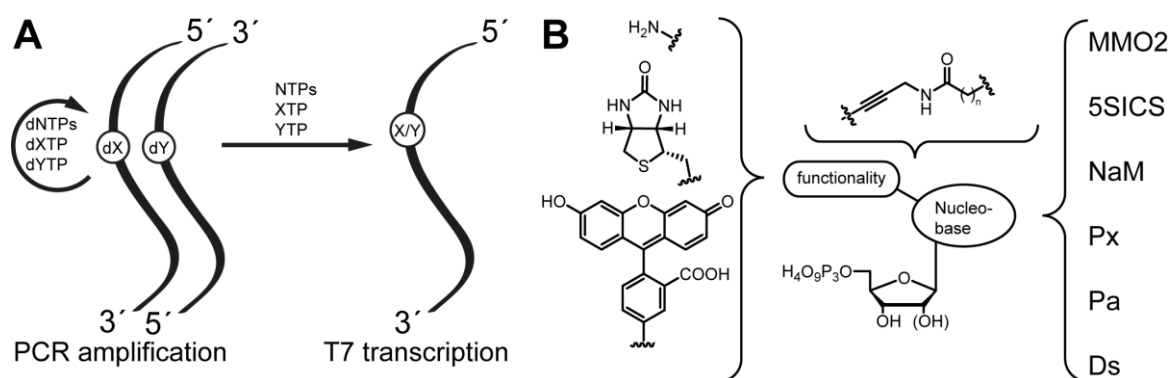
Fig. 41: Different properties are required for successful labeling using an ubp. Nucleotides must be amplified and transcribed in natural-like efficiency and fidelity (A). A general setup for such a functionalized (ribo)nucleoside triphosphate shows a functional group fused to nucleobase via propargylamide-like linkers (B).[241,261,293,294]

As depicted in Fig. 41, functionalities[241,261,293,294] such as terminal amines, biotin for Streptavidine pull-down experiments, or fluorophores (here represented by fluoresceine) are introduced by propargylamide-like linkers. Using this setup, favorable hydrogen-bonding interactions between polymerase and amide carbonyl group of linker can be utilized.[241]

1.4 Electron paramagnetic resonance (EPR) as powerful tool for structural investigations on RNA

The phenomenon of *EPR*, discovered in 1944 by E. K. Zavoisky[295] is based on the absorption in microwave region ($v = 10^4\text{-}10^6$ MHz) by paramagnetic substances. The principle relies on the associated magnetic moment of an unpaired electron. Energy of this momentum is usually described as $m_s = \pm 1/2$ is set to defined energetic levels ($m_s = +1/2$ and $m_s = -1/2$) in an applied magnetic field (see Fig. 42 b).[296] Those states differ by the amount $-\mu_e H_0$ and $+\mu_e H_0$ (μ_e = magnetic moment of spinning electron, H_0 = applied magnetic field) in contrast to status without applied magnetic field H_0. In *EPR* a transition between those two different spin states takes place by absorbing a quantum of radiation of an appropriate frequency. Regarding Eq. 1, the equation can be transposed as equation to magnetic moment *g*. Electron spin resonance (*ESR*) absorption positions can be expressed in terms of observed *g* values (*g-factor*).[295,296]
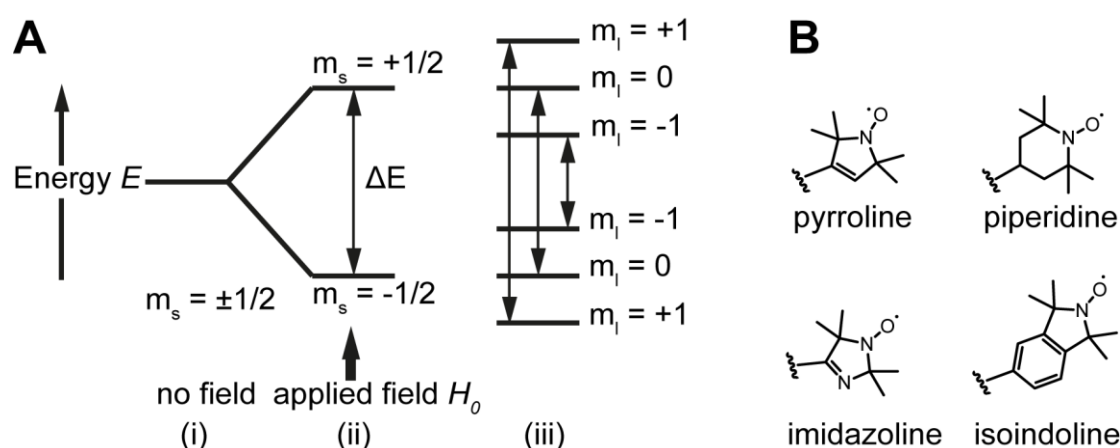
Fig. 42: (A) Schematic representation of *EPR* transition states for an unpaired electron without applied magnetic field (i) and applied magnetic field (ii). Neighboring nuclear spin *I* interacts with electrons in an applied magnetic field resulting in nuclear Zeeman interaction and corresponding energetic leves m_I (iii). (B) Different scaffolds used for nitroxide based labels.

Unpaired electronic spin interacts with neighboring nuclear spin *I*, which is called hyperfine structure or nuclear Zeeman interaction. An unpaired electronic spin couples with a nucleus resulting in a multiplet with $2nI+1$ lines as depicted in Fig. 42 c for $I = 1$ such as the nitrogen atom of a nitroxide spin label resulting in six possible states and three different energies. Those three energetic transitions can be measured. Usually, first derivative *EPR* are represented as it is here, too. A typical absorption *EPR* spectrum would show a bell-shape.

$$\mu_e H_0 - (-\mu_e H_0) = 2\mu_e H_0 = \Delta E = h\nu = g\beta H_0$$

Eq. 1: Correlation of transition energy ΔE regarding microwave and electron spin energy states.[297]

Eq. 1 shows that transition energy ΔE is equal to energy of irradiating microwave hν (h = Planck constant, ν = frequency) on the one hand and the difference between two electron spin energy states $2\mu_e H_0$ on the other hand. Here μ_e represents the magnetic moment of spinning electron and H_0 the applied magnetic field. ΔE is also equal to product of Bohr magneton β, applied magnetic field H_0 and the value of *g* (*g* factor). The value of g depends on the environment of unpaired electron. Thus, g correlates directly with the orientation and mobility of the molecule containing unpaired electron in an applied magnetic field.[296,297]

$$g = \frac{\Delta E}{\beta H_0} = \frac{h\nu}{\beta H_0}$$

Eq. 2: Equation Eq. 1 changed to *g*.

As shown in Eq. 2, irradiating microwave and applied magnetic field reveal informations about the radical's surrounding.

Instrumentally, *EPR* applications can be divided in two different methods. Continuous wave (*cw*) experiments and *pulsed* techniques are used. Using *cw EPR* provides access regarding mobility of spin labels on a molecular level. If molecular motion is fast, anisotropic tensors (*g*) become no longer necessary in Eq. 1 and received spectra differ in line shape in contrast to immobile molecules. Fig. 42 d shows a relative mobile molecule. It can be seen, that all three transitions are nearly equal in height and shape. These characteristics can be observed as a function of temperature dependent immobilization also. For distant measurements, a pulsed technique (pulsed electron double response, *PELDOR*) is used. A defined sequence of microwave pulses focusses the spin orientation. Using Fourier transform mathematics, a distant distribution can be derived from measured relaxation time of oriented spins in certain spatial range.[295–297]

Labeling of oligonucleotides using spin labels can be carried out at different positions as presented in Fig. 43, introduction of spin labels can be carried out at different positions. Similar to former discussed labeling of oligonucleotides using fluorescent tags, spin labels can be attached in an analoguos manner at corresponding nucleobase (Fig. 43 A), phosphate backbone (Fig. 43 B) or ribose moiety (Fig. 43 C).
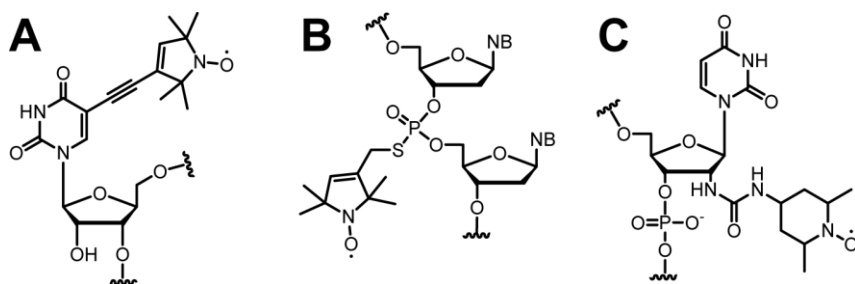
Fig. 43: Spin labels for DNA and RNA can be attached at nucleobase (A), phosphate backbone (B) or ribose moiety (C).[298]

Regarding harsh conditions during DNA or RNA synthesis on solid support,[299,300] postsynthetic labeling strategies are favored. Modern labeling strategies deal with copper catalyzed click-chemistry on solid support[301] or as recently published in solution.[302]

2 Aim of the study

Investigations on functional RNA are still a challenging topic. Gaining more interest by understanding ncRNAs' role in cancer pathways[303] and diseases[304] research on functional and structural RNA increased. Catalytically active RNA molecules like ribozymes and other regulatory RNAs are involved in subcellular structural organization and regulation. Due to their widespread functionality, for example as regulatory elements, the sequence conservation is generally low.[181] Thus, conclusions from sequence to structure and finally to the function of a specific ncRNA are not valid.

There are still huge gaps in our understanding of ncRNAs according to their mechanism and range of function.[181] Modern techniques like next-generation sequencing and bioinformatics approaches are versatile tools to detect ncRNAs in the plethora of unidentified RNA molecules. The still incomplete understanding of higher organisms and diverse roles of RNA in cellular processes[173,305] require new tools for structural and spatiotemporal investigations on this interesting and important biomolecules.

In this thesis, novel tools for site-specific RNA labeling approaches based on click chemistry shall be developed. The archetype of click reactions, the CuAAC shows cytotoxicity due to the requirement of Cu(I) as catalyst. A modern type of click reaction, the *IEDDA* click is additive free and shows higher reaction rates than other click reactions. [87]

Main aim of this thesis is the chemical synthesis of new building blocks. New tetrazine derivatives for additive-free *IEDDA* click labeling will be prepared as well as unnatural ribonucleoside triphosphates suitable for structural investigations on ncRNA using an enzymatic and template directed technique for site-specific introduction.

At first, different tetrazines will be synthesized on various synthetic routes and compared regarding quenching properties and reactivity on modified RNA strands.

Secondly, the chemical synthesis of unnatural nucleotides suitable for DNA or RNA applications will be shown. A six letter based genetic alphabet should increase capacity of information storage in oligonucleotides.[241–245] As most promising unnatural base pair (d)NaM:(d)TPT3 developed in the Romesberg group is suggested.[1,274] Employing this unnatural base pair, the site-specific incorporation of nucleotides via T7 *in vitro* transcription is possible and allows introducing new functionalities in RNA. Thus, this approach should ideally be suited to introduce reporter groups into ncRNA for structural

and functional investigations. Using the excellent requirements of named UBP, a minimal influence into ncRNAs functionality should be given.

In this work, functionalized and unfunctionalized derivatives of this unnatural base pair will be synthesized. A novel approach for the site-specific decoration of RNA with various reporter groups via *in vitro* transcription based on an expanded genetic alphabet will be developed. Following applications in fluorescence based studies as well as first approaches for structural investigations on specific ncRNAs are carried out by introducing spin labels into RNA. This allows the combinantion of enzymatic precision and recognition for unnatural nucleotides with EPR spectroscopy as modern spectroscopic method suitable for structural investigations on biomolecules.[306]

In parallel, synthesis of a canonical nucleoside on mutated atomic level and its usage to decipher the cleavage mechanism on a novel class of catalytic active RNA will be carried out. Twister ribozymes as RNA motif were identified in this decade[212,214] and provoked a discussion about the cleaving mechanism of this class of ncRNA.[212,213,218,220,224,226,307] Using chemical synthesis to reach nucleobases mutated on atomic level enables investigations on the influence of RNAs' conserved sequences on function and mechanism of constructs.

3 Results and discussion

3.1 Asymmetric tetrazine derivatives for *IEDDA* click applications on modified RNA

Novel asymmetric functionalized tetrazine derivatives will be synthesized using different synthetic pathways. After subsequent conjugation with fluorophore Oregon Green 488[TM], comparing studies reveals quenching properties of synthesized conjugates. Furthermore, reactivity on modified RNA strands suitable for *IEDDA* click chemistry will be tested.

3.1.1 Asymmetric meta substituted tetrazine synthesized via [2+2+2] cycloaddition

Starting from 6-methyl-2-pyridinecarbonitrile (*m*-tolunitrile, **45**), a radical bromination at the methyl group was carried out with *N*-bromsuccinimide (*NBS*) yielding brominated compound **46** with 38%. After this, a subsequent amine formation using concentrated ammonia solution in MeOH was carried out. This reaction[308] was also used in diploma thesis and showed excellent results for para-substituted derivatives. In order to avoid secondary or tertiary amines as unwanted byproducts, reactions have to be performed in a strong diluted manner. As shown in Fig. 44, reaction can be also used for meta-substituted compounds, yielding **47** (quant.) and **49** (89%).
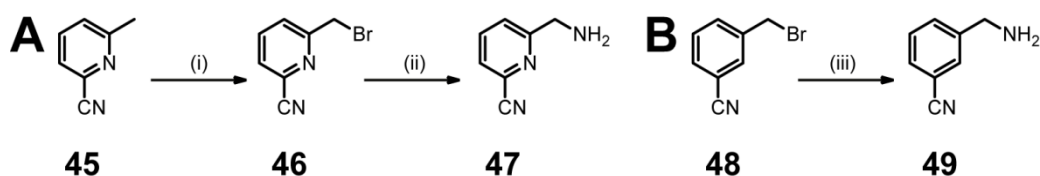
Fig. 44: Synthetic approach for compound 47 (A) and 49 (B) as starting material required for tetrazine synthesis. (i) CCl_4, NBS, AIBN, 75 °C, 4h, 38%; (ii) NH_3 (aq., 25%), MeOH, r.t., o/n, quant. (iii) NH_3 (aq., 25%), MeOH, r.t., o/n, 89%.

Using Pinner-like conditions, the aromatic nitrile **49** was solved in hydrazine solution (aq., 80%) and stirred at 90 °C for 4 h with corresponding counterpart **50** or **52**. The resulted precipitate was filtered of and the oxidation step using sodium nitrite in glacial acetic acid was carried out subsequently if needed. Meta-substituted tetrazine **51** (3%) could be isolated directly after first reaction step without final oxidation. **53** (7% over two steps) was yielded as pink solids after subsequent oxidation as described.
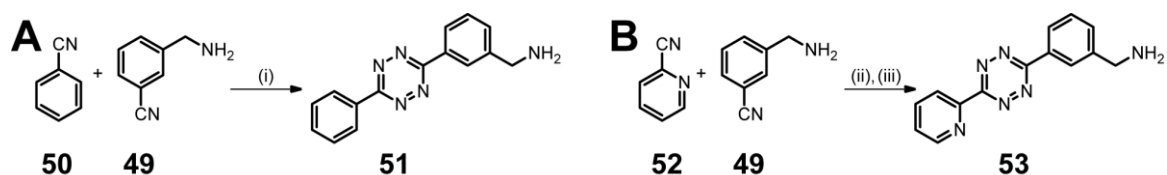
Fig. 45: Synthesis of meta-substituted tetrazine derivatives 51 and 53. Used conditions are Pinner reaction related. (i) H_2NNH_2 (aq. 80%) 90 °C, 5h, 3% and (ii) H_2NNH_2 (aq. 80%), 90 °C, 4h; (iv) $NaNO_2$/MeOH, r.t, 15min 7% over two steps.

In order to improve tetrazine's properties in view of quenching and reaction rates, compound **54** was synthesized. As depicted in Fig. 46, both adjacent aromatic rings are pyridine derivatives. Again, [2+2+2] cycloaddition was carried out under Pinner like conditions yielding the precursor (20%). Subsequent oxidation using glacial acetic acid and $NaNO_2$ was not successful in this case. As an alternative, DDQ in toluene was used and yielded **54** as pink solid.
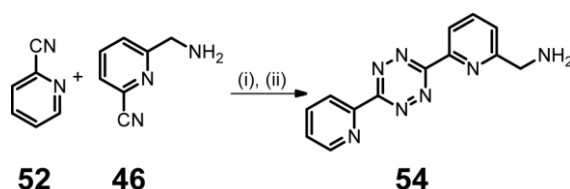
Fig. 46: Synthesis of compound 54 bearing nitrogen in both adjacent aromatic systems. (i) H_2NNH_2 (aq. 80%) 90 °C, 3h, 20%; (ii) DDQ, toluene, r.t., 30min, quant.

3.1.2 Synthesis of tetrazine-fluorophore conjugates suitable for *IEDDA* click chemistry

After synthesis of *meta*-substituted tetrazine derivatives, conjugation with commercially available fluorophore Oregon Green™ 488 was carried out. Tetrazine and Oregon Green™ 488 carboxylic acid succimidyl ester **55** were solved in DMSO in a 1.5:1 ratio. The volatile nitrogenous base NEt_3 was added in a catalytic quantity and reaction mixture was stirred under exclusion of light for one hour. General approach is shown in Fig. 47 A. The solvent and NEt_3 were evaporated under freeze-drying conditions. The crude products were purified via HPL chromatography and analyzed by LC-MS measurement as depicted in Fig. 47 B
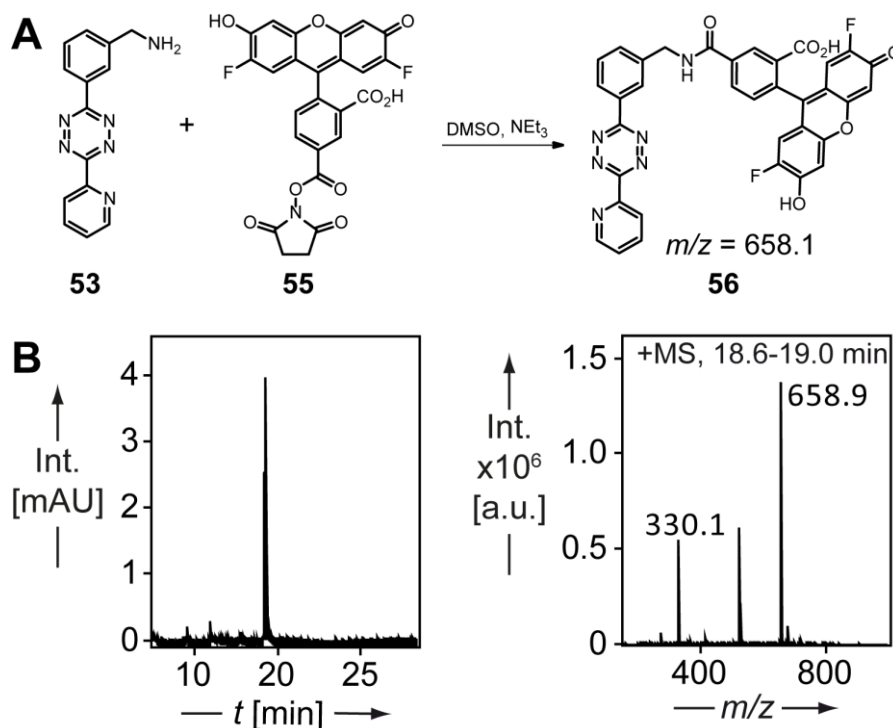
Fig. 47: General approach for tetrazine-fluorophore conjugation exemplary shown for 56 (A) and corresponding LC-MS analysis (B).

Using this technique, two meta-substituted tetrazines fluorophore conjugates **56** (97%) and **58** (97%) were synthesized. Additionally, commercially available derivative 3-(*p*-benzylamino)-1,2,4,5-tetrazine (**4**, *Jena Bioscience*) was conjugated to fluorophore Oregon Green 488™ yielding **57** (98%) as well as biotinylated derivative **59** (98%) for internal reference. Both compounds are depicted in Fig. 48.
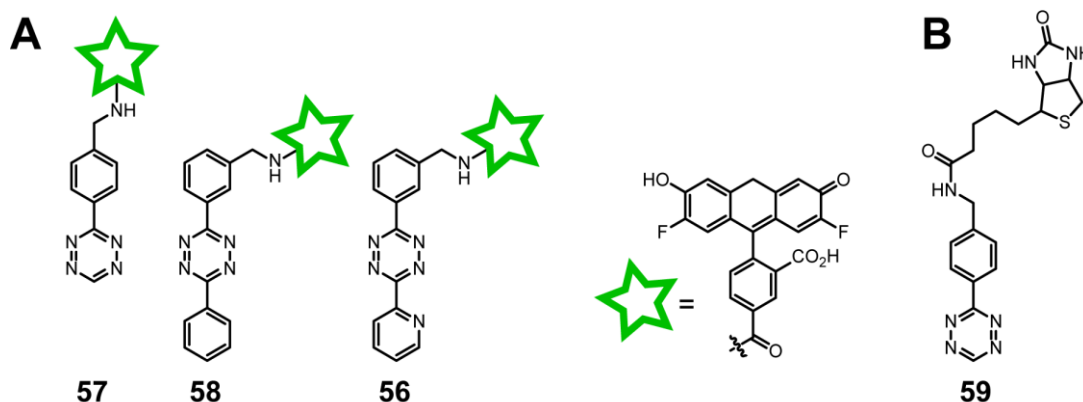
Fig. 48: Synthesized tetrazine-fluorophore conjugates 56 and 58 as well as conjugate 57 used for internal reference (A) and biotinylated compound 59 (B).

Referring to Weissleder[146] and as mentioned in previous sections, *meta* position of the conjugated fluorophore was pointed out as a significant aspect regarding quenching properties of tetrazines.

3.1.3 Synthesis of asymmetric tetrazines using a 1,4-dichloroazine precursor

Alternative multistep synthesic approach[113] was carried out to compare the overall yield with the [2+2+2] one-pot cycloaddition. A publication from 2013 by Wang et al.[91] showed this synthetic pathway[113] for different tetrazines.

Overall yield for a symmetric role model taken from experimental data is 28%. Calculation of overall yield is shown and explained in Fig. 49. After condensing acid hydrazide **61** and acid chloride **60** symmetric hydrazide **62** was yielded with 91%. In a second step, **63** was yielded (51%) after chlorination with PCl_5. Concluding cyclisation with hydrazine and subsequent oxidation yields symmetric tetrazine **7** with 60% over two steps.
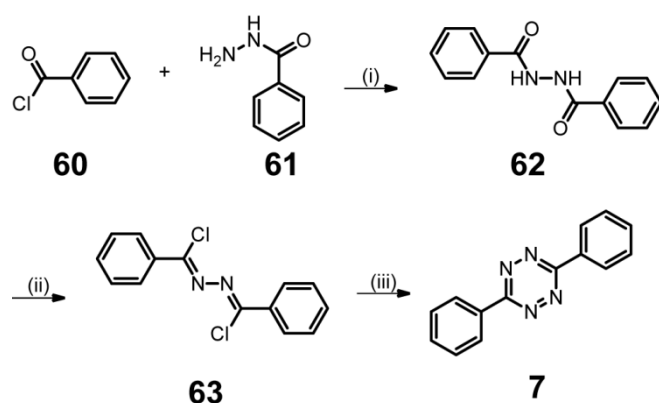
Fig. 49: Synthesis of symmetric tetrazine 7 according to alternative synthetic pathway. (i) NEt_3, DCM, 0 °C to r.t., 15min, 91%; (ii) PCl_5, toluene, 120 °C, 3h, 51%; (iii) H_2NNH_2 (aq. 80%), pyridine, 80 °C, 20min; $NaNO_2$, AcOH, r.t., 10min, 60% (over two steps).

Overall yield from literature is 31%[91] and in good agreement with obtaines experimental data. Experimental overall yield was calculated with 28%.

In order to use this synthetic pathway for functionalized tetrazines suitable for later fluorophore conjugation, *para*-functionalized compound **20a** and *meta*-functionalized compound **51** were chosen. Including an additional protection step to inhibit the reactive primary amine using phthalic anhydride, an overall yield of 25% was achieved for **20a**. As shown in Fig. 50, yield of single synthetic steps is in a similar range like for symmetric compound **7** shown before in Fig. 49. In contrast to this, synthesis of the *meta*-substituted tetrazine **51** failed during chlorination from compound **71** to **72**. Working in an equal reaction setup, no conversion of the substituted hydrazide **71** was achieved.
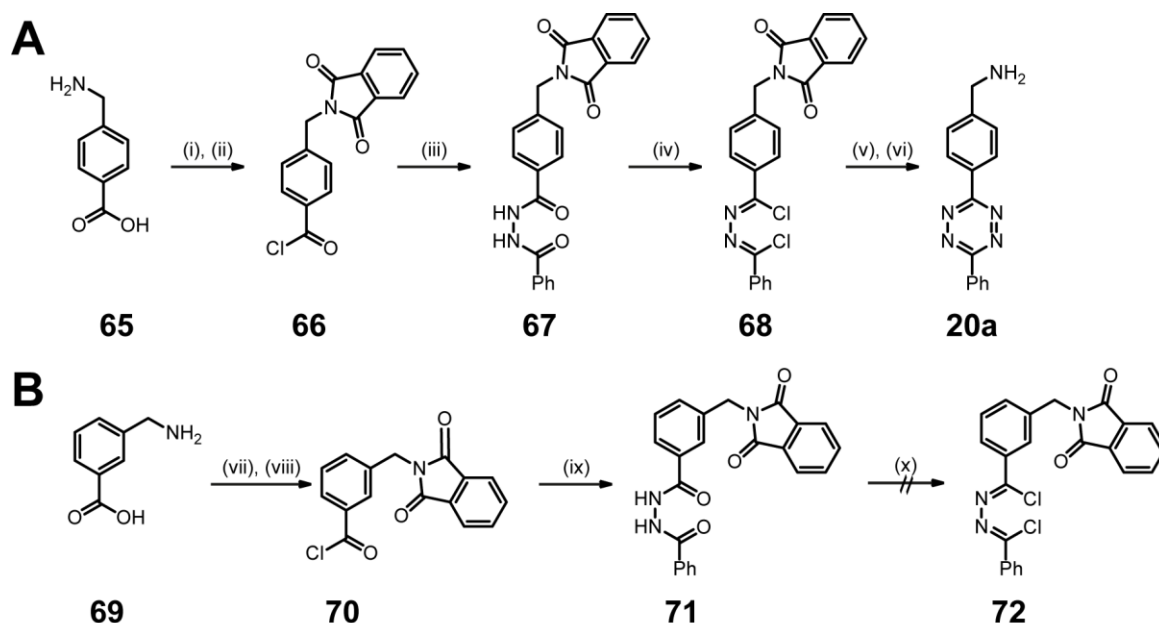
Fig. 50: Synthesis of amine-bearing tetrazines according to procedure published by Baddar et al.[122] Para substituted tetrazine (A) yielded 25% overall. (i) phthalic anhydride, AcOH, reflux, 2 h, 87%; (ii) SOCl$_2$, 90 °C, 2 h, quant.; (iii) benzhydrazide, NEt$_3$, DCM, r.t., 2 h, 56%; (iv) PCl$_5$, toluene, Δ, 3 h, 64%; (v) H$_2$NNH$_2$ (aq., 80%), 90 °C, 3 h; (vi) NaNO$_2$, AcOH, r.t., 20 min, (80% over two steps). Meta substituted tetrazine (B) could not be yielded as product. (vii) phthalic anhydride, AcOH, reflux, 3 h, 70%; (viii) SOCl$_2$, 90 °C, 2 h, 84%; (ix) benzhydrazide, NEt$_3$, DCM, r.t., 2 h, 73%; (x) PCl$_5$, toluene, Δ, no product observed.

Focusing on a comparative handling of asymmetric substituted tetrazines, multistep synthesis turned out to be a drawback seen from the temporal perspective. Dealing with low to moderate yields by a small workload is more efficacious than a big effort receiving moderate yields. This multistep synthesis showed an improved yield for *para*-functionalized compound **20a** in contrast to Pinner-like reaction conditions used in former diploma synthesis.[164] Indeed, literature states very wide ranged overall yields either for [2+2+2] cycloadditions using catalysts[82,89] or multistep synthesis[90,91,113]. A comparing approach, using both methods for desired asymmetric tetrazine should be carried out if increased yield is wanted. If the focus is set on variety or diversity Pinner-like reaction can be named as reaction of choice.

3.2 Biochemical application of synthesized tetrazine-fluorophore conjugates

Former synthesized tetrazine fluorophore conjugates were used in biochemical experiments to test their quenching properties and reactivity on chemically synthesized and *in vitro* transcribed RNA. Additionally, different conjugates were investigated on cellular level to analyze *IEDDA* click on RNA under native conditions.

3.2.1 Comparative quenching study on asymmetric tetrazine-fluorophore conjugates

To an aqueous tetrazine-fluorophore conjugate containing solution, an excess of 5-norbornene-2-methanol **73** was added. Before reaction between norbornene and tetrazine, Oregon Green™ 488 is quenched by corresponding conjugated tetrazine (Fig. 51, contoured star). After *IEDDA* click reaction, fluorescence is recovered (Fig. 51, filled star). Increased fluorescence was compared to the quenched fluorescence before addition and a negative control where only water was added.
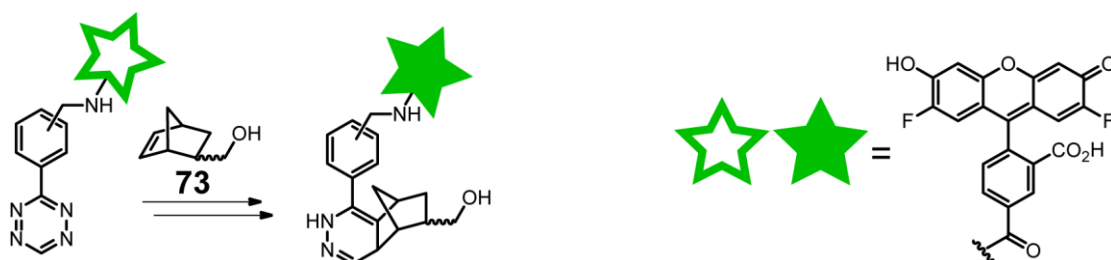
Fig. 51: Schematic presentation of general approach for comparative fluorescence readout.

Normalized turn-on ratios of conjugates **58**, **22**, **57**, and **56** are shown in Fig. 52. Graphs are ordered by increasing turn-on. Tetrazine **58** shows the lowest turn-on. A 2.2-fold increase of fluorescence is not satisfactory for e.g. in-cell applications. Literature-known derivative **22**[101] also exhibited only a 2.7-fold increase upon reaction in this study. In contrast to this, derivative **56** yields a 7.9-fold turn-on refers conjugate **57** increasing fluorescence by a 6.7-fold turn-on to second place. Synthesized tetrazine derivatives tested in a similar manner during former diploma thesis showed results in the range of derivative **58**.
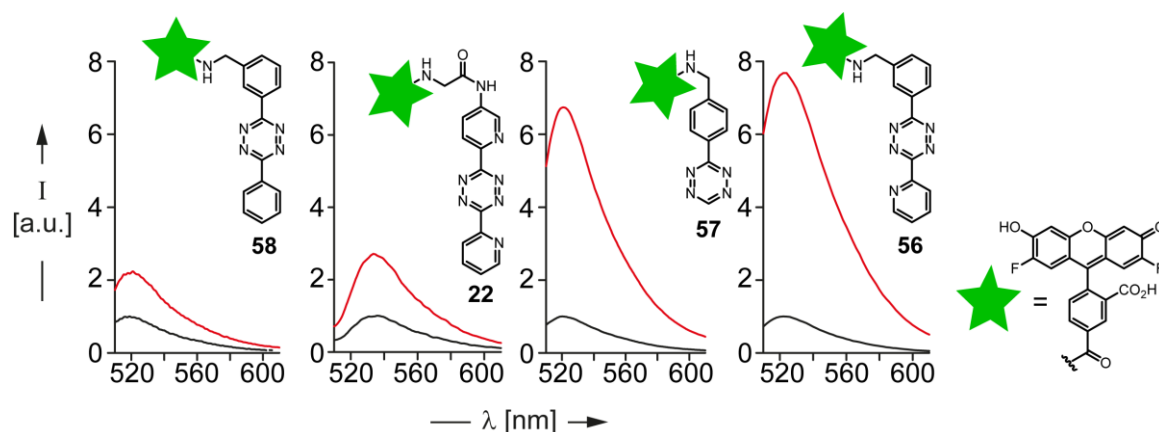
Fig. 52: Fluorescence of tetrazine fluorophore conjugates before (black) and after (red) reaction with 5-norbornene-2-methanol. The curves are normalized to the fluorescence value before reaction with 5-norbornene-2-methanol **73** in H$_2$O (5 µM tetrazine, 100-fold excess of 5-norbornene-2-methanol, 40 min reaction time).

The nearly 8-fold increase of fluorescence for **56** is a very good result. Additional *TBET*[146] influence, as discussed before is missing in every synthesized conjugate caused by conjugates structure. Thus, a comparison to other working groups results stating higher turn-on ratios[146] can not be done directly. Nevertheless, an influence of adjacent (hetero-) aromatic systems is not directly observed. Comparing **58**, **57** and **56** shows that an attached phenyl substituent used for **58** decreases quenching properties, a pyridine substituent used for **56** increases quenching properties in contrast to used internal commercially available reference **57**.

Conjugate **22** published in 2012[101] was used before with other fluorophores[101] and comparing studies regarding turn-on ratios of asymmetric tetrazines have been carried out in other labs, too. But published studies dealt with a comparison of different fluorophores conjugated to one tetrazine. So, investigating the best available turn-on ratio was carried out from another point of view in those studies.[82,154,155] **22** was also used for one of those approaches and showed turn-on ratios for other fluorophores in a range of a 4-fold turn-on.[101]

The shown approach to attach one fluorophore to different asymmetric tetrazine derivatives dealt with focus on influences of different substituents on the immanent quenching properties using a fluorophore suitable for super resolution microscopy. Arguments for Oregon Green™ 488 as fluorophore of choice beside a high photostability and high quantum yield are mentioned before.[155,162,163] The synthesized conjugate **56** showed a great success in respect thereof.

3.2.2 *IEDDA* click of different conjugates on synthetic RNA and subsequent in-cell applications

Biochemical applications of synthesized conjugates were first tested on synthetic RNA. A uridine phosphoramidite modified with a reactive norbornene handle (Fig. 53) was used for *in vitro IEDDA* click reactions. Norbornene bearing uridine phosphoramidite **74** shown in Fig. 53 was synthesized and provided by F. Braun.[309] Solid-phase synthesized RNA containing **74** was reacted with an excess of tetrazine fluorophore conjugates. After successful click reaction, RNA was visualized and analized by polyacrylamide gel electrophoresis (*PAGE*) and mass spectrometry (*MS*) respectively.
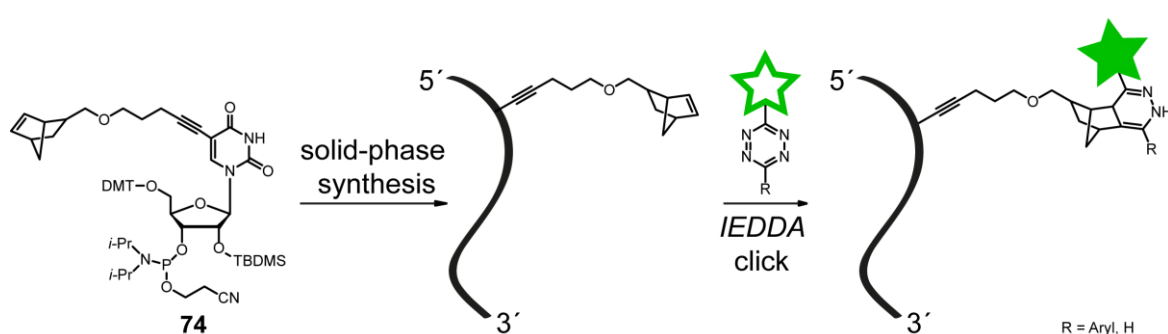
Fig. 53: Schematic representation of first *in vitro IEDDA* click approach. Norbornene-modified uridine **74**[309] was incorporated into RNA via solid-phase synthesis.

As proof, if *IEDDA* click chemistry works also on synthetic RNA, 12 nt long norbornene-uridine containing strand **RNA-U^{NOR}-12** was synthesized using an ABI3400 DNA/RNA synthesizer, clicked with conjugate **57** and analyzed via LC-MS. Mass spectrometry showed a successful click reaction, as it is shown in Fig. 54.
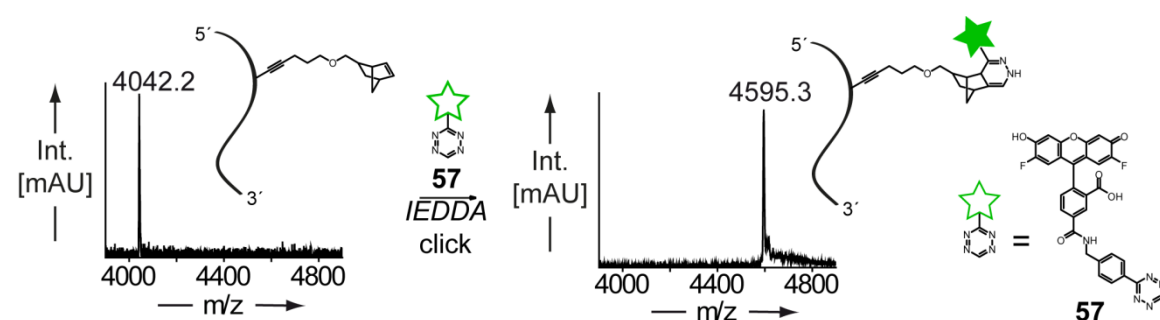
RNA-U^{NOR}-12: 5'-CGA UG**Y** CAG UGG-3'
        Y = **74**

Fig. 54: MALDI-TOF mass spectrum of purified RNA-U^{NOR}-12 before (*m/z*$_{calc.}$ = 4038.7, left) and after (*m/z*$_{calc.}$ = 4593.8, right) *IEDDA* click reaction with two equivalents 74.[309]

After the successful click reaction of **RNA-U^{NOR}-12** with **57**, different conjugates were clicked and analyzed *in vitro* on 24 nt long strand **RNA-U^{NOR}-24** including norbornene

modified uridine **74** at position 2 suitable for *in vitro* click. Results of comparing denaturing *PAGE* are shown in Fig. 55.
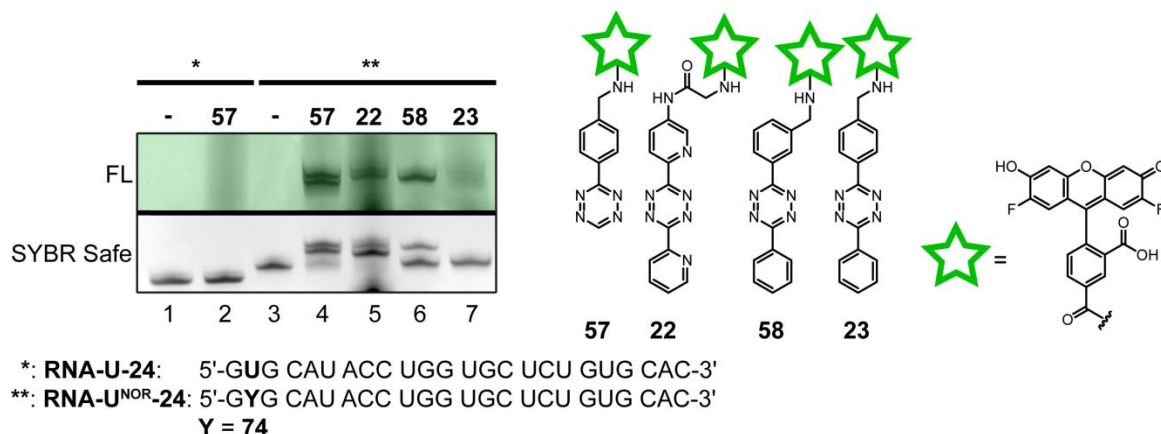
Fig. 55: 20% PAGE analysis of different tetrazines-fluorophore conjugates clicked on norbornene bearing RNA-U^NOR-24. Fluorescent (*FL*) readout is depicted above SYBR Safe stain.[309]

Denaturing *PAGE* analysis of the used tetrazine fluorophore conjugates shows remarkable results after click reaction on **RNA-U^NOR-24**. Lane 1 and lane 2 show unmodified **RNA-U-24** bearing canonical uridine at position 2. **74** as norbornee modified uridine derivative causes a clear shift in PAGE analysis as visible in Fig. 55's lane 3. Reference conjugate **57** shows a nearly quantitative reaction (Fig. 55 lane 4, 96%) with norbornene modified **RNA-U^NOR-24** as well as **22** (Fig. 55 lane 5, 97%) published by Chin and coworkers[101]. The reaction yield was calculated from band intensities. Unfortunately, **22** showed considerable degradation in fluorescence scan (Fig. 55 lane 5). LC-MS analysis showed cleavage of the aliphatic amide bond. In contrast to this, **23** react only in a negligible amount (Fig. 55 lane 6). Tetrazine **58** reacts only with low yield (Fig. 55 lane 7, ~40%). For conjugate **22** and especially for reference **57** two product bands are visible (Fig. 55 lane 4 and lane 5). Verification of product bands was carried out by preparative denaturing *PAGE* and subsequent LC-MS analysis showing similar masses. This implies *PAGE* analysis as sensitive enough to separate isomers arising from *endo-* and *exo-* addition of the tetrazine-fluorophore conjugate. In contrast, conjugate **58** shows only one product band. Assuming steric influences of attached fluorophore in *meta*-position one isomer of cycloaddition is favored.

Turn-on ratios of derivative **23** and literature known derivative **22**[101] show only minor applicability for *IEDDA* clicks.

Subsequent experiments on cellular level were carried out as part of diploma thesis by A. Weber (maiden name A. Pyka)[309] representing first successful application of *IEDDA* click chemistry on RNA in mammalian cells. NCI-H460 cells were transfected with a small

interfering RNA (siRNA) duplex consisting of 21 nt long norbornene-uridine containing **RNA-U^NOR-21** and corresponding unmodified antisense RNA. After 4 h incubation and multiple washings, cells were incubated with either tetrazine fluorophore conjugate **22**, **23**, **57** or **58** for 1 h. Cell fluorescence was analyzed by flow cytometry and data analyzed using *FlowJo* software. Results are shown in Fig. 56.

RNA-U^NOR-21: 5'-GG**Y** GAA GUU CAA GGG CGU GdTdT-3'
Y = 74
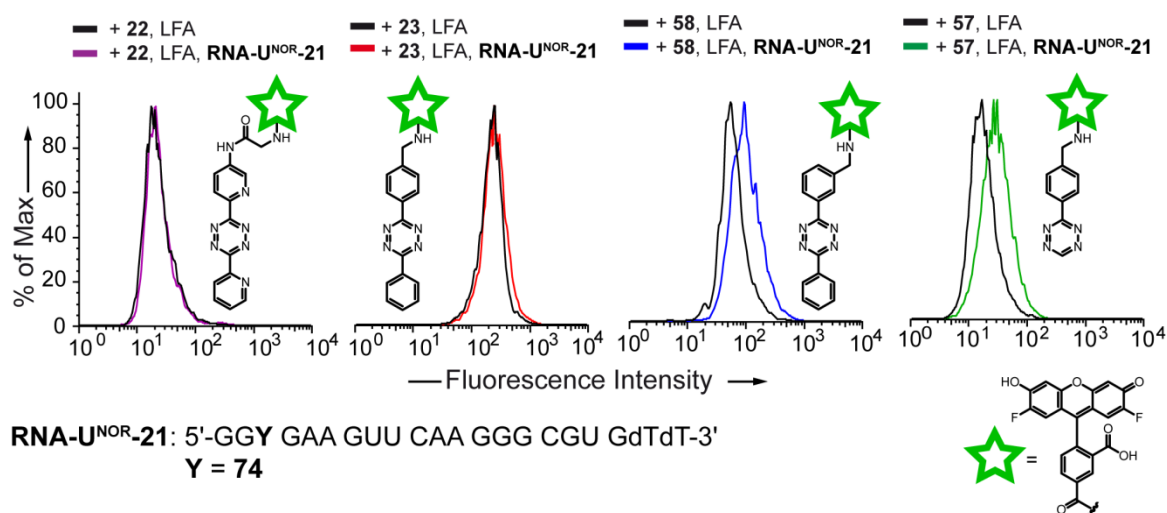
Fig. 56: FACS analysis showing successful in-cell *IEDDA* click using tetrazine-fluorohore derivatives 22, 23, 57, and 58. Percentages given are the population comparison for each experiment determined using SED algorithm (<u>S</u>uper-<u>E</u>nhanced <u>D</u>max subtraction) in comparison to background fluorescence of the cells (black curves, tetrazine and lipofectamine only) and provide a percentage of positive cells found in the sample and not in the background.[309]

Observed results are for the most part similar according to former discussed *in vitro* experiments. Derivative **23** showed in contrast to *in vitro* application increase in fluorescence (20.9%). **22** published by Chin and coworkers showed the weakest result for in cell application (17.4%). As described, a cleavage of aliphatic amide bond occurred during *in vitro* applications and might be assumed in this case, too. Thus, this derivative is not suitable for applications on a cellular level. Nevertheless reference **57** (63.6%) and meta substituted **58** (62.4%) showed good results for in-cell *IEDDA* cycloadditions on mammalian cells.[309]

Furthermore, confocal microscopy experiments were carried out within 12 h past fixation of incubated cells. Fig. 57 shows laser scaning microscope (*LSM*) images of H460 cells with transfected **RNA-U^NOR-21** (A) and untransfected H460 cells (B) as negative control. Both samples were incubated with with conjugate **57** for 1h.
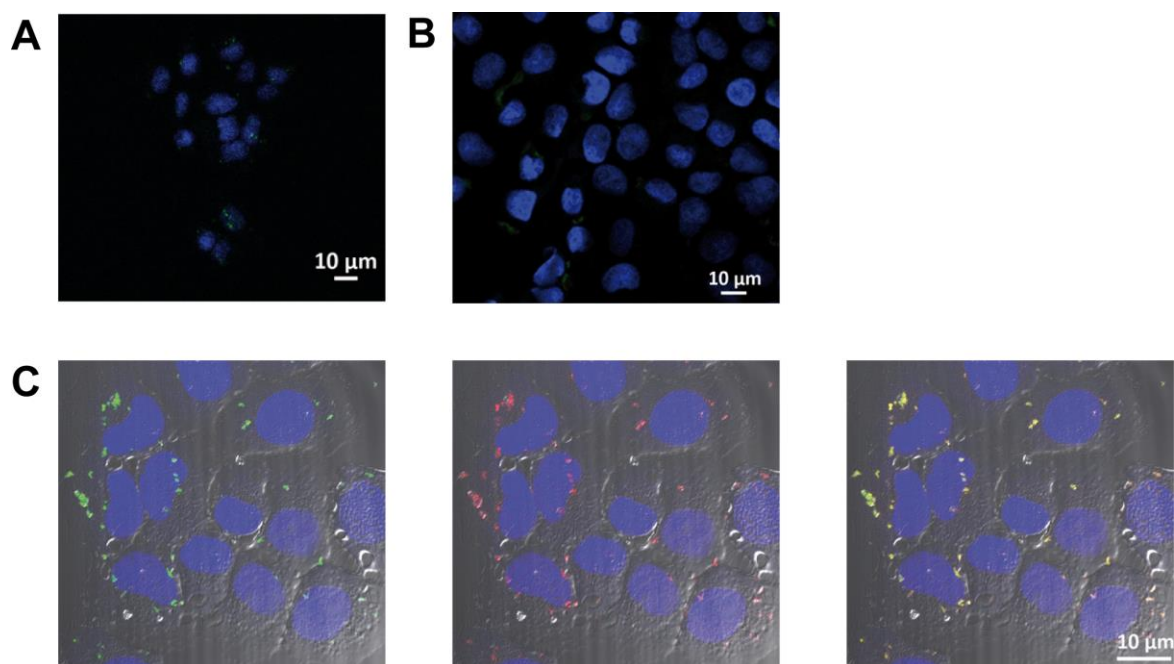
Fig. 57: LSM image of H460 cells transfected with RNA-U^{NOR}-21 (A) and untransfected (B). Both cell samples were subsequently incubated with conjugate **57** for 1h. Shown are green fluorescent channel and nuclei stain channel. Double stranded siRNA labeled with ATTO 647 for colocalization was used, too. Lower images show DIC and 405 nm exitation channel in combination with green (left), red (middle), and both channels (C) after successful *IEDDA* click.[309]

Transfected norbornene-modified RNA is still concentrated in lipid vesicels in the cytoplasm from transfection carrier. Shown in Fig. 57 C are a merged image of differential interference contrast (*DIC*), nuclei stain (4,6-diamidino-2-phenylindole, *DAPI*, 405 nm excitation signal), green fluorescence channel (488 nm excitation signal) and red fluorescent channel (633 nm excitation channel). An ATTO 647-labeled antisense RNA was used for colocalization.[309] Increased fluorescence of labeled RNA can be clearly detected. Synthesized novel conjugate **7^{OG}** is applicable as well *in vitro* as on a cellular level and shows good results in its quenching properties and *IEDDA* properties. However, internal reference XX turned out to be best in experiments carried out. Main observed advantage of **58** in contrast to **57** is the steric influence resulting in only one product band (see Fig. 55).

3.2.3 *IEDDA* click on transcribed RNA using an unnatural ribonucleoside triphosphate

Through cooperation and as succession, unnatural norbornene bearing ribonucleoside triphosphate **76** was synthesized and used for further *in vitro IEDDA* click applications of synthesized conjugate **56**. Further information on synthesis is described in literature[310,311] and in section 3.3.1. In an analogue manner as described before, *IEDDA* click chemistry was carried out on *in vitro* transcribed RNA. Transcribed oligonucleotides were characterized by LC-MS analysis and according data are listed in appendix.
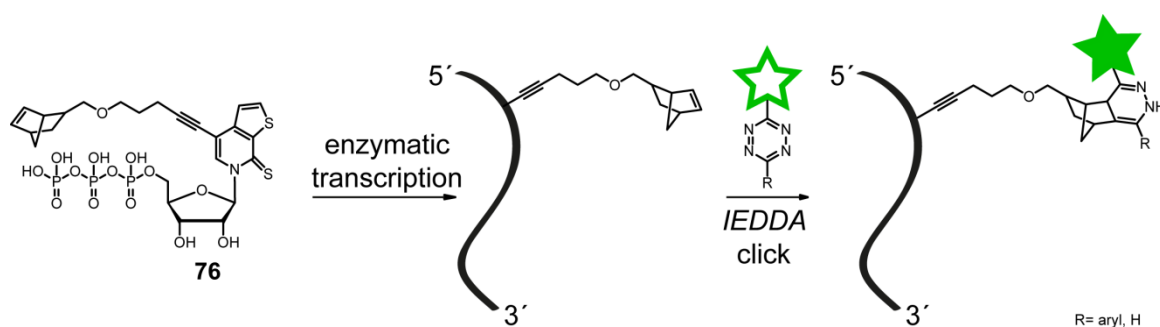
Fig. 58: Analoguous *in vitro IEDDA* click approach. Norbornene-modified unnatural ribonucleoside triphosphate 76 was incorporated into RNA via T7 *in vitro* transcription. [310]

Transcribed 30 nt long **RNA-TPT3^{NOR}-1** bearing one TPT3 based modification of **76** at position 8 was incubated with conjugates **56** and **57** for 1 h using a three-fold excess of corresponding conjugates. After incubation, click products were separated by PAGE and analyzed using fluorescent read-out and SYBR-safe stain.
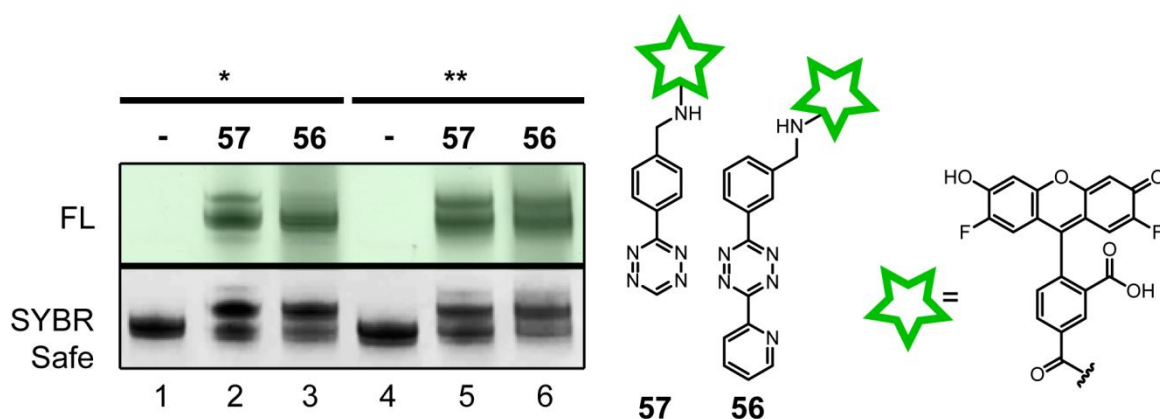
*: RNA-TPT3^{NOR}-1: 5'-GGA GAU C**Y**U CCA CGA GGA UUC CCG **U**CA CAG-3'
: RNA-TPT3^{NOR}-2: 5'-GGA GAU CY**U CCA CGA GGA UUC CCG **Y**CA CAG-3'
                    Y = 76

Fig. 59: *IEDDA* click of conjugates on transcribed RNA. After T7 *in vitro* transcription **RNA-TPT3^{NOR}-1** and **RNA-TPT3^{NOR}-2** was clicked with a three-fold exzess of tetrazine fluorophore conjugates **56** and **57**. Fluorescent (*FL*) readout is depicted above SYBR Safe stain.[310]

Fig. 59 shows results of tested conjugates **56** and **57** on **RNA-TPT3^{NOR}-1** and **RNA-TPT3^{NOR}-2**. **57** was internal reference again. Comparing band intensities of clicked and unclicked RNA shows lower results for internal reference **57** in contrast to former reaction on **RNA-U^{NOR}-24**. Using even longer time for click incubation only 72% product was detected for **57** (similar results on **RNA-TPT3^{NOR}-1** and **RNA-TPT3^{NOR}-2**) and 50% (**RNA-TPT3^{NOR}-2**) or 61% (**RNA-TPT3^{NOR}-1**) for **56**. Again, **57** shows two product bands and *meta*-substituted conjugate **56** shows one product band as discussed before. Showing a site-specific introduction of more than one tetrazine on multiple modified RNA is shown in Fig. 59, too. **RNA-TPT3^{NOR}-2** shows two product bands either for **56** and **57**.

Increased fluorescence shown with tetrazine-fluorophore conjugate **56** was remarkable. Again, the advantage of a meta-substitution is pointed out by only one resulting product band in contrats to internal reference **57** (see Fig. 59).Fine tuning as reported in literature[41,87,88] is sensitively influenced by many aspects and not straight-forward. Regarding synthetic aspects, either one-pot synthesis or multistep synthesis yields an overall outcome of about 30% caused by statistical distribution[82,101,114,115,117] or loss during single synthetic steps of linear synthesis[90,91]. A maximum yield of 45% was found for **9** in literature.[39,312,313] Additives for an increased yield[93,121] had been used during former diploma thesis[164], but advertised increased yields could not be verified. different Synthesized tetrazine derivatives were successfully yielded in a good cost-value ratio. They showed different properties in their turn-on and quenching characteristics as expected. In-cell applications were carried out and minimized tools for bio-orthogonal labeling approaches on a cellular level were investigated in a first comparing manner.

Worthwhile investigations comparing tetrazine fluorophore conjugates suitable for *IEDDA* click chemistry could be done in an assay-based approach. Comparing first the plethora of tetrazine derivatives in miscellaneous media on different dienophiles in a time dependent manner would show the preferred reaction partner for appropriate tetrazine and media. Those results have to be transferred to an assay using various fluorophores conjugated to the tetrazines. This would show, which fluorophore is best for desired tetrazine-media combination. Furthermore, a fine tuning in linker systems might be elaborated. For cyclopropenes used as dienophile such a study was published in 2017.[314] Trindade and coworkers compared the stability and the reactivity of cyclopropenes in *IEDDA* reactions with regard to the linker system attached. Similar investigations can be done for the tetrazines, too. Reviewing the presented system, no *TBET* is possible. Using other fluorophores e.g. boron-dipyrromethene based ones showed better results as published in 2013[146]. In contrast to direct attachment using

TBET assisted quenching outdoing all other fluorophores, another *ex vivo* experiment[315] showed the lowest results for *BODIPY* in contrast.

With hindsight it can be ascertained, that advantages of *IEDDA* click reaction imply detriments also. Rapid synthesis of novel tetrazine derivatives is possible by a low yielding reaction pathway. Increasing yield by adding divalent triflates can be possible or using a multistep synthetic pathway respectively. Changing substituents to increase reactivity is possible and was applied in a successful manner converting moderate reacting derivative **51** into highly reactive derivative tetrazine **53** using pyridine instead of phenyl.

With regard to results of Weissleder and coworkers from 2010, when they used derivative **9** conjugated to three different fluorophores in a comparing study to determine turn-on ratios for an *IEDDA* reaction in PBS and FBS obtained results showed a large range. A 1.5-fold increased turn-on efficiency for Oregon Green™ 488 and nearly two-fold increased turn-on efficiency for a *BODIPY* derivative were published in literature.[155] A similar situation is shown beforehand in Fig. 55 and Fig. 59. Using equal reaction conditions and a tetrazine used for reference turn-on ratios ranged between a quantitative *IEDDA* click for **RNA-U^NOR-24** and ~70% for **RNA-TPT3^NOR-1**.

IEDDA cycloaddition is the fastest click reaction at present and can be modulated in many respects. Using advantages and possibilities it holds a plethora of applications either *ex vivo* or *in vivo*. Adjusting *IEDDA* reaction for one's system is caused by many factors. Synthesized asymmetric tetrazines showed extraordinary turn-on properties and are applicable for in vitro and in cell applications, but used internal reference **9** turned out to be high level standard during project term either for *in vitro* or *in cellulo* applications, too.

3.3 An unnatural base pair and its functionalized nucleotides for site-specific RNA labeling

Chemical synthesis of unnatural nucleotides suitable for DNA or RNA applications will be carried out. Based on most promising *ubp* (d)**NaM**:(d)**TPT3**, functionalized building blocks for a six letter genetic alphabet are synthesized and applied on non-coding RNA. Thus, novel insights on transcription properties and *IEDDA* click chemistry on unnatural nucleobases are achieved.

3.3.1 Synthesis of a norbornene-functionalized unnatural ribonucleoside triphosphate

As follow up from an existing molecule developed in the Kath-Schorr group, final synthetic step and in vitro applications were carried out. Based on **TPT3**, which was discussed beforehand as unnatural nucleotide[277] functionalized ribonucleoside **76** was synthesized. The unnatural nucleobase is recognized as part of DNA *ubp* d**TPT3**:d**NaM** and was successfully used for *in vitro* studies on DNA.[277] **76** presents functionalized ribose derivative suitable for T7 *in vitro* transcription after conversion into ribonucleoside triphosphate.
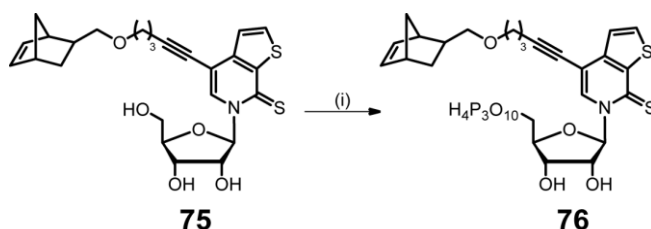
Fig. 60: Synthesis of ribonucleoside triphosphate 76. (i) OP(OMe)$_3$, POCl$_3$, 0 °C, 6 h / NBu$_3$, (*n*-Bu$_3$NH)$_2$H$_2$P$_2$O$_7$, 0 °C, 15 min, TEAB, 15%.

Triphosphate synthesis of **76** (see Fig. 60) was accomplished according to a procedure published by Tor[59] in 2007. Gaining the unnatural nucleotide **76** with 15 % yield after the described purification steps was moderate compared to literature. As described in a review by Burgess and Cook in 2000[316], there is an abundance of synthetic routes to gain nucleotides as well as a wide range of given yields depending on the synthetic route. Steady optimization of workflow was achieved. First approaches using the precipitation of the crude product as sodium salt as described in the synthetic procedure for this nucleotide based on the publication of Huang and coworkers[317] were not pursued any further. Elaborated procedure skipping the precipitation as sodium salt pellet and

directly clean crude reaction mixture via preparative HPLC was successfully applied to obtain pure triphosphate **76** as it is shown in Fig. 61.
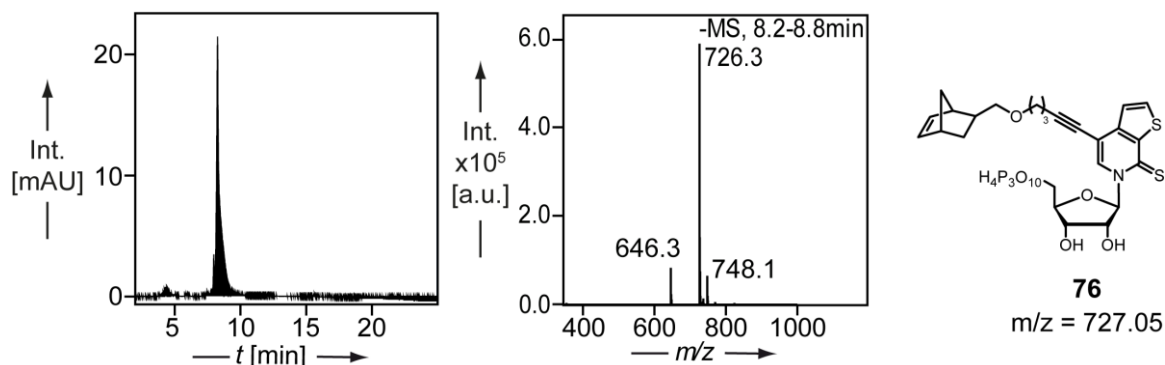
Fig. 61: LC-MS analysis of 76 after preparative HPL chromatographic purification. Shown are UV trace (left λ=254 nm) and corresponding ESI⁻ spectrum of peak eluting at t_R = 8.2 min. [310]

3.3.2 T7 *in vitro* transcription using an unnatural ribonucleoside triphosphate suitable for *IEDDA* click chemistry

Using the *ubp* counterpart d**NaM** as commercially available *CEP* suitable for solid phase synthesis, DNA template strands were designed to test T7 *in vitro* transcription conditions for enzymatically transcribed RNA bearing an unnatural norbornene-modified nucleotide. DNA strands containing one or two **NaM** nucleobases were synthesized via solid phase synthesis as well as one unmodified strand as canonical control.
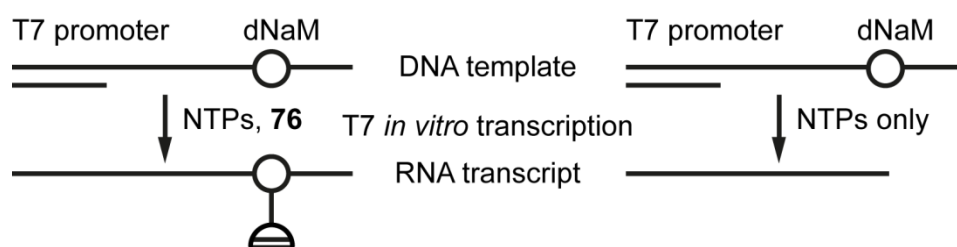
Fig. 62: General approach for T7 in vitro transcription using 76 and dNaM-CEP as *ubp*.

The general approach is depicted in Fig. 62. Assuming a reconition of **76** by T7 RNA polymerase as counterpart of dNaM in corresponding DNA template strand, full length transcript should be only yielded if **76** is added to transcription. Otherwise, truncation of transcript occurs. Transcriptions were carried out to T7 protocol described in material and methods. Time extension of *in vitro* transcriptions overnight showed no significant improvement and therefore standard transcription reaction was set to 4 h.
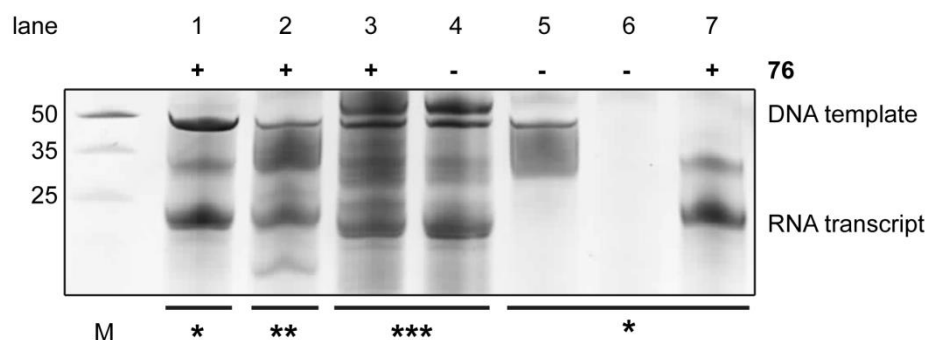
lane	1	2	3	4	5	6	7	
	+	+	+	−	−	−	+	**76**

*: **DNA-NaM-1**: 5'-CTG TG**A** CGG GAA TCC TCG TGG A**X**G ATC TCC TAT AGT GAG TCG TAT TA-3'
RNA-TPT3^{NOR}-1: 5'-GGA GAU C**Y**U CCA CGA GGA UUC CCG **U**CA CAG-3'

: **DNA-NaM-2: 5'-CTG TG**X** CGG GAA TCC TCG TGG A**X**G ATC TCC TAT AGT GAG TCG TAT TA-3'
RNA-TPT3^{NOR}-2: 5'-GGA GAU C**Y**U CCA CGA GGA UUC CCG **Y**CA CAG-3'

***: **DNA-NaM-0**: 5'-CTG TG**A** CGG GAA TCC TCG TGG A**C**G ATC TCC TAT AGT GAG TCG TAT TA-3'
RNA-TPT3^{NOR}-0: 5'-GGA GAU C**G**U CCA CGA GGA UUC CCG **U**CA CAG-3'

X = dNaM; Y = 76

Fig. 63: Denaturing *PAGE* analysis showing crude *in vitro* transcriptions of DNA templates containing dNaM. Lanes 1-3 show crude T7 in vitro transcriptions of DNA templates containing one or two dNaM and without dNaM nucleotides in presence of canonical NTPs and **76** yielding full length transcript. Lane 4 and lane 5 show crude *in vitro* transcriptions in absence of **76**. Missing full length RNA transcript in lane 5 is obvious. Lane 6 shows a DNase digestion of lane 5. Lane 7 shows DNase digestion of lane 1. [310]

In Fig. 63 proof of concept is shown by denaturing *PAGE* analysis. Full length transcripts of the modified RNA transcripts are as obvious as the unmodified transcripts. Obtaining modified transcripts was achieved in moderate to good yields. Preparative *PAGE* purification showed 36% full length transcript **RNA-TPT3^{NOR}-1** from template **DNA-NaM-1** and 16% full length transcript **RNA-TPT3^{NOR}-2** from template **DNA-NaM-2** compared to unmodified transcript **RNA-TPT3^{NOR}-0** from template **DNA-NaM-0**. Truncation occurs at position 23 for transcripts where the unnatural nucleotide is incorporated. Literature states a reduced yield caused by modified triphosphates[241] and unspecific incorporation of canonical NTPs is excluded.

Successful single and double incorporation of **76** can be visualized in a better way using biotinylated tetrazine derivative **59**. Biotin is often used for pull-down experiments taking advantage of the high affinity between streptavidin and biotin.[318] Here, biotin itself is large enough to show a difference using PAGE analysis. Results are shown in Fig. 64.
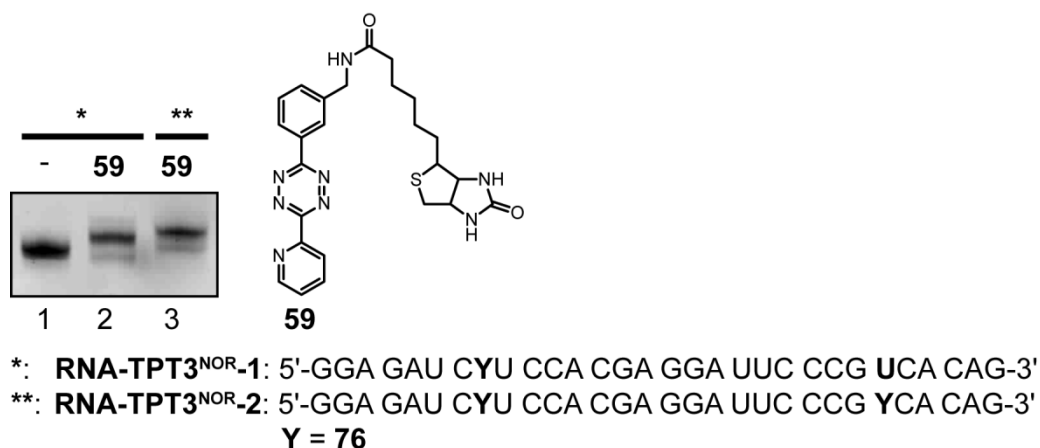
Fig. 64: Denaturing 20% *PAGE* analysis after *IEDDA* click between 3 equiv. of biotinylated tetrazine 59 and RNA-TPT3^{NOR}-1 and RNA-TPT3^{NOR}-2 respectively. [310]

RNA-TPT3^{NOR}-1 and **RNA-TPT3^{NOR}-2** were reacted with biotinylated tetrazine conjugate **59**. *PAGE* analysis points out the single (86% lane 2, calculated from band intensities) and double (84% lane 3, calculated from band intensities) labeled RNA strands by their different migration behavior.

Additional *PAGE* analysis of canonical RNA transcripts using *IEDDA* click technique shows no fluorescent activity for **RNA-TPT3^{NOR}-0** in contrast to modified RNA transcripts. This shows that no unspecific incorporation of **76** opposite canonical nucleotides takes place. If so, incorporation is in a similar infinitesimal amount as the other way round.

IEDDA click approaches using different tetrazine derivatives conjugated to Oregon Green^{TM} 488 on transcribed **RNA-TPT3^{NOR}-1** and resulting dates are shown and discussed beforehand in Fig. 59 in view of click efficiency of tetrazine derivatives.

A short excerpt of Fig. 59 is shown again in Fig. 65 below. As discussed beforehand, *IEDDA* click chemistry can be carried out between tetrazines and strained alkenes such as norbornene. **76** is equipped with a norbornene handle for such an application. Thus, only **76** can react to added compounds **56** and **57** and show a signal in fluorescence read-out.
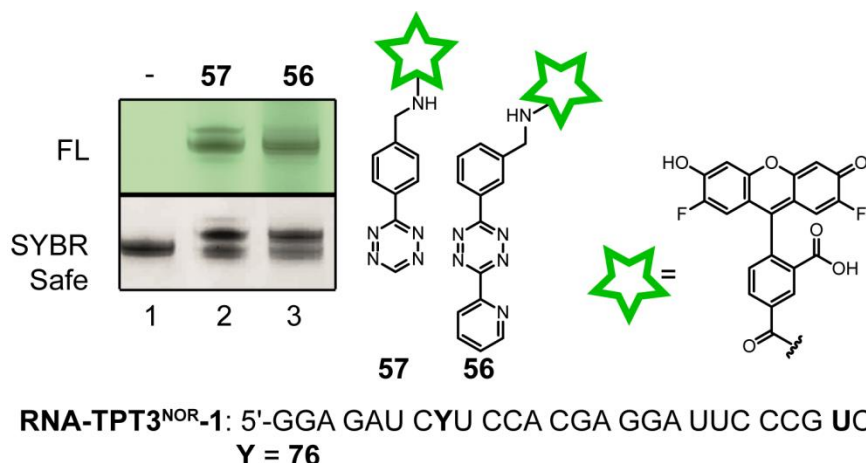
Fig. 65: Excerpt of fig. 59 showing successful incorporation of norbornene modified nucleotide 76 by *IEDDA* click chemistry. [310]

In addition, transcribed RNA was verified by LC-MS analysis. Unmodified RNA transcripts differ in mass by 204 a.u. caused by nucleobase of **76** in contrast to used adenine for unmodified RNA. Unmodified RNA weights $m/z = 9866.8$ as 5′-triphosphate (TP) and modified RNA bearing one **76** weights in contrast $m/z = 10070.8$ as 5′-triphosphate (TP) which was clearly identified by LC-MS analysis as shown in Table 4. Furthermore, the 5′-diphosphate (DP) and the 5′-monophosphate (MP) of the transcripts were identified in the crude transcription using LC-MS. In addition **RNA-TPT3^NOR-2** having two **76** incorporated was also verified by LC-MS and deconvoluted masses of the RNA transcripts match with the calculated ones within the tolerance range. This shows that specific incorporation of **76** as counterpart of the *ubp* **TPT3**/**NaM** using d**NaM**-containing DNA templates takes place and false incorporation of canonical ribonucleosides might only occur to a neglectible amount. Opposite the lack of false incorporation of canonical triphosphates a possible false incorporation of **76** was also refuted as shown in literature.[310,319]

RNA sequence	$m/z_{calculated}$	$m/z_{measured}$
RNA-TPT3^{NOR}-1 5'-GGA GAU C**Y**U CCA CGA GGA UUC CCG UCA CAG-3'	5'-OH: 9830.8 5'-MP: 9910.8 5'-DP: 9990.8 5'-TP: 10070.8	5'-OH: 9831.5 5'-MP: 9911.0 5'-DP: 9990.8 5'-TP: 10070.0
RNA-TPT3^{NOR}-2 5'-GGA GAU C**Y**U CCA CGA GGA UUC CCG**Y**CA CAG-3'	5'-OH: 10073.9 5'-MP: 10153.8 5'-DP: 10233.8 5'-TP: 10313.8	5'-OH: 10074.9 5'-MP: 10155.1 5'-DP: 10235.1 5'-TP 10314.4
RNA-TPT3^{NOR}-0 5'-GGA GAU CGU CCA CGA GGA UUC CCG UCA CAG-3'	5'-MP: 9706.9 5'-DP: 9786.8 5'-TP:9866.8	5'-MP: 9706.7 5'-DP: 9786.7 5'-TP: 9866.2

Table 4: ESI-MS data of transcribed oligonucleotides RNA-TPT3^{NOR}-1, RNA-TPT3^{NOR}-2 and RNA-TPT3^{NOR}-0 bearing unnatural nucleotide 76 marked as Y in sequence or canonical uridine.[310]

Using unnatural norbornene-modified ribonucleotide **76**, first *in vitro* applications were carried out using different tetrazine conjugates.[310] As previously shown, *IEDDA* reaction is not affected by nucleobase's molecular structure and is as active as other norbornene modified-nucleotides, like e.g. uridine.[309]

3.3.3 Synthesis of unnatural desoxynucleoside triphosphates dNaM-TP and dTPT3-TP

Unnatural ribonucleoside triphosphates are incorporated by T7 *in vitro* transcription. This recommends DNA with corresponding unnatural counterpart as template. Short DNA template strands can be received by solid phase synthesis and phosphoramidite chemistry. Annealing a single stranded DNA primer to template DNA can be used to incorporate required T7 promoter sequence and unnatural nucleosides allowing a mismatch in the primer – plasmid duplex. Subsequent PCR amplification yields DNA duplex containing an *ubp*. For this step, both parts of *ubp* **NaM**:**TPT3** are recommended.

The single synthetic steps of the unmodified and deoxygenated **TPT3** derivative suitable for DNA applications are described in material and methods.[274] Pyridone **79** synthesized by F. Eggert was coupled to 1-chloro-3,5-di-*O*-toluoyl-2-deoxy-D-ribofuranose **78** in a Hilbert-Johnson-like reaction yielding **80** with 41%. Yield of this synthetic step could be improved in contrast to literature by longer reaction time. Starting from ribose **77**, toluoyl protected deoxygenated ribose **78** was synthesized according to literature[320] in three steps with an overall yield of 65%. As mentioned by Lhomme[320] in according literature, the sugar derivative tends to hydrolyses and turns into an off-white to greyish crystalline

solid. Thionation of pyridine moiety was carried out using Lawesson's reagent. Chromatographic isolation of thionated product was done after subsequent deprotection of **80** yielding nucleoside **81** with 7% after two steps. Unfortunately, literature stated yields[274] could not be reached for these steps. Formation to the desired nucleotide **82** was performed using the literature known synthetic pathway for triphosphates as described by Kovács and Ötvös[321] yielding nucleoside triphosphate with 6%.[321]
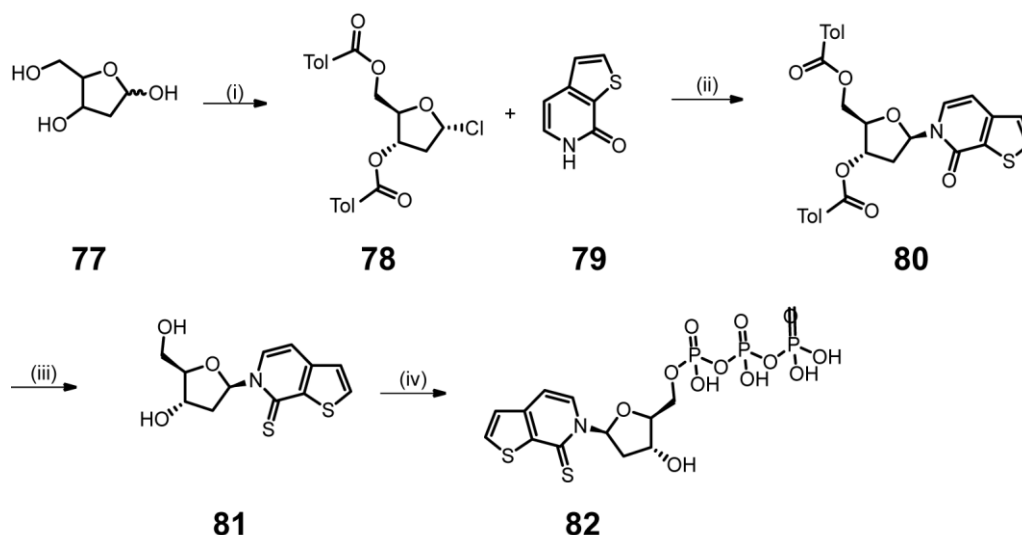
Fig. 66: Synthesis of dTPT3-TP (82) according to Romesberg and coworkers. [274,320] (i) HCl (1.25 M in MeOH), MeOH r.t., 2 h / p-toluoylchloride, pyridine, 0 °C to r.t., o/n / HCl (sat. in AcOH), AcOH, r.t., 65% (over three steps); (ii) BSA, SnCl$_4$, DCM, 0 °C to r.t., o/n, 41%; (iii) Lawesson's reagent, Tol, 120 °C, 4 h / MeOH, NaOEt (21 w/v in EtOH) r.t., 2h, 6.5% (over two steps); (iv) OP(OMe)$_3$, POCl$_3$, 0 °C, 6 h / NBu$_3$, (n-Bu$_3$NH)$_2$H$_2$P$_2$O$_7$, 0 °C, 15min, TEAB, 6%.

Corresponding counterpart of *ubp* **NaM**:**TPT3** was done in a literature known straight forward synthesis.[271] After protecting deoxygenated ribose using a silyl-protection group 1,3-Dichloro-1,1,3,3-tetraisopropyldisiloxane (*TIDPS*), 3′- and 5′-protected ribose derivative **84** was yielded with 40%. Then, 2-methoxynaphthalene **83** is coupled to **84**. Using *n*-BuLi as metalation reagent and the methoxy group at position two as moderate "directed *ortho* metalation" (*DOM*) the lithiated intermediate of **83** reacts in a subsequent step with the protected lactole **84** to open intermediate **85**. As second step a Mitsunobu reaction forms the closed protected nucleoside precursor. Subsequent deprotection is carried out under standard conditions, using TBAF in THF yielding **86** with 12% over three steps. Overall yield is in literature stated range[271] and improving synthesis was not required.

Triphosphate synthesis was carried out to the procedure described by Kovács and Ötvös[321] yielding dNaM-TP **87** with 11%.
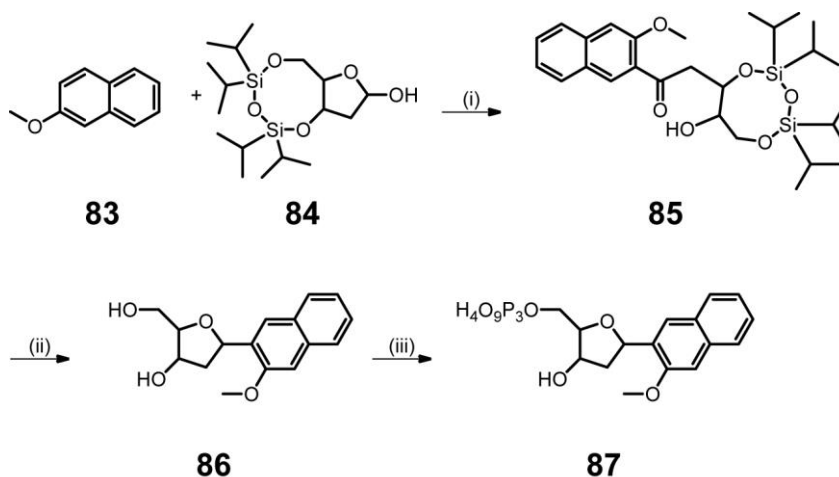
Fig. 67: Synthesis of dNaM-TP (87) according to Romesberg and coworkers.[271] (i) *n*-BuLi, THF, 0 °C to r.t., 1 h / 32 (in THF), -10 °C to r.t., o/n; (ii) *n*-Bu$_3$P, TMAD, THF, 0 °C to r.t., o/n / TBAF * 3H$_2$O, r.t., 2 h, 12% over three steps; (iii) OP(OMe)$_3$, POCl$_3$, 0 °C, 6 h / NBu$_3$, (*n*-Bu$_3$NH)$_2$H$_2$P$_2$O$_7$ (0.5 M in DMF), 0 °C, 15 min, TEAB, 11%.

Subsequent biochemical applications of synthesized unnatural nucleotides were carried out by coworkers. In successful PCR amplification experiments building blocks of *ubp* were introduced in DNA strands for latter T7 *in vitro* transcription.[319]

3.3.4 Reverse transcription of RNA bearing an unnatural ribonucleoside triphosphate

Site-specific incorporation of unnatural ribonucleoside triphosphate **76** was proven by reverse transcription also. The general workflow is depicted in Fig. 68 (A) below. [γ-^{32}P]-labeled 15 nt DNA primer (**DNA-RT-1**) complementary to **RNA-TPT3^{NOR}-1** was used for reverse transcription. Unnatural ribonucleoside triphosphate is incorporated at position 23 of transcribed RNA. In unmodified control consisting of canonical nucleotides, AMV reverse transcriptase generates full length complemantary DNA (*cDNA*) of 30 nt. Successsful incorporation of **76** blocks AMV reverse polymerase at position 23 of cDNA. As references a solid-phase synthesized 22 nt long DNA primer (**DNA-RT-2**) was used.

RNA-TPT3^{NOR}-0: 5'-GGA GAU C**G**U CCA CGA GGA UUC CCG **U**CA CAG-3'
RNA-TPT3^{NOR}-1: 5'-GGA GAU C**Y**U CCA CGA GGA UUC CCG **U**CA CAG-3'
DNA-RT-1: 5'-CTG TGA CGG GAA TCC-3'
DNA-RT-2: 5'-CTG TGA CGG GAA TCC TGG A-3'
Y = 76
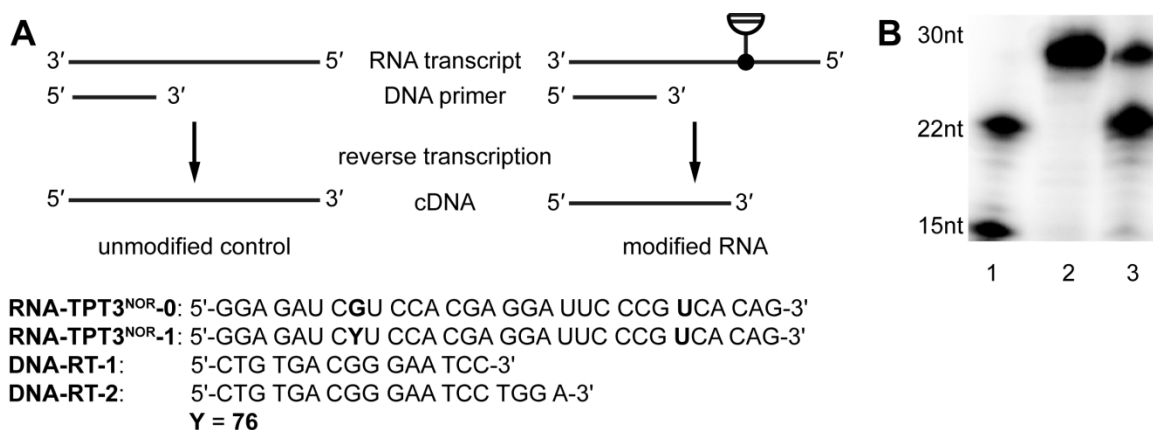
Fig. 68: Reverse transcription of RNA-TPT3^{NOR}-1. Depicted is the general workflow (A) and radioactive read-out of reverse transcription using AMV reverse transcriptase (B). Lane 1: 15 nt and 22 nt long DNA primer used as reference; lane 2: reverse transcription of unmodified RNA; lane 3: reverse transcription of modified RNA containing 76. The reaction is stalled at position of unnatural nucleobase 76.[310]

PAGE analysis of the reverse transcription (Fig. 68 B) shows, that unmodified RNA transcript **RNA-TPT3^{NOR}-0** is transcribed in cDNA by full length which is observed in lane 2. Blocking of the AMV reverse transcriptase occurs at position 22 when RNA contains unnatural nuclebase XX as it can be observed in Fig. 68 B, lane 3. A 30 nt long cDNA transcript of modified RNA was observed by longer incubation times. It is assumed, that AMV reverse transcriptase incorporates minor amounts of natural nucleotides opposite **76** and an erroneous cDNA is produced.[310]

In a similar experimental setup reverse transcription using **87** for cDNA synthesis was tested.

RNA-TPT3^{NOR}-1: 5'-GGA GAU C**Y**U CCA CGA GGA UUC CCG **U**CA CAG-3'
DNA-RT-1: 5'-CTG TGA CGG GAA TCC-3'
DNA-RT-2: 5'-CTG TGA CGG GAA TCC TGG A-3'
Y = 76
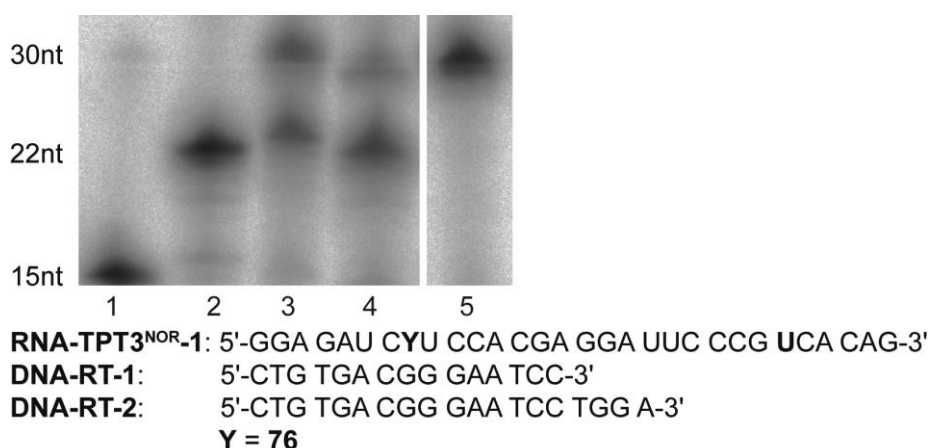
Fig. 69: Reverse transcription of RNA-TPT3^{NOR}-1 to test 87 in cDNA synthesis. Lane 1: DNA-RT-1; Lane 2: DNA-RT-2; Lane 3: reverse transcription of RNA-TPT3^{NOR}-1 with 87; Lane 4: reverse transcription of RNA-TPT3^{NOR}-1 w/o 87; lane 5: reverse transcription of canonical RNA-TPT3^{NOR}-0. Full gel is shown in appendix.

AMV reverse transcriptase still shows truncation at position 22. Band intensity shows a higher truncation amount for cDNA approach without addition of compound **87** (Fig.

69 lane 4). Thus, incorporation of **87** occurs, but AMV reverse transcriptase struggles with cDNA synthesis from RNA containing an unnatural nucleotide. Similar behavior during reverse transcription was observed by Benner and coworkers, too.[322] Using a similar experimental setup, to test *ubp* **Z**:**P**, they reported skipping or mismatching of an uncomplemented nucleotide for Superscript III reverse. Further experiments, to test and validate in which way enzymes are unable to cope with unnatural nucleotides during reverse transcription might reveal a better insight. Here, reverse transcription experiments should only validate site-specificity of unnatural ribonucleoside triphosphates.

3.3.5 Synthesis of NaM-TP as ribonucleoside triphosphate counterpart for dTPT3

This part shows synthetic approaches and of a ribonucleoside triphosphate using unnatural nucleobase **NaM** suitable for *in vitro* transcription. A particular decrease in stability for e.g. RNA duplexes or stem regions in ncRNA constructs can be assumed lacking Watson-Crick-like H-bonds, but aiming for **NaM**-TP present unavoidable mismatches on RNA level will be avoided. Synthesis carried out to literature will be described in the following.

The synthetic approach towards triphosphates commences by the synthesis of the nucleoside as building block in this case, too. For the unnatural nucleoside **NaM** – based on 2-methoxynaphthalene like previously described d**NaM** – two synthetic strategies are possible.[293,323]

Both approaches start with a directed ortho metalation of 2-methoxynaphthalene or 2-bromo-3-methoxynaphthalene using butyl lithium derivatives, followed by a nucleophilic addition to a protected lactone. According to procedure[323] published in 2009 benzyl protected lactone **92** was used for several attempts. Synthesis of **92** was carried out according to literature-known pathways[324–327]. 1'-Methyl protected ribose **89** was protected at 2'-OH, 3'-OH and 5'-OH using benzyl bromide and sodium hydride in DMF yielding **90**. Deprotection of 1'-OH was carried out using hydrochloric acid in 1,4-dioxane. Lactone formation of **92** was carried out by an Albright-Goldman oxidation using acetic anhydride and DMSO.[324–327]
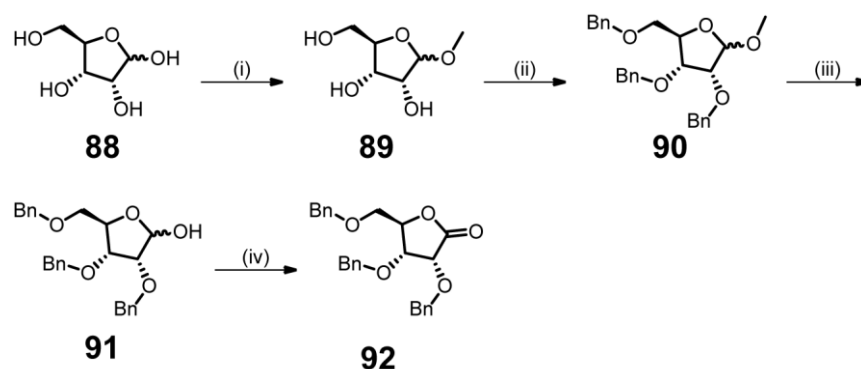
Fig. 70: Synthesis of compound 48. (i) Dowex 50 (H⁺-form), MeOH, 4 °C, o/n, 72%; (ii) NaH, BnBr, DMF, 0 °C to r.t., o/n, 56%; HCl (aq., 0.2 M), 1,4-dioxane, 100 °C, 3h, n/a; (iv) Ac2O, DMSO, 4 °C, 48h, 53% over two steps.

Subsequent three in one-pot syntheses of **NaM** nucleoside using **92** and 2-methoxynaphthalene **83** failed during final deprotection.

Synthesis of **NaM** is described referring to R_f values of intermediates.[323] The intermediates **94** and **95** could have been isolated by additional purification steps using column chromatography according those R_f-values. An exact verification by ^{1}H-NMR was impossible. The second intermediate **95** could be verified by mass spectrometry. Nevertheless, the final step of this synthesis did not lead to compound **96**. Benzyl deprotection using boron tribromide as solution in DCM showed no positive result. Using BBr$_3$ as pure reagent revealed to a decomposition of the isolated intermediate **95**. As alternative pathway a deprotection strategy using Pd/C and hydrogen was tried.
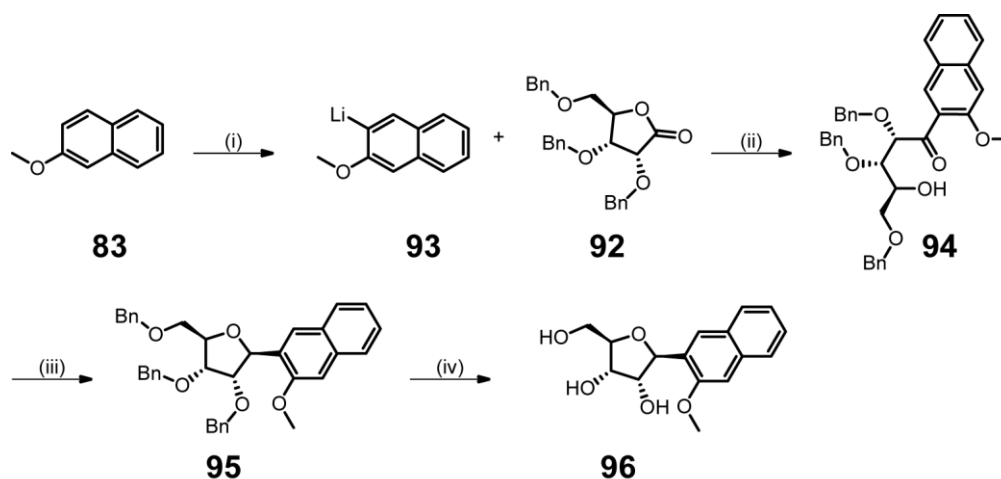
Fig. 71: Synthetic pathway for 49 according to Romesberg and coworkers.[323] (i) *n*-BuLi, THF, -40 °C to r.t.; (ii) THF, -12 °C to r.t., 3 h; (iii) HSiEt$_3$, BF$_3$*Et$_2$O, MeCN, -40 °C to r.t., 2 h; (iv) BBr$_3$, DCM, -78 °C, 5 h.

The described procedure[323] uses benzyl ethers as protecting groups for 2'-OH, 3'-OH, and 5'-OH of lactone **92**. Benzyl ether is one of the most robust and most used protecting groups.[328] Formation of primary and secondary benzyl ethers are well known in literature and a plethora of procedures can be found. A widespread amount of

references describes cleavage of this protecting group, too. Reductive hydrolysis using Pd/C and a hydrogen saturated solvent is a common and well-established way. Studies regarding solvent effects, reaction rates for different aliphatic or aromatic ethers as well as possible occurring problems can be reviewed.[329–332] As an alternative, the widely used ether-cleaving reagent BBr_3 can be used. Advantageous is the possibility to cleave specific ethers under mild conditions without affecting other functional groups. Furthermore, specific ethers can be cleaved without affecting other ethers by adjusted reaction conditions.[328,333] Standard procedures describe reaction conditions at low temperatures in DCM. The cleavage is initiated by a nucleophilic attack at the boron atom by the ether oxygen and results in a bromide and an alkoxydibromoborane, which is converted into a hydroxyl group during workup.[334,335] Modern computationally aided mechanistic investigations prefer an intermolecular reaction pathway in contrast to the former postulated reaction sequence. Both pathways are shown in Fig. 72. The preferred mechanism either monomolecular or bimolecular depends on the steric properties of the substituents.[335]
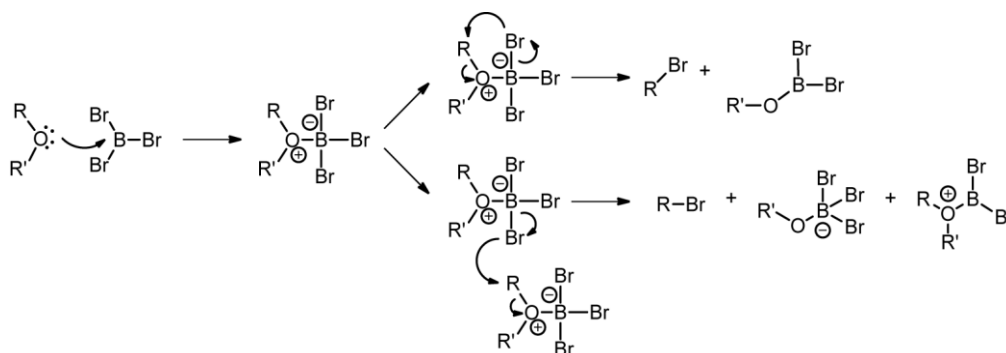
Fig. 72: Proposed monomolecular (upper pathway) and bimolecular (lower pathway) mechanism for BBr_3-ether cleavage.[335]

Silva and coworkers also address a possible reaction inhibition due to steric hindrance which might be the reason for reported unable BBr_3-mediated ether cleavage.[328] A Br^- donation prevents to stop the bimolecular reaction pathway. This could explain the failed attempts using BBr_3 for ether deprotection, but not the failed deprotection using reductive hydrolysis. Literature describes several procedures, which differ slightly in reaction conditions, but can be summarized as palladium-catalyzed hydrogenation delivering the corresponding alcohol and toluene. Regarding obtained products after the described approaches does not lead to an explicit source of errors. A decomposed product after the usage of pure BBr_3 can be attributed to harsh reaction conditions. The other approaches using BBr_3 as solution in DCM as well as the palladium-catalyzed hydrogenation showed no result at all. Literature research obtained other possible deprotection strategies for ether cleavage, like the use of boron trichloride[336] or the

usage of ozone[337]. Referring to former work of G. Mund[338] a similar questionability occurred. Fortunately another synthetic route was published by Romesberg and coworkers in 2016.[293]

An alternative pathway[293] of **NaM** synthesis was carried out. As shown Fig. 73 functionalizations at position 7 can be introduced before nucleoside synthesis.[293] Regarding synthetic steps, same pathway can be used for unfunctionalized 2-methoxynaphthalene.
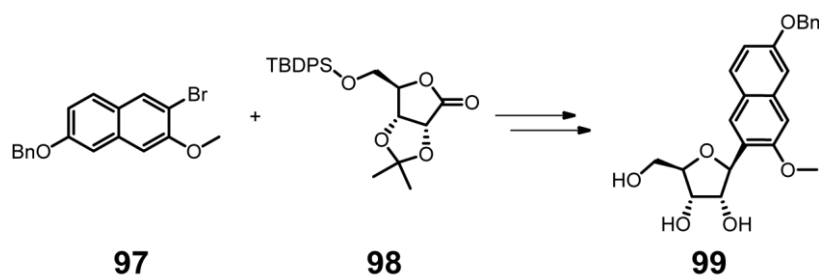
Fig. 73: NaM derivative synthesized by Romesberg and coworkers in 2016 using an alternative lactone protection strategy.[293]

A brominated methoxynaphthalene was ortholithiated with *t*-BuLi and subsequently reacted with a 2′-OH, 3′-OH acetonide protected and 5′-TBDPS protected lactone. The second step of the synthesis is analogous to the prior mentioned synthetic pathway a Lewis acid-induced deoxygenation of the anomeric carbon. Deprotection strategy is changed. Silyl ether at 5′-OH is removed with TBAF as fluoride source. Deprotection of bridging 2′-OH, 3′-OH acetonide can be carried out by acetic acid (aq., 70%) under conditions near reflux.[293] This synthetic route was transferred on unmodified NaM as ribonucleoside.

Using *ortho*-metalation with *t*-BuLi in THF for 2-methoxynaphthalene **93** is carried out in a similar way to procedure from 2009[323]. Taking into account to adjust reaction time with regard to changed basicity using *t*-BuLi instead of *n*-BuLi was done. Mitsunobu reaction is consistent to former pathway yielding cyclic nucleoside. The required deprotection steps as described above were unnecessary. Ring closure of open intermediate **102** was carried out using BF_3*Et_2O. This Lewis acid is able to deprotect acetonide groups, too. Silyl ether cleavage appears in a Lewis acid mediated way also.[271,293] Fully deprotected nucleoside **96** was yielded in three attempts in an average of 20% without additional deprotection steps described in literature.[293]
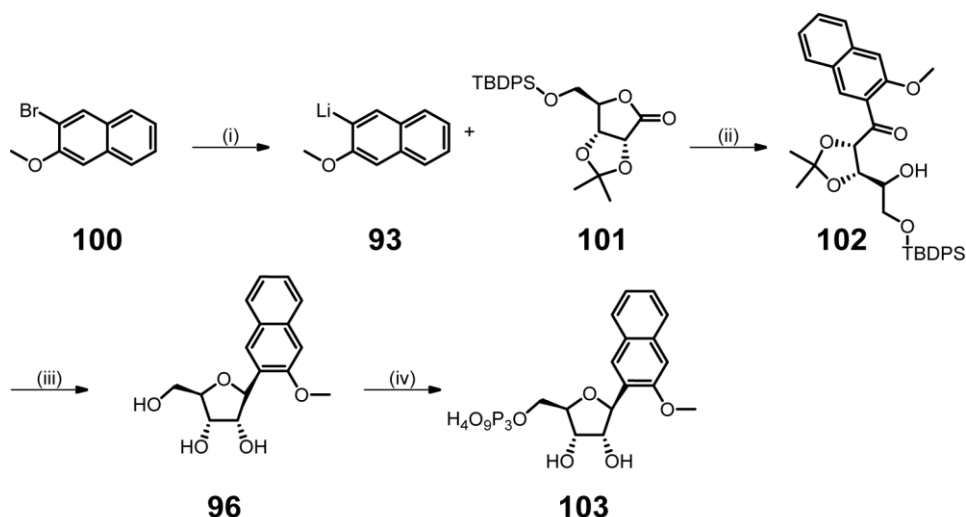
Fig. 74: Synthetic pathway for NaM nucleoside according to Romesberg and coworkers.[293]
(i) *t*-BuLi, THF, -78 °C, 15min; (ii) THF -78 °C, 3h; (iii) HSiEt$_3$, BF$_3$*Et$_2$O, MeCN, -40 °C, 1h, 20% over three steps. (iv) OP(OMe)$_3$, POCl$_3$, 0 °C, 6 h / NBu$_3$, (*n*-Bu$_3$NH)$_2$H$_2$P$_2$O$_7$ (0.5 M in DMF), 0 °C, 30 min, TEAB, 10%.

The conversion from nucleoside **96** to triphosphate **NaM**-TP **103** was carried out in the same manner as described before using the established synthetic route based on the Kovács and Ötvös[321] yielding 103 with 10% as fourfold triethylammonia salt. Shown in Fig. 75 is the UV trace of a crude triphosphate reaction before preparative HPLC workup. Depicted are the peaks referring to nucleoside triphosphate (TP), diphosphate (DP) and monophosphate (MP) of **103**. Also depicted is the used proton sponge (PS). Despite huge differences in retention times, proton sponge tends to "smear" during HPL chromatographic workup and there-fore a second HPLC purification is needed usually.
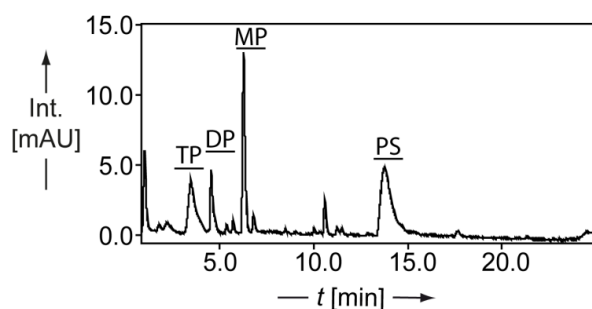
Fig. 75: UV-trace of crude triphosphate synthesis yielding 103 before preparative HPL chromatographic purification. Ribonucleoside triphosphate (TP), diphosphate (DP) and monophosphate (MP) are marked. Proton sponge (PS) used during triphosphate synthesis is also depicted in shown chromatogram.

After preparative HPL chromatographic purification, NaM-TP **103** was isolated as clean compound. Fig. 76 shows LC-MS analysis of clean NaM-TP. Retention times agree with retention times shown before in Fig. 75. Peak eluting at t_R = 2min in Fig. 76 shows no distinct mass pattern and is assigned to salt and buffer components used during purification.
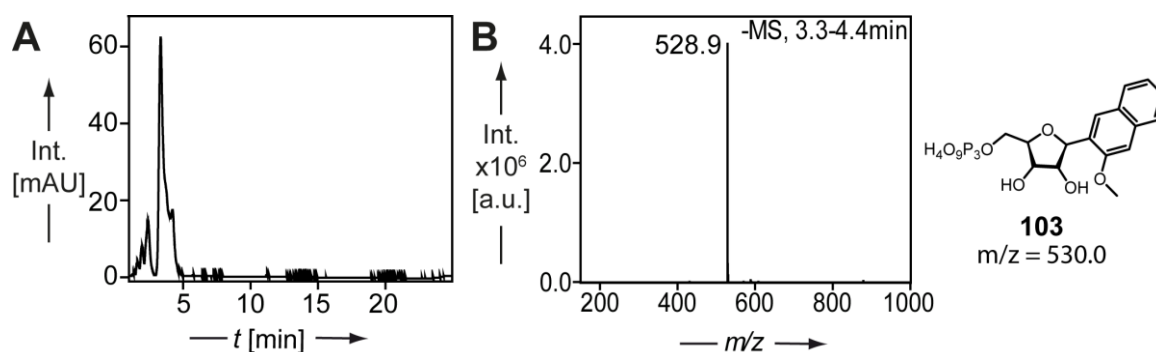
Fig. 76: LC-MS analysis of NaM-TP. Shown are UV trace (A, λ = 254 nm) and corresponding ESI⁻ spectrum (B) of peak eluting at t_R = 3.3min.

3.3.6 Transcriptions using NaM-TP

In 2016 it was stated in literature, that the nucleobase **NaM** is well suited as a directing part of RNA transcription. DNA templates bearing d**NaM** are excellently transcribed to RNA bearing **5SICS** or **TPT3** as unnatural counterpart. Nonetheless it is also stated, that a DNA template for an *in vitro* transcription containing d**5SICS** is not suitable for functionalized **NaM** derivative transcription in a good manner.[293]

In vitro transcriptions using d**5SICS**-modified DNA templates and **103** were carried out according to the protocol stated in material and methods.

Using literature known template sequences[274,277,311], two DNA templates were chemically synthesized. **DNA-CXT^NaM** and **DNA-CXT^5SICS** bearing either d**NaM** or d**5SICS** at position 31. Here, **DNA-CXT^5SICS** with d**5SICS** as counterpart for **103** was used. The T7 *in vitro* transcripts were only purified by G-25 column cleaning after DNase digestion and submitted as crude transcription to *PAGE* analysis. If **103** is incorporated successfully, 17 nt long full length RNA will be yielded. Otherwise truncation at position 13 occurs.

DNA-CXT⁵ˢᴵᶜˢ:　　　5'-CAC T**X**C TCG GGA TTC CCT ATA GTG AGT CGT ATT AT-3'
RNA-CXT⁵ˢᴵᶜˢ-NaM: 5'-GGG AAU CCC GAG **Y**AG UG-3'
X = d5SCIS; **Y** = **103**
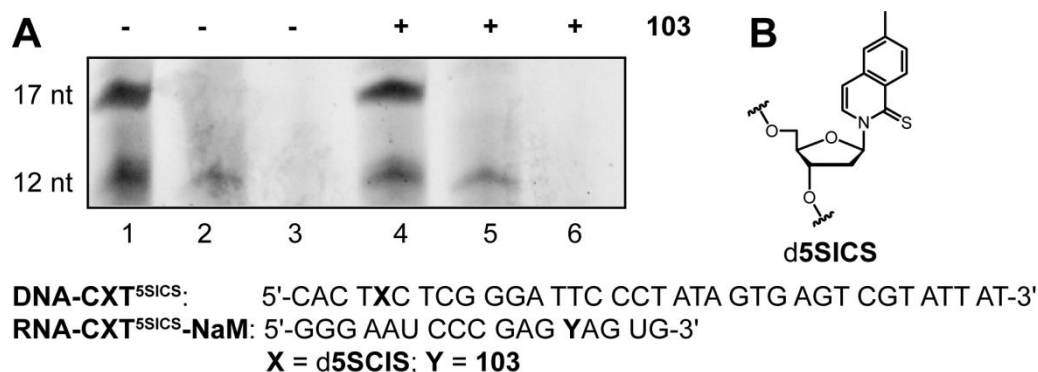
Fig. 77: 20% denat. *PAGE* depicting a **DNA-CXT⁵ˢᴵᶜˢ** directed *in vitro* transcription (A). Lane 1: **DNA-CXT5ˢᴵᶜˢ** transcription w/o **103**, Lane 2: DNase digestion of transcription from lane 1, Lane 3: G-25 purification of lane 2, Lane 4: **DNA-CXT⁵ˢᴵᶜˢ** transcription w/ **103**, Lane 5: DNase digestion of transcription from lane 4, Lane 6: G-25 purification of lane 4. Full gel is shown in appendix. (B) Chemical structure of unnatural nucleotide incorporated in **DNA-CXT⁵ˢᴵᶜˢ**.

Two different batches of **103** have been tested on template-directed *in vitro* transcription in parallel. Fig. 77 shows a 20% denat, *PAGE* analysis of a transcription using **DNA-CXT⁵ˢᴵᶜˢ** as template and **103**. *PAGE* analysis shows no significant difference to the negative control. Moreover, neither in the negative control nor in the positive transcription reaction a band is left after size exclusion purification using G-25 columns. G-25 columns used for desalting have a manufacturer related advice, that oligonucleotides lower than 10 nt are held back. If **103** would have been incorporated, a 17 nt long full length transcript would be achieved. The 13 nt truncation fragment seems to be held back by column material.

A comparing study using **DNA-CXTᴺᵃᴹ** and **DNA-CXT⁵ˢᴵᶜˢ** was carried out. Both templates are modified at position 31. One template bears a d**NaM** nucleotide suitable for the incorporation of **TPT3**-TP derivatives; the other is suitable for possible incorporation of **103** using a d**5SICS**-*CEP* (see **Fig. 77** B). Crude transcriptions were DNase digested and submitted to LC-MS to verify the transcription products by mass.

Fig. 78 shows an UV-trace of crude **DNA-CXTᴺᵃᴹ** directed T7 *in vitro* transcription using **TPT3ᶜᴾ**-TP[311] **104** as unnatural ribonucleoside triphosphate (A). The deconvoluted masses of the truncated fragment (B) and the full length transcript (C) of cycloprooene containing **RNA-CXTᴺᵃᴹ-CP** are in agreement with calculated values and can be clearly assigned. **104** was synthesized by F. Eggert[311] and is used in this work for T7 *in vitro* transcriptions. In contrast to former used phosphoramdite **74** and ribonucleoside triphosphate **76** cyclopropene bearing **104** possesses increased handle reactivity and a decreased size of strained alkene.
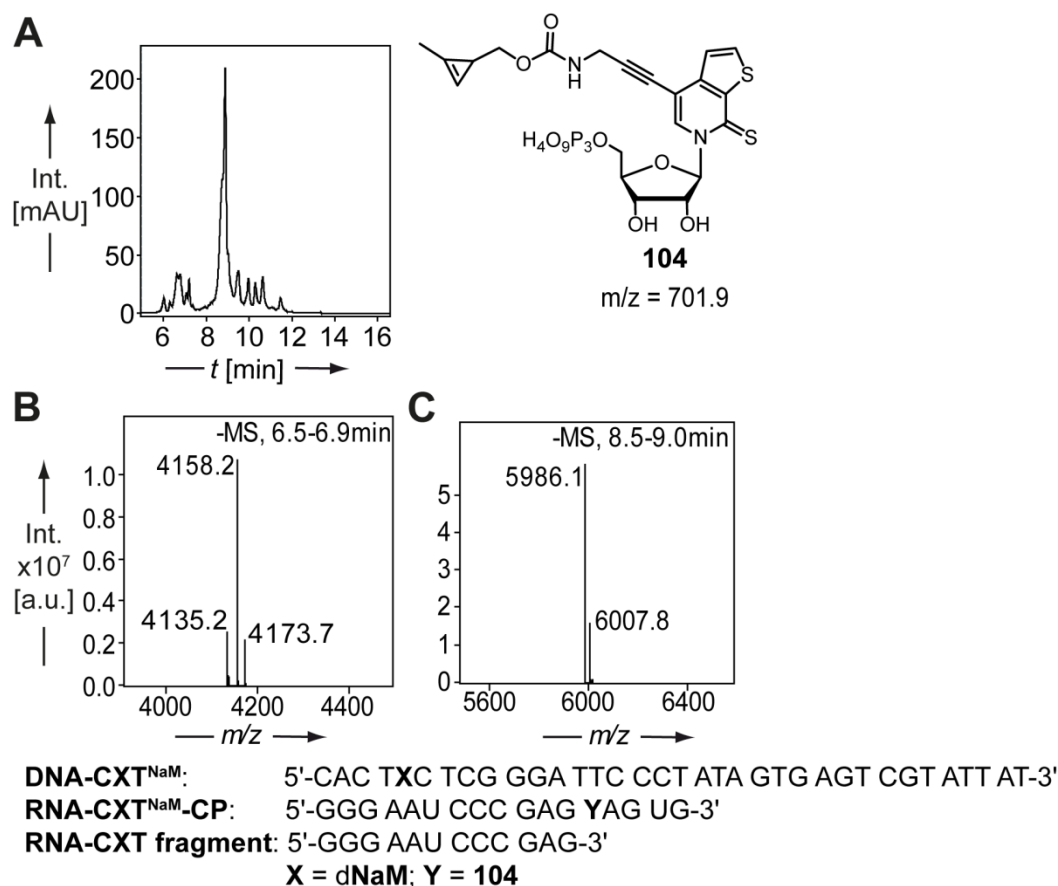
Fig. 78: LC-MS analysis of an *in vitro* transcription using DNA-CXT^NaM template and TPT3^CP-TP. UV trace (A) shows truncation at t_R = 6.7 min and full length transcript at t_R = 8.7 min. Deconvoluted ESI^- spectra of truncation (B) and full length RNA (C) correspond with calculated masses. Both spectra show additional sodium adducts of RNA.

The masses shown in Fig. 78 correspond with calculated values of the 5′-TP of truncated fragment in addition with one (m/z = 4135.4) or two (m/z = 4157.4) sodium ions. Also full length transcript matches with computed values for sodium adducts ([M-2H+Na]^- m/z = 5985.3; [M-2H+Na]^- m/z = 6008.3) of the 5′-TP. This method of analysis perfectly fits with (un)modified **TPT3** ribonucleoside derivatives incorporated into RNA strands. Regarding **NaM** as unnatural nucleobase, values listed in Fig. 79 shows masses of uracil, adenine, and unmodified **TPT3** as comparison.

Nucleobase	Mass	+Na	+2Na	+3Na
Uracil	112.0	135.0	158.0	181.0
Adenine	135.1	158.0	181.0	204.0
NaM	158.1	181.1	204.1	227.0
TPT3	166.0	189.0	212.0	235.0

Fig. 79: Structural comparison of nucleobases U, A, NaM, and TPT3 (left) and table of corresponding calculated masses (right). Greyed out are similar masses caused by sodium adducts. Shown are only nucleobases. Sugar moieties are not depicted.

This mass pattern raises difficulty in a verification of nucleotide incorporation. Sodium pattern between uracil and adenine might be surmounted by the fact, that RNAPs recognizes the right nucleotide counterpart *in vitro* and *in vivo* for canonical base pairs, but proving the incorporation of an unnatural, synthetic nucleotide, whose RNA incorporation is not proved beyond doubt are aggravating circumstances in this regard.

Relevant citation ends up in a dichotomy. On the one hand (d)**NaM** is named part of the most promising *ubp*[274] and was used in first semi-synthetic organism.[1] On the other hand Romesberg and coworkers stigmatize **NaM** nucleoside on RNA level.[271,293] With high transcription fidelity[323], transcription yields with ribonucleoside **NaM** decreases massively in contrast to canonical controls[323]. In 2016 transcriptions experimets, using three **NaM**-TP derivatives were published[293] showing an overall average below 60% of yielded full length transcript for used derivatives.[293]

Using mass spectrometric analysis to verify **NaM** incorporation into RNA offered an inconclusive result. Crude transcription of **DNA-CXT^5SICS** showed a truncation at position 12. LC-MS analysis is shown in Fig. 80. In comparison, truncated fragments can be verified by mass and elute at similar retention times. The truncated RNA fragment either in Fig. 78 B or in Fig. 80 B is measured as sodium adduct with $m/z = 4135.4$ or the twofold adduct with $m/z = 4157.4$. Deviation of measured and calculated values is caused by deconvoluting software. No "free" RNA fragment triphosphate was observed. Considering Fig. 80 C and Fig. 80 D the masses conclude a possible full length transcript of the **RNA-CXT^5SICS-NaM**. According to calculated values, Fig. 80 C might show the full length RNA ending up as triphosphate strand with an adenosine false incorporation ($m/z = 5768$). In agreement with the shown truncation fragments and measured full length RNA shown in Fig. 79, there is an equal probability for the sodium adduct of a transcript bearing an uridine at position 13 ($m/z = 5745+23 = 5768$). Deconvoluted mass $m/z = 5807$ indicates a potassium adduct ($m/z = 5807-39 = 5768$). Taking a look at Fig. 80 D masses show a possible successful **RNA-CXT^5SICS-NaM** transcript with incorporation of **103** ($m/z = 5791$) or the sodium adduct of a 17 nt long RNA with mentioned adenosine misincorporation ($m/z = 5791$). Indicating correct sequence of RNA are deconvoluted masses of $m/z = 5733.9$ and $m/z = 5632.1$ representing sodium adduct of 5'-DP ($m_{calc}[DP] = 5711.4$; $m_{calc}[DP+Na]=5733.4$) and 5'-MP ($m_{calc}[MP] = 5631.4$) of full length RNA. Again, sodium adduct of 5'-TP ($m_{calc}[TP+Na] = 5813.4$) and potassium adduct ($m_{calc}[TP+K] = 5829.4$) is observed.
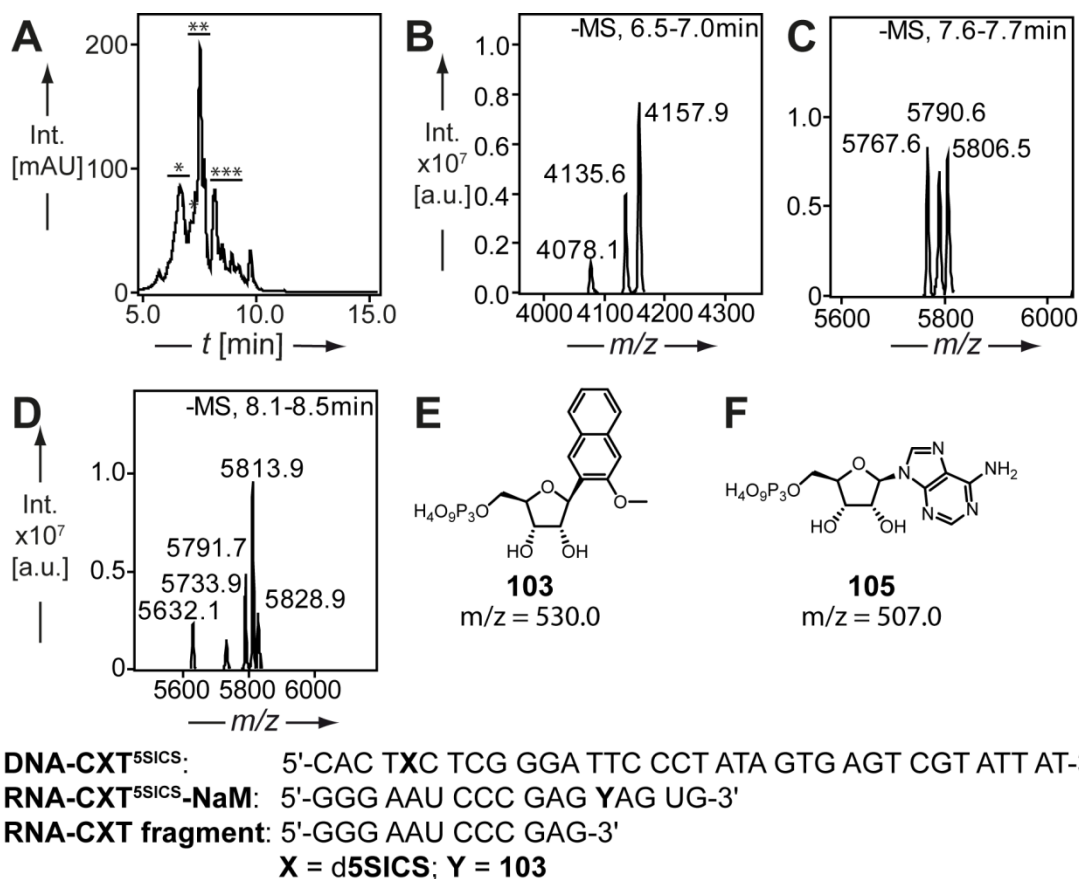
Fig. 80: LC-MS analysis of crude *in vitro* transcription using DNA-CXT[5SICS] template and 103. UV trace (A, λ = 254 nm) shows three peaks, representing truncated 12 nt long fragment (*) eluting at t_R = 6.5-7.0 min, full length 17 nt RNA transcript with a false incorporation of adenosine (**) eluting at t_R = 7.6-7.7 min and a full length 17 nt RNA transcript eluting at t_R = 8.1-8.5 min(***). Deconvoluted masses of truncated fragment (B), false incorporated full length RNA (C) and full length RNA (D) correspond with calculated masses. Structures of **NaM**-TP **103** (E) and Adenosine-TP **105** (F) are depicted with corresponding masses.

Integration of deconvoluted peaks shows a ratio of truncation in contrast to full length transcript. Assuming 100% RNA by adding up three marked peaks (*, **, ***) truncation occurs with 45%. False incorporation of adenosine takes place in 39% and putative correct RNA in 16%. Definite conclusions about correct incorporation of **103** can not be done with this set of data.

3.3.7 Enzymatic digest to nucleosides of NaM containing RNAtranscripts

As an alternative to former dicussed methods, an enzymatic digestion to nucleosides with subsequent HPL chromatographic analysis[339,340] was performed. A schematic presentation of the workflow is shown below in Fig. 81. After enzymatic digestion of RNA with S1 nuclease in a first step and in a second step a composition of alkaline phosphatase, snake venom phosphodiesterase and benzonase nuclease single nucleosides are analyzed by HPLC separation. For RNA consisting of canonical

ribonucleosides four signals are expected. If NaM-TP is successfully transcribed during T7 *in vitro* transcription, five signals are expected.
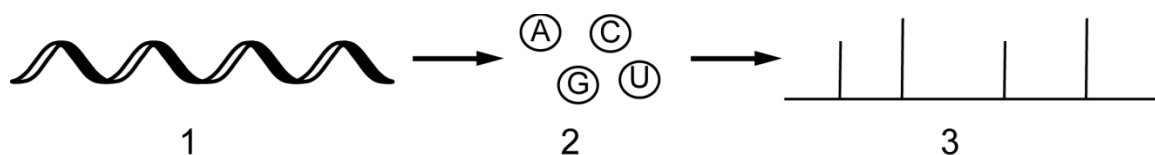
Fig. 81: Schematic presentation of digests worklow for canonical RNA. After enzymatic digest of RNA (1), single nucleosides (2) will be analyzed and identified via HPLC (3).[339,340]

Using an unmodified solid phase synthesized strand as role model, HPL chromatographic retention times of individual nucleosides were determined and validated. Furthermore, single injection of unnatural ribonucleoside **NaM** (Fig. 82 C) was done to determine retention time. In order to clarify incorporation for **53**, *in vitro* transcribed RNA putatively containing **NaM** was digested to ucleosides and analyzed via HPLC, too. Corresponding HPLC UV traces are shown in appendix also. As shown in Fig. 82 (C), **49** shows a unique time point (t_R = 23.9 min) for used conditions. Comparing UV traces of the digestion down to the nucleosides from the RNA strand depicted in Fig. 82 with (D) and without (B) addition of **53** to the transcription, no significant signal at t_R = 23.9 min is observable. Based on literature and based on the obtained data, it is anticipated, that **53** is incorporated.
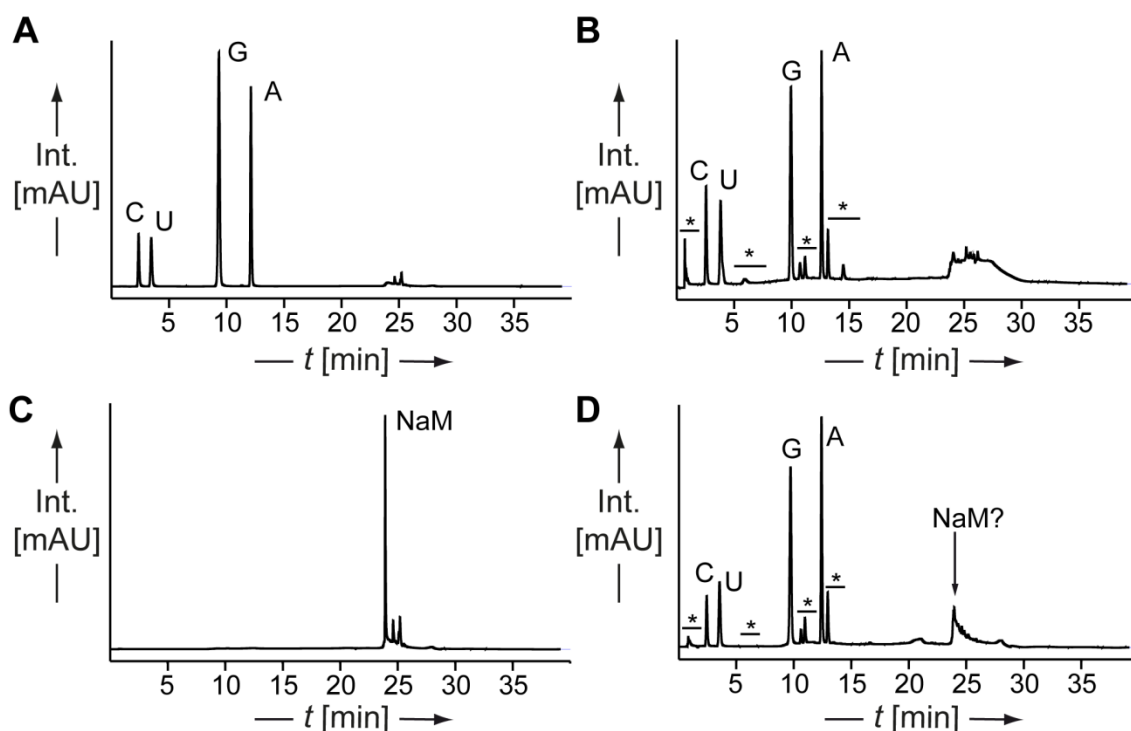
Fig. 82: HPL chromatographic UV traces (260 nm) of enzymatic digestion to the nucleosides. Solid-phase synthesized unmodified RNA-ND^{test} (A) shows retention times for canonical nucleosides C (t_R = 2.4 min), U (t_R = 3.5 min), G (t_R = 9.3 min) and A (t_R = 12.1 min). In contrast, *in vitro* transcribed unmodified **RNA-CXT^A-U** using **DNA-CXT^A** as template (B). Unassigned peaks depicted with (*) unspecifically occur at every nucleoside digestion using *in vitro* transcribed RNA. **103** was measured alone as reference (C) showing a retention time of t_R = 23.9 min. Nucleoside digestion of *in vitro* transcribed **RNA-CXT^{5SICS}-NaM^{53}** using **103** and **DNA-CXT^{5SICS}** (D).

Chemical analysis of **103** consisting of ^{1}H-NMR, ^{31}P-NMR and accurate mass measurement shows a high purity of the ribonucleoside triphosphate. Triethylammonium adducts caused by used HPL chromatographic purification process does not affect incorporation fidelity during enzymatic *in vitro* transcription. Purification of other synthesized triphosphates was carried out in a similar manner. **TPT3** derivatives were treated in the same way and show good results in biochemical applications. Resuming analytical techniques, neither electrophoretic analysis nor mass spectrometric measurement clarifies incorporation of **103**. Digestion of transcribed RNA to nucleosides showed no unambiguous result, too.

A detailed verification of NaM-TP incorporation into RNA via T7 *in vitro* transcription was carried out by K. Kurscheidt[341] using a reverse transcription approach. Data sets of K. Kurscheidt coincide in general with obtained data from LC-MS analysis of *in vitro* transcribed RNA (see Fig. 80) showing only moderate incorporation of **NaM**-TP **103**. Further experiments validating incorporation of unnatural ribonucleoside triphosphates have to be carried out in this case.

3.4 Distance measurement on RNA using different labeling approaches based on *IEDDA* click and unnatural nucleotides

The prepared tetrazine-fluorophore conjugates showed great results regarding *IEDDA* click applications on RNA. The next approach is the idea to combine the fastest known click reaction with a powerful tool for structural investigations on biomolecules. A tetrazine-spin-label conjugate was synthesized and clicked on a selfcomplementary RNA duplex, using a site-specific incorporated modified unnatural ribonucleoside triphosphate as reactive handle. Furthermore, unnatural nucleotide building blocks were modified with different spin labeled linker systems to increase rigidity for more precise distance maesurements.

3.4.1 Tetrazine spin label conjugates for structural investigations on RNA

Successful *in vitro* transcriptions using an unnatural ribonucleoside carrying a cyclopropene modified **TPT3** suitable for *IEDDA* click-chemistry have been carried out and established workflow was published by Kath-Schorr and coworkers.[311] Setting a new focus on spatial and structural investigations adapting this technique, compound **107** was synthesized in a similar manner like tetrazine-fluorophore conjugates before. **TEMPYO-NHS** (**106**) spin label and **4** were conjugated in a base-mediated manner using DMSO as solvent.
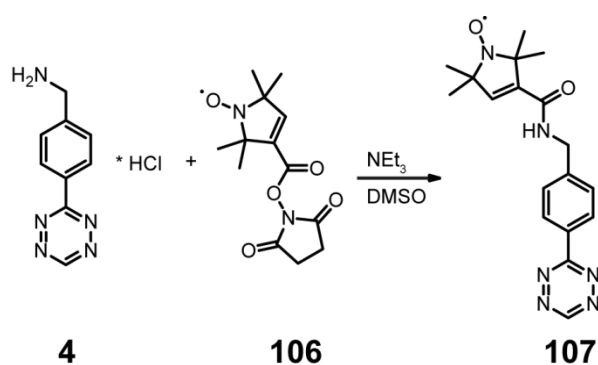
Fig. 83: Conjugation of 23 and TEMPYO-NHS using standard amide chemistry to gain compound 107.

After 1 h reaction time under argon atmosphere and exclusion of sunlight, compound **107** was isolated in a quantitative manner using HPL-chromatography and verified by LC-MS analysis as shown in Fig. 84.
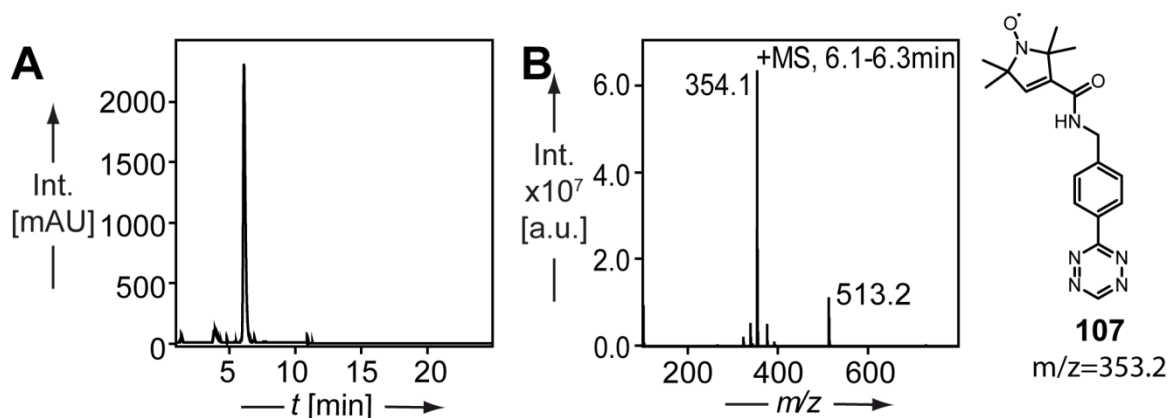
Fig. 84: LC-MS chromatogram of purified compound 107. Shown are UV-trace (λ = 254 nm; A) and corresponding ESI+ (B) of peak eluting at t_R = 6.2 min.

Resulting conjugate **107** shown in Fig. 83 was reacted to a self-complementary RNA construct (**RNA-SC**) adapted from Schiemann and coworkers.[301] They showed distance measurements using EPR spectroscopy with an uridine derivative. Bearing a terminal alkine, molecule undergoes copper catalyzed click chemistry with azide modified spin labels on solid-support forming dӋ depicted in Fig. 85 A.[301]
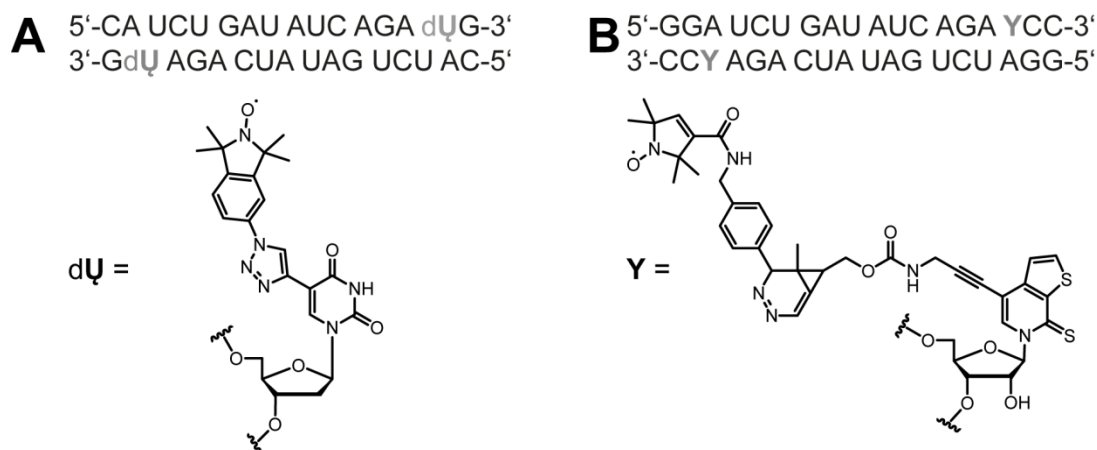
Fig. 85: Self complementary RNA designed by Kerzhner et al.[301] (A) and adapted selfcomplementary RNA used for *IEDDA* click (B). Incorporated and clicked nucleotides are depicted below corresponding sequence.

Overcoming accrued mismatch caused by unnatural ribonucleoside triphosphate **104** opposite to adenine was reduced by an elongation of the sequence at both ends using additional canonical nucleotides as shown in Fig. 85 B. Thus, a frayed duplex was avoided.

A general workflow of this approach is shown in Fig. 86. After T7 *in vitro* transcription of DNA template **DNA-SC** and corresponding T7 promoter, self-complementary RNA transcript **RNA-SC-CP** bearing reactive cyclopropane handle, is hybridized. Subsequent click reaction and purification yields labeled RNAduplex. Click reaction between RNA

and **107** was carried at room temperature. After 1 h reaction time, excess of spin-label tetrazine **107** was removed using spin columns.
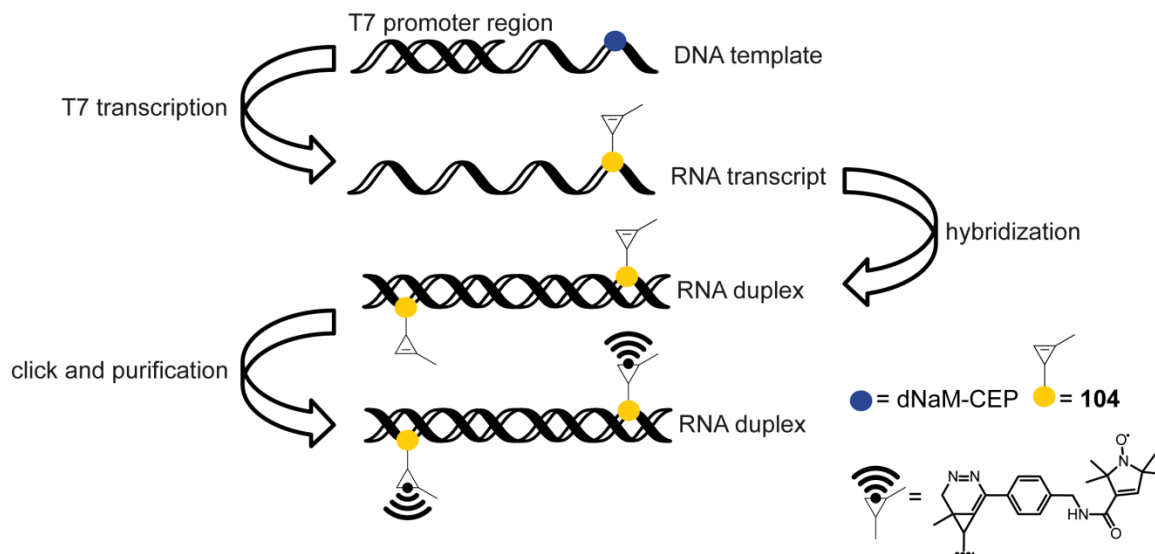
Fig. 86: General workflow for post-transcriptional spin-labeling of *in vitro* transcribed modified RNA duplex using 107.

This method for post transcriptional labeling showed almost quantitative spin labeling of the RNA by room temperature cw-X-band EPR spectroscopy (spin labeling efficiency 94%). Spin label activity of conjugate **107** and clicked RNA was proven using *cw EPR*. Corresponding spectra are shown in Fig. 87.
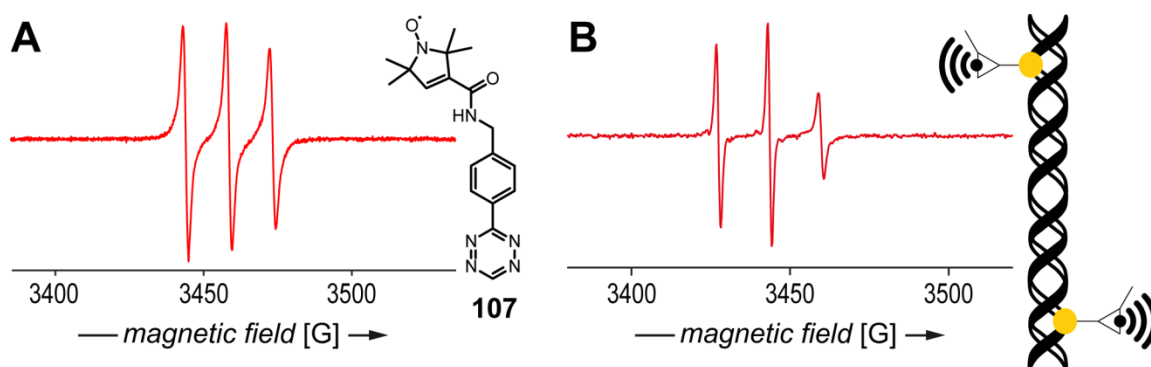
Fig. 87: *Cw-EPR* of compound 107 (A) and clicked RNA-SC-CP (B).

A distance measurement using *PELDOR* technique was implemented by the group of G. Hagelueken at physical chemistry department, Bonn and is shown in Fig. 88. Tikhonov regulated spectrum (Fig. 88 C) shows a broad distance distribution. Regarding five degrees of freedom within compound **107** (see Fig. 83) and even more in subsequent click product (see Fig. 85) caused by flexible linker system suitable for *IEDDA* click, a broad distance distributions was anticipated. Spin labels for structural investigations of biomolecules should be incorporated as rigidly as possible.[342]
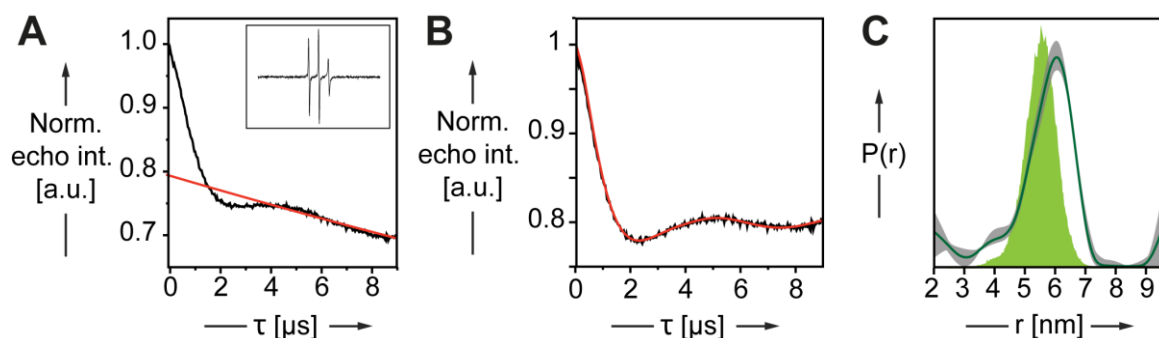
Fig. 88: PELDOR derived distance distribution in labeled RNA duplex. Shown are uncorrected PELDOR time trace (A, the fitted inter-molecular background function is shown as red line), background corrected PELDOR time trace (B) and inter-label distance distributions of RNA duplex (dark green curve) overlaid with the predicted spin-spin distance distribution (green shading) obtained by MD simulation (C).

Comparing measured distances with the distances shown in literature[301] an argumentation based on conjugate orientation can be assumed with reasonable certainty. Published by Kerzhner et al. was a calculated inter-spin distance of 4.78 nm and a measured inter-spin distance of 4.68 nm[301] for similar constructs using post-synthetic clicked uridine derivative shown before in Fig. 85.

Despite the rather flexible and in total 20 atom possessing linker between nitroxide and nucleobase core, a surprisingly well-defined distance distribution with a major peak at 6.1 nm is observed. *Prima facie* one could suppose an accumulation of the clicked linker system into the groove[343] of hybridized RNA duplex, but altered evaluation of received data shows three different distances, which can be assigned to different *IEDDA* products.
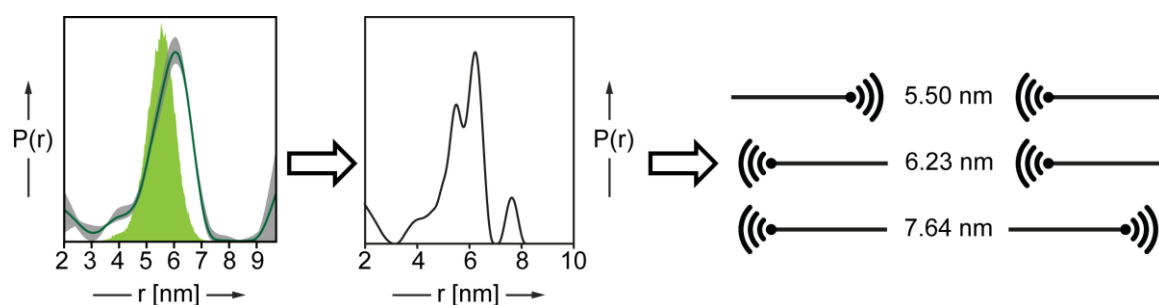
Fig. 89: PELDOR measured distance distribution of RNA duplex (left) composed from three distances (middle) trackable in evaluation. The different distances are caused by different orientations of *IEDDA* products (schematic shown at the right).

Mean between the distance of 5.50 nm and 7.64 nm is 6.57 nm. Measured distance of 6.23 nm deviates by 0.34 nm. Thus, a second effect despite orientation of compound has to be taken into account. Inhibiting flexibility and degrees of freedom in the presented system was done first by designing an exceptional rigid linker that is directly attached to the unnatural nucleoside scaffold of **TPT3**. Synthetic route, as well as *in vitro* applications discussed in the following. Further investigation on this topic would be

interesting for possible applications on larger constructs, e.g. protein-RNA interactions. Presented system has the potential to be a versatile tool for post-transcriptional labeling approaches and also feasible for in cell applications. *IEDDA* click reactions work efficiently on RNA in living cells. Thus, this approach might be a first step towards structural investigations on specific RNAs in its natural habitat.

3.4.2 Synthesis of a rigid spin-label directly attached to an unnatural ribonucleoside triphosphate

As shown before, a structural investigation und RNA using *IEDDA* click chemistry shows broad diatance distributions caused by length and flexibility of the used system. Required rigidity[342] can be achieved by a direct attachment of a spin label to the unnatural nucleobase of **TPT3**. Based on approaches of Olcott and coworkers, synthesizing first proline based stable radicals[344], 2,2,5,5-tetramethyl-pyrrolin-1-oxyl-3-acetylene (*TPA*) was chosen as small and rigid pyrrolin-based label. Having a terminal alkyne moiety, *TPA* is suitable for Palladium catalyzed C-C crosscoupling via Sonogashira reaction.

The synthesis of *TPA* is a synthetic route based on the work of Hopkins and coworker[345], further developed by Kálai[346], well elaborated in detailed protocols by Schiemann[300] or Azarkh[347] and is shown in Fig. 90.
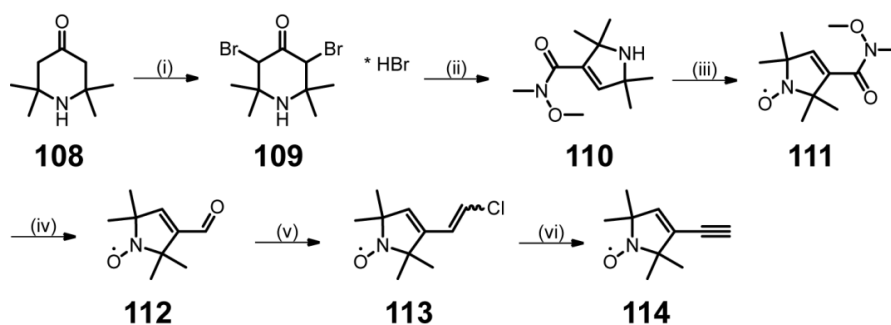
Fig. 90: Synthesis of TPA according to literature[300,348,349]. (i) Br$_2$ (in AcOH), AcOH, r.t., 7h, 72%; (ii) N,O-dimethylhydroxylamine · HCl, H$_2$O, NEt$_3$, r.t., o/n / 50 °C, 6h, 70%; (iii) *m*-CPBA, DCM, 0 °C, 4h, 46%; (iv) DIBAL, Et$_2$O, -40 °C to r.t., 1h / 0 °C to r.t., quant.; (v) *n*-BuLi, THF, -12 °C to r.t., 30min; ClCH$_2$(PPh$_3$)Cl, 0 °C to r.t., 2h, 42%; (vi) KOtBu, THF, 50 °C, 3h, 20%.

Starting with a double bromination of **108** piperidone derivative **109** is yielded. The five-membered ring representing the pyrroline scaffold is arranged in a subsequent Faworskii rearrangement leading to Weinreb amide **110**. In the next step nitroxide **111** is formed using *m*-CPBA. The formation of nitroxide spin labels using *m*-CPBA as oxidation reagent for hindered secondary amines was developed in the 1980s by Lai.[349,350] After that, amide **111** is reduced to the corresponding aldehyde **112** via DIBAL. In literature, alternative reduction strategies are described.[300] Using DIBAL showed quantitative yield

in contrast to other proposed pathways. To reach intended acetylene as functional group, vinyl chloride **113** has to be formed by a Wittig reaction. The geometric isomerism has not to be taken into consideration, because elimination to *TPA* (**114**) finally lacks stereo chemical aspects as visible in Fig. 90.
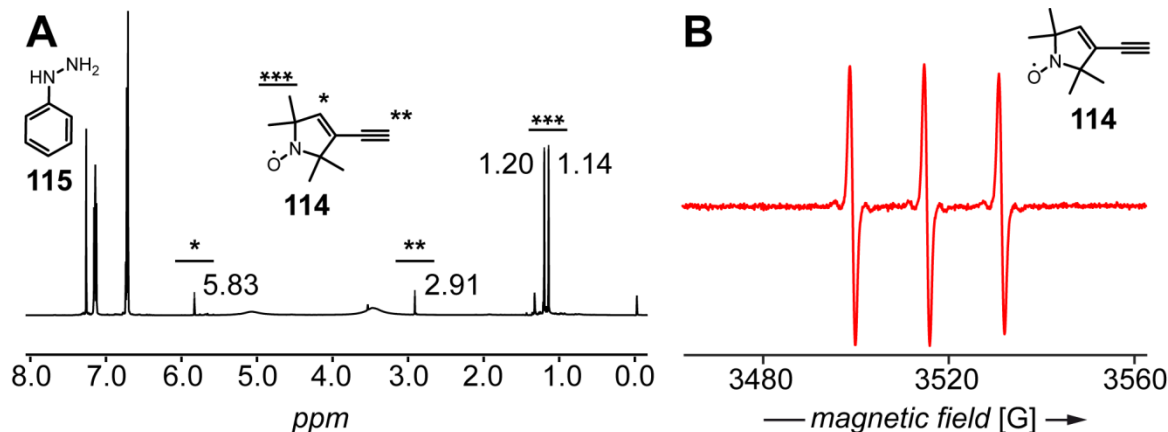
Fig. 91: ^{1}H-NMR spectrum of *in situ* reduced TPA 114 using phenylhydrazine 115. NMR sinals of phenylhydrazine are clearly visible in aromatic NMR range at 7 ppm (A) and corresponding *cw EPR* spectrum of **114** (B).

Paramagnetic substances interfere with NMR measurement. Spin labels have to be reduced *in situ* using phenylhydrazine to preventing paramagnetic nature of the probe and generate corresponding *N*-hydroxy amines. Fig. 91 shows a typical proton NMR spectrum of a reduced compound. Proton signals of used phenylhydrazine are clearly visible. This well established technique can be used when absorptions in the aromatic region are not of interest.[351] During synthesis of compound **119** all paramagnetic species were measured as *N*-hydroxy amine using ^{1}H-NMR or analyzed by mass spectrometry.
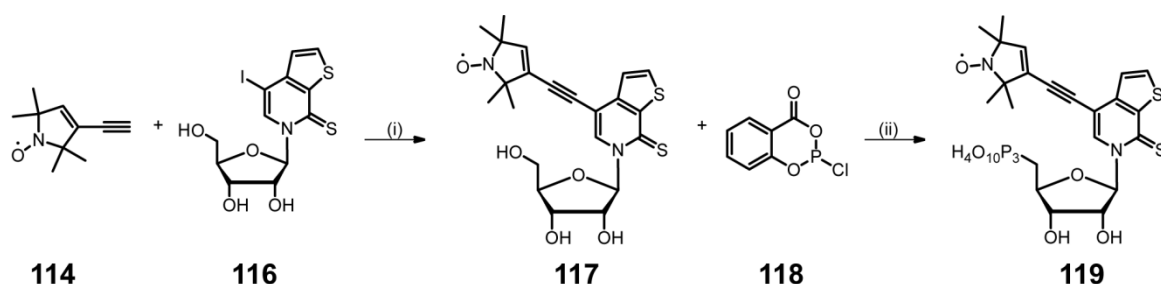
Fig. 92: Synthesis of spin-label bearing ribonucleoside triphosphate 119. (i) CuI, NEt$_3$, Pd(PPh$_3$)$_4$, r.t., o/n, quant.; (ii) Py, 1,4-dioxane, r.t., 40min / NBu3, (*n*-Bu$_3$NH)$_2$H$_2$P$_2$O$_7$, r.t., 40min / I$_2$ (in Py/H$_2$O 98/2 v/v), r.t., 5%.

Spin label **114** and unnatural **TPT3** derivative **116** were combined to the desired labeled nucleoside via Palladium catalyzed C-C cross coupling using Sonogashira reaction conditions (Fig. 92, step i).[311] Required copper(I) species in Sonogashira reactions does not affect the shielded radical. Sonogashira reaction yielded labeled ribonucleoside **117**

in a quantitative manner. Shown in Fig. 93 are LC-MS analysis and the corresponding cw-EPR analysis proving activity and integrity of **117**.
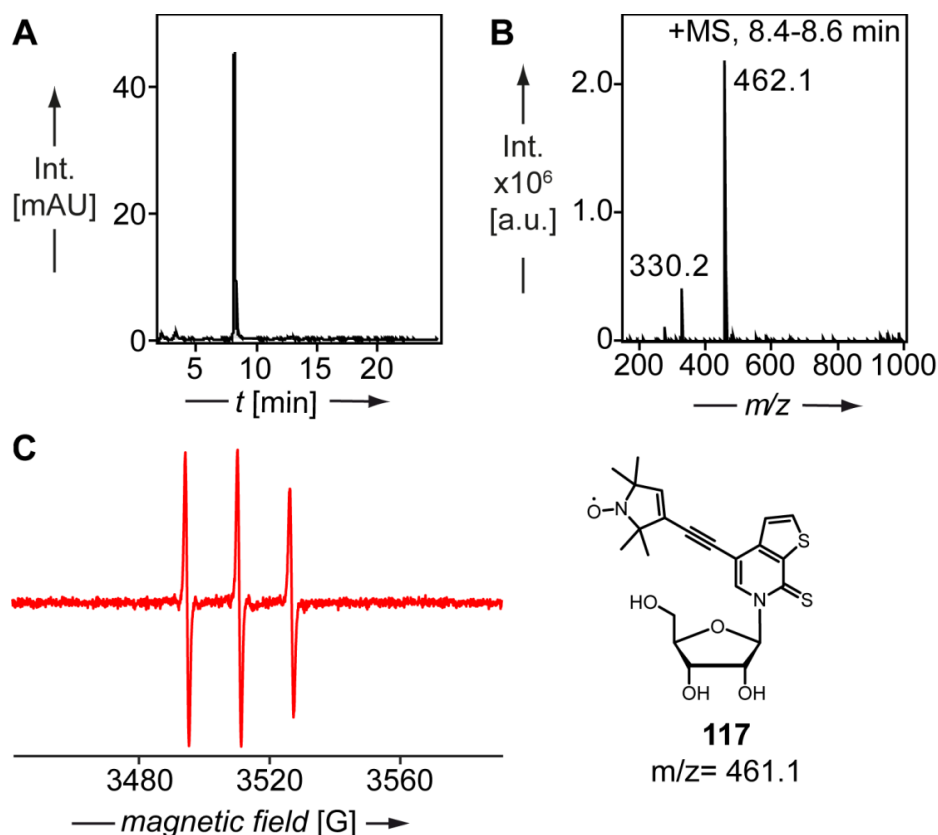
Fig. 93: LC-MS analysis of column chromatographically purified compound 117. UV-trace (A) and corresponding ESI$^+$ spectrum of **119** in peak eluting at t_R = 8.4-8.6 min (B) are shown. CW-EPR of compound **117** is also depicted (C).

Synthesis of ribonucleoside triphosphate **119** was carried out according to protocol of Ludwig[352], yielding 5% product. In this case, a different triphosphate synthesis was chosen. Usual synthetic approaches in this work are grounded on the work of Yoshikawa[353] and Ludwig[352]. Yoshikawa elaborated the monophosphate synthesis from corresponding nucleoside using $POCl_3$ and $OP(OMe)_3$ in 1967. Based on this work, Ludwig developed a synthetic pathway for triphosphate synthesis as displayed in Fig. 94. Those fundamental one-pot-two-step[321] in chemical biology have been refined and improved by Kovács and Ötvös in 1988[321].
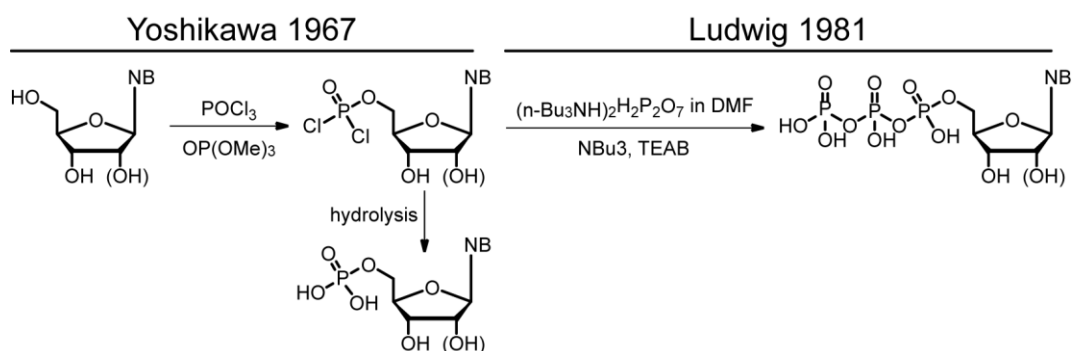
Fig. 94: Overview of developed synthetic steps in triphosphate synthesis by Yoshikawa[353] and Ludwig[352] (NB = nucleobase).

Used alternative was published by Ludwig and Eckstein in 1989[354] (see Fig. 92 and Fig. 95). As shown in Fig. 94 synthesized triphosphates are usually based on chlorophosphate derivatives. In order to avoid those highly reactive phosphodichloridate species, Lugwig and Eckstein used salicylic chlorophosphite **118**. This intermediate can be converted into the shown trimetaphosphates derivative using triethylammonium buffered pyrophosphate. Using alternative synthetic pathway, generated monophosphate intermediate via benzodioxaphosphirinone derivative yields an activated phosphite, which is less reactive regarding unwanted sidereactions such as hydrolysis like it is depicted in Fig. 94.[354] Additionaly, an increase in yield, better solubility and higher efficiency are stated.[354] A comparable approach of triphosphate synthesis using both reaction pathways gaining **119** is shown in Fig. 95.

An increase in yield could not be verified clearly. Yielded product was approximately similar and synthetic pathways can be read up in experimental part. The UV-trace using Eckstein's method shows approximately a similar amount of impurities (see Fig. 95 B) and HPL chromatographic purification is recommended in both cases. In summary, triphosphate synthesis using either Kovács and Ötvös'[321] or Ludwig and Eckstein's[354] method is a challenging and complex synthetic step. Both methods yield compound **119** and both methods need a certain time of preparation and workup. Taking subjective opinion as evaluation criterion, Kovács and Ötvös'[321] method is favoured caused by gained experience.
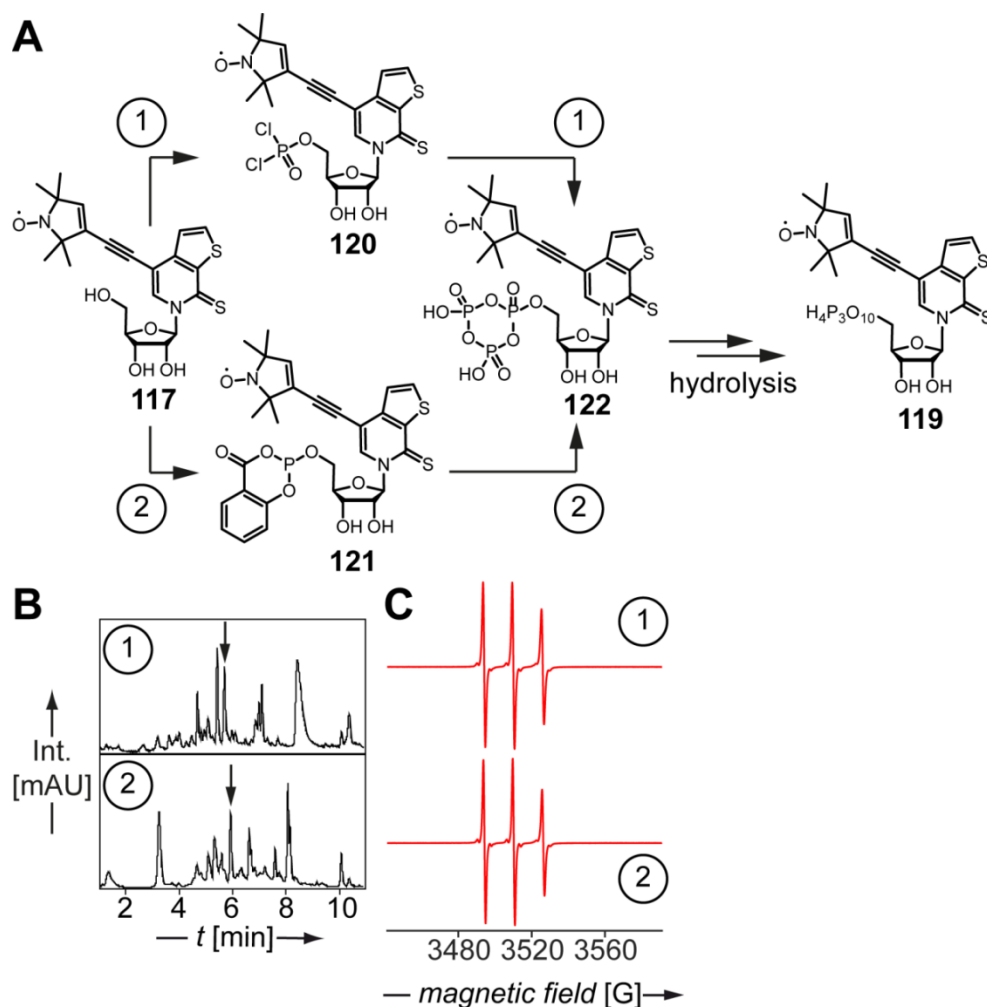
Fig. 95: Intermediates during triphosphate synthesis (A) either on synthetic pathway elaborated by Kovács and Ötvös[321] (1) or Ludwig and Eckstein[354] (2). Ribonucleoside triphosphate is finally yielded by hydrolysis of cyclic triphosphate intermediate. Comparing LC-MS UV-traces of crude triphosphate synthesis (B) shows product **119** eluting at $t_R = 5.9$ min either using synthetic pathway of Kovács and Ötvös[321] (upper UV trace, 1) or alternatively by Ludwig's and Eckstein's method[354] (lower UV trace, 2). Spin label interity is not affectec by any of used methods as corresponding cw-EPR spectra reveal (C).

3.4.3 TPA as rigid linker system causes incorporation problems using T7 RNA Polymerase

Using standard protocols for template-directed *in vitro* T7 transcription was taken to yield RNA transcripts bearing **119**. In a similar fashion, procedures were used for *ubp*-based RNA suitable for post-transcriptional *IEDDA* chemistry like discussed in sections before.

Depicted in Fig. 96 is the general used approach described above. A DNA template bearing d**NaM**-*CEP* as part of *ubp* **NaM**:**TPT3** is used for *in vitro* transcription. Using canonical NTPs and unnatural, spin label-modified ribonucleoside triphosphates based on **TPT3** yields a site-specifically labeled RNA transcript. This transcript is finally

hybridized achieving RNA duplex formation suitable for interstrand distant distribution. T7 *in vitro* transcriptions were performed in a 100 µL scale with final concentrations of 40 mM Tris·HCl pH 7.9, 25 mM MgCl$_2$, 5 mM DTT, 2.5 mM each canonical triphosphate, 1 mM unnatural triphosphate (**119**), 3 µM template DNA and primer, 0.5 U µL^{-1} RNasin (*Promega*), 3 ng µL^{-1} iPP (*Roche*), and 5 U µL^{-1} T7 RNA polymerase (*self-made*, AA sequence conforms with GenBank[6]: AY264774.1), which was added to the mixture endmost. Primer and templates were annealed for 2 min at 95 °C and slowly cooled to room temperature. The transcription mixture was for 4 h at 37 °C. Subsequent DNase 1 digestion was performed by the addition of 10 µL 10 x DNase 1 buffer (*New England Biolabs*) and 5 µL DNase 1 (2 U/µL, *New England Biolabs*).Samples were incubated for 30 min at 37 °C.
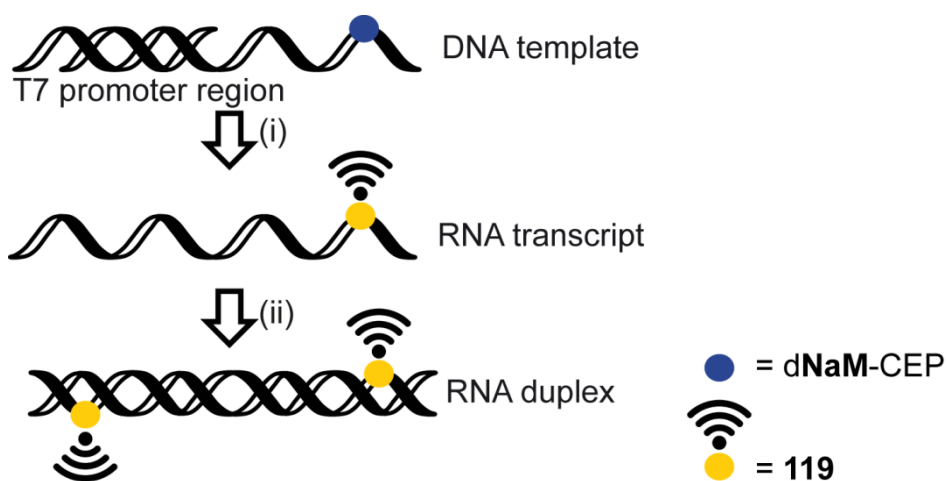
Fig. 96: General approach for template-directed *in vitro* transcription using ribonucleoside triphosphates based on TPT3. DNA template synthesized by solid phase bearing d**NaM**-*CEP* and T7 promoter region is transcribed into corresponding RNA with canonical NTPs and **119** (i). RNA strands are hybridized subsequently to RNA duplex for interstrand distance distribution (ii).

In order to reveal rapid results, first approaches were carried out using **DNA-CXT^{NaM}** template. Resulting RNA is not self-complementary, but transcription protocol are well established and used as role model or internal reference, respectively. Derivative **119** with a rigid linker showed moderate to modest incorporation rates during *in vitro* transcriptions yielding **RNA-CXT^{NaM}-RL** as shown in Fig. 97. Using established protocols, only a minor amount full length RNA transcript was yielded. HPL chromatographically purified RNA strands were identified by mass spectrometric analysis subsequently.

DNA-CXT^{NaM}: 5'-CAC TXC TCG GGA TTC CCT ATA GTG AGT CGT ATT AT-3'
RNA-CXT^{NaM}-RL: 5'-GGG AAU CCC GAG YAG UG-3'
X = dNaM; Y = 119
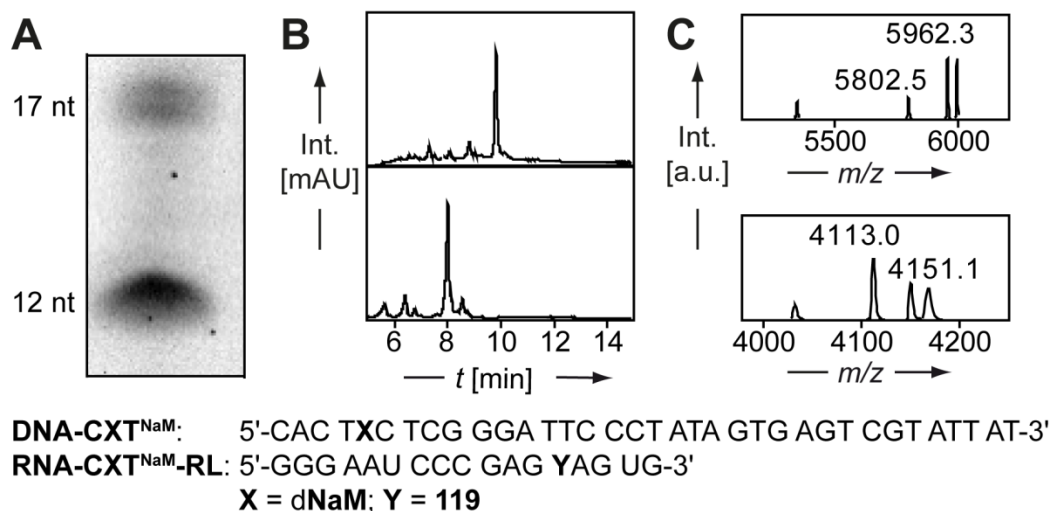
Fig. 97: 15% denat. *PAGE* showing *in vitro* transcription approach using 119 on template DNA-CXT^{NaM} (A). Truncated 12 nt fragment of **RNA-CXT^{NaM}-RL** and 17 nt full length transcript **RNA-CXT^{NaM}-RL** were isolated and measured by LC-MS. Analysis of peaks eluting at t_R = 7.9-8.1 min (B, lower UV-trace) and t_R = 9.7-10.0 min (B, upper UV-trace) showed successful incorporation of compound **119** (C, upper graph) and truncation before incorporation of **119** (C, lower graph) after deconvolution. Full spectra are shown in appendix.

Using established protocols, only a minor amount full length RNA transcript was yielded. HPL chromatographically purified RNA strands were identified by mass spectrometric analysis subsequently and calculated masses of truncation fragments agree with measured masses for truncation before **119** is incorporated as shown in Table 5.

Using **DNA-CXT^{NaM}** as well established role model compared to self-complementary **DNA-SC^{NAM}** reveals, that a sequence-dependent decreased incorporation can be excluded. Used DNA templates differ in length and flanking nucleotides. In both cases transcription shows a high truncation ratio. Truncation appears at position 13 of resulting transcript using template **DNA-CXT^{NaM}** as shown before and at position 15 of corresponding RNA using **DNA-SC^{NaM}**.

	RNA sequence	m_{calc}	Measured (*m/z*)
RNA-CXT^{NaM}-RL truncation	5′-GGG AAU CCC GAG-3′	5'-TP: 4113.0	4113.0
RNA-CXT^{NaM}-RL	5′-GGG AAU CCC GAG **Y**AG UG-3′	5'-MP: 5802.3.	5802.5
		5'-TP: 5962.3	5962.3
RNA-SC-RL truncation	5′-GGA UCU GAU AUC AGA-3′	5'-OH: 4800.0	4796.9
		5'-MP: 4880.0	4876.8
		5'-DP: 4960.0	4956.8
		5'-TP: 5040.0.	5036.8
RNA-SC-RL	5′-GGA UCU GAU AUC AGA **Y**CC-3′	5'-OH: 5933.4	5933.9
		5'-MP: 6013.4	6014.2
		5'-DP: 6093.4	6094.2
		5'-TP: 6173.4.	6173.8

Table 5: Table representing ESI data of transcribed RNA-CXT^{NaM}-RL and RNA-SC-RL. Truncated fragments and full length transcripts (**Y** = **119**) were analyzed via LC-MS. Calculated and measured data were compared to verify incorporation of compound **119**. Full spectra are shown in appendix.

Incorporation of **119** is nonetheless successful and spin-label integrity is not affected by transcription conditions according to the *cw* X-band *EPR* spectra shown in Fig. 98. Two different DNA templates were used. Template A (CXT) was used before to investigate incorporation efficiency of other unnatural ribonucleoside triphosphates and template B (sc_epr) was adapted from Schieman and coworkers[301] and used for *IEDDA* click-chemistry using spin labeled tetrazine derivative **107** (see Fig. 85).

DNA-CXT^{NaM}: 5'-CAC T**X**C TCG GGA TTC CCT ATA GTG AGT CGT ATT AT-3'
RNA-CXT^{NaM}-RL: 5'-GGG AAU CCC GAG **Y**AG UG-3'
DNA-SC: 5'-GG**X** TCT GAT ATC AGA TCC TAT AGT GAG TCG TAT TAT-3'
RNA-SC-RL: 5'-GGA UCU GAU AUC AGA **Y**CC-3'
X = d**NaM**; **Y** = **119**
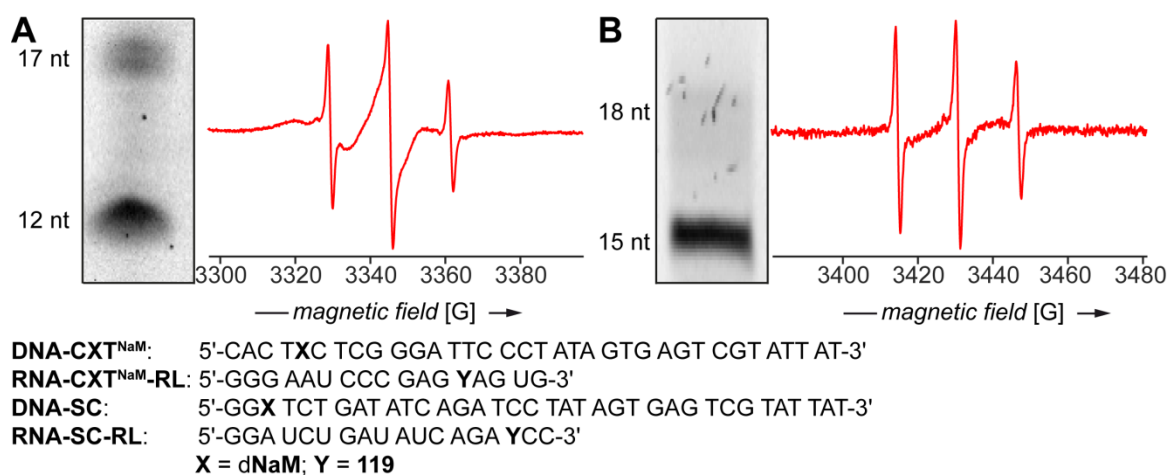
Fig. 98: *Cw* X-band epr spectra of full-length RNA transcripts using DNA-CXT^{NaM} (A) or DNA-SC (B) as template and 119 as unnatural ribonucleoside triphosphate for T7 *in vitro* transcription. Shown PAGE analysis of T7 *in vitro* transcriptions visualizes ratio of full length (upper bands) versus truncation (lower bands)

PELDOR applications for distance measurement could not be done lacking a suitable amount of labeled RNA necessary for aspired applications. Demonstrating incorporation efficiency of unnatural was done before using other modified **TPT3** derivatives like **76** and **104**.[310,311] By taking into consideration that spin label-modified unnatural nucleotide

119 is incorporated successfully, but only in a low manner adapted transcription protocols were tested. Differing temperature and reaction times showed no improvement. In contrast to the sordid full length transcription yields and high amount of truncated RNA using **119**, other unnatural nucleotides bearing longer and also bulky modifications show good to excellent incorporation behavior.[310,311,319]

Thus, it is reasonable to assume that synthesized compound **119** is not suitable for *in vitro* transcription approaches with T7 RNAP. In addition, a rough *in silico* visualization was done using molecular modeling software PyMOL (v. 1.8.4.0).
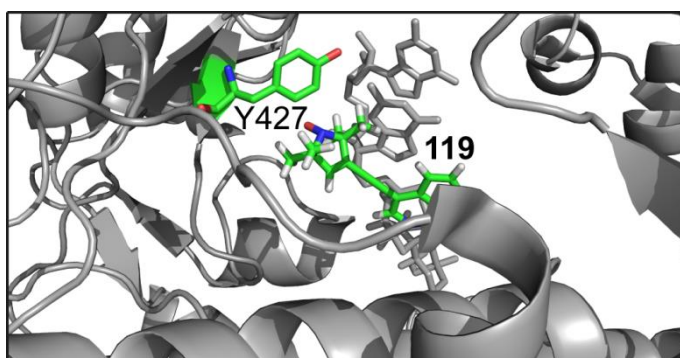
Fig. 99: Computational presentation of unnatural nucleobase 119 in T7 RNAP[240]**.** Colored are only Y427 and **119**. All other amino acids and nucleotides are grayed out.

Using pdb datafiles of T7 RNAP either in initiation complex (pdb: 1QLN[240]) or elongation complex (pdb: 1H38[355]) and molecular structure of synthesized unnatural nuclebase, a very close proximity between nitroxide moiety and tyrosine Y427 of T7 RNAP is observable. Electronic surface of Y427 and nucleobase's nitroxide moiety intersect. **119** is placed at position GTP+1 in corresponding crystal structure of T7 RNAP[240]. This ribonucleobase triphosphate is in priming position at the catalytic active site.[240,355,356] Shown discrepancy of nucleobase and enzyme corroborates structural disadvantage of **119**.

3.4.4 Synthesis of a slight flexible linker system suitable for T7 *in vitro* transcription

The modest incorporation of **119** and broad distance distrinution using tetrazine spin label conjugate **107** requires a compromise between recommended rigidity for *EPR*-based distance applications and a needed flexibility for *in vitro* transcriptions. TEMPYO-NHS was used in combination with propargylamine.
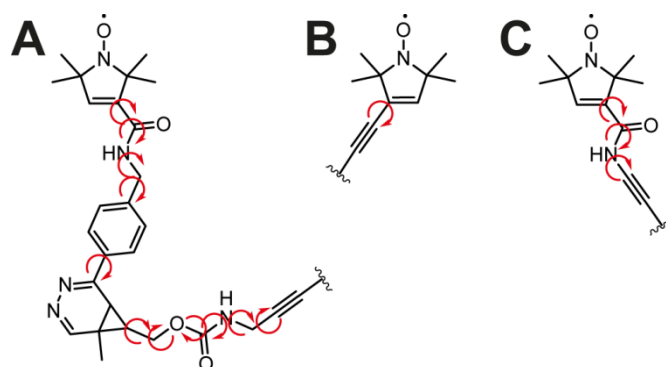
Fig. 100: Comparison of the used pyrrolin-based spin label compounds and the number of their rotational degrees of freedom. Tetrazine spin label-conjugate **107** after *IEDDA* reaction with 104 (A) shows eleven degrees of freedom. In contrast to this, *TPA* based label **119** (B) inherits only one degree of freedom. As a good compromise novel and wanted *TEMPYO*-based spin label (C) shows three degrees of freedom.

As shown above in Fig. 100 C, rigidity of the used spin label derivative is levelled down due to the increase of mobile single bonds in the molecule. This decreases spatial high accuracy of the strictly rigid *TPA* based label in a certain manner. Synthesis of wanted label is shown in Fig. 101 and starts with an amide coupling between **106** and propargylamine is the initiation yielding **124** in a quantitative manner after filtrating off resulting byproduct succimimide. As second step a Sonogashira cross-coupling reaction under similar conditions as described in 3.4.2 can be carried out. Sonogashira like conditions for Pd catalyzed C-C cross-coupling are well elaborated and yielded nucleoside **125** with 66% after standard workup. The final synthetic step to gain nucleotide **126** (13%) was carried out similar to Kovács & Ötvös' method[321] as described for other triphosphates.
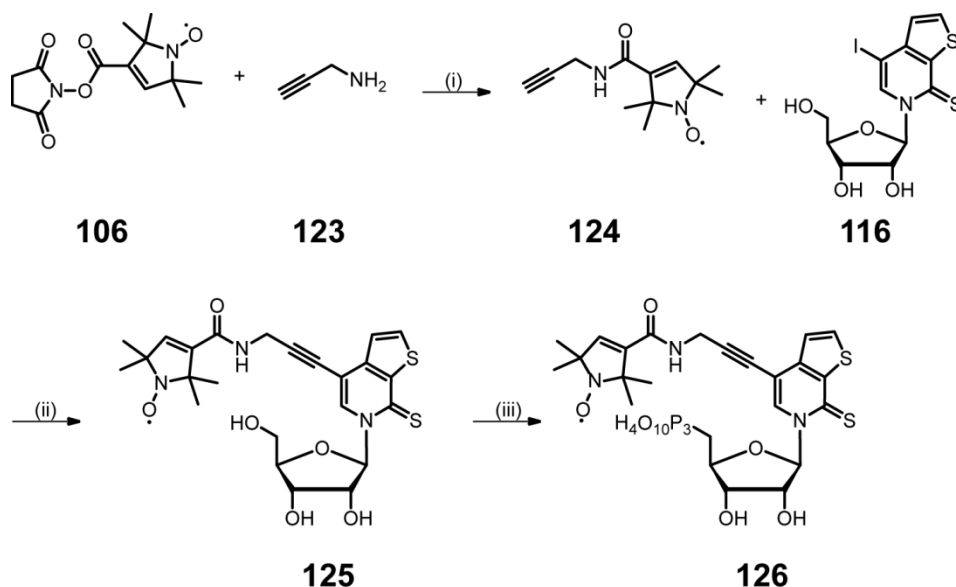
Fig. 101: Synthetic pathway for compound 45. (i) NEt_3, DCM, r.t. 2h, quant.; (ii) CuI, NEt_3, $Pd(PPh_3)_4$, DMF, r.t., o/n, 66%; (iii) $OP(OMe)_3$, $POCl_3$, 0 °C, 3h / NBu_3, $(n\text{-}Bu_3NH)_2H_2P_2O_7$ (0.5 M in DMF), 0 °C, 30min, TEAB, 13%.

Beforehand mentioned disturbing interactions of spin label compounds bearing shielded free radicals are shown in Fig. 102 exemplary for compound **124**. Chemical shifts [ppm] of protons in a certain distance to radical are not strongly affected by free radicals in ^{1}H-NMR analytics. Neighboring groups such as shielding methyl groups (Fig. 102 signal a) are affected by this effect. Fine structure of the peaks can not be investigated, too. Terminal alkyne proton (Fig. 102 signal d) shows under reduced conditions a triplet structure at 3.07 ppm ($^4J = 2.5$ Hz). Similar data are observable for bridging –(CH$_2$)– group (Fig. 102 signal c). Showing a doublet of a doublet with a geminal coupling constant of $^2J = 5$ Hz and long range coupling of $^2J = 2.5$ Hz under reduced conditions, only a broad singlet is observed in upper image. Disturbing effects of free radicals are detectable on integration of signal intensity, too. Using DMSO-d_6 prevents literature-known precipitation of corresponding *N*-hydroxy amine.[351]
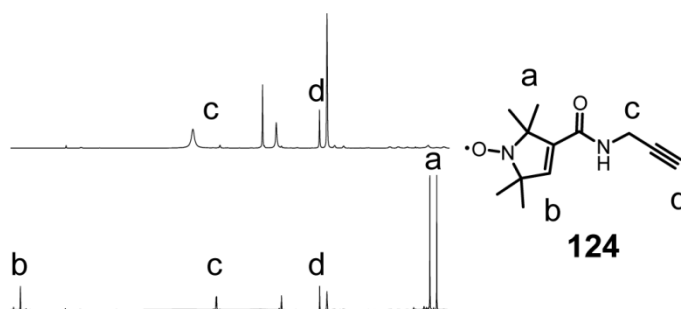
Fig. 102: ^{1}H-NMR measurement of compound 124 before (upper spectrum) and after (lower spectrum) *in situ* **reduction using 115.** Full spectra are shown in appendix.

Verifying spin label activity of **126** was carried out after triphosphate synthesis using cw-EPR by the group of Prof. O. Schiemann at physical chemistry department of Bonn and is shown in Fig. 103. *EPR* measurements using X-band show, that stable radical attached to unnatural nucleotide is not affected by synthetic steps carried out during nucleotide synthesis.
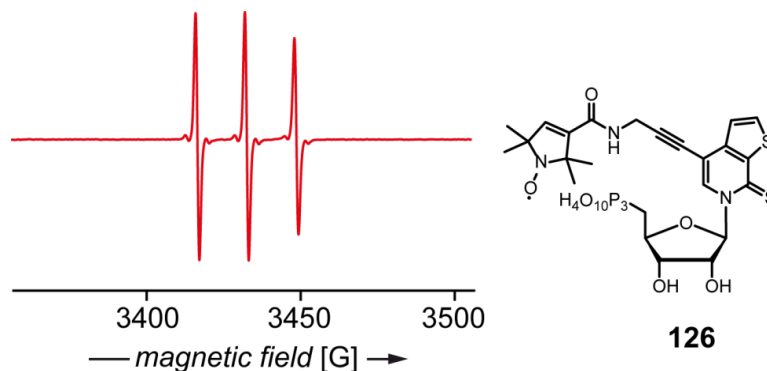
Fig. 103: Cw-EPR of compound 126.

3.4.5 Linker systems suitable for T7 *in vitro* transcriptions need a certain size

Using compound **126** as spin label-modified unnatural nucleotide possessing certain flexibility in T7 *in vitro* transcriptions shows only minor truncation in contrast to former discussed compound **119**. Full length transcript was analysed by LC-MS. Deconvoluted mass spectrum (Fig. 104 B) displays incorporation of **126**, but more important is the result, that full length transcript can be achieved in a high yielding way and **126** is incorporated successfully.

A

126 + -

18 nt
15 nt

B

Int. [a.u.]

6230.6
6150.9
6071.1
5991.1

5500   6000   6500

— m/z →

C

3400   3450   3500

— magnetic field [G] →
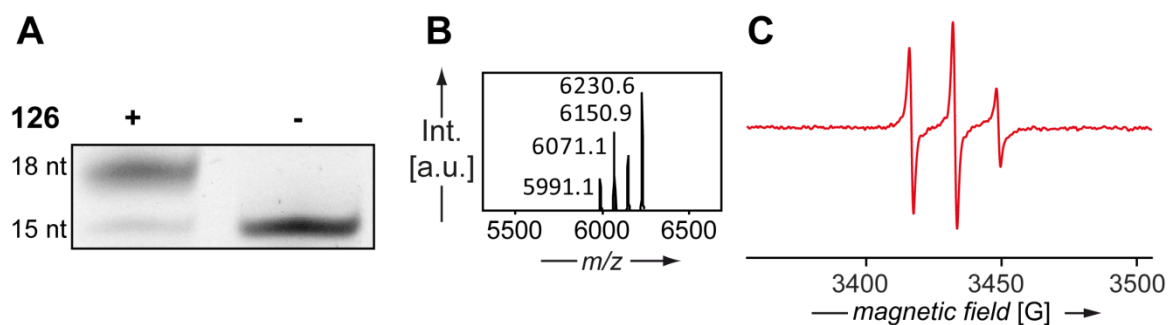
DNA-SC: 5'-GG**X** TCT GAT ATC AGA TCC TAT AGT GAG TCG TAT TAT-3'
RNA-SC-FL: 5'-GGA UCU GAU AUC AGA **Y**CC-3'
                    X = d**NaM**; **Y** = **126**

Fig. 104: Sucessful incorporation of 126 into RNA via T7 *in vitro* transcription. 20% denat. *PAGE* analysis of an *in vitro* transcription using unnatural nucleotide **126** (A; Lane 1: Successful *in vitro* transcription using **126** on template **DNA-SC**. Lane 2: T7 *in vitro* transcription on **DNA-SC** w/o **126**). Deconvoluted masses of full length **RNA-SC-FL** with compound **126** incorporated (B; M_{calc}: 5′-OH: 5990.4; 5′-MP: 6070.4; 5′-DP: 6150.4; 5′-TP: 6230.4) and corresponding cw-EPR of full length transcript (C). Full gel and spectrum are depicted in appendix.

Yielding full length RNA transcript in similar conditions like for compound **76**[310] and **104**[311], one assumes, that the rigid linker system of **119** is not applicable for *in vitro* transcription. Regarding former used linker systems, like mentioned before, which are commonly used for *in vitro* transcriptions with good to excellent yields[310,311], structural aspects have to be discussed. Comparing overall length of the used linkers, the one used for **119** is the shortest. In an unfolded manner, molecular systems used for norbornene- and for cyclopropane-modified nucleotides **76** and **104** show lengths up to 12 Å. Calculating approximate lengths was carried out with Chem3D pro v7.0.0 used on molecular drawings manufactured in ChemDraw v16.0.1.4. In particular for **104**, 11.9 Å measured from C_{Ar} to C_{CPMe} and 10.3 Å or 10.7 Å from C_{Ar} up to the double bond. Compound **76** shows a distance of 11.8 Å (C_{Ar} to C_{Bridge}) and 11.1 Å or 11.3 Å from 11C_{Ar} to the carbon atoms forming the strained alkene. The rigid system used for spin label attachment in **119** shows an overall length in a magnitude around 7 Å. Regarding chemical structures, it is obvious, that compound **119** and its precursor own a rigid length. Measured to the first flexible position in other mentioned systems, a length of roughly 5 Å is observed.
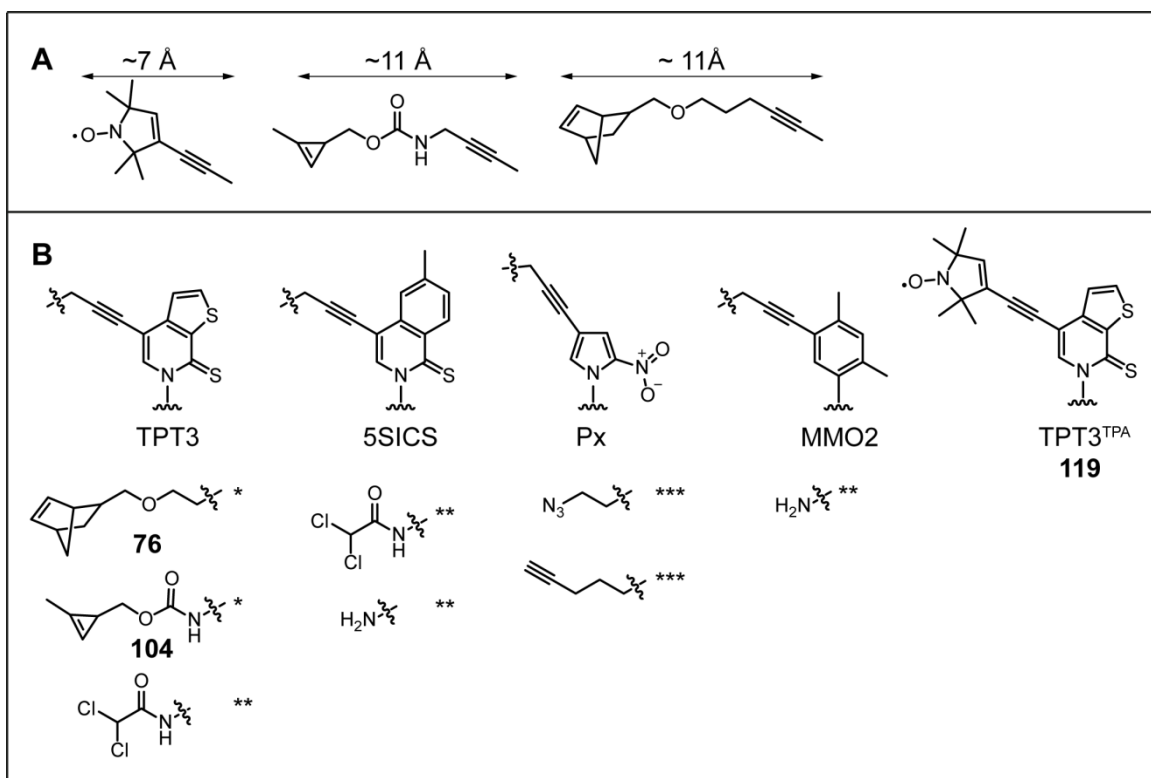
Fig. 105: (A) Used linker systems and their approximate length. (Calculated with Chem3D pro v7.0.0). (B) Unnatural functionalized nucleotide derivatives synthesized by the Kath-Schorr group (*), Romesberg and coworkers (**) as well as Hirao and coworkers (***). In contrast nucleobase of 119 is depicted as rigid derivative showing only weak incorporation rates.[241,310,311,357] Shown are only nucleobases. Sugar moieties are not depicted.

Referred to literature, the T7 RNAP has overcome the structural state from initiation to elongation complex[240], which usually appears at +10 nt after T7 promoter region fused to corresponding DNA template. Regarding the not natural molecular size of **119** combined with the intrinsic rigidity of the used system, it is assumed, that the synthesized ribonucleotide does not fit in the active site of T7 RNAP. This assumption seems to be hardened after synthesizing **126**. Incorporating this unnatural ribonucleotide does not present a major problem for used T7 RNAP. Thus, a size limitation in the range of 6 Å or certain flexibility in the used linker systems is required. In comparison to other unnatural nucleotides either published by Hirao and coworkers[259], the Romesberg group[242,274] or the Kath-Schorr group[310,311] a functionalization of the unnatural nucleotide is usually based on the same linker system. Reactive group are introduced via C-C cross-coupling using an iodine moiety at the nucleoside and a terminal alkyne at respective linker. In every case, a flexible –CH$_2$– group is positioned next to the triple bond.
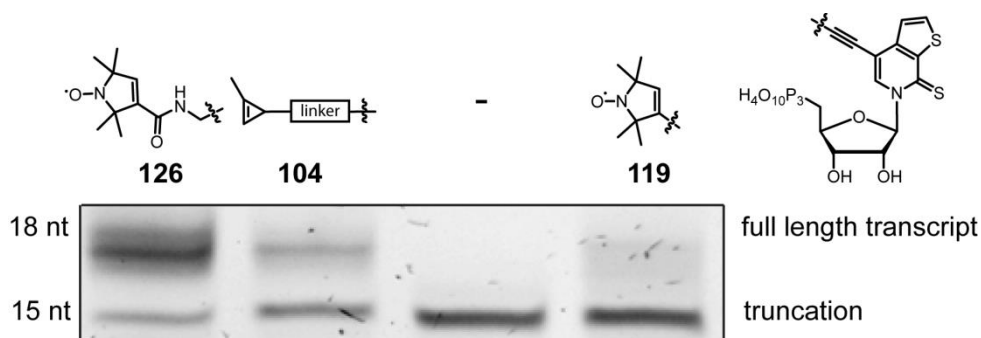
Fig. 106: 20% denat. *PAGE* showing incorporation versus truncation using different unnatural nucleotides for template directed *in vitro* transcription using DNA-SC receiving corresponding RNA trasncrips. Lane 1: 126, Lane 2: 104, Lane 3: w/o unnatural nucleotide, Lane 4: 119

As shown in Fig. 106 a comparing *PAGE* analysis shows tendencies of incorporation of **TPT3** derivatives. The negative control (Fig. 106 lane 3) shows only truncation at position 15 of 18 nt long **RNA 4^{NaM}**. A fluorescent readout using AIDA image analyzer (version 4.27) results in insignificant values. False incorporation of **TPT3** derivatives shown by Eggert et al. appears within the detection limits of used fluorescence-based assay.[319] Same results were obtained in this case, too. Incorporation values using **119** is in an array of 15% – 20%. Average incorporation rate of **TPT3** derivatives **104** and **126** is usually above 90%.

3.4.6 *Cw-EPR* and *PELDOR* measurements of RNA containing compound 126

Using flexible system of **126** resulted in a successful incorporation of the unnatural nucleotide as stated before. Integrity of hybridized RNA duplex was verified by circular dichroism (CD) spectroscopy. Mismatch of unnatural nucleotide opposite a canonical base (Fig. 107) and resulting decrease of stability was investigated by thermal denaturation experiments, discussed in the following. Experimental procedure of CD spectroscopic and thermal denaturation analysis is described in material and methods and shown in Fig. 108.
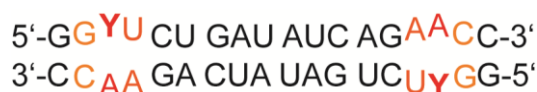
Fig. 107: Assumed duplex widening for RNA-SC-FL caused by the Y:A (Y = 126)mismatch only regarding the flanking base pairs related the their inherent hydrogen bonds.

Regarding asymmetric structure of nucleic acids, caused by stacking interactions of nucleosides circular dichroism is given. A CD spectrum can easily distinguish among A-

form, B-form and Z-form double helices therefor. A-form RNA CD spectra exhibit a maximum near $\lambda = 260$ nm.[358–360] This significant maximum is measured in both hybridized duplexes, **RNA 4^A** and **RNA 4^{45}**. Thermal denaturation of unmodified duplex **RNA 4^A** takes place at $T_m = 69.7\pm2.0$ °C and for modified duplex **RNA 4^{45}** at $T_m = 47.5\pm0.9$ °C. Thus, a difference in melting temperatures of $\Delta T_m = 22.2$ °C is observed. Regarding RNA sequence and it's **126** : A mismatch at position 15 an destabilization of hybridized duplex is inevitable. This mismatch leads to measured decrease in melting temperature of about 11.1 °C (see Fig. 108). Nevertheless, duplex formation is still given verified by the CD spectroscopic investigations.
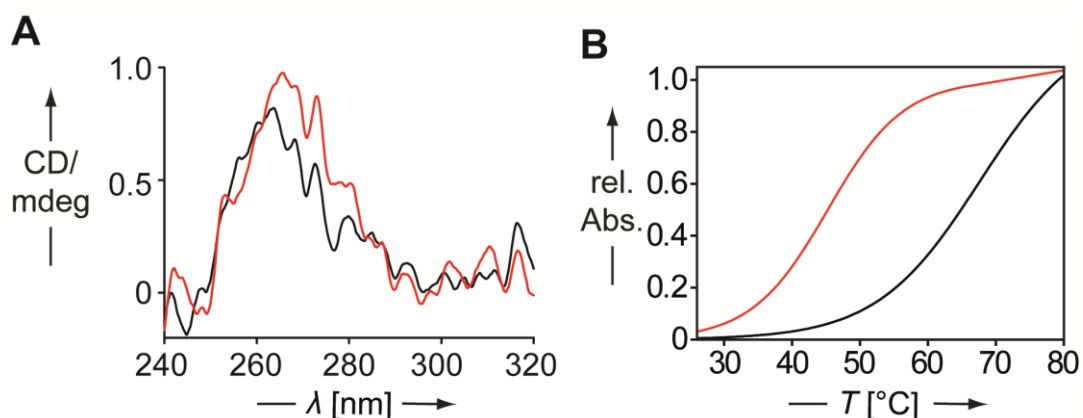
Fig. 108: Left: CD spectroscopic analysis of RNA 4^{45} (red) and unmodified RNA 4^A (black). Significant A-form RNA maximum at $\lambda = 260$ nm is clearly visible. Right: Thermal denaturation of RNA 4^{45} (red) and unmodified RNA 4^A (black). Melting temperature of RNA 4^{45} ($T_m = 47.5\pm0.9$ °C) differs in contrast to unmodified RNA 4^A ($T_m = 69.7\pm2.0$ °C) about $\Delta T_m = 22$ °C.

Literature states destabilization of duplex RNAs caused by structural perturbation of spi labels in a range from $T = 4$ °C up to $T = 10$ °C per label.[300,301] Those labels are attached to canonical nucleobases covalently before solid phase synthesis or by click-chemistry in a post-transcriptional way.[300,301] This means, Watson-Crick like hydrogen bonding can still be formed. In this case, using unnatural hydrophobic nucleobases without ability to form hydrogen bonding to the counterpart a decrease in melting temperature of $\Delta T = 11.1$ °C per mismatch is a promising result.

Transcribed RNA bearing spin labeled unnatural nucleotides was handled as described in material and methods. Standard conditions do not affect the label activity and as mentioned before usage of reducing additives during biochemical applications e.g. Dithiothreitol (*DTT*) does not influence the label activity as well. Further handling took place according general scheme for spin labeled RNA duplex shown in Fig. 96 and used for RNA constructs bearing unnatural nucleotides suitable for *IEDDA* reaction also. Purification of marked RNA via preparative *PAGE* and subsequent electro elution was

also carried out as stated in material and methods, but as annotated, RNA was purified in the further course using reverse phase HPLC with gradients described in material and methods.

Cw-EPR measurements were carried out to prove label activity and lowered label mobility in RNA (Fig. 109 A). Structural investigations on hybridized RNA duplex were carried out according to the procedure given in material and methods using *PELDOR* technique. Performed PELDOR experiments resulted in a sharp distance distribution with a well-defined peak at 4.97 nm shown in Fig. 109 C. Since the duplexes are self-complementary, the low modulation depth of the time traces (Fig. 109 B) can be explained by the unavoidable formation of hairpin structures containing just one spin label.[361] The *in silico* spin labeling software mtsslWizard[362] was used to predict inter-spin distances accounting for flexibility of the nitroxide group. The unnatural nucleobase **TPT3** was positioned as **126** : A base pair with Watson-Crick geometry in this model.

According to former experiments using a copper catalyzed post-synthetic labeling technique on solid-phase synthesized RNA[301] the shown technique using *in vitro* transcription owns a major advantage. Enzymatic transcribed RNA is not limited in length as it occurs for synthetic RNA.[21–24]
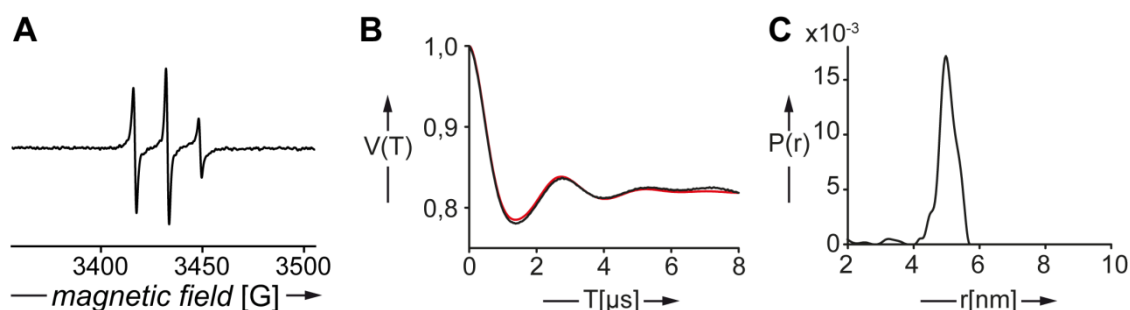
Fig. 109: (A) *Cw-EPR* **of hybridized RNA 4**[45] **duplex bearing 126 at position 15. (B) Background-substracted time trace of** *PELDOR* **measurement of 45 incorporated RNA 4**[45] **duplex. (C) Corresponding distance distribution of** *PELDOR* **measurement.**

To apply this novel technique to measure interstrand distances in a long and highly structured RNA, CPEB3 ribozyme was transcribed for an intrastrand measurement. The HDV-like self-cleaving RNA was labeled at position +10 and +50 with **45**. To prevent major structural impact provoked by mismatches in the stem region labeling appeared in loop *P2* and *P4* of the construct. Thus, stem integrity is still given and folding of catalytic active RNA construct should not be affected. Transcribed RNA showed insufficient distance distribution unfortunately. Fig. 110 shows measured distance distribution as well as background corrected time domain.
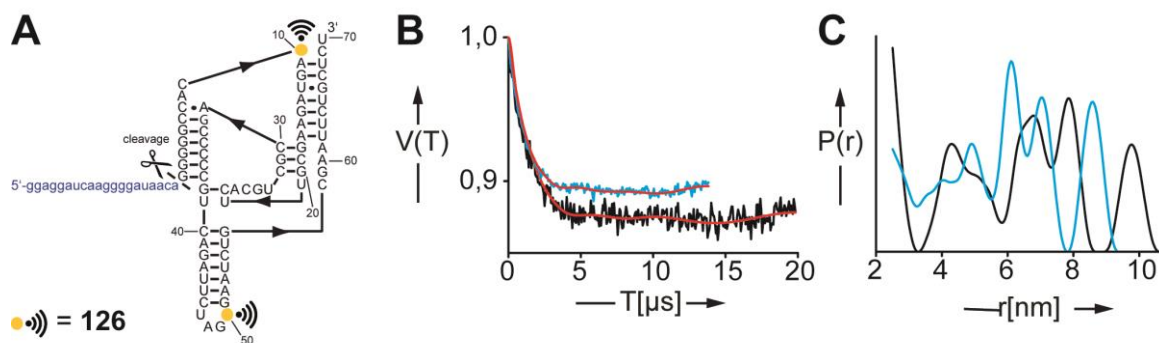
Fig. 110: (A) *In vitro* **transcribed CPEB3 ribozyme construct. Cleavage site is depicted by black scissor pictogram. 20 nt long cleavage fragment is displayed in blue. Background substracted time trace (B) and distance distributions (C) of the CPEB3 ribozyme direct after transcription (black, 35% cleaved) and after 4 h cleaving (blue, 49% cleaved) using 10 mM MgCl₂.**

Referring to literature for HDV ribozyme[363], a distance change before and after cleaving is measurable. Those results are based on two-strand construct used for *FRET* experiments.[363] Thus, a structural or conformational change in CPEB3 between uncleaved and cleaved state can be assumed, too. Using 10 mM MgCl$_2$ leads to another relation of cleaved and non-cleaved fraction. As shown in Fig. 110 a change in distance distribution is observable. Regrettably, a clear distance is not visible. It is assumed, that the labeled loop regions of CPEB3 ribozyme are too flexible to gain a clear distance distribution.

Nevertheless, Fig. 110 B shows intrastrand modulation. Both labels are incorporated successfully for the first time via T7 *in vitro* transcription into a fully functionable catalytic RNA. This the only known strategy so far for the direct, site-specific introduction of spin labels into RNA via *in vitro* transcription and therefor shown results represents first site-specifically labeled ribozyme suitable for EPR and PELDOR based investigations without solid phase synthesis or ligation strategy. This will give access to novel information on the structure of large non-coding RNA molecules. The structural impact by introducing an unnatural nucleobase into the RNA has to be studied in every case, and further experiments using labeled stem regions as comparison have to be carried out. Assuming less flexibility as in labeled loop regions, a more accurate distance distribution should be achieved.

3.5 1-Deazaadenosinephosphoramidite as atomic mutagenesis for mechanistic studies on twister ribozyme

The identification of twister ribozymes as RNA motif renewed the discussion about the cleaving mechanism of this class of ncRNA. In a challenging straight forward synthesis an adenosine derivative is synthesized for cleavage studies on a catalytic RNA construct. The ribonucleoside phosphoramidite lacks a nitrogen atom in the purine scaffold and reveals novel insights in cleavage mechanism.

3.5.1 Synthesis of 1-Deazaadenosine

The general synthesis of the adenosine analogue 1-deazaadenosine (1) was done according to the procedures of Petrelli[234] and Geroni[233].

To describe the synthetic strategy generally, design of purine scaffold lacking nitrogen at position 1 was done first. In the second part of the synthetic pathway, modified cyanoethylphosphoramidite is prepared for later use in solid phase synthesis of RNA using a cascade of protection and deprotection steps based on a strategy elaborated by Beigelman in 2002.[235]
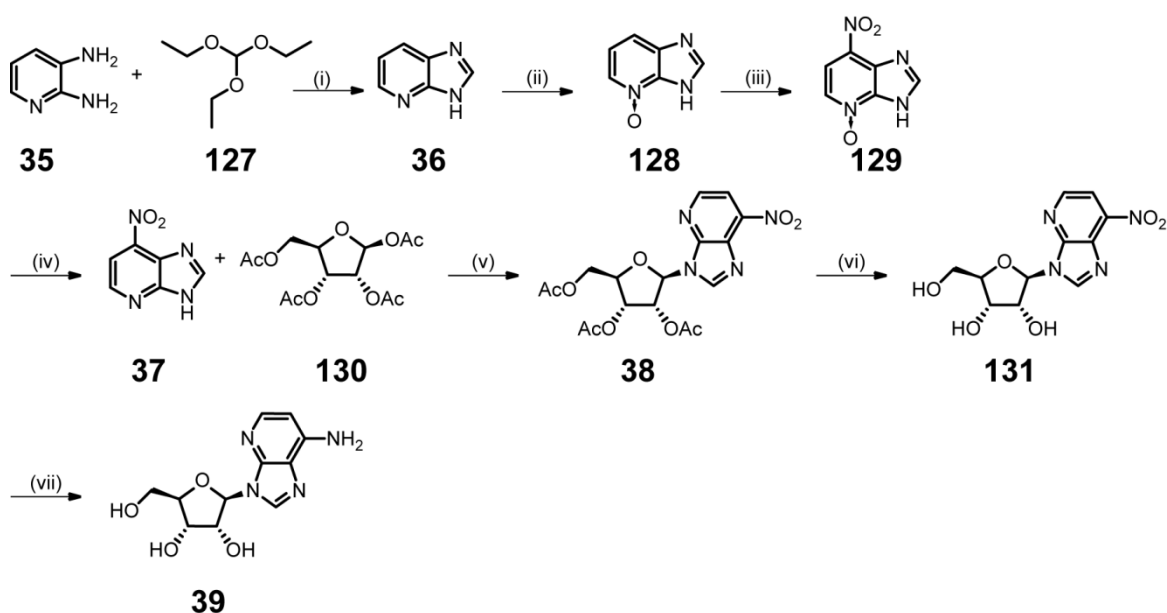
Fig. 111: Detailed synthetic scheme for 1-Deazaadenosine 39 synthesis according to the procedures adapted by Genroni[233], Petrelli[234]. (i) reflux, 3 h / HCl (aq., conc.), reflux, 1 h, 75%; (ii) m-CPBA, AcOH, r.t., 48 h, 58%; (iii) HNO3 (fum.), TFA, 90 °C, 3 h, 75%; (iv) PCl3, MeCN, 0 °C, 3 h, 68%; (v) 1,2,3,5-tetra-O-acetyl-β-D-ribofuranose, SnCl4, MeCN, r.t., o/n, 91%; (vi) NH3/MeCN, r.t. 24 h, quant.; (vii) Pd/C, H2, MeCN, r.t., o/n, 60%.

A detailed synthetic scheme is shown in Fig. 111 and will be explained in the following paragraphs. Starting with a multistep condensation between 2,3-diaminopyridine **35** and triethylorthoformate **127**, the 1-deazapurine scaffold **36** was yielded in literature given amounts. Amine at position 3 is protected as *N*-oxide using *m*-CPBA in glacial acetic acid yielding **128**. In the next synthetic step, nitration at position 7 was carried out with a mixture of fuming nitric acid and triflouracetic acid and **129** was isolated in literature known and reproduceable yields. After nitration, **129**'s amine oxide was deprotected using PCl$_3$ as trivalent phosphorus compound taking advance of strong phosphorus oxygen double bond formation as driving force. As next step the 1-deazaadenine precursor **37** was condensed to 1,2,3,5-tetra-*O*-acetyl-β-D-ribofuranose **130** using a modified version of the Fischer-Helferich method with stannic chloride.[235,364] Using longer reaction times turned out to enhance product yield. Literature[233] states a reaction time of 7 h yielding 82% product. Overnight reaction time showed an increase of yield up to 91% of **38**.

Subsequent deprotection of **38**'s acetyl groups under basic conditions yielded the unprotected nucleoside precursor **131** in a quantitative manner. Heterogenic reduction of the nitro group to corresponding amine was carried out using Palladium on carbon and H$_2$. Thus, the free nucleoside 1-deazaadenosine **39** was yielded.
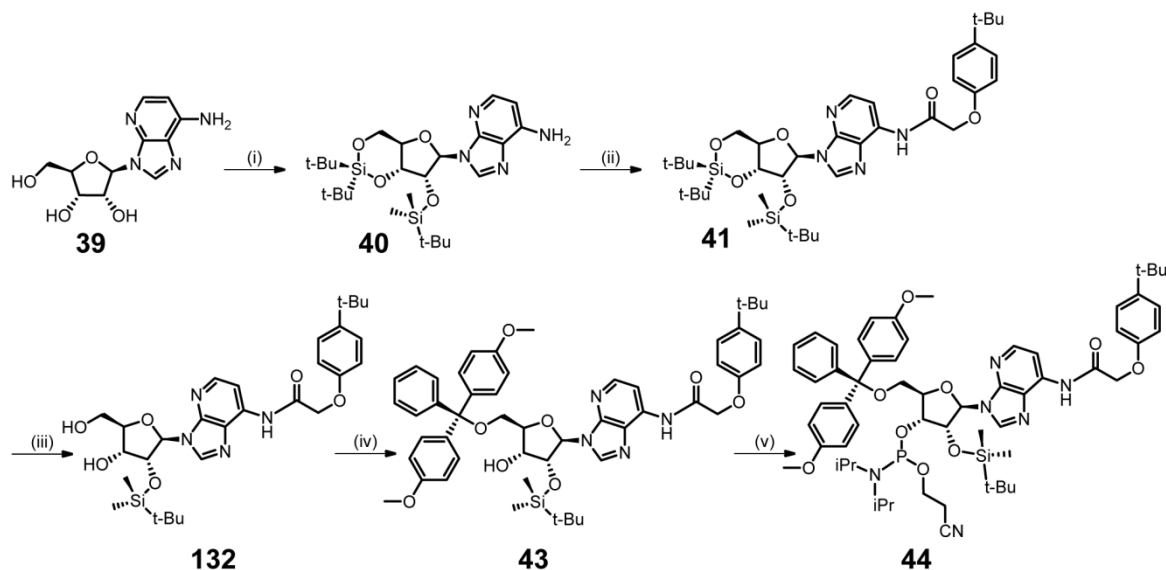
Fig. 112: Detailed synthetic scheme of protection strategy according to Beigelman[235] **yielding 44.** (i) di-*tert*-butylsilylbis(trifluoromethanesulfonate), DMF, 0 °C to r.t., o/n/ imidazole, *tert*-butyldimethylsilyl-Cl, r.t., >3 h, 71%; (ii) *tert*-butylphenoxyacetyl-Cl, pyridine, 0 °C to r.t., o/n, 74%; (iii) HF*pyridine, pyridine, DCM, 0 °C to r.t., 30 min, 65%; (iv) dimethylaminopyridine, dimethoxytrityl-Cl, pyridine, 0 °C to r.t., o/n, 65%; (v) diisopropylethylamine, N,N-diisopropylchlorophosphoramidite, DCM, 0 °C, 10 min, 93%.

To achieve cyanoethylphosphoramidite **44** suitable for solid phase synthesis, a multistep protection route published by Beigelman and coworkers in 2002[235] was adapted.

First, 5′-OH as well as 3′-OH of **39** was protected by a twofold triflic functionalized silyl protecting group. Using di-*tert*-butylsilyl bis(trifluoromethanesulfonate) is advised by Beigelman due to proportionate mild deprotection conditions. Without purification, the 5′- and 3′-protected ribose was processed for 2′-protection on same conditions with *tert*-butyldimethylsilyl (*TBS*) group yielding 71% of **40** after purification. The exocyclic amine of the modified nucleobase was protected with tert-butylphenoxyacetyl chloride (*TAC*) to corresponding acetyl amide to prevent unwanted side reactions during later solid phase synthesis. **41** was yielded with 74%.

Next, 5′-OH and 3′-OH of **41** have to be deprotected with HF*pyridine to get partly protected nucleoside **132**, which can be transferred to 5′-dimethoxytrityl *(DMT)* protected nucleoside **43** with a yield of 42% over two steps. In a final step, required phosphoramidite **44** was synthesized with 93% yield.

The protecting and deprotecting cascade carried out in second part of synthesis yielded **44** as nucleotide suitable for solid-phase RNA synthesis. In Fig. 113, protection groups and their common abbreviations are depicted. Dimethoxytrityl (*DMT*) at 5′-OH, tert-butyldimethylsilyl (*TBS*) at 2′-OH and tert-butylphenoxyacetyl (*TAC*) at exocyclic amine of adenine were used to transfer nucleoside 1-deazaadenosine **39** into nucleotide **44**. Using solid support, **44** can be incorporated into functional RNA in a site-specific manner.

44
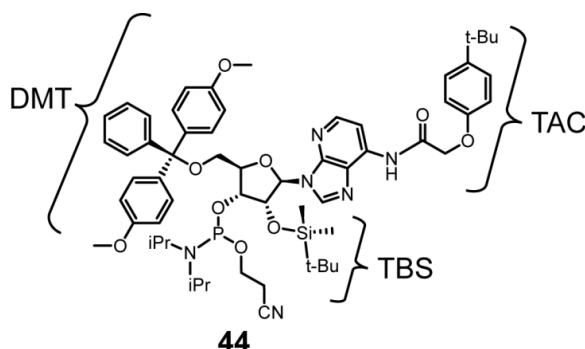
Fig. 113: Required protection groups for 44.

It is mentionable, that the synthetic circumstances of the last three steps in this synthetic route are crucial. Indeed silyl ethers are very common protecting groups. Selective protection and deprotection using different silyl ethers is often mentioned in literature. Also the advantages of different alcohols protected with either different or sometimes even the same silyl group, exploiting reagents and conditions to control different reactivity of the functional groups. Methods of selective desilylation are very useful, but not applicable for every system. As described by Crouch[365] in 2004 concerning selectively deprotection of silyl groups with fluorine sources, as well as the stability of

TBS groups towards fluorine sources the described and used deprotection strategy will be successful. Unfortunately tailoring deprotection conditions are needed due to potential concurrently deprotection of the *TBS* at 2′-OH.
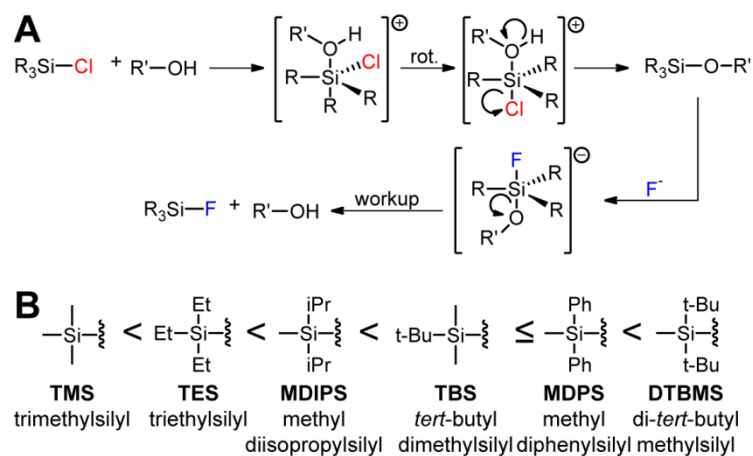
Fig. 114: (A) Mechanism for used silyl protection and deprotection strategy. (B) Stability of different silyl groups used as common protection groups for hydroxyl groups.

The mechanistic characteristic of silyl protection and deprotection is a pentacoordinated intermediate (see Fig. 114 A). Silyl cations are unstable, so synthetic steps in silyl ether chemistry appear in a S_N2 like manner. Additionally, strong Si-F bond act as driving force for fluoride-based deprotection of silyl ethers (see Fig. 114 A). The steric and electronic effects of substituents on the silicon and on the parent alcohol are often in focus during deprotection steps. As general rule of thumb bulky substituents either at the silicon or on the parent alcohol carbon decreases the reactivity of the Si-O bond. Shown in Fig. 114 B are some common silyl protection groups used for formation of silyl ethers and their relative stability against hydrolysis. The depicted classification is valid either for acid catalyzed or for base catalyzed hydrolysis.[365–367] Protection and deprotection cascade based on literature[235] showed that given stability of secondary *TBS* ethers was disproven at a first approach. According to referred literature[235], fluoride mediated deprotection was carried out over a period of 2 h. However, no significant difference in reactivity or stability was observed between the *TBS* group at 2′-position and the di(*tert*-butyl)silyl group bridging 5′- and 3′-position after purification of the reaction. Beigelman advises against alternative protection pathways using e.g. tetraisopropyldisiloxane (*TIPDS*)[235] as carried out for d**NaM** synthesis in this thesis. This would recommend other fluoride sources associated with harsher conditions. In order to avoid a full detachment of silyl ethers once more, a shorter time period under similar conditions was successful to isolate the gained product **63** accepting lower yield. Main advantage using silyl ether protection strategies for nucleoside precursors are significant ^{1}H-NMR signals of adjacent bulky

substituents. Like Fig. 115 shows exemplary for **62**, steric demanding *tert*-butyl groups show distinctive characteristic shifts and can be identified in an easy manner.
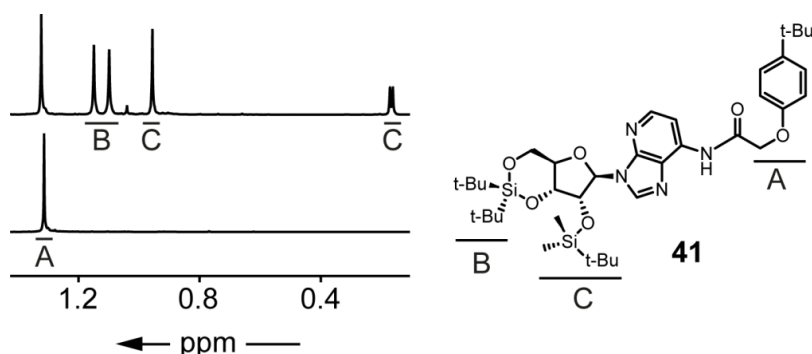
Fig. 115: Failed tailored deprotection of 62's di(*tert*-butyl)silyl protection group (B) using HF*pyridine. The TBS (C) protected 2′-OH got deprotected simultaneously as recognized in subsequent ^{1}H-NMR analysis. The significant *t*-Bu signals of protecting group (B) and (C) disappeared after treatment with the fluorine source. The *t*-Bu signal of the acetyl amide protection of the exocyclic amine (A) is apparent and verified its unscathed survival.

Furthermore, as described by Greene[328] *TBS* groups are able to migrate. Usually migration occurs under basic conditions, but migrations do occur under acidic conditions, too. With regard to Bigelow[368] who observed, that *TBS* groups possess the ambition of frequent migration[368].

Taking onto account, that the ongoing synthetic pathway – in this case 5′-*DMT* protection – is under basic conditions, unwanted *TBS* migration occurred. Separation of 2′-*TBS* and 3′-*TBS* protected nucleotide precursors can be carried out via column chromatography and additional identification by ^{1}H-NMR regarding the chemical shifts of the two *TBS* methyl groups.
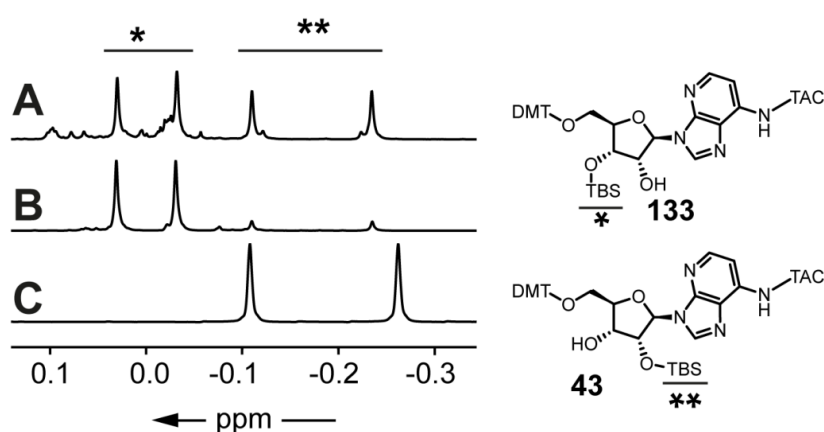
Fig. 116: Extracted ^{1}H-NMR analysis showing the significant CH₃- signals of a 3′-TBS (*) and a 2′-TBS (**) protection. After 5′-DMT protection under basic conditions a mixture of compounds was yielded, shown in corresponding spectrum (A). After a refined column chromatographic separation, a clean fraction of unwanted byproduct **133** bearing a 3′-TBS protection (B) and desired site-specific 2′-TBS protected phosphoramidite precursor **43** (C) was isolated.

Schöllhorn describes a migration for the *TBS* as well as for the sterically demanding *tert*-butyldiphenylsilyl (*TBDPS*) groups. The intramolecular migration is more pronounced for the less stable *TBS* group under base catalysis. Because of the reversibility of 1,2-silyl migration via a cyclic intermediate by a pentacoordinate silicon, an equilibrium between 2′- and 3′- protected compound **64** occurs.[369] The mechanism of this migration is comparable to the general mechanism of a Brook rearrangement, describing a 1,2-rearrangement of silicon from carbon to oxygen.[370]
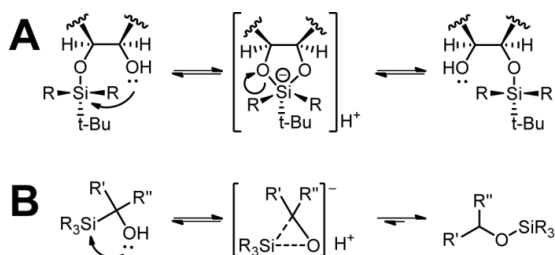
Fig. 117: Showing the general mechanism of 1,2-silyl migration for a 1,2-diol (A) using a five-membered cyclic intermediate and the general mechanism of the Brook rearrangement (B). Brook rearrangements usually occur from a secondary or tertiary carbon to adjacent oxygen atoms forming a cyclic intermediate under base catalysis.

Refined column chromatographic separation and verification by ^{1}H-NMR was carried out after *DMT* protection of 5′-OH under basic conditions as described in experimental procedure. Storage conditions at -20 °C under an inert atmosphere suppressed a *de novo* silyl migration at the *CEP*-precursor and the final synthetic step had been carried out under appropriate conditions taking proper *CEP* handling into consideration.

Overall yields published in literature could not be reached in this work, but regarding the fact, that no convergent synthesis can be performed using this straight forward approach an overall yield of 3% after 11 challenging steps achieving modified phosphoramidite precursor XX is in a satisfactory range. Final synthetic step achieving (XX) for chemical synthesis of RNA was carried out as decribed in Fig. 112 and Chemical Methods part of this work. Purification of CEP (XX) yielded 93%, suitable for solid-phase synthesis.

3.5.2 Chemical synthesis of RNA containing 1-Deazaadenosine

Biochemical analysis of the twister ribozyme using the synthesized **RNA-TW** was performed by Lilley and coworkers. Cleavage studies as well as crystallization experiments on twister ribozyme can be carried out on different constructs as discussed before.[212–214] Cleavage experiments using synthesized compound **44** will be done using a two piece construct. Shown in Fig. 118 A is the 28 nt long synthetic **RNA-TW**, which is used as ^{32}P-labeled substrate in latter discussed cleavage studies.

A

-10   -1 +1   +10

5'-ACC AGC GGC AGA AUG CAG CUU UAU UGC C-3'

B

ES 2   O. sativa

Fig. 118: Striven RNA sequence of synthesized RNA-TW containing 44 (A), where 44 is highlighted in red at position +1. Two piece ES 2 twister ribozyme construct used in cleavage experiments (B, left) as well as *O. sativa* twister ribozyme used in former crystalization studies (B, right).

Required oligonucleotides were synthesized using TBS phosphoramidite chemistry implemented on an Applied Biosystems 394 synthesizer. RNA was synthesized using UltraMILD ribonucleotide phosphoramidites with 2′-TBS protection (*Link Technologies*). Oligoribonucleotides were deprotected in 1:1 ammonia/methylamine at 60 °C for 20 min and evaporated to dryness. They were redissolved in 115 µL DMSO (anhydr.), 60 µL triethylamine and 75 µL triethylamine trihydrofluoride (*Aldrich*) and incubated at 65 °C for 2.5 h to remove t-BDMS groups, and normally recovered by butanol precipitation. Synthesized RNA containing **44** was passed through a NAP 10 column (*GE Life Sciences*), recovered by ethanol precipitation and verified by LC-MS.

RNA-TW: 5′-ACC AGC GGC AG**Y** AUG CAG CUU UAU UGC CdT-3′

Y = 44

Fig. 119: Mass spectrometric analysis of RNA-TW. UV-chromatogram (A, λ=254 nm) and deconvoluted ESI⁻ trace (B) of the peak eluting at 13 min (calculated for synthetic RNA: 9241.5; found: m/z = 9241.6). Sequence of synthesized and analyzed RNA contains a dT at 3′-end for synthetic convenience as shown.

Corresponding UV trace (λ = 254 nm) and deconvoluted mass spectrum of synthetic RNA XX are shown in Fig. 119. For synthetic convenience an additional thymine was added to the 3′-end[371] of synthesized 28 nt long **RNA-TW** resulting in sequence shown in Fig. 119 C. Further biochemical applications carried out by Lilley and coworkers are briefly described in the following and will be discussed in a simplified manner.

3.5.3 Biochemical applications using 1-Deaazaadenosine for mechanistic investigations on twister ribozyme

Crystal structure and an assumed chemical mechanisms of the twister ribozyme were published in 2014.[212–214] Twister as RNA motif was first identified during bioinformatics research of non-coding RNA databases[213,214] and as discussed beforehand two possible cleavage mechanisms can be assumed for this class of catalytic RNA and were major point of discourse. [212–214] On the one hand general acid-base catalysis and on the other hand metal-ion-mediated catalysis can be assumed. The crystal structure and first mechanistic studies of twister ribozyme catalysis carried out indicate acid-base catalysis, but assumed mechanism could not be validated.[212,214]

Both mechanisms are possible *prima facie*, due to the fact that structural investigations on RNA via crystallization are only snapshots of the structure and do not reflect conformational changes during dynamic processes like cleaving.
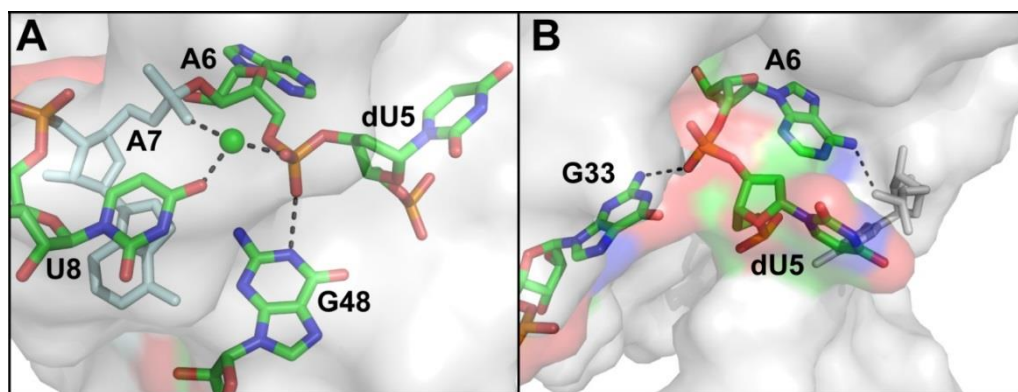
Fig. 120: Crystal structure of catalytic center of twister ribozyme. Left: Cleavage site in *env22* twister ribozyme published by Micura and coworkers in 2014. Divalent cation (green) at cleavage site stabilizes structural conditions of the ribozyme.[213] Right: Crystal structure of twister ribozyme from *O. sativa*, published by Lilley and coworkers. dU5 is far from required in-line trajectory orientation. G33 donates hydrogen to scissile phosphate of A6, which is held in *syn* conformation by C16 and C17 (greyed out).[371]

The crystallized structures of the *env22* twister ribozyme indicates as previously mentioned a metal-ion catalyzed mechanism[213] in contrast to earlier biochemical studies which assume rather a structural than a catalytic role for divalent metal ions in the twister structure[218]. As stated by Micura and coworkers in 2014[213] varying Mg^{2+} concentrations as well as usage of other divalent metal ions influence the cleavage activity of the twister ribozyme. Underpinnings are similarities to the hairpin ribozyme and the absence of the recommended in-line alignment necessary for the acid-base catalysis shown in Fig. 120. An assured statement concerning the assumed mechanism was neither done by Lilley nor Micura.[204,213,224] Even studies comparing pH- and metal ion effects on the ribozyme activity reveal only suggestions.[218]

In Fig. 120 crystal structures of catalytic centers published by Micura and coworkers[213] (A) as well as Lilley and coworkers[212] (B) are shown. Micura and coworkers advocating a metal-ion catalyzed route, corroborated this hypothesis in 2015.[224] It was assumed, that divalent ions are directly involved in catalysis and accelerate cleavage.[224] Nevertheless, they had to admit that the precise role of highly conserved adenine remains incompletely understood.[224] Using adenosine derivatives in two-strand *ES 2* construct showed clarifying results.

In twister ribozyme's double-pseudoknot structure highly conserved nucleotides in loop 1 (L1) and loop 4 (L4) form the active site of the self-cleaving RNA.[371] These nucleotides are written in red in Fig. 121. In 54 nt long crystallized ribozyme of *O. sativa*[212] and in two-piece *ES 2*[371] ribozyme bearing modified adenosine nucleotides cleavage activity and global fold are given.
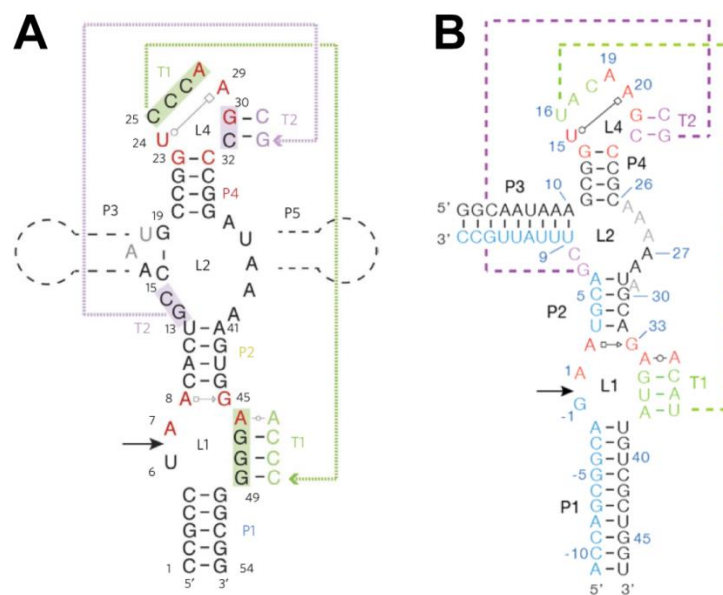
Fig. 121: Comparing sequence and secondary structure of the twister ribozyme. The 54 nt long crystallized ribozyme of *O. sativa* (A)[212] lacking P3 and P5 helix and the two-piece ES2 ribozyme (B)[371] used in cleavage experiments, with the substrate strand **RNA-TW** in blue. Cleavage occurs at the arrowed positions. Highly conserved nucleotides are written in red.

Admittedly, required in-line geometry (see Fig. 22 A) for acid-base mechanism is not given, but G33 (see Fig. 120) shows in substitution experiments strong influence on pH-dependent catalytic activity, like guanosines in hairpin[204] or VS[372] ribozyme. *In silico* experiments underline these results.[373] Regarding the high conservation of adenosine at position one (A7 in Fig. 121 A and A1 in Fig. 121 B) in the plethora of found twister ribozymes and a substitution of this nucleotide in the P1 stem inhibits the cleavage activity, adenosine is essential for ribozyme activity.[371] To reinforce the hypothesized mechanism and to further investigate the role of A1 in *ES 2* construct in cleavage mechanism three adenosine derivatives were needed in a pH-dependant cleavage study. A schematic presentation of experimental setup is depicted in Fig. 122. The experiments showed adenosine at position +1 in *ES 2* construct acting as general acid in twister ribozyme.[371] Substitution of adenosine by N3C adenosine abolishes catalytic activity. Thus, highly acidic nitrogen at position 3 is involved in catalytic mechanism as it is geometrically impossible for the more basic nitrogen at position one in nucleobase to approach the leaving group.[371]
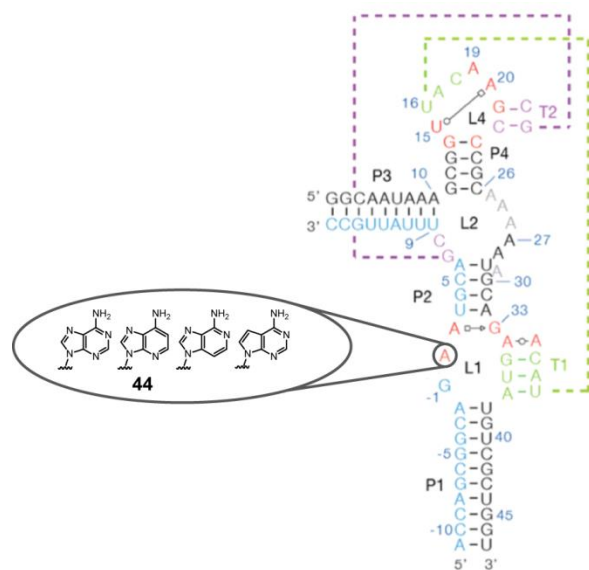
Fig. 122: Schematic experimental setup of pH-dependant catalytic activity study using different adenosine derivatives.[371]

High conservation of specific adenosine highlightet in Fig. 122 in about 2700 putative twister ribozymes underline the importance of this nucleotide in catalytic activity.[371] Atomis mutagenesis of the nucleobase scaffold at this position showed that pH dependence of cleavage arises from adenosine's nitrogen at position 3. Bell shaped pH dependence with apparent pK_a values as well as activity magnitude in substitution experiments verify a concerted acid-base catalysis in twister ribozyme.[371]

Lilley and coworkers proved by means of the synthesized phosphoramidite an increased protonation occurring at N3.[371] This unusual objective fact can be outlined by the local environment of A1 in the ribozyme structure and altered relative basicity of A1's nitrogen atoms related to this structural characteristic. The structural characteristic of A1 and N3's related importance in A1 was pointed out in 2017, too.[220] Nevertheless metal ions either monovalent or divalent possess a certain role regarding stabilization of the RNA structure and enhance activity as well.[371] Further investigations on this extraordinary self-cleaving RNA have been carried out by several groups to understand its peculiarities.[219,228,307,373,374]

However, additional studies are required to complete our understanding of the mechanism for twister ribozymes that use a combination of catalytic strategies.[220]

4 Conclusion and outlook

The understanding of ncRNAs mechanism and range of function is still not complete. Thus, novel tools to introduce reporter groups into various large non-coding RNA molecules are required to allow structural and functional investigations on those RNAs. In this thesis, the basis for site-specific modifications of RNAs with virtually any length via *in vitro* transcription is laid.

In the context of this thesis, novel compounds were synthesized and techniques for site-specific labeling of RNA have been developed and established.

In detail, different novel *meta*-functionalized 3,6-bis-aromatic tetrazine were synthesized and successfully applied in *IEDDA* click chemistry after conjugation to fluorescent dyes. After proof of concept, tetrazines inherent quenching properties were tested. Here, a novel derivative showed increased quenching properties in contrast to other synthesized derivatives and commercial available tetrazine derivatives. Furthermore labeling approaches on synthetic RNA strands using synthesized conjugates for *IEDDA* click chemistry were successfully applied both *in vitro* and in cells.

Transferring *IEDDA* click chemistry to structural investigations on biomolecules, a spin-label tetrazine was synthesized. This molecule opens a wide field of applications using basic chemical synthesis in combination with the fastest click reaction. After successful application on short RNA strands, developments of this technique for large constructs as well as in-cellapplications are strongly recommended. Structural features of biomolecules in its native surrounding can be investigated with this technique.

In the second part of this thesis, (ribo)nucleoside building blocks were synthesized which allow to expanded the genetic alphabet. The synthesized deoxynucleoside triphosphates were used in effective PCR amplification. Synthesized, alkene functionalized unnatural ribonucleoside triphosphates were successfully incorporated into RNA by *in vitro* transcription and posttranscriptionally modified by *IEDDA* click chemistry. This technique represents a new pathway for site-specific RNA labeling using an unnatural base pair, which is recognized and transcribed by T7 RNA polymerase. Due to the fact, that an expanded genetic alphabet on RNA level is an uncharted scientific topic, about future possibilities can only be speculated.

The approach was then extended to site-specifically incorporate spin-labelsinto RNA by *in vitro* transcription. For this, the required building blocks were synthesized and used for *in vitro* transcription. Successful distance measurements in RNA duplexes by EPR-

spectroscopy were shown. This new methods allow the facile site-specific labeling of long RNA constructs with spin-labels via *in vitro* transcription. By synthesis of unnatural ribonucleoside triphosphates with different linker systems, a compromise between recommended flexibility and rigidity was found. Rigidity is required for precise distance measurements and flexibility is provided by enzymes structure.

In the last part of this thesis, a chemically modified adenosine analoq was synthesized which helped to clarify the cleavage mechanism of a novel ribozyme class. This adenosine analoq was suitably protected as phosphoramidite for solid phase RNA synthesis and subsequently incorporated into the sequence of the twister ribozyme. PH-dependent cleavage assays with the wild-type ribozyme and the ribozyme bearing adenosine analogs al catalytically essential nucleobase positions were performed in collaboration with the Lilley group, Dundee, UK. This work allowed deciphering the cleavage mechanism of the twister ribozyme.

In summary, the novel nucleotides and tetrazine derivatives prepared and employed in this thesis are potent chemical tools for site-specific RNA labeling. Applications of this versatile toolbox for in cell labeling are imaginable and worthwhile.

5 Materials and methods

5.1 Chemical Methods

5.1.1 General chemical methods

5.1.1.1 Reagents and solvents

All commercially available chemicals and solvents were handled according to the suppliers' recommendations and used without further purification. Additional purification steps, special storage conditions and handling are described in according synthetic sections.

Chemicals were bought from *ABCR*; *Alfa Aesar*; *Applichem*; *BASF*; *Bachem*; *Carbosynth*; *Fluka*; *Riedel-de-Haën*; *Sigma-Aldrich*; *Grüssing*; *VWR*; *Carl Roth*; *TCI*; *Acros Organics*; *Thermo Fisher Scientific*; *Merck*; *Carbolution* and *Fluorochem*.

5.1.1.2 Schlenk line

Water and air sensitive chemicals were handled under Schlenk conditions using Argon (N46, *Air Liquide*) counter flow as well as heat-dried and Argon-flushed apparatus. Syringes and cannulas were Argon-flushed, too.

5.1.1.3 Thin layer chromatography (TLC)

As stationary phase for thin layer chromatography silica gel-coated aluminum plates were used and monitored under UV light for visualization. The TLC plates were commercially available by *Merck* (TLC Silica Gel 60 F_{254}, 20 x 20 cm) and *Sigma-Aldrich* (Silica gel on TLC Al foils, 4 x 8 cm).

Staining reagents were prepared according to literature-known recipes. Used staining reagents were *p*-Anisaldehyde (1.00 mL *p*-anisaldehyde, 1.00 mL sulfuric acid (97%), 18.0 mL EtOH), bromocresol green (0.10 g bromocresol green, 5.00 mL 0.1 M NaOH (aq.), 500 mL EtOH), potassium permanganate reagent (2.00 g potassium permanganate, 20.0 g potassium carbonate, 0.25 g sodium hydroxide, 300 mL H_2O), and Seebach stain (2.50 g phosphomolybdic acid, 1.00 g $Ce(SO_4)_2$, 6.00 mL sulfuric acid (97%), 94.0 mL H_2O).[375,376]

5.1.1.4 Column chromatography

The stationary phase for column chromatography was Geduran® Si 60 0.063 – 0.200 mm silica gel (*Merck*). The used mobile phases for column chromatography are stated in the corresponding sections.

5.1.1.5 Nuclear magnetic resonance spectroscopy (NMR)

NMR spectroscopy was recorded on either an Avance I 300 MHz (^{1}H: 300 MHz, ^{13}C: 75 MHz, ^{31}P: 121 MHz), an Avance I 400 MHz (^{1}H: 400 MHz, ^{13}C: 101 MHz, ^{31}P: 162 MHz), an Avance I 500 MHz (Oxford Magnet, ^{1}H: 500 MHz, ^{13}C: 126 MHz, ^{31}P: 202 MHz) or an Avance III HD Ascend 700 MHz (^{1}H: 700 MHz, ^{13}C: 176 MHz, ^{31}P: 283 MHz) from *Bruker*.

Chemical shifts (δ) are given in ppm and spectra are calibrated to the particular deuterated solvent residue signal or the natural ^{13}C signal of the deuterated solvent according to literature values[377] as listed below. ^{31}P spectra are calibrated to phosphoric acid (85%) as external standard.

solvent	^{1}H-NMR, δ_H [ppm]	^{13}C-NMR, δ_C [ppm]
$CDCl_3$	7.26	77.16
DMSO-d_6	2.50	39.52
D_2O	4.79	-
CD_3OD	3.31	49.00
CD_2Cl_2	5.32	53.84

The following abbreviations were used for the multiplicities: s = singlet, d = doublet, t = triplet, m = multiplet, br = broad. The coupling constants are given in Hertz [Hz] and specified as absolute values. The spectra were analyzed using MestReNova v8.0.1-10878 (*Mestrelab Research S.L.*).

5.1.1.6 Mass spectrometry

High resolution mass spectrometric (HR MS) analysis was performed on a MAT 95 XL (*Thermo Finnigan*) using electron ionization (EI). HR MS using electrospray ionization (ESI) was performed either on a micrOTOF-Q (*Bruker Daltonik*) or an Orbitrap XL (*Thermo Fisher Scientific*).

5.1.1.7 High-performance liquid chromatography (analytical)

Purification and separation of either small molecules or oligonucleotides in an analytical manner or in small scales was performed on an 1100 series HPLC system (*Agilent*) using an EC150/4.6 Nucleodur® 100-5 C$_{18}$ ec column (*Macherey-Nagel*) at a flow rate of 1 mL/min. Additives and adjusted gradients are given in the appropriate sections.

5.1.1.8 High-performance liquid chromatography (preparative)

Preparative purification of nucleotides was performed on a 1200 series system (*Agilent*) in combination with a Gemini® 5 µm NX-C18 110 Å, 75×30 mm, AXIA™ packed column (*Phenomenex*). The mobile phase was formed by a gradient from 0 → 40% B in 6 min using 0.1 M TEAB (aq., HPLC grade) as eluent A and MeCN (HPLC grade) as eluent B. Flow rate 40 mL/min.

5.1.1.9 High-performance liquid chromatography mass spectrometry (LC-MS)

Mass spectrometry measurements were performed on a HCT esquire (*Bruker Daltonik*) in combination with an 1100 series HPLC (*Agilent*). As stationary phase a Zorbax Narrow Bore SB C18 (2.1×50 mm, 5 µm) column (*Agilent*) was used. Used mobile phases are listed below.

Application	Mobile phase A	Mobile phase B
Small molecules	0.1%(v/v) formic acid	MeCN
	0.1%(w/v) NH$_4$OAc	
Nucleosides/Nucleotides	0.1%(w/v) NH$_4$OAc	id.
Oligonucleotides	100 mM HFIP/ 10 mM TEA	id.

All additives were commercially available as LC-MS grade additive and diluted in ddH$_2$O according to the table above.

Used software was a proprietary bundle provided by *Bruker Daltonik* (esquireConrol v.6.2; HyStar v.3.2; Compass DataAnalysis v.4.2).

5.1.1.10 Lyophilization

All announced freeze-drying applications were performed on an ALPHA 2-4 LDplus (*Martin Christ*). Oligonucleotide samples were desalted using G-25 spin columns (*GE*

Healthcare) before freeze-drying. HPLC samples were diluted with ddH$_2$O to lower the MeCN amount below at least 30%.

5.1.2 Synthesis and physical data of asymmetric tetrazines

5.1.2.1 General synthesis of asymmetric aminomethyl-functionalized 1,2,4,5-tetrazines used during diploma thesis

To benzonitrile or 2-pyridinecarbonitrile (1.0 eq., 9.71 mmol/9.61 mmol, 1.00 g) a 1.2-fold excess of the required aminomethyl functionalized aromatic nitrile (1.2 eq., 11.7 mmol/11.5 mmol) was added and the mixture was dissolved in hydrazine hydrate (aq., 80%, 5.00 mL). After stirring the reaction mixture at 90 °C for 4 to 5 h and subsequent cooling to room temperature the orange to reddish precipitate was filtered off, washed with ice-cold water (2 x 2 mL) and dried under reduced pressure. The crude solid is solved in glacial acetic acid (5 mL to 6 mL). After addition of $NaNO_2$ (1.00 eq., 9.71 mmol/9.61 mmol, 670 mg/663 mg) the reaction is stirred for 15 min at room temperature. The solvent was removed under reduced pressure and the crude product is purified by column chromatography. As general trend, a mobile phase of DCM/MeOH (4/1 v/v) is required and the desired aminomethyl-1,2,4,5-tetrazine derivative ($R_f \approx 0.2$) can be yielded as pinkish solid.

5.1.2.2 Synthesis of 6-bromomethyl-pyridine-2-carbonitrile (46)

2-Cyano-6-methylpyridine (1.0 eq., 12.7 mmol, 1.50 g) was solved in CCl_4 (28 mL) and heated to 70 °C. After the addition of NBS (1.2 eq., 15.2 mmol, 2.71 g) the reaction mixture was stirred for ten minutes at 70 °C and subsequently the AIBN (0.05 eq., 0.64 mmol, 0.10 g) was added. The reaction was stirred for four hours at 75 °C, cooled to room temperature and the precipitate was filtered off. The solvent was removed under reduced pressure and the crude product was purified via column chromatography (DCM). **46** (4.83 mmol, 0.95 g, 38%) was yielded as off-white solid.
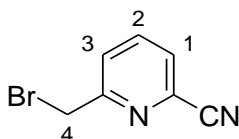
Chemical formula: $C_7H_5BrN_2$; **MW**: 197.0; **R$_f$** (DCM): 0.3.
¹H-NMR (CDCl$_3$, 400 MHz, r.t.): δ [ppm] = 7.86 (t, $^3J_{H2H3/H2H1}$ = 7.8 Hz, 1H, H2), 7.70 (d, $^3J_{H1H2}$ = 8.0 Hz, 1H, H1), 7.63 (d, $^3J_{H3H2}$ = 7.7 Hz, 1H, H3), 4.55 (s, 2H, H4).
MS (EI): [M]$^{+\cdot}$ 197.0 (100), 198.0 (8), 199.0 (98), 200.0 (8).

5.1.2.3 Synthesis of 6-aminomethyl-pyridine-2-carbonitrile (47)

46 (1.0 eq., 4.83 mmol, 0.95 g) was dissolved in MeOH (10.0 mL) and NH_3 (aq., 25%, 20.0 mL). Reaction was stirred overnight at room temperature. The solvent was removed

under reduced pressure and the crude product was used without further purification. **47** (4.69 mmol, 1.00 g, 97%) was yielded as off-white bromide salt.
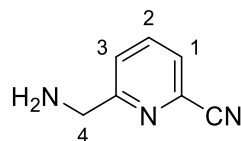
Chemical formula: $C_7H_7N_3$; **MW**: 133.2 / 213.2 (Br salt).

^{1}H-NMR (DMSO-d_6, 400 MHz, r.t.): δ [ppm] = 8.15 (t, $^3J_{H2H3/H2H1}$ = 7.8 Hz, 1H, H2), 8.08 (d, $^3J_{H1H2}$ = 6.8 Hz, 1H, H1), 7.85 (d, $^3J_{H3H2}$ = 7.9 Hz, 1H, H3), 4.31 (s, 2H, H4).

5.1.2.4 Synthesis of 3-aminomethylbenzonitrile (49):

3-Bromomethylbenzonitrile (1.0 eq., 10.71 mmol, 2.10 g) was solved in MeOH (20 mL) and NH_3 (aq., 25%, 40 mL).The reaction was stirred over night at room temperature. The solvent was removed under reduced pressure and the crude product was used without further purification. **49** (9.48 mmol, 2.02 g, 89%) was yielded as off-white bromide salt.
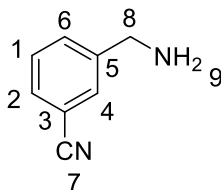
Chemical formula: $C_7H_5BrN_2$; **MW**: 132.1 / 213.1 (Br salt).

^{1}H-NMR (DMSO-d_6, 400 MHz, r.t.): δ [ppm] = 8.37 (s/br, 2H; H9), 7.98 (s, 1H, H4), 7.85 (m, 2H, H1, H2), 7.66 (d, $^2J_{H6H1}$ = 7.9 Hz, 1H, H6), 4.13 (s, 2H, H8).

^{13}C-NMR (DMSO-d_6, 75 MHz, r.t.): δ [ppm] = 135.5 (C5), 134.0 (C6), 132.7 (C4), 132.2 (C2), 129.8 (C1), 118.5 (C7), 111.4 (C3), 41.4 (C8).

MS (EI): [M]$^{+.}$ 132.1.

5.1.2.5 Synthesis of 3-(6-phenyl-1,2,4,5-tetrazin-3-yl)-benzenemethanamine (51):

Benzonitrile (1.0 eq., 9.79 mmol, 1.01 g) and **49** (1.2 eq., 11.35 mmol, 1.50 g) were solved in hydrazine hydrate (aq., 80%, 5 mL). The solution was stirred at 90 °C for 5 h. After cooling to room temperature, the orange precipitate was filtered off, washed with cold water and dried under reduced pressure. The crude solid was dissolved in methanol, concentrated onto silica gel and **51** (0.24 mmol, 64 mg, 2% yield) was isolated by column chromatography (DCM/MeOH, 4:1, v/v) as pink solid.
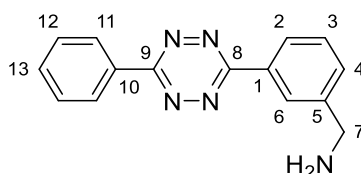
Chemical formula: $C_{15}H_{13}N_5$; **MW**: 263.3; **R$_f$** (DCM/MeOH, 5:1 v/v): 0.2.

¹H-NMR (DMSO-d_6, 500 MHz, r.t.): δ = 8.58 (s, 1H, H6), 8.55 (dd, $^3J_{H6H7}$ = 7.7 Hz, $^4J_{H6H8}$ = 1.7 Hz, 2H, H11), 8.44 (d, $^2J_{H4H3}$ = 7.7 Hz, 1H, H2), 7.70 (m, 4H, H4, H12, H13), 7.64 (t, $^2J_{H3H4/H3H2}$ = 7.7 Hz, 1H, H3), 3.96 (s, 2H, H7).

¹³C-NMR (DMSO-d_6, 126 MHz, 298 K): δ = 163.4 (C9), 163.3 (C8), 132.6 (C13), 131.9 (C10, C1), 131.7 (C4), 129.5 (C12), 129.3 (C3), 127.6 (C11), 126.5 (C6), 125.9 (C2), 44.8 (C7).

HR MS (EI): calc. for [M]$^{+\cdot}$ 263.1171; found m/z = 263.1172.

5.1.2.6 Synthesis of 3-(6-(pyridin-2-yl)-1,2,4,5-tetrazin-3-yl)-benzenemethanamine (53)

2-Pyridinecarbonitrile (1.0 eq., 7.58 mmol, 790 mg) and **49** (1.2 eq., 9.10 mmol, 1.93 g as Br-salt) were solved in hydrazine hydrate (aq., 80 %, 5.00 mL) and stirred for 4 h at 90 °C. After cooling to room temperature, the orange precipitate was filtered off and washed with ice-cold water (2 x 3 mL). The crude precursor was dried *in vacuo* and afterwards solved in glacial acetic acid (6.00 mL). As oxidizing agent, sodium nitrite (522 mg, 7.57 mmol, 1.0 eq) was added and the reaction mixture was stirred for 15 min at room temperature. The solvent was evaporated under reduced pressure and the oxidized crude product dried *in vacuo*. Purification via column chromatography (DCM/MeOH, 85/15, v/v) gave **53** (0.05 mmol, 14.0 mg, 7%) as pink solid.
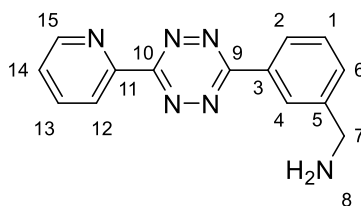
Chemical formula: $C_{14}H_{12}N_6$; **MW**: 264.3; **R$_f$** (DCM/MeOH, 85/15, v/v): 0.2.

¹H-NMR (DMSO-d$_6$, 400 MHz, r.t.): δ [ppm] = 8.93 (d, $^3J_{H15H14}$ = 4.0 Hz, 1H, H15), 8.63 (s, 1H, H4), 8.58 (d, $^3J_{H12H13}$ = 7.8 Hz, 1H, H12), 8.47 (d, $^3J_{H2H1}$ = 7.8 Hz, 1H, H2), 8.16 (td, $^3J_{H13H14/H13H12}$ = 7.8 Hz, $^4J_{H13H15}$ = 1.7 Hz, 1H, H13), 7.78 – 7.66 (m, 3H, H1, H6, H14), 4.02 (s, 2H, H7).

¹³C-NMR (DMSO-d$_6$, 75 MHz, r.t.): δ [ppm] = 163.5 (C9, C10), 163.3 (C10, C9), 150.6 (C15), 150.2 (C11), 141.8 (C3), 137.8 (C13), 132.4 (C14, C5), 131.7 (C5, C14), 129.5 (C1), 127.2 (C4), 126.6 (C2), 126.6 (C6), 124.0 (C12), 44.1 (C7).

119

HR MS (ESI$^+$): calc. for [M+H]$^+$: 265.1096; found: m/z = 265.1201.

5.1.2.7 Synthesis of 3-(6-(pyridin-2-yl)-1,2,4,5-tetrazin-3-yl)-benzenemethanamine (54)

2-Pyridinecarbonitrile (1.0 eq., 1.90 mmol, 200 mg) and **47** (1.2 eq., 2.28 mmol, 486 mg as Br-salt) were solved in hydrazine hydrate (aq., 80 %, 5 mL) and stirred for 3 h at 90 °C. After cooling to room temperature, the orange precipitate was filtered off and washed with ice-cold water (2 x 3 mL). The crude intermediate was dried *in vacuo* and purified via column chromatography (DCM/MeOH, 4/1, v/v) yielding the dihydrotetrazine precursor (0.39 mmol, 105.0 mg, 20 %) as red solid. The dihydrotetrazine was solved in toluene (anhydr., 2.5 mL) under an argon atmosphere. As oxidizing agent, DDQ (2.0 eq., 0.78 mmol, 177 mg) solved in toluene (anhydr., 1 mL) was added slowly and the reaction mixture was stirred for 30 min at room temperature. The solvent was evaporated under reduced pressure. The oxidized product **54** (0.39 mmol, 105 mg, quant.) was dried *in vacuo* and yielded as pink solid.
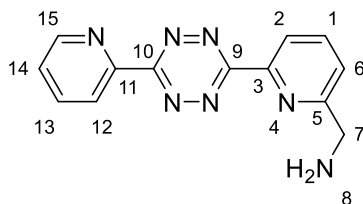
Chemical formula: $C_{13}H_{11}N_7$; **MW**: 265.3; **R$_f$** (DCM/MeOH, 4/1, v/v): 0.2.

^{1}H-NMR (DMSO-d_6, 400 MHz, r.t.): δ [ppm] = 8.96 (d, $^3J_{H15H14}$ = 4.7 Hz, 1H, H15), 8.62 (dd, $^3J_{H12H13}$ = 8.1 Hz, $^3J_{H6H1}$ = 8.1 Hz, 2H, H6, H12), 8.50 (s/br, 2H, H8), 8.25 (t, $^3J_{H1H2/H1H6}$ = 7.8 Hz, 1H, H1), 8.18 (td, $^3J_{H13H12/H13H14}$ = 7.8 Hz, $^4J_{H13H15}$ = 1.7 Hz, 1H, H13), 7.84 (d, $^3J_{H2H1}$ = 7.7 Hz, 1H, H2), 7.76 (ddd, $^3J_{H14H13}$ = 7.6 Hz, $^3J_{H14H15}$ = 4.7 Hz, $^4J_{H14H12}$ = 1.1 Hz, 1H, H14), 4.41 (s, 2H, H7).

^{13}C-NMR (DMSO-d_6, 101 MHz, r.t.): δ [ppm] = 163.4 (C9, C10), 163.1 (C10, C9), 151.0 (C15), 138.9 (C1), 137.9 (C13), 126.8 (C14), 125.6 (C2), 124.5 (C6, C12), 124.0 (C12, C6), 43.0 (C7).

HR MS (ESI$^+$): calc. for [M+H]$^+$: 266.1149; found: m/z = 266.1155.

5.1.2.8 General procedure for the synthesis of tetrazine-fluorophore conjugates

The tetrazine, in general 0.1 mg (0.54 µmol for **4**, 0.38 µmol for **51**, and 0.38 µmol for **53**) and Oregon Green® 488 carboxylic acid succinimidyl ester, 5-isomer (0.13 mg, 0.25 µmol) or biotin N-hydroxysuccinimide ester (0.09 mg, 0.25 µmol) were dissolved in

dimethylsulfoxide (anhydr., 50.0µL) and triethylamine (anhydr., 1.50 µL). The solution was stirred under exclusion of light at room temperature. The reaction progress was monitored by LC-MS. The product were obtained in quantitavive manner (**56**: 0,25 µmol, 0,16 mg, 97%; **57**: 0,25 µmol, 0.142 mg, 98%; **58**: 0,24 µmol, 0.16 mg, 97; **59**: 0,25 µmol, 0.12 mg, 98%) and purified by reverse phase HPLC using a gradient from 15% to 80% acetonitrile (HPLC grade) in water (*MilliQ*) in 25 min. The identity and purity of the conjugates were confirmed by LC-MS.

According spectra are shown in 7.2.

5.1.2.9 Synthesis of 2-benzoylhydrazide benzoic acid (62)

The synthesis was adapted to the procedure described by Plowright.[378] In DCM (750 mL) benzhydrazide (1.00 eq., 50.0 mmol, 6.81 g) was dissolved, basified with NEt_3 (2.10 eq., 110 mmol, 15.2 mL) and cooled to 0 °C. Under ice-cold conditions benzoyl chloride (1.0 eq., 50.5 mmol, 5.87 mL) was added drop wise. The reaction was warmed to room temperature; the colorless precipitate was filtered off and dried *in vacuo*. **62** (45.5 mmol, 10.92 g, 91%) was yielded as colorless solid.
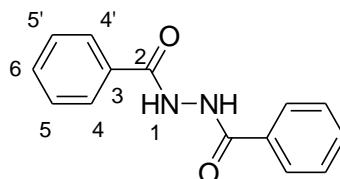
Chemical formula: $C_8H_{12}O_5$; **MW**: 240.3.

^{1}H-NMR (DMSO-d_6, 400 MHz, r.t.): δ [ppm] = 10.51 (s, 2H, H1), 7.94 (dd, $^3J_{H4H6}$ = 8.3 Hz, $^4J_{H4H6}$ = 1.2 Hz, 4H, H4, H4'), 7.65 – 7.56 (m, 2H, H6), 7.56 – 7.50 (m, 4H, H5, H5').

^{13}C-NMR (DMSO-d_6, 101 MHz, r.t.): δ [ppm] = 165.81 (C2), 132.58 (C3), 131.82 (C6), 128.48 (C5, C5'), 127.43 (C4, C4').

5.1.2.10 Synthesis of bis(α-chlorobenzylidene)hydrazine (63)

The synthesis was carried out to the procedure described by Chen.[91] Under an atmosphere of argon, **62** (1.0 eq., 8.32 mmol, 2.00 g) and PCl_5 (2.2 eq., 18.3 mmol, 3.81 g) were solved in Tol (25 mL) and stirred for 3 h at 120 °C. After cooling to room temperature, the solvent was removed under reduced pressure. The crude residue was washed with water (2 x 10 mL) and dried *in vacuo*. The product was purified by recrystallization from EtOH and DCM. **63** (4.22 mmol, 1.17 g, 51%) was yielded as colorless solid.
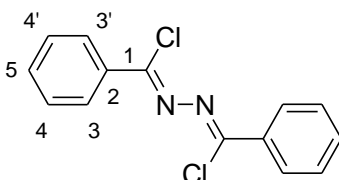
Chemical formula: $C_8H_{12}O_5$; **MW**: 277.2.

¹H-NMR (CD_2Cl_2, 400 MHz, r.t.): δ [ppm] = 8.17 – 8.10 (m, 4H, H3, H3'), 7.63 – 7.54 (m, 2H, H5), 7.53 – 7.48 (m, 4H, H4, H4').

¹³C-NMR (CD_2Cl_2, 101 MHz, r.t.): δ [ppm] = 144.72 (C1), 134.19 (C2), 132.50 (C5), 129.17 (C3, C3'), 129.04 (C4, C4').

MS (EI): [M]$^{+\cdot}$ 275.9 (70), 277.9 (43), 279.9 (7); [M-C_7H_5ClN] 137.9 (100).

5.1.2.11 Synthesis of 3,6-diphenyl-1,2,4,5-tetrazine (2)

63 (1.0 eq., 1.44 mmol, 0.40 g) was solved in hydrazine hydrate (aq., 80%, 5 mL) and pyridine (1 mL). The reaction was stirred for 20 min at 80 °C. After cooling to room temperature, the crude product was filtered off, washed with ice-cold water (2 x 5 mL) and dried *in vacou*. The crude product was directly solved in AcOH (5 mL) and $NaNO_2$ (1.1 eq., 1.58 mmol, 0.11 g) was added slowly at room temperature. After stirring for ten minutes the solvent was removed by reduced pressure and **2** (0.87 mmol, 0.20 g, 60%) was yielded as pink solid.
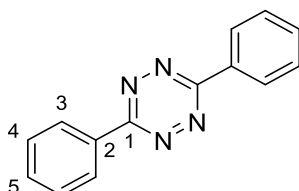
Chemical formula: $C_{14}H_{10}N_4$; **MW**: 234.3

¹H-NMR (DMSO-d_6, 500 MHz, r.t.): δ [ppm] = 8.56 – 8.53 (m, 4H, H3), 7.74 – 7.68 (m, 6H, H4, H5).

¹³C-NMR (DMSO-d_6, 126 MHz, r.t.): δ [ppm] = 163.34 (C1), 132.62 (C5), 131.85 (C2), 129.48 (C3, C3'), 127.56 (C4, C4').

5.1.2.12 Synthesis of 4-((1,3-dioxo-1,3-dihydroisoindol-2-yl)methyl)benzoic acid (66i)

4-(Aminomethyl)-benzoic acid (1.0 eq., 6.66 mmol, 1.00 g) was dissolved in AcOH (12.0 mL) and after the addition of phthalic anhydride (1.5 eq., 9.92 mmol, 1.47 g) the reaction was refluxed for 2 h. After cooling to room temperature the solvent was removed under reduced pressure. Purification of the product was done via column

chromatography (Cy/EE, 1/1, v/v) and after drying *in vacou*. **66i** (5.80 mmol, 1.63 g, 87%) was yielded as colorless solid.
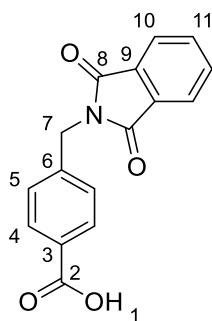
Chemical formula: $C_{16}H_{11}NO_4$; **MW**: 281.3; R_f (Cy/EE, 1/1 v/v): 0.6.

^{1}H-NMR (DMSO-d_6, 400 MHz, r.t.): δ [ppm] = 12.91 (s/br, 1H, H1), 7.93 – 7.84 (m, 6H, H4, H10, H11), 7.42 (d, $^3J_{H5H4}$ = 8.5 Hz, 2H, H5), 4.84 (s, 2H, H7).

^{13}C-NMR (DMSO-d_6, 101 MHz, r.t.): δ [ppm] = 167.67 (C8), 166.98 (C2), 141.53 (C6), 134.61 (C11), 131.56 (C9), 129.88 (C3), 129.62 (C4), 127.36 (C5), 123.29 (C10), 40.64 (C7)

MS (EI): [M]$^{+.}$ 281.0 (100), 282.0 (17).

5.1.2.13 Synthesis of 4-((1,3-dioxo-1,3-dihydroisoindol-2-yl)methyl)benzoic acid chloride (66)

66i (1.0 eq., 1.78 mmol, 0.50 g) was dissolved in $SOCl_2$ (19 eq., 34.5 mmol, 25 mL) and refluxed for 4 h at 90 °C. After cooling to room temperature the solvent was distilled off. The crude product was washed with DCM (2 x 10 mL) and dried *in vacou*. **66** (1.77 mmol, 0.53 g, 99%) was yielded as off-white solid in a quantitative way.
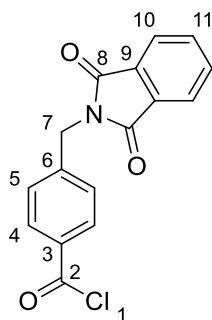
Chemical formula: $C_{16}H_{10}ClNO_4$; **MW**: 299.7.

^{1}H-NMR (DMSO-d_6, 400 MHz, r.t.): δ [ppm] = 10.43 (s/br, 1H, H1), 8.17 – 7.78 (m, 6H, H4, H10, H11), 7.41 (d, $^3J_{H5H4}$ = 8.5 Hz, 2H, H5), 4.83 (s, 2H, H7).

MS (EI): [M]$^{+.}$ 299.0 (30), 301.0 (10); [M-Cl]$^.$ 264.1 (100).

Explanatory remark: Product was verified by mass spectrometry (EI) with reference to the isotopic fingerprint of chloride. Due to solubility problems DMSO-d_6 had to be used for NMR measurements and the acid chloride was hydrolyzed during measurements.

5.1.2.14 Synthesis of *N'*-(4-(1,3-dioxo-1,3-dihydro-isoindol-2-ylmethyl)-benzoyl)-hydrazide benzoic acid (67)

The synthesis was carried out to the procedure described by Chen.[91] **66** (1.0 eq., 3.50 mmol, 1.05 g) was dissolved in DCM (15 mL) and drop wise added to a stirred solution of benzhydrazide (1.1 eq., 3.85 mmol, 0.52 g) and NEt$_3$ (1.9 eq., 6.65 mmol, 0.92 mL) solved in DCM (50 mL) and stirred for 2 h at room temperature. The colorless precipitate was filtered off, washed with DCM (2 x 20 mL) and dried *in vacou*. **67** (1.98 mmol, 0.79 g, 56%) was yielded as colorless solid.

Chemical formula: C$_{23}$H$_{17}$N$_3$O$_4$; **MW**: 399.4

^{1}H-NMR (DMSO-*d$_6$*, 400 MHz, r.t.): δ [ppm] = 10.49 (s, 2H, H11, H12), 7.99 – 7.81 (m, 8H, H1, H2, H7, H16), 7.59 (t, $^3J_{H17H16}$ = 7.3 Hz, 1H, H17), 7.53 (d, $^3J_{H15H16}$ = 7.7 Hz, 2H, H15), 7.46 (d, $^3J_{H8H7}$ = 8.3 Hz, 2H, H8), 4.86 (s, 2H, H5).

13C-NMR (DMSO-*d$_6$*, 101 MHz, r.t.): δ [ppm] = 167.70 (C4), 165.78 (C10, C13), 165.51 (C10, C13), 140.47 (C6), 134.58 (C1), 132.55 (C3), 131.83 (C14, C9), 131.71 (C9, C14), 131.59 (C17), 128.49 (C15), 127.78, 127.41 (C16), 127.31 (C7), 123.27 (C2), 40.62 (C5).

HR MS (EI): calc. for [M]$^{+.}$ 399.1219; found: *m/z* = 399.1217.

5.1.2.15 Synthesis of *N'*-(chlorophenylmethylene)-(4-(1,3-dioxo-1,3-dihydro-isoindol-2-ylmethyl) benzenecarbohydrazonoyl chloride (68)

The synthesis was carried out to the procedure described by Chen.[91] Under an inert atmosphere **67** (1.0 eq., 0.99 mmol, 0.40 g) was dissolved in Tol (15 mL) and PCl$_5$ (2.5 eq., 2.48 mmol, 0.52 g) was added. The reaction mixture was refluxed for 3 h. After cooling to room temperature, the solvent was removed under reduced pressure, the crude product washed with cold water (5 mL), recrystallized from EtOH and DCM and dried *in vacuo*. **68** (0.64 mmol, 0.28 g, 64%) was yielded as off-white solid.
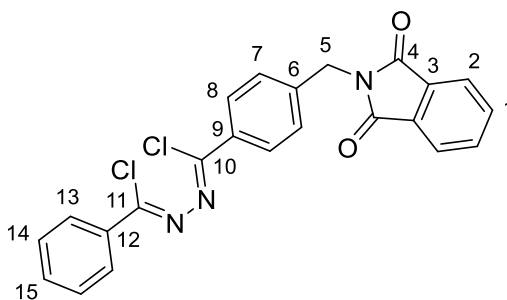
Chemical formula: $C_{23}H_{15}Cl_2N_3O_2$; MW: 436.3

1H-NMR (DMSO-d_6, 400 MHz, r.t.): δ [ppm] = 10.49 (s, 2H, H11, H12), 7.99 – 7.81 (m, 8H, H1, H2, H7, H16), 7.59 (t, $^3J_{H17H16}$ = 7.3 Hz, 1H, H17), 7.53 (d, $^3J_{H15H16}$ = 7.7 Hz, 2H, H15), 7.46 (d, $^3J_{H8H7}$ = 8.3 Hz, 2H, H8), 4.86 (s, 2H, H5).

13C-NMR (DMSO-d_6, 101 MHz, r.t.): δ [ppm] = 167.70 (C4), 165.78 (C10, C13), 165.51 (C10, C13), 140.47 (C6), 134.58 (C1), 132.55 (C3), 131.83 (C14, C9), 131.71 (C9, C14), 131.59 (C17), 128.49 (C15), 127.78, 127.41 (C16), 127.31 (C7), 123.27 (C2), 40.62 (C5).

MS (EI): $[M]^{+\cdot}$ 435.0 (93), 437.0 (59), 439 (9); $[M-C_7H_5ClN]^{\cdot}$ 297.0 (100).

Explanatory remark: Product was verified by mass spectrometry (EI) with reference to the isotopic fingerprint of chloride. Due to solubility problems DMSO-d_6 had to be used for NMR measurements and the acid chloride was hydrolyzed during measurements.

5.1.2.16 Synthesis 4-(6-phenyl-1,2,4,5-tetrazin-3-yl)-benzenemethanamine (20a)

68 (1.0 eq., 0.63 mmol, 0.28 g) was solved in hydrazine hydrate (aq., 80%, 10 mL) and stirred for 3 h at 90 °C. After cooling to room temperature, the precipitate was filtered off, washed with ice-cold water (5 mL) and dried *in vacuo*. The crude product was directly solved in AcOH (8 mL) and NaNO$_2$ (1.5 eq., 0.95 mmol, 0.66 g) was added slowly. After stirring for 20 min at room temperature, the solvent was removed under reduced pressure and the product was purified by column chromatography (DCM/MeOH, 4/1, v/v). **20a** (0.50 mmol, 0.13 g, 80%) was yielded as pink solid.
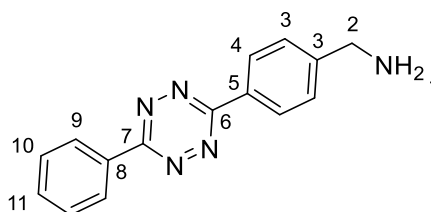
Chemical formula: $C_{15}H_{13}N_5$; MW: 263.3

1H-NMR (DMSO-d_6, 400 MHz, r.t.): δ [ppm] = 8.53 (dd, $^3J_{H9H10}$ = 7.5, $^4J_{H9H11}$ = 1.9 Hz, 2H, H9), 8.48 (d, $^3J_{H4H3}$ = 8.2 Hz, 2H, H4), 7.74 – 7.62 (m, 5H, H3, H10, H11), 3.94 (s/br, 2H, H1), 3.89 (s, 2H, H2).

5.1.2.17 Synthesis of 3-((1,3-dihydro-1,3-dioxo-2*H*-isoindol-2-yl)methyl)-benzoic acid (70i)

3-(aminomethyl)-benzoic acid (1.0 eq., 6.66 mmol, 1.00 g) was dissolved in AcOH (25 mL) and after the addition of phthalic anhydride (3.0 eq., 19.8 mmol, 2.93 g) the reaction was refluxed for 3 h. After cooling to room temperature the solvent was removed under reduced pressure. Purification of the product was done via column chromatography (DCM) and after drying *in vacuo*. **70i** (4.66 mmol, 1.31 g, 70%) was yielded as colorless solid.
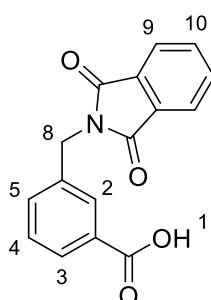
Chemical formula: $C_{16}H_{11}NO_4$; **MW**: 281.1; **R$_f$** (DCM): 0.7.

^{1}H-NMR (DMSO-*d$_6$*, 400 MHz, r.t.): δ [ppm] = 13.43 (s/br, 1H, H1), 8.31 – 8.19 (m, 2H, H9), 8.15 – 8.04 (m, 2H, H10), 7.79 – 7.72 (m, 2H, H3, H5), 7.66 – 7.62 (m, 2H, H2, H4), 3.79 (s, 2H, H8).

5.1.2.18 Synthesis of 3-((1,3-dihydro-1,3-dioxo-2*H*-isoindol-2-yl)methyl)-benzoyl chloride (70)

70i (1.0 eq., 3.56 mmol, 1.00 g) was dissolved in SOCl$_2$ (3.87eq., 13.8 mmol, 10 mL) and refluxed for 1 h at 90 °C. After cooling to room temperature the solvent was distilled off. The crude product was washed with DCM (2 x 5 mL) and dried *in vacuo*. **70** (2.99 mmol, 0.90 g, 84%) was yielded as off-white solid.
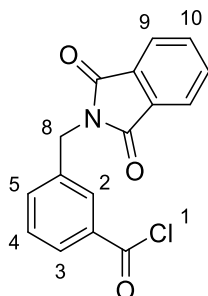
Chemical formula: $C_{16}H_{10}ClNO_4$; **MW**: 299.7.

¹H-NMR (DMSO-d_6, 400 MHz, r.t.): δ [ppm] = 10.43 (s/br, 1H, H1), 8.17 – 7.78 (m, 6H, H4, H10, H11), 7.41 (d, $^3J_{H5H4}$ = 8.5 Hz, 2H, H5), 4.83 (s, 2H, H7).

5.1.2.19 Synthesis of *N'*-(3-(1,3-dioxo-1,3-dihydro-isoindol-2-ylmethyl)-benzoyl)-hydrazide benzoic acid (71)

The synthesis was carried out to the procedure described by Chen.[91] **70** (1.0 eq., 2.99 mmol, 0.90 g) was dissolved in DCM (10 mL) and drop wise added to a stirred solution of benzhydrazide (1.1 eq., 3.59 mmol, 0.49 g) and NEt3 (2.0 eq., 5.98 mmol, 0.83 mL) in DCM (30 mL) and stirred for 2 h at room temperature. The colorless precipitate was filtered off and washed with DCM (2 x 20 mL) and dried *in vacuo*. **71** (2.18 mmol, 0.87 g, 73%) was yielded as colorless solid.
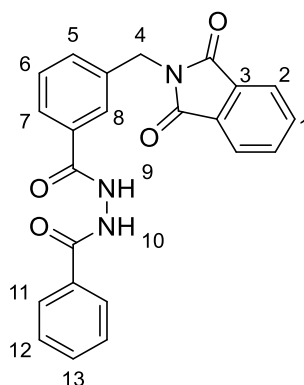
Chemical formula: $C_{23}H_{17}N_3O_4$; **MW**: 399.4

¹H-NMR (DMSO-d_6, 400 MHz, r.t.): δ [ppm] = 10.49 (s, 2H, H11, H12), 7.99 – 7.81 (m, 8H, H1, H2, H7, H16), 7.59 (t, $^3J_{H17H16}$ = 7.3 Hz, 1H, H17), 7.53 (d, $^3J_{H15H16}$ = 7.7 Hz, 2H, H15), 7.46 (d, $^3J_{H8H7}$ = 8.3 Hz, 2H, H8), 4.86 (s, 2H, H5).

5.1.3 Synthesis of 1′-(β-D-Ribofuranosyl)6H-thieno-[2,3-c]-4-[5-(5-norbornene-2-exo-methoxy)-pent-1-ynyl]pyridine-7-thione-5′-triphosphate (76)

The synthesis was adapted to the procedure described by Tor.[59] All solutions were freshly prepared or distilled under Argon atmosphere and/or stored over molecular sieve (4 Å). Under an inert atmosphere nucleoside **75** (1.0 eq., 0.09 mmol, 42 mg) and proton sponge (1.0 eq., 0.09 mmol, 18.4 mg) were solved in $OP(OMe)_3$ (0.50 mL) and cooled to 0 °C. After the slow addition of $POCl_3$ (2.5 eq., 0.22 mmol, 0.02 mL) the reaction was stirred for 6 h under ice-cold conditions. NBu_3 (10.5 eq., 0.95 mmol, 0.22 mL) and (n-$Bu_3NH)_2H_2P_2O_7$ (0.5 M in DMF, 5.4 eq., 0.47 mmol, 0.95 mL) were added simultaneously in a rapid manner and the reaction was subsequently stirred for 15 min at 0 °C. The reaction was stopped by the addition of TEAB (1.0 M, 6.30 mL). Extraction with EE (20 mL) and evaporation of the aqueous layer at room temperature gave the crude product. The crude product was dissolved in H_2O (16 mL) and transferred into centrifuge tubes. After the addition of NaCl (aq., 3.0 M, 1.80 mL) and EtOH (abs., 54.0 mL) the tubes were shaken vigorously. The solution was cooled to -80 °C for one hour and afterwards centrifuged for 40 min at 3200 rcf. The supernatant was removed and after freeze drying the crude product was yielded as sodium salt pellet. Triphosphate **76** (14.1 µmol, 10.2 mg, 15%) was purified via HPLC (analytical cleaning: 10 → 22%B in 20 min; A: 20 mM NH_4OAc; B: 20 mM NH_4OAc/MeCN 1/1 *v/v*).
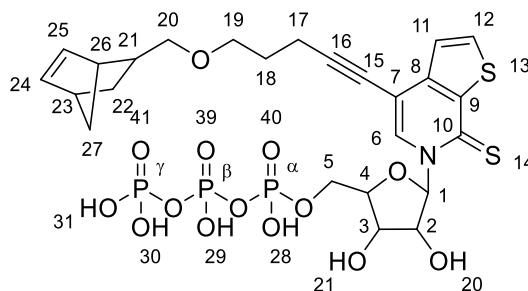
Chemical formula: $C_{25}H_{29}NO_{14}P_3S_2$; **MW**: 725.6

^{1}H-NMR (D_2O, 400 MHz, r.t.): δ [ppm] = 8.41 (s; 1H; H6), 8.14 (d, $^3J_{H12H11}$ = 5.3 Hz, 1H, H12), 7.62 (d, $^3J_{H11H12}$ = 5.3 Hz, 1H, H11), 7.16 (d, $^3J_{H1H2}$ = 2.1 Hz, 1H, H1), 6.06 (dd, $^3J_{H24H25}$ = 5.4 Hz, $^3J_{H24H23}$ = 2.9 Hz, 1H, H24, H25), 5.99 (dd, $^3J_{H25H24}$ = 5.5 Hz, $^3J_{H25H26}$ = 2.6 Hz, 1H, H25, H24), 4.50 - 4.40 (m, 5H, H2, H3, H4, H5a, H5b), 3.82 - 3.70 (m, 2H, H19), 3.49 (m, 1H, H20a, H20b), 3.37 (td, $^2J_{H20bH20a}$ = 10.0 Hz, $^3J_{H20bH21}$ = 1.7 Hz, 1H, H20b, H20a), 2.75 (s, 1H, H26, H23), 2.67 (t, $^3J_{H17H18}$ = 6.8 Hz, 2H, H17), 2.66 (s, 1H, H23, H26), 1.97 (p, $^3J_{H18H17}$ = 6.6 Hz, $^3J_{H18H19}$ = 6.6 Hz, 2H, H18), 1.64 - 1.57 (m, 1H, H21), 1.21 – 1.08 (m, 4H, H27a, H27b, H22a, H22b).

31P-NMR (D$_2$O, 162 MHz, r.t.): δ [ppm] = -10.19 (d, $^2J_{P\gamma P\beta}$ = 20.0 Hz, Pγ), -10.73 (d, $^2J_{P\alpha P\beta}$ = 20.4 Hz, Pα), -22.55 (dd, $^2J_{P\beta P\alpha}$ = 20.1 Hz, $^2J_{P\beta P\gamma}$ = 20.1 Hz, Pβ).

HR MS (ESI$^-$): calc. for [M]$^{2-}$ 373.5075; found: m/z = 373.5044.

5.1.4 Synthesis of dTPT3-TP

5.1.4.1 Synthesis of 1′-chloro-3′,5′-di-*O*-(*p*-chlorbenzoyl)-2′-deoxy-*α/β*-ribose (78)

The synthesis was adapted from literature.[320] Under an inert atmosphere, 2′-deoxyribose (1.0 eq., 37.3 mmol, 5.00 g) was solved in MeOH (anhydr., 80 mL) and HCl (1.25 N in MeOH, 1.30 mL) was added. The resulting mixture was stirred for 1 h at room temperature. After neutralization with pyridine (35 mL) the solution was evaporated to dryness. Co-evaporation with pyridine (15 mL) was carried out twice. Reaction control by TLC (DCM/MeOH, 10/1, v/v, R_f = 0.2) showed quantitative conversion to methylated intermediate. Without further purification, intermediate was solved in pyridine (80 mL) and chilled to 0 °C. Toluolchloride (2.4 eq., 89.5 mmol, 11.8 mL) was added slowly under ice-cold conditions and the reaction was warmed to room temperature overnight. The solution was poured on a mixture of H_2O/DCM (250 mL, 2/3, v/v). After phase separation the organic layer was washed with $NaHCO_3$ (aq., sat, 100 mL), H_2O (100 mL), H_2SO_4 (3 N, 100 mL) and H2O (100 mL). After drying over $MgSO_4$ and removal of solvent under reduced pressure, the resulting oily intermediate was dissolved in glacial acetic acid (26 mL). The solution was added slowly to a saturated solution of HCl in acetic acid (40.8 mL, prepared by adding 6.60 mL acetyl chloride to a solution of 32.8 mL glacial acetic and 1.60 mL water). Precipitated crystals were filtered off, washed with cold Et_2O (50.0 mL) and dried *in vacuo*. The protected ribose derivative **78** (9.35 g, 24.1 mmol, 65%) was yielded as colorless crystalline solid.
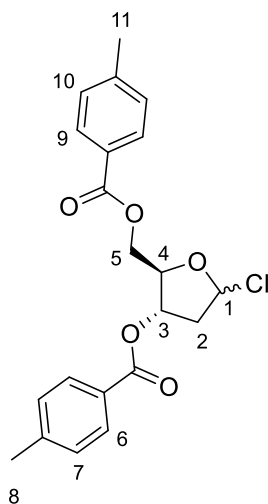
Chemical formula: $C_{21}H_{21}ClO_5$; **MW**: 388.8.

^{1}H-NMR (CDCl$_3$, 400 MHz, r.t.): δ [ppm] = 7.99 (d, $^3J_{H6H7/H9H10}$ = 8.2 Hz, 2H, H6, H9), 7.90 (d, $^3J_{H9H10/H6H7}$ = 8.2 Hz, 2H, H9, H6), 7.26 (d, $^3J_{H7H6/H10H9}$ = 8.0 Hz, 2H, H7, H10), 7.24 (d, $^3J_{H10H9/H7H6}$ = 8.0 Hz, 2H, H10, H7), 6.47 (d, $^3J_{H1H2}$ = 5.1 Hz, 1H, H1), 5.61 – 5.54 (m, 1H, H3), 4.86 (dt, $^3J_{H4H5}$ = 4.2 Hz, $^3J_{H4H5}$ = 3.1 Hz, 1H, H4), 4.68 (dd, $^2J_{H5H5}$ = 12.1 Hz,

$^3J_{H5H4}$ = 3.3 Hz, 1H, H5), 4.60 (dd, $^2J_{H5H5}$ = 12.1 Hz, $^3J_{H5H4}$ = 4.3 Hz, 1H, H5), 2.92 – 2.71 (m, 1H, H2), 2.42 (s, 3H, H8, H11), 2.41 (s, 3H, H11, H8).

5.1.4.2 Synthesis of 2-Hydroxymethyl-5-methoxy-tetrahydro-furan-3,4-diol (80)

The synthesis was carried out to the procedure described by Romesberg.[274] Under an inert atmosphere, thieno(2,3-*c*)pyridin-7(6*H*)-one **79** (1.0 eq., 3.31 mml, 500 mg) was solved in DCM (anhydr., 20 mL) and stirred for 5 min at room temperature. After the BSA (1.1 eq., 3.64 mmol, 0.89 mL) addition the solution was stirred for 40 min, ribose derivative **78** (1.5 eq., 4.97 mmol, 1.93 g) was added and the reaction mixture was cooled to 0 °C. Under ice-cold conditions SnCl$_4$ (0.5 eq., 1.66 mmol, 0.19 mL) was added dropwise and the reaction was warmed to room temperature overnight. The reaction was diluted with EE (50 mL) and water (50 mL). After phase separation the organic layer was washed with water (40 mL) and saturated aqueous NaCl (25 mL). Subsequently the organic layer was dried over MgSO$_4$ and the solvent was removed under reduced pressure. Product **80** was purified by column chromatography (Cy/EE, 6/4, v/v) and yielded as colorless solid (1.34 mmol, 674 mg, 41%).
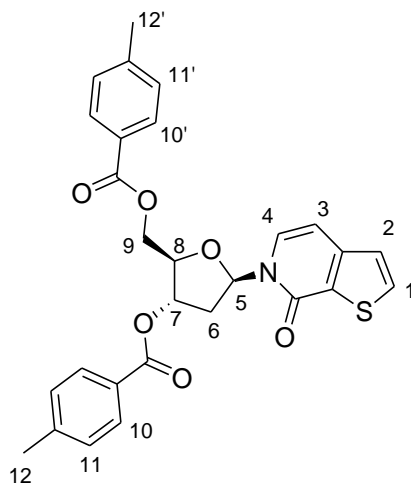
Chemical formula: C$_{26}$H$_{21}$NO$_6$S; **MW**: 475.5; **R$_f$** (Cy/EE 6:4 v/v): 0.5.

^{1}H-NMR (CDCl$_3$, 400 MHz, r.t.): δ [ppm] = 7.97 (d, $^3J_{H10H11/H10'H11}$ = 8.2 Hz, 2H, H10, H10'), 7.91 (d, $^3J_{H10H11/H10'H11'}$ = 8.2 Hz, 2H, H10, H10'), 7.70 (d, $^3J_{H4H3}$ = 5.1 Hz, 1H, H2), 7.56 (d, $^3J_{H4H3}$ = 7.3 Hz, 1H, H4), 7.28 (d, $^3J_{H11H10/H11'H10'}$ = 8.1 Hz, 2H, H11, H11'), 7.22 (d, $^3J_{H11H10/H11'H10'}$ = 8.0 Hz, 2H, H11, H11'), 7.17 (d, $^3J_{H3H4}$ = 5.1 Hz, 1H, H1), 6.89 – 6.76 (m, 1H, H5), 6.57 (d, $^3J_{H3H4}$ = 7.3 Hz, 1H, H3), 5.65 (dt, $^3J_{H8H7}$ = 6.7 Hz, $^3J_{H8H6/H7H8}$ = 1.9 Hz, 1H, H8), 4.76 (dd, $^2J_{H9H9}$ = 12.1 Hz, $^3J_{H9H8}$ = 3.4 Hz, 1H, H9), 4.71 (dd, $^2J_{H9H9}$ = 12.1 Hz, $^3J_{H9H8}$ = 3.6 Hz, 1H, H9), 4.63 – 4.59 (m, 1H, H7), 2.96 – 2.88 (m, 1H, H6), 2.44 (s, 3H, H12, H12'), 2.40 (s, 3H, H12, H12'), 2.38 – 2.33 (m, 1H, H6).

5.1.4.3 Synthesis of 2-Hydroxymethyl-5-methoxy-tetrahydro-furan-3,4-diol (81, dTPT3)

The synthesis was carried out according to a procedure described by Romesberg.[274] Under inert gas atmosphere the toluoyl protected nucleoside precursor **80** (1.0 eq., 0.99 mmol, 500 mg) and Lawesson's reagent (1.2 eq., 1.19 mmol, 481 mg) were solved in toluene (anhydr., 10.0 mL). The reaction mixture was stirred at 120 °C. After 4 h reaction TLC (Cy/EE, 60/40, v/v) showed no further conversion, so the solvent was removed under reduced pressure and the crude product was dried *in vacuo*. Verification was only carried out by crude mass spectrometry (**MS** (ESI$^+$): calc. for [M+Na]$^+$ 542.1, found m/z = 542.1). The crude product was submitted to the next step without further purification. Therefore it was solved in MeOH (anhydr., 10.0 mL) under an Argon atmosphere. NaOEt (21% w/v in EtOH, 13.7 mL) was added dropwise at room temperature and the reaction was stirred for 2 h. Subsequently the crude mixture was dried *in vacuo* and purified by column chromatography (Cy/EE, 3/7, v/v) to yield the unprotected nucleoside **81** (0.064 mmol, 18.2 mg, 6.5% over two steps) as yellow oil.
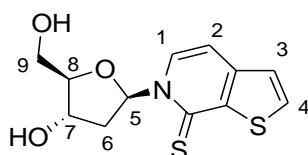
Chemical formula: $C_{12}H_{13}NO_3S_2$; **MW**: 283.4; **R$_f$** (Cy/EE, 3/7, v/v): 0.3.

^{1}H-NMR (MeOD, 400 MHz, r.t.): δ [ppm] = 8.45 (d, $^3J_{H1H2}$ = 7.2 Hz, 1H, H1), 7.98 (d, $^3J_{H4H3}$ = 5.3 Hz, 1H, H4), 7.37 (d, $^3J_{H3H4}$ = 5.3 Hz, 1H, H3), 7.35 (d, $^3J_{H5H6}$ = 6.4 Hz, 1H, H5), 7.27 (d, $^3J_{H2H1}$ = 7.3 Hz, 1H, H2), 4.44 (dt, $^3J_{H7H6}$ = 6.4 Hz, $^3J_{H7H8}$ = 4.3 Hz, 1H, H7), 4.09 – 4.04 (m, 1H, H8), 3.92 (dd, $^2J_{H9H9}$ = 12.1 Hz, $^3J_{H9H8}$ = 3.2 Hz, 1H, H9), 3.84 (dd, $^2J_{H9H9}$ = 12.1 Hz, $^3J_{H9H8}$ = 3.9 Hz, 1H, H9), 2.75 (ddd, $^2J_{H6H6}$ = 13.7 Hz, $^3J_{H6H5}$ = 6.3 Hz, $^3J_{H6H7}$ = 4.4 Hz, 1H, H6), 2.17 – 2.10 (m, 1H, H6).

HR MS (ESI$^+$): calc. for $C_{12}H_{14}NO_3S_2$: 284.0410, measured 284.0405.

5.1.4.4 Synthesis of dTPT3-TP (82)

The synthesis was carried out analogous to the procedure described by Romesberg.[274] All reagents were freshly prepared or freshly distilled under Argon atmosphere and further dried over molecular sieve (4Å). Under an inert atmosphere nucleoside **81** (1.0 eq., 0.05 mmol, 13.0 mg) and proton sponge (1.0 eq., 0.05 mmol, 11.0 mg) were solved in OP(OMe)$_3$ (anhydr., freshly dist., stored over molecular sieve 4Å, 0.23 mL) and cooled to 0 °C. After the slow addition of POCl$_3$ (anhydr., freshly dist., 2.5 eq., 0.12 mmol, 0.01 mL) the reaction was stirred for 6 h under ice-cold conditions. NBu$_3$ (anhydr., stored over molecular sieve 4Å, 10.5 eq., 0.48 mmol, 0.12 mL) and (*n-*

Bu$_3$NH)$_2$H$_2$P$_2$O$_7$ (0.5 M in DMF) (5.4 eq., 0.25 mmol, 0.50 mL) were added simultaneously in a rapid manner and the reaction was subsequently stirred for 30 min at 0 °C. The reaction was stopped by the addition of TEAB (1.0 M, 3.5 mL). The reaction mixture was freeze-dried and triphosphate **82** (1.47 mg, 2.81 µmol, 6%) was purified via HPLC cleaning (preparative cleaning: 10 → 40%B in 10 min; analytical cleaning: 10 → 22%B in 15 min; A: 0.1 M TEAB; B: MeCN).
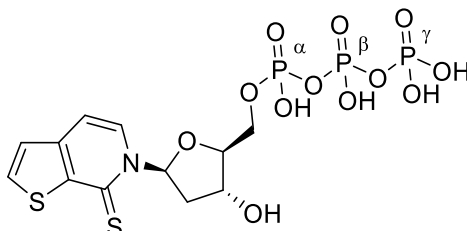
Chemical formula: C$_{14}$H$_{20}$NO$_{10}$P$_3$S$_2$; **MW**: 523.3

^{31}P-NMR (D$_2$O, 162 MHz, r.t.): δ [ppm] = -9.75 (d, $^2J_{P\gamma P\beta}$ = 19.7 Hz, Pγ), -10.68 (d, $^2J_{P\alpha P\beta}$ = 19.8 Hz, Pα), -22.39 (dd, $^2J_{P\beta P\alpha}$ = 19.8 Hz, $^2J_{P\beta P\gamma}$ = 19.8 Hz, Pβ).

5.1.5 Synthesis of dNaM-TP

5.1.5.1 Synthesis of 2-deoxy-3,5-*O*-(1,1,3,3-tetrakis(1-methylethyl)-1,3-disiloxanediyl)-D-*erythro*-pentofuranoside (84)

Under an inert atmosphere 2-deoxyribose (1.0 eq., 22.4 mmol, 3.00 g) was solved in pyridine (anhydr., 60 mL) and cooled to 0 °C. TIDPS-Cl$_2$ (1.2 eq., 26.9 mmol, 8.52 mL) was added dropwise under ice-cold conditions. The reaction was warmed to room temperature overnight. After diluting the reaction mixture with EE (50 mL) and water (50 mL), extracting the aqueous layer and phase separation, organic layer was washed with NaCl (aq., sat., 25 mL), and the solvent was removed under reduced pressure. The crude product was purified via column chromatography (Cy/EE, 4/1, *v/v*) to yield the protected ribose **84** (9.01 mmol, 3.39 g, 40%) as colorless oil. ^{1}H-NMR analytics show two datasets due to hemiacetal formation. Verification was carried out only by mass spectrometry.
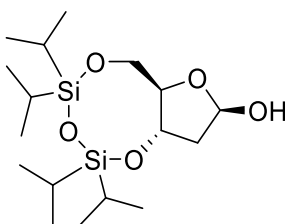
Chemical formula: C$_{17}$H$_{36}$O$_5$Si$_2$; **MW**: 376.2, **R$_f$** (Cy/EE, 4:1 *v/v*) = 0.4.

MS (ESI$^+$): calculated for [M+Na]$^+$: 399.2; found: *m/z* = 399.2

5.1.5.2 Synthesis of 1,4-anhydro-2-deoxy-1-*C*-(3-methoxy-2-naphthalenyl)-D-*erythro*-pentitol (86, dNaM)

The synthesis was carried out analogous to a procedure described by Romesberg.[271] Under an inert atmosphere the silylether protected sugar **84** (1.0 eq., 2.66 mmol, 1.00 g) was solved in THF (anhydr., 2.50 mL). Simultaneously methoxy naphthalene was solved in THF (anhydr., 20 mL) and cooled to 0 °C. Under ice-cold conditions *n*-BuLi (3.1 eq., 8.25 mmol, 5.20 mL) was added dropwise and the reaction was warmed to room temperature. After stirring for 1 h at room temperature, the reaction was cooled to -10 °C and the solved sugar derivative was added dropwise. Subsequent warming to room temperature was performed overnight. The reaction was diluted using EE (50 mL) and NH$_4$Cl (aq., sat., 50 mL). After phase separation, the organic layer was washed with NaCl (aq., sat.), dried over MgSO$_4$, and the solvent was removed under reduced pressure. As described by Romesberg and coworkers, the crude residue was purified via

column chromatography (Cy/EE, 3/1, v/v) and the intermediate of the nucleoside **85** was isolated as yellowish oil (**R_f** = 0.3, 0.66 mmol, 353 mg, 25%). The isolated intermediate (350 mg) was dissolved in THF (anhydr., 10 mL) under an inert atmosphere. After the addition of *n*-Bu$_3$P (1.5 eq. according to the isolated intermediate, 0.99 mmol, 0.24 mL) the resulting solution was cooled to 0 °C and TMAD (1.5 eq. according to the isolated intermediate, 0.99 mmol) was added at 0 °C. After warming to room temperature overnight TBAF trihydrate (5.0 eq. according to the isolated intermediate, 3.13 mmol, 1.04 g) was added. The reaction was stirred at room temperature for 2 h, before the crude product was diluted with NaHCO$_3$ (50 mL) and extracted with EE (3 x 50 mL). After phase separation, the organic layer was washed with NaCl (aq., sat.) and dried over MgSO$_4$. After removal of solvent under reduced pressure, product **86** (0.31 mmol, 84 mg, 12% over two steps) was purified by column chromatography (EE) and isolated as colorless solid.
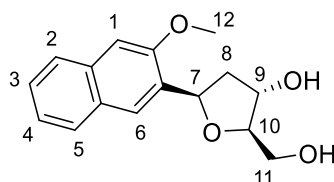
Chemical formula: C$_{16}$H$_{18}$O$_4$; **MW**: 274.3; **R_f** (EE) = 0.4

^{1}H-NMR (MeOD, 500 MHz, r.t.): δ [ppm] = 7.99 (t, $^4J_{H6H5}$ = 0.9 Hz, 1H, H6), 7.75 (m, 2H, H2, H5), 7.38 (ddd, $^3J_{H3H2}$ = 8.2 Hz, $^3J_{H3H4}$ = 6.9 Hz, $^4J_{H3H1}$ = 1.3 Hz, 1H, H3), 7.30 (ddd, $^3J_{H4H5}$ = 8.1 Hz, $^3J_{H4H3}$ = 6.9 Hz, $^4J_{H4H6}$ = 1.3 Hz, 1H, H4), 7.21 (s, 1H, H1), 5.49 (dd, $^3J_{H7H8}$ = 10.0 Hz, $^3J_{H7H8}$ = 5.7 Hz, 1H, H7), 4.33 – 4.30 (m, 1H, H9), 4.02 – 3.97 (m, 1H, 9), 3.94 (s, 3H, H12), 3.82 – 3.67 (m, 2H, H11), 2.48 – 2.41 (m, 1H, H8), 1.88 – 1.79 (m, 1H, H8).

5.1.5.3 Synthesis of dNaM-TP (87)

The synthesis was carried out analogous to the procedure described by Romesberg.[271] The nucleoside was purchased by Berry & Associates. All solutions were freshly prepared or distilled under Argon atmosphere and/or stored over molecular sieve (4 Å). Under an inert atmosphere nucleoside **86** (1.0 eq., 0.10 mmol, 25 mg) and proton sponge (1.0 eq., 0.10 mmol, 19.5 mg) were solved in OP(OMe)$_3$ (0.53 mL) and cooled to 0 °C. After the slow addition of POCl$_3$ (2.5 eq., 0.23 mmol, 0.02 mL) the reaction was stirred for 6 h under ice-cold conditions. NBu$_3$ (11.0 eq., 1.01 mmol, 0.24 mL) and (n-Bu$_3$NH)$_2$H$_2$P$_2$O$_7$ (0.5 M in DMF, 5.5 eq., 0.50 mmol, 1.00 mL) were added simultaneously in a rapid manner and the reaction was subsequently stirred for 30 min at 0 °C. The reaction was stopped by the addition of TEAB (1.0 M, 7.15 mL). The reaction mixture

was freeze-dried and triphosphate **87** (0.01 mmol, 5.10 mg, 11%) was purified via HPLC (preparative cleaning: 10 → 40%B in XX min; analytical cleaning: 10 → 22%B in XX min; A: 0.1 M TEAB (aq.); B: MeCN).
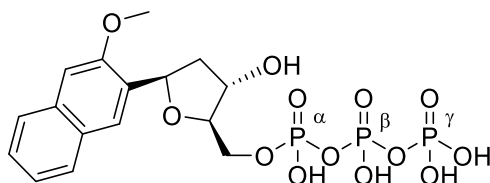
Chemical formula: $C_{16}H_{21}O_{14}P_3$; **MW**: 514.0

^{31}**P-NMR** (D$_2$O, 500 MHz, r.t.): δ [ppm] = -9.71 (d, $^2J_{P\gamma P\beta}$ = 22.0 Hz, Pγ), -10.44 (d, $^2J_{P\alpha P\beta}$ = 20.0 Hz, Pα), -22.43 (dd, $^2J_{P\beta P\alpha}$ = 20.4 Hz, $^2J_{P\beta P\gamma}$ = 20.4 Hz, Pβ)

HR MS (ESI$^-$): calc. for [M-H]$^-$: 513.0122; found: m/z = 513.0119.

5.1.6 Synthesis of NaM-TP

5.1.6.1 Synthesis of 2-Hydroxymethyl-5-methoxy-tetrahydro-furan-3,4-diol (89)

Under an argon atmosphere β-D-ribofuranose (1.0 eq., 33.3 mmol, 5.00 g) was dissolved in MeOH (anhydr., 50 mL) and cooled to 0 °C. Under argon counters current DOWEX® 50 (H^+ form, 15%, w/w, 0.75 g) was added slowly and the reaction mixture was stirred overnight at 4 °C. The resin was filtered off and washed with MeOH. The solvent was removed under reduced pressure and the crude product was dried *in vacuo*. After purification via column chromatography (EE/EtOH, 4/1, v/v) **89** (24.0 mmol, 3.93 g, 72%) was isolated as colorless oil.
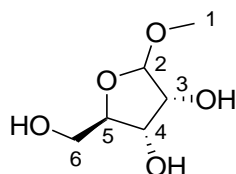
Chemical formula: $C_6H_{12}O_5$; **MW**: 164.2; **R$_f$** (EE/EtOH, 4/1, v/v): 0.6.

^{1}H-NMR (MeOD, 400 MHz, r.t.): δ [ppm] = 4.74 (d, $^3J_{H2H3}$ = 1.0 Hz, 1H, H2), 4.02 (dd, $^3J_{H4H5}$ = 6.9, $^3J_{H4H3}$ = 4.7 Hz, 1H, H4), 3.93 (td, $^3J_{H5H4/H5H6}$ = 6.7 Hz, $^3J_{H5H6}$ = 3.5 Hz, 1H, H5), 3.86 (dd, $^3J_{H3H4}$ = 4.6 Hz, $^3J_{H3H2}$ = 1.0 Hz, 1H, H3), 3.71 (dd, $^2J_{H6H6}$ = 11.8 Hz, $^3J_{H6H5}$ = 3.5 Hz, 1H, H6), 3.53 (dd, $^2J_{H6H6}$ = 11.8 Hz, $^3J_{H6H5}$ = 6.4 Hz, 1H, H6), 3.34 (s, 3H, H1).

5.1.6.2 Synthesis of 2-Hydroxymethyl-5-methoxy-tetrahydro-furan-3,4-diol (90)

The synthesis was carried out to the procedure described by Brown.[325] Under an atmosphere of argon ribose **89** (1.0 eq., 14.0 mmol, 2.20 g) was dissolved in DMF (anhydr., 30 mL) and cooled to 0 °C. Under argon counters current NaH (60% in mineral oil, 6.0 eq., 83.7 mmol, 3.35 g as dispersion) was added portion wise at 0 °C and the reaction mixture was stirred under ice-cold conditions for 30 minutes. The reaction was warmed to room temperature overnight under stirring. The reaction was quenched with water (3.00 mL) and the crude product was dried *in vacuo*. The dried solid was dissolved in DCM (30 mL), washed with HCl (aq., 0.5%, 50 mL), $NaHCO_3$ (aq., sat., 30 mL), water (50 mL), and NaCl (aq., sat., 50 mL). After the layers have been separated, the organic layer was dried over $MgSO_4$ and the solvent was removed under reduced pressure. The crude product was purified by column chromatography (DCM) and **90** (7.79 mmol, 3.38 g, 56%) was isolated as colorless oil.
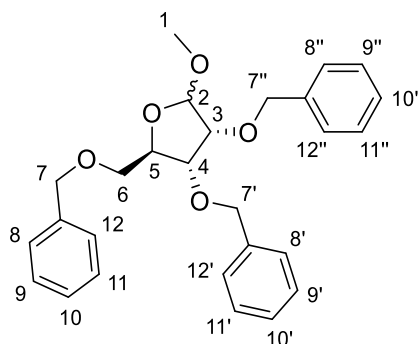
Chemical formula: $C_{27}H_{30}O_5$; **MW**: 434.5; **R$_f$** (DCM): 0.5.

¹H-NMR (CDCl$_3$, 400 MHz, r.t.): δ [ppm] = 7.41 – 7.23 (m, 15H, H8, H8′ H8″, H9, H9′, H9″, H10, H10′, H10″, H11, H11′, H11″, H12, H12′, H12″), 4.93 (d, $^3J_{H2H3}$ = 1.3 Hz, H2), 4.68 (d, $^2J_{H7'H7'/H7''H7''/H7H7}$ = 12.1 Hz, 1H, H7′,H7″, H7), 4.62 (d, $^2J_{H7''H7''/H7'H7'/H7H7}$ = 12.1 Hz, 1H, H7″, H7′, H7), 4.58 – 4.54 (m, 3H, H7, H7′, H7″), 4.46 (d, $^2J_{H7H7/H7'H7'/H7''H7''}$ = 11.9 Hz, 1H, H7, H7′, H7″), 4.35 (ddd, $^3J_{H5H4}$ = 7.1 Hz, $^3J_{H5H6}$ = 5.8 Hz, $^3J_{H5H6}$ = 3.7 Hz, 1H, H5), 4.03 (dd, $^3J_{H4H5}$ = 7.1 Hz, $^3J_{H4H3}$ = 4.7 Hz, 1H, H4), 3.85 (dd, $^3J_{H3H4}$ = 4.7 Hz, $^3J_{H3H2}$ = 1.2 Hz, 1H, H3), 3.62 (dd, $^2J_{H6H6}$ = 10.6 Hz, $^3J_{H6H5}$ = 3.8 Hz, 1H, H6), 3.52 (dd, $^2J_{H6H6}$ = 10.6 Hz, $^3J_{H6H5}$ = 5.8 Hz, 1H, H6), 3.32 (s, 3H, H1).

5.1.6.3 Synthesis of 2-Hydroxymethyl-5-methoxy-tetrahydro-furan-3,4-diol (92)

The synthesis was carried out to the procedure described by Fletcher and Codée.[326] The fully protected ribose **90** (1.0 eq., 8.57 mmol, 3.73 g) was dissolved in 1,4-dioxane (70 mL) and 0.2 M HCl (aq., 34 mL). The reaction was gently boiled for 3 h at 100 °C. The solution was neutralized with NaHCO$_3$ (aq., sat.) after cooling to room temperature and subsequently extracted with DCM (3 x 75 mL). The organic layer was separated, washed with saturated aqueous NaCl and dried over MgSO$_4$. After removal of the solvent, the crude product was dried *in vacuo* and used for the next step without further purification. The crude intermediate was solved in DMSO (anhydr., 12 mL) under an atmosphere of argon and cooled to 4 °C. Acetic anhydride (8.00 mL) was added slowly and the reaction was stirred at 4 °C for 48 h. The reaction was poured on ice cold water (150 mL) and extracted with EE (3 x 75 mL). The organic layer was washed with water (3 x 50 mL) and NaHCO$_3$ (aq., sat., 75 mL). The organic layer was then dried over MgSO$_4$ and the solvent was removed under reduced pressure. The crude product was purified by column chromatography (DCM) to yield lactone **92** (4.60 mmol, 1.93 g, 53% over two steps) as colorless amorphous solid.
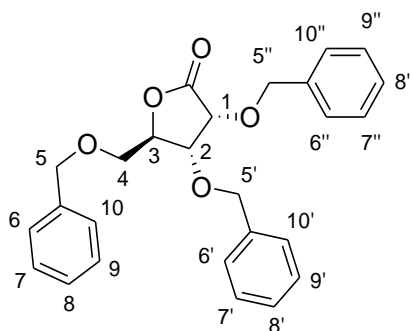
Chemical formula: $C_{26}H_{26}O_5$; **MW**: 418.5; **R$_f$** (DCM): 0.5.

^{1}H-NMR (CDCl$_3$, 400 MHz, r.t.): δ [ppm] = 7.42 – 7.13 (m, 15H, H6, H7, H8, H9, H10, H6′, H7′, H8′, H9′, H10′, H6″, H7″, H8″, H9″, H10″), 4.95 (d, $^2J_{H5'H5'/H5''H5''/H5H5}$ = 12.0 Hz, 1H, H5′, H5″, H5), 4.75 (d, $^2J_{H5''H5''/H5'H5'/H5H5}$ = 11.9 Hz, 1H, H5″, H5′, H5), 4.70 (d, $^2J_{H5H5/H5'H5'/H5''H5''}$ = 11.9 Hz, 1H, H5, H5′, H5″), 4.59 – 4.52 (m, 2H, H3, H5′, H5″, H5), 4.50 (d, $^2J_{H5H5/H5'H5'/H5''H5''}$ = 11.9 Hz, 1H, H5, H5′, H5″), 4.45 – 4.38 (m, 2H, H1, H5, H5′, H5″), 4.10 (dd, J = 5.7 Hz, $^3J_{H2H3}$ = 2.0 Hz, 1H, H2), 3.67 (dd, $^2J_{H4H4}$ = 11.0 Hz, $^3J_{H4H3}$ = 2.9 Hz, 1H, H4), 3.56 (dd, $^2J_{H4H4}$ = 11.0 Hz, $^3J_{H4H3}$ = 2.7 Hz, 1H, H4).

5.1.6.4 Synthesis of (1S)-1,4-Anhydro-1-C-(3-methoxy-2-naphthalenyl)-D-ribitol (96, NaM)

The reaction was carried out to the procedure published by Romesberg and co-workers.[323] Under an atmosphere of argon, the protected 2-methoxynaphthalene **83** (1.8 eq., 0.90 mmol, 151 mg) was dissolved in THF (anhydr., 1.00 mL) and cooled to -40 °C. Under these conditions, *n*-BuLi (1.6 M, 1.8 eq., 0.60 mL) was added dropwise, the reaction mixture was warmed to room temperature and stirred at room temperature for 2 h. Then the reaction was chilled to -12 °C and protected lactone **92** (1.0 eq., 0.50 mmol, 200 mg) was added in an argon countercurrent. The reaction was slowly heated to room temperature and after 1 h stirring at room temperature, the reaction was extracted using EE (25 mL) after NH$_4$Cl (aq., sat., 5 mL) addition. The organic layer was dried over MgSO$_4$ and evaporated under reduced pressure. This crude mixture was dissolved in MeCN (anhydr., 10 mL) under an inert atmosphere. After cooling to -40 °C, HSiEt$_3$ (1.9 eq., 0.95 mmol, 0.15 mL) and subsequent BF$_3$·OEt$_2$ (1.0 eq., 0.50 mmol, 0.51 mL) were added slowly. After warming to ice-cold conditions, the reaction was stopped by the addition of NaHCO$_3$ (aq., sat., 5.00 mL) and extracted with Et$_2$O (10 mL). After drying over MgSO$_4$ and removing the solvent under reduced pressure, the crude mixture was used without further purification. Under inert conditions, the intermediate was solved in DCM (anhydr., 10.0 mL) and cooled to -78 °C. The addition of BBr$_3$ (1.0 eq., 0.50 mmol, 0.08 mL) was carried out at -78 °C and the reaction was kept for three hours at this temperature while being stirred. After the addition of a MeOH/DCM

(1/1, v/v, 5.00 mL) mixture as well as pyridine (1.50 mL) and the evaporation to dryness, the crude product should be purified by column chromatography.
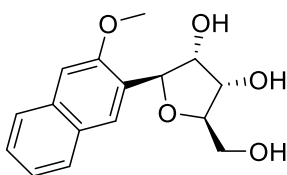
Chemical formula: $C_{16}H_{18}O_5$; **MW**: 290.3

Explanatory remark: The product could not be isolated. Isolated intermediates, relevant data and difficulties are discussed in main text.

5.1.6.5 Synthesis of 6-Hydroxymethyl-2,2-dimethyl-dihydro-furo[3,4-*d*][1,3]dioxol-4-one (101i)

In an overnight reaction D(+)-ribono-1,4-lactone (1.0 eq., 27.0 mmol, 4.00 g) and *p*-toluenesulfonic acid monohydrate (0.06 eq., 1.58 mmol, 0.30 g) were suspended at room temperature in acetone (20.0 eq., 540 mmol 39.7 mL). After quenching the reaction with $NaHCO_3$ (0.10 eq., 2.70 mmol, 0.23 g) the solids were filtered off and the filtrate was dried under reduced pressure. After column chromatography (Cy/EE, 1/2, v/v) the acetonide protected product **101i** (13.0 mmol, 2.44 g, 48%) was dried *in vacuo* and yielded as colorless oil.
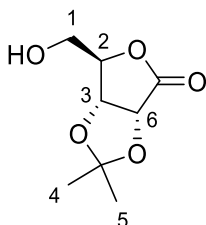
Chemical formula: $C_8H_{12}O_5$; **MW**: 188.2; **R$_f$** (Cy/EE, 1:2 v/v): 0.6.

1H-NMR (CDCl₃, 400 MHz, r.t.): δ [ppm] = 4.83 (d, $^3J_{H6H3/H3H6}$ = 5.6 Hz, 1H, H3, H6), 4.78 (d, $^3J_{H3H6/H6H3}$ = 5.6 Hz, 1H, H6, H3), 4.63 (t, $^3J_{H2H1}$ = 2.0 Hz, 1H, H2), 3.99 (dd, $^2J_{H1H1}$ = 12.2 Hz, $^3J_{H1H2}$ = 2.3 Hz, 1H, H1), 3.81 (dd, $^2J_{H1H1}$ = 12.2 Hz, $^3J_{H1H2}$ = 1.8 Hz, 1H, H1), 1.48 (s, 3H, H4, H5), 1.38 (s, 3H, H5, H4).

5.1.6.6 Synthesis of 6-(tert-Butyl-diphenyl-silanyloxymethyl)-2,2-dimethyl-dihydro-furo[3,4-*d*][1,3]dioxol-4-one (101)

Under an atmosphere of argon, imidazole (2.00 eq., 10.64 mmol, 0.73 g) and lactone **101i** (1.0 eq., 5.32 mmol, 1.00 g) were dissolved in DCM (15 mL). After cooling to 0 °C the TBDPS-Cl (1.1 eq., 5.85 mmol, 1.52 mL) was added drop wise. The reaction was warmed slowly to room temperature and after 3 h the reaction was stopped by the addition of H_2O (10 mL). The phases were separated, the aqueous layer was extracted

with EE (3 x 15 mL), the combined organic layers were dried over Na_2SO_4 and the solvent was evaporated under reduced pressure. The crude product was purified by column chromatography (Cy/EE, 1/4, v/v), dried *in vacuo* and **101** (5.31 mmol, 2.27 g, 99%) was yielded as colorless oil.
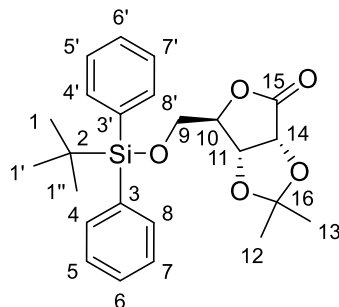
Chemical formula: $C_8H_{12}O_5$; **MW**: 426.6; **R$_f$** (Cy/EE, 4/1, v/v): 0.6.

^{1}H-NMR (CDCl$_3$, 400 MHz, r.t.): δ [ppm] = 7.65 – 7.57 (m, 4H, H5, H5′, H7, H7′), 7.50 – 7.36 (m, 6H, H4, H4′, H6, H6′, H8, H8′), 4.90 (d, $^3J_{H14H11/H11H14}$ = 5.6 Hz, 1H, H14, H11), 4.74 (d, $^3J_{H11H14/H14H11}$ = 5.6 Hz, 1H, H11, H14), 4.58 (t, $^3J_{H10H9}$ = 1.9 Hz, 1H, H10), 3.92 (dd, $^2J_{H9H9}$ = 11.5 Hz, $^3J_{H9H10}$ = 2.3 Hz, 1H, H9), 3.76 (dd, $^2J_{H9H9}$ = 11.5 Hz, $^3J_{H9H10}$ = 1.5 Hz, 1H, H9), 1.49 (s, 3H, H12, H13), 1.40 (s, 3H, H13, H12), 1.05 (s, 9H, H1, H1′, H1″).

HR MS (EI): calc. for [M-CH$_3$]$^{+\cdot}$ 411.1622; found: *m/z* = 411.1627.

5.1.6.7 Synthesis of 2-(*tert*-Butyl-diphenyl-silanyloxy)-1-(5-[hydroxy-(3-methoxy-naphthalen-2-yl)-methyl]-2,2-dimethyl-[1,3]dioxolan-4-yl)-ethanone (102)

The synthesis was carried out analogous to a procedure described by Romesberg.[293] Under an atmosphere of argon, 2-bromo-3-methoxynaphthalene (2.00 eq., 5.64 mmol, 1.34 g) was dissolved in THF (anhydr., 12 mL) and cooled to -78 °C. The *t*-BuLi (1.8 eq., 5.1 mmol, 3.00 mL) was added drop wise and the solution was stirred for 15 minutes under this conditions. The protected lactone **51** (1.0 eq., 2.82 mmol, 1.20 g) was solved in THF (anhydr., 7 mL) under an inert atmosphere and then added slowly to the reaction mixture at -78 °C. The reaction was then stirred for 3 h at this temperature. The reaction was stopped after reaction control via TLC by adding NH$_4$Cl (aq., sat., 10 mL). After warming to room temperature the phases were separated, the aqueous layer was extracted with EE (3 x 10 mL), the combined organic layers were dried over Na_2SO_4 and the solvent was removed under reduced pressure. The crude product was dried *in vacuo* and **52** was obtained as colorless solid/foam and used without further purification. ^{1}H-NMR analytics of the crude product was carried out to verify the intermediate.
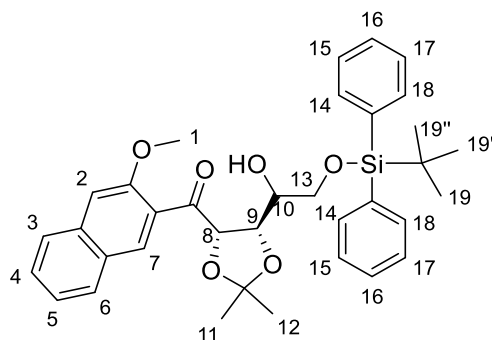
Chemical formula: $C_{35}H_{40}O_6Si$; **MW**: 584.8; **R$_f$** (Cy/EE, 4/1, v/v): 0.4.

^{1}H-NMR (CDCl$_3$, 400 MHz, r.t.): δ [ppm] = 7.82 – 7.73 (m, 7H, Ar), 7.47 – 7.32 (m, 10H, Ar), 5.05 (d, $^3J_{H8H9/H9H8}$ = 5.8 Hz, 1H, H8, H9), 5.02 – 4.97 (m, 1H, H10), 4.93 – 4.85 (m, 1H, H9, H8), 4.55 – 4.45 (m, 2H, H13), 4.01 (s, 3H, H1)1.29 (s, 3H, H12, H11), 1.20 (s, 3H, H11, H12), 1.16 (s, 9H, H19, H19′, H19″).

5.1.6.8 Synthesis of 2-Hydroxymethyl-5-(3-methoxy-naphthalen-2-yl)-tetrahydro-furan-3,4-diol (96, NaM)

The synthesis was carried out analogous to the procedure described by Romesberg.[293] Under an atmosphere of argon, intermediate **52** (1.00 eq., 2.82 mmol, 0.50 g) was dissolved in MeCN (anhydr., 36.0 mL) and cooled to -40 °C. Et$_3$SiH (1.7 eq., 4.79 mmol, 0.73 mL) was added slowly. The BF$_3$·Et$_2$O (1.1 eq., 2.92 mmol, 0.37 mL) was added drop wise after stirring the reaction for 10 min at -40 °C. Subsequently the reaction was stirred for an additional hour at the temperature as stated above. The reaction was quenched by the addition of K$_2$CO$_3$ (aq., sat., 15 mL). The phases were separated, the aqueous layer was extracted with EE (3 x 15 mL), the combined organic layers were dried over Na$_2$SO$_4$, and the solvent was evaporated under reduced pressure. The crude product was purified by column chromatography (EE), dried *in vacuo* and the fully deprotected product **49** (0.58 mmol, 0.17 g, 20%) was yielded as colorless oil.
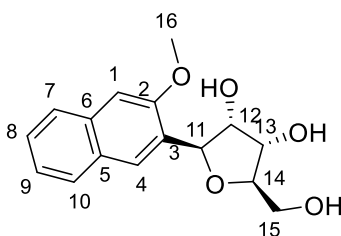
Chemical formula: $C_8H_{12}O_5$; **MW**: 290.3; **R$_f$** (EE): 0.4.

^{1}H-NMR (CDCl$_3$, 500 MHz, r.t.): δ [ppm] = 7.94 (s, 1H, H4), 7.77 (d, $^3J_{H7H8}$ = 8.1 Hz, 1H, H7), 7.71 (d, $^3J_{H10H9}$ = 8.1 Hz, 1H, H10), 7.42 (t, $^3J_{H9H10}$ = 7.5 Hz, 1H, H9), 7.32 (t, $^3J_{H8H7}$ = 7.5 Hz, 1H, H8), 7.06 (s, 1H, H1), 5.38 (d, $^3J_{H11H12}$ = 2.4 Hz, 1H, H11), 4.48 –

4.39 (m, 1H, H12), 4.28 (dd, $^3J_{H13H12}$ = 7.8 Hz, $^3J_{H13H14}$ = 4.3 Hz, 1H, H13), 4.05 – 4.01 (m, 2H, H14), 3.93 – 3.87 (m, 1H, H15), 3.84 (s, 3H, H16), 3.71 (dd, $^2J_{H15H15}$ = 12.0 Hz, $^3J_{H15H14}$ = 3.8 Hz, 1H, H15).

¹³C-NMR (CDCl₃, 126 MHz, r.t.): δ [ppm] = 154.50 (C2), 134.04 (C6), 128.70 (C5), 127.96 (C7), 127.07 (C4), 126.86 (C3), 126.45 (10), 126.42 (C9), 124.02 (C8), 105.05 (C1), 81.89 (14), 79.07 (C11), 73.33 (C13), 72.34 (C12), 62.50 (C15), 55.48 (C16).

HR MS (ESI⁻): calc. for [M-2H+Na]⁻ 313.1046; found: *m/z* = 313.1054.

5.1.6.9 Synthesis of NaM-TP (103)

The synthesis was carried out analogous to the procedure described by Romesberg. All solutions were freshly prepared or distilled under Argon atmosphere and/or stored over molecular sieve (4 Å). Under an inert atmosphere nucleoside **49** (1.0 eq., 0.14 mmol, 40.6 mg) and proton sponge (1.0 eq., 0.14 mmol, 30.0 mg) were solved in OP(OMe)₃ (0.35 mL) and cooled to 0 °C. After the slow addition of POCl₃ (2.5 eq., 0.36 mmol, 0.03 mL) the reaction was stirred for 6 h under ice-cold conditions. NBu₃ (10.5 eq., 1.52 mmol, 0.36 mL) and (*n*-Bu₃NH)₂H₂P₂O₇ (0.5 M in DMF; 5.4 eq., 0.76 mmol, 1.52 mL) were added simultaneously in a rapid manner and the reaction was subsequently stirred for 30 min at 0 °C. The reaction was stopped by the addition of TEAB (1.0 M, 10 mL). The reaction mixture was freeze-dried and triphosphate **53** (0.01 mmol, 12.4 mg, 10%) was purified via HPLC (preparative cleaning: 10 → 40%B in 10 min; analytical cleaning: 10 → 22%B in 15 min; A: 0.1 M TEAB; B: MeCN) as fourfold triethylammonia salt.
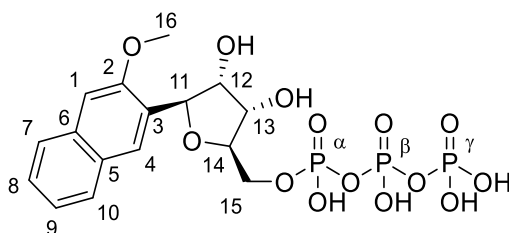
Chemical formula: C₁₆H₂₁O₁₄P₃; **MW**: 530.3

¹H-NMR (CDCl₃, 500 MHz, r.t.): δ [ppm] = 8.06 (s, 1H, H4), 7.95 (d, $^3J_{H7H8}$ = 8.1 Hz, 1H, H7), 7.90 (d, $^3J_{H10H9}$ = 8.2 Hz, 1H, H10), 7.55 (t, $^3J_{H9H10}$ = 6.9 Hz, 1H, H9), 7.46 (t, $^3J_{H8H7}$ = 6.8 Hz, 1H, H8), 7.41 (s, 1H, H1), 5.68 (s, 1H, H11), 5.41 (td, $^3J_{H13H12}$ = 6.0 Hz, $^3J_{H13H14}$ = 4.0 Hz, 1H, H13), 5.34 – 5.22 (m, 1H, H12), 4.68 (s, 1H, H14), 4.32 – 4.21 (m, 2H, H15), 3.05 (s, 3H, H16).

³¹P-NMR (D₂O, 202 MHz, r.t.): δ [ppm] = -6.38 (d, $^2J_{PγPβ}$ = 21.0 Hz, Pγ), -10.84 (d, $^2J_{PαPβ}$ = 19.6 Hz), -22.54 (dd, $^2J_{PβPα}$ = 20.5 Hz, $^2J_{PβPγ}$ = 20.5 Hz, Pβ)

HR MS (ESI⁻): calc. for [M]⁻: 529.0071; found: *m/z* = 529.0071.

5.1.7 Synthesis of spin-labelled compounds

5.1.7.1 Synthesis of 1-Oxyl-2,2,5,5-tetramethyl-2,5-dihydro-1*H*-pyrrole-3-carboxylic acid 4-(1,2,4,5)tetrazin-3-yl-benzylamide (107)

TEMPYO-NHS (1.5 eq., 33.5 µmol, 9.43 mg) and **4** (1.0 eq., 22.4 µmol, 5.00 mg) were dissolved in a solution of NEt$_3$ (anhydr., 1.5 eq, 33.5 mmol, 4.60 µL) and DMSO (anhydr., 500 µL) under an atmosphere of argon and exclusion of light. After 1 h the reaction mixture was diluted with water (5 mL) and rapidly frozen in liquid nitrogen. After freeze-drying the crude product was purified via HPLC (20 → 95%B in 20 min; A: ddH$_2$O; B: MeCN) and **107** (21.5 µmol, 7.59 mg, 95%) was yielded in a quantitative manner.
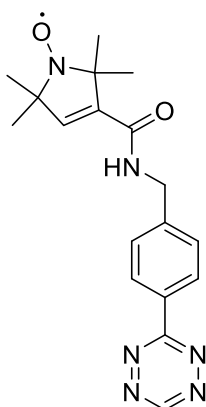
Chemical formula: C$_{18}$H$_{21}$N$_6$O$_2$·; **MW**: 353.4
HR MS (ESI$^+$): calc for [M]$^+$·: 353.1721; found: *m/z* = 353.1709.

5.1.7.2 Synthesis of 3,5,-dibromo-2,2,6,6-tetramethylpiperidin-4-one hydrobromide (109)

The synthesis was carried out analogous to the procedure described by Drescher.[347] Triacetoneamine (1.0 eq., 322 mmol, 50 g) was dissolved at room temperature in acetic acid (195 mL) and bromine (2.0 eq., 640 mmol, 102 g) dissolved in acetic acid (140 mL) was added dropwise over a period of 7 h. The crude product was filtered of and washed with acetic acid (50 mL), water (50 mL) and Et$_2$O (3 x 50 mL). The solid product was dried *in vacuo* and **109** (232 mmol, 91.2 g, 72%) was yielded as off-white solid.
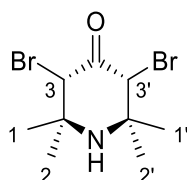
Chemical formula: C$_9$H$_{15}$Br$_2$NO; **MW**: 313.0
^{1}H-NMR (DMSO-*d$_6$*, 400 MHz, r.t.): δ [ppm] = 5.46 (s, 2H, H3, H3′), 1.64 (s, 6H, H1, H1′), 1.53 (s, 6H, H2, H2′).

The second dataset to the *trans*-isomer: 5.52 (s, 2H, H3, H3′), 1.73 (s, 6H, H1, H1′), 1.36 (s, 6H, H2, H2′).

MS (EI): [M]$^{+\cdot}$ 310.8 (12), 312.8 (24), 314.8 (11); [C$_3$H$_6$O]$^{\cdot}$ 58.0 (100).

5.1.7.3 Synthesis of 2,2,5,5-Tetramethyl-2,5-dihydro-1*H*-pyrrole-3-carboxylic acid methoxy-methyl-amide (110)

The synthesis was carried out analogous to the procedure described by Drescher.[347] A solution of H$_2$O (31 mL) and *N,O*-Dimethylhydroxylamine hydrochloride (1.2 eq., 46.4 mmol, 4.59 g) was cooled to 0 °C. To this solution NEt$_3$ (4.3 eq., 165.5 mmol, 16.7 g) was added slowly at 0 °C and stirred for 10 min under ice-cold conditions. After warming to room temperature, **109** (1.0 eq., 38.7 mmol, 15.5 g) was added spatula-wise over a time frame of about 6 h. The reaction mixture was stirred over night at room temperature and additionally for 6 h at 50 °C. After the reaction was cooled down to room temperature and the pH was adjusted to pH ≈ 10 with NaOH (aq., 30% w/v) the reaction mixture was extracted with EE (3 x 50 mL). The organic layer was concentrated under reduced pressure to a volume of about 75 mL and diluted with HCl (aq., 2M, 75 mL). The organic layer was discarded and the aqueous layer was basified again to pH ≈ 10 by NaOH (aq., 30% w/v) under ice-cold conditions. The basified solution was extracted with EE (3 x 50 mL). The combined organic layers were washed with NaCl (aq., sat., 50.0 mL), dried over anhydrous MgSO$_4$ and finally dried *in vacuo*. The product **110** (27.1 mmol, 5.74 g, 70%) was yielded as brown oil that crystallizes.
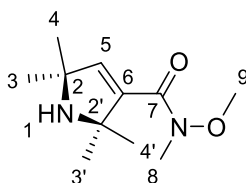
Chemical formula: C$_{11}$H$_{20}$N$_2$O$_2$; **MW**: 212.2

^{1}H-NMR (CDCl$_3$, 500 MHz, r.t.): δ [ppm] = 6.07 (s, 1H, H5), 3.58 (s, 3H, H9), 3.19 (s, 3H, H8), 1.36 (s, 6H, H4, H4′), 1.25 (s, 6H, H3, H3′).

^{13}C-NMR (CDCl$_3$, 500 MHz, r.t.): δ [ppm] = 166.45 (C7), 140.85 (C5), 139.05 (C6), 68.60 (C2, C2′), 64.48 (C2′, C2), 61.01 (C8), 33.38 (C9), 30.32 (C3, C3′), 30.06 (C4, C4′).

5.1.7.4 Synthesis of 3-(*N*-methoxy-*N*-methylcarbamoyl)-2,2,5,5-tetramethyl-1-oxy-pyrroline (111)

The synthesis was carried out analogous to the procedure described by Drescher.[347] After solving **110** (1.0 eq., 24.7 mmol, 5.25 g) in DCM (40 mL) the reaction mixture was cooled to 0 °C and *m*-CPBA (2.0 eq., 49.5 mmol, 8.46 g) was added slowly. The reaction

was stirred for 4 h under ice-cold conditions and finally quenched by the addition of ice-cold water (~20 mL). The phases were separated, the aqueous layer was extracted with DCM (3 x 20 mL), the combined organic layers were washed with $NaHCO_3$ (aq., sat., 30 mL) and NaCl (aq., sat., 30 mL). Subsequently the organic layer was dried over anhydrous Na_2SO_4, the solvent was removed under reduced pressure and after column chromatography (Cy/EE, 1/1, v/v) **111** (11.4 mmol, 2.59 g, 46%) was isolated as orange crystals.
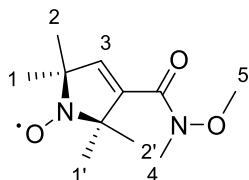
Chemical formula: $C_{11}H_{19}N_2O_3^{\cdot}$; **MW**: 227.3; R_f (Cy/EE, 1/1, v/v): 0.45 - 0.5.
^{1}H-NMR (CDCl$_3$, 400 MHz, r.t., *in situ* reduced by phenylhydrazine): δ [ppm] = 6.25 (s, 1H, H3), 3.61 (s, 3H, H5), 3.20 (s, 3H, H4), 1.54 (s, 6H, H2, H2′), 1.44 (s, 6H, H1, H1′). The spectrum was calibrated to TMS. Residul peaks are caused by phenylhydrazine.

5.1.7.5 Synthesis of 3-formyl-2,2,5,5-tetramethyl-1-oxy-pyrroline (112)

The synthesis was adapted from the procedure described by Drescher.[347] Under an atmosphere of argon, **111** (1.0 eq., 5.72 mmol, 1.30 g) was solved in Et$_2$O (10 mL) and cooled to -40 °C. DIBAL (1 M in hexanes, 1.2 eq., 6.90 mmol, 6.90 mL) was added slowly at -40 °C and the reaction was warmed to 0 °C. After 1 h of stirring under ice-cold conditions, the reaction mixture was poured into HCl (aq. 2 M, 10 mL) at 0 °C and warmed to room temperature. The phases were separated. The aqueous layer was extracted with EE (3 x 15 mL) and the combined organic layers were dried over Na_2SO_4. After solvent evaporation under reduced pressure the crude product was purified via column chromatography (Cy/EE, 1/1, v/v) and **112** (5.60 mmol, 943 mg, 98%) was isolated as yellow crystals.
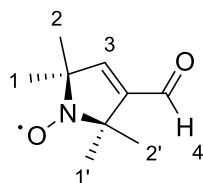
Chemical formula: $C_9H_{14}NO_2^{\cdot}$; **MW**: 168.2; R_f (Cy/EE, 1/1, v/v): 0.8.
^{1}H-NMR (CDCl$_3$, 400 MHz, r.t., *in situ* reduced by phenylhydrazine): δ [ppm] = 5.57 (s, 1H, H3), 1.65 (s, 6H, H2, H2′), 1.39 (s, 6H, H1, H1′).
The spectrum was calibrated to TMS. Residul peaks are caused by phenylhydrazine.
HR MS (EI): calc for [M]$^{\cdot}$: 168.1025; found: m/z = 168.1027.

5.1.7.6 Synthesis of 3-(2-chloroethyl)-2,2,5,5-tetramethyl-1-oxy-pyrroline (113)

The synthesis was carried out analogous to the procedure described by Drescher.[347] In an argon atmosphere chloromethyltriphenylphosphoniumchloride (1.1 eq., 13.1 mmol, 4.54 g) was solved in THF (anhydr., 15 mL) and cooled to -12 °C. After drop wise addition of n-BuLi (2.5 M in hexanes, anhydr., 1.1 eq., 13.1 mmol, 5.23 mL) the reaction was warmed to room temperature and stirred for 30 min. After cooling the reaction to 0 °C again, an ice-cold solution of **112** (1.0 eq., 11.9 mmol, 2.00 g) in THF (anhydr., 10 mL) was added drop wise. The reaction was warmed to room temperature once more. After 2 h the reaction was stopped by the addition of water (2 mL). After phase separation, extraction of the aqueous layer with EE (3 x 15 mL), drying over Na_2SO_4, and solvent evaporation the crude product was purified by column chromatography (Cy/EE, 9/1, v/v). The purified product **113** (5.00 mmol, 1.00 g, 42%) was isolated as yellow solid.
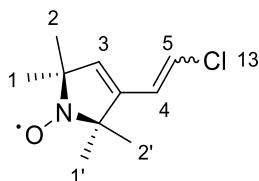
Chemical formula: $C_{10}H_{15}ClNO^{\cdot}$; **MW**: 200.7; **R$_f$** (Cy/EE, 9/1, v/v): 0.7.

¹H-NMR (CDCl₃, 400 MHz, r.t., *in situ* reduced by phenylhydrazine): δ [ppm] =

cis-isomer 6.26 (d, $^3J_{H5H4}$ = 13.7 Hz, 1H, H5), 6.23 (s, 1H, H3), 6.18 (dd, $^3J_{H4H5}$ = 13.8, $^4J_{H4H3}$ = 0.9 Hz, 1H, H4), 1.21 (s, 6H, H2, H2'), 1.15 (s, 6H, H1, H1').

trans-isomer 6.14 (dd, $^3J_{H5H4}$ = 8.0, $^5J_{H5H3}$ = 0.5 Hz, 1H, H5), 5.83 (dd, $^3J_{H4H5}$ = 8.0, $^4J_{H4H3}$ = 1.0 Hz, 1H, H4), 5.48 (s, 1H, H3), 1.20 (s, 6H, H2, H2'), 1.15 (s, 6H, H1, H1').

The spectrum was calibrated to TMS. Residul peaks are caused by phenylhydrazine.

5.1.7.7 Synthesis of 3-ethynyl-2,2,5,5-tetramethyl-1-oxy-pyrroline (114)

The synthesis was adapted from the procedure described by Drescher.[347] Under an atmosphere of argon, **113** (1.0 eq., 5.00 mmol, 1.00 g) was solved in THF (anhydr., 15 mL) at room temperature. In a counter flow of argon, KO^{t}Bu (2.9 eq., 14.50 mmol, 1.63 g) was added and the reaction mixture was stirred for 3 h at 50 °C. After cooling to room temperature NH_4Cl (1 M, 3 mL) was added. After phase separation, the aqueous layer was extracted with Et₂O (3 x 15 mL), the combined organic layers were washed with water (25 mL) and NaCl (aq., sat., 25 mL), dried over anhydrous Na_2SO_4, and solvent was removed under reduced pressure. The crude product was purified via

column chromatography (Cy/EE, 9/1, v/v) and **114** (1.02 mmol, 168 mg, 20%) was isolated as yellow solid.
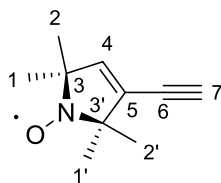
Chemical formula: $C_{10}H_{14}NO^{\cdot}$; **MW**: 164.2; **R$_f$** (Cy/EE, 9/1, v/v): 0.4.

^{1}H-NMR (CDCl$_3$, 500 MHz, r.t., *in situ* reduced by phenylhydrazine): δ [ppm] = 5.83 (s, 1H, H4), 2.91 (s, 1H, H7), 1.20 (s, 6H, H2, H2′), 1.14 (s, 6H, H1, H1′).

The spectrum was calibrated to TMS. Residul peaks are caused by phenylhydrazine.

^{13}C-NMR (CDCl$_3$, 500 MHz, r.t.): δ [ppm] = 141.19 (C5), 128.45 (C4), 113.31 (C6), 80.37 (C7), 25.46 (C1, C1′), 24.85 (C2, C2′).

5.1.7.8 Synthesis of 6-(3,4-Dihydroxy-5-hydroxymethyl-tetrahydro-furan-2-yl)-4-(1-oxyl-2,2,5,5-tetramethyl-2,5-dihydro-1-oxy-pyrrol-3-ylethynyl)-6*H*-thieno[2,3-*c*]pyridine-7-thione (117)

The synthesis was adapted from the procedure described by Kath-Schorr.[310,311] Under an atmosphere of argon **TPT3^I 116** (1.0 eq., 0.16 mmol, 68.0 mg), **114** (1.2 eq., 0.19 mmol, 31.2 mg) and CuI (0.7 eq., 0.11 mmol, 21.0 mg) were dissolved in dry DMF (10 mL) and the resulting solution was degassed with a stream of argon. Previosly degassed NEt$_3$ (anhydr., 3.0 eq., 0.48 mmol, 48.6 mg, 0.07 mL) was added subsequently. After the addition of Pd(PPh$_3$)$_4$ (0.1 eq., 0.02 mmol, 23.1 mg), the mixture was stirred overnight at room temperature under exclusion of light. The solvent was removed *in vacuo* and the residue was purified by column chromatography (DCM/MeOH, 9/1, v/v). Nucleoside **117** (0.15 mmol, 70.8 mg, 96%) was isolated as yellow solid in a quantitative manner.
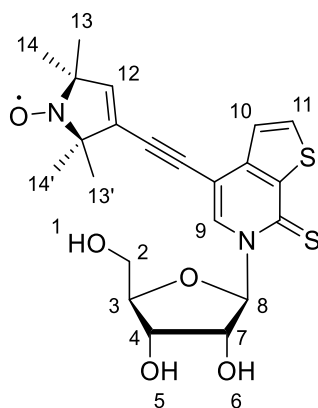
Chemical formula: $C_{22}H_{25}N_2O_5S_2^{\cdot}$; **MW**: 461.1; **R$_f$** (DCM/MeOH, 9:1 v/v): 0.5.

¹H-NMR (CDCl₃, 400 MHz, r.t., *in situ* reduced by phenylhydrazine): δ [ppm] = 8.44 (s, 1H, H9), 7.76 (d, $^3J_{H11H10}$ = 5.4 Hz, 1H, H11), 7.34 (d, $^3J_{H10H11}$ = 5.4 Hz, 1H, H10), 6.78 (d, $^3J_{H8H7}$ = 1.25 Hz, 1H, H8), 5.91 (s, 1H, H12), 4.26 (dd, $^3J_{H3H4}$ = 4.8 Hz, $^3J_{H3H2}$ = 2.0 Hz, 1H, H3), 4.20 – 4.13 (m, 2H, H4, H7), 4.10 (dd, $^2J_{H2H2}$ = 11.8 Hz, $^3J_{H2H3}$ = 2 Hz, 1H, H2), 3.90 (dd, $^2J_{H2H2}$ = 12.0 Hz, $^3J_{H2H3}$ = 2 Hz, 1H, H2), 1.29 (s, 6H, H13, 13′), 1.20 (s, 6H, H14, 14′).

The spectrum was calibrated to TMS. Residul peaks are caused by phenylhydrazine.

HR-MS (ESI⁺): calculated for (C₂₂H₂₅N₂O₅S₂·): 461.1205; found: *m/z* = 461.1197.

5.1.7.9 Synthesis of 4-(1-Oxyl-2,2,5,5-tetramethyl-2,5-dihydro-1-oxy-pyrrol-3-ylethynyl)-(3-(6-(β-D-ribofuranos-5'-triphosphate-1'-yl)-6*H*-thieno[2,3-*c*]pyridine-7-thione (119)

The synthesis was adapted from the procedure described by Marx.[379] In an inert atmosphere of argon nucleoside **117** (1.0 eq., 0.24 mmol, 110 mg) was dissolved in pyridine (anhydr., 0.43 mL) and 1,4-dioxane (anhydr., 1.28 mL). At room temperature a solution of 2-chloro-4*H*-1,2,3-dioxaphosphirine-4-one (1 M in dioxane, anhydr., 1.0 eq., 0.24 mmol, 0.24 mL) was added slowly and the reaction mixture was stirred for 40 min. After a simultaneous addition of NBu₃ (anhydr., stored over molecular sieve 4 Å, 1.0 eq., 0.24 mmol, 0.57 mL) and (*n*-Bu₃NH)₂H₂P₂O₇ (0.5 M in DMF, anhydr., 1.5 eq., 0.36 mmol, 0.72 mL) the reaction was stirred for additional 40 min. Subsequently an I₂ solution (1% in Py/H₂O, 98/2) was added drop wise until no discoloration occurs. The excess of iodine was removed by adding few drops of an aqueous 5% solution of NaHSO₃. The solvent was removed under reduced pressure. The crude product was dissolved in H₂O and lyophilized. Purification of **119** (8.41 mg, 0.01 mmol, 5%) was carried out via preparative HPLC (15% → 50% B in 12 min; A: 0.1% NH₄Cl(aq.), B: MeCN) and **119** was isolated as yellow solid.
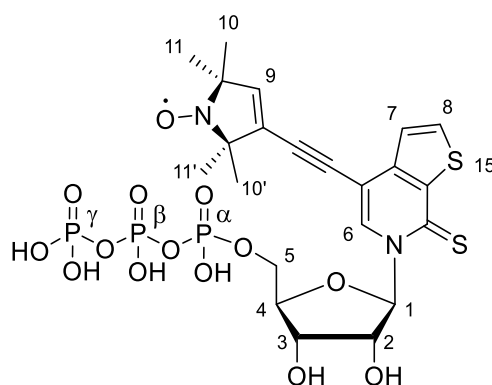
Chemical formula: C₂₂H₂₈N₂O₁₄P₃S₂·; **MW**: 701.5

¹H-NMR (D₂O, 400 MHz, r.t.): δ [ppm] = 8.66 (H6), 7.65 (H7), 7.31 (H8), 6.06 (H1), 5.35 (H9), 5.24 (H3, H2), 4.96 (H2, H3), 4.48 (H4), 3.87 (H5), 3.72 (H5), 1.49 (H10, H10′), 1.42 (H11, H11′).

An integrative analysis was not possible due to the paramagnetic spin label and its influence on proton NMR.

³¹P-NMR (D₂O, 162 MHz, r.t.): δ [ppm] = -10.24 ($^2J_{P\gamma P\beta}$ = 19.5 Hz, Pγ), -11.95 (d, $^2J_{P\alpha P\beta}$ = 20.3 Hz, Pα), -22.50 (dd, $^2J_{P\beta P\alpha}$ = 20.1 Hz, $^2J_{P\beta P\gamma}$ = 20.1 Hz, Pβ).

HR-MS (ESI⁻): calculated for (C₂₂H₂₅N₂O₅S₂Na): 721.9931; found: m/z = 721.9936.

5.1.7.10 Synthesis of 4-(1-Oxyl-2,2,5,5-tetramethyl-2,5-dihydro-1-oxy-pyrrol-3-ylethynyl)-(3-(6-(β-D-ribofuranos-5'-triphosphate-1'-yl)-6*H*-thieno[2,3-*c*]pyridine-7-thione (119)

The synthesis was adapted to the procedure described by Srivatsan.[59] All reagents were freshly prepared or freshly distilled under Argon atmosphere and further dried over molecular sieve (4 Å). Under an inert atmosphere nucleoside **117** (1.0 eq., 0.05 mmol, 25.0 mg) and proton sponge (1.0 eq., 0.05 mmol, 25.0 mg) were solved in OP(OMe)₃ (anhydr., freshly dist., stored over molecular sieve 4 Å, 0.30 mL) and cooled to 0 °C. After the slow addition of POCl₃ (anhydr., freshly dist., 2.5 eq., 0.14 mmol, 0.01 mL) the reaction was stirred for 6 h under ice-cold conditions. NBu₃ (10.5 eq., 0.57 mmol, 0.78 mL) and (*n*-Bu₃NH)₂H₂P₂O₇ (0.5 M in DMF, 5.5 eq., 0.29 mmol, 0.58 mL) were added simultaneously in a rapid manner and the reaction was subsequently stirred for 30 min at 0 °C. The reaction was stopped by the addition of TEAB (1.0 M, 5 mL). The reaction mixture was freeze-dried and triphosphate **119** (0.003 mmol, 2,3 mg, 6%) was purified via HPLC (preparative cleaning: 15% → 50% B in 12 min; A: 0.1% NH₄Cl(aq.), B: MeCN) and yielded as yellow solid.
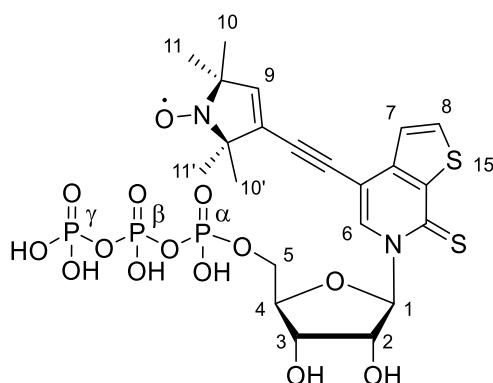
Chemical formula: C₂₂H₂₈N₂O₁₄P₃S₂⁻; **MW**: 701.5

¹H-NMR (D₂O, 400 MHz, r.t.): δ [ppm] = 8.78 (H6), 7.58 (H7), 7.16 (H8), 6.06 (H1), 4.48 (H4), 4.16 (H5), 4.01 (H5), 1.54 (H10, H10′), 1.43 (H11, H11′).

An integrative analysis was not possible due to the paramagnetic spin label and its influence on proton NMR.

^{31}P-NMR (D$_2$O, 162 MHz, r.t.): δ [ppm] = -10.16 ($^2J_{PγPβ}$ = 19.9 Hz, Pγ), -10.72 (d, $^2J_{PαPβ}$ = 21.9 Hz, Pα), -22.54 (dd, $^2J_{PβPα}$ = 20.5 Hz, $^2J_{PβPγ}$ = 20.5 Hz, Pβ).

MS (ESI$^+$): calculated for [M+H]$^+$: 7.4; found: m/z = 711.4.

5.1.7.11 Synthesis of 1-Oxyl-2,2,5,5-tetramethyl-2,5-dihydro-1*H*-pyrrole-3-carboxylic acid prop-2-ynylamide (124)

In a flame dried round bottom flask a mixture of propargylamine **123** (1.5 eq., 3.20 mmol, 0.20 mL) and TEMPYO-NHS ester **106** (1.0 eq., 2.13 mmol, 600 mg) was diluted in DCM (anhydr., 6 mL) under argon atmosphere. After stirring the reaction for 2 h at room temperature the colorless precipitate was filtered off and washed twice with DCM. Subsequently the solvent was removed under reduced pressure and the residue was dried *in vacou*. Product **124** (2.11 mmol, 467 mg, 99%) was yielded as yellowish solid in a quantitative manner.
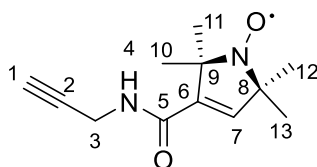
Chemical formula: C$_{12}$H$_{17}$N$_2$O$_2$·; **MW**: 221.3

^{1}H-NMR (400 MHz, CDCl$_3$; r.t., *in situ reduced* by phenylhydrazine): δ [ppm] = 6.00 (s, 1H, H7), 4.72 (s/br, 1H, H4), 3.99 (s, 2H, H3), 2.16 (t, $^4J_{H1H3}$ = 2.3 Hz, 1H, H1), 1.35 (s, 6H, H10, H13), 1.22 (s, 6H, H11, H12).

The spectrum was calibrated to TMS. Residul peaks are caused by phenylhydrazine.

^{13}C-NMR (101 MHz, CDCl$_3$; r.t., *in situ* reduced by phenylhydrazine): δ [ppm] = 163.94 (C5), 140.02 (C6), 137.42 (C7), 129.09 (C8, C9), 128.40, (C9, C8), 79.40 (C2), 71.92 (C1), 29.16 (C3), 24.71 (C11, C12), 24.35 (C10, C13).

The spectrum was calibrated to TMS. Residul peaks are caused by phenylhydrazine.

HR-MS (ESI$^-$): calculated for (C$_{12}$H$_{18}$N$_2$O$_2$):222.1363; found: m/z = 222.1361.

5.1.7.12 Synthesis of 1-Oxyl-2,2,5,5-tetramethyl-2,5-dihydro-1*H*-pyrrole-3-carboxylic acid (3-(6-(β-D-ribofuranos-1'-yl)-7-thioxo-6,7-dihydrothieno[2,3-*c*]pyridin-4-yl)-prop-2-ynyl)-amide (125)

The synthesis was adapted from the procedure described by Kath-Schorr.[310,311] Under an atmosphere of argon **TPT3^I 116** (1.0 eq., 0.69 mmol, 295 mg), **124** (1.3 eq., 0.87 mmol, 193 mg) and CuI (0.7 eq., 0.51 mmol, 98 mg) were dissolved in dry DMF

(20 mL) and the resulting solution was degassed with a stream of argon. Previously degassed NEt$_3$ (anhydr., 3.0 eq., 2.10 mmol, 213 mg, 0.30 mL) was added subsequently. After the addition of Pd(PPh$_3$)$_4$ (0.1 eq., 0.07 mmol, 80.9 mg), the mixture was stirred overnight at room temperature under exclusion of light. The solvent was removed *in vacuo* and the residue was purified by column chromatography (DCM/MeOH, 9/1, v/v). The received product **125** (0.47 mmol, 252 mg, 66%) was isolated as beige solid.
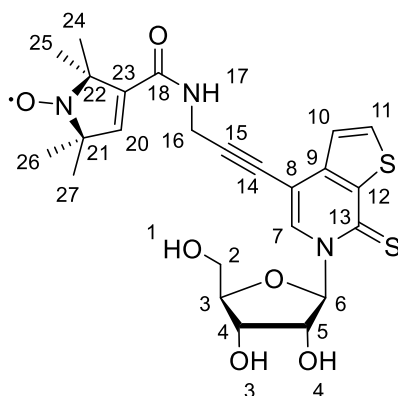
Chemical formula: C$_{22}$H$_{25}$N$_2$O$_5$S$_2$·; **MW**: 518.6; **R$_f$** (DCM/MeOH, 9:1 v/v): 0.4.

^{1}H-NMR (MeOD, 400 MHz, r.t., *in situ* reduced by phenylhydrazine): δ [ppm] = 8.75 (s, 1H, H7), 7.94 (d, $^3J_{H11H10}$ = 5.4 Hz, 1H, H11), 7.42 (d, $^3J_{H10H11}$= 5.4 Hz, 1H, H10), 6.89 (d, $^3J_{H6H5}$ = 1.4 Hz, 1H, H6), 6.23 (s, 1H, H20), 4.22 (s, 2H, H16), 4.19 (dd, $^3J_{H3H4}$ = 4.4 Hz, $^3J_{H3H2}$ = 1.6 Hz, 1H, H3), 4.15 – 4.12 (m, 2H, H4, H5), 4.02 (dd, $^2J_{H2H2}$ = 12.5 Hz, $^3J_{H2H3}$ = 2.0 Hz, 1H, H2), 3.82 (dd, $^2J_{H2H2}$ = 12.6 Hz, $^3J_{H2H3}$ = 2.3 Hz, 1H, H2), 1.31 (s, 6H, H24, H27), 1.19 (s, 6H, H25, H26).

The spectrum was calibrated to TMS. Residul peaks are caused by phenylhydrazine.

^{13}C-NMR (MeOD, 101 MHz, r.t., *in situ* reduced by phenylhydrazine) δ [ppm] = 174.22 (C13), 167.23 (C18), 145.75 (C12), 140.55 (C23), 139.26 (C11), 135.63 (C7), 129.88 (C8, C9),124.99 (C10), 105.84 (C14), 96.39 (C6), 91.58 (C15), 85.68 (C3), 71.22 (C2), 60.67 (C1), 30.20 (C16), 25.42 (C24, C25, C26, C27), 25.41 (C24, C25, C26, C27), 25.31 (C25, C26), 25.30 (C24, C27).

The spectrum was calibrated to TMS. Residul peaks are caused by phenylhydrazine.

HR-MS (ESI$^+$): calculated for (C$_{25}$H$_{29}$N$_3$O$_6$S$_2$·): 519.1492; found: *m/z* = 519.1504.

5.1.7.13 Synthesis of 1-Oxyl-2,2,5,5-tetramethyl-2,5-dihydro-1*H*-pyrrole-3-carboxylic acid (3-(6-(β-D-ribofuranos-5'-triphosphate-1'-yl)-7-thioxo-6,7-dihydrothieno[2,3-*c*]pyridin-4-yl)-prop-2-ynyl)-amide (126)

The synthesis was adapted to the procedure described by Srivatsan.[59] All reagents were freshly prepared or freshly distilled under Argon atmosphere and further dried over molecular sieve (4 Å). Under an inert atmosphere nucleoside **125** (1.0 eq., 0.15 mmol,

78.0 mg) and proton sponge (1.0 eq., 0.15 mmol, 32.0 mg) were solved in $OP(OMe)_3$ (anhydr., freshly dist., stored over molecular sieve 4 Å, 0.75 mL) and cooled to 0 °C. After the slow addition of $POCl_3$ (anhydr., freshly dist., 2.5 eq., 0.38 mmol, 0.04 mL) the reaction was stirred for 3 h under ice-cold conditions. NBu_3 (10.5 eq., 1.58 mmol, 0.38 mL) and $(n\text{-}Bu_3NH)_2H_2P_2O_7$ (0.5 M in DMF, 5.5 eq., 0.83 mmol, 1.66 mL) were added simultaneously in a rapid manner and the reaction was subsequently stirred for 30 min at 0 °C. The reaction was stopped by the addition of TEAB (1.0 M, 11 mL). The reaction mixture was freeze-dried and triphosphate **126** (0.02 mmol, 21 mg, 13% as threefold TEAB salt) was purified via HPLC (preparative cleaning: 0%B → 40%B in XX min; A: 0.1 M TEAB; B: MeCN) and yielded as colorless solid.
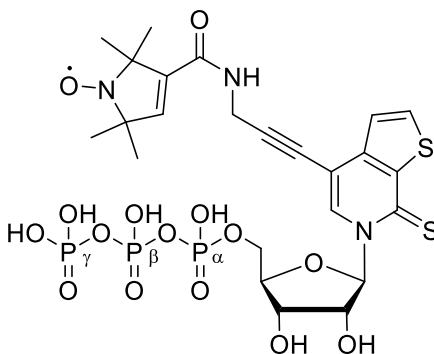
Chemical formula: $C_{24}H_{31}N_3O_{15}P_3S_2^-$; **MW**: 758.6

^{31}P-NMR (D_2O, 162 MHz, r.t.): δ [ppm] = -6.37 (d, $^2J_{P\gamma P\beta}$ = 21.1 Hz, Pγ), -11.54 (d, $^2J_{P\alpha P\beta}$ = 20.4 Hz), -22.53 (dd, $^2J_{P\beta P\alpha}$ = 20.4 Hz, $^2J_{P\beta P\gamma}$ = 20.4 Hz, Pβ)

HR-MS (ESI$^-$): calculated for ($C_{24}H_{30}N_3O_{15}P_3S_2$):757.0337; found: m/z = 757.0304.

5.1.8 Synthesis of 1-Deazaadenosinecyanoethylphosphoramidite

5.1.8.1 Synthesis of Imidazo[4,5-b]pyridine (36)

The synthesis was carried out analogous to the procedure described by Petrelli and coworkers.[234] A reaction mixture of 2,3-diaminopyridine **35** (1.0 eq., 91.6 mmol, 10.0 g) in triethyl orthoformate **127** (6.7 eq., 600 mmol, 100 mL) was refluxed for three hours. After the removal of the solvent at reduced pressure, the residue was refluxed in HCl (aq., conc., 100 mL) for one hour. After cooling to room temperature, the reaction mixture was neutralized with solid Na_2CO_3 and extracted with EE (3 x 100 mL). The combined organic layers were dried over Na_2SO_4 and the solvent was removed under reduced pressure. The crude product was dissolved in EtOH (100 mL) and treated with charcoal. The charcoal was filtered off and after the evaporation of the solvent the product was dried *in vacou* to yield **36** (8.19 g, 68.7 mmol, 75%) as colorless needles.
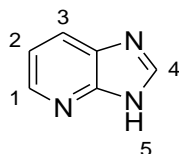
Chemical formula: $C_6H_5N_3$; **MW**: 119.1

1H-NMR (DMSO-d_6, 400 MHz, r.t.): δ [ppm] = 8.44 (s, 1H, H4), 8.35 (d, $^3J_{H1H2}$ = 3.7 Hz, 1H, H1), 8.01 (d, $^3J_{H3H2}$ = 7.8 Hz, 1H, H3), 7.22 (dd, $^3J_{H2H3}$ = 8.0 Hz, $^3J_{H2H1}$ = 4.7 Hz, 1H, H2).

5.1.8.2 Synthesis of imidazo[4,5-b]pyridine-N-oxide (128)

The synthesis was carried out analogous to the procedure described by Herdewijn and coworkers.[60] 3H-imidazo[4,5-*b*]pyridine **36** (1.0 eq., 68.7 mmol, 8.19 g) was dissolved in AcOH (120 mL) and *m*-CPBA (1.5 eq., 103 mmol, 17.8 g) was added. The reaction mixture was stirred at room temperature for 48 h. Subsequently the precipitate was filtered off and washed with EE (2 x 30 mL). The crude product was recrystallized from EtOH and finally dried *in vacuo*. **128** (39.7 mmol, 5.36 g, 58%) was yielded as off-white solid.
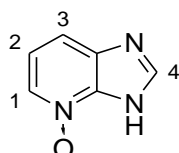
Chemical formula: $C_6H_5N_3O$; **MW**: 135.1

1H-NMR (DMSO-d_6, 400 MHz, r.t.): δ [ppm] = 8.45 (s, 1H, H4), 8.22 (dd, $^3J_{H1H2}$ = 6.3 Hz, $^4J_{H1H3}$ = 0.9 Hz, 1H, H1), 7.65 (dd, $^3J_{H3H2}$ = 8.2 Hz, $^4J_{H3H1}$ = 0.9 Hz, 1H, H3), 7.22 (dd, $^3J_{H2H3}$ = 8.2 Hz, $^3J_{H2H1}$ = 6.3 Hz, 1H, H2).

5.1.8.3 Synthesis of 7-nitro-3*H*-imidazo[4,5-*b*]pyridine 4-oxide[234] (129)

The synthesis was carried out analogous to the procedure described by Petrelli and coworkers.[234] Imidazo[4,5-*b*]pyridine-*N*-oxide **128** (1.0 eq., 39.7 mmol, 5.36 g) was solved in TFA (40 mL) and HNO$_3$ (fum., 26 mL) was added drop wise. After the addition of the acid, the reaction mixture was stirred for three hours at 90 °C. After cooling to room temperature the reaction mixture was poured into crushed ice and subsequently neutralized with NH$_3$ (aq., 25%). During neutralization, the temperature was kept at room temperature. The crude solid product was filtered off, washed with ice-cold water (25 mL) and dried *in vacuo*. Product **129** (68.7 mmol, 8.19 g, 75%) was yielded as slightly yellow solid.
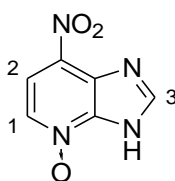
Chemical formula: C$_6$H$_4$N$_4$O$_3$; **MW**: 180.1

^{1}H-NMR (DMSO-*d$_6$*, 400 MHz, r.t.): δ [ppm] = 8.73 (s, 1H, H3), 8.62 (d, $^3J_{H1H2}$ = 5.4 Hz, 1H, H1), 7.93 (d, $^3J_{H2H1}$ = 5.4 Hz, 1H, H2).

5.1.8.4 Synthesis of 7-nitro-3*H*-imidazo[4,5-*b*]pyridine (37)

The synthesis was adapted by the procedure described by Geroni and coworkers.[233] **56** (1.0 eq., 5.55 mmol, 1.00 g) was solved in MeCN (anhydr., 20 mL) under an atmosphere of argon. The reaction mixture was chilled to 0 °C and PCl$_3$ (9.1 eq., 50.3 mmol, 4.40 mL) was added drop wise. After 3 h stirring under ice-cold conditions, the reaction mixture was poured on crushed ice and neutralized with Na$_2$CO$_3$. The precipitated product was filtered off and dried *in vacuo*. **57** (3.77 mmol, 618 mg, 68%) was yielded as slightly yellow solid and used for the next step without further purification.
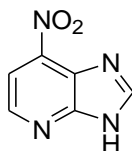
Chemical formula: C$_6$H$_4$N$_4$O$_2$; **MW**: 164.1

5.1.8.5 Synthesis of 7-nitro-3-(2,3,5-tri-*O*-acetyl-   *β*-ribofuranosyl)-3*H*-imidazo[4,5-*b*]pyridine (38)

The synthesis was carried out analogous to the procedure described by Geroni and coworkers.[233] Under an argon atmosphere, **37** (1.0 eq., 4.89 mmol, 0.88 g) and 1,2,3,5-tetra-*O*-acetyl-β-D-ribofuranose (1.0 eq., 4.89 mmol, 1.56 g) were dissolved in MeCN (anhydr., 49 mL). At room temperature $SnCl_4$ (0.8 eq., 3.91 mmol, 1.02 g) was added dropwise. The reaction was stirred at room temperature overnight. After neutralization with $NaHCO_3$ (aq., sat.) the reaction mixture was extracted with chloroform (3 x 40 mL). The combined organic layers were dried over $NaSO_4$ and the solvent was removed under reduced pressure. The crude solid product was purified via column chromatography (MeOH/DCM, 5/95, v/v). After removal of the eluent, the product was dried *in vacuo* and the protected nucleoside **38** (4.48 mmol, 1.89 g, 91%) was yielded as yellow viscous liquid.
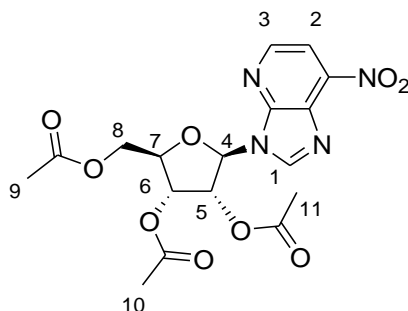
Chemical formula: $C_{17}H_{18}N_4O_9$; **MW**: 422.3; **R$_f$** (MeOH/DCM, 5/95 v/v): 0.5.

¹H-NMR (MeOD, 400 MHz, r.t.): δ [ppm] = 8.85 (s, 1H, H1), 8.73 (d, $^3J_{H3H2}$ = 5.3 Hz, 1H, H3), 8.09 (d, $^3J_{H2H3}$ = 5.4 Hz, 1H, H2), 6.46 (d, $^3J_{H4H5}$ = 4.8 Hz, 1H, H4), 6.13 (dd, $^3J_{H5H4}$ = 5.8 Hz, $^3J_{H5H6}$ = 4.8 Hz, 1H, H5), 5.78 (t, $^3J_{H6H5//H6H7}$ = 5.4 Hz, 1H, H6), 4.55 – 4.39 (m, 3H, H7, H8), 2.17 (s, 3H, H9, H10, H11), 2.09 (s, 3H, H10, H11, H9), 2.08 (s, 3H, H11, H9, H10).

5.1.8.6 Synthesis of 7-nitro-3-*β*-D-ribofuranosyl-3*H*-imidazo[4,5-*b*]pyridine (131)

The synthesis was carried out analogous to the procedure described by Geroni and coworkers.[233] Under an argon atmosphere, **38** (1.0 eq., 4.48 mmol, 1.89 g) was dissolved in MeOH (anhydr., 60 mL). The reaction mixture was saturated with gaseous ammonia and subsequently set aside for 24 h at room temperature. After removing the solvent at reduced pressure product was dried *in vacuo* and **131** (4.46 mmol, 1.32 g, 99%) was yielded as colorless solid in a quantitative manner.
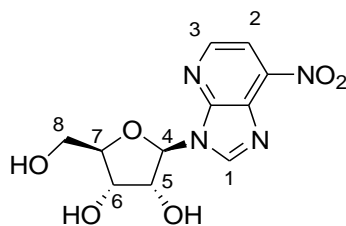
Chemical formula: $C_{11}H_{12}N_4O_6$; **MW**: 296.2

1H-NMR (MeOD, 400 MHz, r.t.): δ [ppm] = 9.00 (s, 1H, H1), 8.67 (d, $^3J_{H3H2}$ = 5.3 Hz, 1H, H3), 8.06 (d, $^3J_{H2H3}$ = 5.3 Hz, 1H, H2), 6.26 (d, $^3J_{H4H5}$ = 5.1 Hz, 1H, H4), 4.73 (t, $^3J_{H5H4/H5H6}$ = 5.1 Hz, 1H, H5), 4.39 (dd, $^3J_{H6H5}$ = 5.2 Hz, $^3J_{H6H7}$ = 4.0 Hz, 1H, H6), 4.30 – 4.16 (m, 1H, H7), 3.92 (dd, $^2J_{H8H8}$ = 12.3 Hz, $^3J_{H8H7}$ = 2.9 Hz, 1H, H8), 3.80 (dd, $^2J_{H8H8}$ = 12.3 Hz, $^3J_{H8H7}$ = 3.1 Hz, 1H, H8).

5.1.8.7 Synthesis of 7-nitro-3-*β*-D-ribofuranosyl-3*H*-imidazo[4,5-*b*]pyridine (39)

The synthesis was carried out analogous to the procedure described by Geroni and coworkers.[233] Under an argon atmosphere, **59** (1.0 eq., 4.48 mmol, 1.89 g) and Pd/C (10%, 1.9 eq,. 3.29 mmol, 0.35 g) were dissolved in MeOH (anhydr., 50.0 mL). The reaction mixture was saturated with gaseous hydrogen and subsequently stirred for 12 hours at room temperature with hydrogen at 30 psi. After filtering of the Pd/C over Celite® 545, the solvent was removed at reduced pressure and the crude product was purified via column chromatography (DCM/MeOH, 4/1, v/v). After removal of the eluent, the product was dried *in vacuo* and the nucleoside **60** (0.80 g, 2.69 mmol, 60%) was yielded as colorless solid.
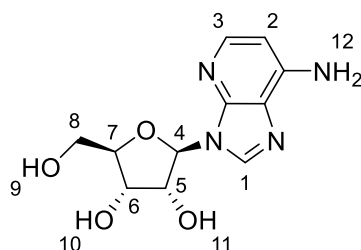
Chemical formula: $C_{11}H_{14}N_4O_4$; **MW**: 266.3; **R_f** (DCM/MeOH, 4/1 v/v): 0.6.

1H-NMR (MeOD, 500 MHz, r.t.): δ [ppm] = 8.24 (s, 1H, H1), 7.78 (d, $^3J_{H3H2}$ = 5.6 Hz, 1H, H3), 6.47 (s, 2H, H12), 6.39 (d, $^3J_{H2H3}$ = 5.6 Hz, 1H, H2), 6.03 (dd, $^3J_{H4H5}$ = 8.7 Hz, $^4J_{H4H5}$ = 3.4 Hz, 1H, H4), 5.87 (d, $^3J_{H10H6}$ = 6.5 Hz, 1H, H10), 5.35 (d, $^3J_{H9H8}$ = 6.4 Hz, 1H, H9), 5.12 (dd, $^3J_{H11H5}$ = 4.3 Hz, 1H, H11), 4.74 – 4.67 (m, 1H, H5), 4.17 – 4.10 (m, 1H, H6), 4.04 – 3.98 (m, 1H, H7), 3.71 – 3.62 (m, 1H, H8), 3.57 – 3.50 (m, 1H, H8).

HR-MS (APCI⁺): calculated for ($C_{11}H_{15}N_4O_4$): 267.1088; found: *m/z* = 267.1086.

5.1.8.8 Synthesis of 3-(2,2-di-*tert*-butyl-7-((*tert*-butyldimethylsilyl)oxy)-hexahydrofuro(3,2-*d*)(1,3,2)dioxasilin-6-yl)-3*H*-imidazo(4,5-*b*)pyridin-*7*-amine (40)

The synthesis was adapted to the procedure described by Beigelmann and coworkers.[235] Under an argon atmosphere 1-deazaadenosine (**39**, 1.0 eq., 1.88 mmol, 500 mg) was dissolved in DMF (anhydr., 5.00 mL), cooled to 0 °C and di-*tert*-butylsilylbis(trifluoromethanesulfonate) (1.5 eq., 2.82 mmol, 1.24 g) was added dropwise. Stirring at 0 °C was continued for 4 h. The reaction was warmed to room temperature overnight and reaction control was done via TLC (EE/MeOH, 85/15, v/v). Again, the solution was cooled to 0 °C, imidazole (3.0 eq., 3.77 mmol, 0.38 g) solved in DMF (anhydr., 2.00 mL) was added and after stirring for several minutes under ice-cold conditions, the reaction was warmed to room temperature. *tert*-Butyldimethylsilylchloride (2.0 eq., 3.77 mmol, 0.57 g) solved in DMF (anhydr., 2.00 mL) was added and the solution was stirred for several hours until reaction control via TLC showed no further conversion. The crude mixture was dried *in vacuo* and purified via column chromatography (EE). **40** (1.33 mmol, 0.69 g, 71%) was yielded as colourless solid.
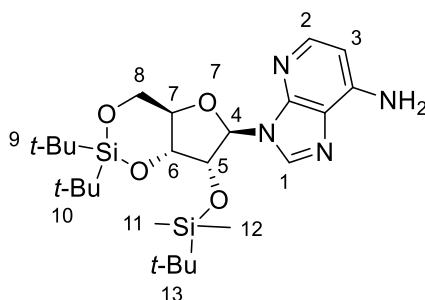
Chemical formula: $C_{25}H_{44}N_4O_4Si_2$; **MW**: 520.8; **R_f** (EE): 0.7.

^{1}H-NMR (MeOD; 400 MHz; r.t.): δ [ppm] = 8.21 (s, 1H, H1), 7.92 (d, $^3J_{H5H6}$ = 5.6 Hz, 1H, H2), 6.52 (d, $^3J_{H6H5}$ = 5.6 Hz, 1H, H3), 6.05 (s, 1H, H4), 4.78 (d, $^3J_{H5H6}$ = 5.2 Hz, 1H, H5), 4.68 (dd, $^2J_{H6H7}$ = 9.4 Hz, $^3J_{H6H5}$ = 5.3 Hz, 1H, H6), 4.46 – 4.41 (m, 1H, H7), 4.20 – 4.12 (m, 1H, H8), 4.06 (dd, $^2J_{H8H8}$ = 10.4 Hz, $^3J_{H8H7}$ = 9.0 Hz, 1H, H8), 1.14 (s, 9H, H9, H10), 1.09 (s, 9H, H10, H9), 0.93 (s, 9H, H13), 0.14 (s, 6H, H11, H12).

5.1.8.9 Synthesis of 2-(4-*tert*-butylphenoxy)-*N*-(3-(2,2-di-*tert*-butyl-7-((*tert*-butyldimethylsilyl)oxy)-hexahydrofuro(3,2-*d*)(1,3,2)dioxasilin-6-yl)-3*H*-imidazo(4,5-*b*)pyridin-7-yl)acetamide (41)

In an inert argon atmosphere **40** (1.0 eq., 0.19 mmol, 100 mg) was dissolved in pyridine (anhydr., 2.00 mL) and cooled to 0 °C. Under this ice-cold conditions, (4-*tert*-butylphenoxy)-acetyl chloride (1.3 eq., 0.24 mmol, 53.8 mg) was added drop wise. After the solution was warmed to room temperature and stirred overnight, the reaction was

quenched by adding water (0.5 mL) and MeOH (0.5 mL). Subsequently the solvents were evaporated under reduced pressure, the crude product was purified via column chromatography (Cy/EE, 50/50, v/v) and **41** (0.14 mmol, 0.11 g, 74%) was yielded as colorless solid.
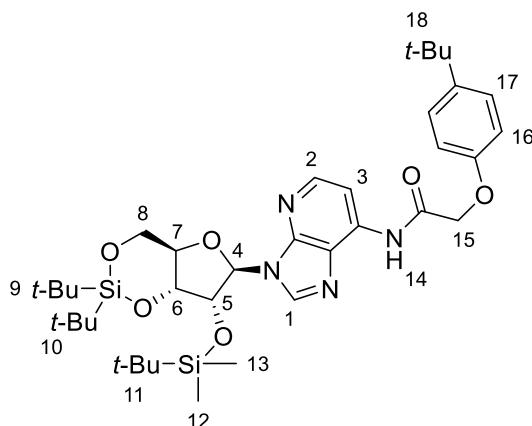
Chemical formula: $C_{37}H_{58}N_4O_6Si_2$; **MW**: 711.1; **R$_f$** (Cy/EE, 1/1, v/v): 0.9.

^{1}H-NMR (MeOD; 400 MHz; r.t.): δ [ppm] = 8.43 (s, 1H, H1), 8.33 (d, $^3J_{H5H6}$ = 5.5 Hz, 1H, H2), 8.25 (d, $^3J_{H6H5}$ = 5.5 Hz, 1H, H3), 7.39 (d, $^3J_{H17H16}$ = 9.0 Hz, 2H, H17), 7.07 (d, $^3J_{H16H17}$ = 9.0 Hz, 2H, H16), 6.12 (s, 1H, H4), 4.87 (1H, H5, overlapping with H$_2$O signal), 4.86 – 4.82 (m, 1H, H6), 4.80 (s, 2H, H15), 4.50 – 4.41 (m, 1H, H7), 4.25 – 4.16 (m, 1H, H8), 4.13 – 4.04 (m, 1H, H8), 1.32 (s, 9H, H18), 1.15 (s, 9H, H9, H10), 1.10 (s, 9H, H10, H9), 0.96 (s, 9H, H11), 0.17 (s, 3H, H12, H13), 0.16 (s, 3H, H13, H12).

MS (ESI$^+$): calculated for [M+H]$^+$: 711.4; found: *m/z* = 711.4.

5.1.8.10 Synthesis of *N*-(3-(3-((*tert*-butyldimethylsilyl)oxy)-4-hydroxy-5-(hydroxymethyl)oxolan-2-yl)-3*H*-imidazo(4,5-*b*)pyridin-7-yl)-2-(4-*tert*-butylphenoxy)acetamide (132)

The synthesis was adapted from a procedure of Beigelman and Coworkers.[235] **41** (1.0 eq., 0.98 mmol, 0.70 g) was dissolved in DCM (anhydr., 14 mL) under argon atmosphere and chilled to 0 °C. After the drop wise addition of HF * pyridine (0.3 eq., 0.24 mmol, 0.05 g) mixed with pyridine (anhydr., 0.5 mL) and stirring for 3 h at 0 °C the reaction was quenched by adding methoxytrimethylsilane (1.5 mL), warmed to room temperature and stirred for 30 min. The solution was diluted with water (15 mL). The organic layer was separated, the aqueous layer was extracted with DCM (2 x 15 mL) and the combined organic layers were dried *in vacuo.* After column chromatography (Cy/EE, 1/1, v/v) **132** (0.64 mmol, 0.36 g, 65%) was yielded as colorless solid.
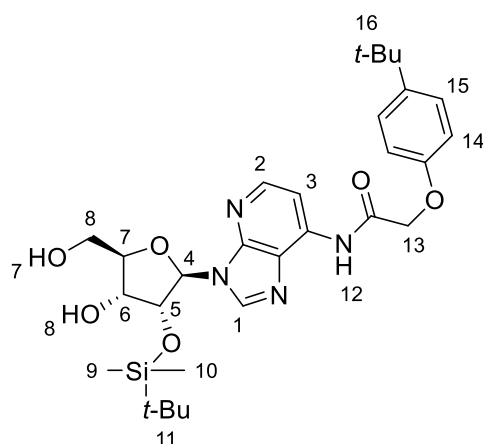
Chemical formula: $C_{29}H_{42}N_4O_6Si$; **MW**: 570.7; **R$_f$** (Cy/EE, 1/1, v/v): 0.5.

^{1}H-NMR (MeOD; 400 MHz; r.t.): δ [ppm] = 8.55 (s, 1H, H1), 8.34 – 8.30 (m, 2H, H2, H3), 7.41 (d, $^3J_{H15H14}$ = 8.9 Hz, 2H, H15), 7.09 (d, $^3J_{H14H15}$ = 8.8 Hz, 2H, H14), 6.09 (d, $^3J_{H4H5}$ = 6.8 Hz, 1H, H4), 5.05 (dd, $^3J_{H5H4}$ = 6.6 Hz, $^3J_{H5H6}$ = 5.2 Hz, 1H, H5), 4.82 (s, 2H, H13), 4.32 (d, $^3J_{H6H5}$ = 4.9 Hz, 1H, H6), 4.26 (d, $^3J_{H7H8}$ = 1.7 Hz, 1H, H7), 3.94 (dd, $^2J_{H8H8}$ = 12.6 Hz, $^3J_{H8H7}$ = 2.2 Hz, 1H, H8), 3.80 (dd, $^2J_{H8H8}$ = 12.6 Hz, $^3J_{H8H7}$ = 2.0 Hz, 1H, H8), 1.33 (s, 9H, H16), 0.79 (s, 9H, H11), -0.11 (s, 3H, H9, H10), -0.26 (s, 3H, H10, H9).

5.1.8.11 Synthesis of *N*-(3-(5-((bis(4-methoxyphenyl)(phenyl)methoxy)methyl)-3-((*tert*-butyldimethylsilyl)oxy)-4-hydroxyoxolan-2-yl)-3H-imidazo(4,5-b)pyridin-7-yl)-2-(4-*tert*-butylphenoxy)acetamide[235] (43)

The synthesis was adapted from Beigelman and coworkers.[235] Under an atmosphere of argon, **132** (1.0 eq., 0.46 mmol, 265 mg) and DMAP (0.9 eq., 0.41 mmol, 50.0 mg) were dissolved in pyridine (anhydr., 4.00 mL). DMT-Cl (173 mg, 0.51 mmol, 1.1 eq.) was dissolved in DCM (anhydr., 0.50 mL) under argon atmosphere. Both solutions were cooled down to 0 °C and the DMT-chloride solution was added drop wise to dissolved **132** under ice cold conditions. The reaction mixture was warmed to room temperature and stirred overnight. Subsequently, the solvents were evaporated under reduced pressure and **43** (0.34 mmol, 0.29 g, 74%) was yielded by column chromatography (Cy/EE, 3/1 v/v) as colorless solid.
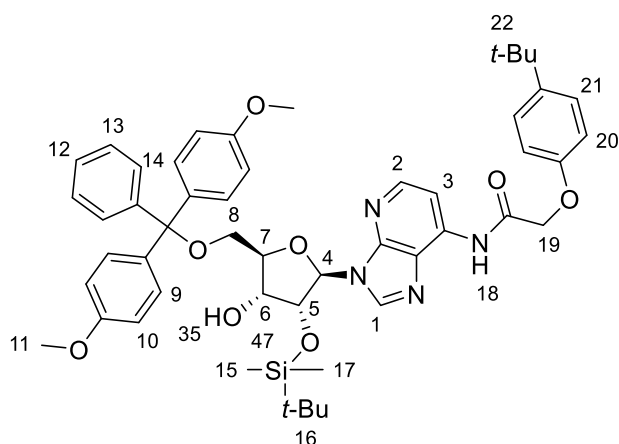
Chemical formula: $C_{50}H_{60}N_5O_8Si$; **MW**: 873.1; R_f (Cy/EE, 7/3, v/v): 0.36; (3'-TBS R_f: 0.44).

¹H-NMR (CDCl₃; 500 MHz; r.t.): δ [ppm] = 9.58 (s/br, 1H, H18), 8.26 – 8.23 (m, 2H, H2, H3), 8.16 (s, 1H, H1), 7.47 (d, $^3J_{H21H20}$ = 7.3 Hz, 2H, H21), 7.38 – 7.33 (m, 5H, H9, H12), 7.26 (m, 4H, H14 and H13 overlapping with solvent residual peak), 7.02 (d, $^3J_{H20H21}$ = 8.9 Hz, 2H, H20), 6.81 (d, $^3J_{H24H23}$ = 8.9 Hz, 4H, H10), 6.11 (d, $^3J_{H4H5}$ = 5.4 Hz, 1H, H4), 5.09 (t, $^3J_{H5H4/H5H6}$ = 5.2 Hz, 1H, H5), 4.69 (s, 2H, H19), 4.36 – 4.31 (m, 1H, H6), 4.29 – 4.24 (m, 1H, H7), 3.78 (s, 3H, H11), 3.78 (s, 3H, H11), 3.55 (dd, $^2J_{H8H8}$ = 10.6 Hz, $^3J_{H8H7}$ = 3.3 Hz, 1H, H8), 3.36 (dd, $^2J_{H8H8}$ = 10.6 Hz, $^3J_{H8H7}$ = 4.1 Hz, 1H, H8), 1.31 (s, 9H, H22), 0.82 (s, 9H, H16), -0.04 (s, 3H, H15, H17), -0.18 (s, 3H, H17, H15).

5.1.8.12 Synthesis of *N*-(3-(5-((bis(4-methoxyphenyl)(phenyl)methoxy)methyl)-3-((*tert*-butyldimethylsilyl)oxy)-4-hydroxyoxolan-2-yl)-3*H*-imidazo(4,5-b)pyridin-7-yl)-2-(4-*tert*-butylphenoxy)acetamide (44)

The nucleotide precursor **43** (1.0 eq., 0.10 mmol, 86 mg) and DiPEA (1.1 eq., 0.11 mmol, 0.02 mL) were dissolved in DCM (anhydr., 2.00 mL) under an argon atmosphere, cooled to 0 °C, then frozen in liquid nitrogen and degassed two times. Subsequently the solution was warmed to 0 °C, 2-cyanoethyl *N,N*-diisopropylchlorophosphoramidite (1.1 eq., 0.11 mmol, 0.02 mL) was added drop wise. After stirring for 10 min at 0 °C, warming to room temperature and stirring for 2 h at room temperature, the reaction mixture was dried *in vacuo*. The crude product was used without further purification except a filtration column (Cy/EE/NEt₃, 12/12/1, v/v/v) under inert conditions to yield the posphorsamidite **44** (0.09 mmol, 100.2 mg, 90% crude product) as colorless resin.[380]
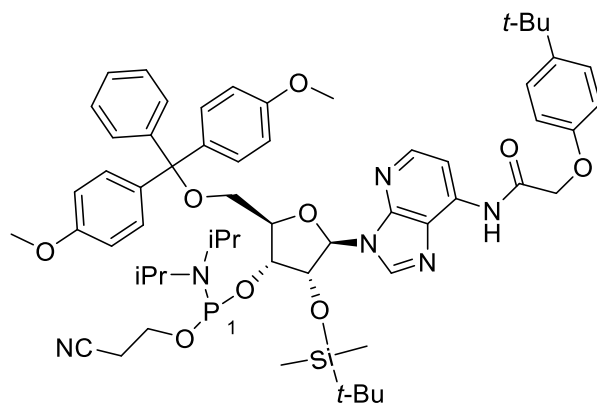
Chemical formula: $C_{59}H_{77}N_6O_9PSi$; **MW**: 1073.3

^{31}**P-NMR** (CDCl$_3$ filtered over Al$_2$O$_3$; 202 MHz; r.t.): δ [ppm] = 150.9 (P1), 148.9 (P1).

MS (ESI$^+$): calculated for [M+Na]$^+$ 1095.5, measured 1095.5.

5.2 Biochemical methods

5.2.1.1 General handling of oligonucleotides and enzymes

Unmodified DNA templates and primers employed in this study were purchased by *Biomers.net* or *Metabion*. All X-TP modified oligonucleotides have been purchased by *Ella Biotech*. Purchased lyophilized RNA and DNA strands were diluted in autoclaved water according to the manufacturers' manuals. All used enzymes (in general T7 RNAP (*homemade*), RNasin and RNasin plus (*Promega*), and inorganic pyrophosphatase (ipp, *Roche*)), were handled according to the manufacturers' manuals. General storage conditions for oligonucleotide strands and enzymes were -20 °C.

5.2.1.2 *In vitro* transcription

Unless otherwise stated, *in vitro* transcriptions were performed in a 100 µL scale with final concentrations given in table below. Primer and templates were annealed for 2 min at 95 °C and slowly cooled to room temperature. The transcription mixture was incubated if not otherwise stated for 4 h at 37 °C. Subsequent DNase 1 digestion was performed by the addition of 10 µL 10 x DNase 1 buffer (*New England Biolabs*) and 5 µL DNase 1 (2 U/µL, *New England Biolabs*).Samples were incubated for 30 min at 37 °C followed by enzyme inactivation for 2 min at 95 °C. Spin-label containing samples were not exposed to enzyme inactivation, because of spin-labels' thermal fragility. X-TP refers to the used unnatural or modified ribonucleotides and will be announced in the corresponding sections.

Reagent	Final concentration
Tris·HCl (pH = 7.9)	40 mM
$MgCl_2$	25 mM
DNA template	3 mM
DNA primer	3 mM
NTP-mix	2.5 mM
X-TP	1 mM
DTT	5 mM
iPP (0.2 U/µL)	0.04 U/µL
RNasin (40 U/µL	0.50 U/µL
T7 RNAP (50 U/µL)	5.00 U/µL

Table 6: Pipetting scheme for a 100 µL in vitro transcription.

Inorganic pyrophosphatase (iPP) was purchased by *Roche*, RNasin was purchased by *Promega* and T7 RNAP was self-made (AA sequence conforms with GenBank AY264774.1)[381].

163

5.2.1.3 Polyacrylamide gel electrophoresis (*PAGE*):

Gel electrophoresis was used to separate and purify nucleic acids.

All samples were diluted in RNA loading buffer in a 1/1 ratio to the sample volume and denatured at 95 °C for 2 min before gel loading. Gels were prepared as described in the pipetting scheme below. Gel polymerization took place for at least 1 h. The gel electrophoresis was carried out in running chambers filled with 1 x TBE buffer. The gel pockets were cleaned with 1 x TBE buffer before sample loading.

solution	Volume
Rotiphorese sequencing gel concentrate (*Roth*) (25 % Bis/AA in 8.3 M urea)	40 mL
8.3 M urea in ddH$_2$O	5 mL
8.3 M urea in 10 x TBE	5 mL
10 % APS (*Roth*) in ddH$_2$O (v/v)	400 µL
TEMED (*Alfa Aesar*)	20 µL

Table 7: Pipetting scheme for a 20 % preparative polyacrylamide gel preparation (50 mL volume).

Polyacrylamide gels for analytical applications were prepared according to the table above in a 5 mL scale. The gel size was 83 x 73 x 0.75 mm for electrophoresis using a Mini Protean tetra cell system (*Bio-Rad*$^®$). Used conditions for analytical gel electrophoresis were 300 V for 45 min. (12 % gels) up to 75 min (20 % gels).

Analytical polyacrylamide gels were stained with SybrSafe® (*Life Technologies*) and visualized by UV illumination using a Genoplex gel documentation system (*VWR*). Fluorescence scanning was done using a Phosphorimager FLA-3000 (*Fujifilm*) with an excitation wavelength of $\lambda_{excitation} = 473$ nm and an emission wavelength of $\lambda_{emission} = 520$ nm.

Preparative purification via polyacrylamide gels was done in a 52 mL gel approach for a 160 x 175 x 1.5 mm sized maxi gel using custom made electrophorese chambers. Used conditions for preparative gel electrophoresis were 400 V for 180 min (15 % gels) up to 240 min (20 % gels).

5.2.1.4 Electro elution

Separated oligonucleotides using preparative gel electrophoresis were isolated via electro elution. A custom made electro eluter was used for this method. The architecture of the used device is based on a "UEA AnalyticalElectroeluter" by *IBI Technologies* and is publicly available in *Molecular Biology and Genomics*, **2007**, Academic Press, p. 52.

The procedure is based on a salt trap. The Plexiglas chamber is filled with 1 x TBE buffer, the excised gel pieces of interest are placed in a designated recess and the v-shaped channel is filled with 170 µL of an 8 M aqueous NH_4OAc solution. This high salt cushion traps the eluted nucleic acids. Oligonucleotide elution took place at 150 V for 60 minutes. After the elution was performed, the v-shaped channel is blocked on both ends and the RNA-containing high salt solution is transferred into a 1.5 mL reaction tube for EtOH precipitation.[382]

5.2.1.5 Ethanol precipitation

Oligonucleotides purified by electro elution were furthermore purified as described in the section below. For the precipitation three volumes of cold (-20 °C) EtOH (abs.) were added and the sample was stored at -20 °C overnight. Afterwards the samples were centrifuged at 4 °C for 40 min at high speed (13.000 rcf). The supernatant was taken of; the resulting pellets were freeze dried, resolved in 50 µL ddH$_2$O, desalted with G-25 spin columns, and finally freeze-dried for storage.

5.2.1.6 Concentration measurements of oligonucleotides

DNA as well as RNA quantification has been carried out in solution using UV absorbance. For concentration determination of the oligonucleotide the Lambert-Beer equation was employed by

$$A = \lg\left(\frac{I_0}{I_1}\right) = \epsilon_\lambda \cdot c \cdot d$$

A: absorbance at a given wavelength (also called optical density (OD)),
I_1: intensity of the transmitted light
I_0: intensity of the incident light
ϵ: molar absorption coefficient at a given wavelength [$l \cdot mol^{-1} \cdot cm^{-1}$]
c: concentration [$mol \cdot l^{-1}$]
d: path length [cm]

Concentration measurements were performed on a NanoDrop UV-spectrophotometer 2000c (*Thermo Scientific*) and concentrations were obtained from A_{260} value and software assisted calculated using online software tool Oligo Calculator v3.27. Canonical nucleobases were plotted for respective X-TPs.[383]

5.2.1.7 Enzymatic digestion to nucleosides

Enzymatic digestion of RNA to nucleosides was carried out with 100 pmol RNA solved in 45 µL ddH$_2$O. After the addition of 5 µL S1 endonuclase reaction buffer (5 x, *Life Technologies*) the reaction mixture was shortly mixed and subsequently spun down. 0.5 µL S1 endonuclease (100 U/µL, *Life Technologies*) was added and the samples were incubated at 37 °C for 60 min and 800 rpm using a thermal shaker (*Eppendorf*). Then, 5.7 µL of alkaline phosphatase reaction buffer (10 x, *Promega*), 0.5 µL alkaline phosphatase (CIAP, 1 U/µL, *Promega*), 0.5 µL phosphodiesterase 1 from *crotalus adamanteus venom* (5 mU/µL, *Sigma Aldrich*) and 0.5 µL Benzonase nuclease (250 U/µL, *Sigma Aldrich*) were added. The samples were incubated for 120 min at 37 °C and 800 rpm. Subsequently the samples have been heated up to 95 °C for 3 min and finally centrifuged at 12.000 rcf for 3 min. 20 µL supernatant were taken off for HPLC analysis.

5.2.1.8 Posttrancriptional labeling of RNA using tetrazine conjugates

Modified RNA-bearing strained alkenes were incubated with an excess of tetrazine conjugates (3-fold) at room temperature for 1 h in aqueous solution. Ensuing *PAGE* analysis was carried out without further purification. Prior to LC-MS analysis labeled RNA was purified by ZipTip C18 pipette tips (*Merck Millipore*) or G-25 columns.

5.2.1.9 Reverse transcription of modified RNA (radioactively labeled)

1.5 pmol DNA primer was labeled with [γ-^{32}P]-ATP (PerkinElmer) using T4 polynucleotide kinase (10 U/µL, *New England Biolabs*) and T4 PNK reaction buffer (10 x, New England Biolabs) according to manufacturers' protocol. Labeled DNA was then annealed to 10 pmol RNA by slow cooling from 95 °C to 42 °C. Using extension buffer with 10 mM DTT containing 0.75 mM dNTPs and 1 µL AMV reverse Transcriptase (10 U/µL, *Promega*), the reaction was incubated at 42 °C for 45 min. The transcriptase was heat inactivated at 70 °C for 10 min. Subsequently, 1 µl RNase H (5 U/µL, *New England Biolabs*) was added and incubated at 37 °C for 20 min followed by heat inactivation at 70 °C for 10 min. The reaction was fractionated by denaturing 20% *PAGE* and analyzed using a Phosphorimager FLA-3000 (*Fujifilm*).[310]

5.2.1.10 Buffers and solutions

Used buffers and their composition which were not purchased by commercial suppliers are listed below:

Name	Composition	Concentration
1 x TBE	Tris	89 mM
Adjusted to pH=7.6	Boric acid	89 mM
using HCl	EDTA	2 mM
RNA loading buffer	Formamide	95%
	Urea (8.3 M, aq.)	5%
	EDTA	20 mM

5.2.1.11 Manufacturer-related buffers:

Manufacturer related buffers were purchased by the announced suppliers and used according to the manufacturer's manuals.

DNase 1 buffer (10x, *New England Biolabs*; B0303S)

Alkaline phosphatase buffer (10x, *Promega*; M1821)

S1 endonuclease buffer (5x, Thermo Fisher; Y02292)

T4 polynucleotide kinase reaction buffer (10x, *New England Biolabs*; B0201S)

AMV reverse transcriptase buffer (10x, *Promega*; M0277S/M0277L)

Pwo proofreading polymerase buffer (10x, Genaxxon; M3002.0000)

Tth DNA polymerase buffer (10x, *Promega*; M2105)

Novagen KOD XL (10x, *Fisher scientific*; 710873)

Vent R (exo-) (10x; *New England Biolabs*; M0257S)

5.2.1.12 Enzymes used for PCR

Taq (*New England Biolabs*), OneTaq (*New England Biolabs*), Pwo (*Genaxxon*), KOD XL (*Novagen*), Vent R (exo-) (*New England Biolabs*), Tth (*Promega*)

5.2.1.13 CD Spectroscopy

Oligonucleotides (50 µM) were hybridized in by heating to 95 °C for 2 min and cooling (1 °C/min) to room temperature. CD experiments were recorded on a J-810 spectropolarimeter (*JASCO*) at 25 °C (0.1 cm cell) by averaging over 10 scans over a wavelength range of 220 nm to 340 nm, with a measuring speed of 100 nm/min and a response time of 0.1 s. Buffer spectra were subtracted from the averaged data obtained.

5.2.1.14 Melting curves

Thermal denaturation experiments of modified and unmodified oligonucleotides were carried out on a V-630 Bio UV-Vis spectrophotometer (*JASCO*). The samples were dissolved in 200 µL phosphate buffer (145 mM NaCl, 10 mM NaH_2PO_4, 10 mM Na_2HPO_4) and after short vigorous stirring transferred into micro-cuvettes (*HELLMA*). The temperature range for melting curve measurement was set from 20 °C to 80 °C with a ramp rate of 1.0 °C/min.

5.3 List of DNA templates and related RNA transcripts

List of solid-phase synthesized RNA strands containing norbornene-modified uridine **X = 74**:

RNA-U^{NOR}-12

5′-CGA UG**X** CAG UGG-3′

RNA-U^{NOR}-24

5′-G**X**G CAU ACC UGG UGC UCU GUG CAC-3′

RNA-U^{NOR}-21

5′-GG**X** GAA GUU CAA GGG CGU GdTdT-3′

Solid-phase synthesized RNA strands containing canonical uridine as control

RNA-U-24

5′-G**U**G CAU ACC UGG UGC UCU GUG CAC-3′

List of solid-phase synthesized T7 primer sequences:

DNA-T7-1

5′-TAA TAC GAC TCA CTA TAG G-3′

DNA-T7-2

5′-ATA ATA CGA CTC ACT ATA GGG-3′

List of solid-phase synthesized DNA templates containing one, two or no **X** = d**NaM** and corresponding transcripts containing one, two or no norbornene-modified TPT3 derivative **Y = 76**:

DNA-NaM-0

5′-CTG TGA CGG GAA TCC TCG TGG A**C**G ATC TCC TAT AGT GAG TCG TAT TA-3′

RNA-TPT3^{NOR}-0

5′-GGA GAU C**G**U CCA CG**Y** GGA UUC CCG UCA CAG-3′

DNA-NaM-1

5′-CTG TGA CGG GAA TCC TCG TGG A**X**G ATC TCC TAT AGT GAG TCG TAT TA-3′

RNA-TPT3^{NOR}-1

5′-GGA GAU C**Y**U CCA CG**Y** GGA UUC CCG UCA CAG-3′

DNA-NaM-2

5′-CTG TG**X** CGG GAA TCC TCG TGG A**X**G ATC TCC TAT AGT GAG TCG TAT TA-3′

RNA-TPT3^{NOR}-2

5′-GGA GAU C**Y**U CCA CG**Y** GGA UUC CCG **Y**CA CAG-3′

List of solid-phase synthesized DNA sequences used for reverse transcription experiments:

DNA-RT-15

5′-CTG TGA CGG GAA TCC-3′

DNA-RT-22

5′-CTG TGA CGG GAA TCC TCG TGG A-3′

List of solid-phase synthesized DNA templates containing either d**NaM** or d**5SICS** at position 31 and corresponding transcripts containing either TPT3 derivatives or NaM:

DNA-CXT^{5SICS}

5′-CAC T**X**C TCG GGA TTC CCT ATA GTG AGT CGT ATT AT-3′

X = d**5SICS**

RNA-CXT^{5SICS}

5′-GGG AAU CCC GAG **Y**AG UG-3′

Y = **103**

DNA-CXT^{NaM}

5′-CAC T**X**C TCG GGA TTC CCT ATA GTG AGT CGT ATT AT-3′

X = d**NaM**

RNA-CXT^{NaM}-CP

5′-GGG AAU CCC GAG **Y**AG UG-3′

Y = **104**

RNA-CXT^{NaM}-RL

5′-GGG AAU CCC GAG **Y**AG UG-3′

Y = **119**

RNA-CXT^{NaM}-FL

5′-GGG AAU CCC GAG **Y**AG UG-3′

Y = **126**

List of solid-phase synthesized RNA sequence used for enzymatic digest to nucleosides:

RNA-ND^{test}

5′-G**A** UCU GAU AUC AGA UC-3′

List of solid-phase synthesized DNA template and corresponding self-complementary transcripts:

DNA-SC

5′-GG**X** TCT GAT ATC AGA TCC TAT AGT GAG TCG TAT TAT-3′

X = d**NaM**

RNA-SC-CP

5′-GGA UCU GAU AUC AGA **Y**CC-3′

Y = **104** (**TPT3^{CP}**-TP)

RNA-SC-RL

5′-GGA UCU GAU AUC AGA **Y**CC-3′

Y = **119** (<u>r</u>igid <u>l</u>inker)

RNA-SC-FL

5′-GGA UCU GAU AUC AGA **Y**CC-3′

Y = **126** (<u>f</u>lexible <u>l</u>inker)

Solid-phase synthesized RNA strands containing canonical adenosine as control

RNA-SC-A

5′-GG**A** UCU GAU AUC AGA UCC-3′

List of solid-phase synthesized DNA template and corresponding transcript for labelled CPEB3 ribozyme:

DNA-CPEB3

5′-AGA GCA GAA TTC GCA GAT TC**X** CTA GAA TCT GAC GGG GGC TGC GAC GTG AAC GCT TCT ACT **X**GT GGC CCC CTG TTA TCC CCT TGA TCC TCC TAT AGT GAG TCG TAT TA-3′

RNA-CPEB3

5′-GGA GGA UCA AGG GGA UAA CAG GGG GCC AC**Y** AGU AGA AGC GUU CAC GUC GCA GCC CCC GUC AGA UUC UAG **Y**GA AUC UGC GAA UUC UGC UCU-3′

Solid-phase synthesized RNA containing atomic mutated adenosine:

RNA-TW

5′-ACC AGC GGC AG**X** AUG CAG CUU UAU UGC CdT-3′

(X = **44)**

6 Literature

(1) Malyshev, D. a; Dhami, K.; Lavergne, T.; Chen, T.; Dai, N.; Foster, J. M.; Corrêa, I. R.; Romesberg, F. E. A Semi-Synthetic Organism with an Expanded Genetic Alphabet. *Nature* **2014**, *509* (7500), 385–388.

(2) Shapiro, J. A. Revisiting the Central Dogma in the 21st Century. *Ann. N. Y. Acad. Sci.* **2009**, *1178*, 6–28.

(3) Crick, F. Central Dogma of Molecular Biology. *Nature* **1970**, *227*, 561–563.

(4) Romano, G.; Veneziano, D.; Acunzo, M.; Croce, C. M. Small Non-Coding RNA and Cancer. *Carcinogenesis* **2017**, *38* (5), 485–491.

(5) Inamura, K. Major Tumor Suppressor and Oncogenic Non-Coding RNAs: Clinical Relevance in Lung Cancer. *Cells* **2017**, *6* (2), 12.

(6) *Catalytic RNA*, 2nd ed.; Eckstein, F., Lilley, D. M. J., Eds.; Springer-Verlag Berlin, Heidelberg: Heidelberg, 1997; Vol. 10.

(7) Mattick, J. S.; Makunin, I. V. Non-Coding RNA. *Hum. Mol. Genet.* **2006**, *15* (1), 17–29.

(8) Montange, R. K.; Batey, R. T. Riboswitches: Emerging Themes in RNA Structure and Function. *Annu. Rev. Biophys.* **2008**, *37* (1), 117–133.

(9) Noller, H. F. RNA Structure: Reading the Ribosome. *Science (80-.).* **2005**, *309* (5740), 1508–1514.

(10) Ke, A.; Doudna, J. A. Crystallization of RNA and RNA-Protein Complexes. *Methods* **2004**, *34* (3), 408–414.

(11) Mooers, B. H. M. Crystallographic Studies of DNA and RNA. *Methods* **2009**, *47* (3), 168–176.

(12) Weeks, K. M. Advances in RNA Structure Analysis by Chemical Probing. *Curr. Opin. Struct. Biol.* **2010**, *20* (3), 295–304.

(13) Sigurdsson, S. T.; Tuschl, T.; Eckstein, F. Probing RNA Tertiary Structure: Interhelical Crosslinking of the Hammerhead Ribozyme. *RNA* **1995**, *1*, 575–583.

(14) Akasaka, K. *Experimental Approaches of NMR Spectroscopy*; Japan, T. N. S. of, Ed.; Springer Nature Singapore Pte Ltd.: Kobe, Japan, 2018.

(15) Fürtig, B.; Richter, C.; Wöhnert, J.; Schwalbe, H. NMR Spectroscopy of RNA. *ChemBioChem* **2003**, *4* (10), 936–962.

(16) Varani, G.; Aboul-ela, F.; H-T Allain, F. NMR Investigation of RNA Structure. *Prog. Nucl. Magn. Reson. Spectrosc.* **1996**, *29*, 51–127.

(17) Ferré-D'Amaré, A. R.; Doudna, J. A. Use of Cis- and Trans-Ribozymes to Remove 5′ and 3′ Heterogeneities from Milligrams of in Vitro Transcribed RNA. *Nucleic Acids Res.* **1996**, *24* (5), 977–978.

(18) Grosshans, C. A.; Cech, T. R. A Hammerhead Ribozyme Allows Synthesis of a New Form of the Tetrahymena Ribozyme Homogeneous in Length with a 3' End Blocked for Transesterification. *Nucleic Acids Res.* **1991**, *19* (14), 3875–3880.

(19) Lu, K.; Yasuyuki, M.; Summers, M. F. Isotope Labeling Strategies for NMR Studies of RNA. *J. Biomol. NMR* **2010**, *46*, 113–125.

(20) Qin, P. Z.; Pyle, A. M. Site-Specific Labeling of RNA with Fluorophores and Other Structural Probes. *Methods* **1999**, *18*, 60–70.

(21) Custom RNA Oligos | Sigma-Aldrich https://www.sigmaaldrich.com/technical-documents/articles/biology/custom-rna-oligos.html (accessed Nov 16, 2017).

(22) metabion | RNA Longmers http://www.metabion.com/products/dna-and-rna-custom-oligonucleotides/rna-custom-oligos/rna-longmers/ (accessed Nov 16, 2017).

(23) Standard DNA Synthesis and Purification | Sigma-Aldrich https://www.sigmaaldrich.com/technical-documents/articles/biology/standard-dna-synthesis.html (accessed Nov 16, 2017).

(24) metabion | DNA Oligos - single tube http://www.metabion.com/products/dna-and-rna-custom-oligonucleotides/dna-custom-oligos/dna-oligos-single-tube-

format/#productTab-3 (accessed Nov 16, 2017).

(25) Sakamoto, T.; Otsu, M.; Kawai, G. NMR Studies on RNA. *Exp. Approaches NMR Spectrosc. Methodol. Appl. to Life Sci. Mater. Sci.* **2017**, 439–459.

(26) England, T. E.; Bruce, A. G.; Uhlenbeck, O. C. Specific Labeling of 3′ Termini of RNA with T4 RNA Ligase. *Methods Enzymol.* **1980**, *65* (1977), 65–74.

(27) Liu, Y.; Sousa, R.; Wang, Y. X. Specific Labeling: An Effective Tool to Explore the RNA World. *BioEssays* **2016**, *38* (2), 192–200.

(28) Hilario, E. End Labeling Procedures. *Mol. Biotechnol.* **2004**, *28* (1), 77–80.

(29) Paredes, E.; Evans, M.; Das, S. R. RNA Labeling, Conjugation and Ligation. *Methods* **2011**, *54* (2), 251–259.

(30) Nuovo, G. J. Co-Labeling Using In Situ PCR: A Review. *J. Histochem. Cytochem. Histochem Cytochem* **2001**, *49* (11), 1329–1339.

(31) Proudnikov, D.; Mirzabekov, A. Chemical Methods of DNA and RNA Fluorescent Labeling. *Nucleic Acids Res.* **1996**, *24* (22), 4535–4542.

(32) Wicke, L.; Engels, J. W. Postsynthetic on Column RNA Labeling via Stille Coupling. *Bioconjug. Chem.* **2012**, *23*, 627–642.

(33) Ganesh, V.; Sudhir, V. S.; Kundu, T.; Chandrasekaran, S. 10 Years of Click Chemistry: Synthesis and Applications of Ferrocene-Derived Triazoles. *Chem. - An Asian J.* **2011**, *6* (10), 2670–2694.

(34) Breinbauer, R.; Köhn, M. Azide-Alkyne Coupling: A Powerful Reaction for Bioconjugate Chemistry. *ChemBioChem* **2003**, *4* (11), 1147–1149.

(35) El-Sagheer, A. H.; Brown, T. Click Chemistry with DNA. *Chem. Rev.* **2010**, *39*, 1388–1405.

(36) Tron, G. C.; Pirali, T.; Billington, R. A.; Canonico, P. L.; Sorba, G.; Genazzani, A. A. Click Chemistry Reactions in Medicinal Chemistry: Applications of the 1,3-dipolar Cycloaddition between Azides and Alkynes. *Med. Res. Rev.* **2008**, *28* (2), 278–308.

(37) Lim, R. K. V; Lin, Q. Bioorthogonal Chemistry: Recent Progress and Future Directions. *Chem. Commun.* **2010**, *46*, 1589–1600.

(38) Franke, R.; Doll, C.; Eichler, J. Peptide Ligation through Click Chemistry for the Generation of Assembled and Scaffolded Peptides. *Tetrahedron Lett.* **2005**, *46* (26), 4479–4482.

(39) Zeglis, B. M.; Mohindra, P.; Weissmann, G. I.; Divilov, V.; Hilderbrand, S. A.; Weissleder, R.; Lewis, J. S. Modular Strategy for the Construction of Radiometalated Antibodies for Positron Emission Tomography Based on Inverse Electron Demand Diels–Alder Click Chemistry. *Bioconjug. Chem.* **2011**, *22* (10), 2048–2059.

(40) Zeglis, B. M.; Emmetiere, F.; Pillarsetty, N.; Weissleder, R.; Lewis, J. S.; Reiner, T. Building Blocks for the Construction of Bioorthogonally Reactive Peptides via Solid-Phase Peptide Synthesis. *ChemistryOpen* **2014**, *3* (2), 48–53.

(41) Oliveira, B. L.; Guo, Z.; Bernardes, G. J. L. Inverse Electron Demand Diels–Alder Reactions in Chemical Biology. *Chem. Soc. Rev.* **2017**, *46*, 4885–4950.

(42) Hughes, L. D.; Rawle, R. J.; Boxer, S. G. Choose Your Label Wisely: Water-Soluble Fluorophores Often Interact with Lipid Bilayers. *PLoS One* **2014**, *9* (2), e87649.

(43) Kubik, M. F.; Bell, C.; Fitzwater, T.; Watson, S. R.; Tasset, D. M. Isolation and Characterization of 2'-Fluoro-, 2'-Amino-, and 2'-Fluoro-/Amino-Modified RNA Ligands to Human IFN-Gamma That Inhibit Receptor Binding. *J. Immunol.* **1997**, *159* (1), 259–267.

(44) Allerson, C. R.; Sioufi, N.; Jarres, R.; Prakash, T. P.; Naik, N.; Berdeja, A.; Wanders, L.; Griffey, R. H.; Swayze, E. E.; Bhat, B. Fully 2'-Modified Oligonucleotide Duplexes with Improved in Vitro Potency and Stability Compared to Unmodified Small Interfering RNA. *J. Med. Chem.* **2005**, *48* (4), 901–904.

(45) Singh, S. K.; Koshkin, A. a.; Wengel, J.; Nielsen, P. LNA (Locked Nucleic Acids): Synthesis and High-Affinity Nucleic Acid Recognition. *Chem. Commun.* **1998**, No.

4, 455–456.

(46) Obika, S.; Nanbu, D.; Hari, Y.; Morio, K. I.; In, Y.; Ishida, T.; Imanishi, T. Synthesis of 2'-O,4'-C-Methyleneuridine and -Cytidine. Novel Bicyclic Nucleosides Having a Fixed C3-Endo Sugar Puckering. *Tetrahedron Lett.* **1997**, *38* (50), 8735–8738.

(47) Kaur, H.; Arora, A.; Wengel, J.; Maiti, S. Thermodynamic, Counterion, and Hydration Effects for the Incorporation of Locked Nucleic Acid Nucleotides into DNA Duplexes. *Biochemistry* **2006**, *45* (23), 7347–7355.

(48) Lönnberg, H. Solid-Phase Synthesis of Oligonucleotide Conjugates Useful for Delivery and Targeting of Potential Nucleic Acid Therapeutics. *Bioconjug. Chem.* **2009**, *20* (6), 1065–1094.

(49) Richardson, R. W.; Gumport, R. I. Biotin and Fluorescent Labeling of RNA Using T4 RNA Ligase. *Nucleic Acids Res.* **1983**, *11* (18), 6167–6184.

(50) Alexander, S. C.; Devaraj, N. K. Developing a Fluorescent Toolbox To Shed Light on the Mysteries of RNA. *Biochemistry* **2017**, *56* (5185–5193).

(51) Gramlich, P. M. E.; Warncke, S.; Gierlich, J.; Carell, T. Click-Click-Click: Single to Triple Modification of DNA. *Angew. Chemie - Int. Ed.* **2008**, *47* (18), 3442–3444.

(52) Merkel, M.; Peewasan, K.; Arndt, S.; Ploschik, D.; Wagenknecht, H. A. Copper-Free Postsynthetic Labeling of Nucleic Acids by Means of Bioorthogonal Reactions. *ChemBioChem* **2015**, *16* (11), 1541–1553.

(53) Moore, M. J.; Query, C. C. Joining of RNAs by Splinted Ligation. *Methods Enzymol.* **2000**, *317*, 109–123.

(54) Schoch, J.; Ameta, S.; Jäschke, A. Inverse Electron-Demand Diels–Alder Reactions for the Selective and Efficient Labeling of RNAw. *Chem. Commun.* **2011**, *47* (47), 12536–12537.

(55) Seelig, B.; Jäschke, A. Site-Specific Modification of Enzymatically Synthesized RNA: Transcription Initiation and Diels-Alder Reaction. *Tetrahedron Lett.* **1997**, *38*, 7729–7732.

(56) Srivatsan, S. G.; Tor, Y. Fluorescent Pyrimidine Ribonucleotide: Synthesis, Enzymatic Incorporation, and Utilization. *J. Am. Chem. Soc.* **2007**, *129*, 2044–2053.

(57) Rao, H.; Tanpure, A. A.; Sawant, A. A.; Srivatsan, S. G. Enzymatic Incorporation of an Azide-Modified UTP Analog into Oligoribonucleotides for Post-Transcriptional Chemical Functionalization. *Nat. Protoc.* **2012**, *7* (6), 1097–1112.

(58) Pawar, M. G.; Srivatsan, S. G. Synthesis, Photophysical Characterization, and Enzymatic Incorporation of a Microenvironment-Sensitive Fluorescent Uridine Analog. *Org. Lett.* **2011**, *13* (5), 1114–1117.

(59) Srivatsan, S. G.; Tor, Y. Synthesis and Enzymatic Incorporation of a Fluorescent Pyrimidine Ribonucleotide. *Nat. Protoc.* **2007**, *2* (6), 1547–1555.

(60) Abu El Asrar, R.; Margamuljana, L.; Abramov, M.; Bande, O.; Agnello, S.; Jang, M.; Herdewijn, P. Enzymatic Incorporation of Modified Purine Nucleotides in DNA. *ChemBioChem* **2017**, *18* (24), 2408–2415.

(61) Tabor, S.; Richardson, C. C. DNA Sequence Analysis with a Modified Bacteriophage T7 DNA Polymerase. *Proc. Natl. Acad. Sci.* **1987**, *84* (14), 4767–4771.

(62) Chelliserrykattil, J.; Ellington, A. D. Evolution of a T7 RNA Polymerase Variant That Transcribes 2'-O-Methyl RNA. *Nat. Biotechnol.* **2004**, *22*, 1155–1160.

(63) Wyss, L. A.; Nilforoushan, A.; Williams, D. M.; Marx, A.; Sturla, S. J. The Use of an Artificial Nucleotide for Polymerase-Based Recognition of Carcinogenic O 6 - Alkylguanine DNA Adducts. *Nucleic Acids Res.* **2016**, *44* (14), 6564–6573.

(64) Choi, J.-S.; Dasari, A.; Hu, P.; Benkovic, S. J.; Berdis, A. J. The Use of Modified and Non-Natural Nucleotides Provide Unique Insights into pro-Mutagenic Replication Catalyzed by Polymerase Eta. *Nucleic Acids Res.* **2016**, *44* (3), 1022–1035.

(65) Holstein, J. M.; Schulz, D.; Rentmeister, A. Bioorthogonal Site-Specific Labeling of the 5′-Cap Structure in Eukaryotic MRNAs. *Chem. Commun.* **2014**, *50* (34), 4478–

4481.

(66) Thirumurugan, P.; Matosiuk, D.; Jozwiak, K. Click Chemistry for Drug Development and Diverse Chemical− Biology Applications. *Chem. Rev.* **2013**, *113*, 4905–4979.

(67) Vrabel, M.; Carell, T. *Cycloadditions in Bioorthogonal Chemistry*; Vrabel, M., Carell, T., Eds.; Topics in Current Chemistry Collections; Springer International Publishing: Cham, 2016.

(68) Sletten, E. M.; Bertozzi, C. R. From Mechanism to Mouse: A Tale of Two Bioorthogonal Reactions. *Acc. Chem. Res.* **2011**, *44* (9), 666–676.

(69) Prescher, J. A.; Dube, D. H.; Bertozzi, C. R. Chemical Remodelling of Cell Surfaces in Living Animals. *Nature* **2004**, *430* (August), 873–877.

(70) Baskin, J. M.; Bertozzi, C. R. Bioorthogonal Click Chemistry: Covalent Labeling in Living Systems. *QSAR Comb. Sci.* **2007**, *26* (11–12), 1211–1219.

(71) Sletten, E. M.; Bertozzi, C. R. Bioorthogonal Chemistry: Fishing for Selectivity in a Sea of Functionality. *Angew. Chemie - Int. Ed.* **2009**, *48* (38), 6974–6998.

(72) Kolb, H. C.; Finn, M. G.; Sharpless, K. B. Click Chemistry: Diverse Chemical Function from a Few Good Reactions. *Angew. Chemie - Int. Ed.* **2001**, *40* (11), 2004–2021.

(73) Bertozzi, C. R. A Decade of Bioorthogonal Chemistry. *Acc. Chem. Res.* **2011**, *44* (9), 651–653.

(74) Kolb, H. C.; Sharpless, K. B. The Growing Impact of Click Chemistry on Drug Discovery. *Drug Discov. Today* **2003**, *8* (24), 1128–1137.

(75) Moses, J. E.; Moorhouse, A. D. The Growing Applications of Click Chemistry. *Chem. Soc. Rev.* **2007**, *36* (8), 1249–1262.

(76) Amblard, F.; Cho, J. H.; Schinazi, R. F. Cu(I)-Catalyzed Huisgen Azide-Alkyne 1,3-Dipolar Cycloaddition Reaction in Nucleoside, Nucleotide, and Oligonucleotide Chemistry. **2009**.

(77) Tornøe, C. W.; Christensen, C.; Meldal, M. Peptidotriazoles on Solid Phase: [1,2,3]-Triazoles by Regiospecific Copper(I)-Catalyzed 1,3-Dipolar Cycloadditions of Terminal Alkynes to Azides.

(78) Gierlich, J.; Burley, G. A.; Gramlich, P. M. E.; Hammond, D. M.; Carell, T. Click Chemistry as a Reliable Method for the High-Density Postsynthetic Functionalization of Alkyne-Modified DNA. *Org. Lett.* **2006**, *8* (17), 3639–3642.

(79) Gaetke, L. M.; Chow, C. K. Copper Toxicity, Oxidative Stress, and Antioxidant Nutrients. *Toxicology* **2003**, *189* (1–2), 147–163.

(80) Blackman, M. L.; Royzen, M.; Fox, J. M. Tetrazine Ligation: Fast Bioconjugation Based on Inverse-Electron-Demand Diels-Alder Reactivity. *J Am Chem Soc* **2008**, *130*, 13518–13519.

(81) Devaraj, N. K.; Weissleder, R.; Hilderbrand, S. A. Tetrazine-Based Cycloadditions: Application to Pretargeted Live Cell Imaging. *Bioconjug. Chem.* **2008**, *19* (12), 2297–2299.

(82) Wu, H.; Devaraj, N. K. Inverse Electron-Demand Diels–Alder Bioorthogonal Reactions. *Top. Curr. Chem.* **2016**, *374* (1), 3.

(83) Alvarez-Builla, J.; Vaquero, J. J.; Barluenga, J. Front Matter. In *Modern Heterocyclic Chemistry*; Wiley-VCH Verlag GmbH & Co. KGaA: Weinheim, Germany, 2011; pp I–XIX.

(84) Prokhorov, A. M.; Kozhevnikov, D. N. Triazines and Tetrazines. In *Progress in Heterocyclic Chemistry*; Elsevier, 2014; pp 449–462.

(85) Katritzky, A. R.; Ramsden, C. A.; Joule, J. A.; Zhdankin, V. V. Reactivity of Six-Membered Rings. In *Handbook of Heterocyclic Chemistry*; Elsevier, 2010; pp 242–382.

(86) *Comprehensive Organic Chemistry Experiments for the Laboratory Classroom*; Afonso, C. A. M., Candeias, N. R., Simao, D. P., Trindade, A. F., Coelho, J. A. S., Tan, B., Franzen, R., Eds.; The Royal Society of Chemistry, 2017.

(87) Knall, A.-C.; Slugovc, C. Inverse Electron Demand Diels–Alder (IEDDA)-Initiated

Conjugation: A (High) Potential Click Chemistry Scheme. *Chem. Soc. Rev.* **2013**, *42* (42), 5131–5142.

(88) Brea, R. J.; Devaraj, N. K. Diels-Alder and Inverse Diels-Alder Reactions. In *Chemoselective and Bioorthogonal Ligation Reactions*; Wiley-VCH Verlag GmbH & Co. KGaA: Weinheim, Germany, 2017; pp 67–95.

(89) Alge, D. L.; Donohue, D. F.; Anseth, K. S. Facile and Efficient Lewis Acid Catalyzed Synthesis of an Asymmetric Tetrazine Useful for Bio-Orthogonal Click Chemistry Applications. *Tetrahedron Lett.* **2013**, *54* (41), 5639–5641.

(90) Wang, D.; Chen, W.; Zheng, Y.; Dai, C.; Wang, K.; Ke, B.; Wang, B. 3,6-Substituted-1,2,4,5-Tetrazines: Tuning Reaction Rates for Staged Labeling Applications. *Org. Biomol. Chem.* **2014**, *12* (23), 3950.

(91) Wang, D.; Chen, W.; Zheng, Y.; Dai, C.; Wang, L.; Wang, B. A General and Efficient Entry to Asymmetric Tetrazines for Click Chemistry Applications. *Heterocycl. Commun.* **2013**, *19* (3), 171–177.

(92) Karver, M. R.; Weissleder, R.; Hilderbrand, S. A. Synthesis and Evaluation of a Series of 1,2,4,5-Tetrazines for Bioorthogonal Conjugation. *Bioconjug. Chem.* **2011**, *22*, 2263–2270.

(93) Yang, J.; Karver, M. R.; Li, W.; Sahu, S.; Devaraj, N. K. Metal-Catalyzed One-Pot Synthesis of Tetrazines Directly from Aliphatic Nitriles and Hydrazine. *Angew. Chemie - Int. Ed.* **2012**, *51* (21), 5222–5225.

(94) Sando, S.; Kool, E. T. Imaging of RNA in Bacteria with Self-Ligating Quenched Probes. *J. Am. Chem. Soc.* **2002**, *124*, 9686–9687.

(95) Asare-Okai, P. N.; Agustin, E.; Fabris, D.; Royzen, M. Site-Specific Fluorescence Labelling of RNA Using Bio-Orthogonal Reaction of Trans-Cyclooctene and Tetrazine. *Chem. Commun* **2014**, *50*.

(96) Schoch, J.; Staudt, M.; Samanta, A.; Wiessler, M.; Jäschke, A. Site-Specific One-Pot Dual Labeling of DNA by Orthogonal Cycloaddition Chemistry. *Bioconjug. Chem.* **2012**, *23* (7), 1382–1386.

(97) Schoch, J.; Wiessler, M.; Jäschke, A. Post-Synthetic Modification of DNA by Inverse-Electron-Demand Diels−Alder Reaction. *J. Am. Chem. Soc.* **2010**, *132* (26), 8846–8847.

(98) Liu, D. S.; Tangpeerachaikul, A.; Selvaraj, R.; Taylor, M. T.; Fox, J. M.; Ting, A. Y. Diels−Alder Cycloaddition for Fluorophore Targeting to Specific Proteins inside Living Cells. *J. Am. Chem. Soc.* **2012**, *134*, 792–795.

(99) Lang, K.; Davis, L.; Wallace, S.; Mahesh, M.; Cox, D. J.; Blackman, M. L.; Fox, J. M.; Chin, J. W. Genetic Encoding of Bicyclononynes and Trans -Cyclooctenes for Site-Specific Protein Labeling in Vitro and in Live Mammalian Cells via Rapid Fluorogenic Diels–Alder Reactions. *J. Am. Chem. Soc.* **2012**, *134* (25), 10317–10320.

(100) Lang, K.; Chin, J. W. Cellular Incorporation of Unnatural Amino Acids and Bioorthogonal Labeling of Proteins. *Chem. Rev.* **2014**, *114* (9), 4764–4806.

(101) Lang, K.; Davis, L.; Torres-Kolbus, J.; Chou, C.; Deiters, A.; Chin, J. W. Genetically Encoded Norbornene Directs Site-Specific Cellular Protein Labelling via a Rapid Bioorthogonal Reaction. *Nat. Chem.* **2012**, *4* (4), 298–304.

(102) Karver, M. R.; Weissleder, R.; Hilderbrand, S. A. Bioorthogonal Reaction Pairs Enable Simultaneous, Selective, Multi-Target Imaging. *Angew. Chemie - Int. Ed.* **2012**, *51* (4), 920–922.

(103) Devaraj, N. K.; Upadhyay, R.; Haun, J. B.; Hilderbrand, S. A.; Weissleder, R. Fast and Sensitive Pretargeted Labeling of Cancer Cells through a Tetrazine/Trans-Cyclooctene Cycloaddition. *Angew. Chemie - Int. Ed.* **2009**, *48* (38), 7013–7016.

(104) Hang, H. C.; Linder, M. E. Exploring Protein Lipidation with Chemical Biology. *Chem. Rev.* **2011**, *111* (10), 6341–6358.

(105) Devaraj, N. K.; Thurber, G. M.; Keliher, E. J.; Marinelli, B.; Weissleder, R. Reactive Polymer Enables Efficient in Vivo Bioorthogonal Chemistry. *Acc. Chem. Res.* **2012**, *109* (13), 4762–4767.

(106) Erdmann, R. S.; Takakura, H.; Thompson, A. D.; Rivera-Molina, F.; Allgeyer, E. S.; Bewersdorf, J.; Toomre, D.; Schepartz, A. Super-Resolution Imaging of the Golgi in Live Cells with a Bioorthogonal Ceramide Probe. *Angew. Chemie - Int. Ed.* **2014**, *53* (38), 10242–10246.

(107) Cole, C. M.; Yang, J.; ŠečkuteC, J.; Devaraj, N. K. Fluorescent Live-Cell Imaging of Metabolically Incorporated Unnatural Cyclopropene-Mannosamine Derivatives. *ChemBioChem* **2013**, *14* (2), 205–208.

(108) Prescher, J. A.; Bertozzi, C. R. Chemical Technologies for Probing Glycans. *Cell* **2006**, *126* (5), 851–854.

(109) Png, Z. M.; Zeng, H.; Ye, Q.; Xu, J. Inverse-Electron-Demand Diels–Alder Reactions: Principles and Applications. *Chem. - An Asian J.* **2017**, *12* (17), 2142–2159.

(110) Sauer, J.; Heldmann, D. K.; Hetzenegger, J.; Krauthan, J.; Sichert, H.; Schuster, J. 1 ,2 ,4 ,5-Tetrazine : Synthesis and Reactivity in [4+2] Cycloadditions. *European J. Org. Chem.* **1998**, *1998* (12), 2885–2896.

(111) Foster, R. A. A.; Willis, M. C. Tandem Inverse-Electron-Demand Hetero-/Retro-Diels–Alder Reactions for Aromatic Nitrogen Heterocycle Synthesis. *Chem. Soc. Rev. Chem. Soc. Rev* **2013**, *42* (42), 63–76.

(112) Seitchik, J. L.; Peeler, J. C.; Taylor, M. T.; Blackman, M. L.; Rhoads, T. W.; Cooley, R. B.; Refakis, C.; Fox, J. M.; Mehl, R. A. Genetically Encoded Tetrazine Amino Acid Directs Rapid Site-Specific in Vivo Bioorthogonal Ligation with Trans-Cyclooctenes. *J. Am. Chem. Soc.* **2012**, *134* (6), 2898–2901.

(113) Eicher, T.; Hauptmann, S.; Speicher, A. *The Chemistry of Heterocycles*, Second Edi.; Wiley-VCH Verlag GmbH & Co. KGaA: Weinheim, FRG, 2003.

(114) Pinner, A. Ueber Die Einwirkung von Hydrazin Auf Die Imidoäther. *Berichte der Dtsch. Chem. Gesellschaft* **1897**, *30* (2), 1871–1890.

(115) Pinner Reaction. In *Comprehensive Organic Name Reactions and Reagents*; American Cancer Society: Hoboken, NJ, USA, 2010; pp 2237–2240.

(116) Wieczorek, A.; Werther, P.; Euchner, J.; Wombacher, R. Green- to Far-Red-Emitting Fluorogenic Tetrazine Probes – Synthetic Access and No-Wash Protein Imaging inside Living Cells. *Chem. Sci.* **2017**, *8*, 1506–1510.

(117) Karver, M.; Weissleder, R.; Hilderbrand, S. A.; Wu, H.; Yang, J.; Šečkutė, J.; Devaraj, N. K.; Upadhyay, R.; Haun, J. B.; Hilderbrand, S. A.; et al. Synthesis and Evaluation of a Series of 1 , 2 , 4 , 5- Tetrazines for Bioorthogonal Conjugation Conjugation Center for Systems Biology. *Angew. Chemie* **2011**, *121* (23), 7147–7150.

(118) Liu, H.; Wei, Y. Novel Synthesis of 3,6-Disubstituted-1,2,4,5-Tetrazine Derivatives from Hydrazones by Using [Hydroxyl(Tosyloxy)Iodo]Benzene. *Tetrahedron Lett.* **2013**, *54*, 4645–4648.

(119) Wu, H.; Yang, J.; Šečkutė, J.; Devaraj, N. K. In Situ Synthesis of Alkenyl Tetrazines for Highly Fluorogenic Bioorthogonal Live-Cell Imaging Probes. *Angew. Chemie* **2014**, *126* (23), 5915–5919.

(120) Abdel-Rahman, M. O.; Kira, M. A.; Tolba, M. N. A Direct Synthesis of Dihydrotetrazines. *Tetrahedron Lett.* **1968**, *35*, 3871.

(121) Clavier, G.; Audebert, P. S-Tetrazines as Building Blocks for New Functional Molecules and Molecular Materials. *Chem. Rev.* **2010**, *110*, 3299–3314.

(122) Baddar, F. G.; Al-Hajjar, F. H.; El-Rayyes, N. R. Acetylenic Ketones. Part VI. Reaction of Aroylphenylacetylenes with Hydrazine Derivatives. *J. Heterocycl. Chem.* **1978**, *15* (3), 385–393.

(123) Eicher, T.; Hauptmann, S.; Speicher, A. The Structure of Heterocyclic Compounds. In *The Chemistry of Heterocycles*; Wiley-VCH Verlag GmbH & Co. KGaA: Weinheim, FRG; pp 1–4.

(124) Lang, S. A.; Johnson, B. D.; Cohen, E. Novel Synthesis of Unsymmetrically Substituted S-Tetrazines. *J. Heterocycl. Chem.* **1975**, *12* (6), 1143–1153.

(125) Devaraj, N. K. Advancing Tetrazine Bioorthogonal Reactions through the

Development of New Synthetic Tools. *Synlett* **2012**, *23* (15), 2147–2152.

(126) Reiner, T.; Keliher, E. J.; Earley, S.; Marinelli, B.; Weissleder, R. Synthesis and in Vivo Imaging of a 18F-Labeled PARP1 Inhibitor Using a Chemically Orthogonal Scavenger-Assisted High-Performance Method. *Angew. Chemie - Int. Ed.* **2011**, *50* (8), 1922–1925.

(127) Neves, A. A.; Sto, H.; Wainman, Y. A.; Kuo, J. C.; Fawcett, S.; Leeper, F. J.; Brindle, K. M. Imaging Cell Surface Glycosylation in Vivo Using " Double Click " Chemistry. **2013**.

(128) Willems, L. I.; Li, N.; Florea, B. I.; Ruben, M.; van der Marel, G. a.; Overkleeft, H. S. Triple Bioorthogonal Ligation Strategy for Simultaneous Labeling of Multiple Enzymatic Activities. *Angew. Chemie* **2012**, *124* (18), 4507–4510.

(129) Yang, K. S.; Budin, G.; Tassa, C.; Kister, O.; Weissleder, R. Bioorthogonal Approach to Identify Unsuspected Drug Targets in Live Cells. *Angew. Chemie* **2013**, *125* (40), 10787–10791.

(130) Krueger, A. T.; Kroll, C.; Sanchez, E.; Griffith, L. G.; Imperiali, B. Tailoring Chimeric Ligands for Studying and Biasing ErbB Receptor Family Interactions. *Angew. Chemie* **2014**, *126* (10), 2700–2704.

(131) Hansell, C. F.; O'Reilly, R. K. A "Mix-and-Click" Approach to Double Core–Shell Micelle Functionalization. *ACS Macro Lett.* **2012**, *1* (7), 896–901.

(132) Shieh, P.; Bertozzi, C. R. Organic & Biomolecular Chemistry Design Strategies for Bioorthogonal Smart Probes. *Org. Biomol. Chem.* **2014**, *12*.

(133) Reiner, T.; Zeglis, B. M. The Inverse Electron Demand Diels-Alder Click Reaction in Radiochemistry. *J. Labelled Comp. Radiopharm.* **2014**, *57* (4), 285–290.

(134) Pretze, M.; Pietzsch, D.; Mamat, C. Recent Trends in Bioorthogonal Click-Radiolabeling Reactions Using Fluorine-18. *Molecules* **2013**, *18* (7), 8618–8665.

(135) Zeglis, B. M.; Sevak, K. K.; Reiner, T.; Mohindra, P.; Carlin, S. D.; Zanzonico, P.; Weissleder, R.; Lewis, J. S. A Pretargeted PET Imaging Strategy Based on Bioorthogonal Diels-Alder Click Chemistry. *J. Nucl. Med.* **2013**, *54* (8), 1389–1396.

(136) Taylor, M. T.; Blackman, M. L.; Dmitrenko, O.; Fox, J. M. Design and Synthesis of Highly Reactive Dienophiles for the TetrazineÀtrans-Cyclooctene Ligation. *J. Am. Chem. Soc* **2011**, *133*, 9646–9649.

(137) Bender, A. M.; Chopko, T. C.; Bridges, T. M.; Lindsley, C. W. Preparation of Unsymmetrical 1,2,4,5-Tetrazines via a Mild Suzuki Cross-Coupling Reaction. *Org. Lett.* **2017**, acs.orglett.7b02868.

(138) Ligation, T.; Versteegen, R. M.; Rossin, R.; Hoeve, W.; Janssen, H. M.; Robillard, M. S. Click to Release : Instantaneous Doxorubicin Elimination Upon. **2013**.

(139) Sečkutė, J.; Devaraj, N. K. Expanding Room for Tetrazine Ligations in the in Vivo Chemistry Toolbox. *Curr. Opin. Chem. Biol.* **2013**, *17* (5), 761–767.

(140) Yang, J.; Liang, Y.; Šečkutė, J.; Houk, K. N.; Devaraj, N. K. Synthesis and Reactivity Comparisons of 1-Methyl-3-Substituted Cyclopropene Mini-Tags for Tetrazine Bioorthogonal Reactions. *Chemistry* **2014**, *20* (12), 3365–3375.

(141) Cole, C. M.; Devaraj, N. K.; Yang, J. Live-Cell Imaging of Cyclopropene Tags with Fluorogenic Tetrazine. **2012**.

(142) Meimetis, L. G.; Carlson, J. C. T.; Giedt, R. J.; Kohler, R. H.; Weissleder, R. Ultrafluorogenic Coumarin-Tetrazine Probes for Real-Time Biological Imaging. *Angew. Chemie - Int. Ed.* **2014**, *53* (29), 7531–7534.

(143) Wieczorek, A.; Buckup, T.; Wombacher, R. Rigid Tetrazine Fluorophore Conjugates with Fluorogenic Properties in the Inverse Electron Demand Diels-Alder Reaction. *Org. Biomol. Chem.* **2014**, *12* (24), 4177–4185.

(144) Versteegen, R. M.; Rossin, R.; ten Hoeve, W.; Janssen, H. M.; Robillard, M. S. Click to Release: Instantaneous Doxorubicin Elimination upon Tetrazine Ligation. *Angew. Chemie* **2013**, *125* (52), 14362–14366.

(145) Rieder, U.; Luedtke, N. W. Alkene-Tetrazine Ligation for Imaging Cellular DNA. *Angew. Chemie - Int. Ed.* **2014**, 9322–9326.

(146) Carlson, J. C. T.; Meimetis, L. G.; Hilderbrand, S. a.; Weissleder, R. BODIPY-

Tetrazine Derivatives as Superbright Bioorthogonal Turn-on Probes. *Angew. Chemie Int. Ed.* **2013**, *52* (27), 6917–6920.

(147) Devaraj, N. K.; Weissleder, R. Biomedical Applications of Tetrazine Cycloadditions. *Acc. Chem. Res.* **2011**, *816* (9), 816–827.

(148) Späte, A. K.; Dold, J. E. G. A.; Batroff, E.; Schart, V. F.; Wieland, D. E.; Baudendistel, O. R.; Wittmann, V. Exploring the Potential of Norbornene-Modified Mannosamine Derivatives for Metabolic Glycoengineering. *ChemBioChem* **2016**, *17* (14), 1374–1383.

(149) Gong, Y. H.; Miomandre, F.; Méallet-Renault, R.; Badré, S.; Galmiche, L.; Tang, J.; Audebert, P.; Clavier, G. Synthesis and Physical Chemistry of S-Tetrazines: Which Ones Are Fluorescent and Why? *European J. Org. Chem.* **2009**, No. 35, 6121–6128.

(150) Vemulapalli, G. K.; Cassen, T. Resonance Fluorescence of *s*-Tetrazine and Its Quenching. *J. Chem. Phys.* **1972**, *56* (10), 5120–5127.

(151) McDonald, J. R.; Brus, L. E. Excited State Electronic Structure and Dynamics in Sym-Tetrazine Vapor. *J. Chem. Phys.* **1973**, *59* (9), 4966.

(152) Audebert, P.; Sadki, S.; Miomandre, F.; Clavier, G.; Claude Vernières, M.; Saoud, M.; Hapiot, P. Synthesis of New Substituted Tetrazines: Electrochemical and Spectroscopic Properties. *New J. Chem.* **2004**, *28* (3), 387–392.

(153) Valeur, B. *Molecular Fluorescence*, First Edit.; Wiley-VCH Verlag GmbH: Weinheim, FRG, 2001.

(154) Han, H.-S.; Devaraj, N. K.; Lee, J.; Hilderbrand, S. A.; Weissleder, R.; Bawendi, M. G. Development of a Bioorthogonal and Highly Efficient Conjugation Method for Quantum Dots Using Tetrazine-Norbornene Cycloaddition. *J. Am. Chem. Soc.* **2010**, *132* (23), 7838–7839.

(155) Devaraj, N. K.; Hilderbrand, S. A.; Upadhyay, R.; Mazitschek, R.; Weissleder, R. Bioorthogonal Turn-on Probes for Imaging Small Molecules inside Living Cells. *Angew. Chemie - Int. Ed.* **2010**, *49* (16), 2869–2872.

(156) Dumas-Verdes, C.; Miomandre, F.; Lépicier, E.; Galangau, O.; Vu, T. T.; Clavier, G.; Méallet-Renault, R.; Audebert, P. BODIPY-Tetrazine Multichromophoric Derivatives. *European J. Org. Chem.* **2010**, No. 13, 2525–2535.

(157) Yin, L.-L.; Chen, Z.-Z.; Tong, L.-L.; Xu, K.-H.; Tang, B. Progress on Fluorescent Probes for Thiols. *Chinese J. Anal. Chem.* **2009**, *37*, 1073–1081.

(158) Cheng, F.; Gamble, L. J.; Grainger, D. W.; Castner, D. G. X-Ray Photoelectron Spectroscopy, Time-of-Flight Secondary Ion Mass Spectrometry, and Principal Component Analysis of the Hydrolysis, Regeneration, and Reactivity of N-Hydroxysuccinimide-Containing Organic Thin Films. *Anal. Chem.* **2007**, *79*, 8781–8788.

(159) Herman, B. Absorption and Emission Maxima for Common Fluorophores. *Curr. Protoc. Cell Biol.* **2001**, *00* (1), A.1E.1-A.1E.5.

(160) Borrmann, A.; Milles, S.; Plass, T.; Dommerholt, J.; Verkade, J. M. M.; Wießler, M.; Schultz, C.; van Hest, J. C. M.; van Delft, F. L.; Lemke, E. A. Genetic Encoding of a Bicyclo[6.1.0]Nonyne-Charged Amino Acid Enables Fast Cellular Protein Imaging by Metal-Free Ligation. *ChemBioChem* **2012**, *13* (14), 2094–2099.

(161) Yang, K. S.; Budin, G.; Reiner, T.; Vinegoni, C.; Weissleder, R. Bioorthogonal Imaging of Aurora Kinase A in Live Cells. *Angew. Chemie - Int. Ed.* **2012**, *51* (27), 6598–6603.

(162) Alford, R.; Simpson, H. M.; Duberman, J.; Hill, G. C.; Ogawa, M.; Regino, C.; Kobayashi, H.; Choyke, P. L. Toxicity of Organic Fluorophores Used in Molecular Imaging: Literature Review. *Mol. Imaging* **2009**, *8* (6), 341–354.

(163) Moneron, G.; Medda, R.; Hein, B.; Giske, A.; Westphal, V.; Hell, S. W. Fast STED Microscopy with Continuous Wave Fiber Lasers. *Opt. Express* **2010**, *18* (2), 1302–1309.

(164) Domnick, C. Synthese Neuer Tetrazin-Fluorophor Konjugate Für in Vivo Click an

Norbornen Modifizierten Oligonukleotiden, Universität Bonn, 2013.

(165) Kim, T. G.; Castro, J. C.; Loudet, A.; Jiao, J. G.-S.; Hochstrasser, R. M.; Burgess, K.; Topp, M. R. Correlations of Structure and Rates of Energy Transfer for Through-Bond Energy-Transfer Cassettes. *J. Phys. Chem. A* **2006**, *110* (1), 20–27.

(166) Waldron, C.; Lacroute, F. Effect of Growth Rate on the Amounts of Ribosomal and Transfer Ribonucleic Acids in Yeast. *J. Bacteriol.* **1975**, *122* (3), 855–865.

(167) Palazzo, A. F.; Lee, E. S.; Mekhail, K.; Niu, D.-K.; Miura, P. Non-Coding RNA: What Is Functional and What Is Junk? *Front. Genet.* **2015**, *6*.

(168) Sharp, S. J.; Schaack, J.; Cooley, L.; Burke, D. J.; Soil, D. Structure and Transcription of Eukaryotic TRNA Gene. *Crit. Rev. Biochem. Mol. Biol.* **1985**, *19* (2), 107–144.

(169) Cedergren, R. J.; Sankoff, D.; Larue, B.; Grosjean, H.; Söil, D. The Evolving Trna Molecul. *Crit. Rev. Biochem.* **1981**, *11* (1), 35–104.

(170) Schimmel, P. R.; Schulman, L. Five Specific Protein-Transfer RNA Interaction. *Crit. Rev. Biochem. Mol. Biol.* **1980**, *9* (3), 207–251.

(171) Schimmel, P. RNA Processing and Modifications: The Emerging Complexity of the TRNA World: Mammalian TRNAs beyond Protein Synthesis. *Nat. Rev. Mol. Cell Biol.* **2018**, *19* (1), 45–58.

(172) Noller, H. F. Structure of Ribosomal RNA. *Annu. Rev. Biochem.* **1984**, *53* (1), 119–162.

(173) Ma, L.; Bajic, V. B.; Zhang, Z. On the Classification of Long Non-Coding RNAs. *RNA Biol.* **2013**, *10* (6), 924–933.

(174) Clark, M. B.; Mattick, J. S. Long Noncoding RNAs in Cell Biology. *Semin. Cell Dev. Biol.* **2011**, *22* (4), 366–376.

(175) Ponting, C. P.; Oliver, P. L.; Reik, W. Leading Edge Evolution and Functions of Long Noncoding RNAs. *Cell* **2009**, *136*, 629–641.

(176) Bedoya-Reina, O. C.; Ponting, C. P. Functional RNA Classes: A Matter of Time? *Nat. Struct. Mol. Biol.* **2017**, *24* (1), 7–8.

(177) Tripathi, V.; Ellis, J. D.; Shen, Z.; Song, D. Y.; Pan, Q.; Watt, A. T.; Freier, S. M.; Bennett, C. F.; Sharma, A.; Bubulya, P. A.; et al. The Nuclear-Retained Noncoding RNA MALAT1 Regulates Alternative Splicing by Modulating SR Splicing Factor Phosphorylation. *Mol. Cell* **2010**, *39* (6), 925–938.

(178) Muddashetty, R. S.; Khanam, T.; Kondrashov, A.; Bundman, M.; Iacoangeli, A.; Kremerskothen, J.; Duning, K.; Barnekow, A.; Hüttenhofer, A.; Tiedge, H.; et al. Poly(A)-Binding Protein Is Associated with Neuronal BC1 and BC200 Ribonucleoprotein Particles. *J. Mol. Biol.* **2002**, *321* (3), 433–445.

(179) Kloc, M.; Wilk, K.; Vargas, D.; Shirato, Y.; Bilinski, S.; Etkin, L. D. Potential Structural Role of Non-Coding and Coding RNAs in the Organization of the Cytoskeleton at the Vegetal Cortex of Xenopus Oocytes. *Development* **2005**, *132*, 3445–3457.

(180) Shamovsky, I.; Ivannikov, M.; Kandel, E. S.; Gershon, D.; Nudler, E. RNA-Mediated Response to Heat Shock in Mammalian Cells. *Nature* **2006**, *440* (7083), 556–560.

(181) Mercer, T. R.; Dinger, M. E.; Mattick, J. S. Long Non-Coding RNAs: Insights into Functions. *Nat. Rev. Genet.* **2009**, *10* (3), 155–159.

(182) George, T. P.; Thomas, T. Exon Mapping in Long Noncoding RNAs Using Digital Filters. *Genomics Insights* **2017**, *10*.

(183) Gong, Y.; Huang, H. T.; Liang, Y.; Trimarchi, T.; Aifantis, I.; Tsirigos, A. LncRNA-Screen: An Interactive Platform for Computationally Screening Long Non-Coding RNAs in Large Genomics Datasets. *BMC Genomics* **2017**, *18* (1), 1–18.

(184) Yang, H.; Shang, D.; Xu, Y.; Zhang, C.; Feng, L.; Sun, Z.; Shi, X.; Zhang, Y.; Han, J.; Su, F.; et al. The LncRNA Connectivity Map: Using LncRNA Signatures to Connect Small Molecules, LncRNAs, and Diseases. *Sci. Rep.* **2017**, *7* (1), 1–6.

(185) Pyle, A. M. Looking at LncRNAs with the Ribozyme Toolkit. *Mol. Cell* **2014**, *56* (1),

13–17.

(186) Doudna, J. A.; Cech, T. R. The Chemical Repertoire of Natural Ribozymes. *Nature* **2002**, *418* (6894), 222–228.

(187) Wilson, C.; Szostak, J. W. In Vitro Evolution of a Self-Alkylatlng Ribozyme. *Nature*. 1995, pp 777–782.

(188) Zhang, B.; Cech, T. R. Peptide Bond Formation by in Vitro Selected Ribozymes. *Nature* **1997**, *390* (6655), 96–100.

(189) Müller, S.; Sabine. Special Issue: Ribozymes and RNA Catalysis. *Molecules* **2017**, *22* (5), 789.

(190) Cech, T. R. The RNA Worlds in Context. *Cold Spring Harb. Perspect. Biol.* **2012**, *4* (7), a006742.

(191) Guerrier-Takada, C.; Gardiner, K.; Marsh, T.; Pace, N.; Altman, S. The RNA Moiety of Ribonuclease P Is the Catalytic Subunit of the Enzyme. *Cell* **1983**, *35* (3), 849–857.

(192) Lau, M.; Ferré-D'Amaré, A. Many Activities, One Structure: Functional Plasticity of Ribozyme Folds. *Molecules* **2016**, *21* (11), 1570.

(193) Marraffini, L. A.; Sontheimer, E. J. CRISPR Interference: RNA-Directed Adaptive Immunity in Bacteria and Archaea. *Nat. Rev. Genet.* **2010**, *11* (3), 181–190.

(194) Serganov, A.; Patel, D. J. Ribozymes, Riboswitches and beyond: Regulation of Gene Expression without Proteins. *Nat. Rev.* **2007**, *8*, 776–790.

(195) Adams, P. L.; Stahley, M. R.; Gill, M. L.; Kosek, A. B.; Wang, J.; Strobel, S. A. Crystal Structure of a Group I Intron Splicing Intermediate. *Rna* **2004**, *10* (12), 1867–1887.

(196) Toor, N.; Keating, K. S.; Taylor, S. D.; Pyle, A. M. Crystal Structure of a Self-Spliced Group II Intron. *Science (80-.).* **2008**, *320* (5872), 77–82.

(197) Lee, K.-Y.; Lee, B.-J. Structural and Biochemical Properties of Novel Self-Cleaving Ribozymes. *Molecules* **2017**, *22* (4), 678.

(198) Ward, W. L.; Plakos, K.; Derose, V. J. Nucleic Acid Catalysis: Metals, Nucleobases, and Other Cofactors. *Chem. Rev.* **2014**, *114*, 4318–4342.

(199) Young, K. J.; Gill, F.; Grasby, J. A. Metal Ions Play a Passive Role in the Hairpin Ribozyme Catalysed Reaction. *Nucleic Acids Res.* **1997**, *25* (19), 3760–3766.

(200) Scott, W. G.; Horan, L. H.; Martick, M. The Hammerhead Ribozyme: Structure, Catalysis, and Gene Regulation. *Prog. Mol. Biol. Transl. Sci.* **2013**, *120*, 1–23.

(201) Wilson, T. J.; Lilley, D. M. J. Do the Hairpin and VS Ribozymes Share a Common Catalytic Mechanism Based on General Acid – Base Catalysis ? A Critical Assessment of Available Experimental Data. *Spring* **2011**, 213–221.

(202) Nakano, S. I.; Chadalavada, D. M.; Bevilacqua, P. C. General Acid-Base Catalysis in the Mechanism of a Hepatitis Delta Virus Ribozyme. *Science (80-.).* **2000**, *287* (5457), 1493–1497.

(203) Doherty, E. A.; Doudna, J. A. Ribozyme Structures and Mechanisms. *Annu. Rev. Biophys. Biomol. Struct.* **2001**, *30* (1), 457–475.

(204) Kath-Schorr, S.; Wilson, T. J.; Li, N.-S.; Lu, J.; Piccirilli, J. A.; Lilley, D. M. J. General Acid-Base Catalysis Mediated by Nucleobases in the Hairpin Ribozyme. *J. Am. Chem. Soc.* **2012**, *134* (40), 16717–16724.

(205) Martick, M.; Lee, T.-S.; York, D. M.; Scott, W. G. Solvent Structure and Hammerhead Ribozyme Catalysis. *Chem. Biol.* **2008**, *15*, 332–342.

(206) DeRose, V. J. Metal Ion Binding to Catalytic RNA Molecules. *Curr. Opin. Struct. Biol.* **2003**, *13* (3), 317–324.

(207) Hanna, R.; Doudna, J. A. Metal Ions in Ribozyme Folding and Catalysis. *Curr. Opin. Chem. Biol.* **2000**, *4* (2), 166–170.

(208) Peracchi, A.; Beigelman, L.; Scott, E. C.; Uhlenbeck, O. C.; Herschlag, D. Involvement of a Specific Metal Ion in the Transition of the Hammerhead Ribozyme to Its Catalytic Conformation. *J. Biol. Chem.* **1997**, *272* (43), 26822–26826.

(209) Lee, T. S.; Silva-López, C.; Martick, M.; Scott, W. G.; York, D. M. Insight into the

Role of Mg2+ in Hammerhead Ribozyme Catalysis from X-Ray Crystallography and Molecular Dynamics Simulation. *J. Chem. Theory Comput.* **2007**, *3* (2), 325–327.

(210) Hampel, A.; Cowan, J. A. A Unique Mechanism for RNA Catalysis : The Role of Metal Cofactors in Hairpin Ribozyme Cleavage. *Chem. Biol.* **1997**, *4* (7), 513–517.

(211) Bevilacqua, P. C. Mechanistic Considerations for General Acid-Base Catalysis by RNA: Revisiting the Mechanism of the Hairpin Ribozyme. *Biochemistry* **2003**, *42* (8), 2259–2265.

(212) Liu, Y.; Wilson, T. J.; McPhee, S. A.; Lilley, D. M. J. Crystal Structure and Mechanistic Investigation of the Twister Ribozyme. *Nat. Chem. Biol.* **2014**, *10* (9), 739–744.

(213) Ren, A.; Košuti, M.; Rajashankar, K. R.; Frener, M.; Santner, T.; Westhof, E.; Micura, R.; Patel, D. J. In-Line Alignment and Mg 2+ Coordination at the Cleavage Site of the Env22 Twister Ribozyme. *Nat. Commun.* **2014**, *5*.

(214) Eiler, D.; Wang, J.; Steitz, T. A. Structural Basis for the Fast Self-Cleavage Reaction Catalyzed by the Twister Ribozyme. *Proc. Natl. Acad. Sci. U. S. A.* **2014**, *111* (36), 13028–13033.

(215) Zheng, L.; Mairhofer, E.; Teplova, M.; Zhang, Y.; Ma, J.; Patel, D. J.; Micura, R.; Ren, A. Structure-Based Insights into Self-Cleavage by a Four-Way Junctional Twister-Sister Ribozyme. *Nat. Commun.* **2017**, *8* (1), 1–12.

(216) Weinberg, Z.; Kim, P. B.; Chen, T. H.; Li, S.; Harris, K. A.; Lünse, C. E.; Breaker, R. R. New Classes of Self-Cleaving Ribozymes Revealed by Comparative Genomics Analysis. *Nat. Chem. Biol.* **2015**, *11* (8), 606–610.

(217) Neuner, S.; Falschlunger, C.; Fuchs, E.; Himmelstoss, M.; Ren, A.; Patel, D. J.; Micura, R. Atom-Specific Mutagenesis Reveals Structural and Catalytic Roles for an Active-Site Adenosine and Hydrated Mg2+in Pistol Ribozymes. *Angew. Chemie - Int. Ed.* **2017**, *56* (50), 15954–15958.

(218) Roth, A.; Weinberg, Z.; Chen, A. G. Y. Y.; Kim, P. B.; Ames, T. D.; Breaker, R. R. A Widespread Self-Cleaving Ribozyme Class Is Revealed by Bioinformatics. *Nat. Chem. Biol.* **2014**, *10* (1), 56–60.

(219) Felletti, M.; Stifel, J.; Wurmthaler, L. A.; Geiger, S.; Hartig, J. S. Twister Ribozymes as Highly Versatile Expression Platforms for Artificial Riboswitches. *Nat. Commun.* **2016**, *7*, 12834.

(220) Gebetsberger, J.; Micura, R. Unwinding the Twister Ribozyme: From Structure to Mechanism. *Wiley Interdiscip. Rev. RNA* **2017**, *8* (3), 1–14.

(221) Zhang, M.; Perelson, A. S.; Tung, C.-S. RNA Structural Motifs. In *eLS*; John Wiley & Sons, Ltd: Chichester, UK, 2011.

(222) Rossini, S. *Egyptian Hieroglyphics: How to Read and Write Them*; Egypt Series; Dover Publications, 1989.

(223) Müller, S.; Appel, B.; Balke, D.; Hieronymus, R.; Nübel, C. Thirty-Five Years of Research into Ribozymes and Nucleic Acid Catalysis: Where Do We Stand Today? *F1000 Fac. Rev* **2016**, No. 5.

(224) Košutic, M.; Neuner, S.; Ren, A.; Flür, S.; Wunderlich, C.; Mairhofer, E.; Vušurovic, N.; Seikowski, J.; Breuker, K.; Höbartner, C.; et al. A Mini-Twister Variant and Impact of Residues/Cations on the Phosphodiester Cleavage of This Ribozyme Class. *Angew. Chemie - Int. Ed.* **2015**, *54* (50), 15128–15133.

(225) Ferré-D 'amaré, A. R. The GlmS Ribozyme: Use of a Small Molecule Coenzyme by a Gene-Regulatory RNA. *Q Rev Biophys.* **2010**, *43* (4), 423–447.

(226) Jimenez, R. M.; Polanco, J. A.; Lupták, A. Chemistry and Biology of Self-Cleaving Ribozymes. *Trends Biochem. Sci.* **2015**, *40*, 648–661.

(227) Webb, C.-H. T.; Riccitelli, N. J.; Ruminski, D. J.; Lupták, A. Widespread Occurrence of Self-Cleaving Ribozyme. *Science (80-.).* **2009**, *326* (5955), 953.

(228) Kapinos, L. E.; Operschall, B. P.; Larsen, E.; Sigel, H. Understanding the Acid-Base Properties of Adenosine: The Intrinsic Basicities of N1, N3 and N7. *Chem. - A Eur. J.* **2011**, *17* (29), 8156–8164.

(229) Muth, G. W.; Ortoleva-Donnelly, L.; Strobel, S. A. A Single Adenosine with a Neutral PK(a) in the Ribosomal Peptidyl Transferase Center. *Science (80-.).* **2000**, *289* (5481), 947–950.

(230) Weblet Importer http://www.glenresearch.com/data/ProductInfo.php# (accessed Oct 17, 2018).

(231) ChemGenes Products – 7-Deaza Adenosine CED phosphoramidite https://www.chemgenes.com/products.php?product=ANP-7101&c=4 (accessed Oct 17, 2018).

(232) Plützer, C.; Kleinermanns, K. Tautomers and Electronic States of Jet-Cooled Adenine Investigated by Double Resonance Spectroscopy. *Phys. CHem. Chem. Phys.* **2002**, *4*, 4877–4882.

(233) Cristalli, G.; Franchetti, P.; Grifantini, M.; Vittori, S.; Bordoni, T.; Geroni, C. Improved Synthesis and Antitumor Activity of 1-Deazaadenosine. *J. Med. Chem.* **1987**, *30*, 1686–1688.

(234) Antonini, I.; Cristalli, G.; Franchetti, P.; Grifantini, M.; Martelli, S.; Petrelli, F. Deaza Analogues of Adenosine as Inhibitors of Blood Platelet Aggregation. *J. Pharm. Sci.* **1984**, *73* (3), 366–369.

(235) Serebryany, V.; Beigelman, L. An Efficient Preparation of Protected Ribonucleosides for Phosphoramidite RNA Synthesis. *Tetrahedron Lett.* **2002**, *43* (11), 1983–1985.

(236) Rich, A. On the Problems of Evolution and Biochemical Information Transfer. In *Horizons in Biochemistry*; Kasha, M., Pullman, B., Eds.; Academic Press: New York, NY, 1962; pp 103–126.

(237) Bergstrom, D. E. Unnatural Nucleosides with Unusual Base Pairing Properties. In *Current Protocols in Nucleic Acid Chemistry*; John Wiley & Sons, Inc.: Hoboken, NJ, USA, 2009; p 1.4.1-1.4.32.

(238) Patel, P. H.; Loeb, L. A. DNA Polymerase Active Site Is Highly Mutable: Evolutionary Consequences. *PNAS* **2000**, *97* (10), 5095–5100.

(239) Freemont, P. S.; Friedman, J. M.; Beese, L. S.; Sandersont, M. R.; Steitz, T. A. Cocrystal Structure of an Editing Complex of Klenow Fragment with DNA. *Biochemistry* **1988**, *85* (December), 8924–8928.

(240) Cheetham, G. M. T.; Steitz, T. A. Structure of a Transcribing T7 RNA Polymerase Initiation Complex. *Science (80-.).* **1999**, *286* (5448), 2305–2309.

(241) Seo, Y. J.; Malyshev, D. A.; Lavergne, T.; Ordoukhanian, P.; Romesberg, F. E. Site-Specific Labeling of DNA and RNA Using an Efficiently Replicated and Transcribed Class of Unnatural Base Pairs. *J. Am. Chem. Soc.* **2011**, *133* (49), 19878–19888.

(242) McMinn, D. L.; Ogawa, A. K.; Wu, Y.; Liu, J.; Schultz, P. G.; Romesberg, F. E. Efforts toward Expansion of the Genetic Alphabet: DNA Polymerase Recognition of a Highly Stable, Self-Pairing Hydrophobic Base [10]. *J. Am. Chem. Soc.* **1999**, *121* (49), 11585–11586.

(243) Berger, M.; Ogawa, A. K.; McMinn, D. L.; Wu, Y.; Schultz, P. G.; Romesberg, F. E. Stable and Selective Hybridization of Oligonucleotides with Unnatural Hydrophobic Bases. *Angew. Chemie - Int. Ed.* **2000**, *39* (16), 2940–2942.

(244) Hirao, I.; Kimoto, M. Unnatural Base Pair Systems toward the Expansion of the Genetic Alphabet in the Central Dogma. *Proc. Jpn. Acad.* **2012**, *88* (7), 345.

(245) Hirao, I.; Kimoto, M. A Synthetic Biology Approach to the Expansion of the Genetic Alphabet : Molecular Design of Unnatural Base Pairs of DNA. *TCI Mail* **2012**, No. 148, 2–11.

(246) Hirao, I. Unnatural Base Pair Systems for DNA/RNA-Based Biotechnology. *Curr. Opin. Chem. Biol.* **2006**, *10* (6), 622–627.

(247) Piccirilli, J. A.; Krauch, T.; Moroney, S. E.; Benner, S. A. Enzymatic Incorporation of a New Base Pair into DNA and RNA Extends the Genetic Alphabet. *Nature* **1990**, *343*, 33–37.

(248) Henry, A. A.; Romesberg, F. E. Beyond A, C, G and T: Augmenting Nature's

Alphabet. *Curr. Opin. Chem. Biol.* **2003**, *7* (6), 727–733.

(249) Schwitzer, C.; Moroney, S. E.; Benner, S. A. Enzymatic Incorporation of a New Base Pair into DNA and RNA Extends the Genetic Alphabet. *J. Am. Chem. Soc.* **1989**, *111*, 8322–8323.

(250) Switzer, C. Y.; Moroney, S. E.; Benner, S. A. Enzymatic Recognition of the Base Pair between Isocytidine and Isoguanosinet. *Biochemistry* **1993**, *32*, 10489–10496.

(251) Krosigk, U. Von; Benner, S. A. Expanding the Genetic Alphabet : Pyrazine Nucleosides That Support a Donor À Donor À Acceptor Hydrogen-Bonding Pattern Aromatic and , Therefore , Able to Stack , the Ring System Must Be Joined to the Sugar by a Creases Susceptibility to Oxidation , but Cr. **2004**, *87*, 1299–1324.

(252) Minakawa, N.; Kojima, N.; Hikishima, S.; Sasaki, T.; Kiyosue, A.; Atsumi, N.; Ueno, Y.; Matsuda, A. New Base Pairing Motifs. The Synthesis and Thermal Stability of Oligodeoxynucleotides Containing Imidazopyridopyrimidine Nucleosides with the Ability to Form Four Hydrogen Bonds. *J. Am. Chem. Soc.* **2003**, *125* (33), 9970–9982.

(253) Guckian, K. M.; Krugh, T. R.; Kool, E. T. Solution Structure of a DNA Duplex Containing a Replicable Difluorotoluene-Adenine Pair. *Nat. Struct. Biol.* **1998**, *5* (11), 954–959.

(254) Morales, J. C.; Kool, E. T. Efficient Replication between Non-Hydrogen- Bonded Nucleoside Shape. *Nat. Struct. Biol.* **1998**, *5* (11), 950–954.

(255) Morales, J. C.; Kool, E. T. Minor Groove Interactions between Polymerase and DNA: More Essential to Replication than Watson-Crick Hydrogen Bonds? *J. Am. Chem. Soc.* **1999**, *121*, 2323–2324.

(256) Ishikawa, M.; Hirao, I.; Yokoyama, S. Synthesis of 3-(2-Deoxy-β-D-Ribofuranosyl)Pyridin-2-One and 2-Amino-6- (N,N-Dimethylamino)-9-(2-Deoxy-β-D-Ribofuranosyl)Purine Derivatives for an Unnatural Base Pair. *Tetrahedron Lett.* **2000**, *41* (20), 3931–3934.

(257) Fujiwara, T.; Kimoto, M.; Sugiyama, H.; Hirao, I.; Yokoyama, S. Synthesis of 6-(2-Thienyl)Purine Nucleoside Derivatives That Form Unnatural Base Pairs with Pyridin-2-One Nucleosides. *Bioorganic Med. Chem. Lett.* **2001**, *11* (16), 2221–2223.

(258) Mitsui, T.; Kitamura, A.; Kimoto, M.; To, T.; Sato, A.; Hirao, I.; Yokoyama, S. An Unnatural Hydrophobic Base Pair with Shape Complementarity between Pyrrole-2-Carbaldehyde and 9-Methylimidazo[(4,5)-b]Pyridine. *J. Am. Chem. Soc.* **2003**, *125* (18), 5298–5307.

(259) Okamoto, I.; Miyatake, Y.; Kimoto, M.; Hirao, I. High Fidelity, Efficiency and Functionalization of Ds−Px Unnatural Base Pairs in PCR Amplification for a Genetic Alphabet Expansion System. *ACS Synth. Biol.* **2016**, *5*, 1220–1230.

(260) Kimoto, M.; Matsunaga, K.; Hirao, I. DNA Aptamer Generation by Genetic Alphabet Expansion SELEX (ExSELEX) Using an Unnatural Base Pair System. In *Nucleic Acid Aptamers: Selection, Characterization, and Application*; Mayer, G., Ed.; Springer New York: New York, NY, 2016; pp 47–60.

(261) Kimoto, M.; Sato, A.; Kawai, R.; Yokoyama, S.; Hirao, I. Site-Specific Incorporation of Functional Components into RNA by Transcription Using Unnatural Base Pair Systems. *Nucleic Acids Symp. Ser. (Oxf).* **2009**, No. 53, 73–74.

(262) Betz, K.; Kimoto, M.; Diederichs, K.; Hirao, I.; Marx, A. Structural Basis for Expansion of the Genetic Alphabet with an Artificial Nucleobase Pair. *Angew. Chemie - Int. Ed.* **2017**.

(263) Leconte, A. M.; Hwang, G. T.; Matsuda, S.; Capek, P.; Hari, Y.; Romesberg, F. E.; Hwang, G. T.; Leconte, A. M.; Joubert, N.; Hocek, M.; et al. Discovery, Characterization, and Optimization of an Unnatural Base Pair for Expansion of the Genetic Alphabet. *J. Am. Chem. Soc.* **2008**, *130* (7), 2336–2343.

(264) Wu, Y.; Ogawa, A. K.; Berger, M.; McMinn, D. L.; Schultz, P. G.; Romesberg, F. E. Efforts toward Expansion of the Genetic Alphabet: Optimization of Interbase Hydrophobic Interactions. *J. Am. Chem. Soc.* **2000**, *122* (32), 7621–7632.

(265) Ogawa, A. K.; Wu, Y.; Berger, M.; Schultz, P. G.; Romesberg, F. E. Rational Design of an Unnatural Base Pair with Increased Kinetic Selectivity [14]. *J. Am. Chem. Soc.* **2000**, *122* (36), 8803–8804.

(266) Berger, M.; Luzzi, S. D.; Henry, A. A.; Romesberg, F. E. Stability and Selectivity of Unnatural DNA with Five-Membered-Ring Nucleobase Analogues. *J. Am. Chem. Soc.* **2002**, *124* (7), 1222–1226.

(267) Romesberg, F. E.; Yu, C.; Matsuda, S.; Henry, A. A. Development of a Universal Nucleobase and Modified Nucleobases for Expanding the Genetic Code. *Curr. Protoc. Nucleic Acid Chem.* **2002**, *Chapter 1*, Unit 1.5.

(268) Matsuda, S.; Henry, A. A.; Schultz, P. G.; Romesberg, F. E. The Effect of Minor-Groove Hydrogen-Bond Acceptors and Donors on the Stability and Replication of Four Unnatural Base Pairs. *J. Am. Chem. Soc.* **2003**, *125* (20), 6134–6139.

(269) Matsuda, S.; Romesberg, F. E. Optimization of Interstrand Hydrophobic Packing Interactions within Unnatural DNA Base Pairs. *J. Am. Chem. Soc.* **2004**, *126* (44), 14419–14427.

(270) Leconte, A. M.; Hwang, G. T.; Matsuda, S.; Capek, P.; Hari, Y.; Romesberg, F. E. Discovery, Characterization, and Optimization of an Unnatural Base Pair for Expansion of the Genetic Alphabet. *J. Am. Chem. Soc.* **2008**, *130* (7), 2336–2343.

(271) Seo, Y. J.; Hwang, G. T.; Ordoukhanian, P.; Romesberg, F. E. Optimization of an Unnatural Base Pair toward Natural-like Replication. *J. Am. Chem. Soc.* **2009**, *131* (23), 3246–3252.

(272) Betz, K.; Malyshev, D. a; Lavergne, T.; Welte, W.; Diederichs, K.; Dwyer, T. J.; Ordoukhanian, P.; Romesberg, F. E.; Marx, A. KlenTaq Polymerase Replicates Unnatural Base Pairs by Inducing a Watson-Crick Geometry. *Nat. Chem. Biol.* **2012**, *8* (7), 612–614.

(273) Betz, K.; Malyshev, D. A.; Lavergne, T.; Welte, W.; Diederichs, K.; Romesberg, F. E.; Marx, A. Structural Insights into DNA Replication without Hydrogen Bonds. *J. Am. Chem. Soc.* **2013**, *135* (49), 18637–18643.

(274) Li, L.; Degardin, M.; Lavergne, T.; Malyshev, D. A.; Dhami, K.; Ordoukhanian, P.; Romesberg, F. E.; Degardin, M.; Lavergne, T.; Malyshev, D. A.; et al. Natural-like Replication of an Unnatural Base Pair for the Expansion of the Genetic Alphabet and Biotechnology Applications. *J. Am. Chem. Soc.* **2014**, *136* (3), 826–829.

(275) Feldman, A. W.; Romesberg, F. E. Expansion of the Genetic Alphabet: A Chemist's Approach to Synthetic Biology. *Acc. Chem. Res.* **2018**, *51* (2), 394–403.

(276) Lavergne, T.; Degardin, M.; Malyshev, D. A.; Quach, H. T.; Dhami, K.; Ordoukhanian, P.; Romesberg, F. E. Expanding the Scope of Replicable Unnatural DNA: Stepwise Optimization of a Predominantly Hydrophobic Base Pair. *J. Am. Chem. Soc.* **2013**, *135* (14), 5408–5419.

(277) Dhami, K.; Malyshev, D. A.; Ordoukhanian, P.; Kubelka, T.; Hocek, M.; Romesberg, F. E. Systematic Exploration of a Class of Hydrophobic Unnatural Base Pairs Yields Multiple New Candidates for the Expansion of the Genetic Alphabet. *Nucleic Acids Res.* **2014**, *42* (16), 10235–10244.

(278) Moran, S.; Ren, R. X. F.; Rumney IV, S.; Kool, E. T. Difluorotoluene, a Nonpolar Isostere for Thymine, Codes Specifically and Efficiently for Adenine in DNA Replication. *J. Am. Chem. Soc.* **1997**, *119* (8), 2056–2057.

(279) Dill, K. A. Dominant Forces in Protein Folding. *Biochemistry* **1990**, *29* (31), 7133–7155.

(280) Ogawa, A. K.; Wu, Y.; McMinn, D. L.; Liu, J.; Schultz, P. G.; Romesberg, F. E. Efforts toward the Expansion of the Genetic Alphabet: Information Storage and Replication with Unnatural Hydrophobic Base Pairs. *J. Am. Chem. Soc.* **2000**, *122* (14), 3274–3287.

(281) Matsuda, S.; Leconte, A. M.; Romesberg, F. E. Minor Groove Hydrogen-Bonds

and the Replication of Unnatural Base Pairs. *J. Am. Chem. Soc.* **2007**, *129* (17), 5551–5557.

(282) Morales, J. C.; Kool, E. T. Functional Hydrogen-Bonding Map of the Minor Groove Binding Tracks of Six DNA Polymerases. *Biochemistry* **2000**, *39* (42), 12979–12988.

(283) Feldman, A. W.; Romesberg, F. E. Expansion of the Genetic Alphabet: A Chemist's Approach to Synthetic Biology. *Acc. Chem. Res.* **2018**, *51* (2), 394–403.

(284) Spratt, T. E. Identification of Hydrogen Bonds between Escherichia Coli DNA Polymerase I (Klenow Fragment) and the Minor Groove of DNA by Amino Acid Substitution of the Polymerase and Atomic Substitution of the DNA. *Biochemistry* **2001**, *40* (9), 2647–2652.

(285) Li, Y.; Waksman, G. Crystal Structures of a DdATP-, DdTTP-, DdCTP, and DdGTP- Trapped Ternary Complex of Klentaq1: Insights into Nucleotide Incorporation and Selectivity. *Protein Sci.* **2001**, *10* (6), 1225–1233.

(286) Zhang, Y.; Ptacin, J. L.; Fischer, E. C.; Aerni, H. R.; Caffaro, C. E.; San Jose, K.; Feldman, A. W.; Turner, C. R.; Romesberg, F. E. A Semi-Synthetic Organism That Stores and Retrieves Increased Genetic Information. *Nature* **2017**.

(287) Zhang, Y.; Lamb, B. M.; Feldman, A. W.; Zhou, A. X.; Lavergne, T.; Li, L.; Romesberg, F. E. A Semisynthetic Organism Engineered for the Stable Expansion of the Genetic Alphabet. *Proc. Natl. Acad. Sci.* **2017**, *114* (6), 1317–1322.

(288) Li, C.; Tebo, A. G.; Gautier, A. Fluorogenic Labeling Strategies for Biological Imaging. *Int. J. Mol. Sci.* **2017**, *18* (7).

(289) George, J. T.; Srivatsan, S. G. Posttranscriptional Chemical Labeling of RNA by Using Bioorthogonal Chemistry. *Methods* **2017**, *120*, 28–38.

(290) Verma, S.; Eckstein, F. MODIFIED OLIGONUCLEOTIDES: Synthesis and Strategy for Users. *Annu. Rev. Biochem.* **1998**, *67* (1), 99–134.

(291) Gößringer, M.; Helmecke, D.; Köhler, K.; Schön, A.; Kirsebom, L. A.; Bindereif, A.; Hartmann, R. K. Enzymatic RNA Synthesis Using Bacteriophage T7 RNA Polymerase. In *Handbook of RNA Biochemistry, Second edition*; Hartmann, R. K., Bindereif, A., Westhof, E., Eds.; Wiley-VCH Verlag GmbH & Co. KGaA, 2005; pp 3–21.

(292) Leconte, A. M.; Chen, L.; Romesberg, F. E. Polymerase Evolution: Efforts toward Expansion of the Genetic Code. *J. Am. Chem. Soc.* **2005**, *127* (36), 12470–12471.

(293) Lavergne, T.; Lamichhane, R.; Malyshev, D. A.; Li, Z.; Li, L.; Sperling, E.; Williamson, J. R.; Millar, D. P.; Romesberg, F. E. FRET Characterization of Complex Conformational Changes in a Large 16S Ribosomal RNA Fragment Site-Specifically Labeled Using Unnatural Base Pairs. *ACS Chem. Biol.* **2016**, *11* (5), 1347–1353.

(294) Kimoto, M.; Hikida, Y.; Hirao, I. Site-Specific Functional Labeling of Nucleic Acids by In Vitro Replication and Transcription Using Unnatural Base Pair Systems. *Isr. J. Chem.* **2013**, *53* (6–7), 450–468.

(295) Salikhov, K. M.; Keywords, Z.; Zavoisky, E. K. Zavoisky and the Discovery of EPR. *Resonance* **2015**, *20* (11), 963–968.

(296) Nejatyjahromy, Y.; Schubert, E. Progress in Biological Sciences Demystifying EPR: A Rookie Guide to the Application of Electron Paramagnetic Resonance Spectroscopy on Biomolecules. *Prog. Biol. Sci.* **2014**, *4* (2), 133–152.

(297) Yadav, L. D. S. *Organic Spectroscopy*, 1st editio.; Yadav, L. D. S., Ed.; Springer: Dordrecht, 2005.

(298) Fielding, A. J.; Concilio, M. G.; Heaven, G.; Hollas, M. A. New Developments in Spin Labels for Pulsed Dipolar EPR. *Molecules* **2014**, *19* (10), 16998–17025.

(299) Hughes, R. A.; Ellington, A. D. Synthetic DNA Synthesis and Assembly: Putting the Synthetic in Synthetic Biology. *Cold Spring Harb. Perspect. Biol.* **2017**, *9* (1), a023812.

(300) Schiemann, O.; Piton, N.; Plackmeyer, J.; Bode, B. E.; Prisner, T. F.; Engels, J. W. Spin Labeling of Oligonucleotides with the Nitroxide TPA and Use of PELDOR,

a Pulse EPR Method, to Measure Intramolecular Distances. *Nat. Protoc.* **2007**, *2* (4), 904–923.

(301) Kerzhner, M.; Abdullin, D.; Więcek, J.; Matsuoka, H.; Hagelueken, G.; Schiemann, O.; Famulok, M. Post-Synthetic Spin-Labeling of RNA through Click Chemistry for PELDOR Measurements. *Chem. - A Eur. J.* **2016**, *22* (34), 12113–12121.

(302) Kerzhner, M.; Matsuoka, H.; Wuebben, C.; Famulok, M.; Schiemann, O. High-Yield Spin Labeling of Long RNAs for Electron Paramagnetic Resonance Spectroscopy. *Biochemistry* **2018**, *57* (20), 2923–2931.

(303) Schmitt, A. M.; Chang, H. Y. Long Noncoding RNAs in Cancer Pathways. *Cancer Cell* **2016**, *29* (4), 452–463.

(304) Peng, Y.; Calin, G. A. Crucial Role of Non-Coding RNAs in Disease. *Cancer Lett.* **2018**, *420*, 127–128.

(305) Zhang, Y.; Huang, H.; Zhang, D.; Qiu, J.; Yang, J.; Wang, K.; Zhu, L.; Fan, J.; Yang, J. A Review on Recent Computational Methods for Predicting Noncoding RNAs. *Biomed Res. Int.* **2017**, *2017*.

(306) Babaylova, E. S.; Ivanov, A. V.; Malygin, A. A.; Vorobjeva, M. A.; Venyaminova, A. G.; Polienko, Y. F.; Kirilyuk, I. A.; Krumkacheva, O. A.; Fedin, M. V.; Karpova, G. G.; et al. A Versatile Approach for Site-Directed Spin Labeling and Structural EPR Studies of RNAs. *Org. Biomol. Chem.* **2014**, *12* (19), 3129–3136.

(307) Panja, S.; Hua, B.; Zegarra, D.; Ha, T.; Woodson, S. A. Metals Induce Transient Folding and Activation of the Twister Ribozyme. *Nat. Chem. Biol.* **2017**, No. august, 1–10.

(308) Cai, Sui, X.; Cebon, B.; Litvak, J.; Pararajasingham, K.; Shelton, Emma, J.; Spencer, Jeffrey, R.; Sperandio, D.; Sprengeler, Paul, A.; Tai, Vincent, W.-F.; Yee, Robert, M. Novel Phenyl Derivatives as Inducers of Apoptosis. PCT/US2003/012604, 2003.

(309) Pyka, A. M.; Domnick, C.; Braun, F.; Kath-Schorr, S. Diels-Alder Cycloadditions on Synthetic RNA in Mammalian Cells. *Bioconjug. Chem.* **2014**, *25* (8), 1438–1443.

(310) Domnick, C.; Eggert, F.; Kath-Schorr, S. Site-Specific Enzymatic Introduction of a Norbornene Modified Unnatural Base into RNA and Application in Posttranscriptional Labeling. *Chem. Commun.* **2015**, *51* (39), 8253–8256.

(311) Eggert, F.; Kath-Schorr, S. A Cyclopropene-Modified Nucleotide for Site-Specific RNA Labeling Using Genetic Alphabet Expansion Transcription. *Chem. Commun.* **2016**, *52* (45), 7284–7287.

(312) Masuya, T.; Murai, M.; Ito, T.; Aburaya, S.; Aoki, W.; Miyoshi, H. Pinpoint Chemical Modification of the Quinone-Access Channel of Mitochondrial Complex I via a Two-Step Conjugation Reaction. *Biochemistry* **2017**, *56* (32), 4279–4287.

(313) Kumar, A.; Hao, G.; Liu, L.; Ramezani, S.; Hsieh, J.-T.; Öz, O. K.; Sun, X. Click-Chemistry Strategy for Labeling Antibodies with Copper-64 via a Cross-Bridged Tetraazamacrocyclic Chelator Scaffold. *Bioconjug. Chem.* **2015**, *26* (4), 782–789.

(314) Ravasco, J. M. J. M.; Monteiro, C. M.; Trindade, A. F. Cyclopropenes: A New Tool for the Study of Biological Systems. *Org. Chem. Front.* **2017**, *4*, 1167–1198.

(315) Hama, Y.; Urano, Y.; Koyama, Y.; Bernardo, M.; Choyke, P. L.; Kobayashi, H. A Comparison of the Emission Efficiency of Four Common Green Fluorescence Dyes after Internalization into Cancer Cells. *Bioconjug. Chem.* **2006**, *17* (6), 1426–1431.

(316) Burgess, K.; Cook, D. Syntheses of Nucleoside Triphosphates. *Chem. Rev.* **2000**, *100* (6), 2047–2060.

(317) Caton-Williams, J.; Lin, L.; Smith, M.; Huang, Z. Convenient Synthesis of Nucleoside 5'-Triphosphates for RNA Transcription. *Chem. Commun. (Camb).* **2011**, *47* (28), 8142–8144.

(318) King, J.; Miller, H. R. P.; Bloch, J.; Jarrett, E.; Bazin, H. Structural Origins of High-Affinity Biotin Binding to Streptavidin. **1987**, *391* (1984).

(319) Eggert, F.; Kulikov, K.; Domnick, C.; Leifels, P.; Kath-Schorr, S. Iluminated by

Foreign Letters – Strategies for Site-Specific Cyclopropene Modification of Large Functional RNAs via in Vitro Transcription. *Methods* **2017**, *120*, 17–27.

(320) Rolland, V.; Kotera, M.; Lhomme, J. Convenient Preparation of 2-Deoxy-3,5-Di-O-*p*-Toluoyl-α-D-*Erythro*-Pentofuranosyl Chloride. *Synth. Commun.* **1997**, *27* (20), 3505–3511.

(321) Kovács, T.; Ötvös, L. Simple Synthesis of 5-Vinyl- and 5-Ethynyl-2'-Deoxyuridine-5'-Triphosphate. *Tetrahedron Lett.* **1988**, *29* (36), 4525–4528.

(322) Leal, N. A.; Kim, H. J.; Hoshika, S.; Kim, M. J.; Carrigan, M. A.; Benner, S. A. Transcription, Reverse Transcription, and Analysis of RNA Containing Artificial Genetic Components. *ACS Synth. Biol.* **2015**, *4* (4), 407–413.

(323) Seo, Y. J.; Matsuda, S.; Romesberg, F. E. Transcription of an Expanded Genetic Alphabet. *J. Am. Chem. Soc.* **2009**, *131* (14), 5046–5047.

(324) Xu, G.; Moeller, K. D. Anodic Coupling Reactions and the Synthesis of C-Glycosides --Supporting Information General Procedure and Spectra Data for Electrolysis. *Org. Lett.* **2010**, *12* (11), 2590–2593.

(325) Lou, C.; Xiao, Q.; Brennan, L.; Light, M. E.; Vergara-Irigaray, N.; Atkinson, E. M.; Holden-Dye, L. M.; Fox, K. R.; Brown, T. Synthesis and Properties of Triplex-Forming Oligonucleotides Containing 2'-O-(2-Methoxyethyl)-5-(3-Aminoprop-1-Ynyl)-Uridine. *Bioorg. Med. Chem.* **2010**, *18* (17), 6389–6397.

(326) Van Rijssel, E. R.; Van Delft, P.; Van Marle, D. V; Bijvoets, S. M.; Lodder, G.; Overkleeft, H. S.; Van Der Marel, G. A.; Filippov, D. V; Codeé, J. D. C. Stereoselectivity in the Lewis Acid Mediated Reduction of Ketofuranoses. *J. Org. Chem.* **2015**, *80*, 4553–4565.

(327) Barker, R.; Fletcher, H. G. 2,3,5-Tri-O-Benzyl-D-Nbosyl and -L-Arabinosyl Bromides. *J. Org. Chem.* **1961**, *26*, 4605–4609.

(328) Wuts, P. G. M.; Greene, T. W. *Greene's Protective Groups in Organic Synthesis*, 5th ed.; John Wiley & Sons, Inc., 2014.

(329) ElAmin, B.; Anantharamaiah, G. M.; Royer, G. P.; Means, G. E. Removal of Benzyl-Type Protecting Groups from Peptides by Catalytic Transfer Hydrogenation with Formic Acid. *J. Org. Chem.* **1979**, *44* (19), 3442–3444.

(330) Bashir-Uddin Surfraz, M.; Akhtar, M.; Allemann, R. K. Bis-Benzyl Protected 6-Amino Cyclitols Are Poisonous to Pd/C Catalysed Hydrogenolysis of Benzyl Ethers. *Tetrahedron Lett.* **2004**, *45* (6), 1223–1226.

(331) Nicolaou, K. C.; Mitchell, H. J.; Jain, N. F.; Winssinger, N.; Hughes, R.; Bando, T. Total Synthesis of Vancomycin. *Angew. Chemie Int. Ed.* **1999**, *38* (1–2), 240–244.

(332) Hawker, S.; Bhatti, M. A.; Griffin, K. G. The Removal of Protecting Groups by Catalytic Hydrogenation. *Chim. Oggi* **1992**, *10* (1), 49–51.

(333) Bhatt, M. V.; Kulkarni, S. U. Cleavage of Ethers. *Synthesis (Stuttg).* **1983**, *4*, 249–282.

(334) Ranu, B. C.; Bhar, S. Dealkylation of Ethers. A Review. *Org. Prep. Proced. Int.* **1996**, *28* (4), 371–409.

(335) Sousa, C.; Silva, P. J. BBr3-Assisted Cleavage of Most Ethers Does Not Follow the Commonly Assumed Mechanism. *European J. Org. Chem.* **2013**, No. 23, 5195–5199.

(336) Okano, K.; Okuyama, K.; Fukuyama, T.; Tokuyama, H. Mild Debenzylation of Aryl Benzyl Ether with BCl3 in the Presence of Pentamethylbenzene as a Non-Lewis-Basic Cation Scavenger. *Synlett* **2008**, *2008* (13), 1977–1980.

(337) Angibeaud, P.; Defaye, J.; Gadelle, A.; Utille, J.-P. Mild Deprotection of Benzyl Ether Protective Groups with Ozone. *Synthesis (Stuttg).* **1985**, *12*, 1123–1125.

(338) Mund, G. Synthese Methylierter RNA-Basen Und Deren Einfluss Auf Die Spaltaktivität Des CPEB3 Ribozyms, Rheinische Friedrich-Wilhelms-Universität Bonn, 2014.

(339) Tolle, F. Click-SELEX - A Versatile Approach towards Nucleobase-Modified Aptamers, Rheinische Friedrich-Wilhelms Universität Bonn, 2016.

(340) Andrus, A.; Kuimelis, R. G. Base Composition Analysis of Nucleosides Using

HPLC. *Curr. Protoc. Nucleic Acid Chem.* **2000**, *10.6*, 10.6.1-10.6.6.

(341) Kurscheidt, K. Reverse Transcription of Unnatural Base Pairs, Rheinische Friedrich-Wilhelms-Universität Bonn, 2018.

(342) Tkach, I.; Pornsuwan, S.; Höbartner, C.; Wachowius, F.; Sigurdsson, S. T.; Baranova, T. Y.; Diederichsen, U.; Sicoli, G.; Bennati, M. Orientation Selection in Distance Measurements between Nitroxide Spin Labels at 94 GHz EPR with Variable Dual Frequency Irradiation. *Phys. Chem. Chem. Phys.* **2013**, *15* (10), 3433–3437.

(343) Weeks, K.; Crothers, D. Major Groove Accessibility of RNA. *Science (80-.).* **1993**, *261* (5128), 1574–1577.

(344) Keana, J. F. W. Newer Aspects of the Synthesis and Chemistry of Nitroxide Spin Labels. *Chem. Rev.* **1978**, *78* (1), 37–64.

(345) Spaltenstein, A.; Robinson, B. H.; Hopkins, P. B. Sequence- and Structure-Dependent DNA Base Dynamics: Synthesis, Structure, and Dynamics of Site, and Sequence Specifically Spin-Labeled DNA. *Biochemistry* **1989**, *28* (24), 9484–9495.

(346) Kálai, T.; Balog, M.; Jekö, J.; Hideg, K. Synthesis and Reactions of a Symmetric Paramagnetic Pyrrolidine Diene. *Synthesis (Stuttg).* **1999**, *1999* (06), 973–980.

(347) Azarkh, M.; Singh, V.; Okle, O.; Seemann, I. T.; Dietrich, D. R.; Hartig, J. S.; Drescher, M. Site-Directed Spin-Labeling of Nucleotides and the Use of in-Cell EPR to Determine Long-Range Distances in a Biologically Relevant Environment. *Nat. Protoc.* **2012**, *8* (1), 131–147.

(348) Haugland, M. M.; El-Sagheer, A. H.; Porter, R. J.; Peña, J.; Brown, T.; Anderson, E. A.; Lovett, J. E. 2′-Alkynylnucleotides: A Sequence- and Spin Label-Flexible Strategy for EPR Spectroscopy in DNA. *J. Am. Chem. Soc.* **2016**, *138* (29), 9069–9072.

(349) Lai, J. T. Hindered Amines III: Highly Regioselective Syntheses of 1,3,3,5,5-Pentasubstituted 2-Piperazinones and Their Nitroxyl Radicals. *Synthesis (Stuttg).* **1981**, No. 1, 40–42.

(350) Lai, J. T. Hindered Amines I: 4-Hydroxy-1,3,3,5,5-Pentasubstituted-2-Piperazinones. *Synthesis (Stuttg).* **1984**, No. 2, 124–125.

(351) Lee, T. D.; Keana, J. F. W. W. In Situ Reduction of Nitroxide Spin Labels with Phenylhydrazine in Deuteriochloroform Solution. A Convenient Method for Obtaining Structural Information on Nitroxides Using Nuclear Magnetic Resonance Spectroscopy. *J. Org. Chem.* **1975**, *40* (21), 3145–3147.

(352) Ludwig, J. A New Route to Nucleoside 5'-Triphosphates. *Acta Biochim. Biophys. Acad. Sci. Hung.* **1981**, *16* (3–4), 131–133.

(353) Yoshikawa, M.; Kato, T.; Takenishi, T. A Novel Method for Phosphorylation of Nucleosides to 5'-Nucleotides. *Tetrahedron Lett.* **1967**, No. 50, 5065–5068.

(354) Ludwig, J.; Eckstein, F. Rapid and Efficient Synthesis of Nucleoside 5'-O-(1-Thiotriphosphates), 5'-Triphosphates and 2',3'-Cyclophosphorothioates Using 2-Chloro-4H-1,3,2-Benzodioxaphosphorin-4-One. *J. Org. Chem.* **1989**, *54* (3), 631–635.

(355) Tahirov, T. H.; Temiakov, D.; Anikin, M.; Patlan, V.; Mcallister, W. T.; Vassylyev, D. G.; Yokoyama, S. Structure of a T7 RNA Polymerase Elongation Complex at 2.9 A Resolution. *Nature* **2002**, *420*, 43–50.

(356) Yin, Y. W.; Steitz, T. A. Structural Basis for the Transition from Initiation to Elongation Transcription in T7 RNA Polymerase. *Science (80-.).* **2002**, *298* (5597), 1387–1395.

(357) Kimoto, M.; Yamashige, R.; Matsunaga, K.; Yokoyama, S.; Hirao, I. Generation of High-Affinity DNA Aptamers Using an Expanded Genetic Alphabet. *Nat. Biotechnol.* **2013**, *31* (5), 453–457.

(358) Gray, D. M.; Liu, J. -J; Ratliff, R. L.; Allen, F. S. Sequence Dependence of the Circular Dichroism of Synthetic Double-stranded RNAs. *Biopolymers* **1981**, *20* (7), 1337–1382.

(359) Riazance, J. H.; Baase, W. A.; Johnson, W. C.; Hall, K.; Cruz, P.; Tinoco, I. Evidence for Z-Form RNA by Vacuum UV Circular Dichroism. *Nucleic Acids Res.* **1985**, *13* (13).

(360) Jaeger, J. A.; Santalucia, J.; Tinoco, I. Determination of RNA Structure and Thermodynamics. *Annu. Rev. Biochem* **1993**, *62*, 255–287.

(361) Halbmair, K.; Seikowski, J.; Tkach, I.; Höbartner, C.; Sezer, D.; Bennati, M. High-Resolution Measurement of Long-Range Distances in RNA: Pulse EPR Spectroscopy with TEMPO-Labeled Nucleotides. *Chem. Sci.* **2016**, *7* (5), 3172–3180.

(362) Hagelueken, G.; Ward, R.; Naismith, J. H.; Schiemann, O. MtsslWizard: In Silico Spin-Labeling and Generation of Distance Distributions in PyMOL. *Appl. Magn. Reson.* **2012**, *42* (3), 377–391.

(363) Ke, A.; Zhou, K.; Ding, F.; Cate, J. H. D.; Doudna, J. A. A Conformational Switch Controls Hepatitis Delta Virus Ribozyme Catalysis. *Nature* **2004**, *429*, 201–205.

(364) Cupps, T. L.; Wise, D. S.; Townsend, L. B. A Further Investigation of the Stannic Chloride-Catalyzed Condensation Reaction of 1-Hexene and 1,2,3,5-Tetra-O-Acyl-Beta-D-Ribofuranoses. *Carbohydr. Res.* **1983**, *115*, 59–73.

(365) Crouch, R. D. Selective Monodeprotection of Bis-Silyl Ethers. *Tetrahedron* **2004**, *60* (28), 5833–5871.

(366) Nelson, T. D.; Crouch, R. D. Selective Deprotection of Silyl Ethers. *Synthesis (Stuttg).* **1996**, *9*, 1031–1069.

(367) Crouch, R. D. Selective Deprotection of Silyl Ethers. *Tetrahedron* **2013**, *69*, 2383–2417.

(368) Wuts, P. G. M.; Bigelow, S. S. Application of Allylboronates to the Synthesis of Carbomycin B. *J. Org. Chem.* **1988**, *53*, 5023–5034.

(369) Mulzer, J.; Schöllhorn, B. Multiple 1,2-O,O-Shift of Tert-Butyldiphenylsilyl Groups in Polyols. *Angew. Chemie Int. Ed. English* **1990**, *29* (4), 431–432.

(370) Brook, A. G. Molecular Rearrangements of Organosilicon Compounds. *Acc. Chem. Res.* **1974**, *7*, 77–84.

(371) Wilson, T. J.; Liu, Y.; Domnick, C.; Kath-Schorr, S.; Lilley, D. M. J. The Novel Chemical Mechanism of the Twister Ribozyme. *J. Am. Chem. Soc.* **2016**, *138* (19), 6151–6162.

(372) Suslov, N. B.; DasGupta, S.; Huang, H.; Fuller, J. R.; Lilley, D. M. J.; Rice, P. A.; Piccirilli, J. A. Crystal Structure of the Varkud Satellite Ribozyme. *Nat. Chem. Biol.* **2015**, *11* (11), 840–846.

(373) Gaines, C. S.; York, D. M. Ribozyme Catalysis with a Twist: Active State of the Twister Ribozyme in Solution Predicted from Molecular Simulation. *J. Am. Chem. Soc.* **2016**, *138* (9), 3058–3065.

(374) Ucisik, M. N.; Bevilacqua, P. C.; Hammes-Schiffer, S. Molecular Dynamics Study of Twister Ribozyme: Role of Mg2+ Ions and the Hydrogen-Bonding Network in the Active Site. *Biochemistry* **2016**, *55* (27), 3834–3846.

(375) TLC Visualization Reagents http://lcso.epfl.ch/files/content/sites/lcso/files/load/TLC_Stains.pdf (accessed May 8, 2017).

(376) TLC recipes http://www.modestmolecule.com/useful-resources/my-tlc-recipes, requested 08.05.2017. (accessed May 8, 2017).

(377) Fulmer, G. R.; M Miller, A. J.; Sherden, N. H.; Gottlieb, H. E.; Nudelman, A.; Stoltz, B. M.; Bercaw, J. E.; Goldberg, K. I.; Beckman, M. NMR Chemical Shifts of Trace Impurities: Common Laboratory Solvents, Organics, and Gases in Deuterated Solvents Relevant to the Organometallic Chemist. **2010**.

(378) Boströ, J.; Hogner, A.; Llinà, A.; Wellner, E.; Plowright, A. T. Oxadiazoles in Medicinal Chemistry. *J. Med. Chem.* **2012**, *55*, 1817–1830.

(379) Obeid, S.; Yulikov, M.; Jeschke, G.; Marx, A. Enzymatic Synthesis of Multiple Spin-Labeled DNA. *Angew. Chemie Int. Ed.* **2008**, *47* (36), 6782–6785.

(380) Beigelman, L.; Karpeisky, Alexander Serebryany, V.; Haeberli, P.; Sweedler, D.

Methods of Producing Phosphitylated Compounds. WO 03/072586 A2, 2002.

(381) Benson, D. A.; Karsch-Mizrachi, I.; Lipman, D. J.; Ostell, J.; Wheeler, D. L. GenBank. *Nucleic Acids Res.* **2004**, *33* (Database issue), D34–D38.

(382) Kofoid, E. DNA Electroelution http://rothlab.ucdavis.edu/protocols/dna-electroelution.shtml (accessed May 2, 2017).

(383) Oligo Calc: Oligonucleotide Properties Calculator http://biotools.nubic.northwestern.edu/OligoCalc.html (accessed May 8, 2017).

7 Appendix

7.1 NMR spectra
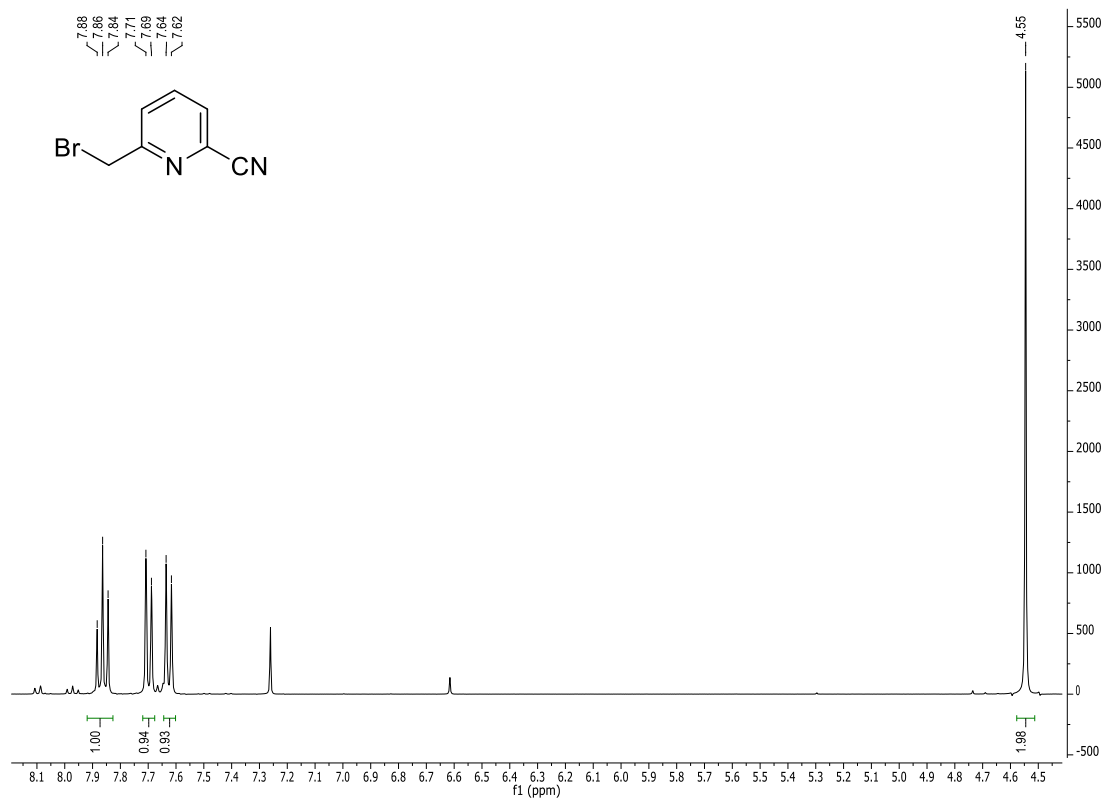
^{1}H NMR of compound **46**: CDCl$_3$; 400 MHz; r.t.
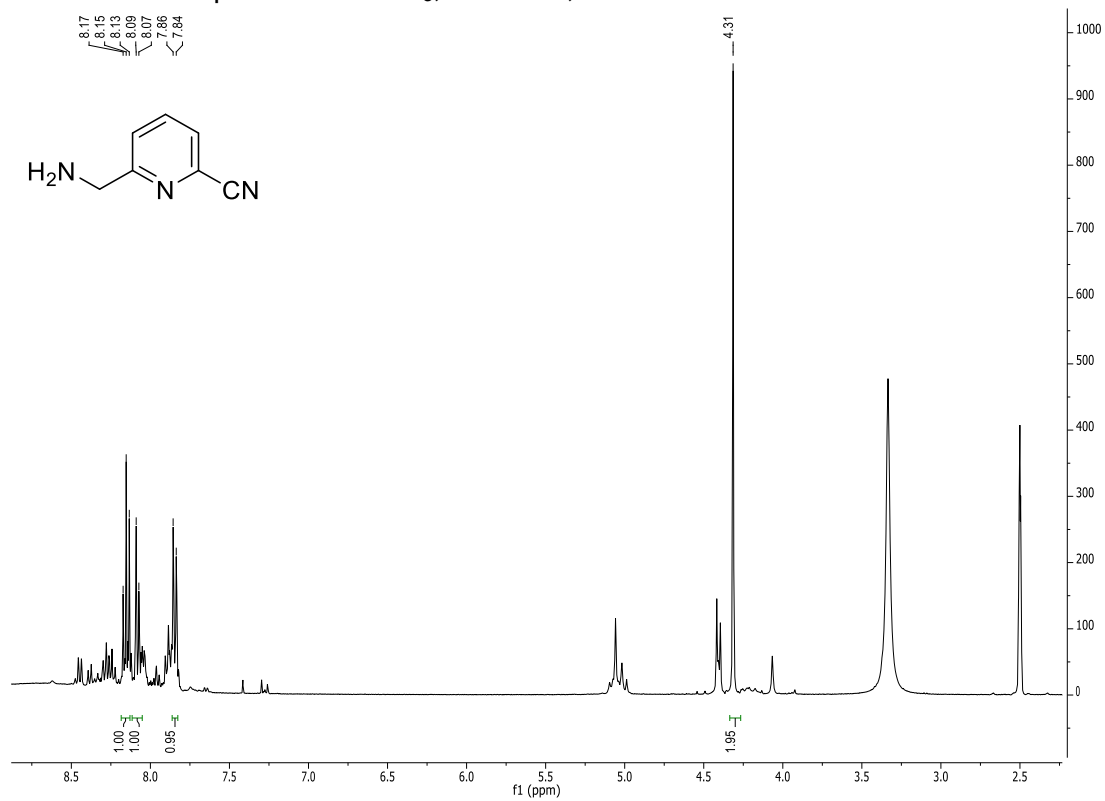
^{1}H NMR of compound **47**: DMSO-d_6; 400 MHz; r.t.
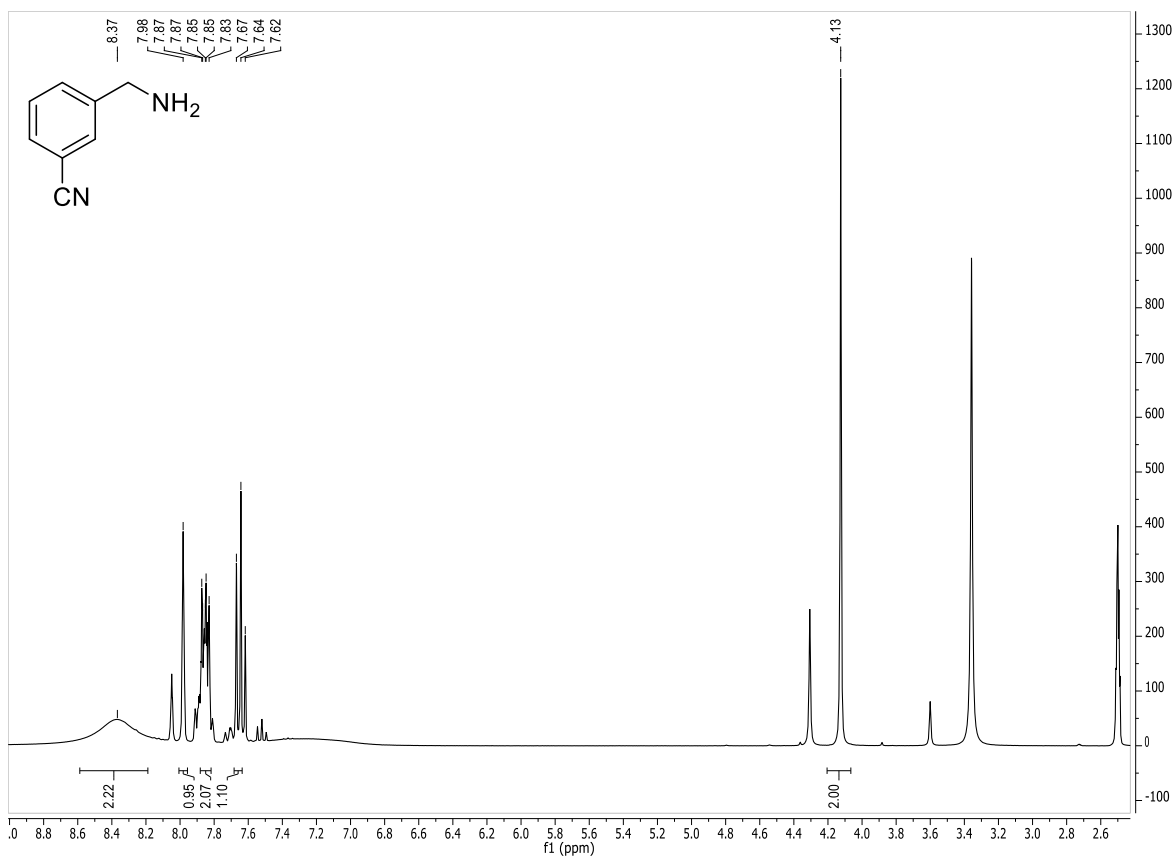
^{1}H NMR of compound **49**: DMSO-d_6; 400 MHz; r.t.
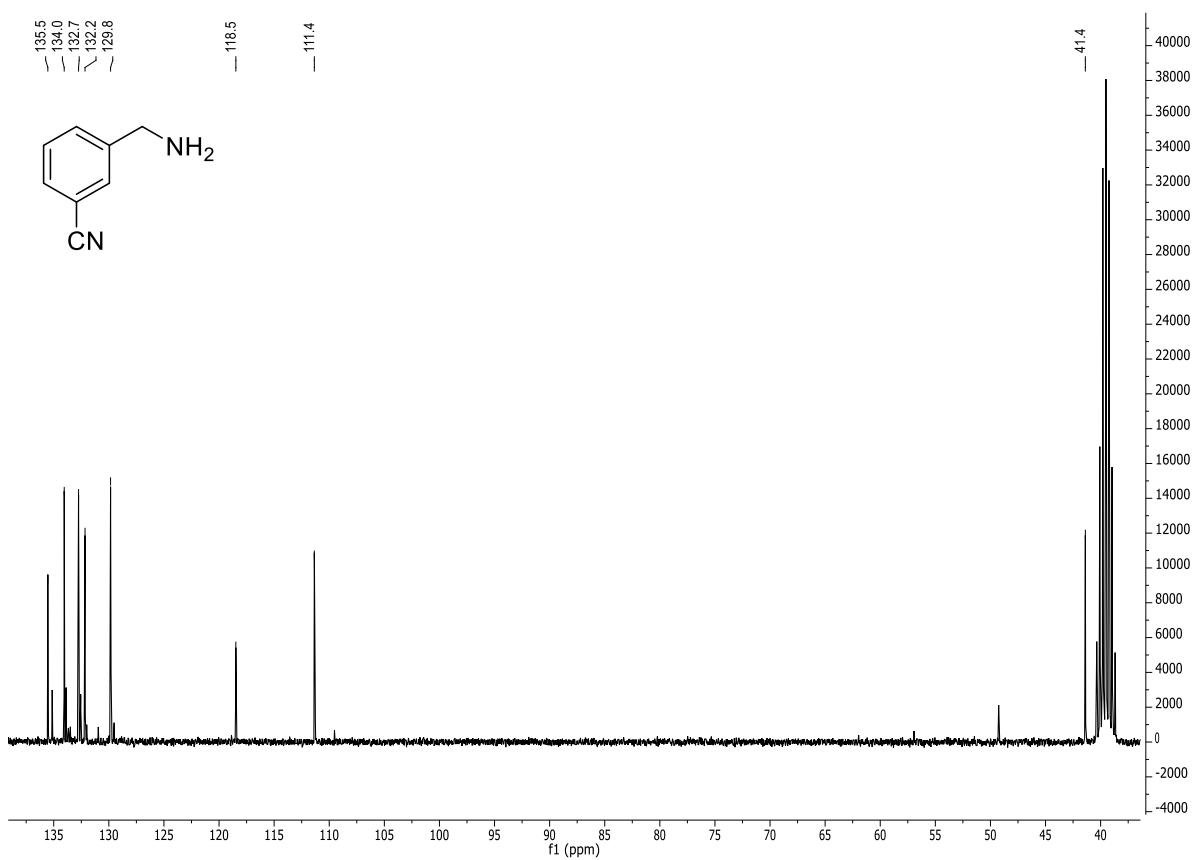
^{13}C NMR of compound **49**: DMSO-d_6; 75 MHz; r.t.
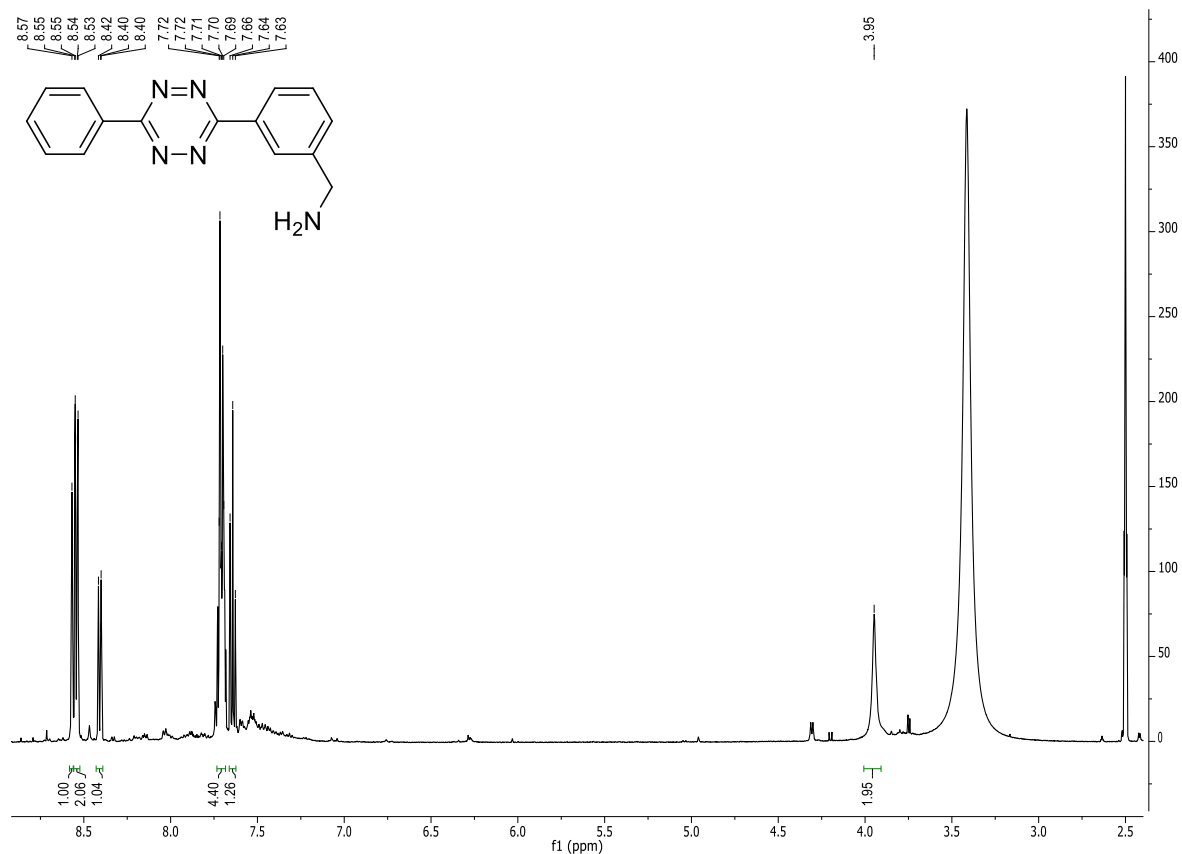
^{1}H NMR of compound **51**: DMSO-d_6; 500 MHz; r.t.
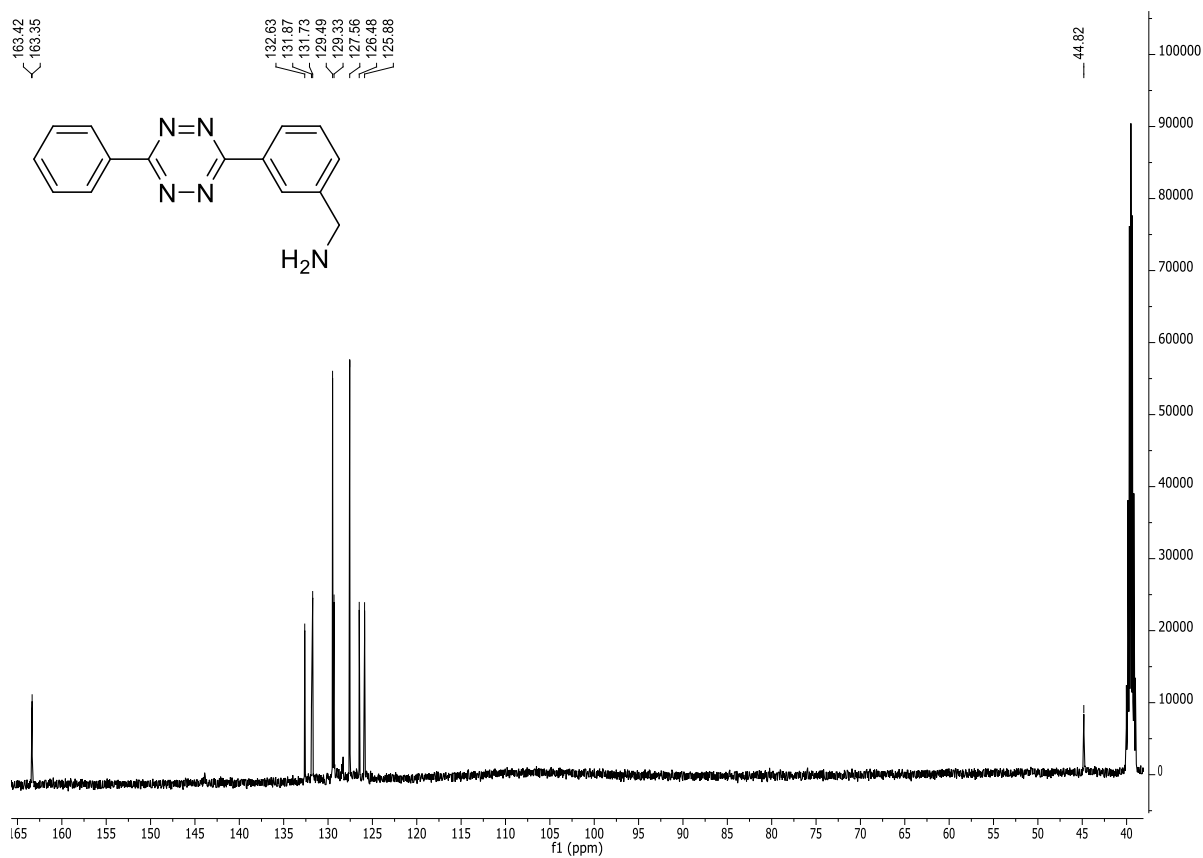
^{13}C NMR of compound **51**: DMSO-d_6; 126 MHz; r.t.
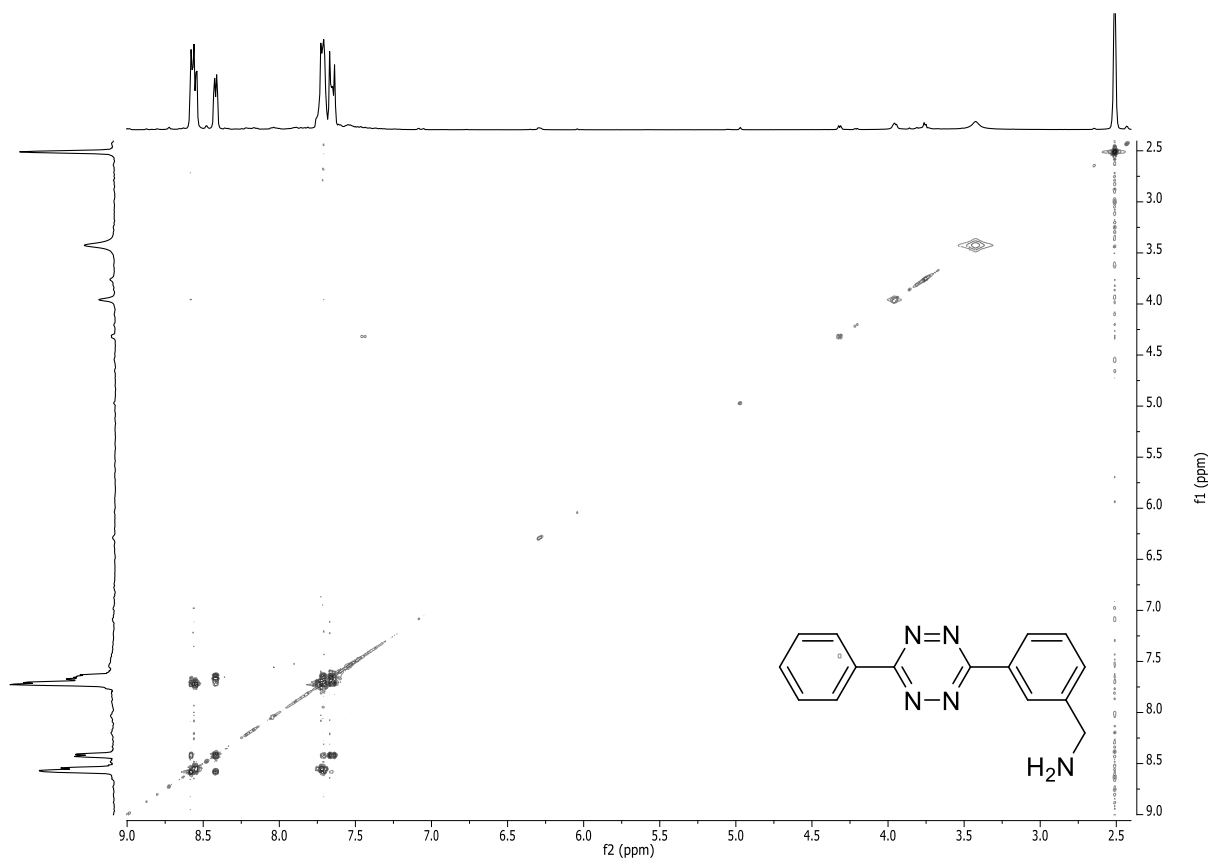
H,H-COSY NMR of compound **51**: DMSO-d_6; 500 MHz; r.t.
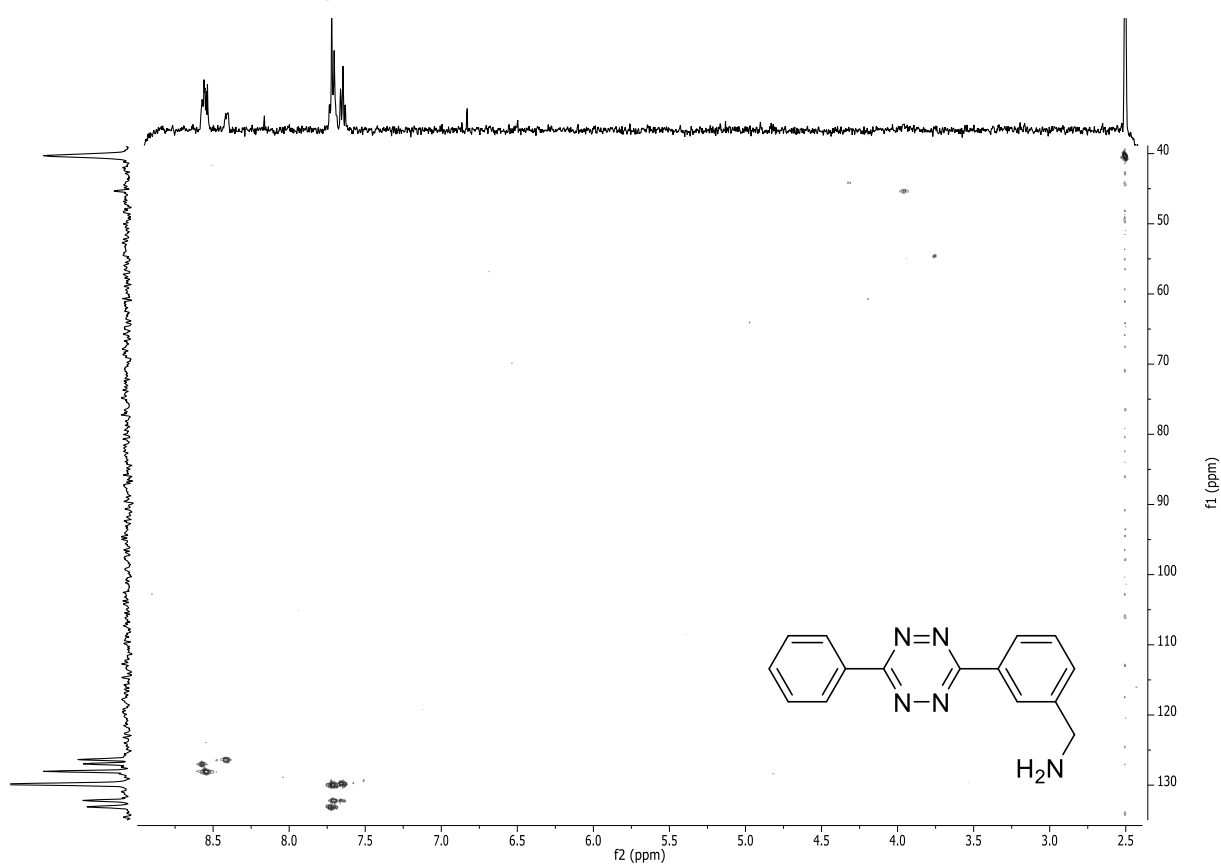
HMQC spectrum of compound **51**: DMSO-d_6; 500 MHz; r.t.
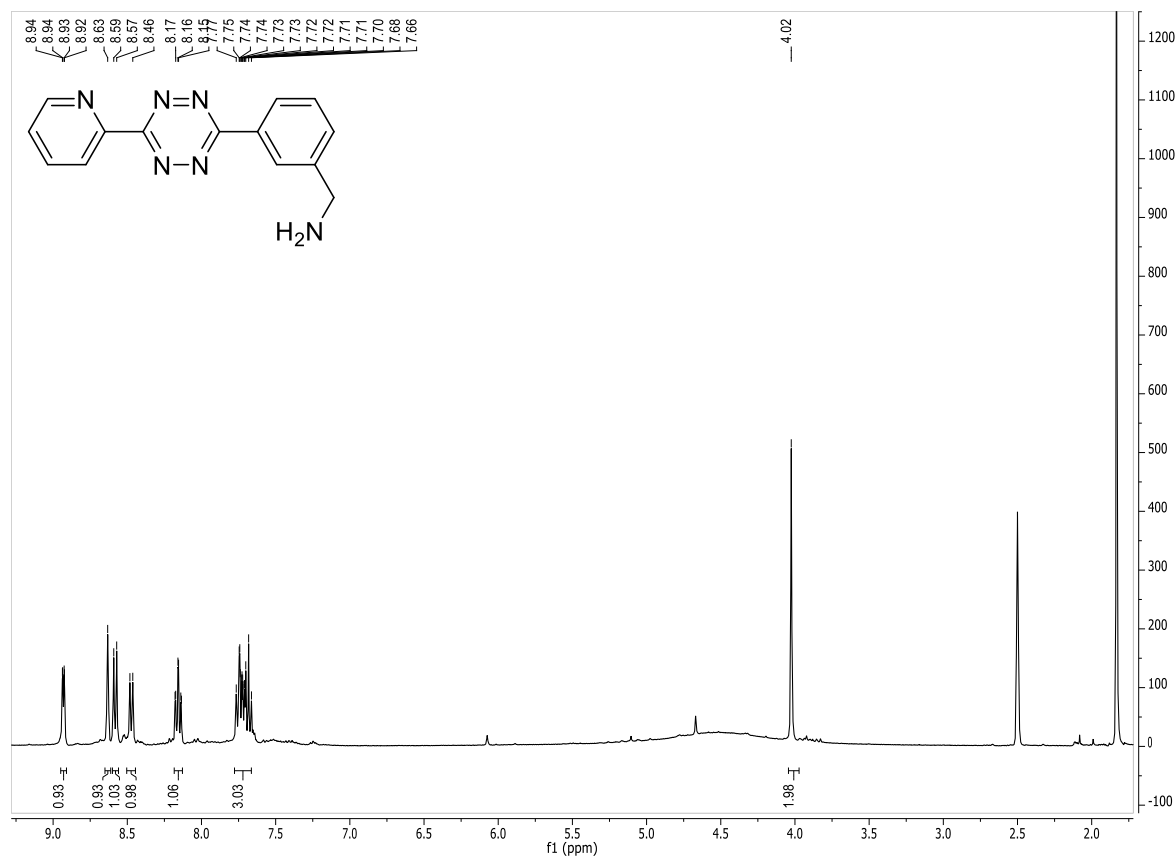
^{1}H NMR of compound **53**: DMSO-d_6; 400 MHz; r.t.
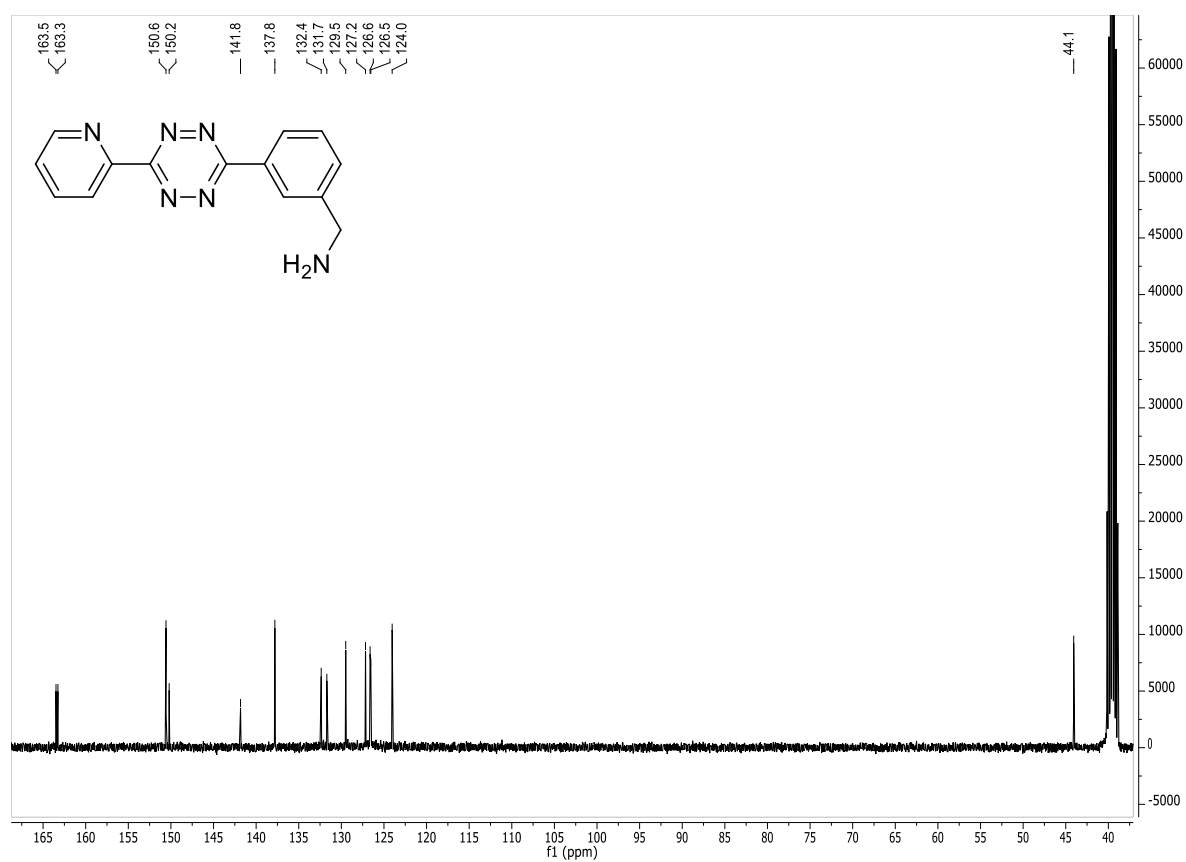
^{13}C NMR of compound **53**: DMSO-d_6; 75 MHz; r.t.
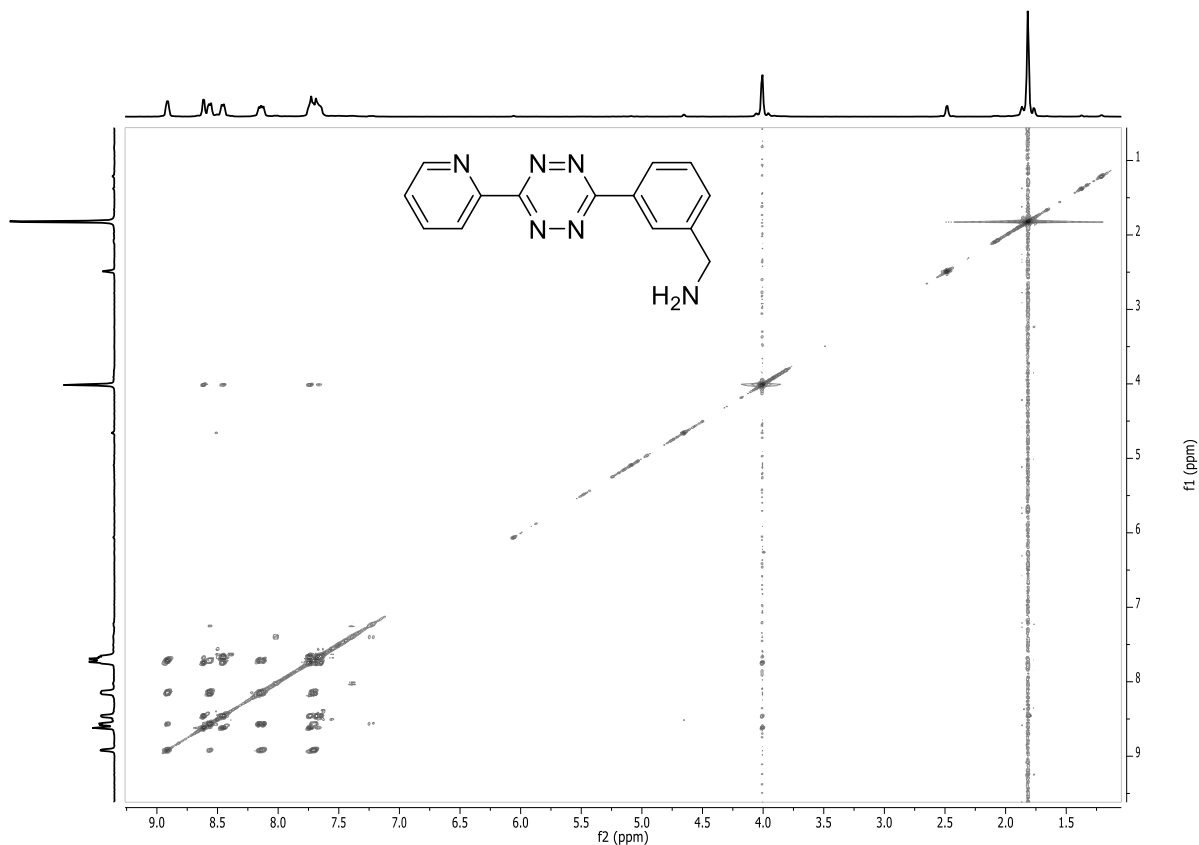
H,H-COSY NMR of compound **53**: DMSO-d_6; 400 MHz; r.t.
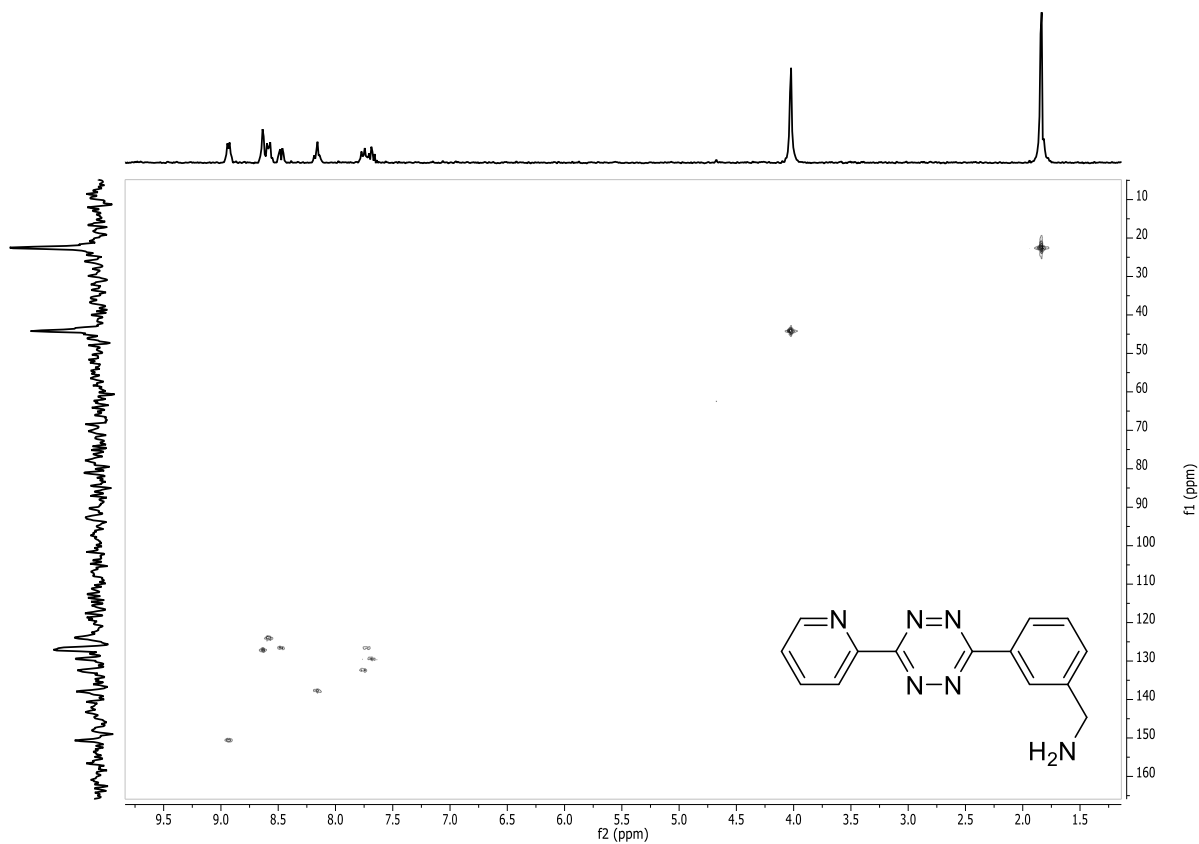
HMQC spectrum of compound **53**: DMSO-d_6; 400 MHz; r.t.
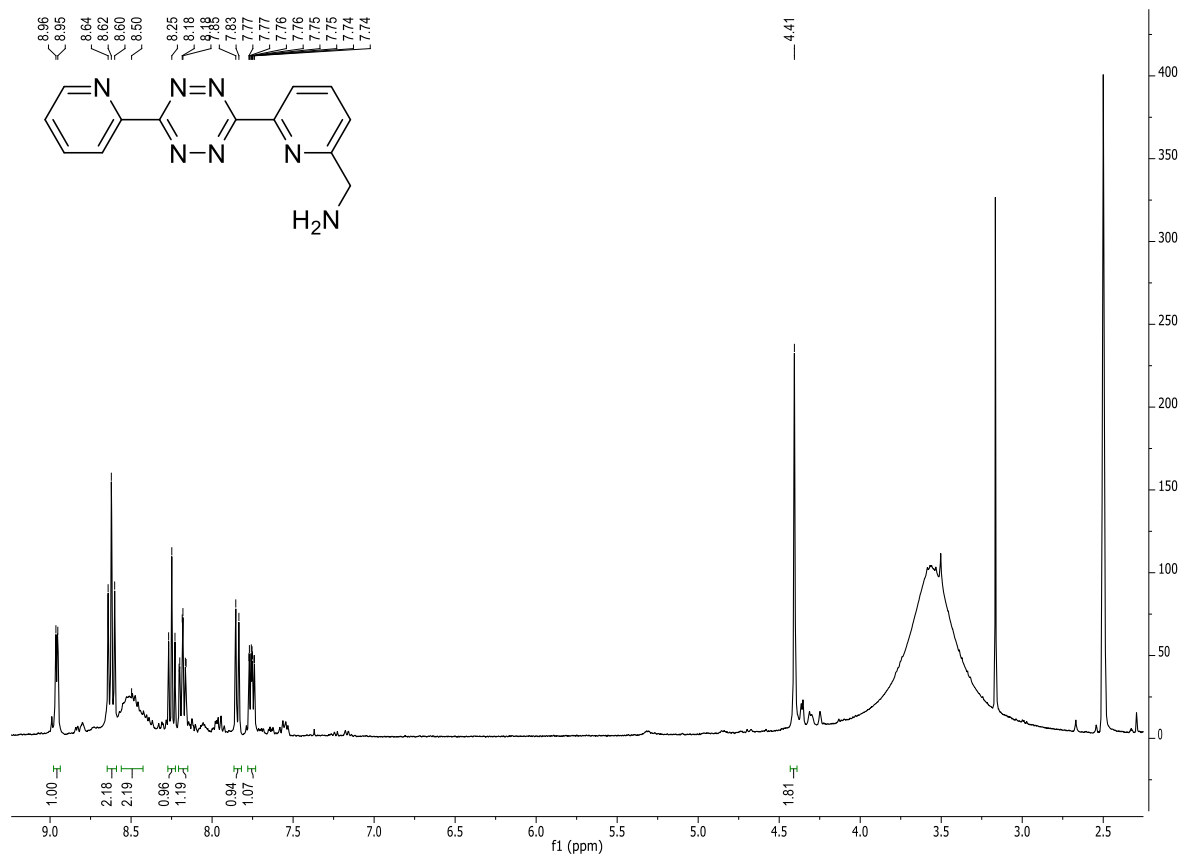
^{1}H NMR of compound **54**: DMSO-d_6; 400 MHz; r.t.
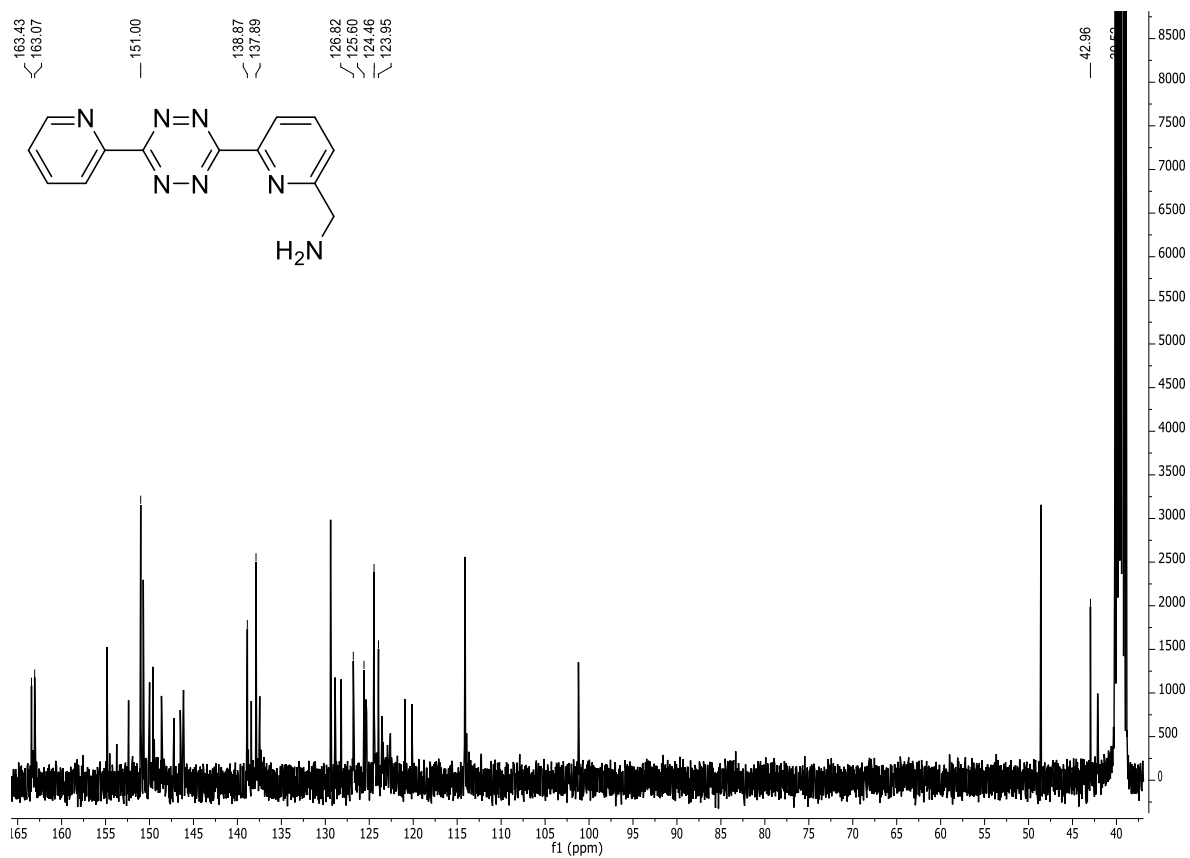
^{13}C NMR of compound **54**: DMSO-d_6; 101 MHz; r.t.
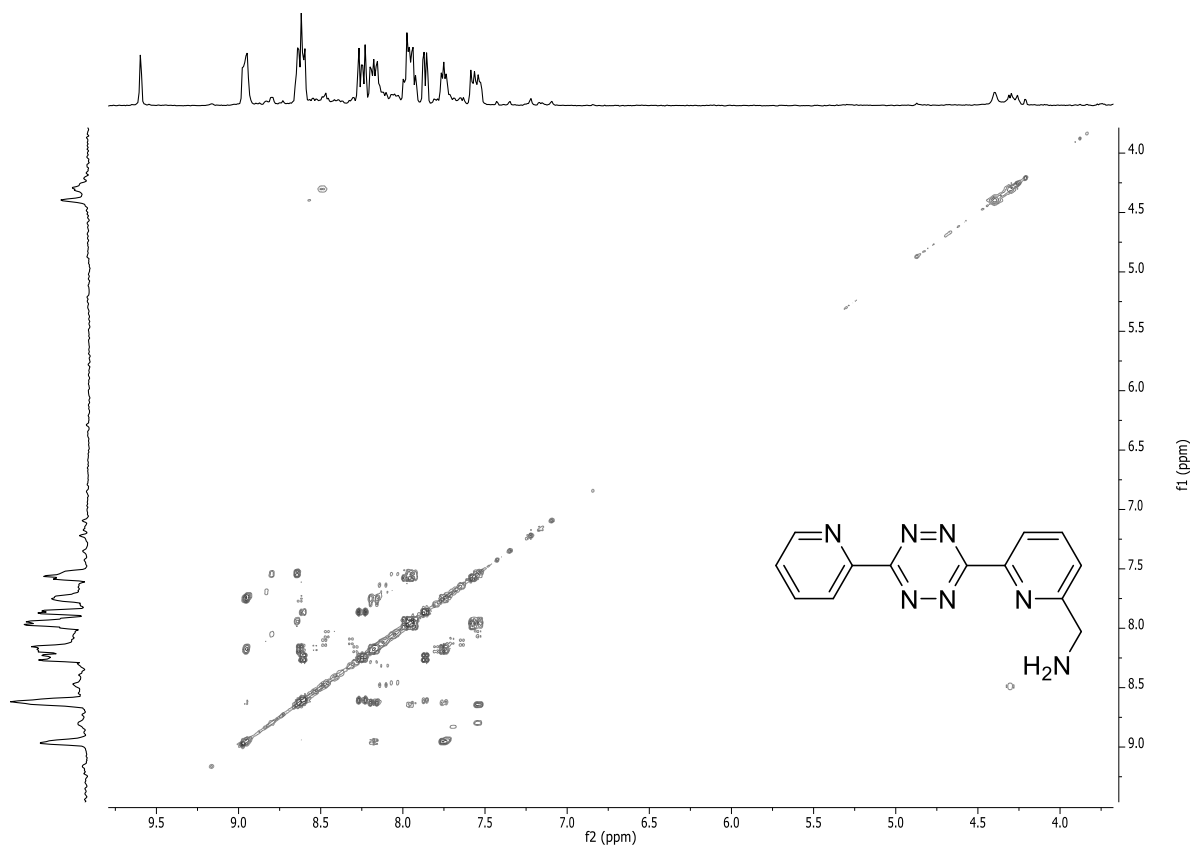
H,H-COSY NMR of compound **54**: DMSO-d_6; 400 MHz; r.t.
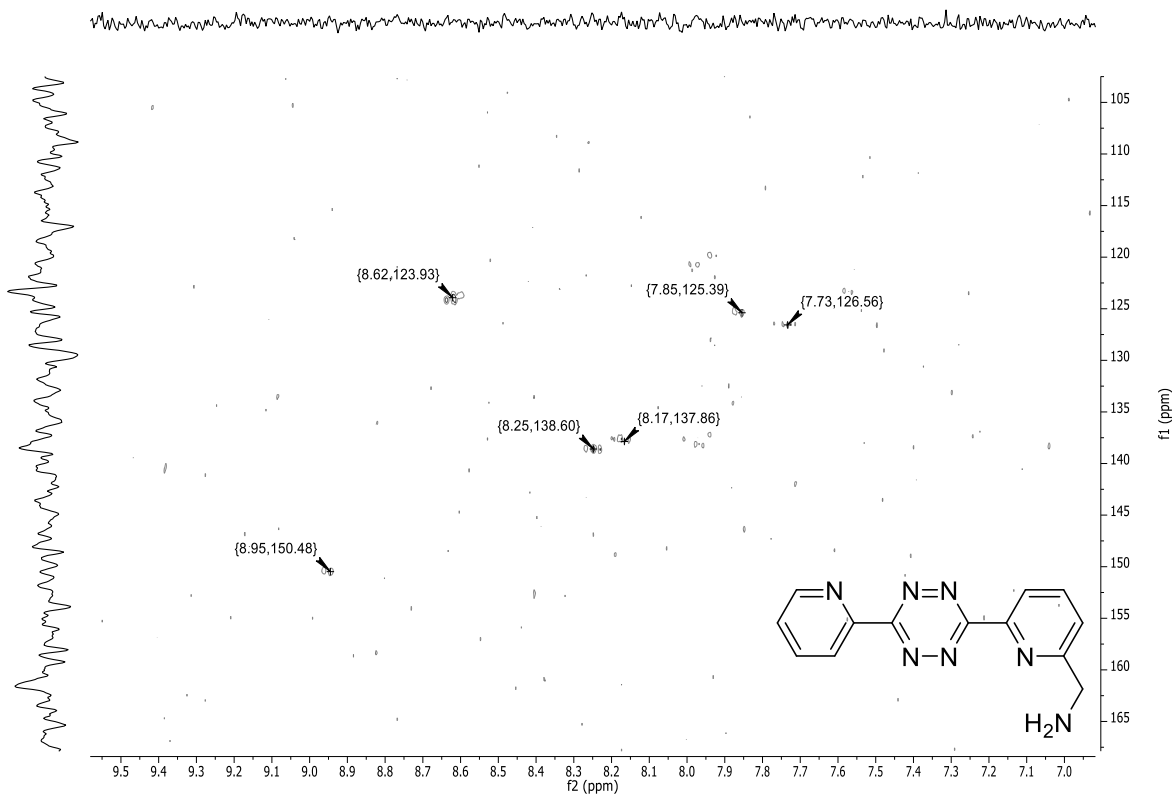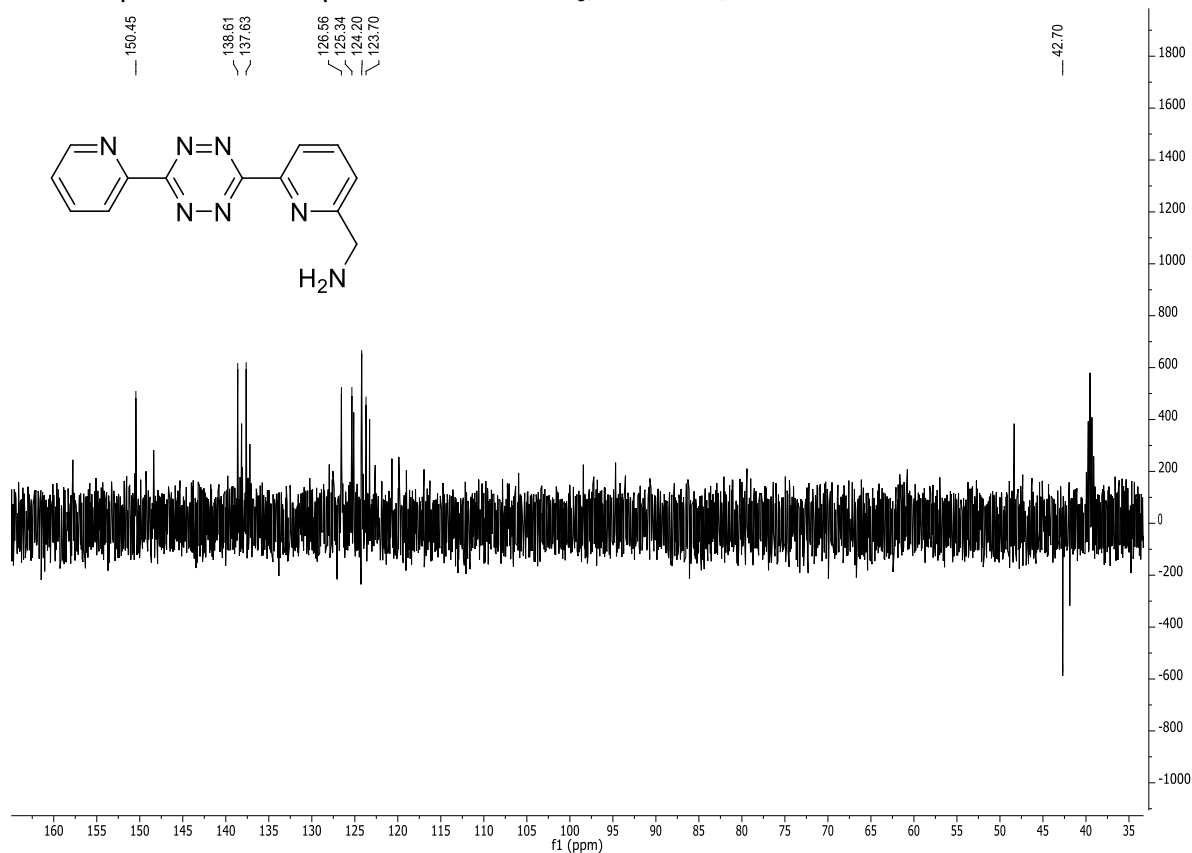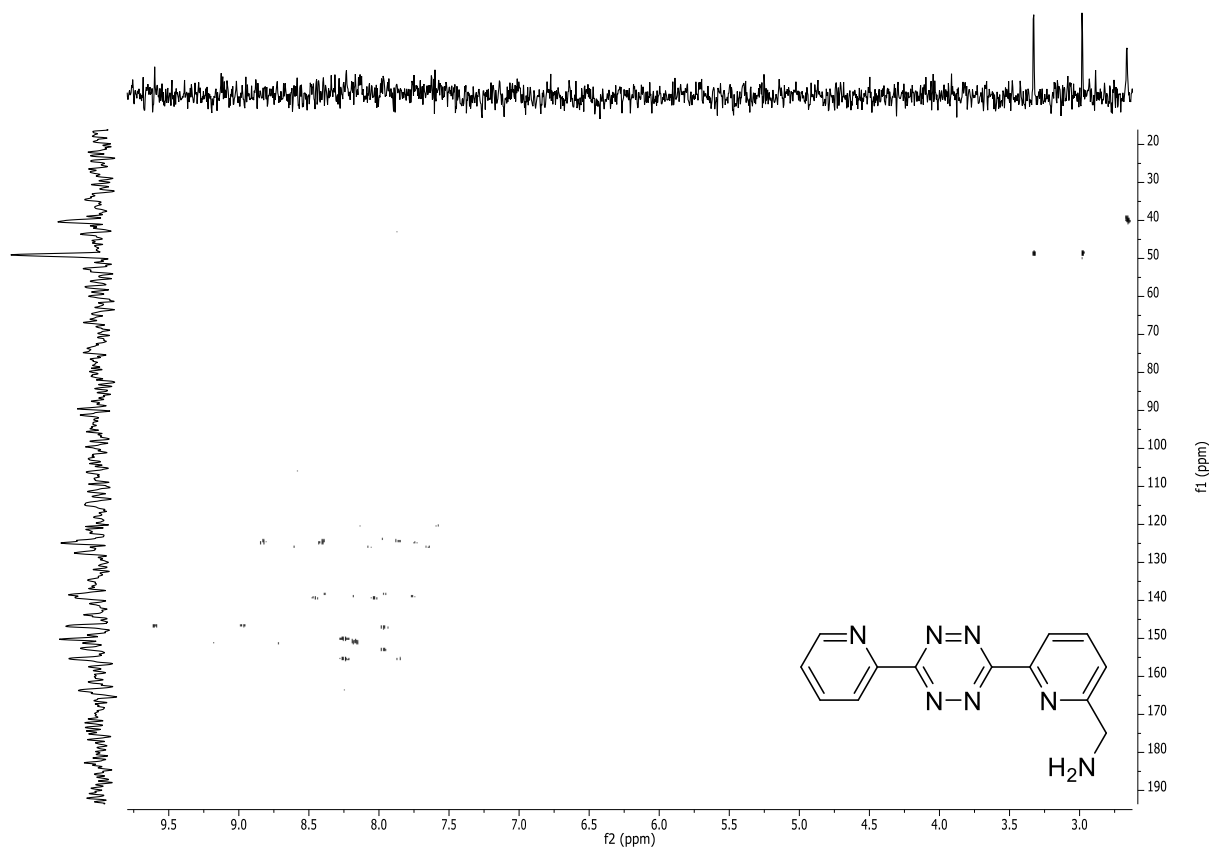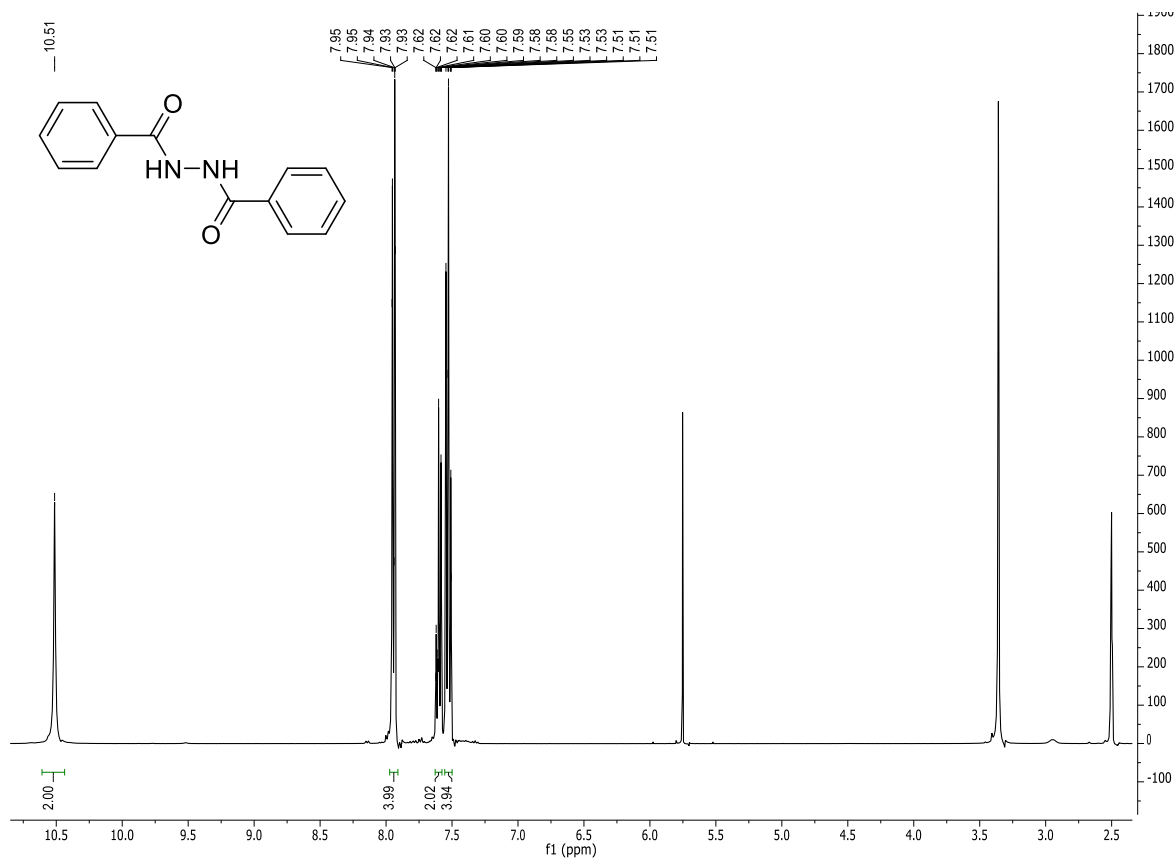
HMQC spectrum of compound **54**: DMSO-d_6; 400 MHz; r.t.

HMBC spectrum of compound **54**: DMSO-d_6; 400 MHz; r.t.

^{13}C-NMR (DEPT 135) of compound **54**: DMSO-d_6; 101 MHz; r.t.

^{1}H NMR of compound **62**: DMSO-d_6; 400 MHz; r.t.

^{13}C NMR of compound **62**: DMSO-d_6; 400 MHz; r.t.

^{1}H NMR of compound **63**: CD$_2$Cl$_2$; 400 MHz; r.t.
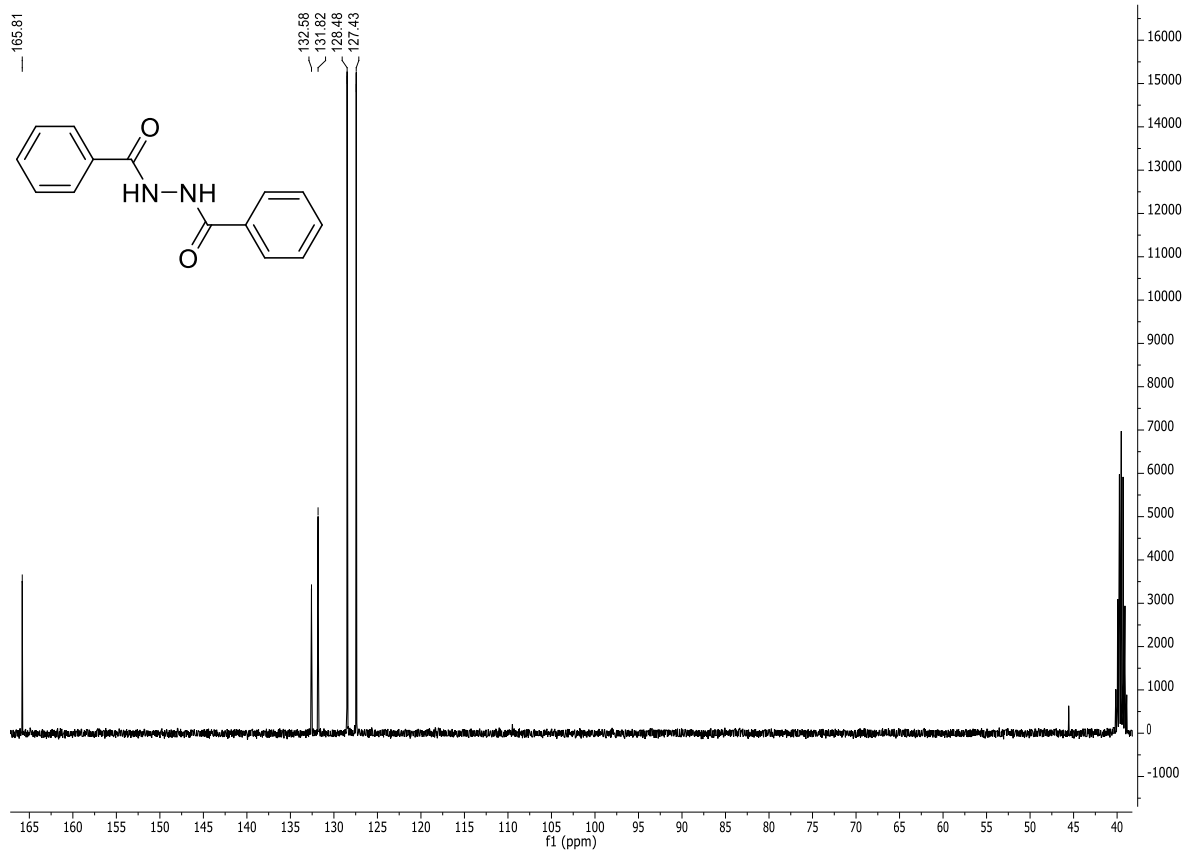
^{13}C NMR of compound **63**: CD$_2$Cl$_2$; 101 MHz; r.t.
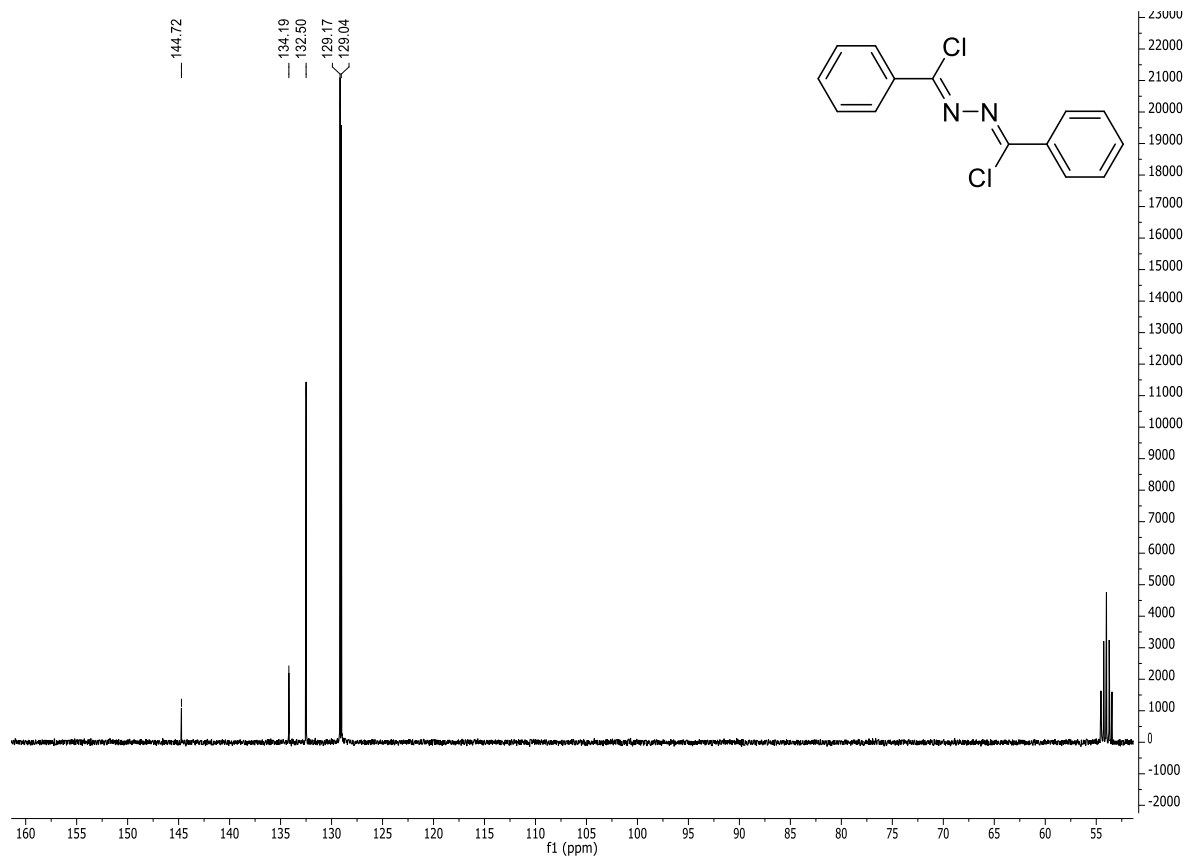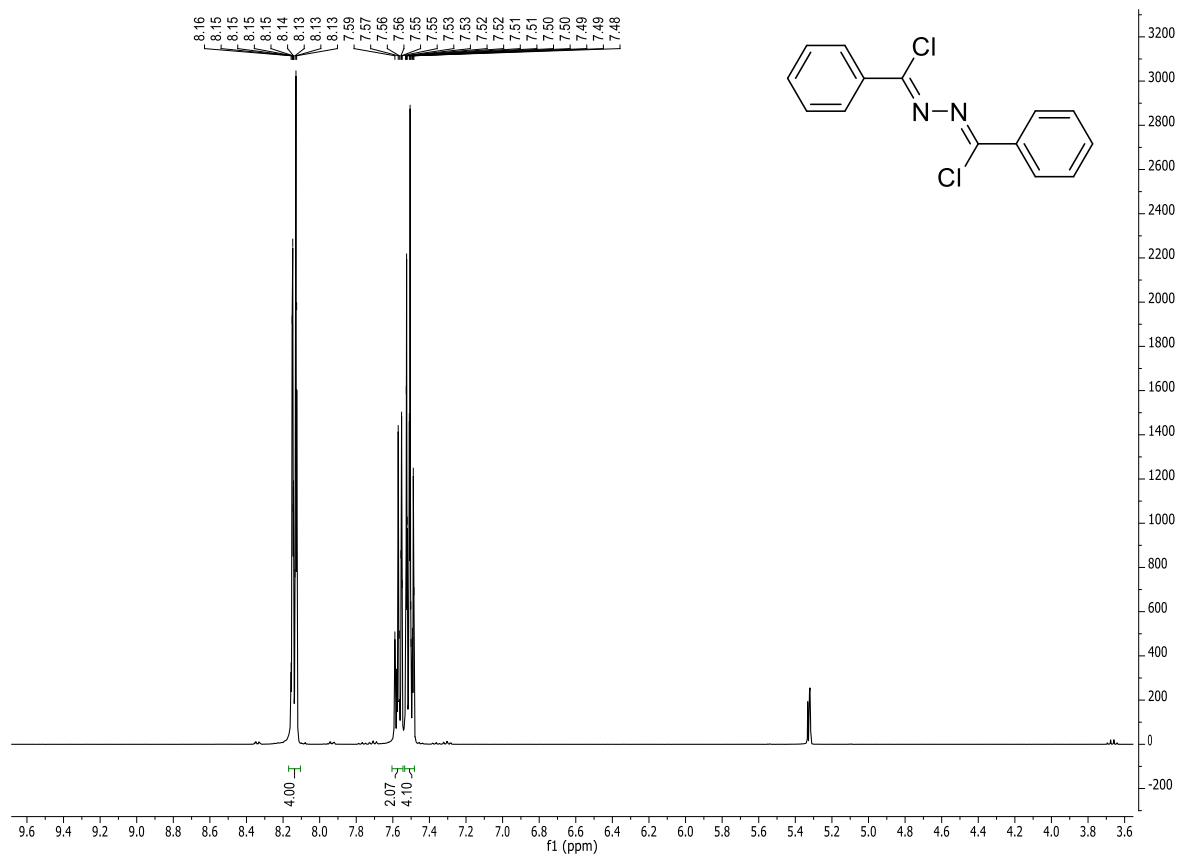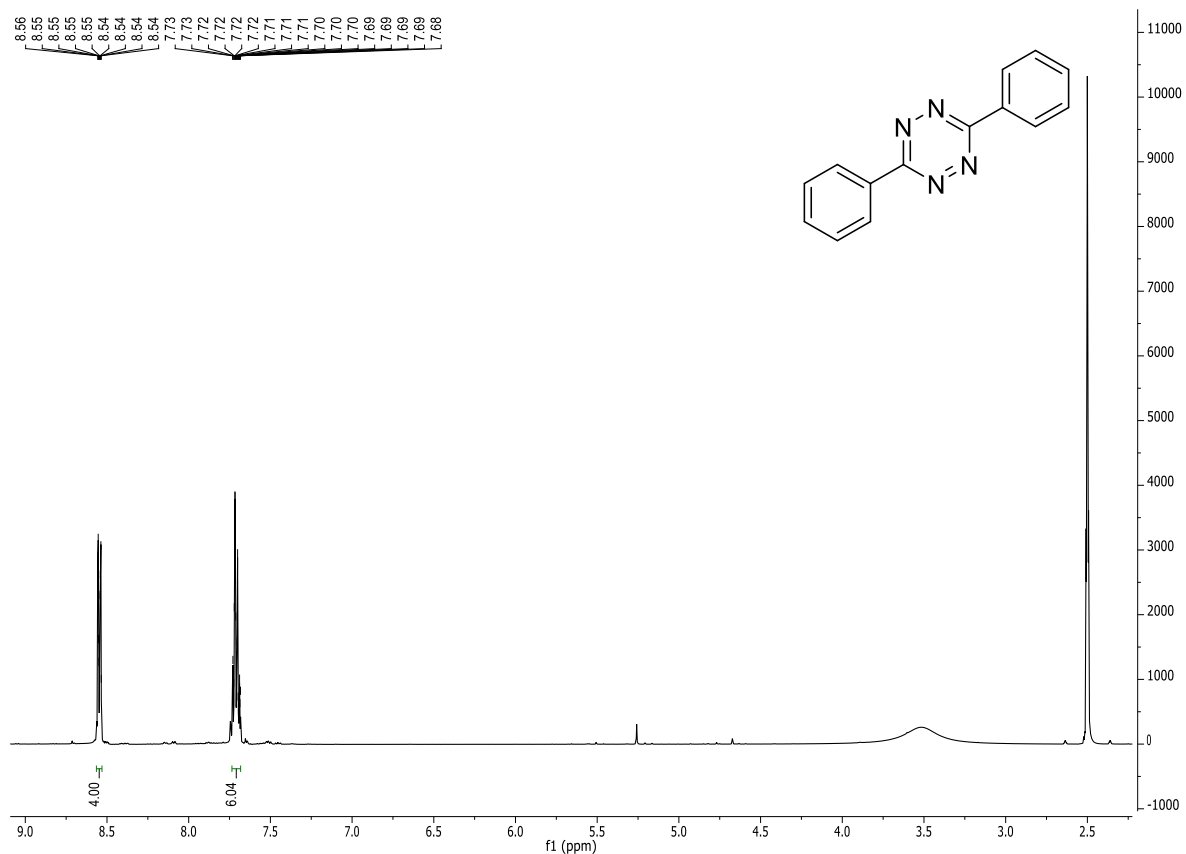
^{1}H NMR of compound **2**: DMSO-d_6; 400 MHz; r.t.
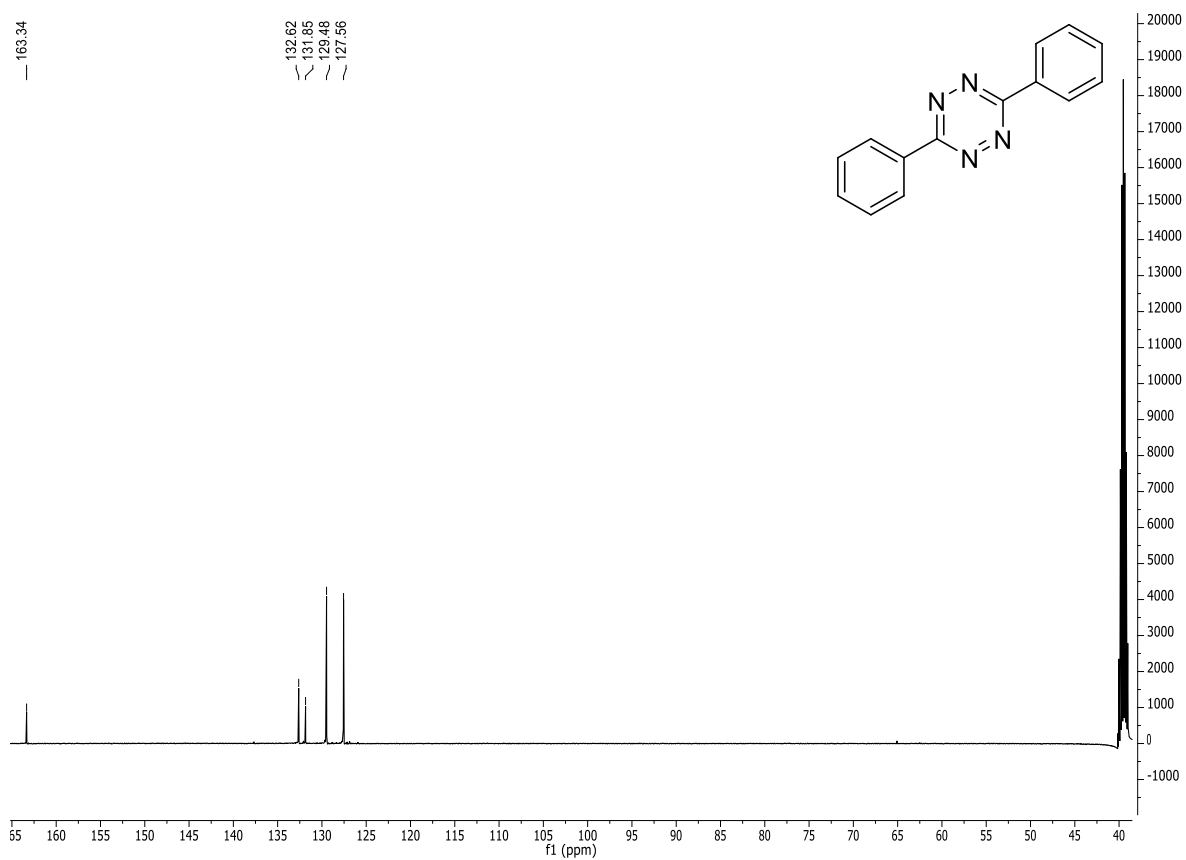
^{13}C NMR of compound **2**: DMSO-d_6; 126 MHz; r.t.
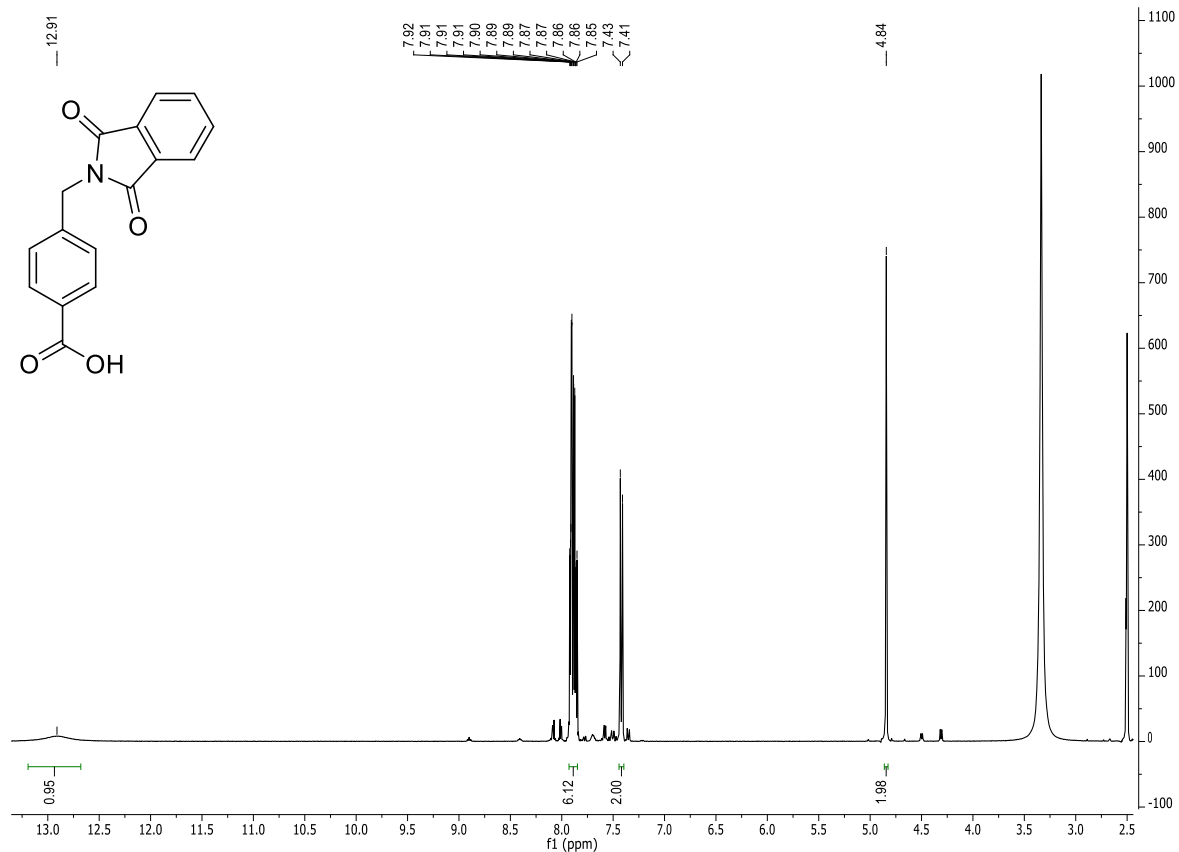
^{1}H NMR of compound **66i**: DMSO-d_6; 400 MHz; r.t.
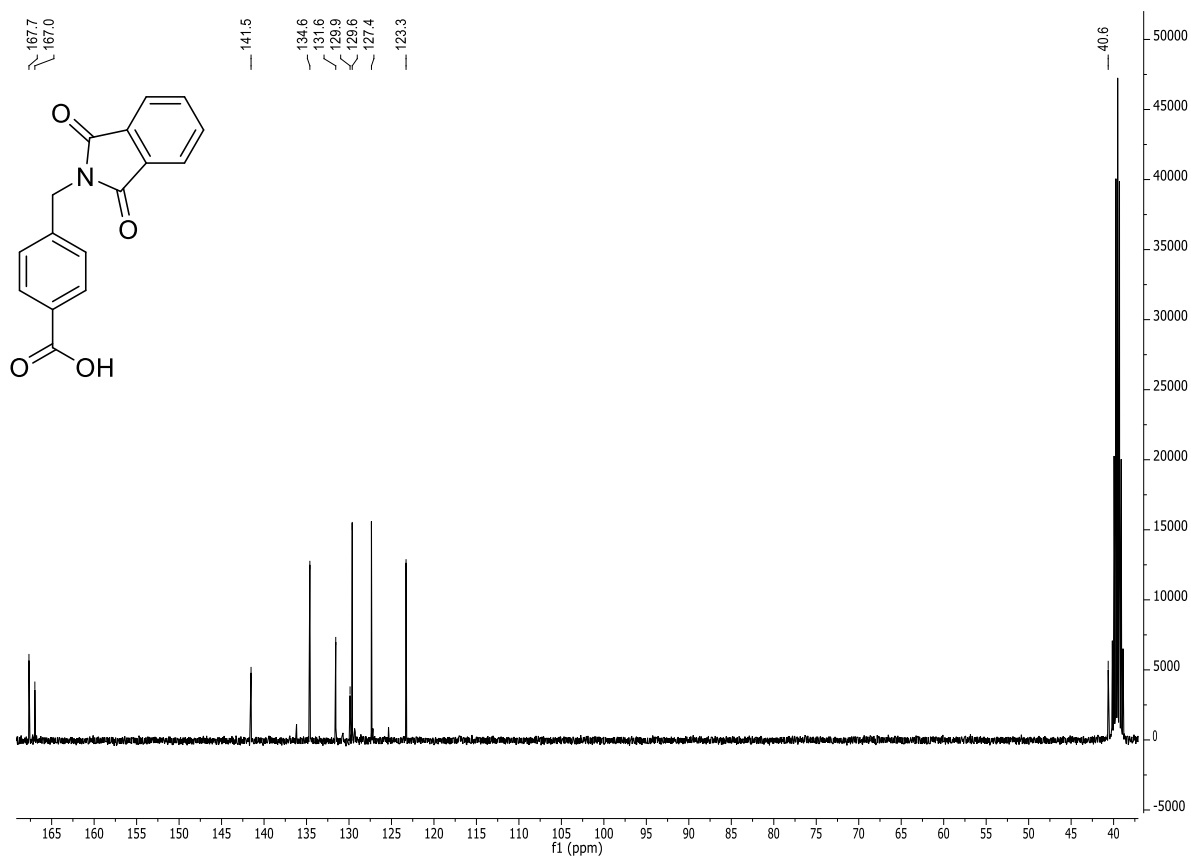
^{13}C NMR of compound **66i**: DMSO-d_6; 101 MHz; r.t.

^{1}H NMR of compound **66**: DMSO-d_6; 400 MHz; r.t.

^{1}H NMR of compound **67**: DMSO-d_6; 400 MHz; r.t.
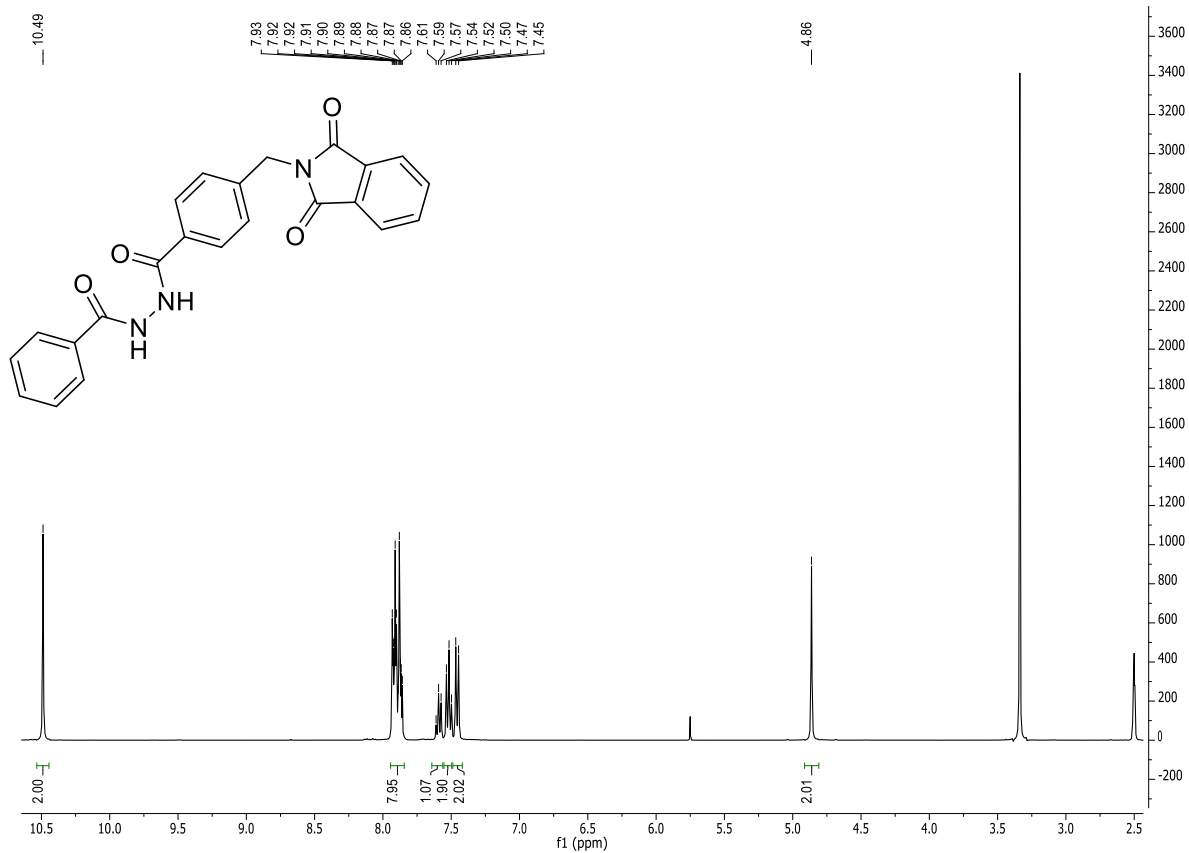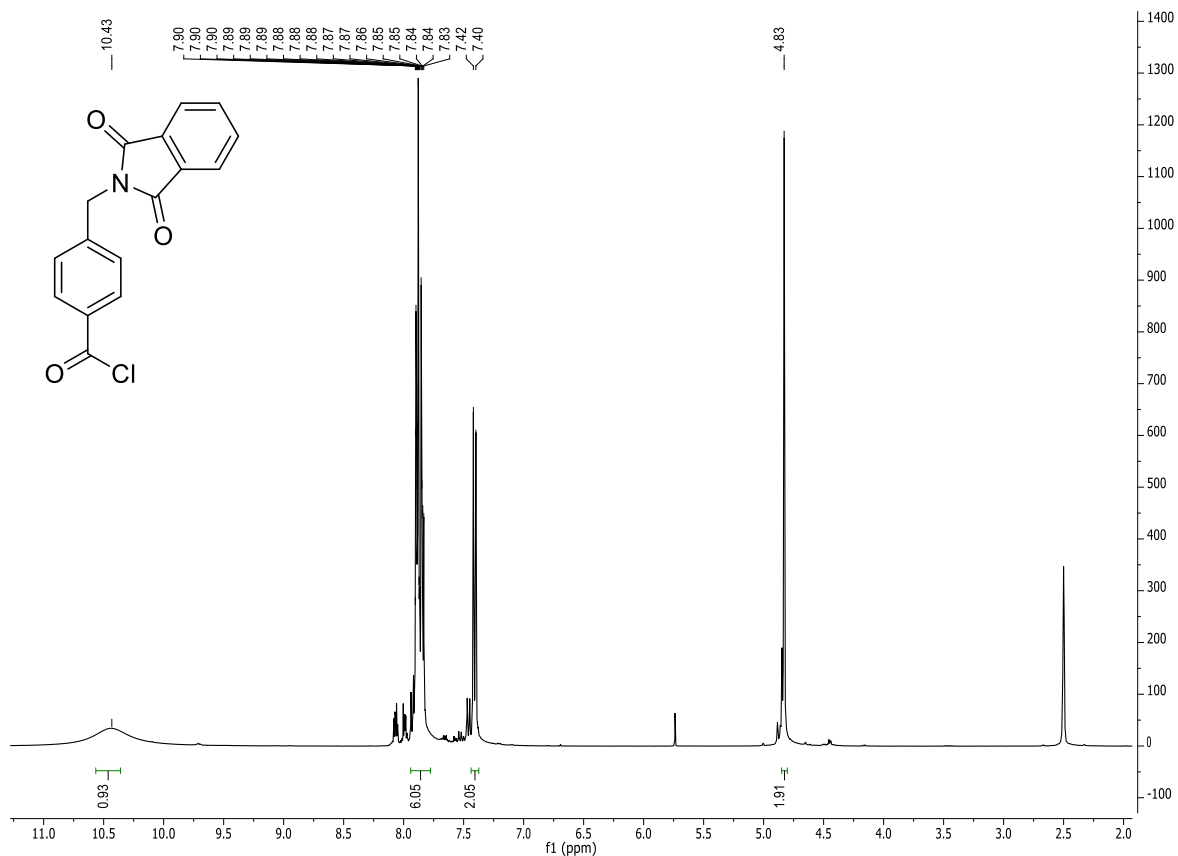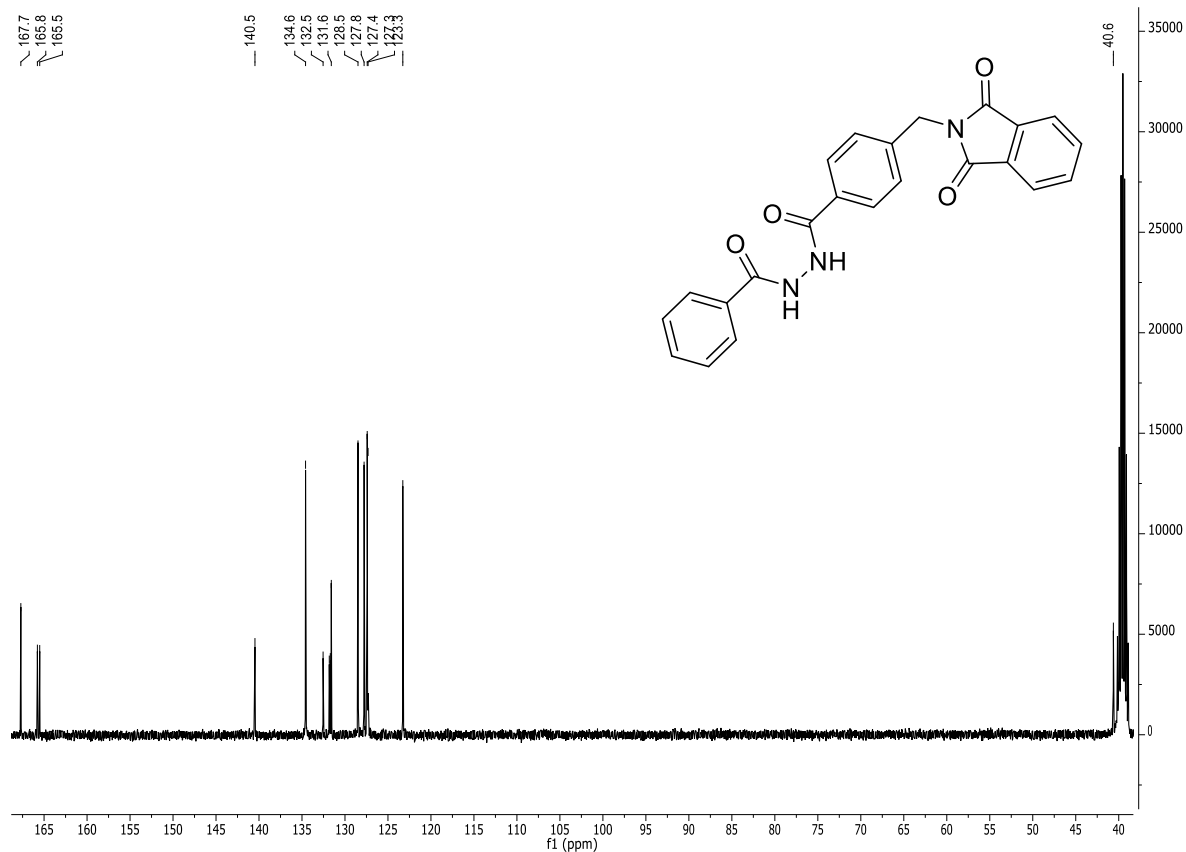
^{13}C NMR of compound **67**: DMSO-d_6; 101 MHz; r.t.
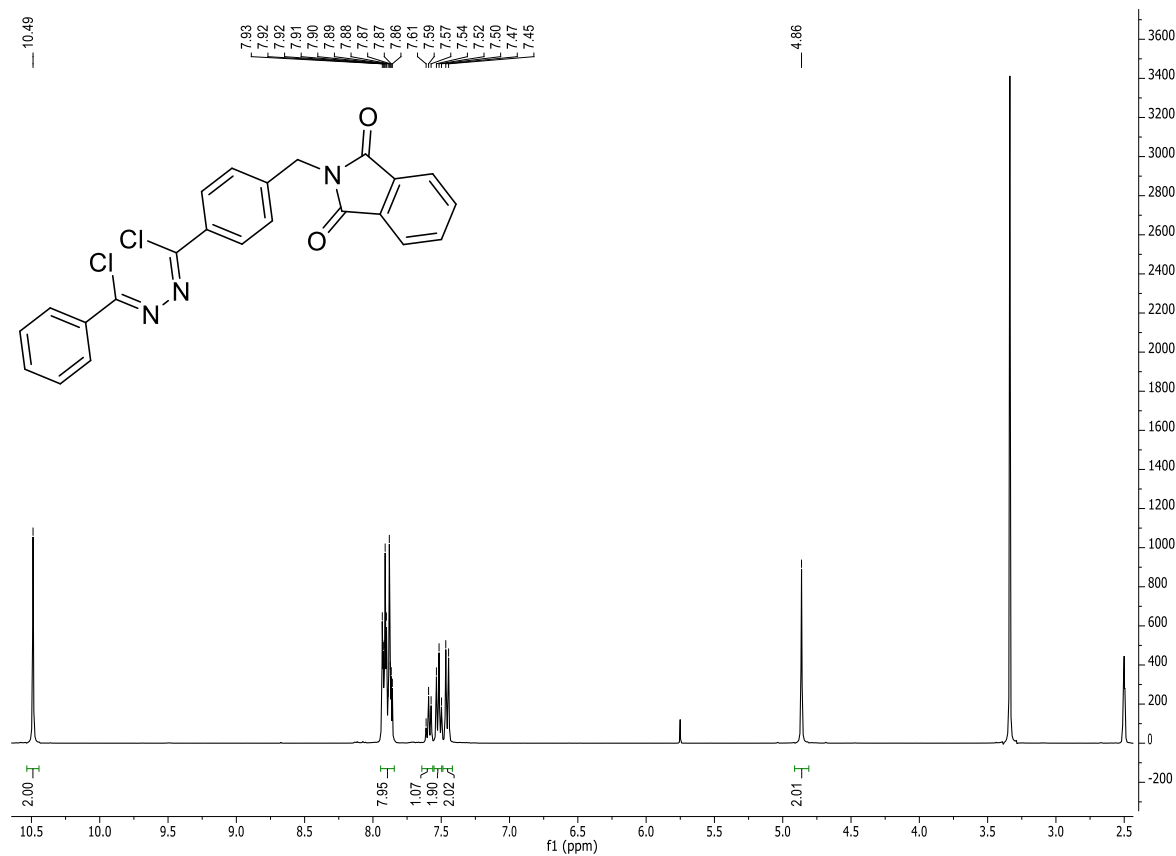
^{1}H NMR of compound **68**: DMSO-d_6; 400 MHz; r.t.
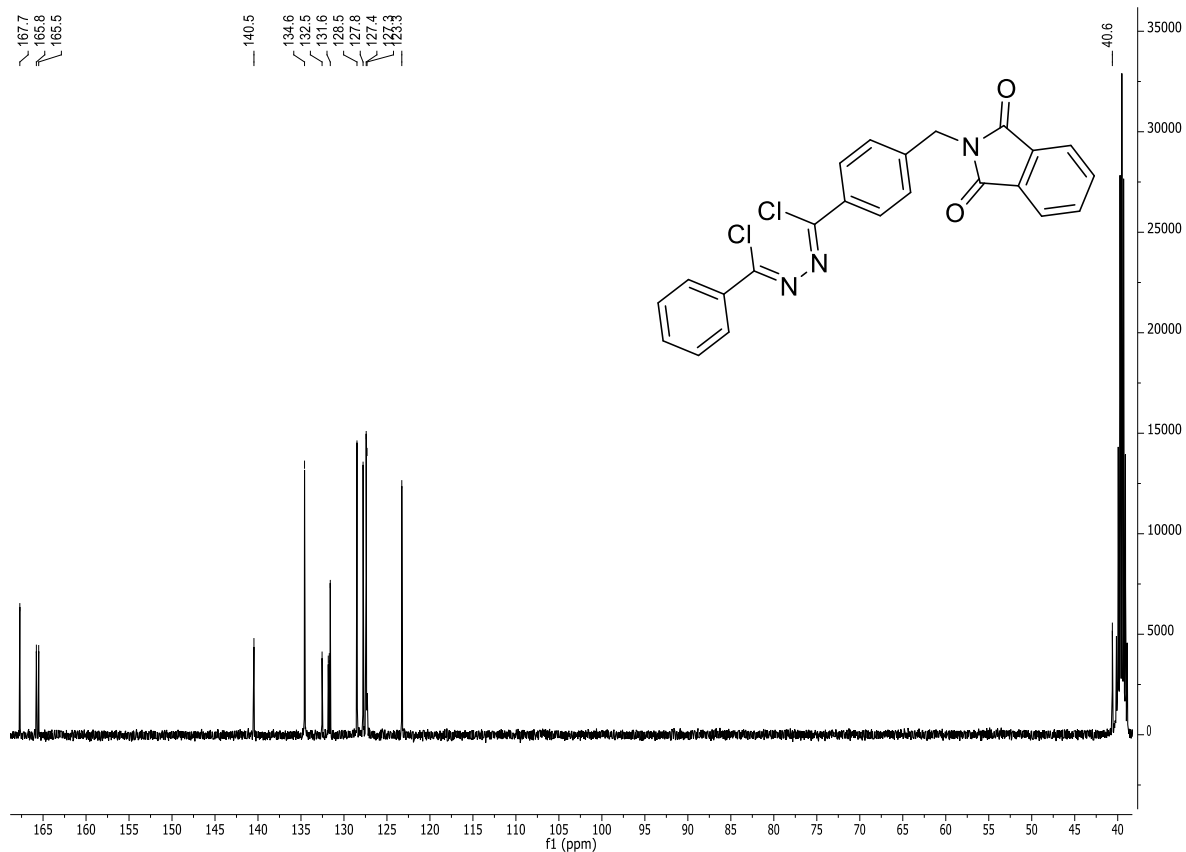
^{13}C NMR of compound **68**: DMSO-d_6; 101 MHz; r.t.
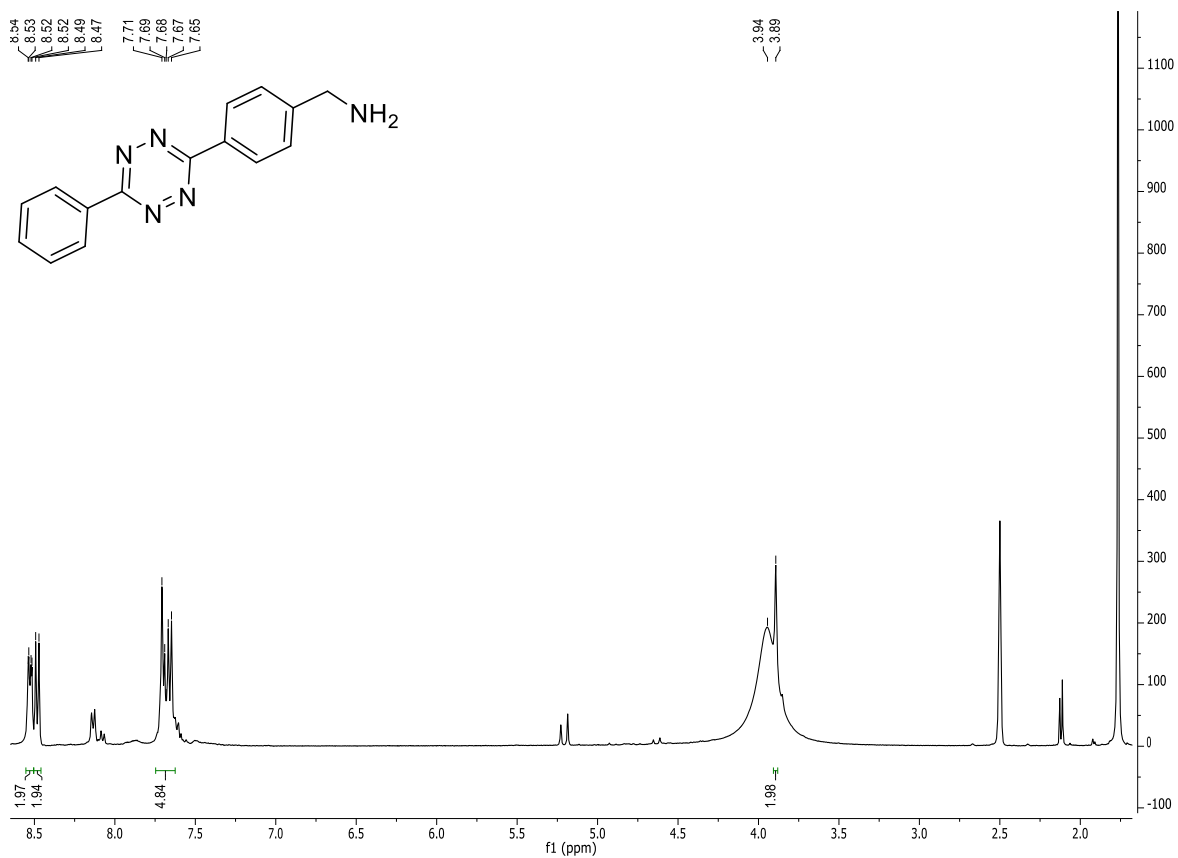
^{1}H NMR of compound **20a**: DMSO-d_6; 400 MHz; r.t.
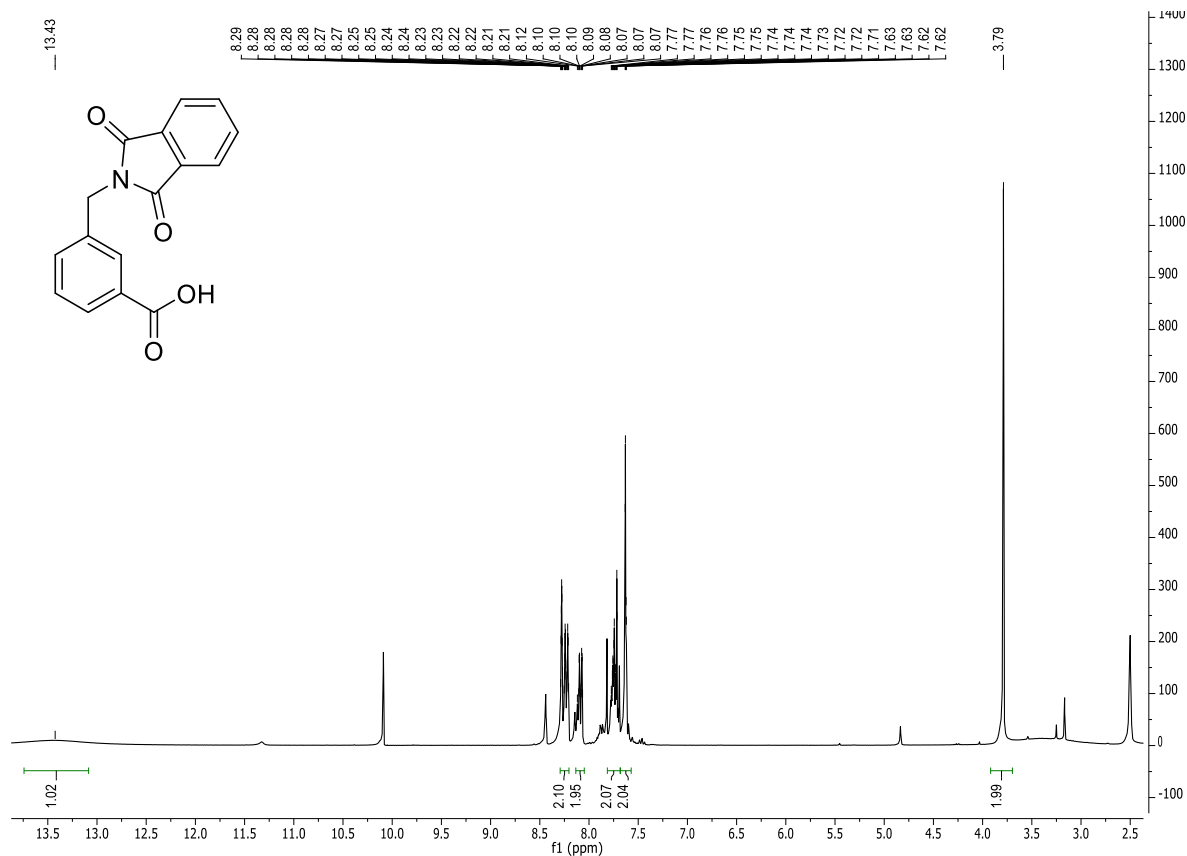
^{1}H NMR of compound **70i**: DMSO-d_6; 300 MHz; r.t.
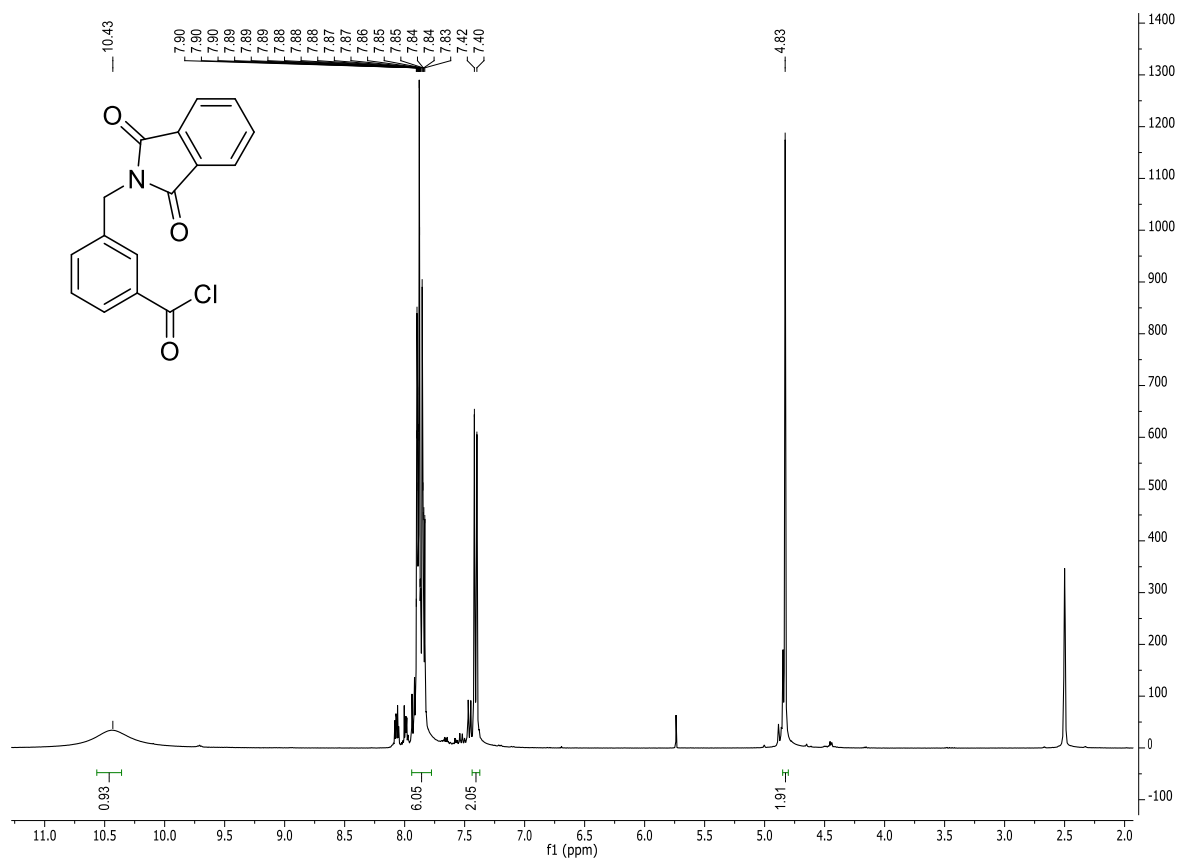
^{1}H NMR of compound **70**: DMSO-d_6; 400 MHz; r.t.

^{1}H NMR of compound **71**: DMSO-d_6; 400 MHz; r.t.

^{13}C NMR of compound **71**: DMSO-d_6; 400 MHz; r.t.
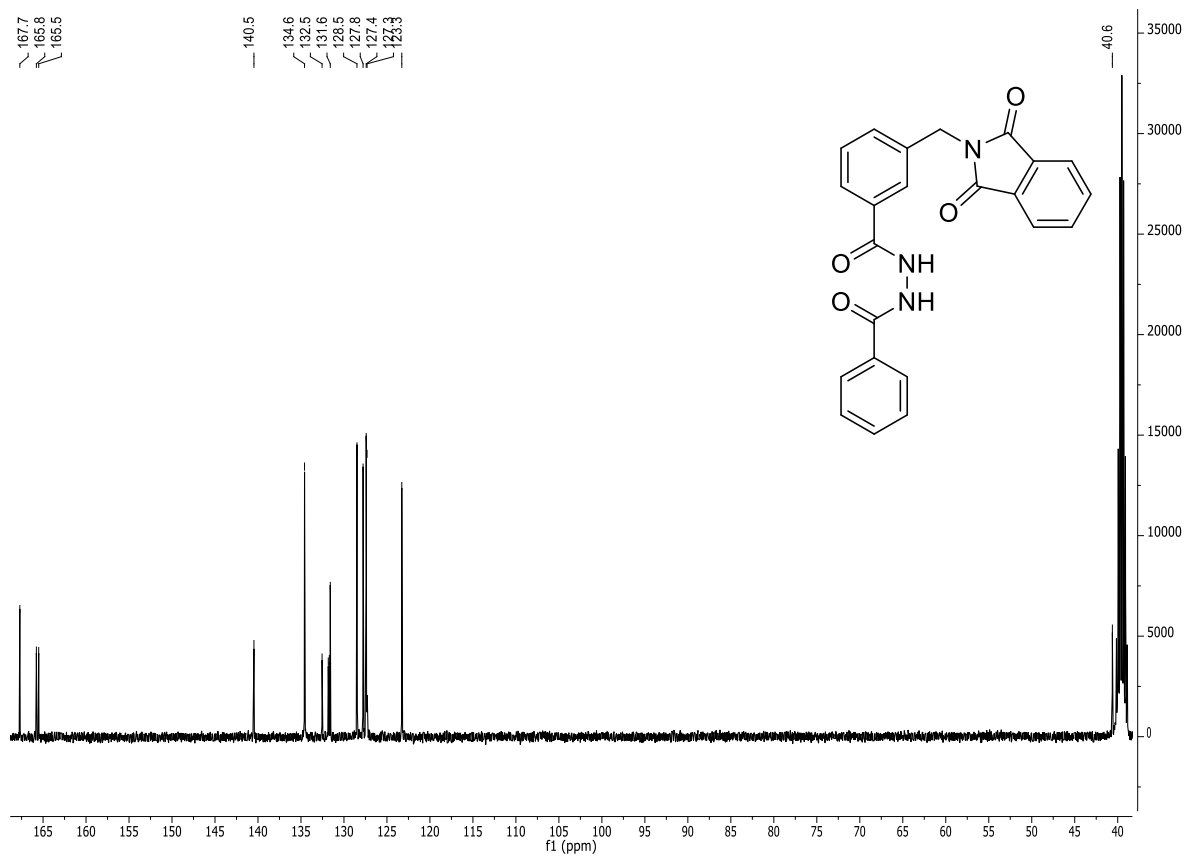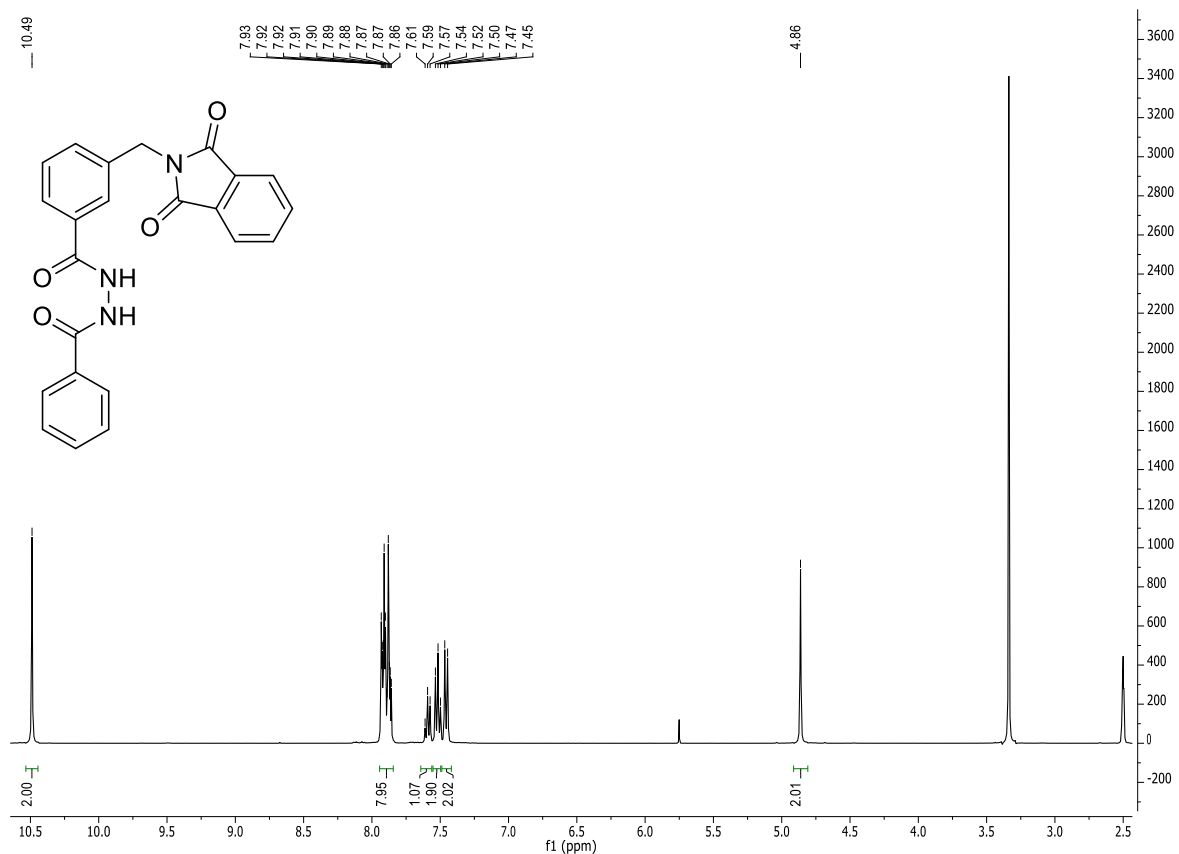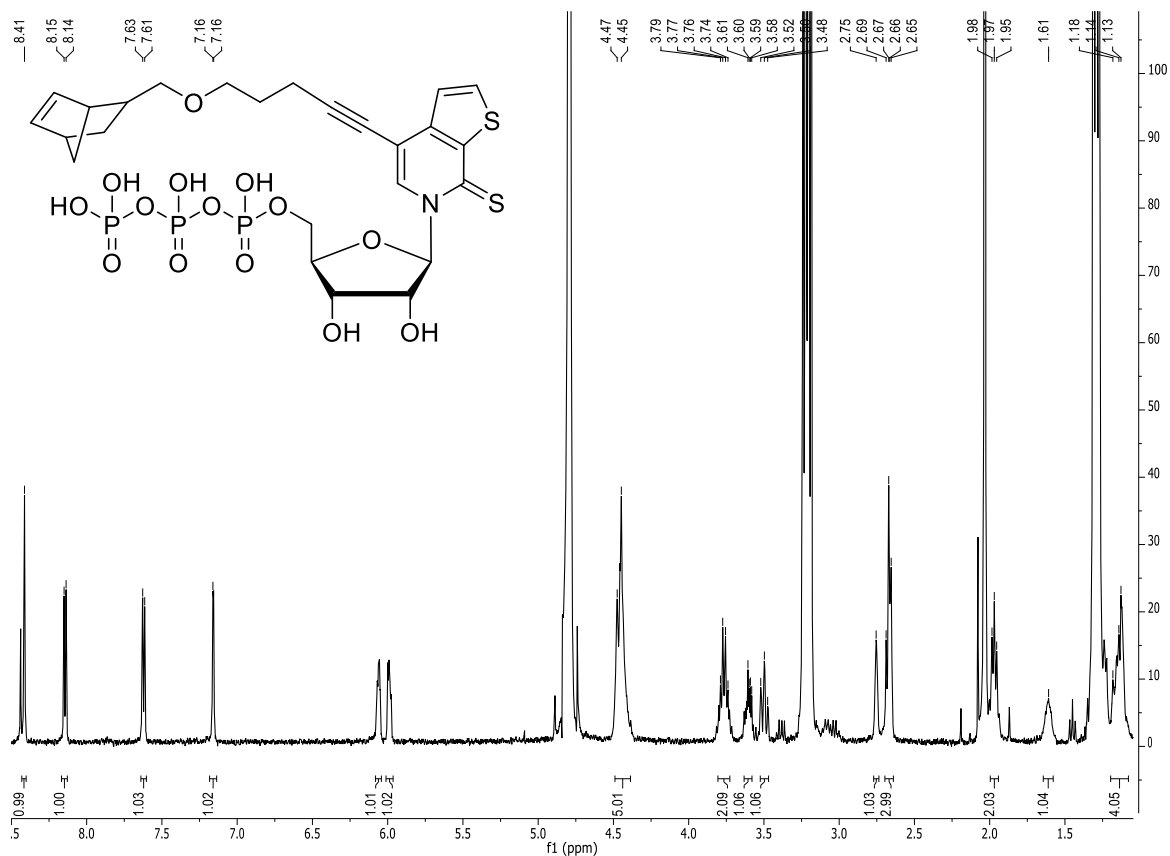
^{1}H NMR of compound **76**: DMSO-d_6; 400 MHz; r.t.
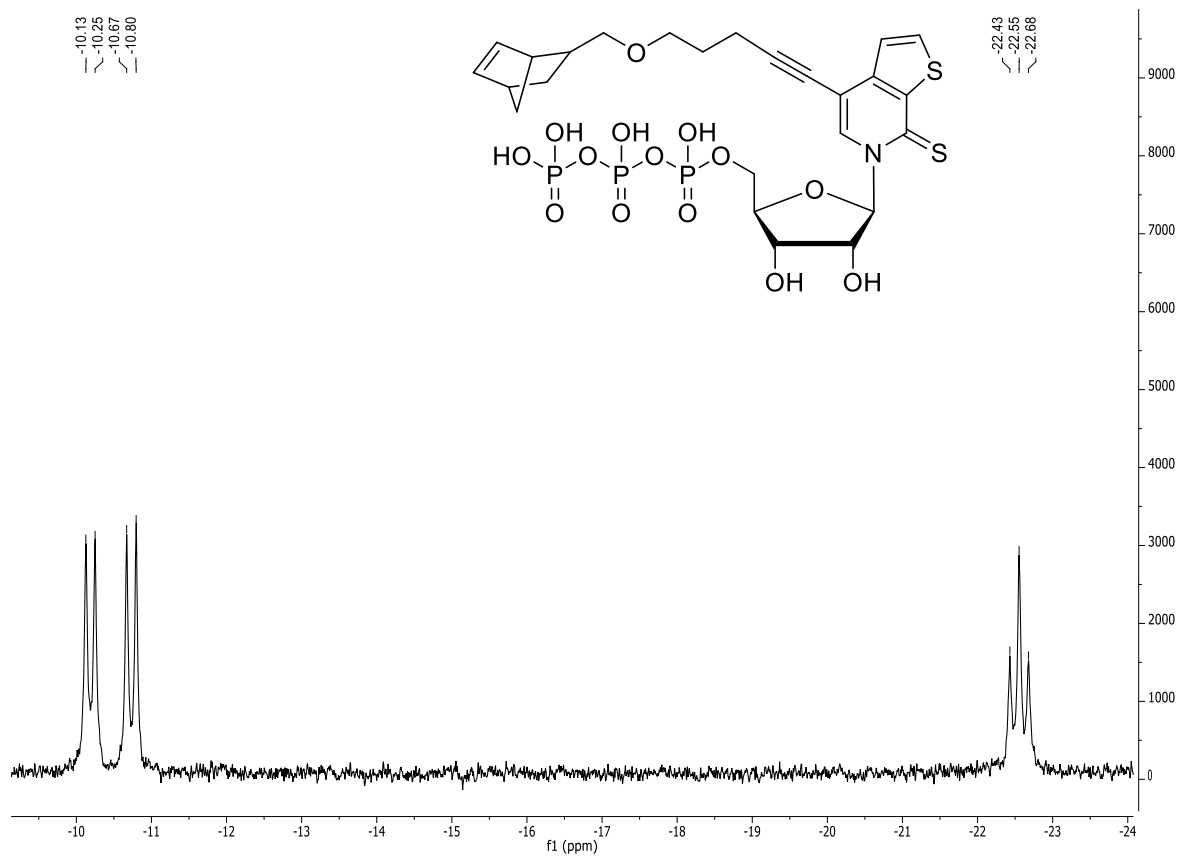
^{31}P NMR of compound **76**: DMSO-d_6; 400 MHz; r.t.
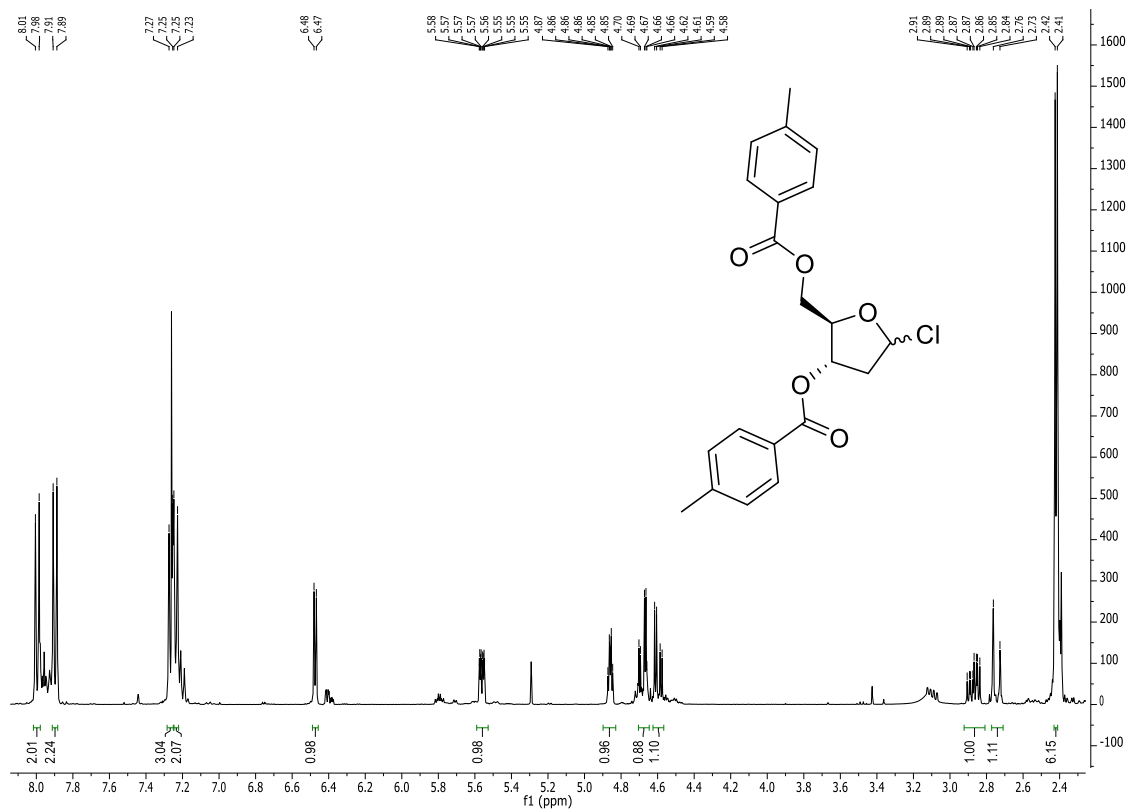
^{1}H-NMR of compound **78**: CDCl$_3$; 400 MHz; r.t.
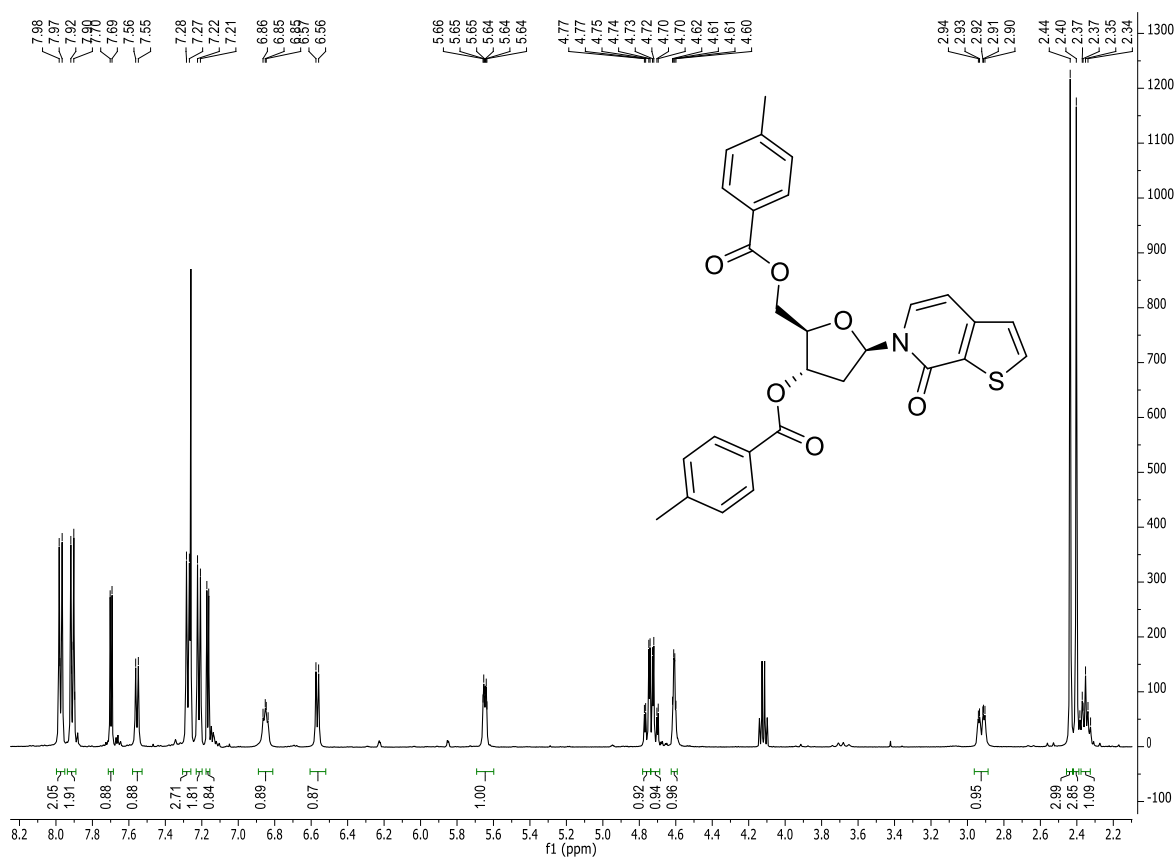
^{1}H-NMR of compound **80**: CDCl$_3$; 400 MHz; r.t.
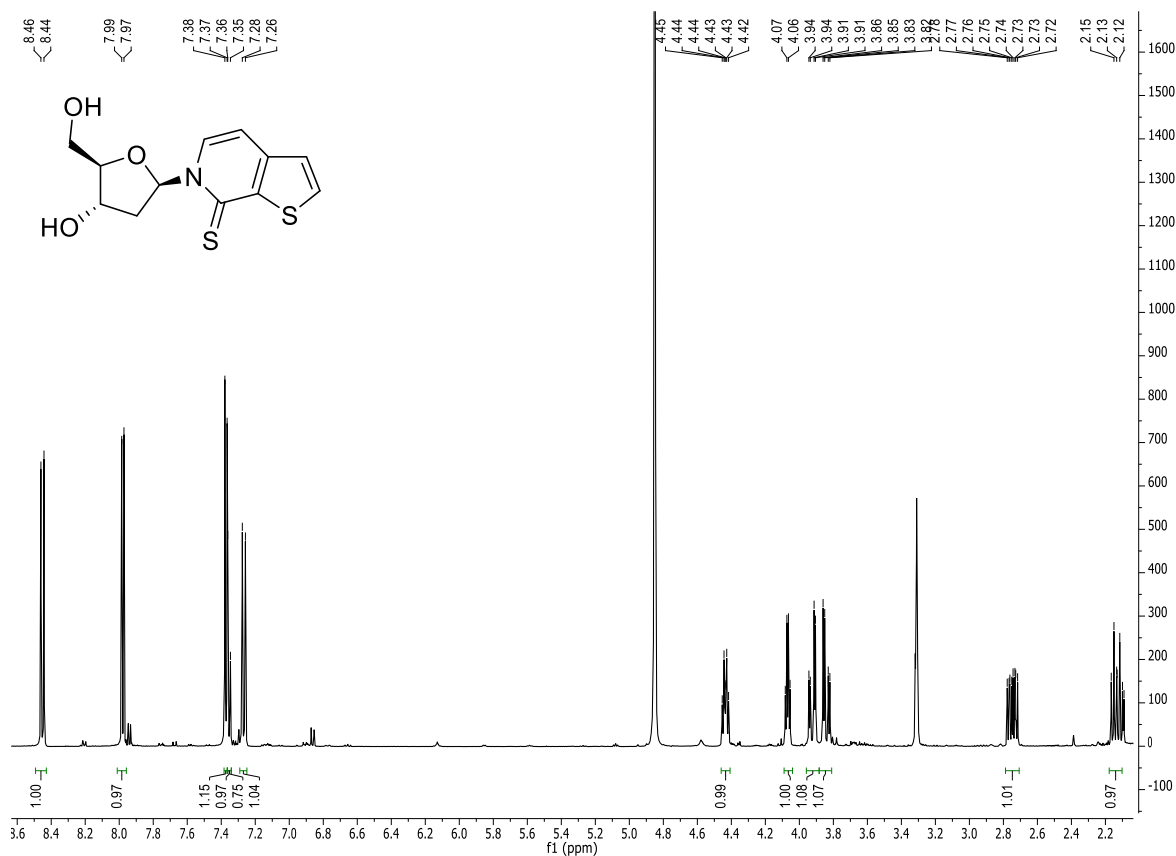
^{1}H-NMR of compound d**TPT3 81**: MeOD; 400 MHz; r.t.
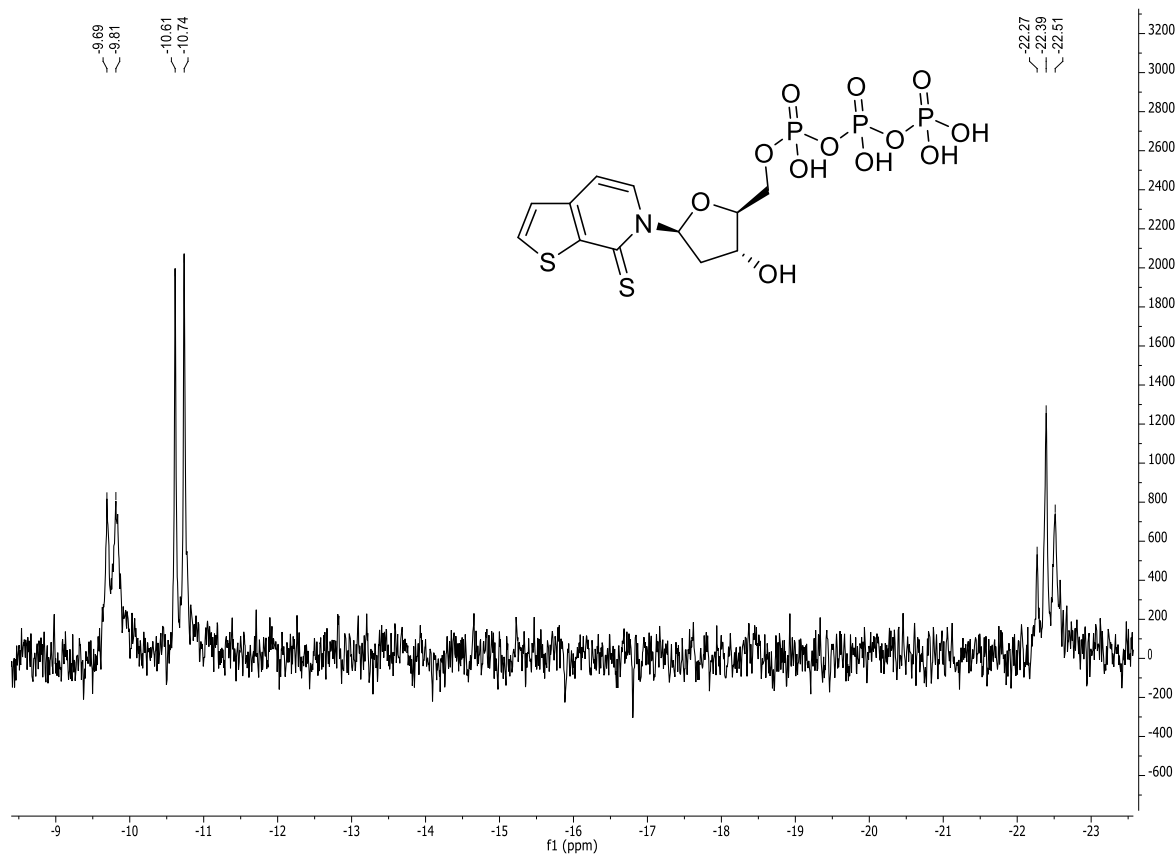
^{31}P-NMR of compound d**TPT3**-TP **82**: D$_2$O; 162 MHz; r.t.
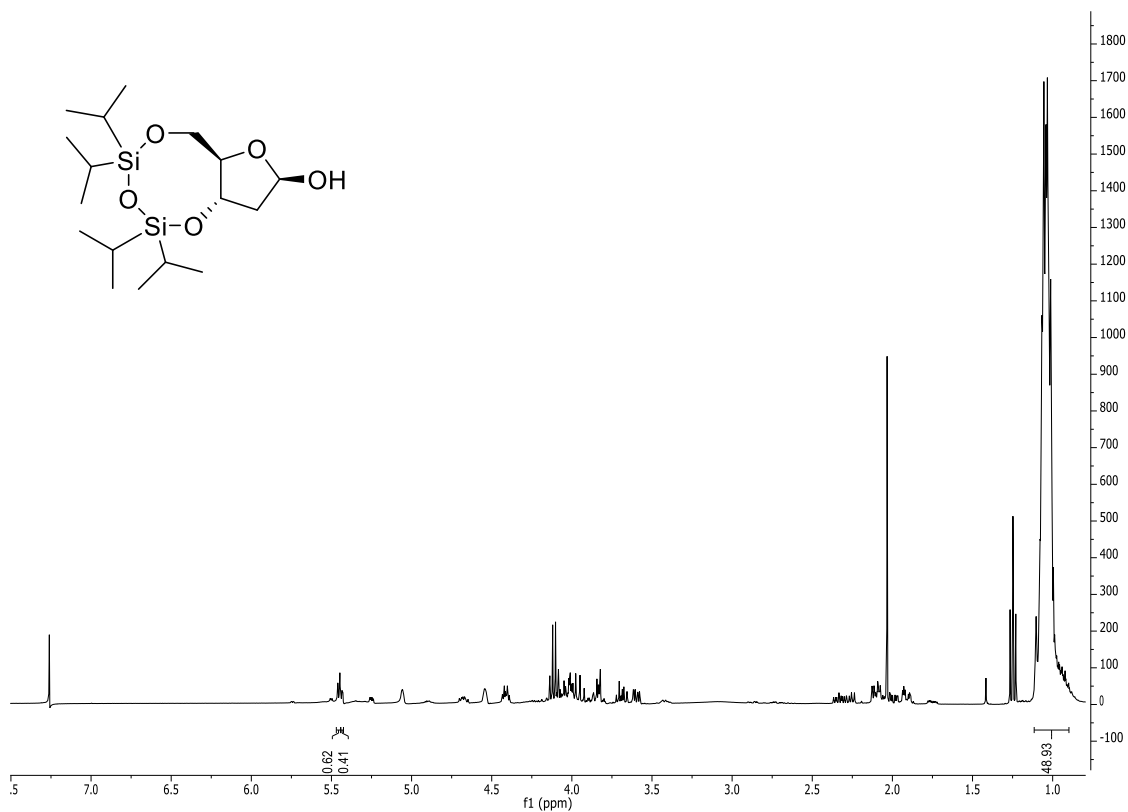
^{1}H NMR of compound **84**: CDCl$_3$; 400 MHz; r.t.
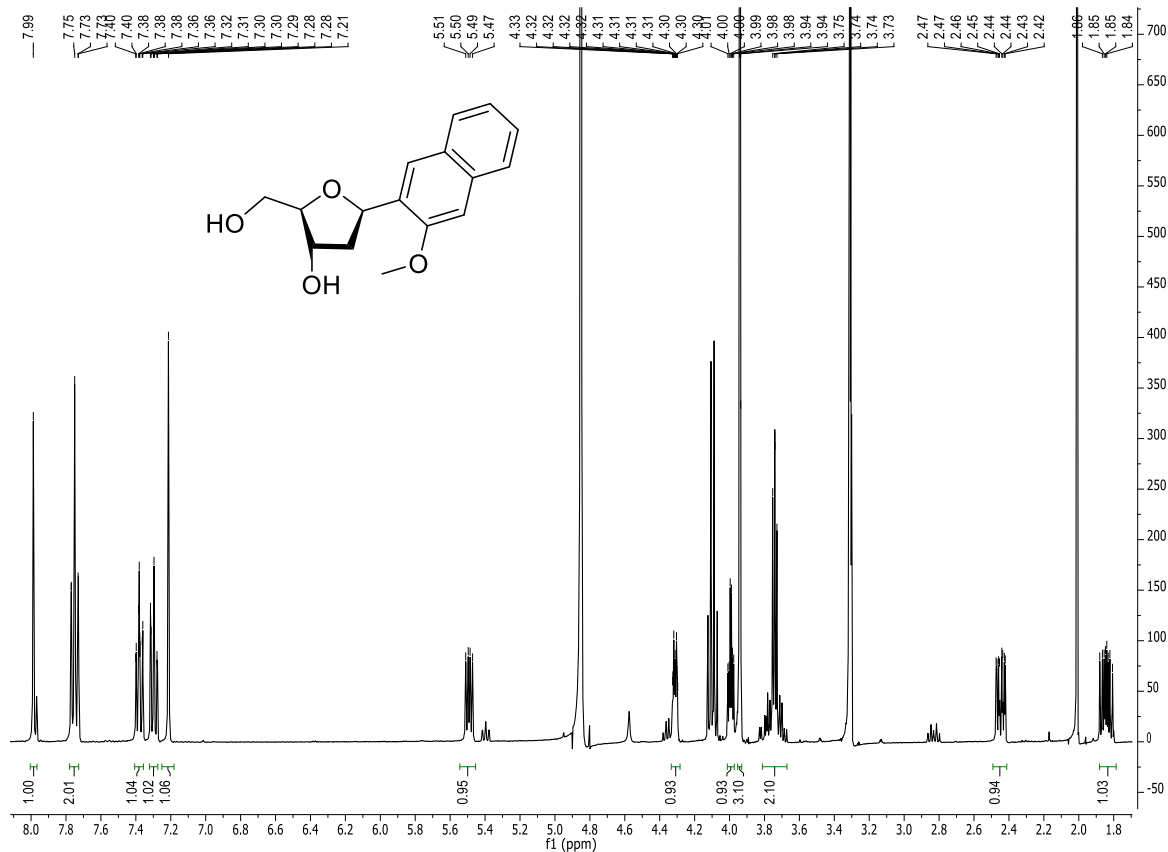
^{1}H NMR of compound d**NaM 86**: MeOD; 500 MHz; r.t.
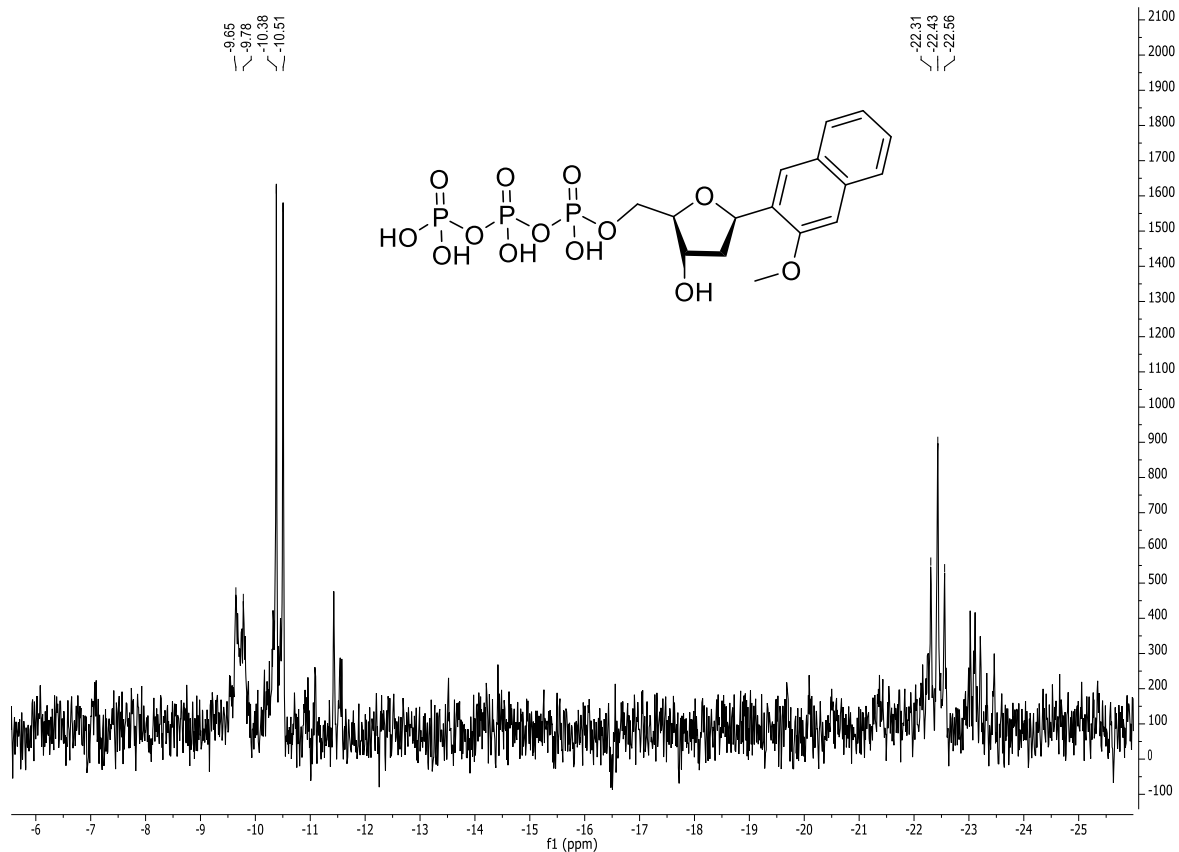
^{31}P-NMR of compound d**NaM**-TP **87**: D$_2$O; 500 MHz; r.t.
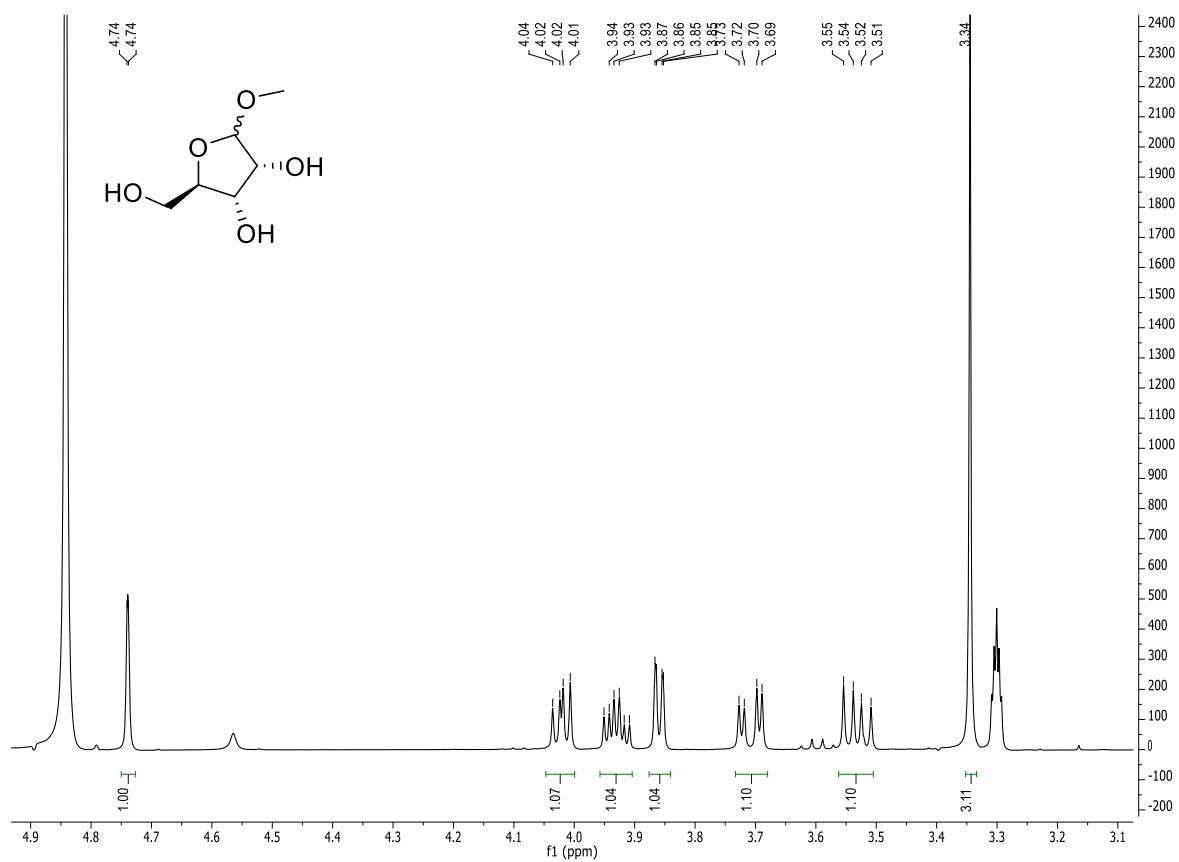
^{1}H-NMR of compound **89**: MeOD; 400 MHz; r.t.

^{1}H-NMR of compound **90**: CDCl$_3$; 400 MHz; r.t.

^{1}H-NMR of compound **92**: CDCl$_3$; 400 MHz; r.t.
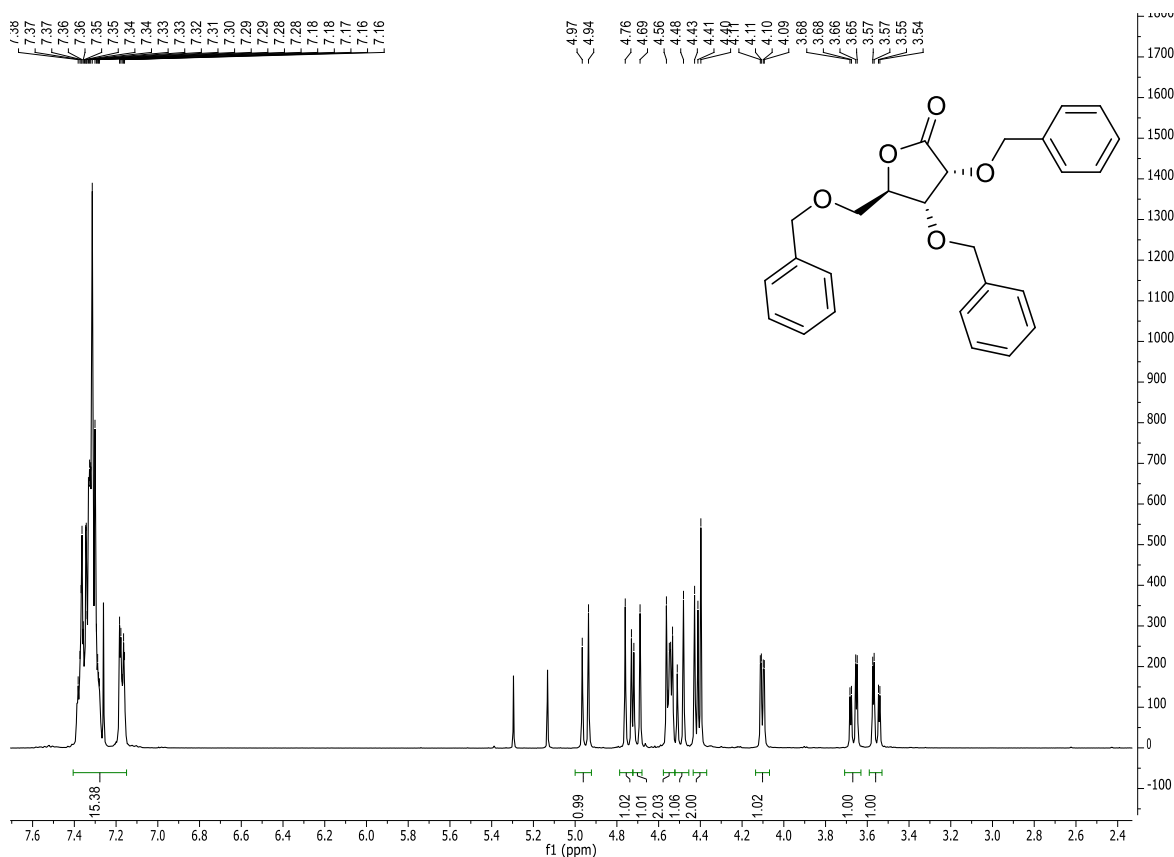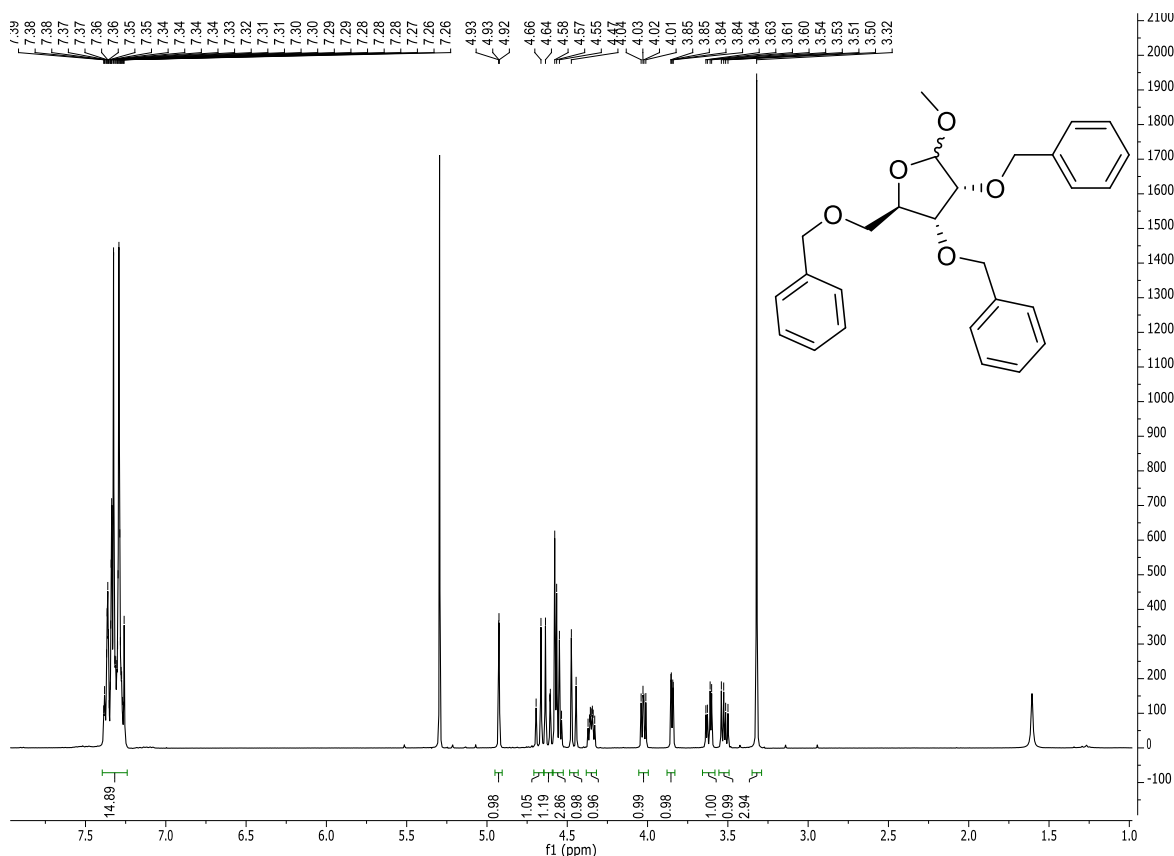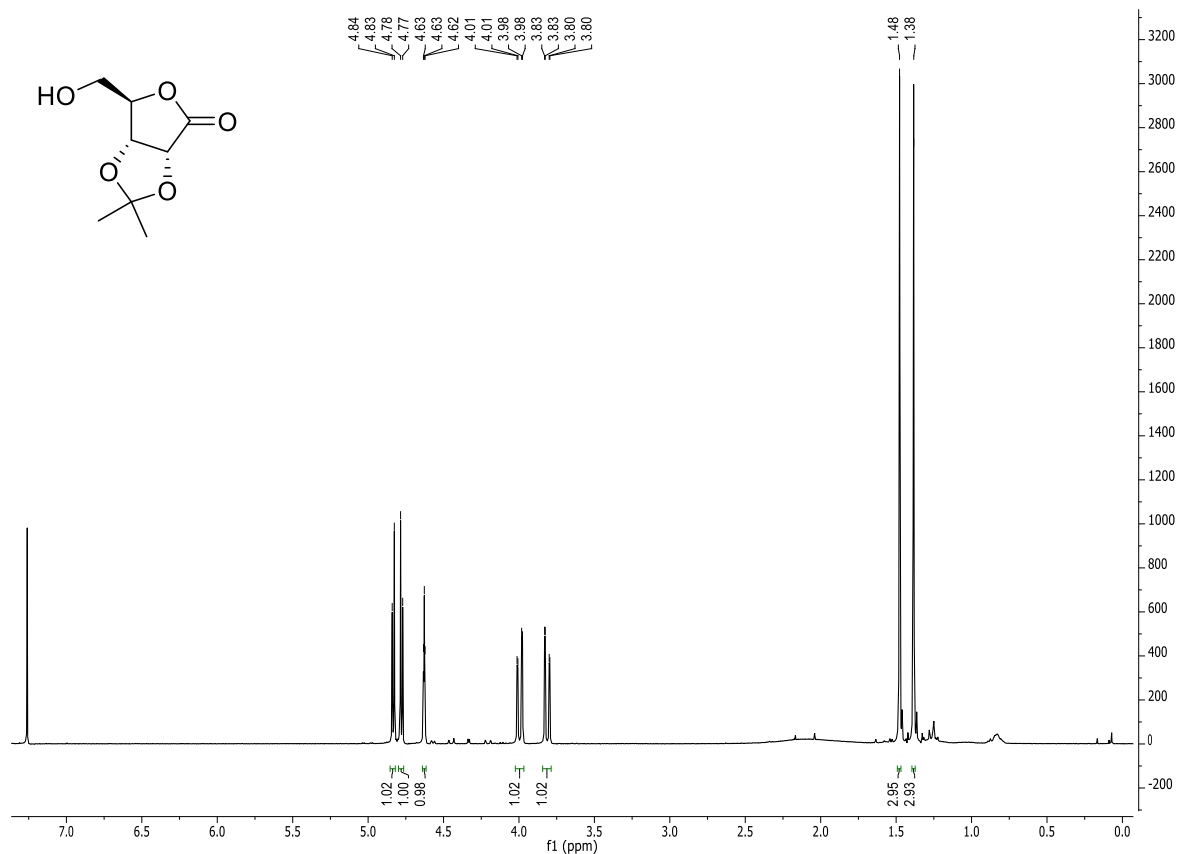
^{1}H-NMR of compound **101i**: CDCl$_3$; 400 MHz; r.t.
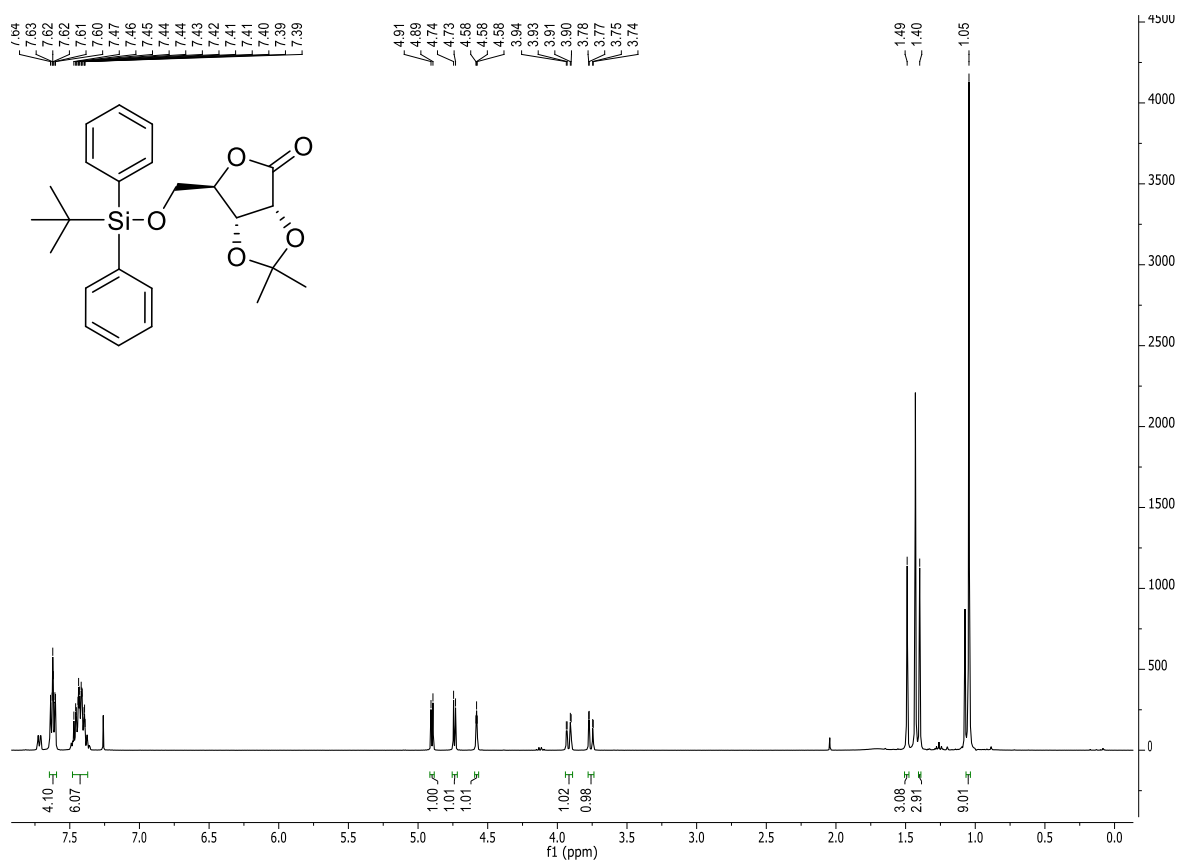
^{1}H-NMR of compound **101**: CDCl$_3$; 400 MHz; r.t.
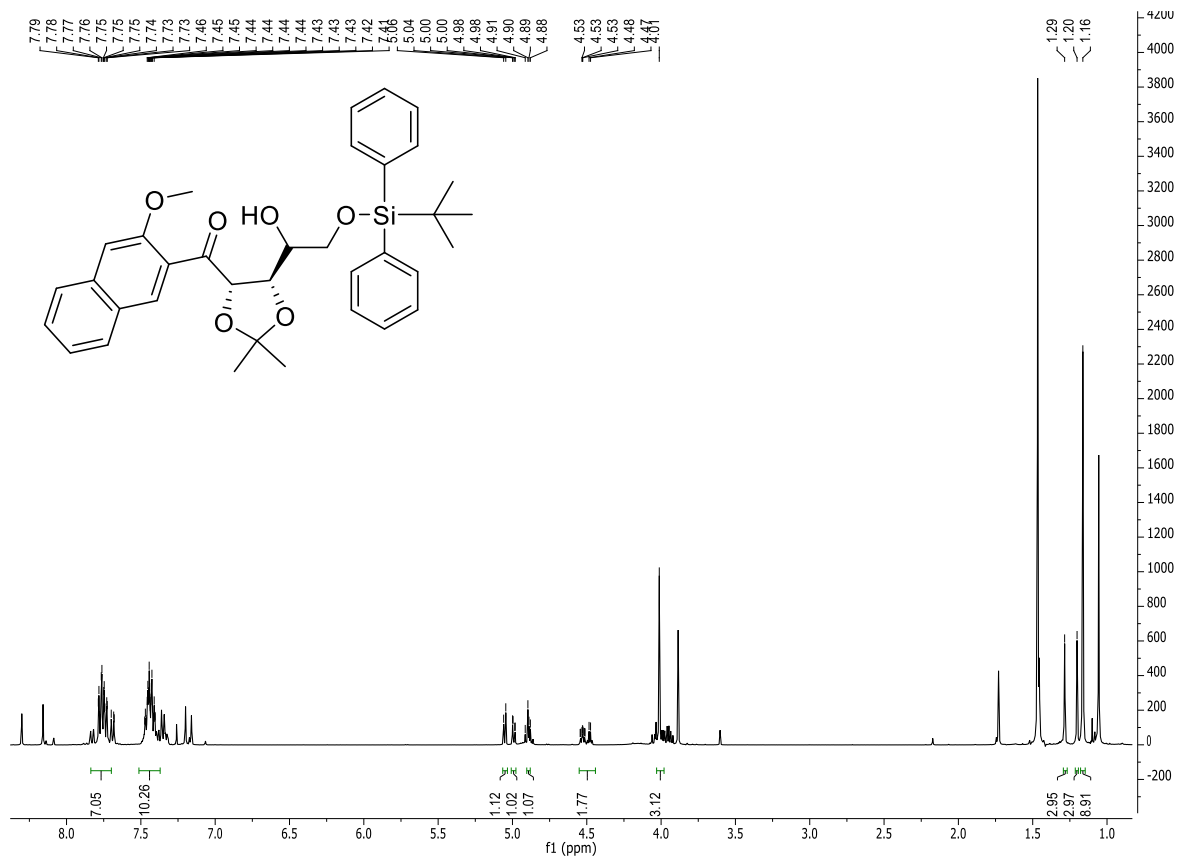
^{1}H-NMR of compound **102**: CDCl$_3$; 400 MHz; r.t.

^{1}H-NMR of compound **NaM 96**: CDCl$_3$; 400 MHz; r.t.

^{13}C-NMR of compound **NaM 96**: CDCl$_3$; 400 MHz; r.t.
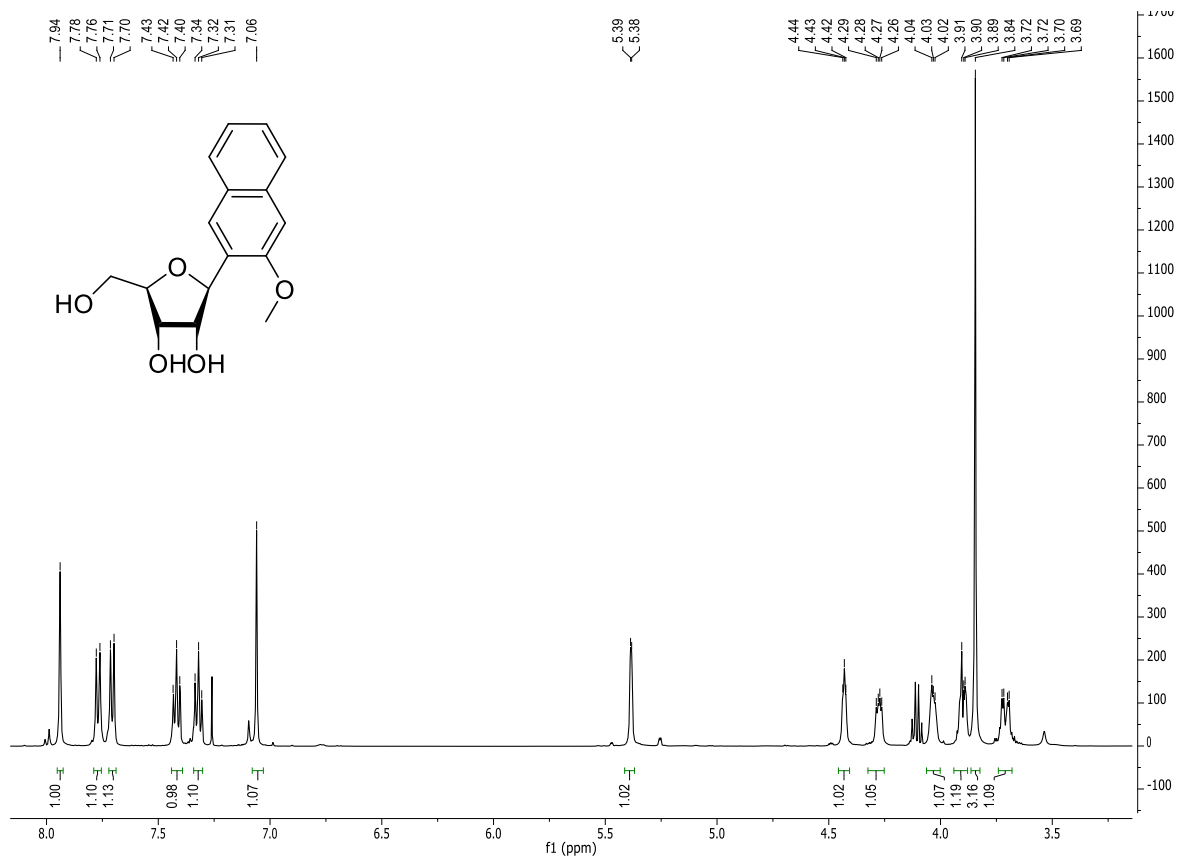
^{1}H-NMR of compound **NaM**-TP **103**: D$_2$O; 202 MHz; r.t.
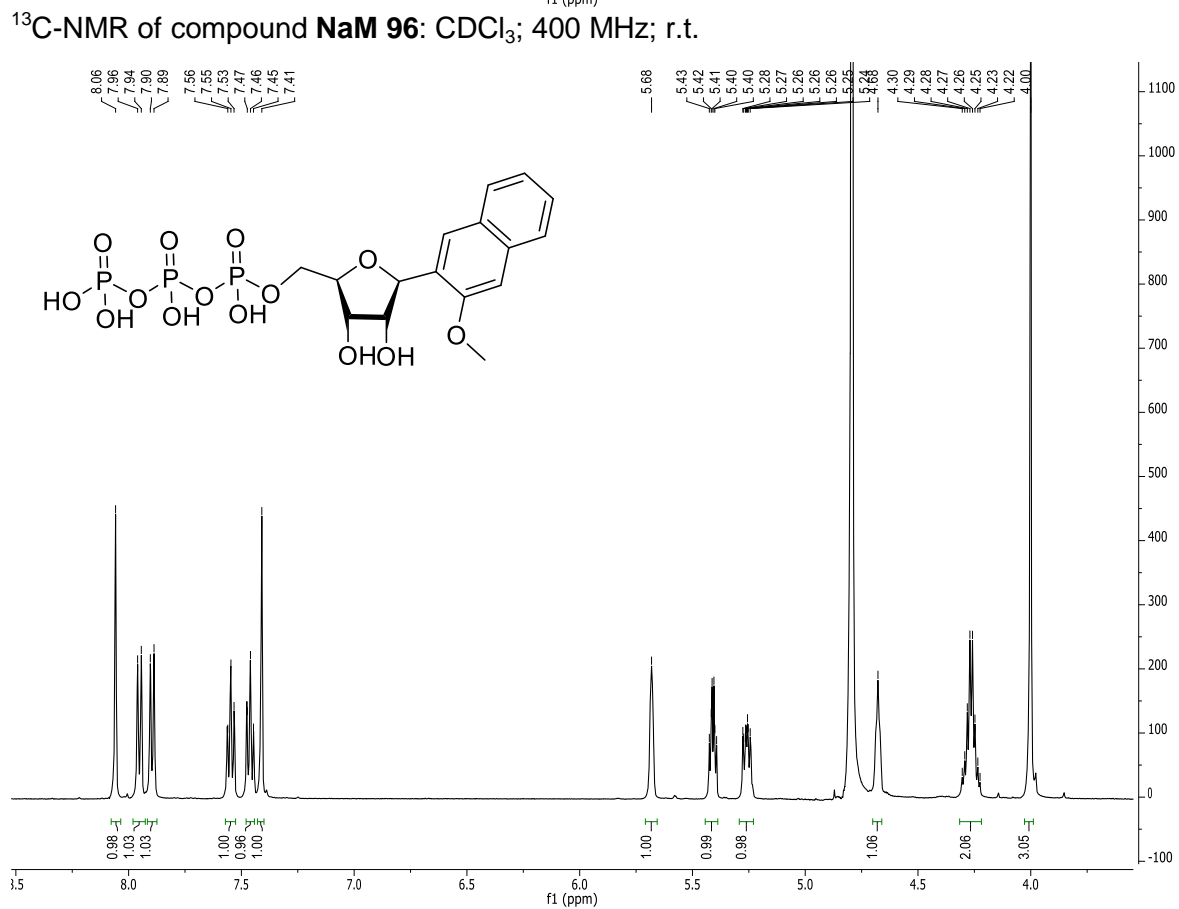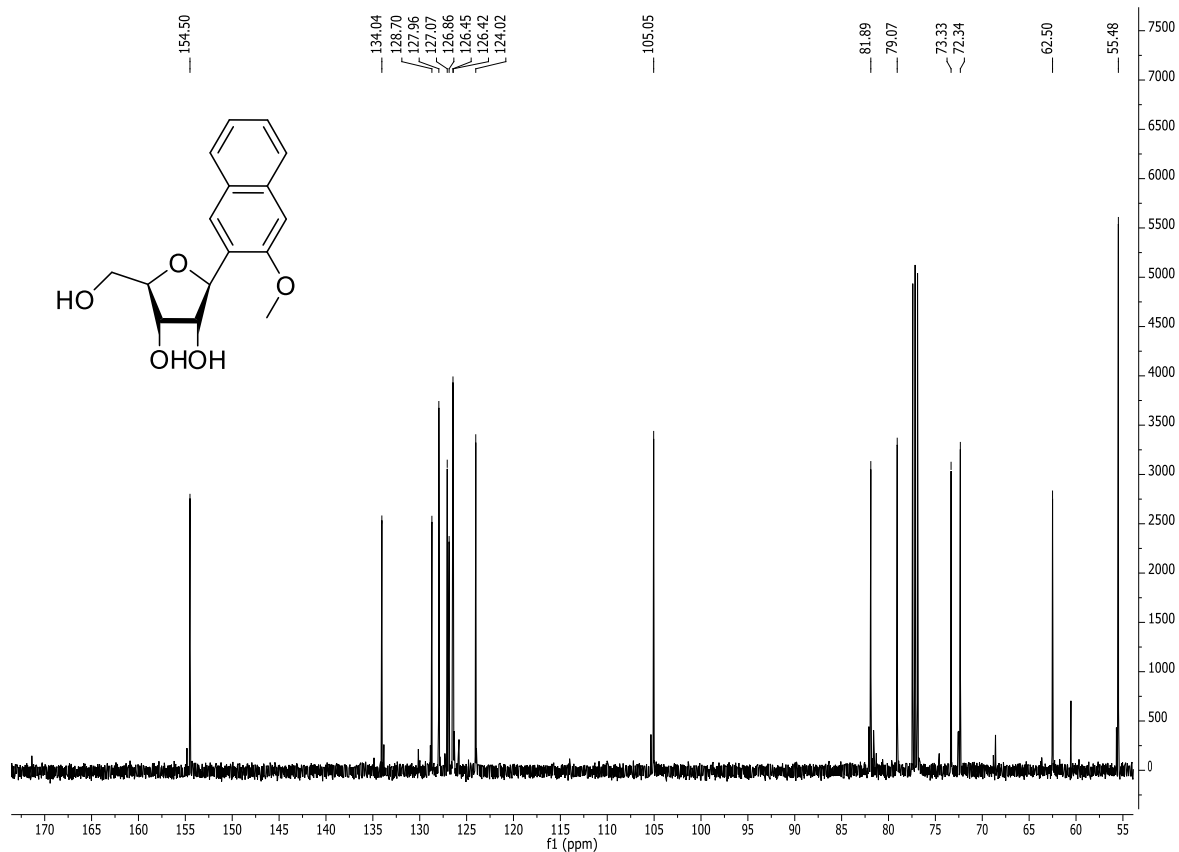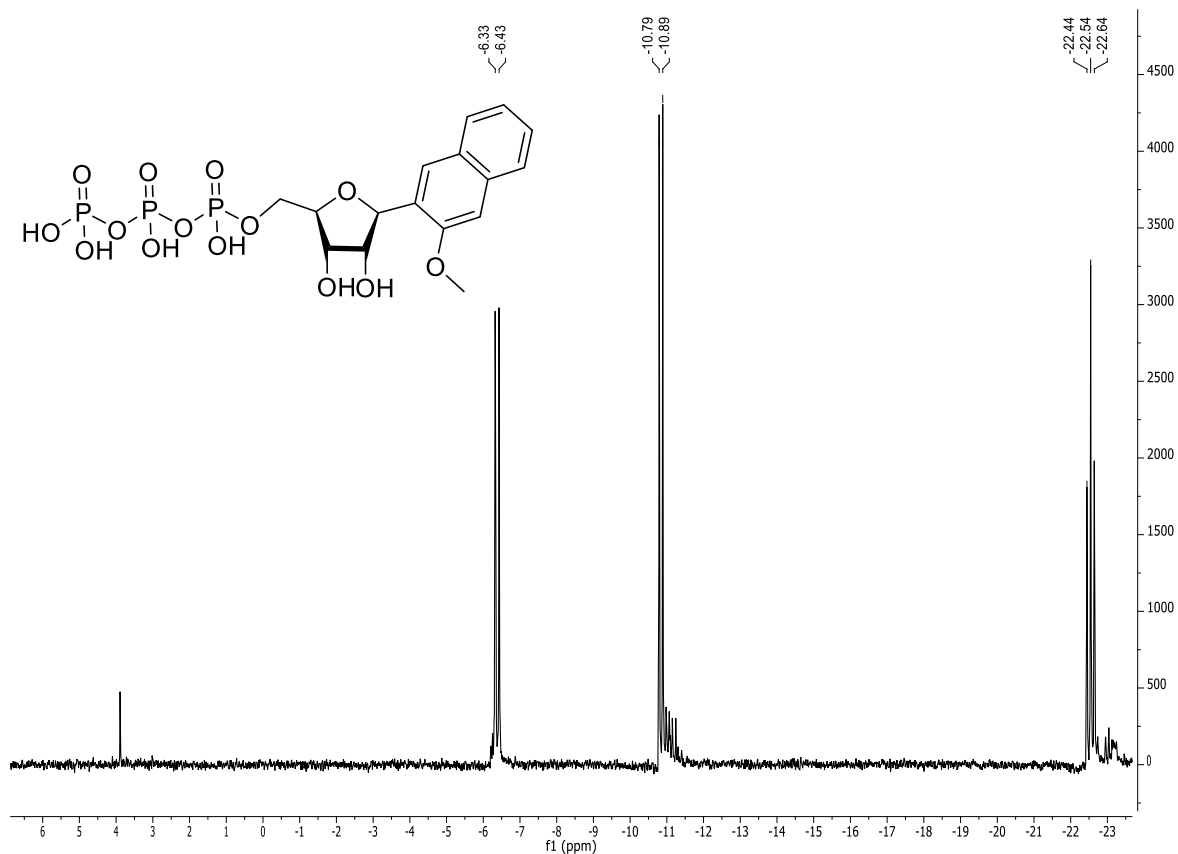
^{31}P-NMR of compound **NaM**-TP **103**: D$_2$O; 500 MHz; r.t.
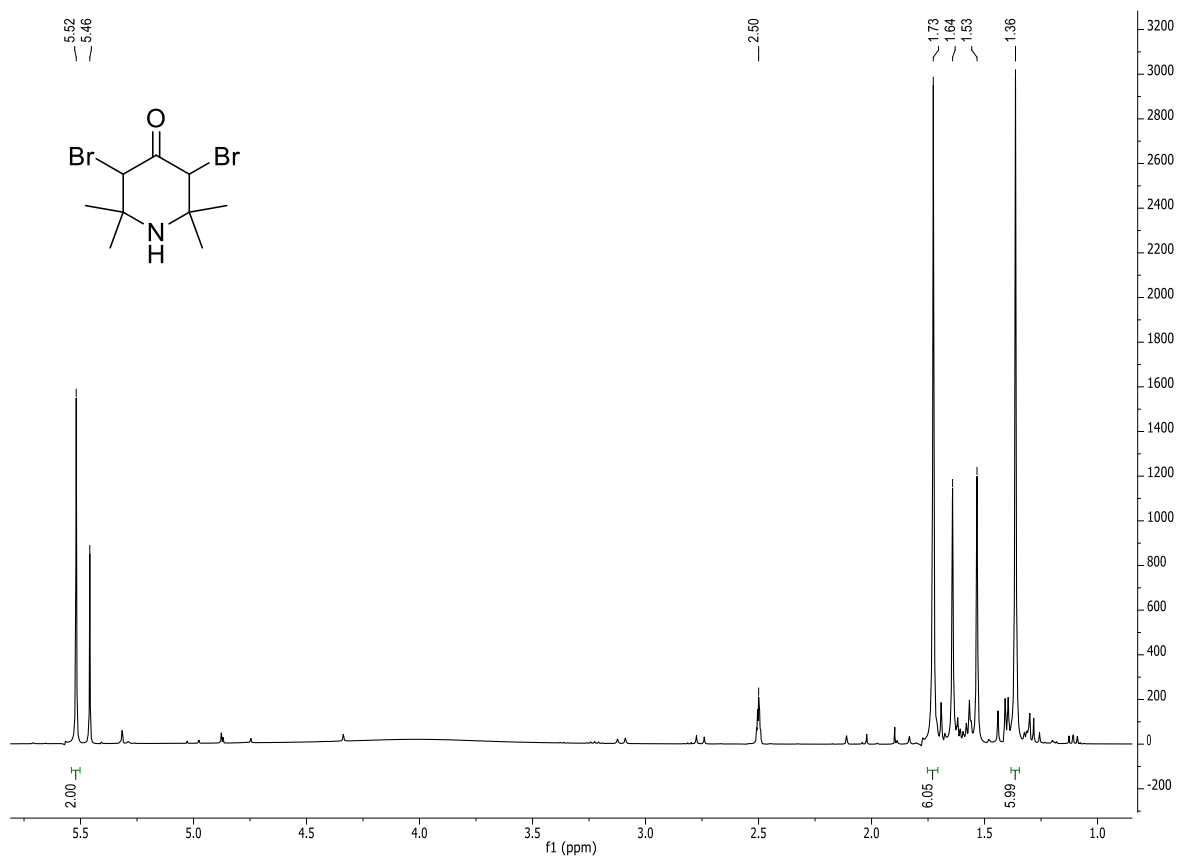
^{1}H-NMR of compound **109**: DMSO-d_6; 400 MHz; r.t.
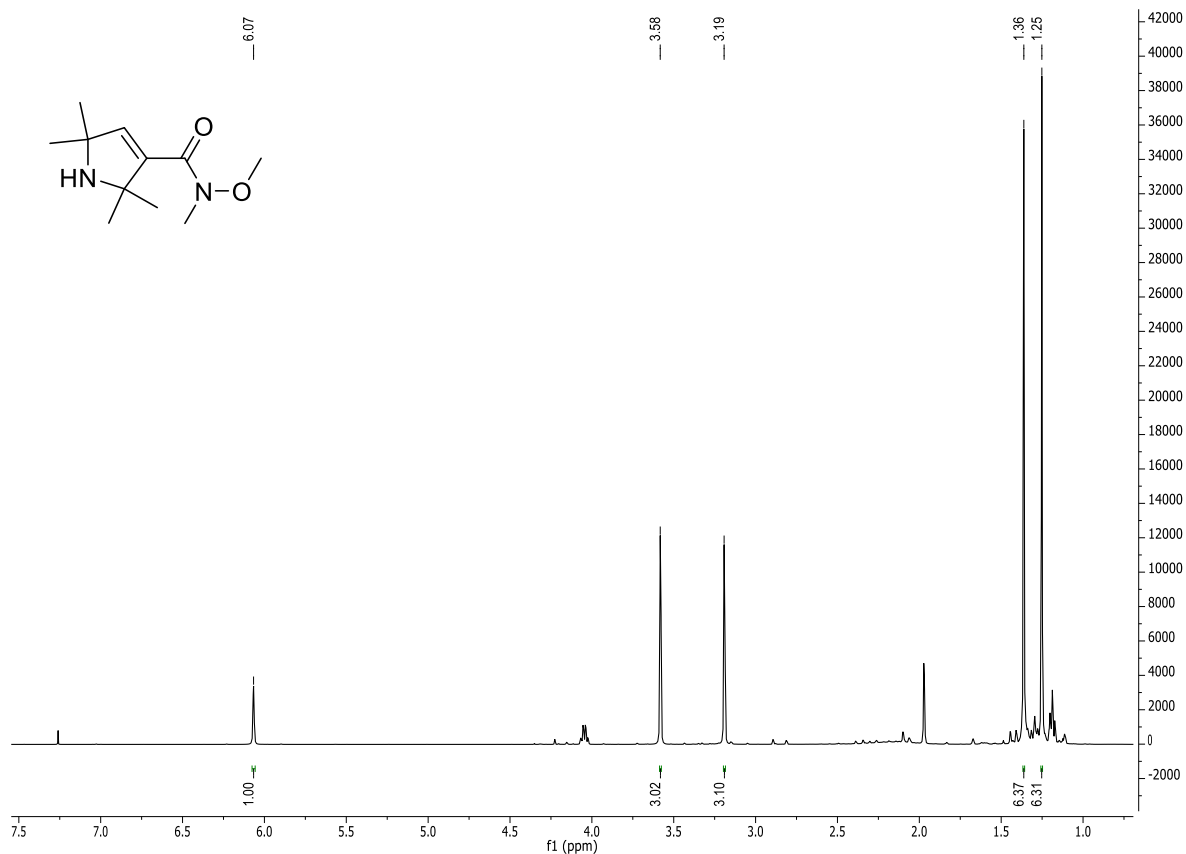
^{1}H-NMR of compound **110**: CDCl$_3$; 500 MHz; r.t.
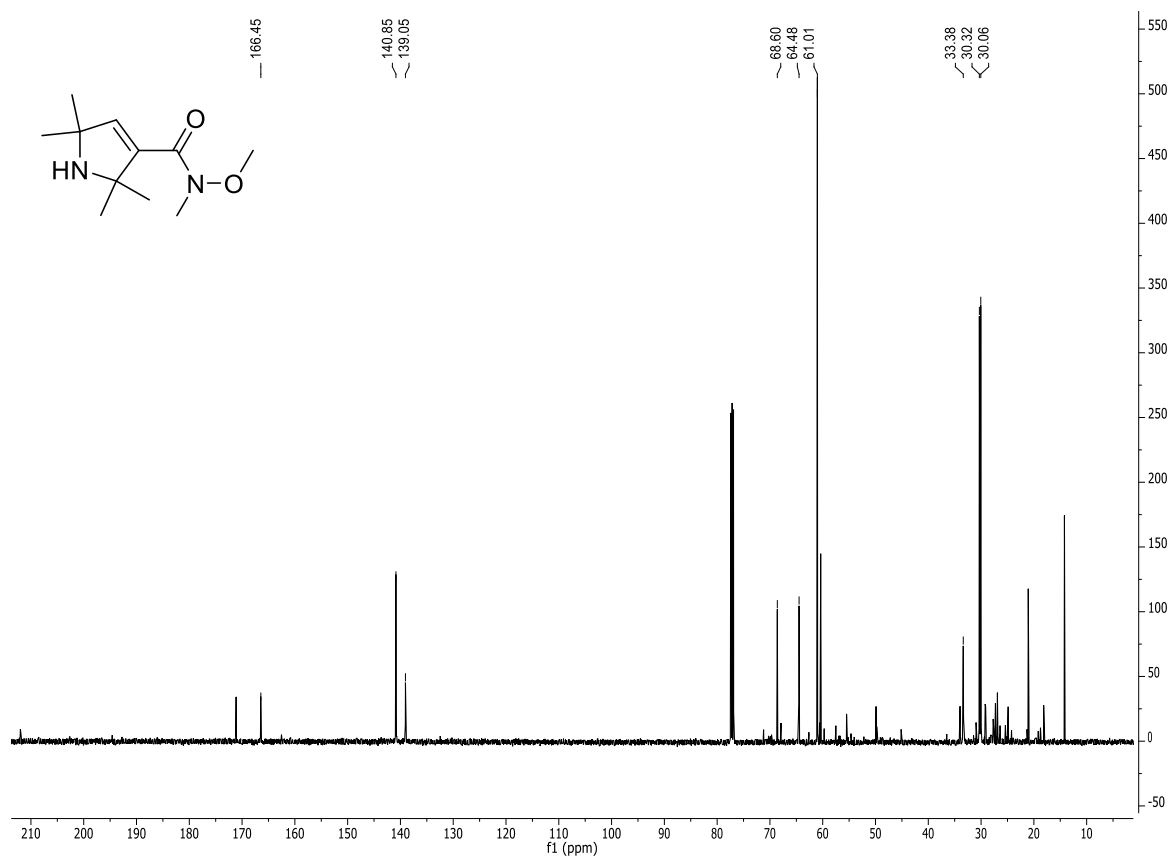
^{13}C-NMR of compound **110**: CDCl$_3$; 500 MHz; r.t.
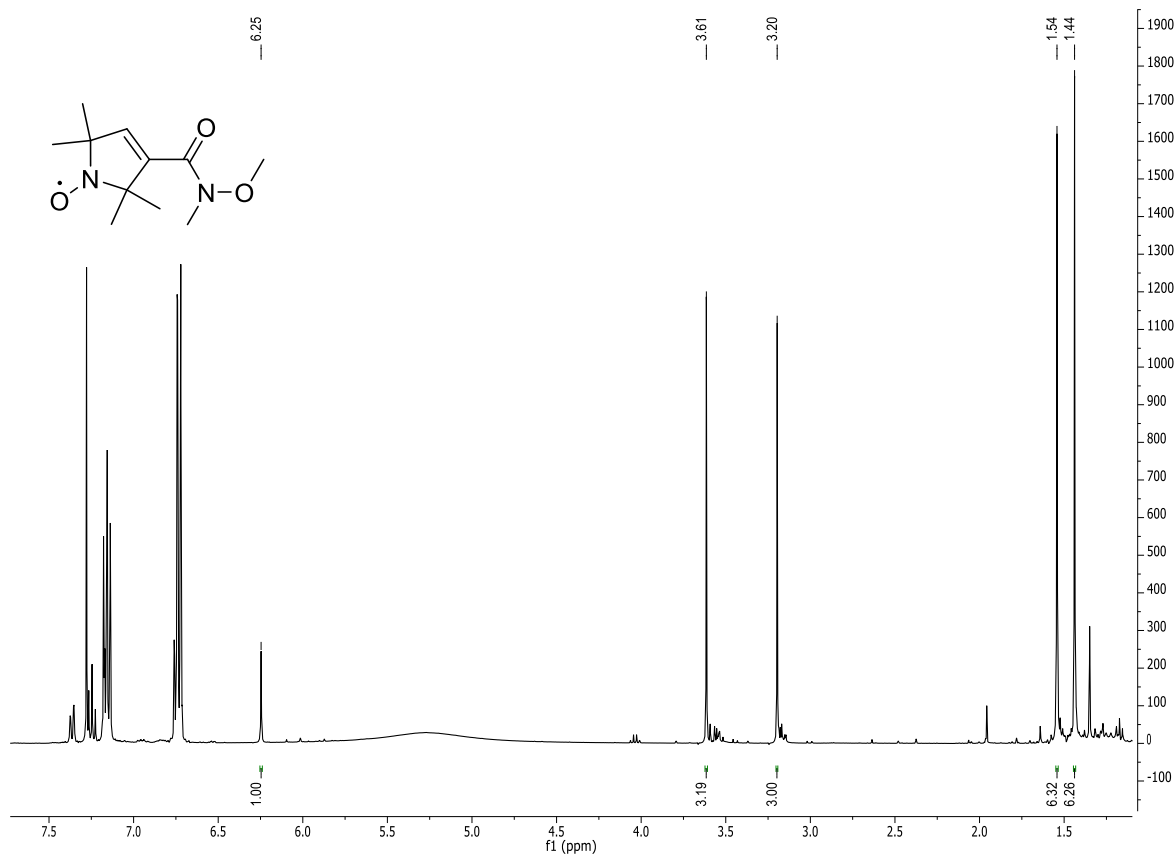
^{1}H-NMR of *in situ* reduced compound **111**: CDCl$_3$; 400 MHz; r.t.
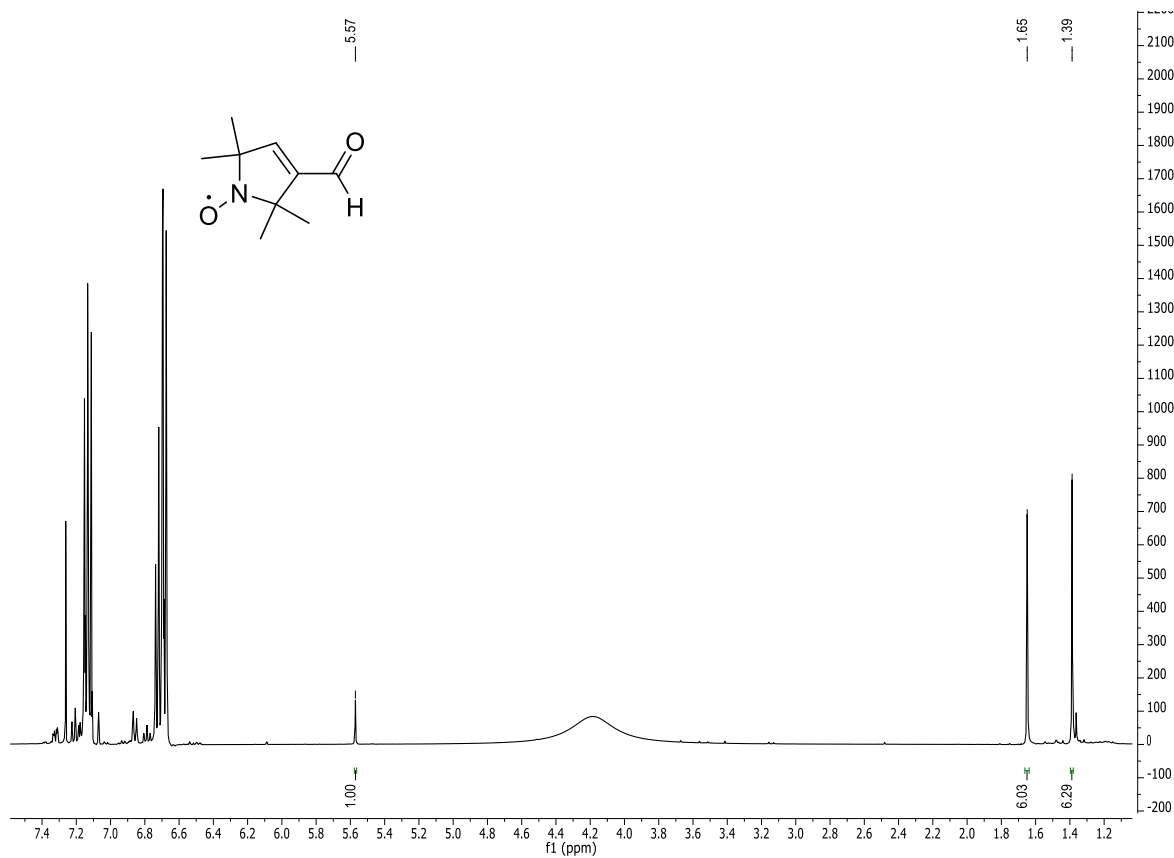
^{1}H-NMR of *in situ* reduced compound **112**: CDCl$_3$; 400 MHz; r.t.
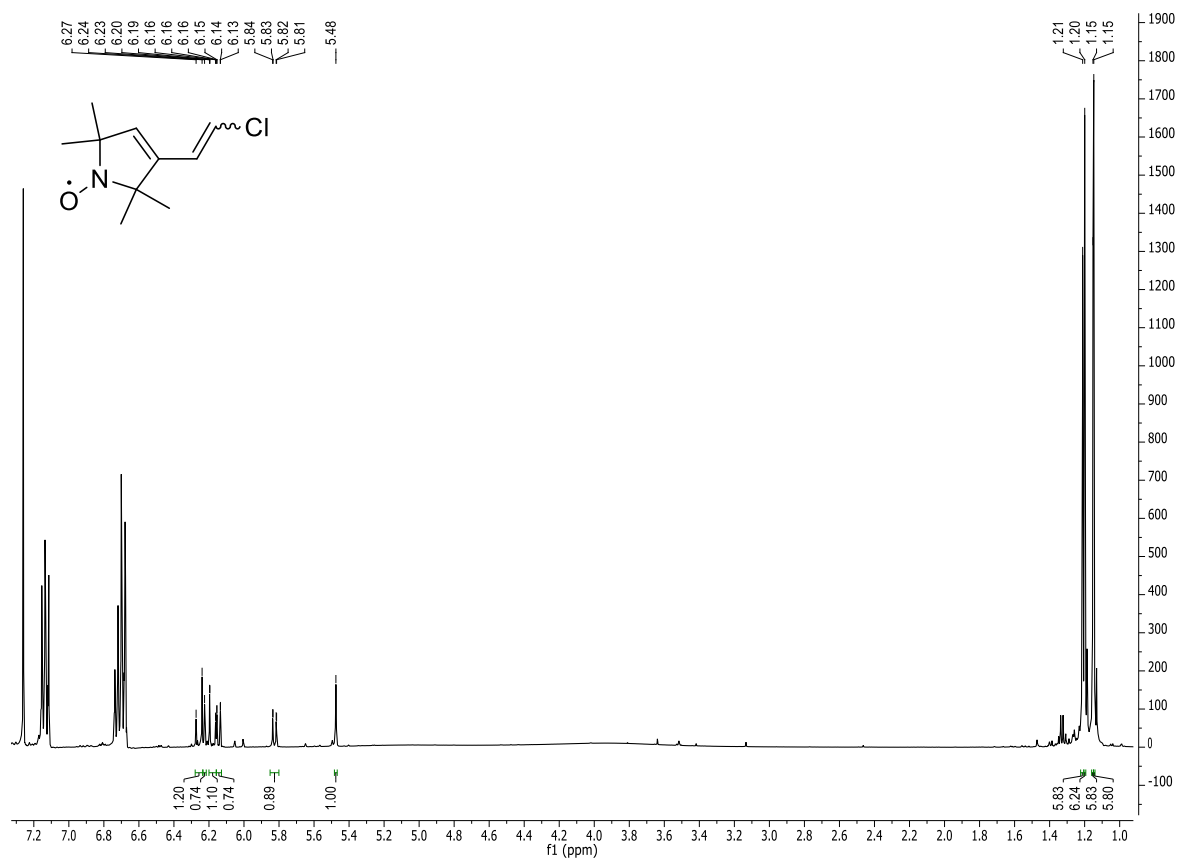
^{1}H-NMR of *in situ* reduced compound **113**: CDCl$_3$; 400 MHz; r.t.
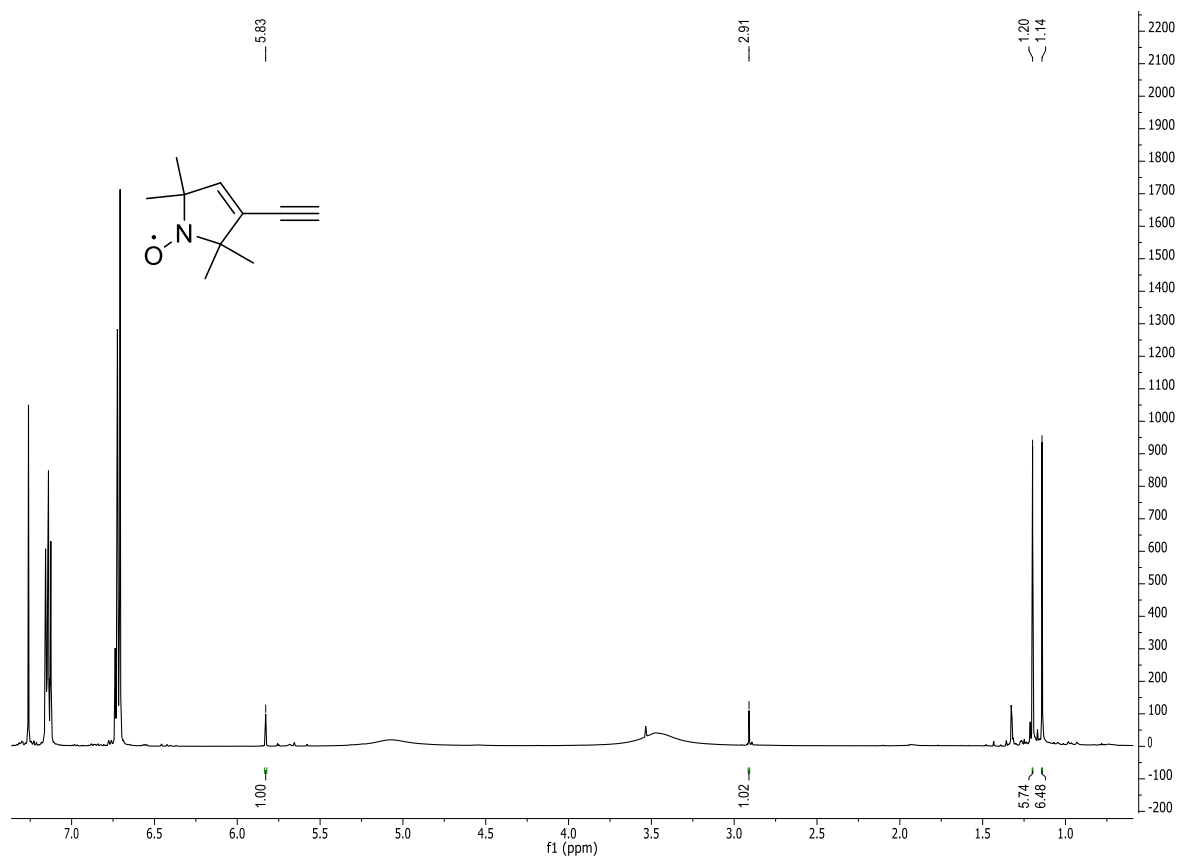
^{1}H-NMR of *in situ* reduced compound **114**: CDCl$_3$; 400 MHz; r.t.
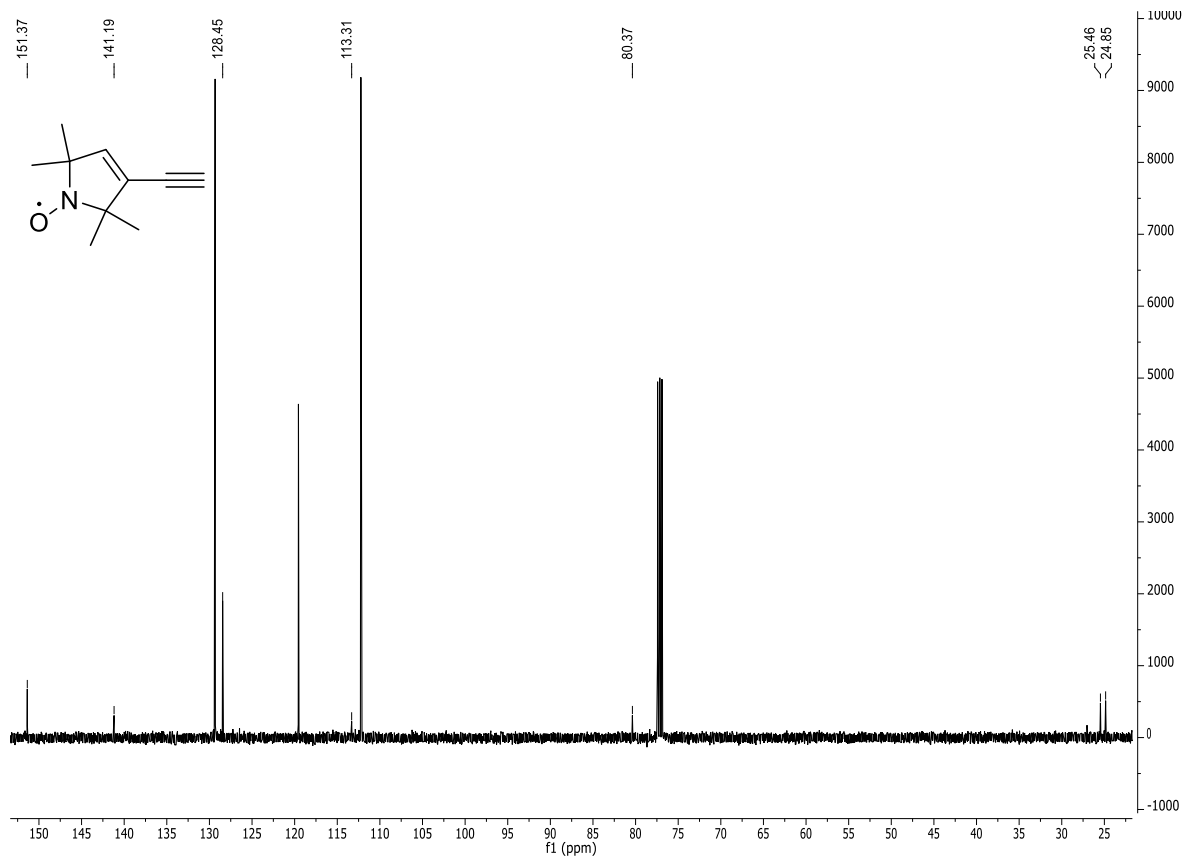
^{13}C-NMR of *in situ* reduced compound **114**: CDCl$_3$; 400 MHz; r.t.
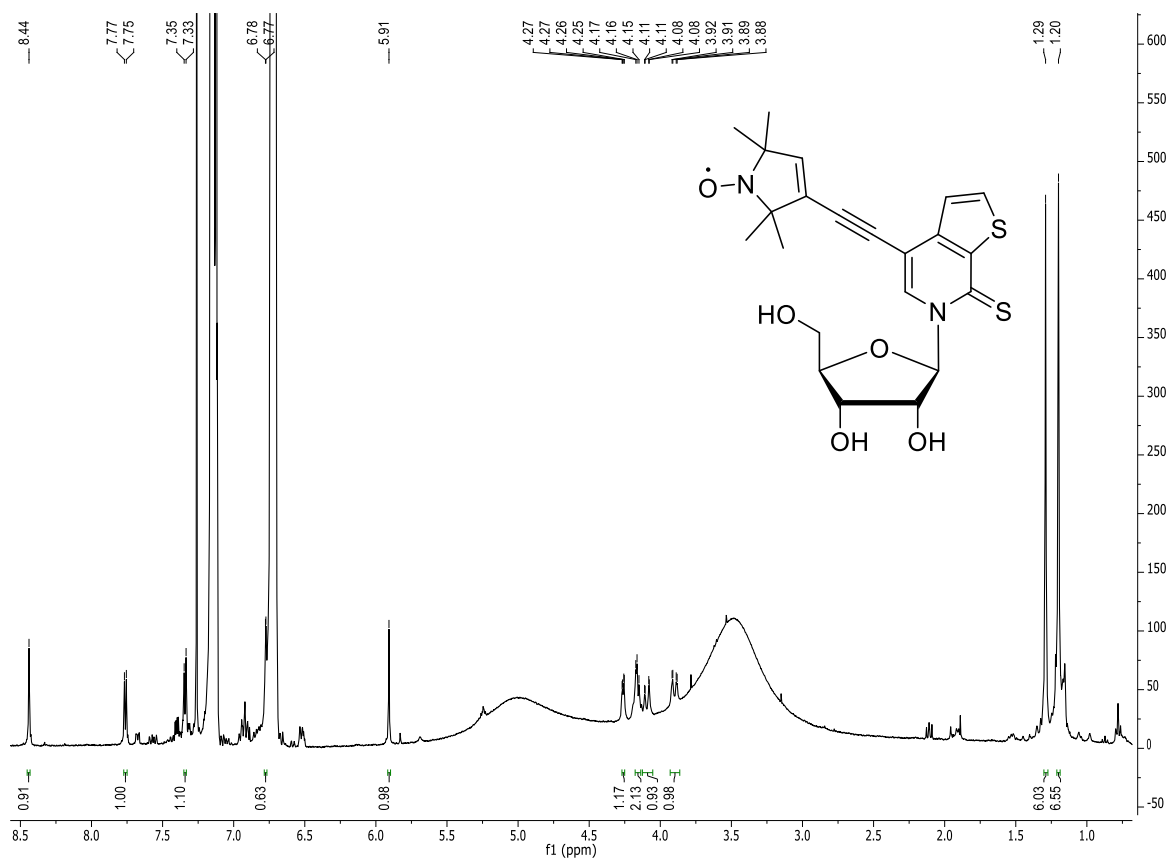
^{1}H-NMR of *in situ* reduced compound **117**: CDCl$_3$; 400 MHz; r.t.

^{1}H-NMR of compound **119**: D$_2$O; 400 MHz; r.t.

^{31}P-NMR of compound **119**: D$_2$O; 400 MHz; r.t.

^{1}H-NMR of compound **119**: D$_2$O; 400 MHz; r.t.

^{31}P-NMR of compound **119**: D$_2$O; 400 MHz; r.t.
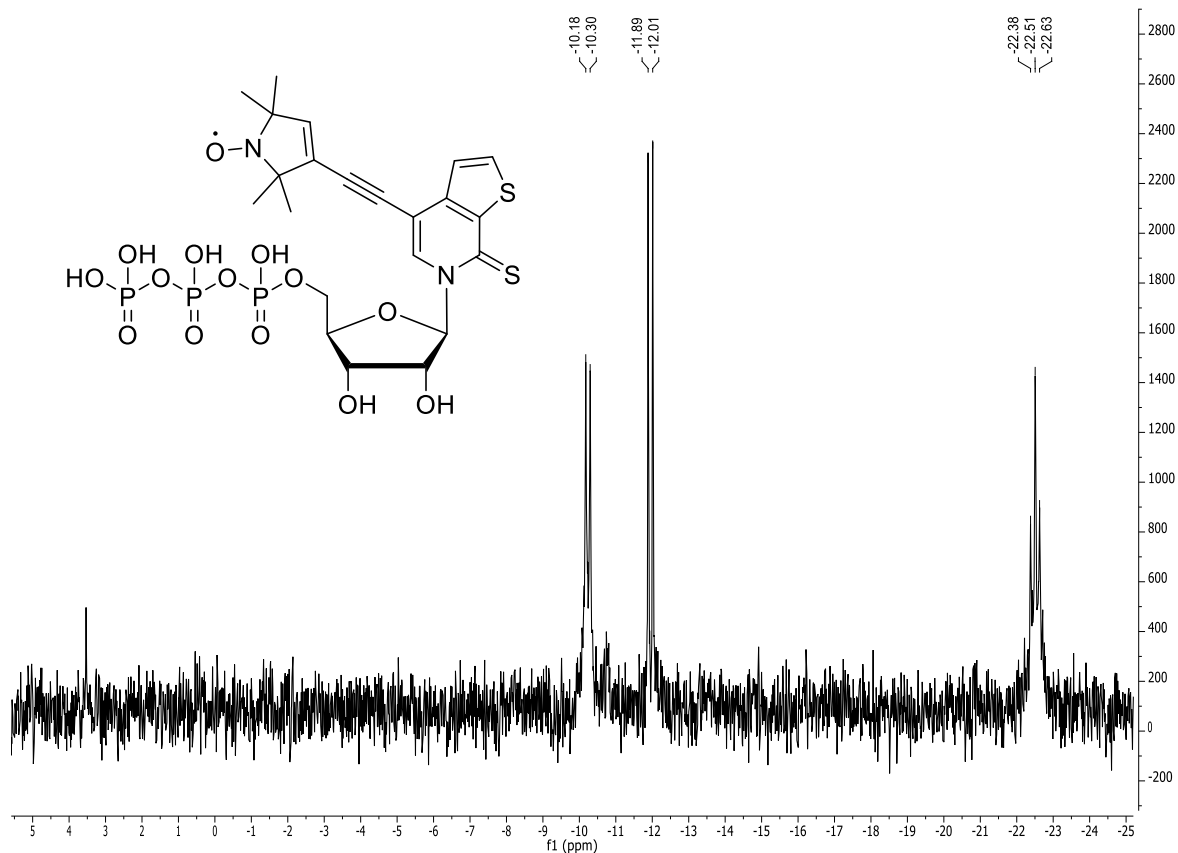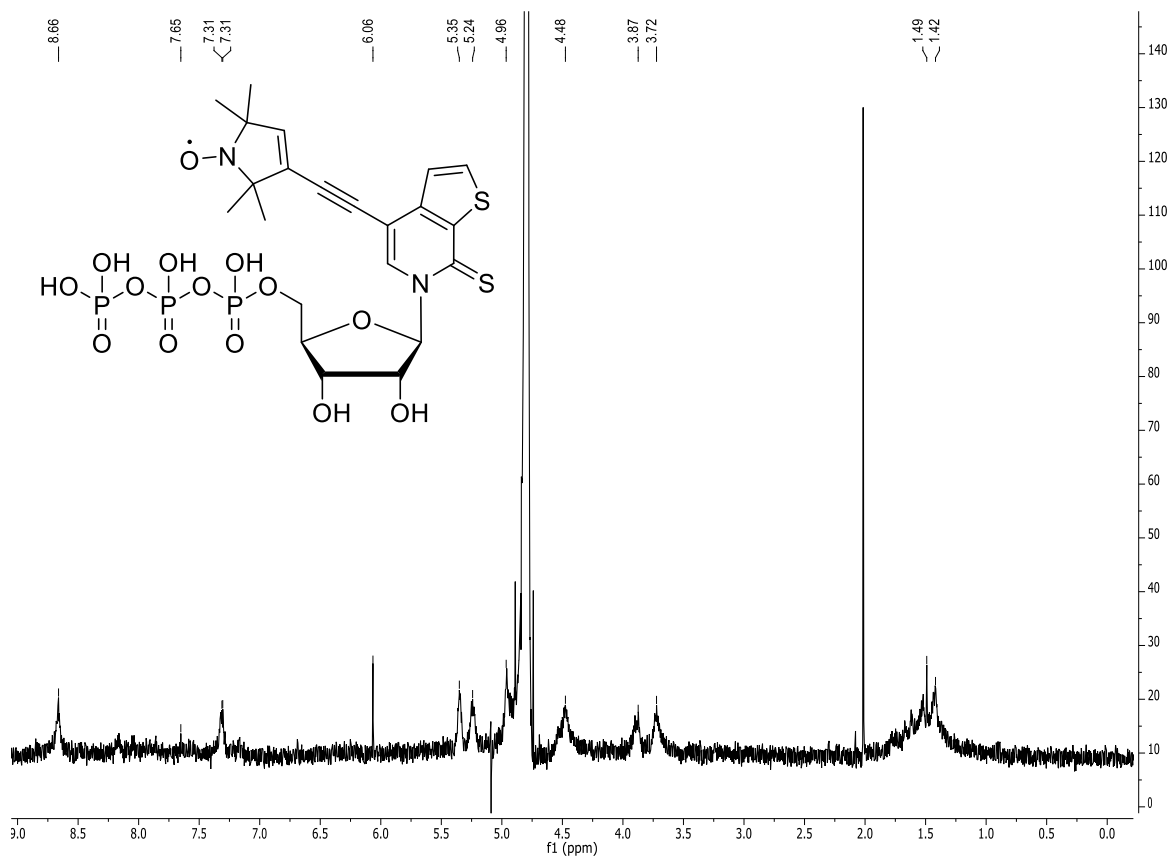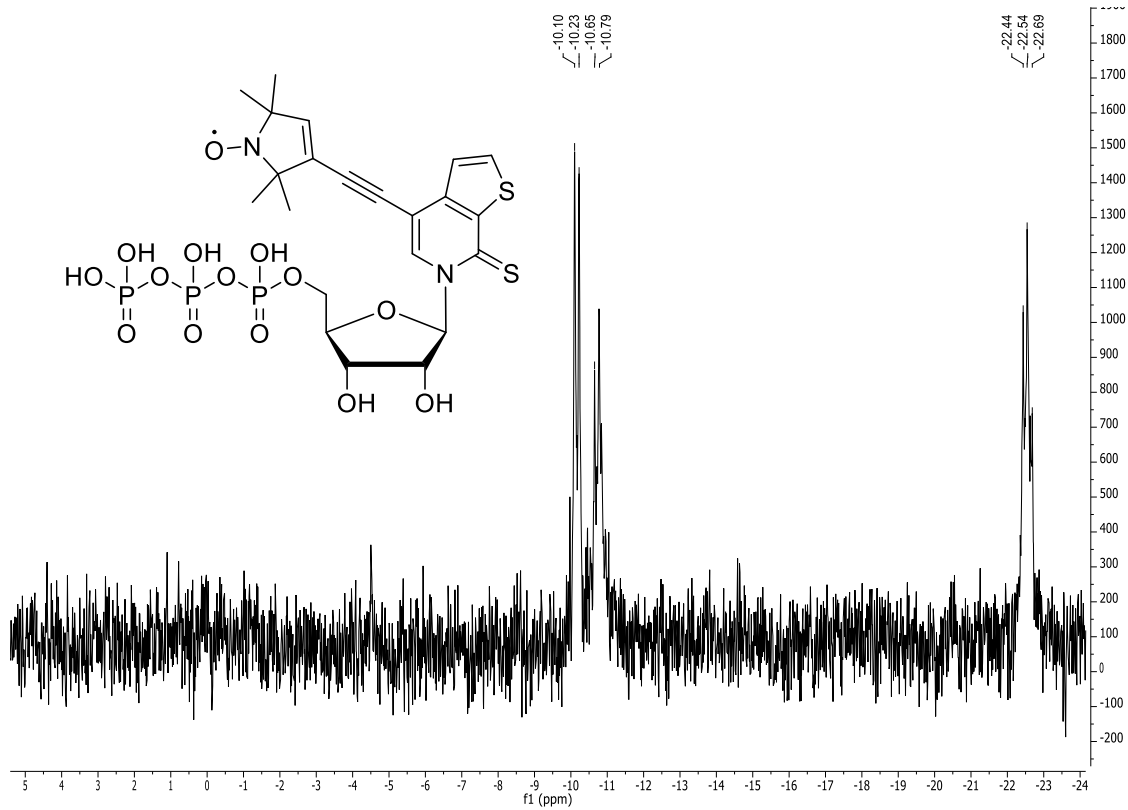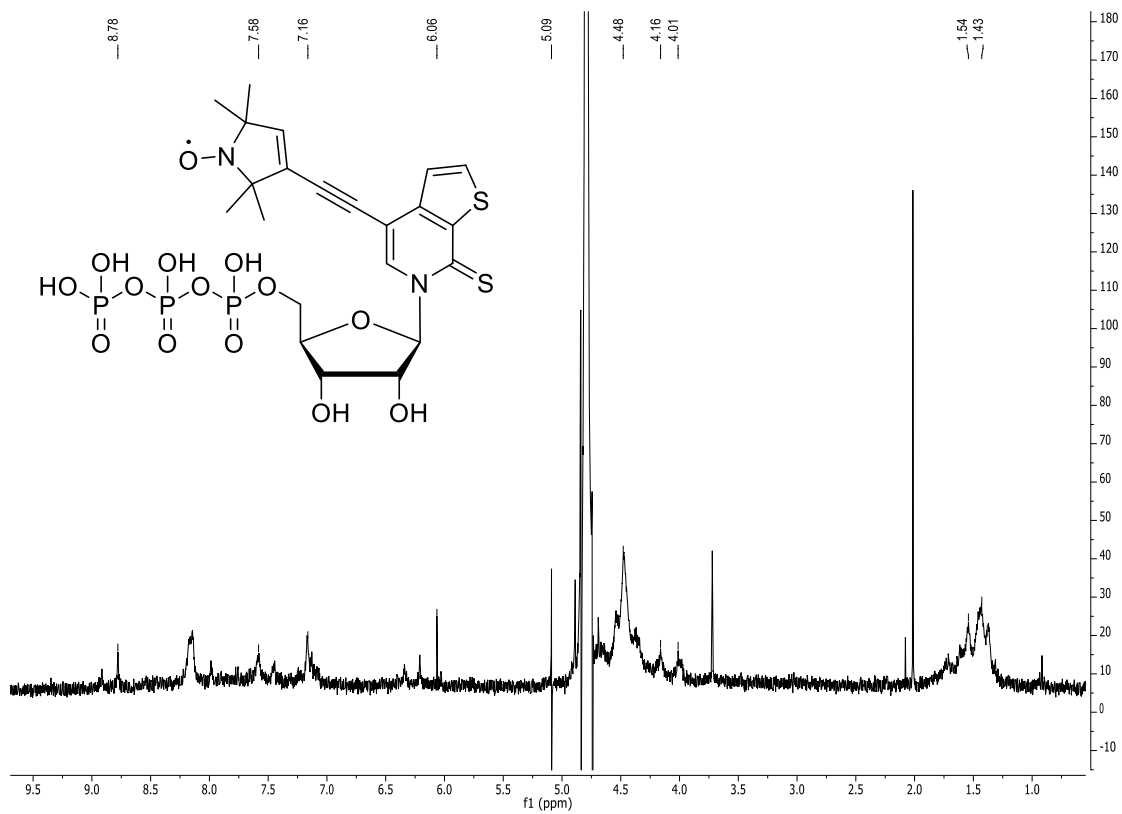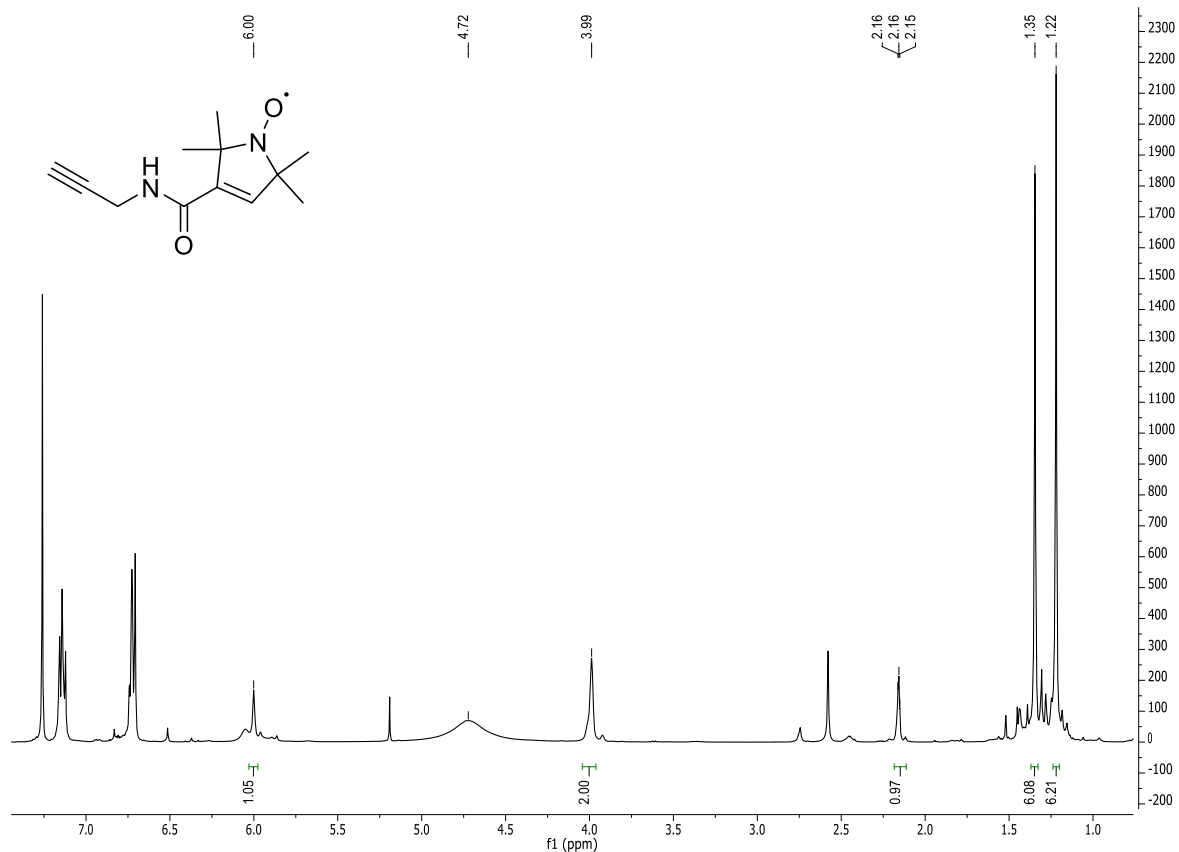
^{1}H-NMR of *in situ* reduced compound **124**: CDCl$_3$; 400 MHz; r.t.
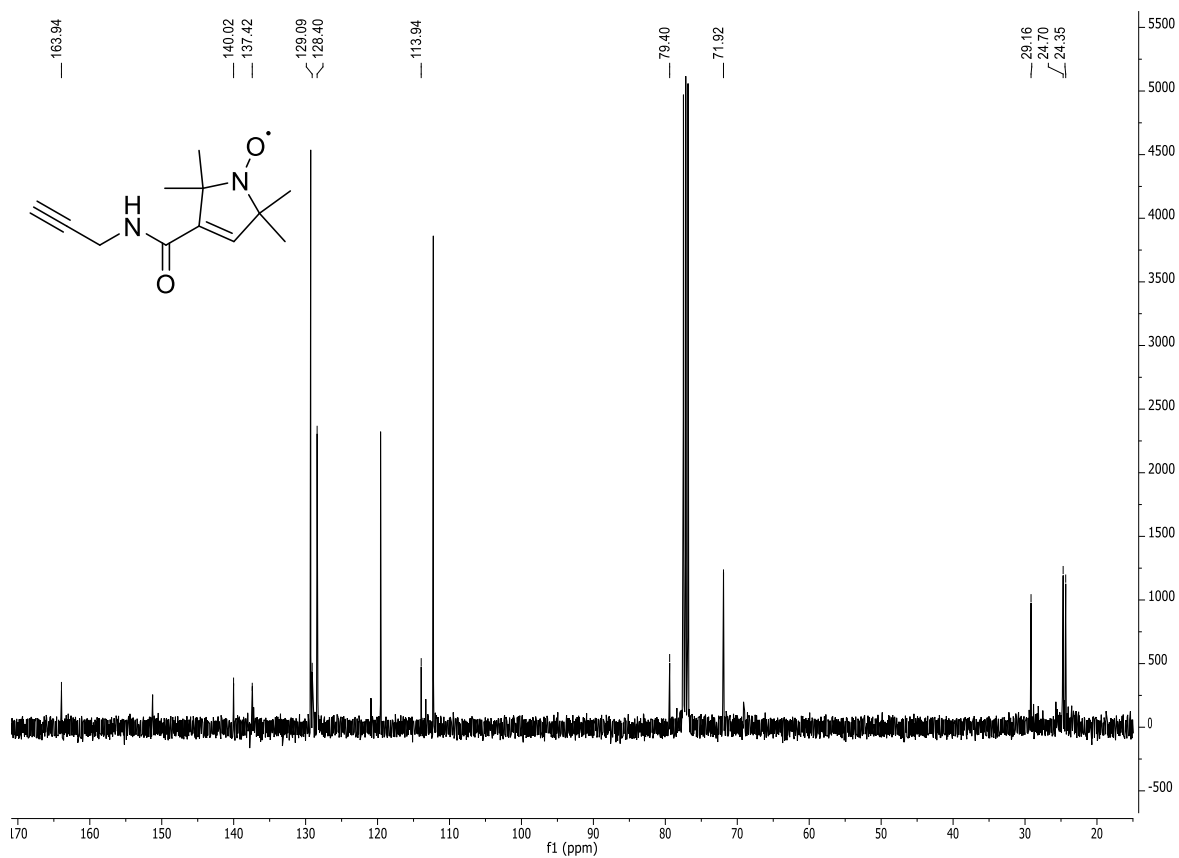
^{13}C-NMR of *in situ* reduced compound **124**: CDCl$_3$; 101 MHz; r.t.
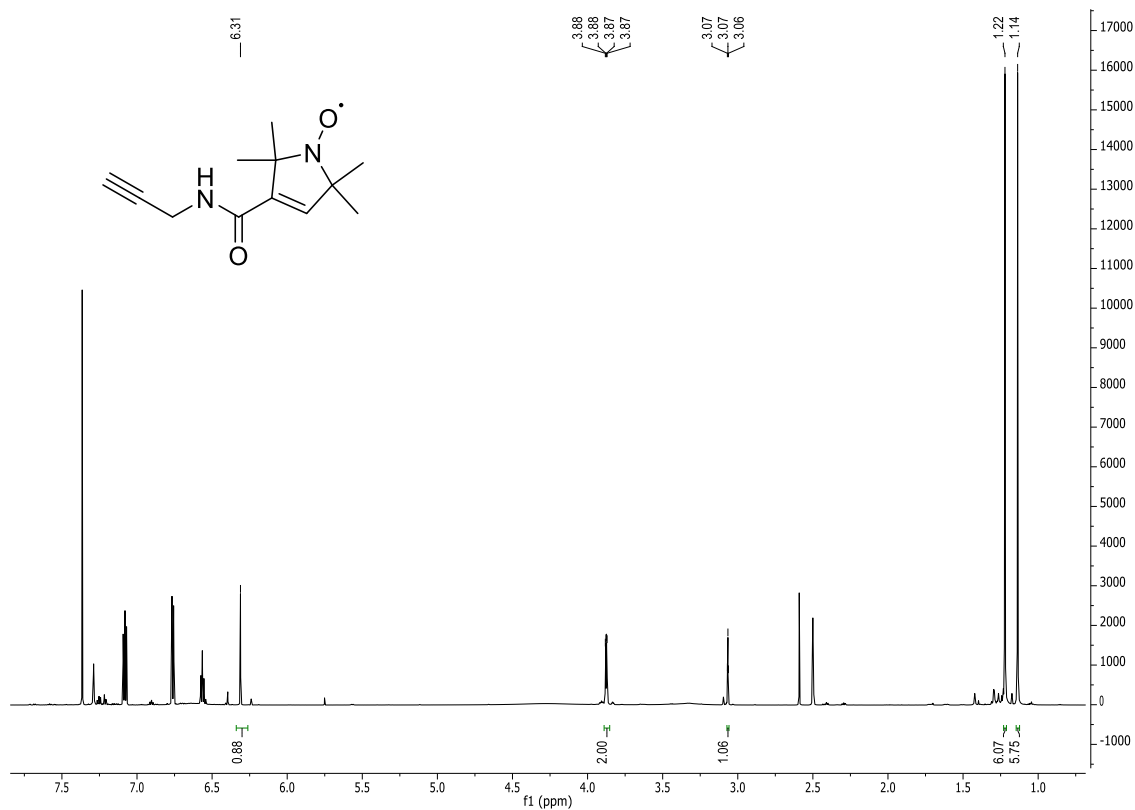
^{1}H-NMR of *in situ* reduced compound **124**: DMSO-d_6; 700 MHz; r.t.
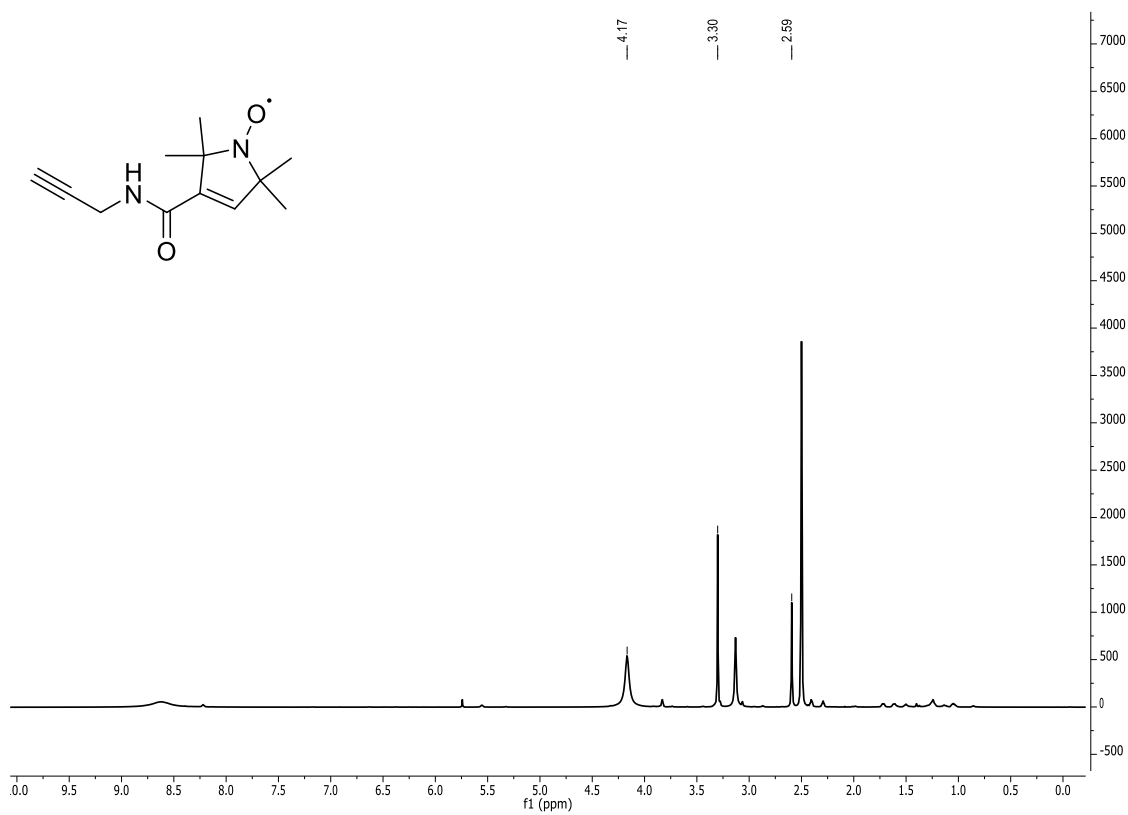
^{1}H-NMR of unreduced compound **124**: DMSO-d_6; 700 MHz; r.t.
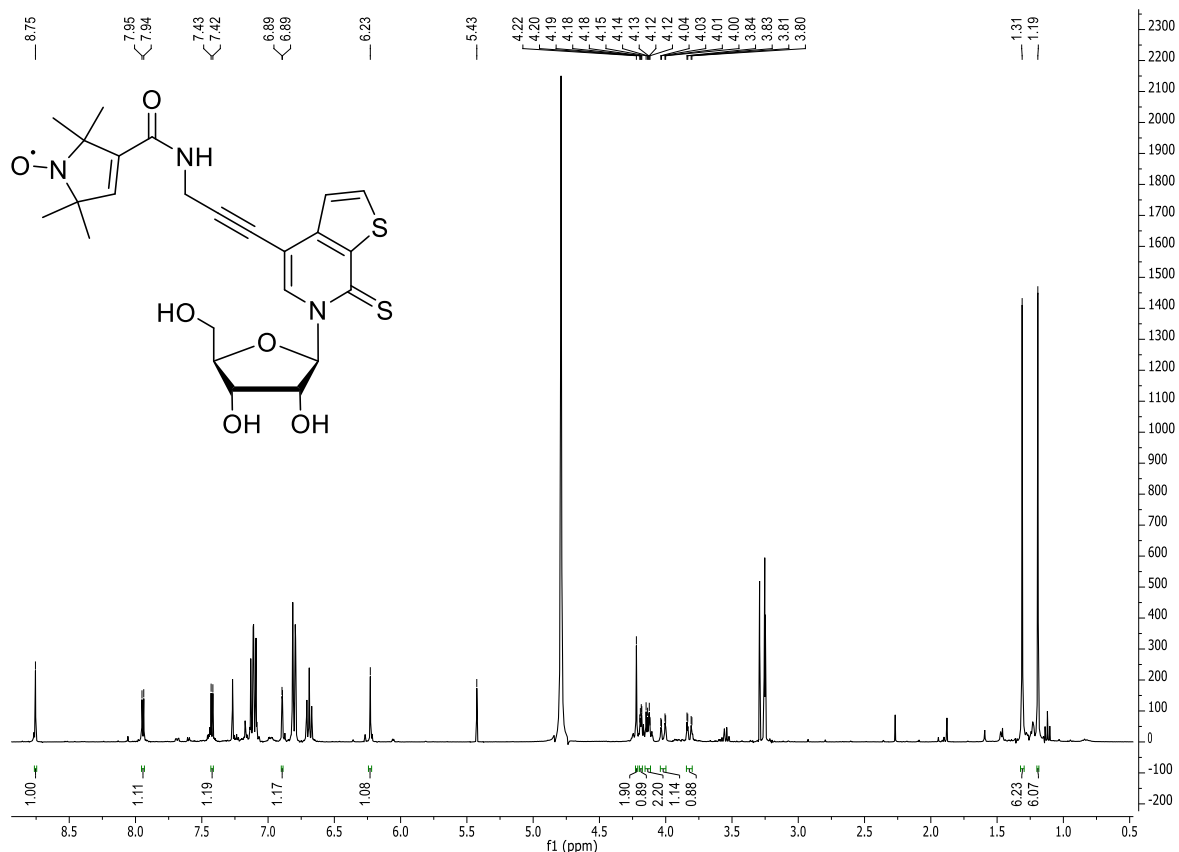
^{1}H-NMR of *in situ* reduced compound **125**: MeOD; 400 MHz; r.t.
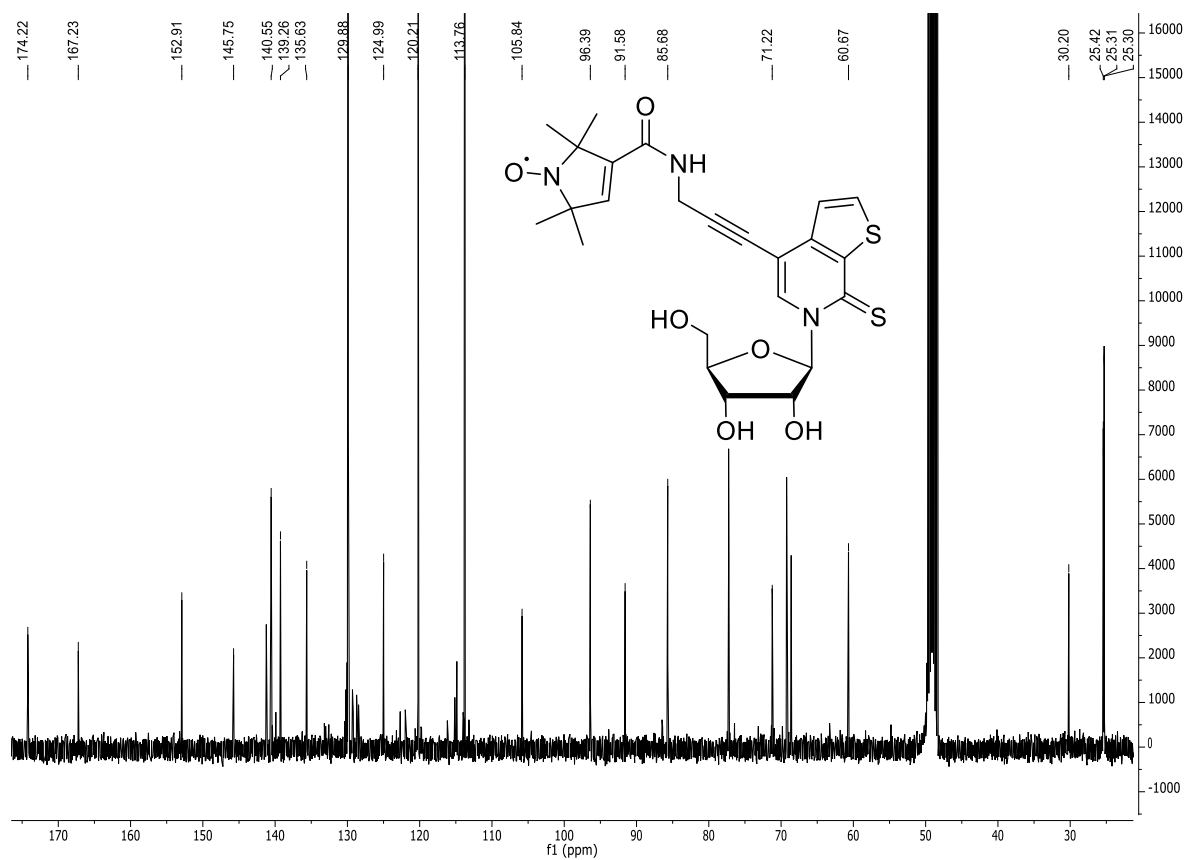
^{13}C-NMR of *in situ* reduced compound **125**: MeOD; 101 MHz; r.t.
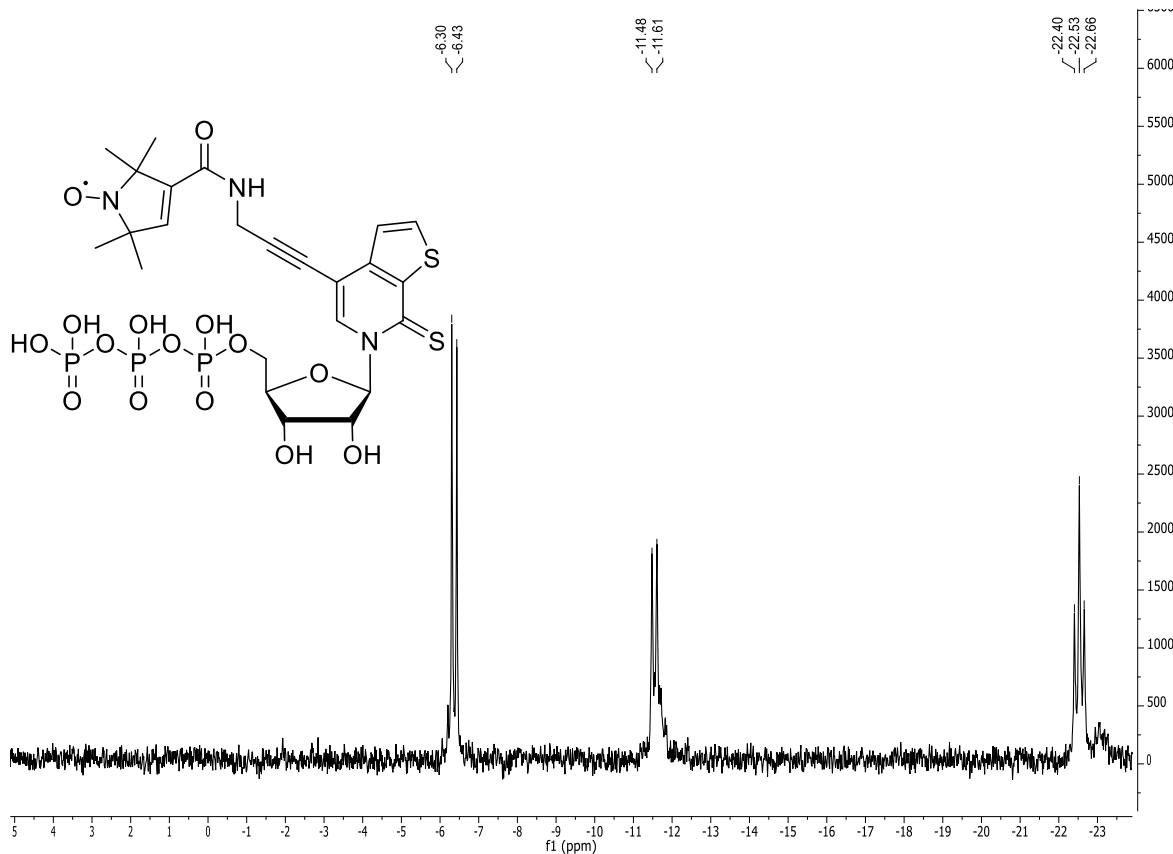
^{31}P-NMR of compound **126**: D$_2$O; 400 MHz; r.t.
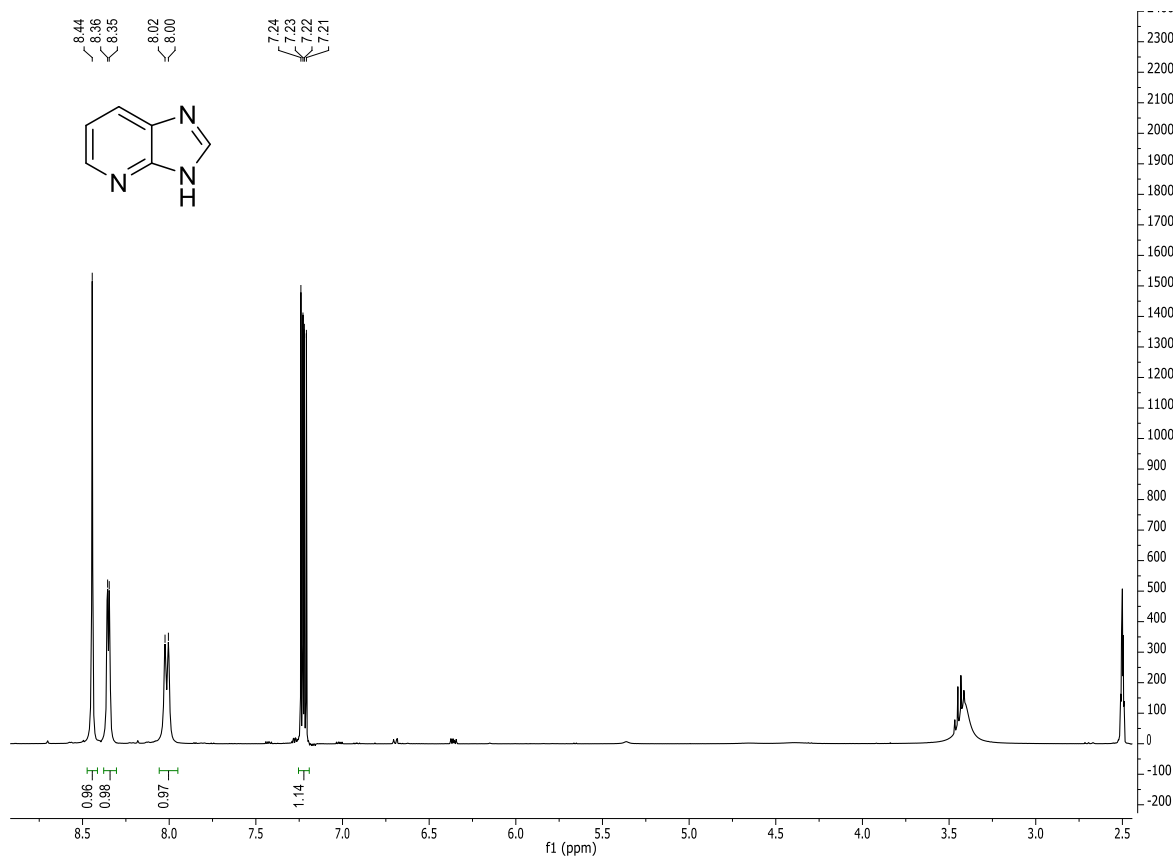
^{1}H-NMR of compound **36**: DMSO-d_6; 400 MHz; r.t.
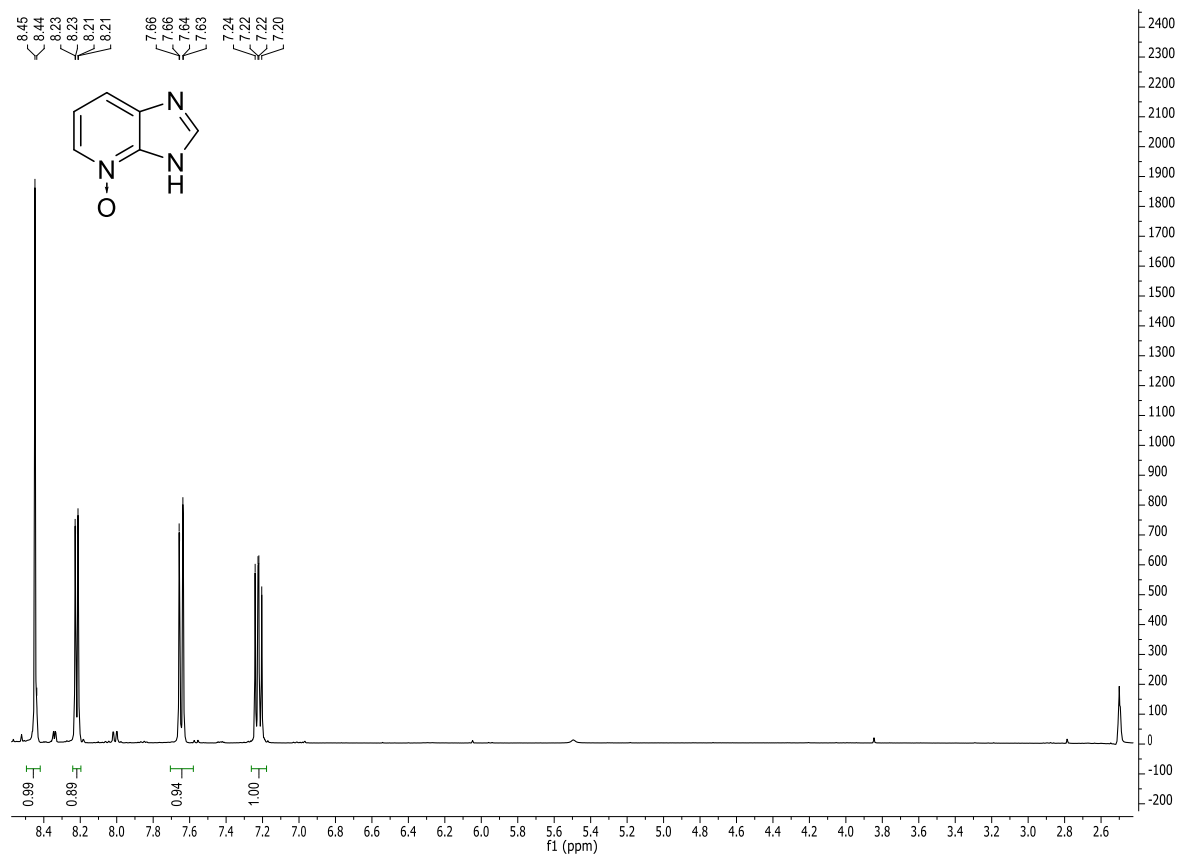
^{1}H-NMR of compound **128**: DMSO-d_6; 400 MHz; r.t.
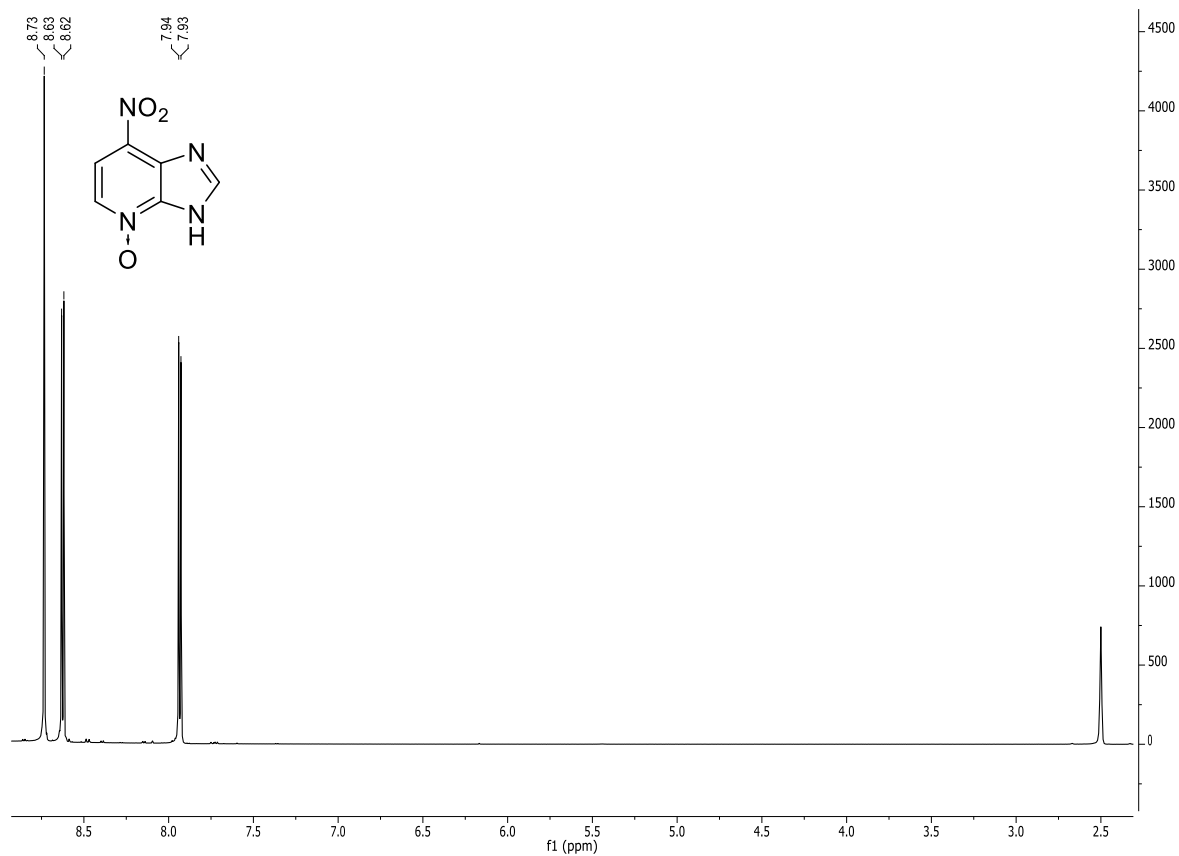
^{1}H-NMR of compound **129**: DMSO-d_6; 400 MHz; r.t.
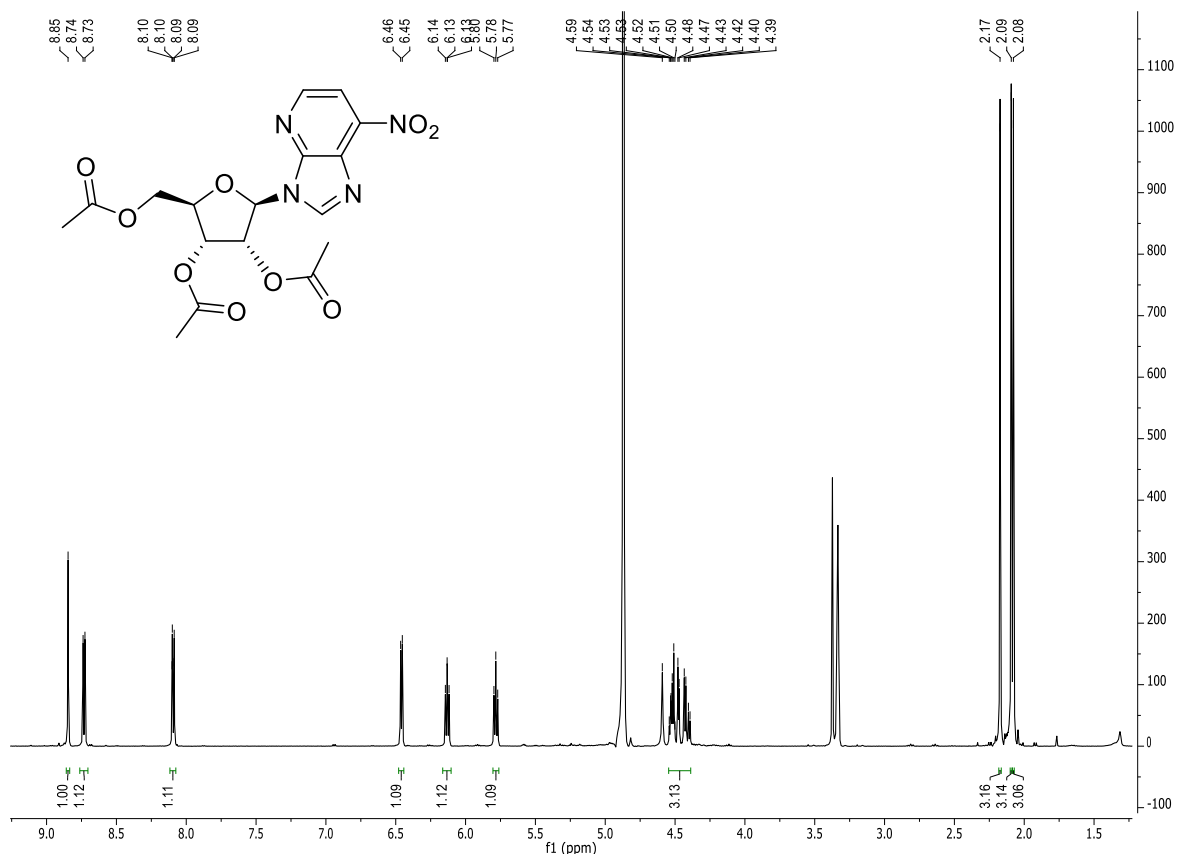
^{1}H-NMR of compound **38**: MeOD; 400 MHz; r.t.
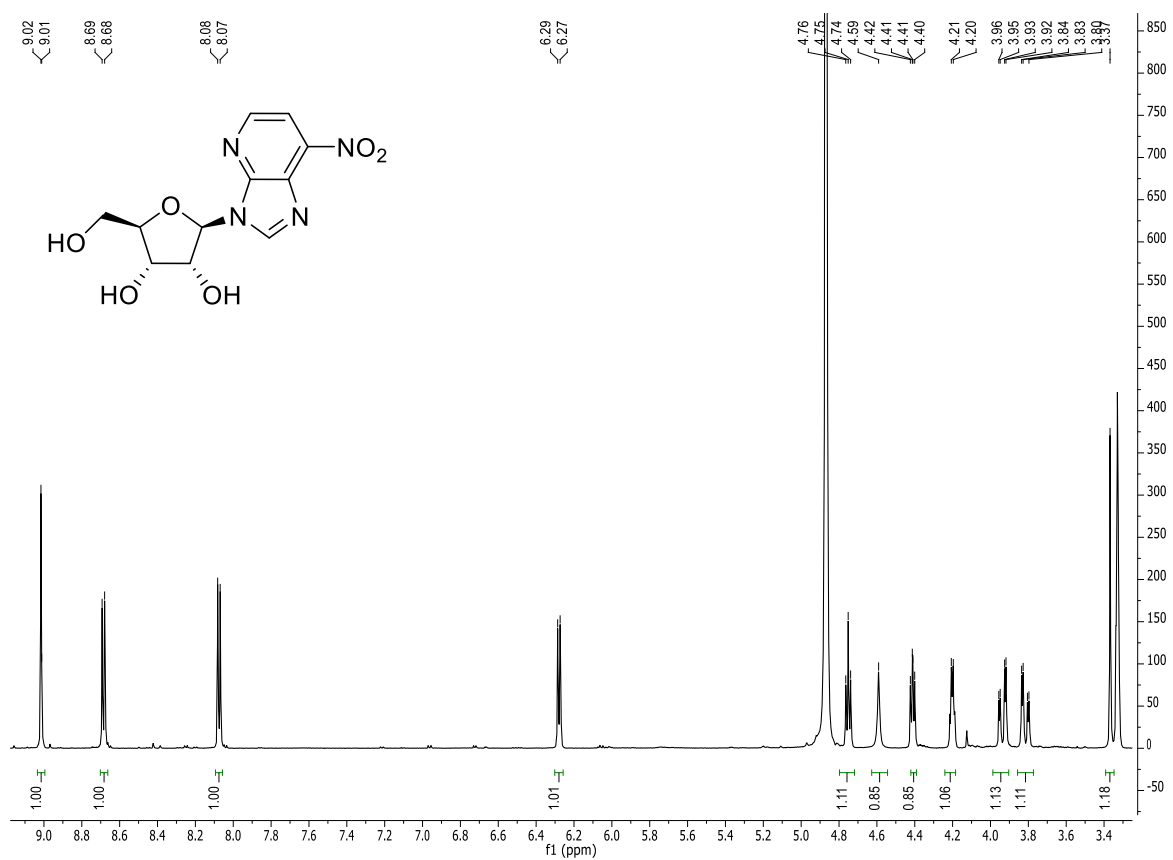
^{1}H-NMR of compound **131**: MeOD; 400 MHz; r.t.
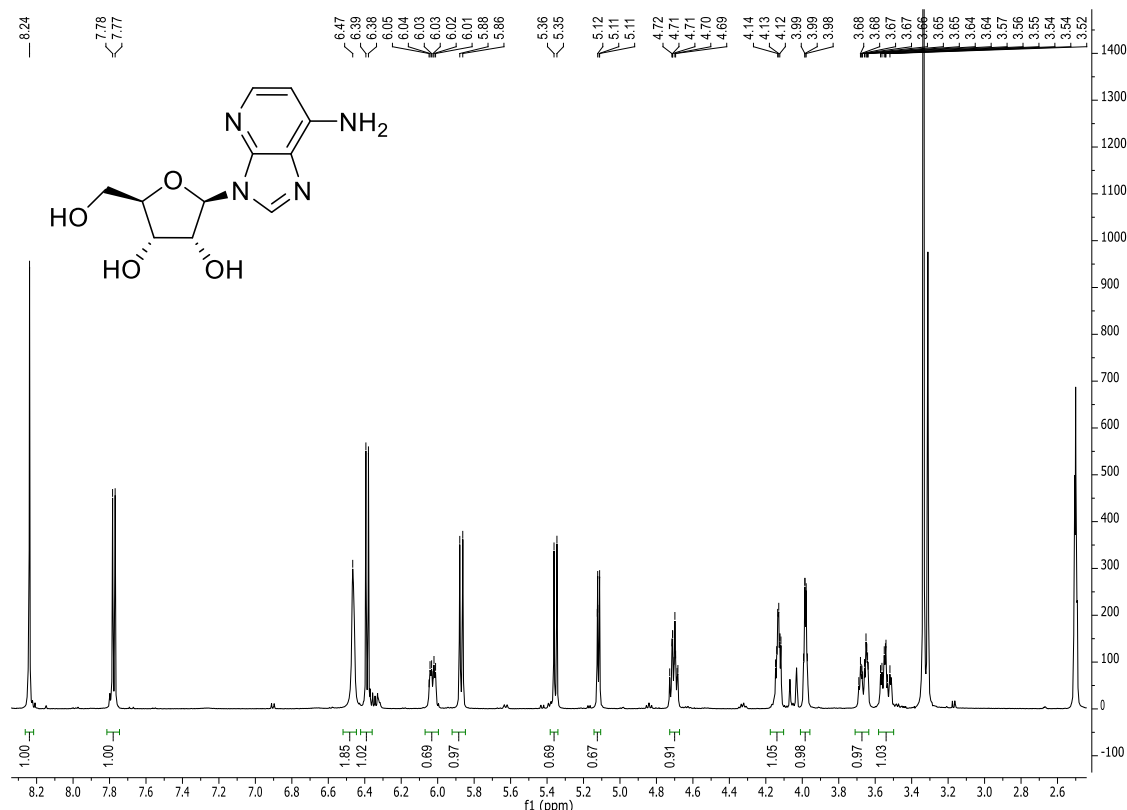
^{1}H-NMR of compound **39**: MeOD; 500 MHz; r.t.
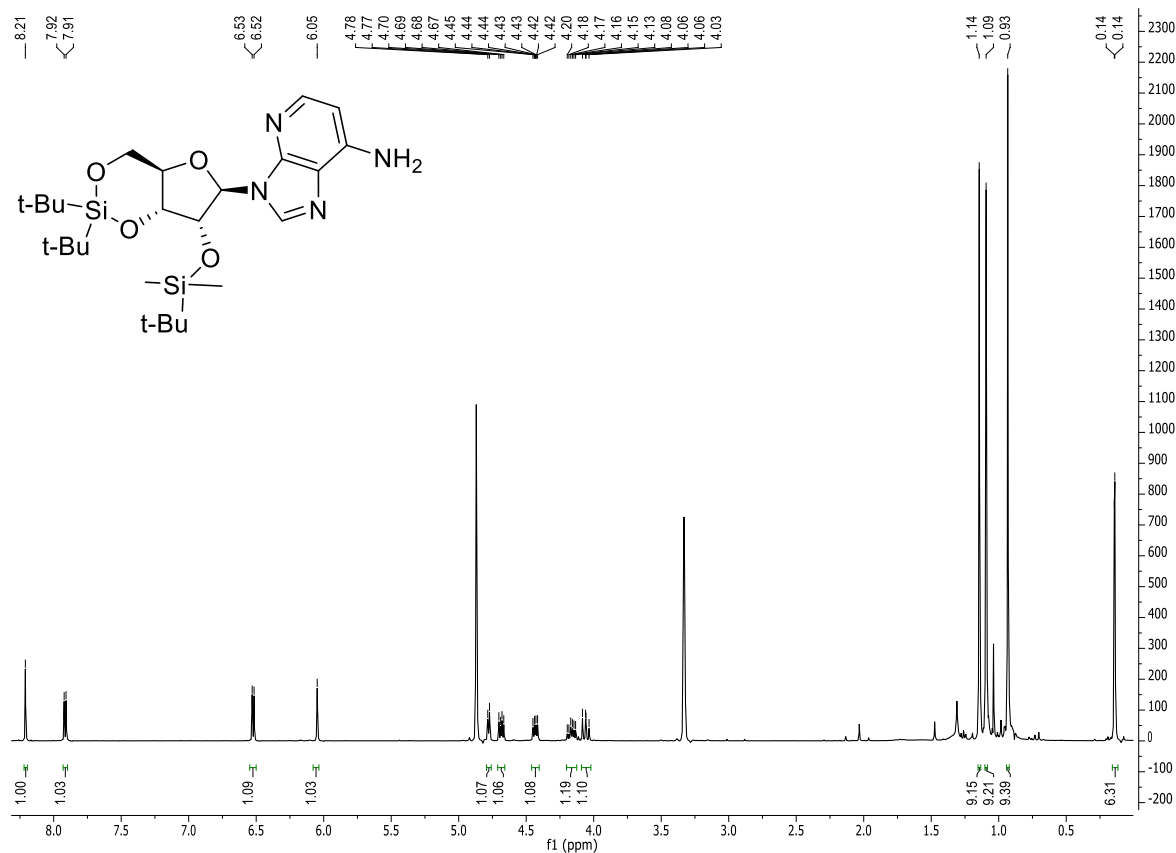
^{1}H-NMR of compound **40**: MeOD; 400 MHz; r.t.

^{1}H-NMR of compound **41**: MeOD; 400 MHz; r.t.

^{1}H-NMR of compound **132**: MeOD; 400 MHz; r.t.
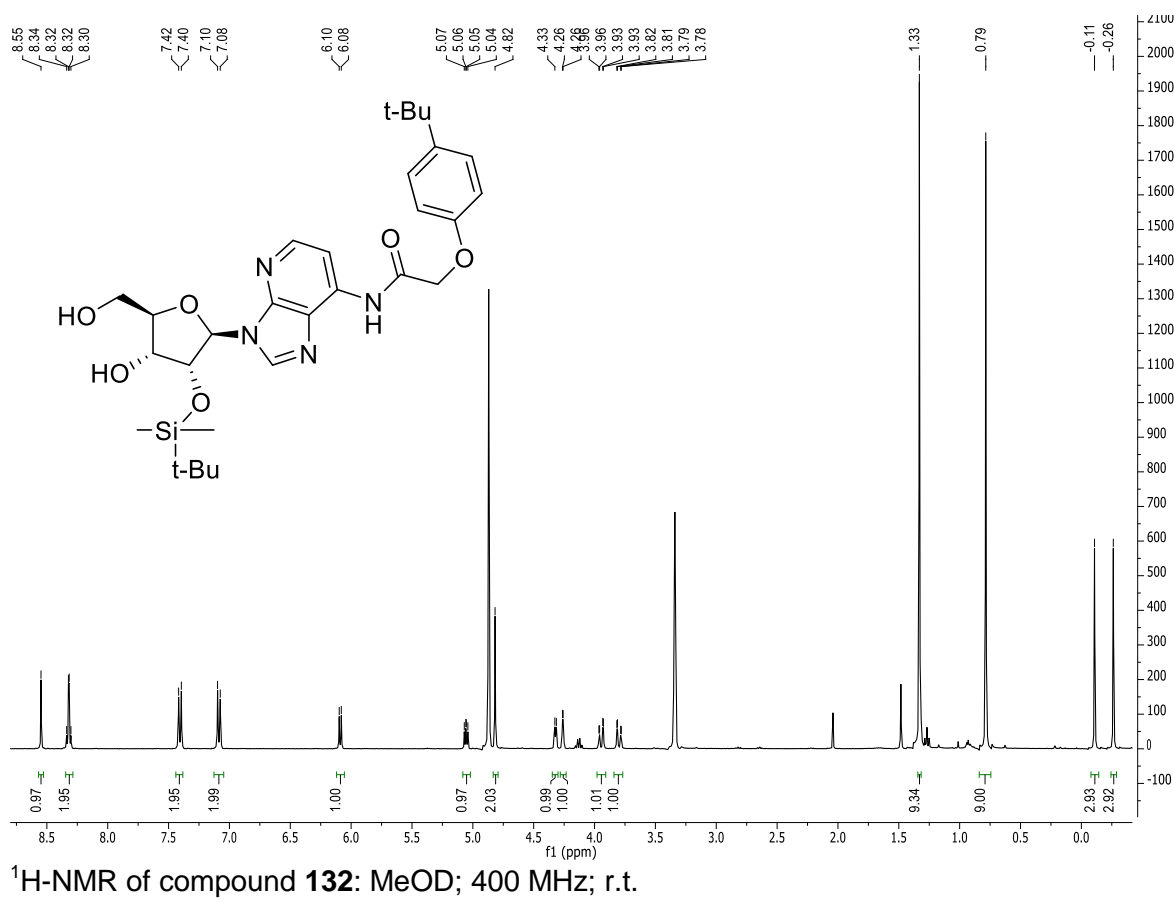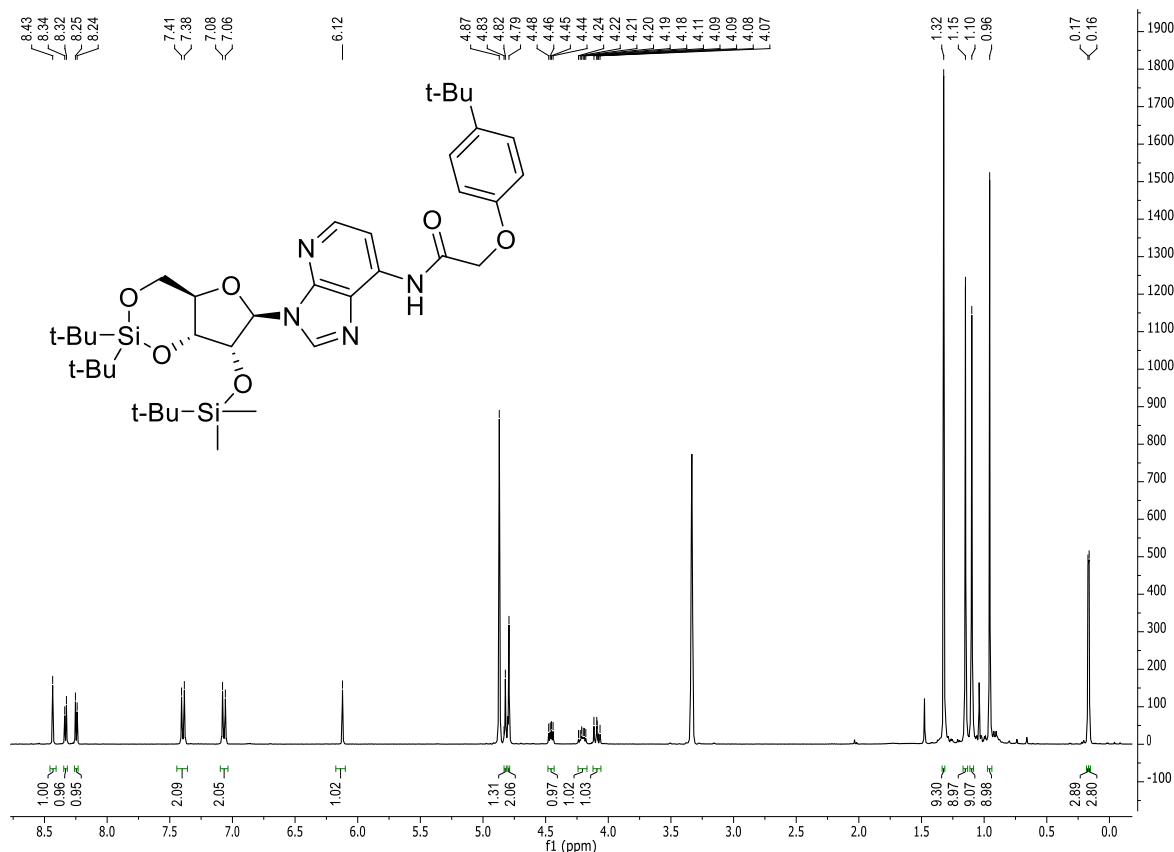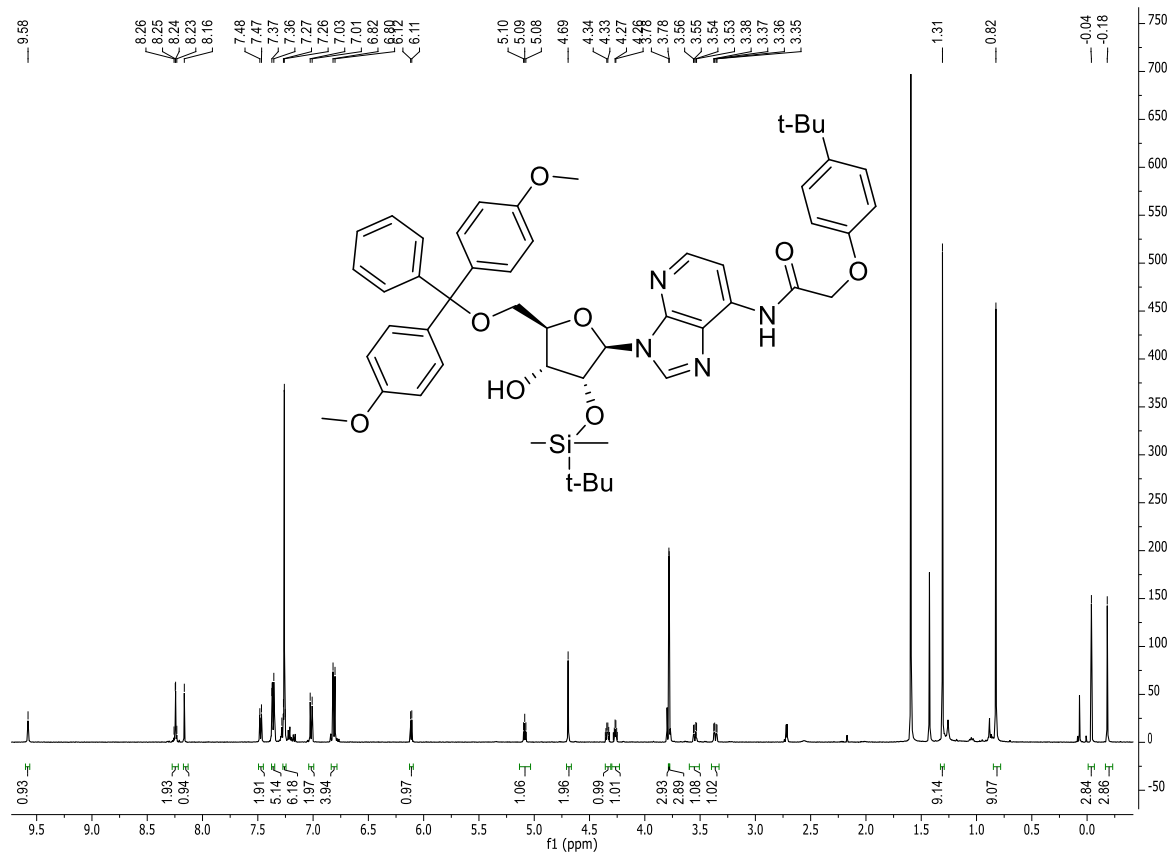
^{1}H-NMR of compound **43**: CDCl$_3$; 500 MHz; r.t.
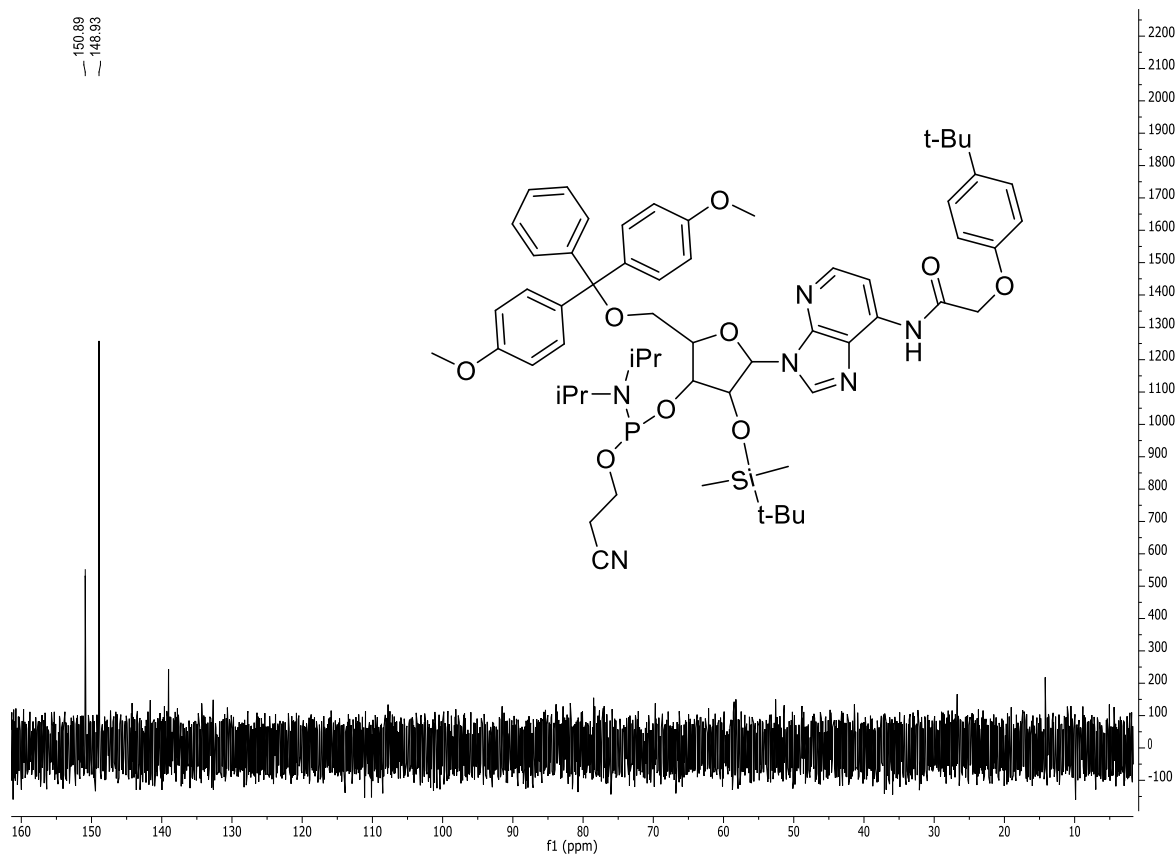
^{31}P-NMR of compound **44**: CDCl$_3$; 202 MHz; r.t.

7.2 LC-MS spectra:
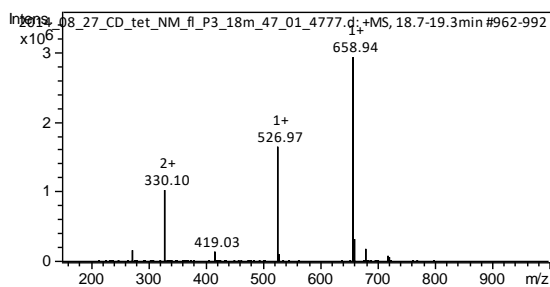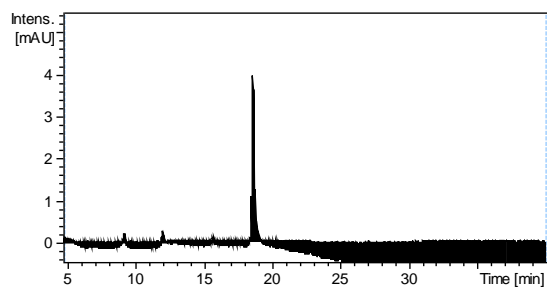
LC-MS spectrum of **56**; r.t., 0%→100% B in 30 min (A: ddH$_2$O + 0.1% FA; B: MeCN).
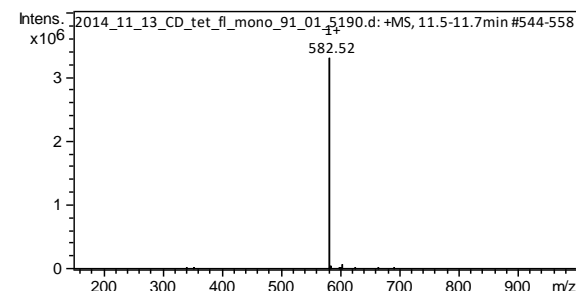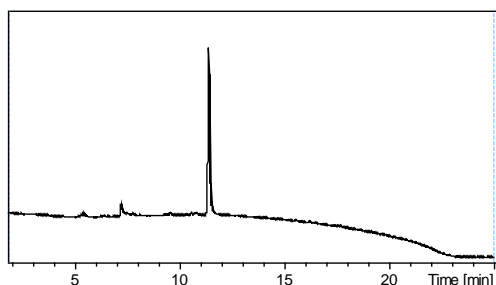
LC-MS spectrum of **57**; r.t., 0%→100% B in 20 min (A: ddH$_2$O + 0.1% FA; B: MeCN).
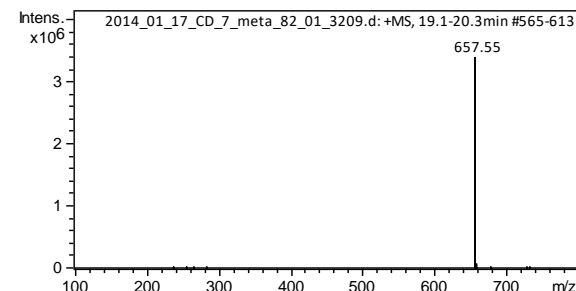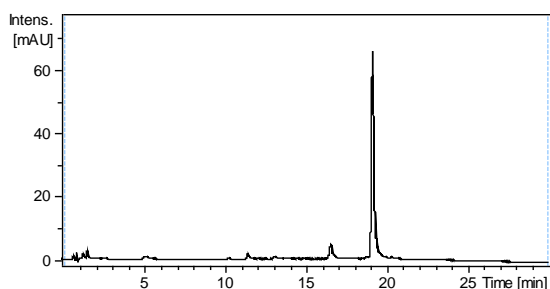
LC-MS spectrum of **58**; r.t., 0%→100% B in 30 min (A: ddH$_2$O + 0.1% FA; B: MeCN).
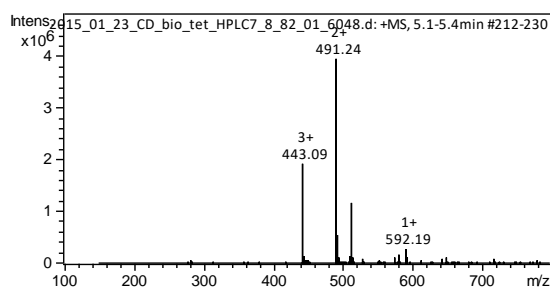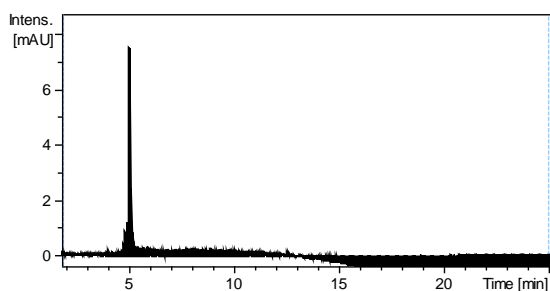
LC-MS spectrum of **59**; r.t., 0%→100% B in 20 min (A: ddH$_2$O + 0.1% FA; B: MeCN).
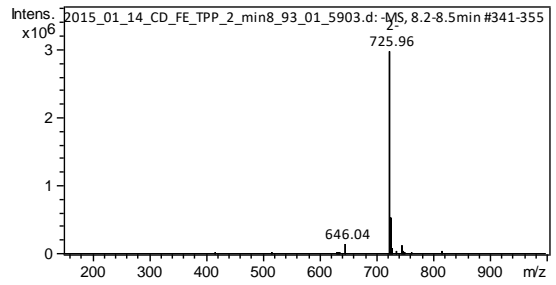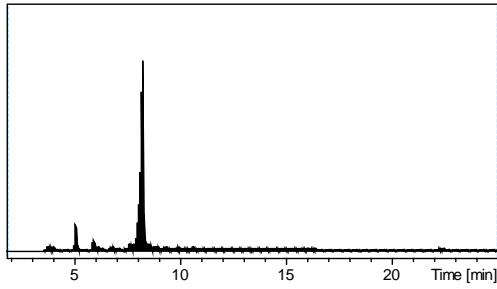
LC-MS spectrum of **76**; r.t., 0%→100% B in 20 min (A: ddH$_2$O + 0.1% NH$_4$OAc; B: MeCN).
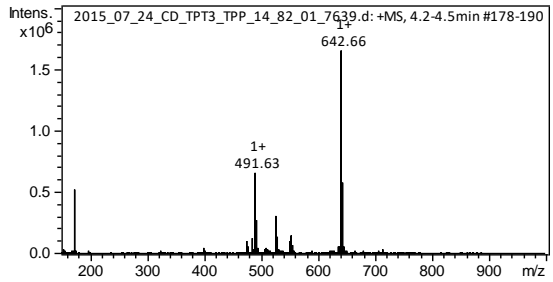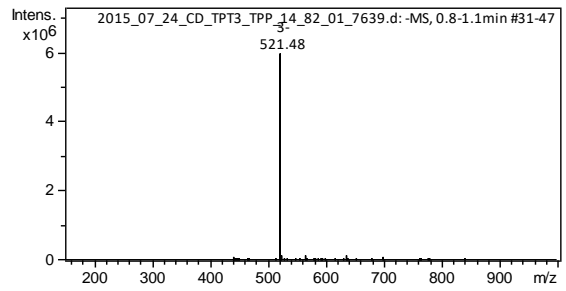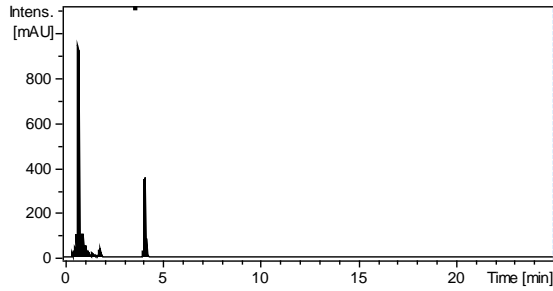
LC-MS spectrum of **82**; r.t., 0%→100% B in 20 min (A: ddH$_2$O + 0.1% NH$_4$OAc; B: MeCN).
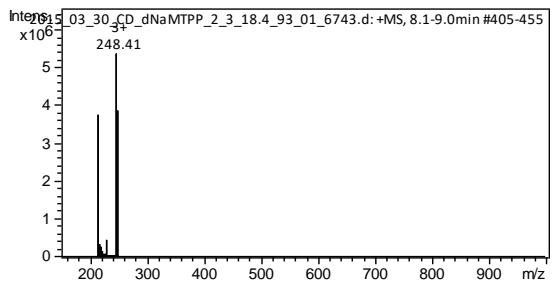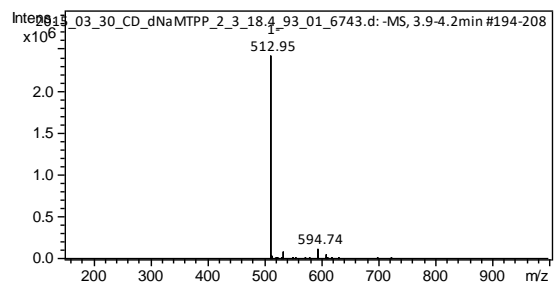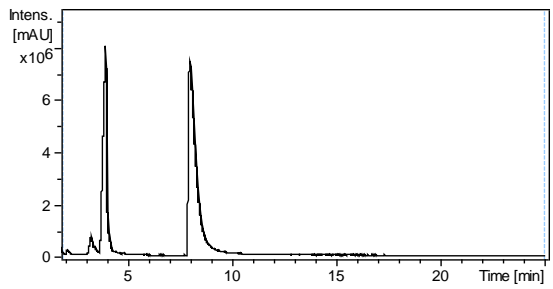
LC-MS spectrum of **87**; r.t., 0%→100% B in 20 min (A: ddH$_2$O + 0.1% NH$_4$OAc; B: MeCN).
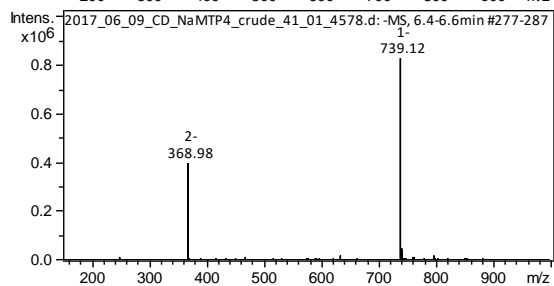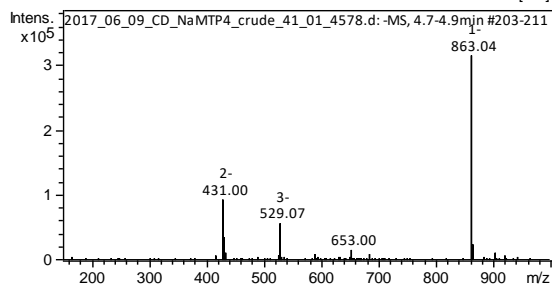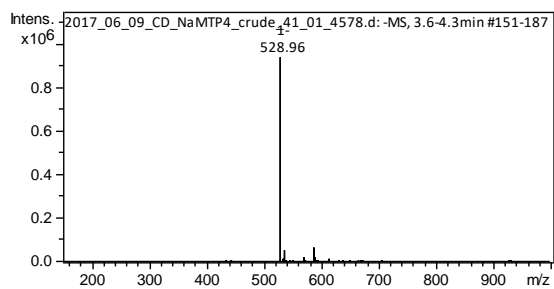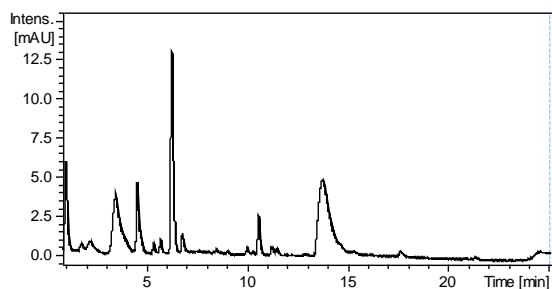
LC-MS spectrum of reaction yielding **103**; r.t., 0%→100% B in 20 min (A: ddH$_2$O + 0.1% NH$_4$OAc; B: MeCN).
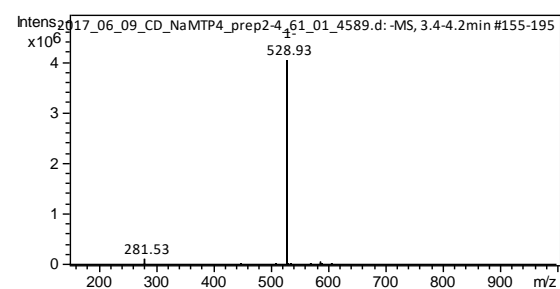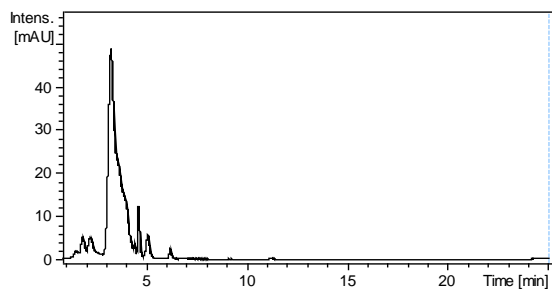
LC-MS spectrum of **103**; r.t., 0%→100% B in 20 min (A: ddH$_2$O + 0.1% NH$_4$OAc; B: MeCN).
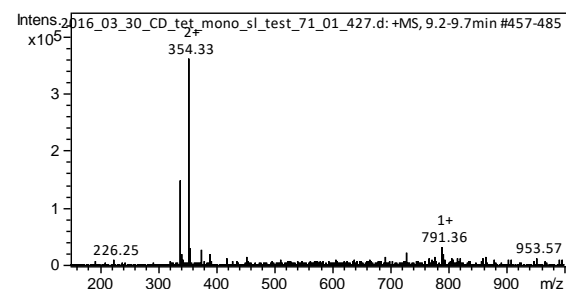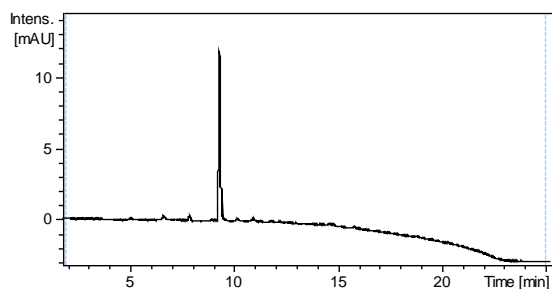
LC-MS spectrum of **107**; r.t., 0%→100% B in 20 min (A: ddH$_2$O + 0.1% NH$_4$OAc; B: MeCN).
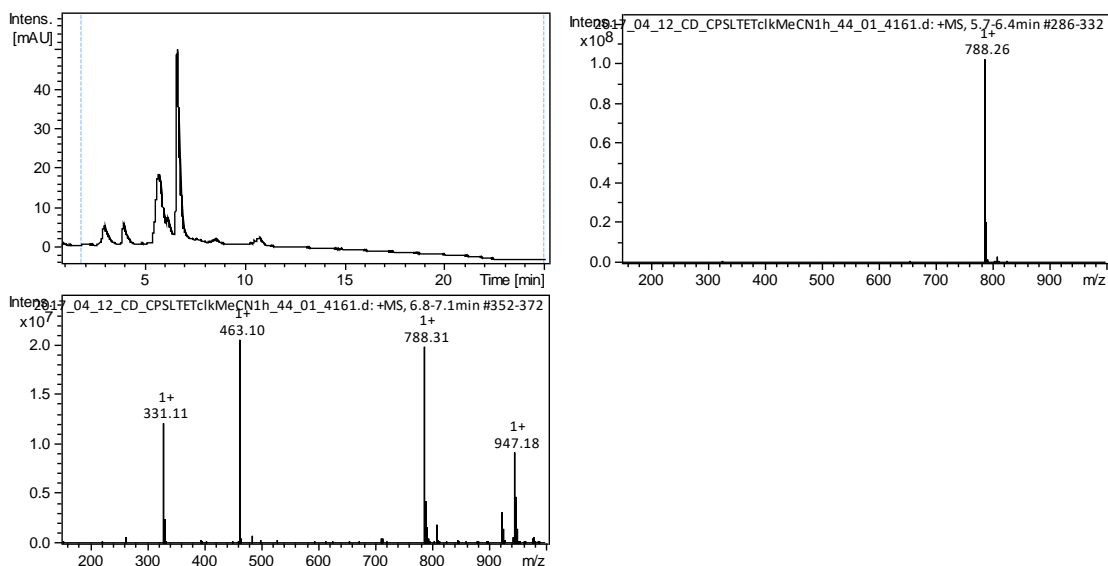
LC-MS spectrum of click product between **104** and **107**; r.t., 0%→100% B in 20 min (A: ddH$_2$O + 0.1% NH$_4$OAc; B: MeCN).
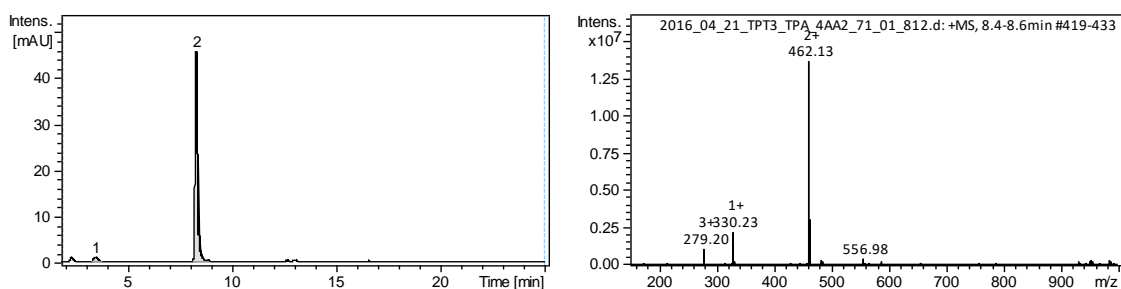
LC-MS spectrum of **117**; r.t., 0%→100% B in 20 min (A: ddH$_2$O + 0.1% NH$_4$OAc; B: MeCN).
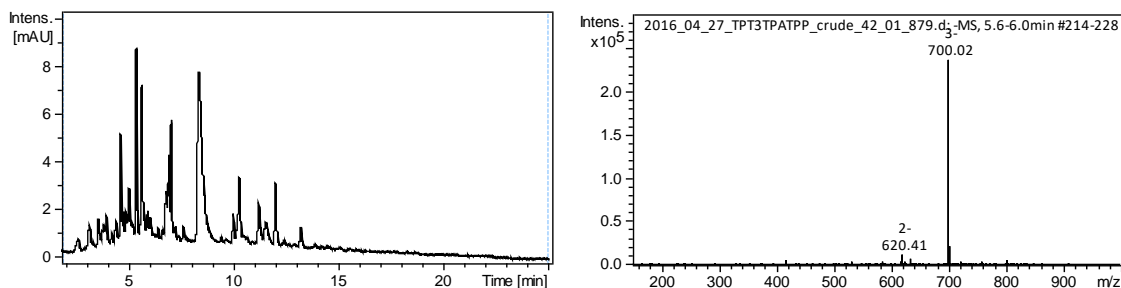
LC-MS spectrum of **119** using synthetic pathway of Kovács and Ötvös; r.t., 0%→100% B in 20 min (A: ddH$_2$O + 0.1% NH$_4$OAc; B: MeCN).
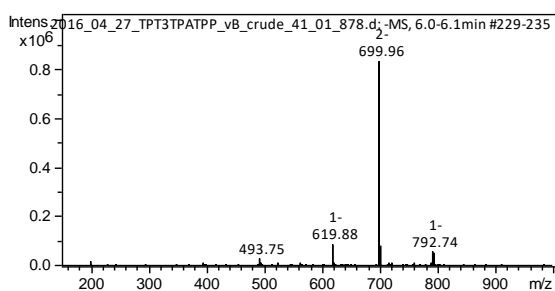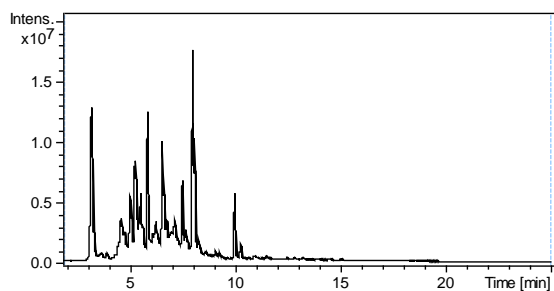
LC-MS spectrum of **119** using synthetic pathway of Lugwig and Eckstein; r.t., 0%→100% B in 20 min (A: ddH$_2$O + 0.1% NH$_4$OAc; B: MeCN).
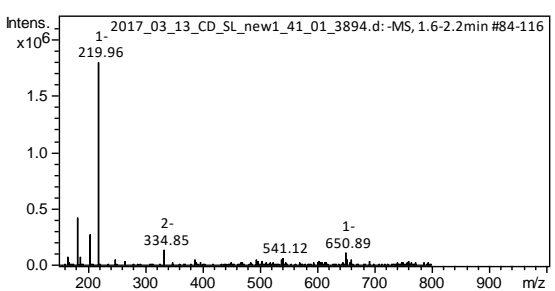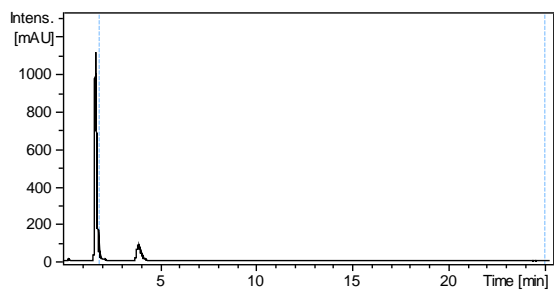
LC-MS spectrum of reaction yielding **124**; r.t., 0%→100% B in 20 min (A: ddH$_2$O + 0.1% NH$_4$OAc; B: MeCN).
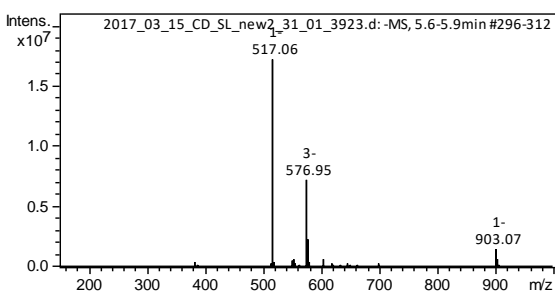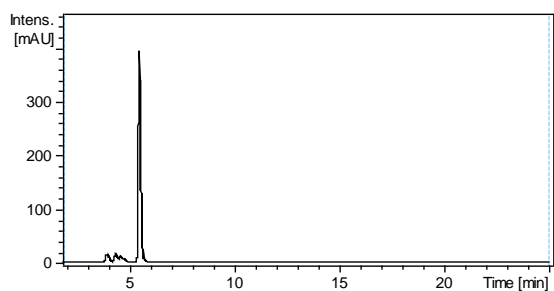
LC-MS spectrum of **125**; r.t., 0%→100% B in 20 min (A: ddH$_2$O + 0.1% NH$_4$OAc; B: MeCN).
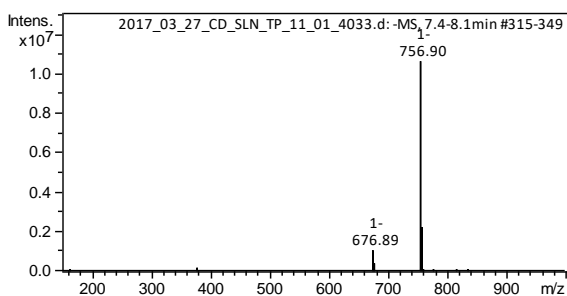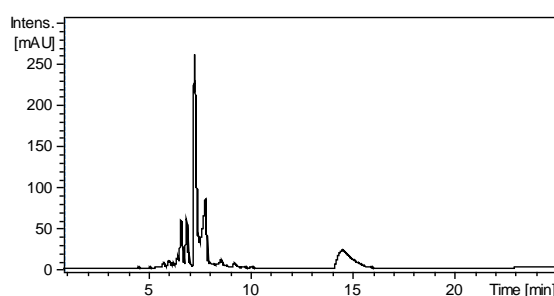
LC-MS spectrum of **126**; r.t., 0%→100% B in 20 min (A: ddH$_2$O + 0.1% NH$_4$OAc; B: MeCN).
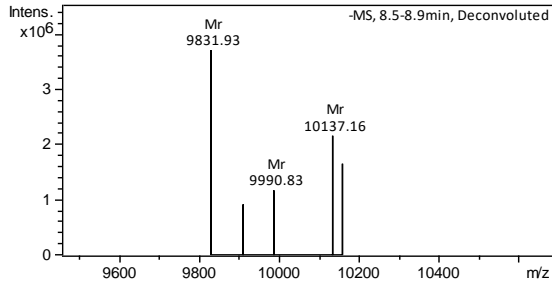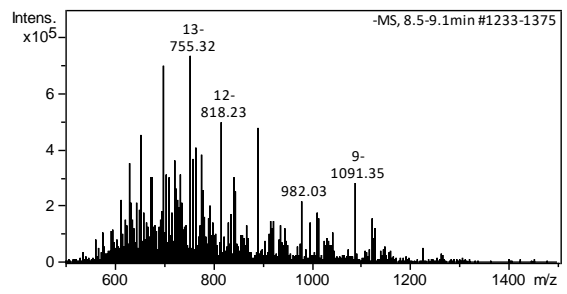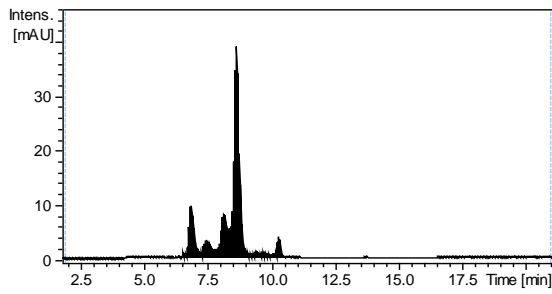
LC-MS spectrum of *in vitro* transcription yielding **RNA-TPT3^{NOR}-1**; r.t., 0%→20% B in 20 min (A: ddH$_2$O 10 mM NEt$_3$ / 100 mM HFIP; B: MeCN).
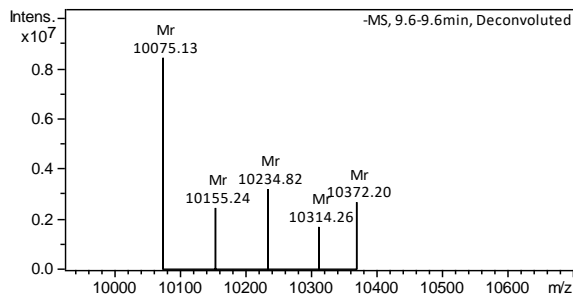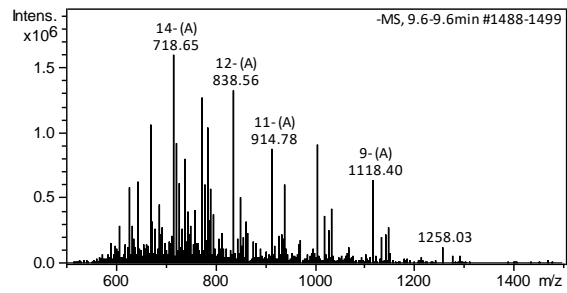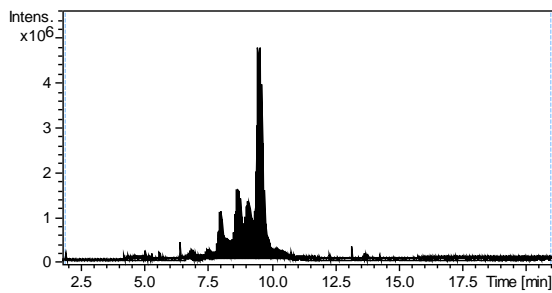
LC-MS spectrum of *in vitro* transcription yielding **RNA-TPT3^{NOR}-2**; r.t., 0%→20% B in 20 min (A: ddH$_2$O 10 mM NEt$_3$ / 100 mM HFIP; B: MeCN).
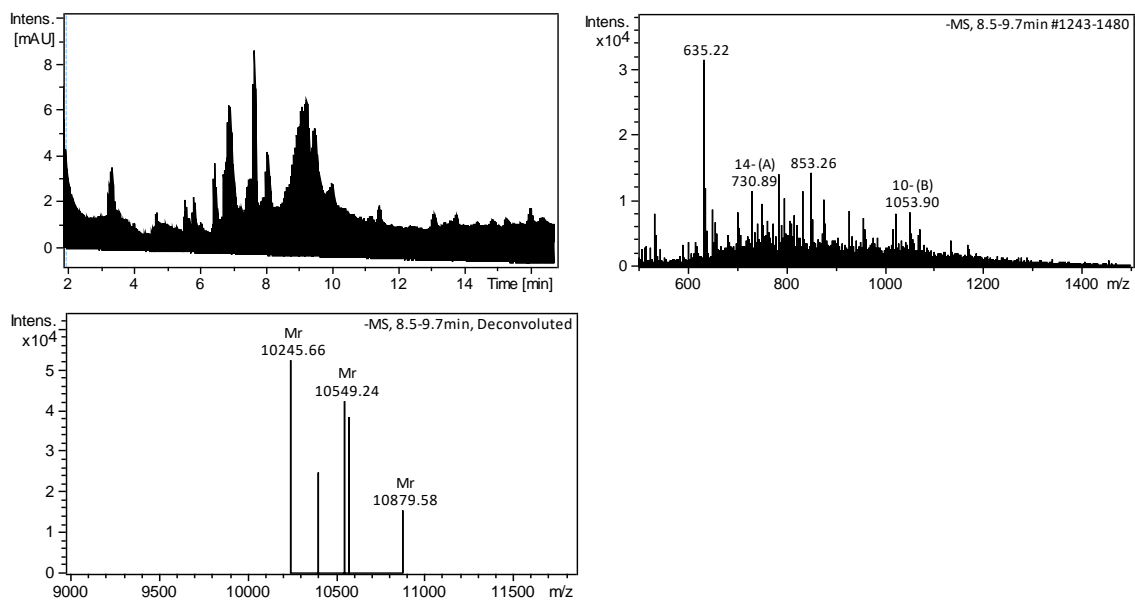
LC-MS spectrum of *in vitro* transcription yielding **RNA-TPT3^{NOR}-1** and click reaction with **59**; r.t., 0%→20% B in 20 min (A: ddH$_2$O 10 mM NEt$_3$ / 100 mM HFIP; B: MeCN).
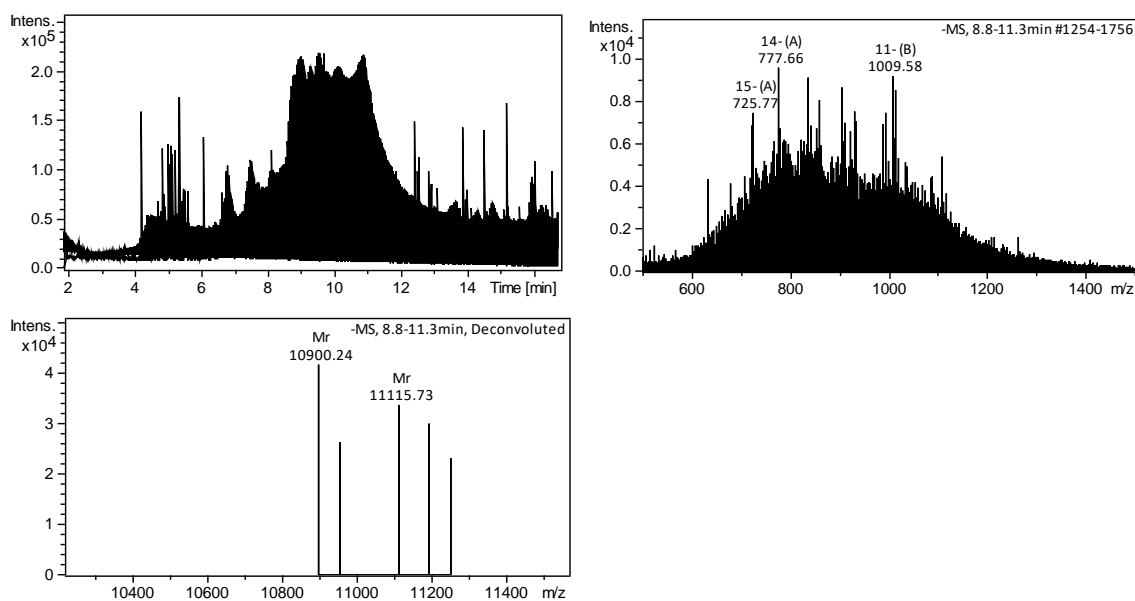
LC-MS spectrum of *in vitro* transcription yielding **RNA-TPT3^{NOR}-2** and click reaction with **59**; r.t., 0%→20% B in 20 min (A: ddH$_2$O 10 mM NEt$_3$ / 100 mM HFIP; B: MeCN).
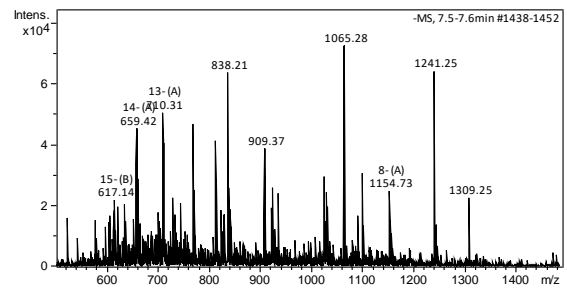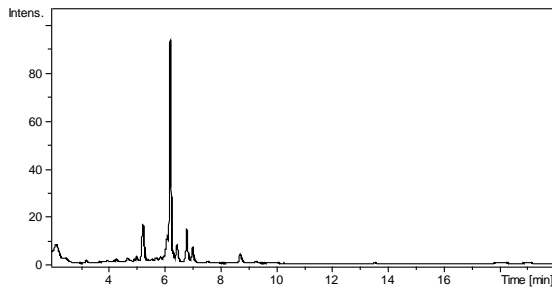
LC-MS spectrum of reverse transcription using **RNA-TPT3^{NOR}-1** and **103**; r.t., 0%→20% B in 20 min (A: ddH$_2$O 10 mM NEt$_3$ / 100 mM HFIP; B: MeCN).
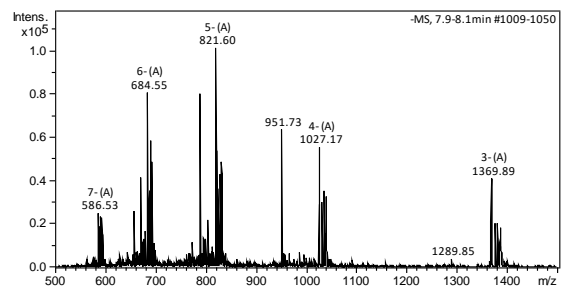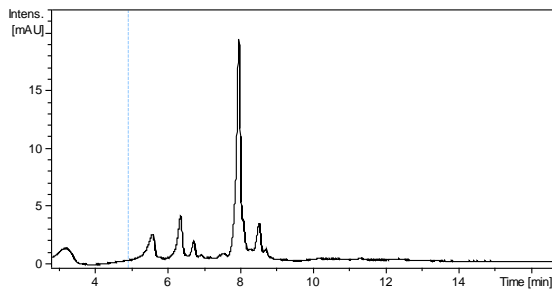
LC-MS spectrum of truncated **RNA-CXT^{NaM}-RL**; r.t., 0%→20% B in 20 min (A: ddH$_2$O + 10 mM NEt$_3$ / 100 mM HFIP; B: MeCN).
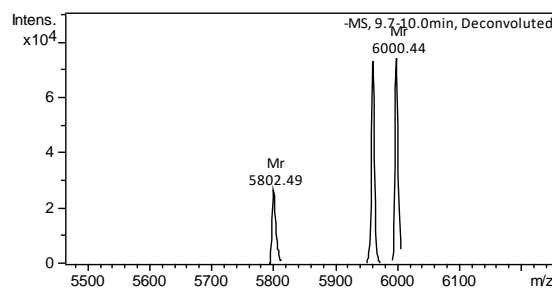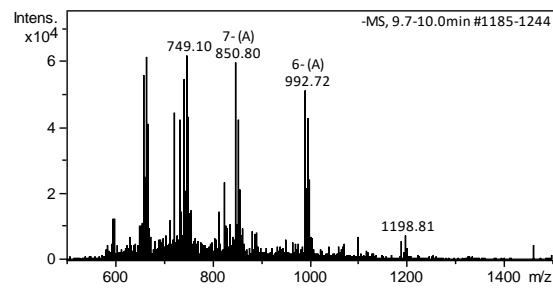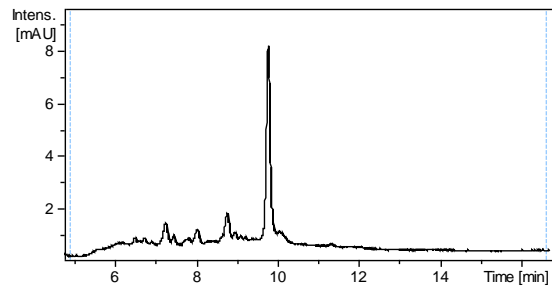
LC-MS spectrum of **RNA-CXT^{NaM}-RL** with **119** incorporated; r.t., 0%→20% B in 20 min (A: ddH$_2$O + 10 mM NEt$_3$ / 100 mM HFIP; B: MeCN).
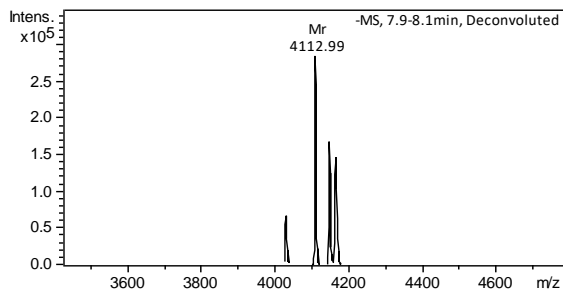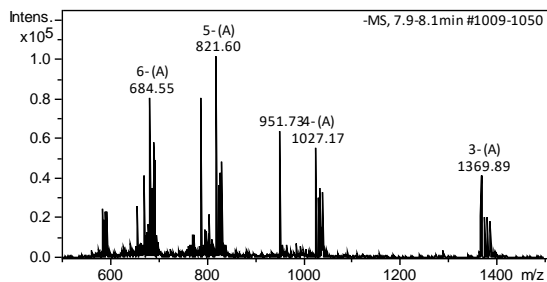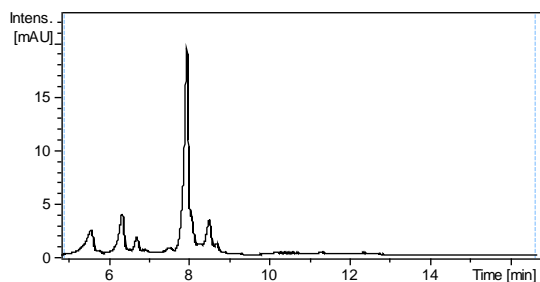
LC-MS spectrum of truncated **RNA-CXT^{NaM}-RL**; r.t., 0%→20% B in 20 min (A: ddH$_2$O + 10 mM NEt$_3$ / 100 mM HFIP; B: MeCN).
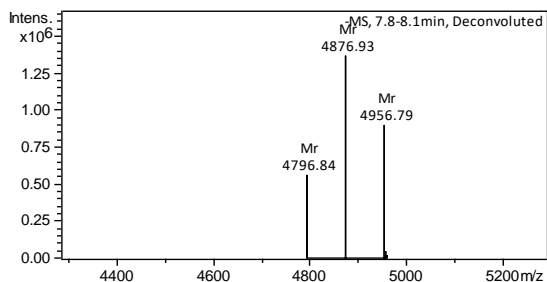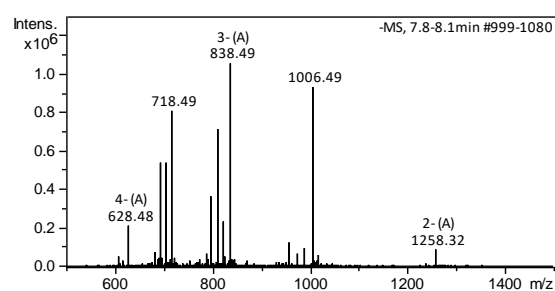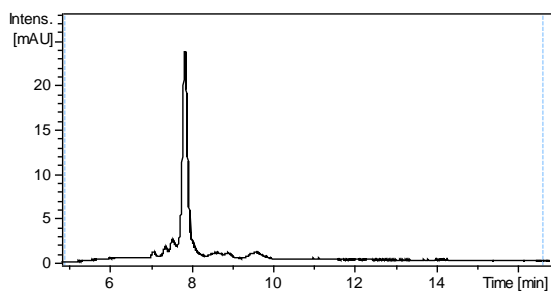
LC-MS spectrum of truncated **RNA-SC-RL**; r.t., 0%→20% B in 20 min (A: ddH$_2$O + 10 mM NEt$_3$ / 100 mM HFIP; B: MeCN).
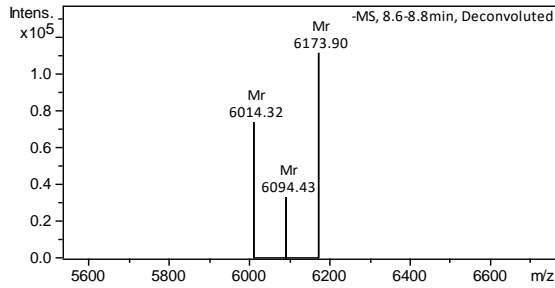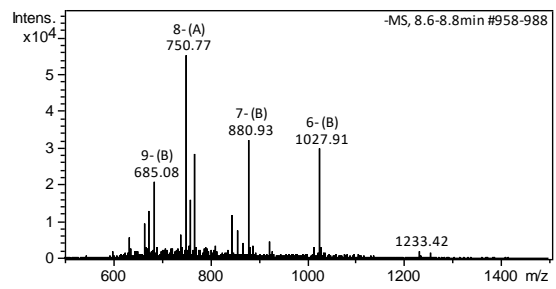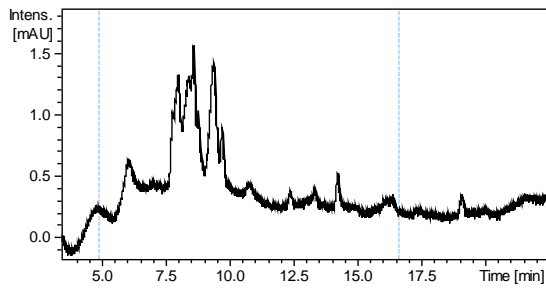
LC-MS spectrum of **RNA-SC-RL** with **119** incorporated; r.t., 0%→20% B in 20 min (A: ddH$_2$O + 0.1% NH$_4$OAc; B: MeCN).
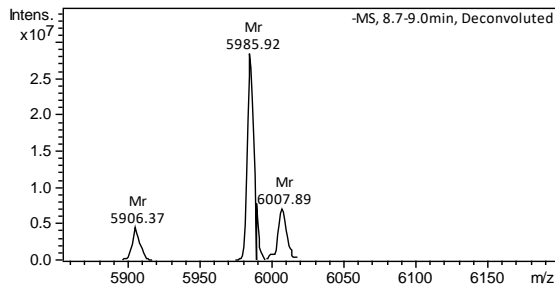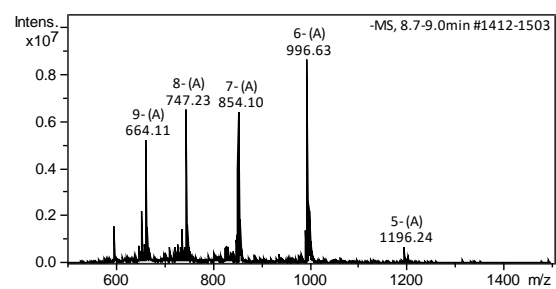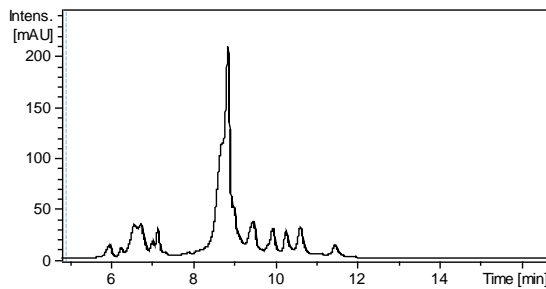
LC-MS spectrum of **RNA-CXT**^{NaM}**-CP** with **104** incorporated; r.t., 0%→20% B in 20 min (A: ddH$_2$O + 10 mM NEt$_3$ / 100 mM HFIP; B: MeCN).
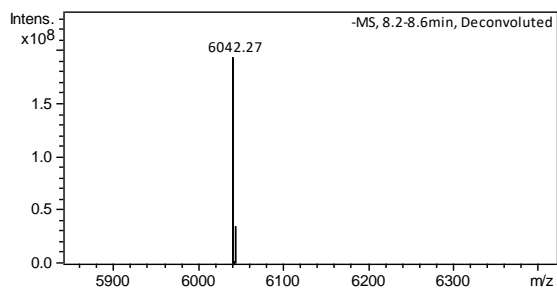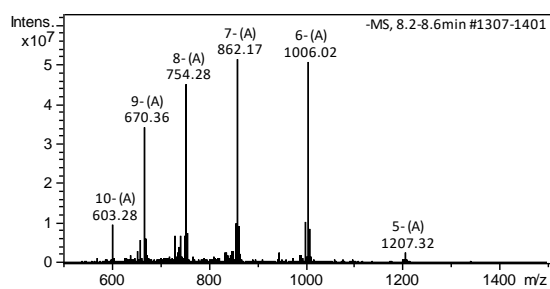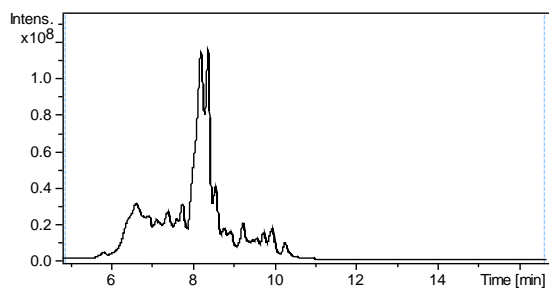
LC-MS spectrum of **RNA-CXT$^{\text{NaM}}$-FL** with **126** incorporated; r.t., 0%→20% B in 20 min (A: ddH$_2$O + 10 mM NEt$_3$ / 100 mM HFIP; B: MeCN).
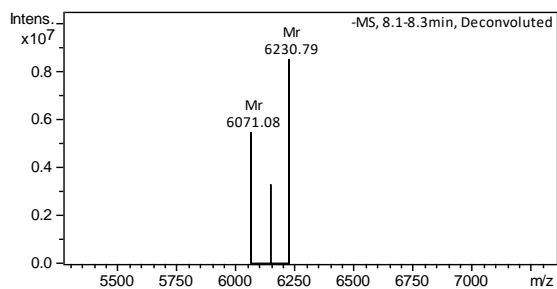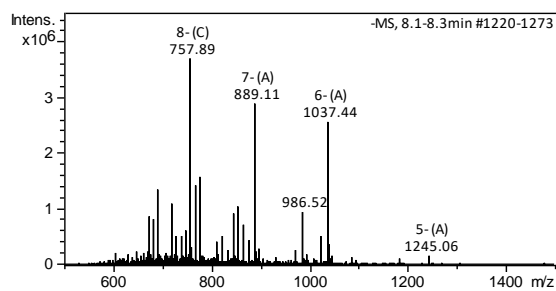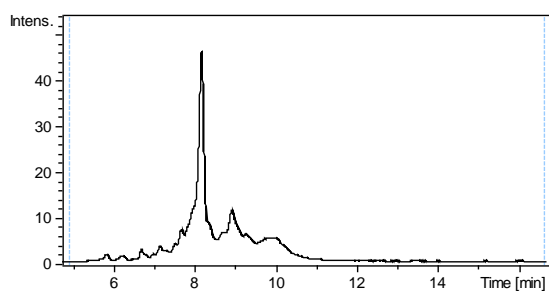
LC-MS spectrum of **RNA-SC-FL** with **126** incorporated; r.t., 0%→20% B in 20 min (A: ddH$_2$O + 0.1% NH$_4$OAc; B: MeCN).
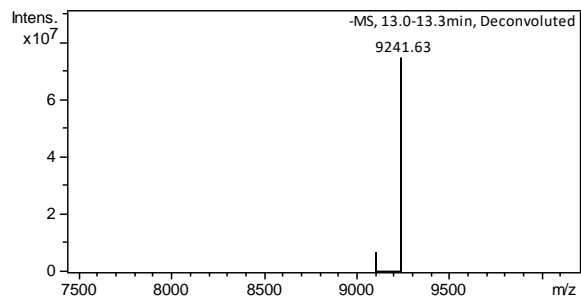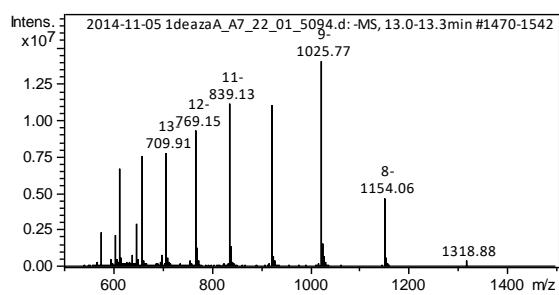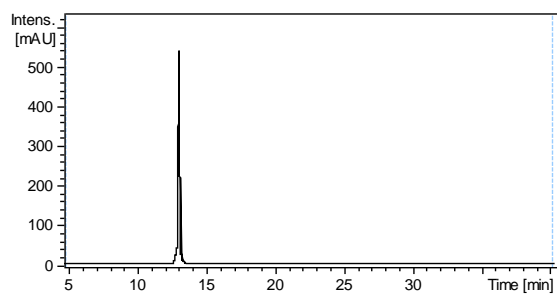
LC-MS spectrum of chemically synthesized **RNA-TW** with **44** incorporated; r.t., 0%→40% B in 40 min (A: ddH$_2$O + 10 mM NEt$_3$ / 100 mM HFIP; B: MeCN).

7.3 (HR) MS spectra:

F: FTMS + p ESI Full ms [80.00-2000.00]
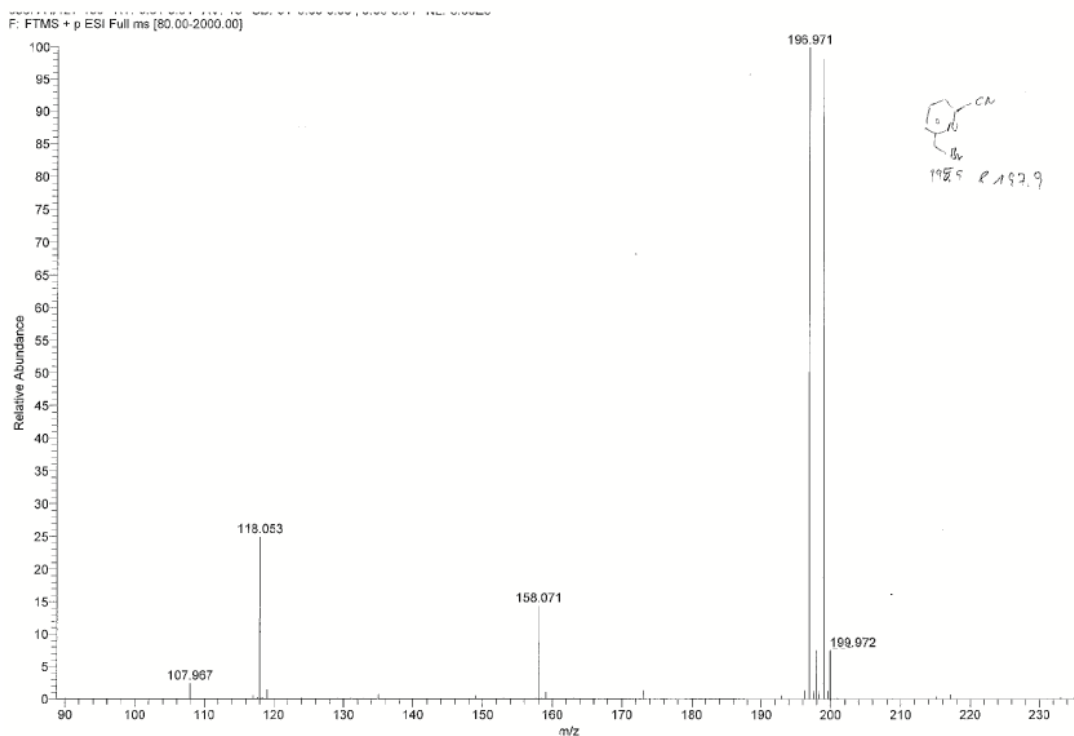
ESI⁺ spectrum of **46**.

SPEC: 447ep (02-Dec-13 12:52:04)   Scans: 1 > 84
Samp: Domnick, CD-6
Oper: PW   Study: Client:
Base: 131.11   Masses: 50.00 > 1000.00   #Peaks: 144
Peak: 1000.0 mmu   Intensity: 2496021   RIC: 10905874
Scan 57 @ 4.01 min (EI +VE +LMR BSCAN (EXP) UP LR NRM)   2.5E+06

ESI⁺ spectrum of **49**.

- 56 -
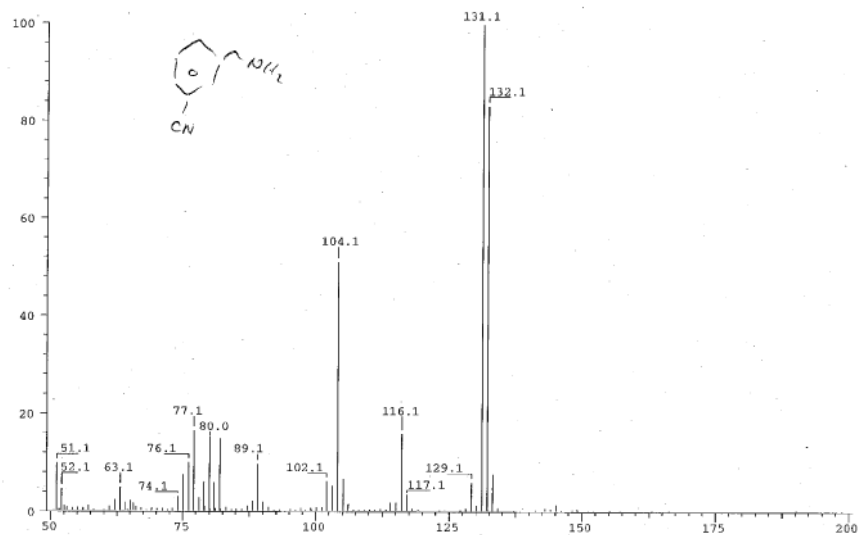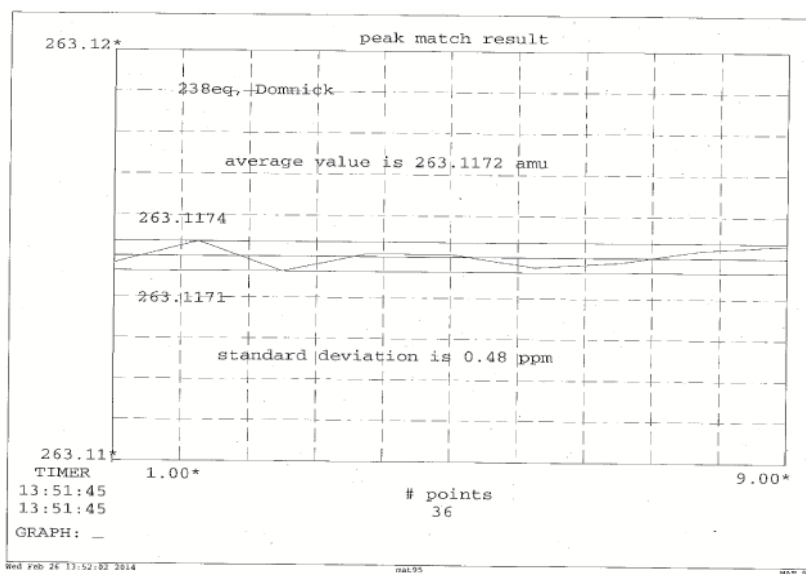
HR-MS (EI) spectrum of **51**.
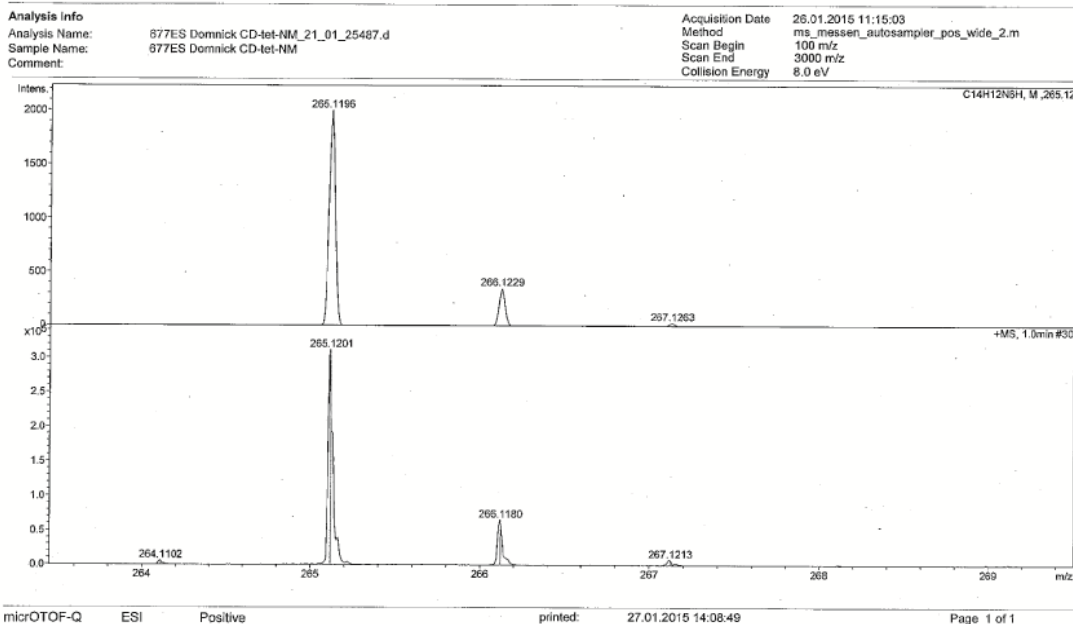
HR-MS (ESI⁺) spectrum of **53**.
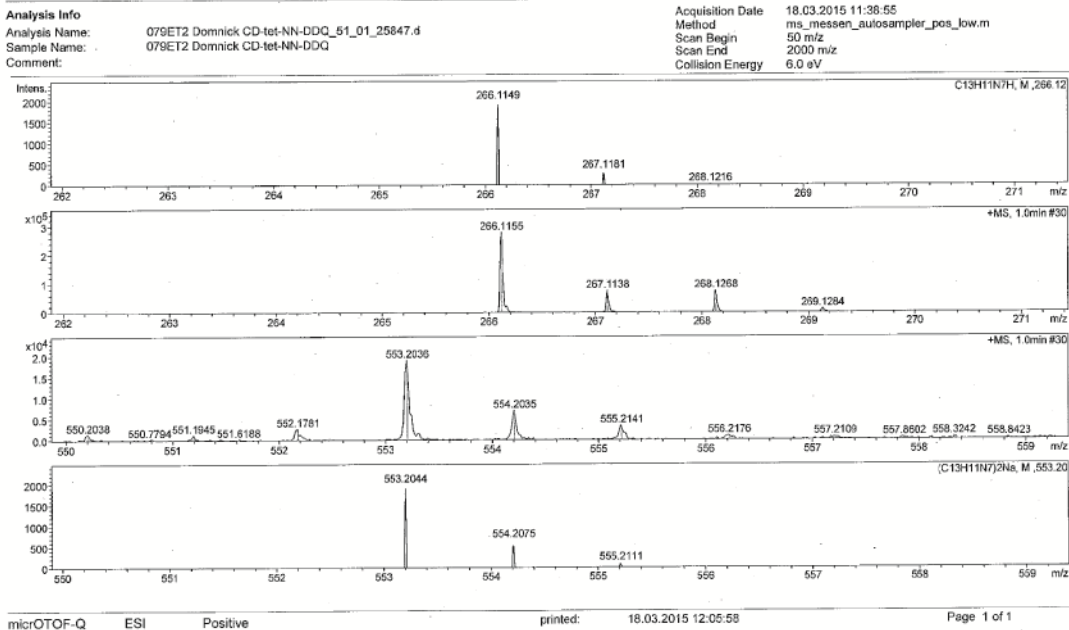
HR-MS (ESI⁺) spectrum of **54**.
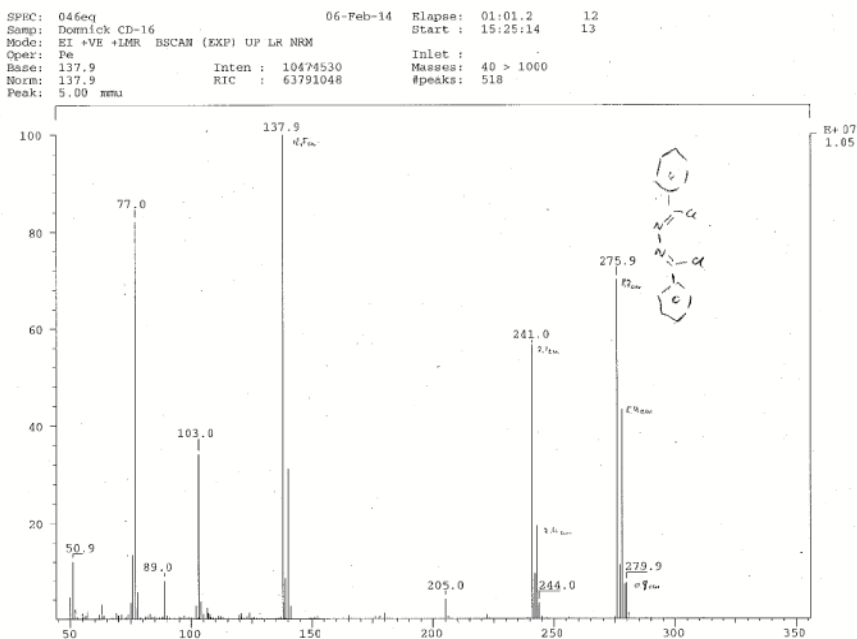
EI spectrum of **63**.

EI spectrum of **2**.

EI spectrum of **66i**.
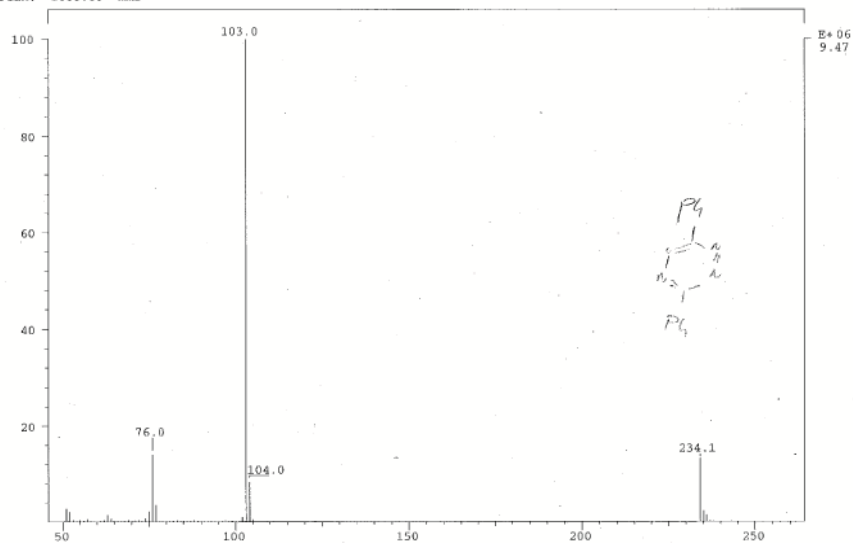
EI spectrum of **66**.

HR-MS (EI) spectrum of **67**.

SPEC: 593eq   02-Apr-14   Elapse: 03:13.3   46
Samp: Domnick, CD-24   Start : 11:51:48   49
Mode: EI +VE +LMR BSCAN (EXP) UP LR NRM
Oper: So   Inlet :
Base: 297.0   Inten : 33475328   Masses: 50 > 1000
Norm: 297.0   RIC   : 340960154   #peaks: 945
Peak: 5.00 mmu
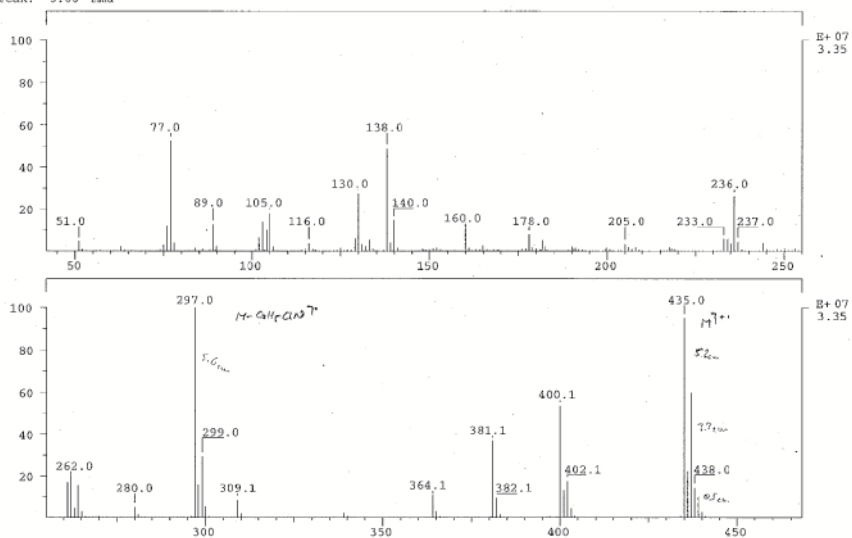
EI spectrum of compound **68**.
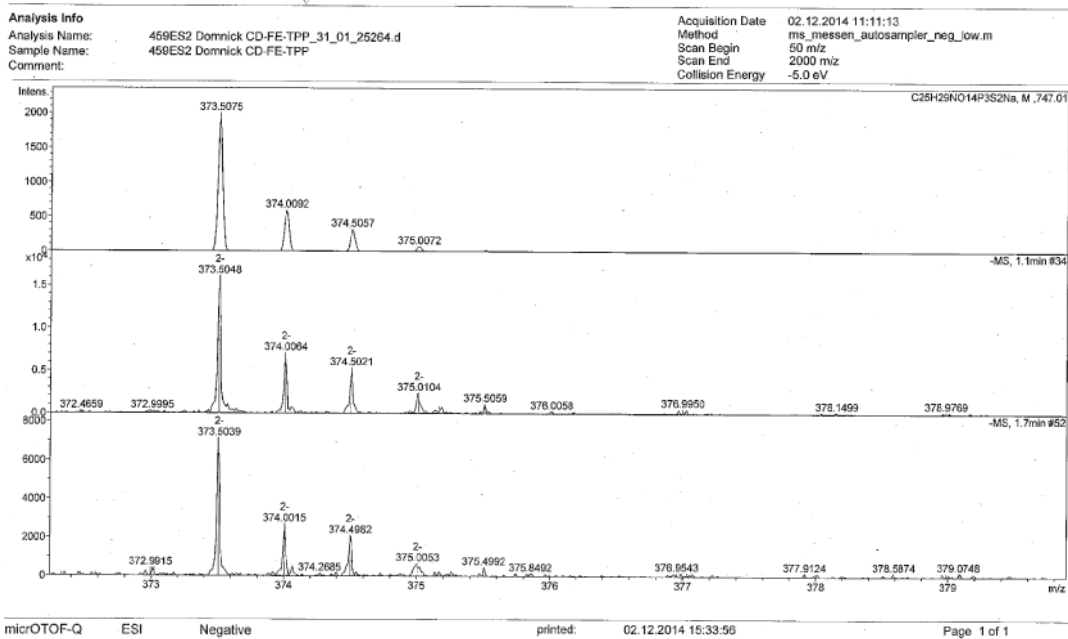
HR-MS (ESI⁻) spectrum of **76**.
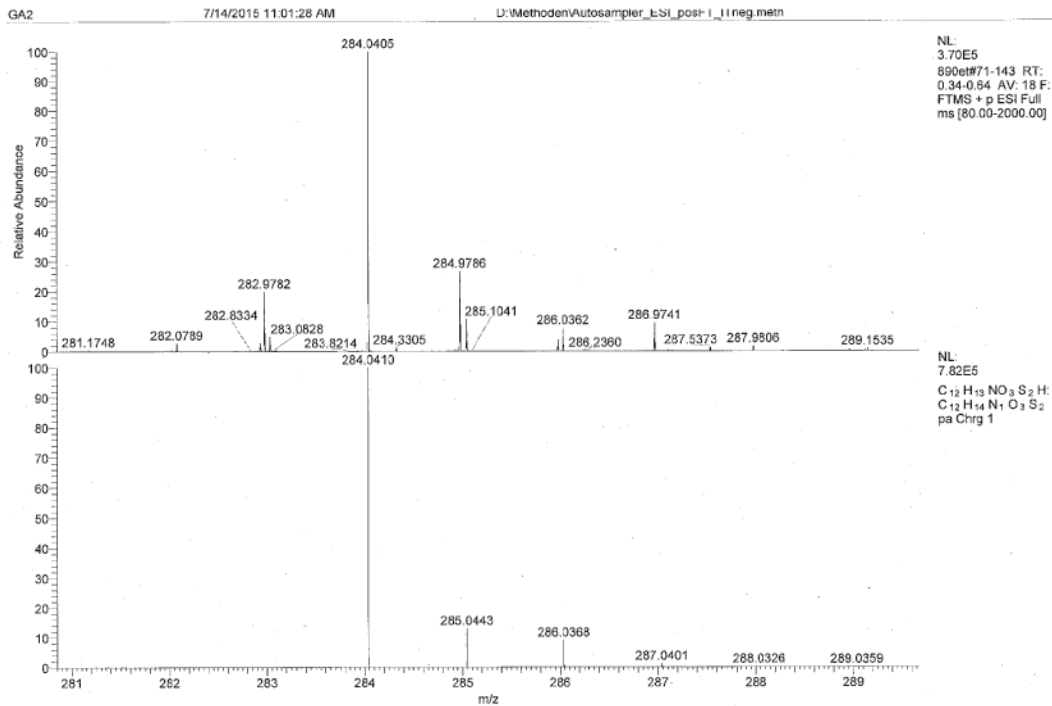
HR-MS (ESI⁺) spectrum of dTPT3 **81**.

ESI⁺ spectrum of **84**.

HR-MS (ESI⁻) spectrum of dNaM-TP **87**.
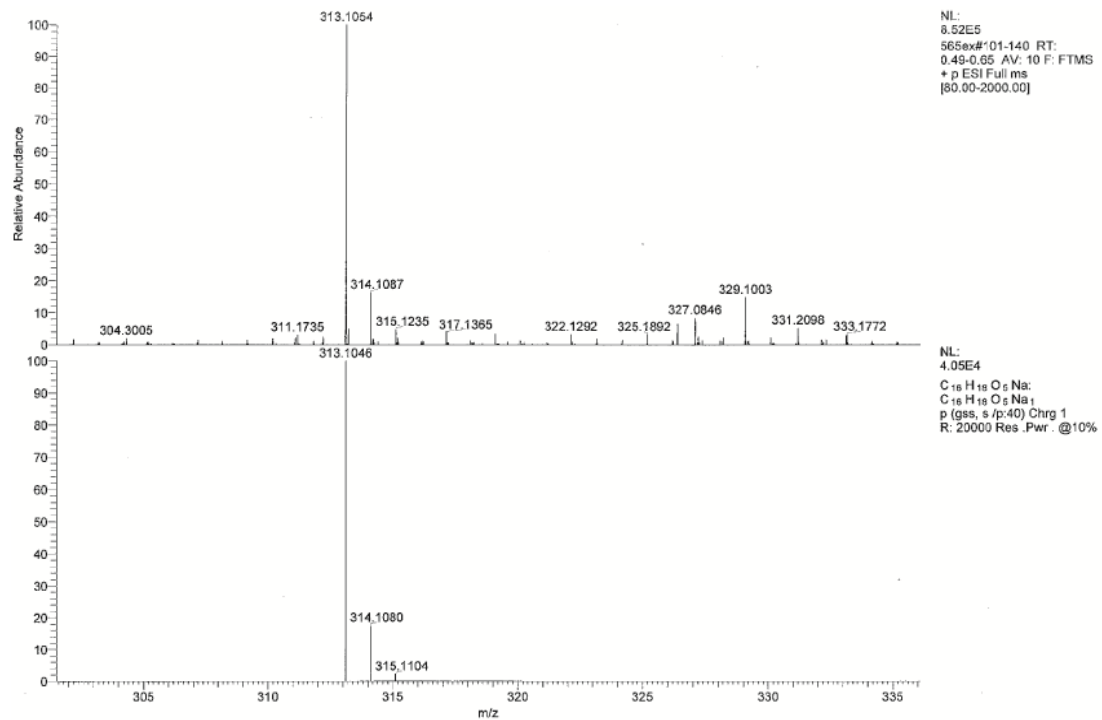
HR-MS (ESI⁺) of **95**.
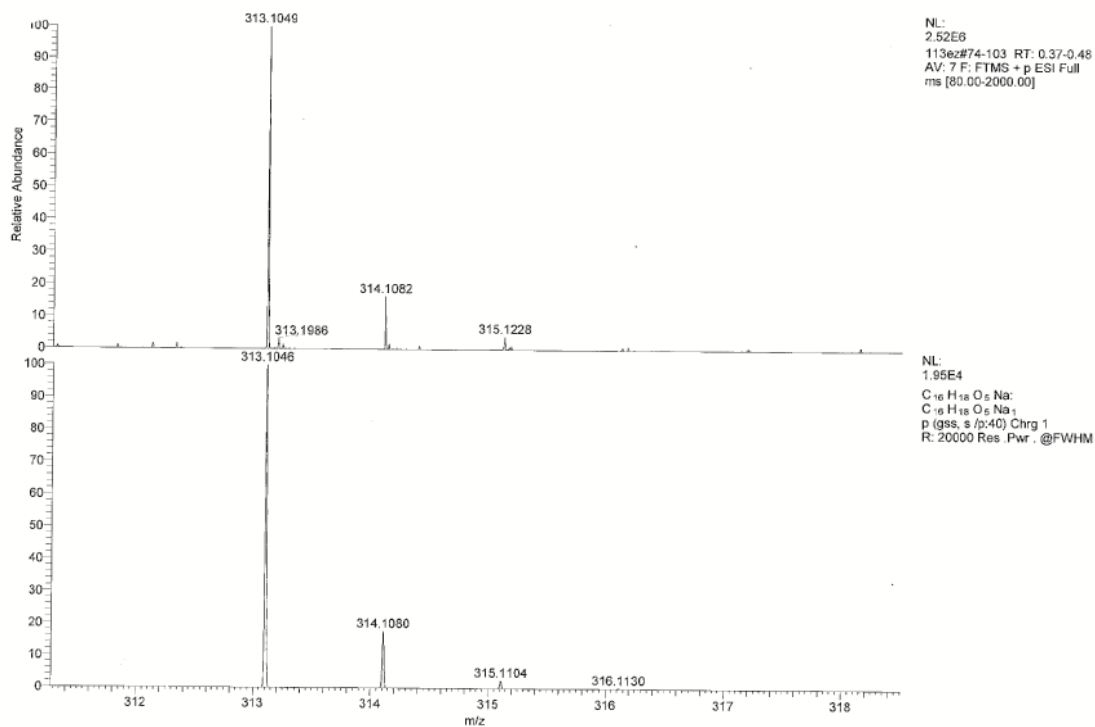
HR-MS (ESI⁺) of **95**(2).
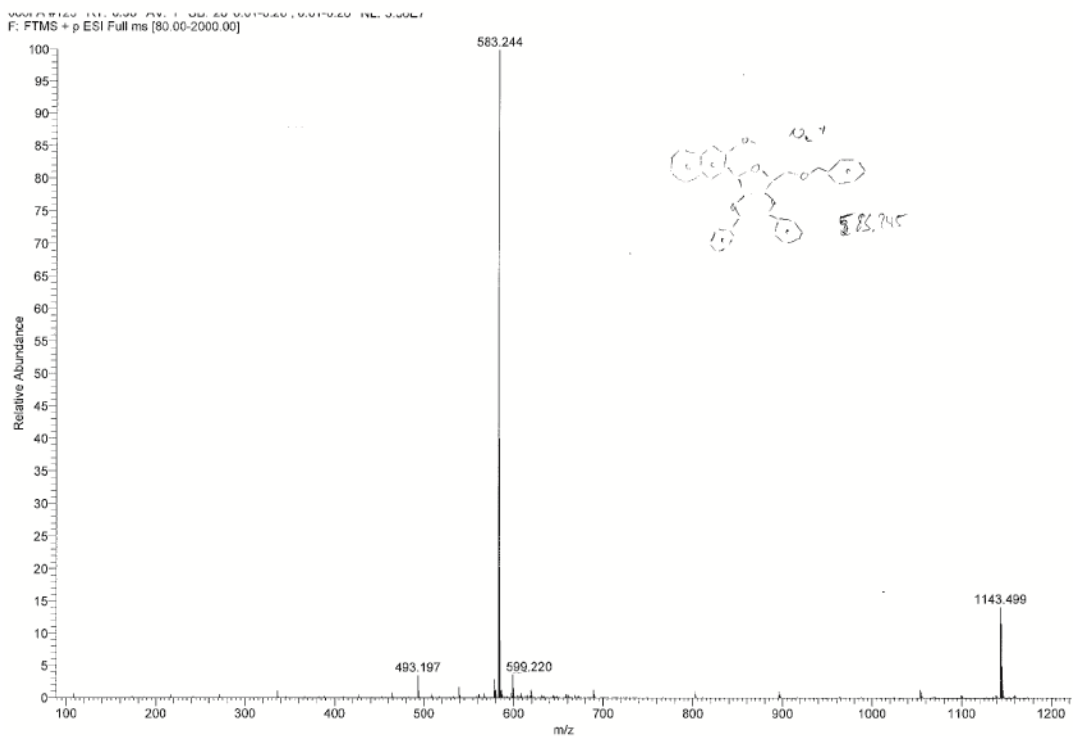
ESI⁺ spectrum of **95**(3).
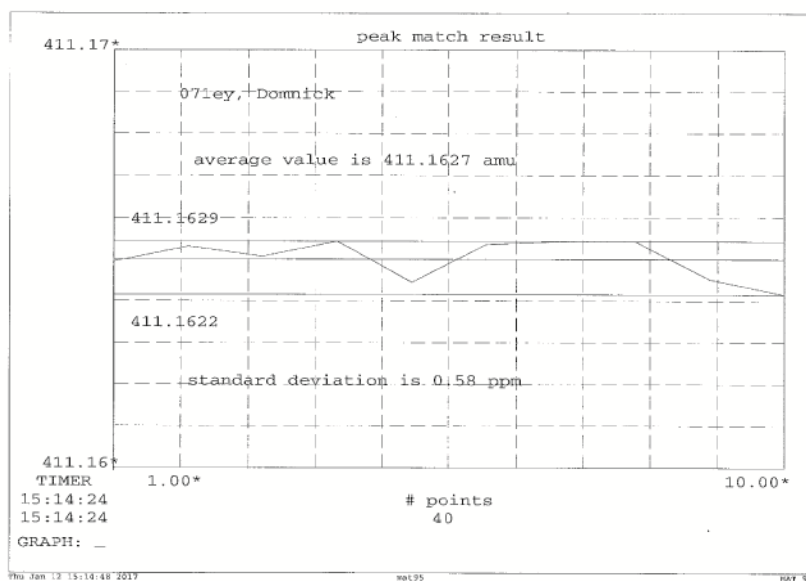
HR-MS (EI) of **101**.
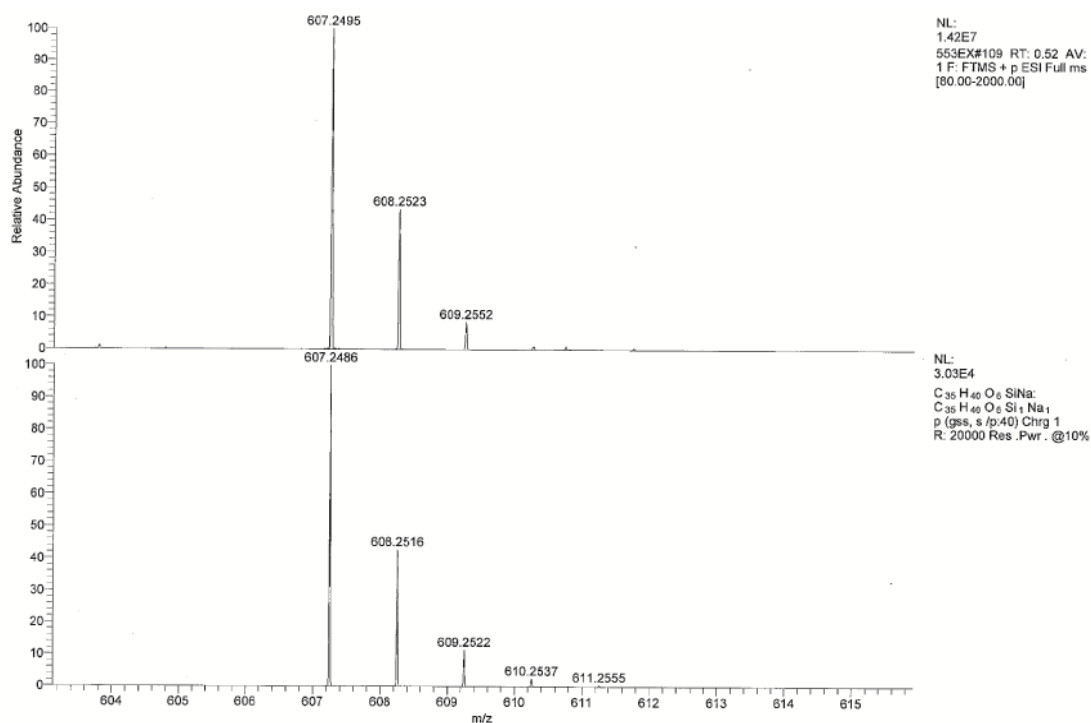
HR-MS (ESI⁺) of **102**.
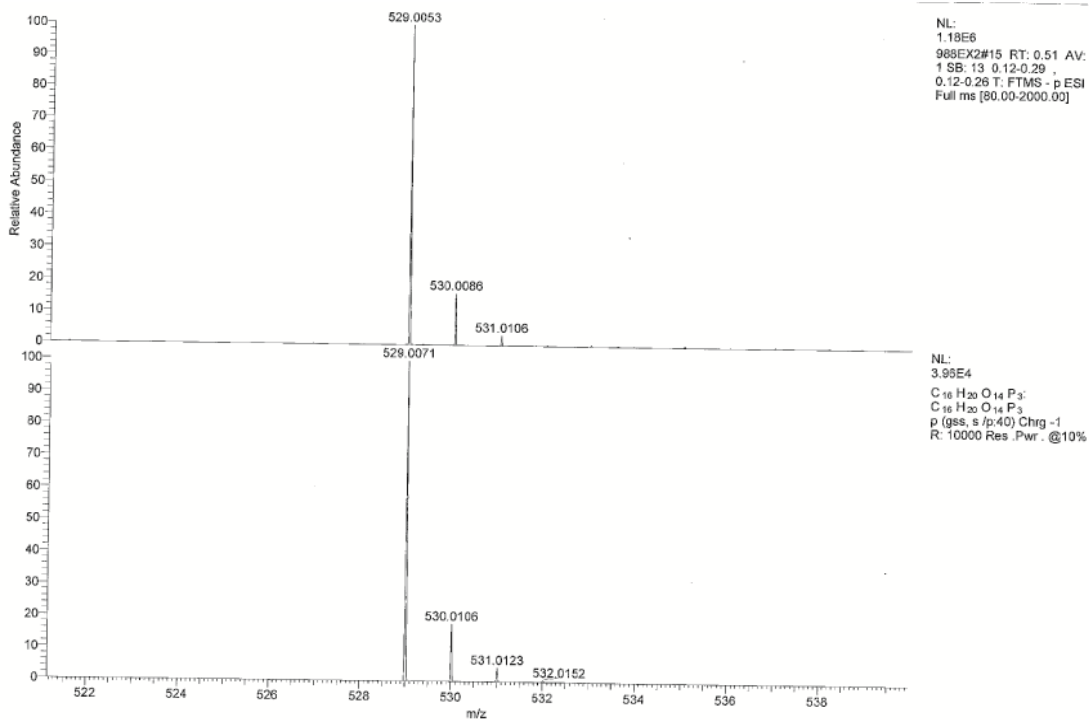
HR-MS (ESI⁻) of NaM-TP **103**.
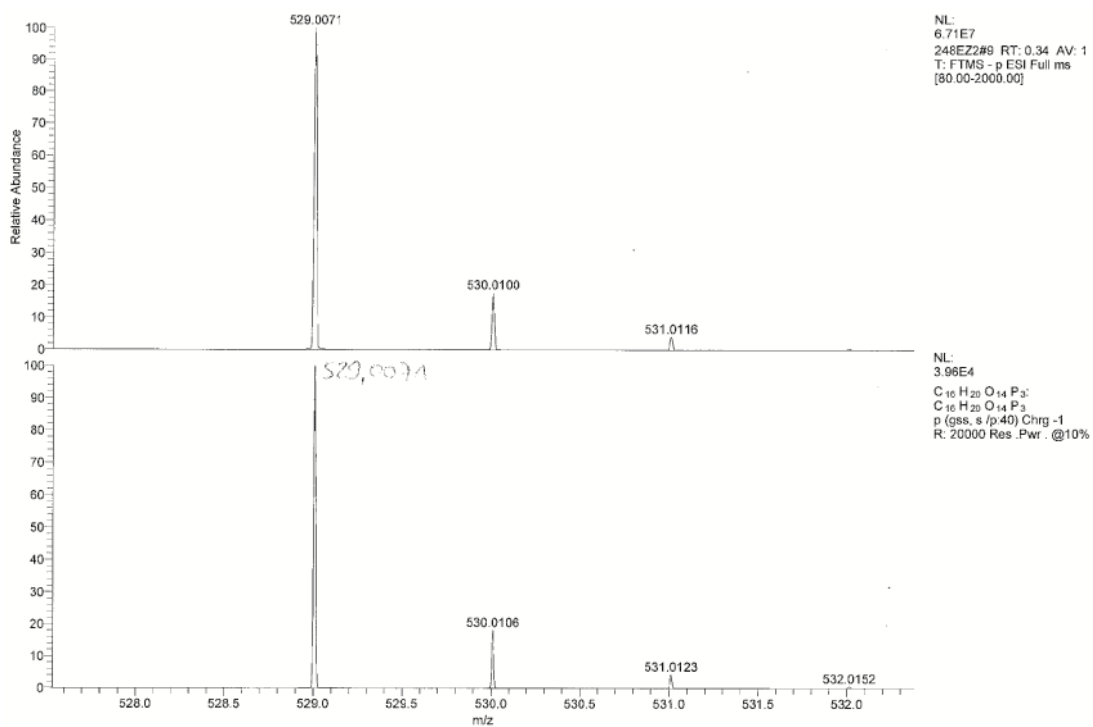
HR-MS (ESI⁻) of NaM-TP **103**(2).
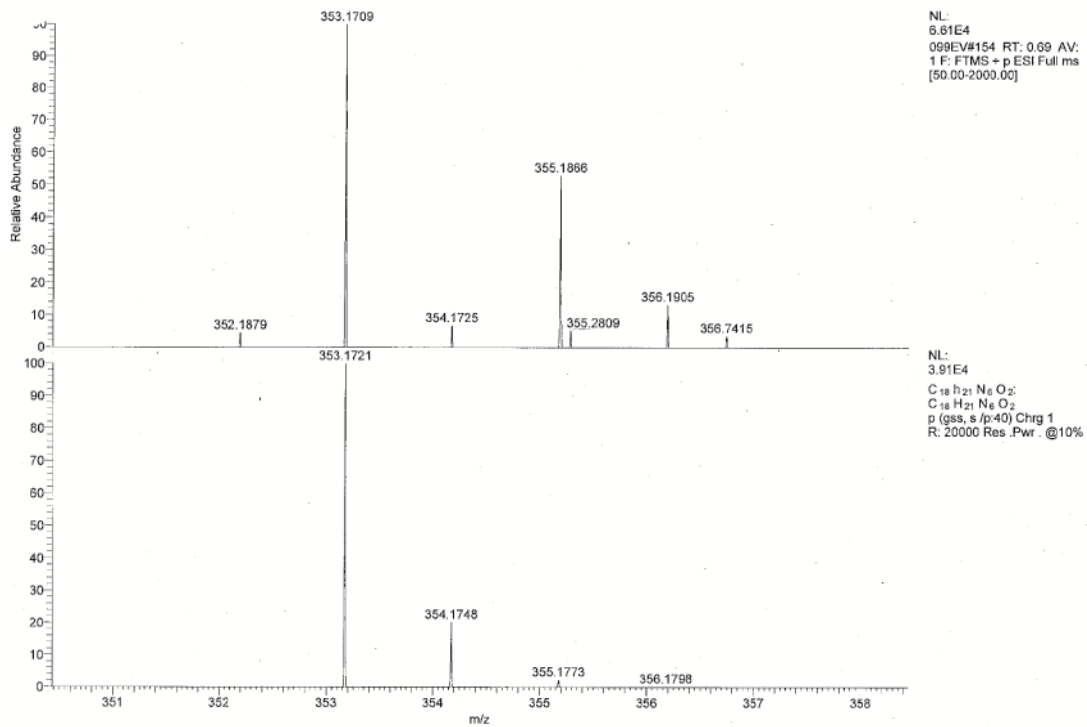
HR-MS (ESI$^+$) of **107**.
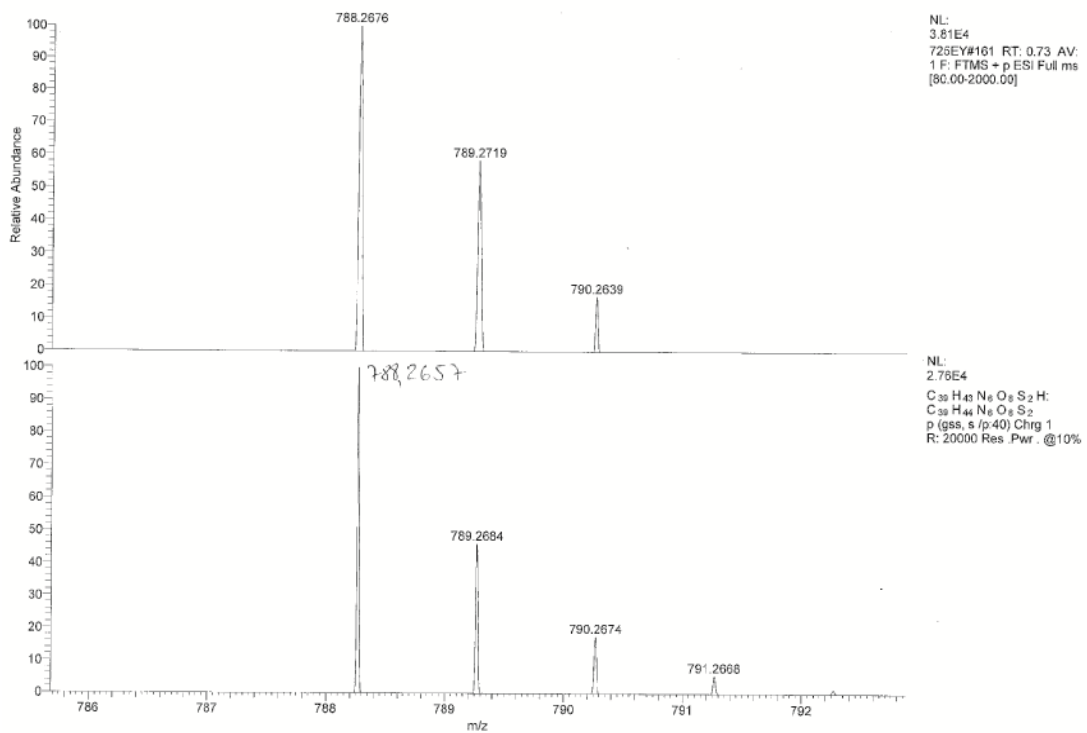
HR-MS (ESI$^+$) spectrum of click product between **TPT3^{CP}-OH**[311] and **107**.
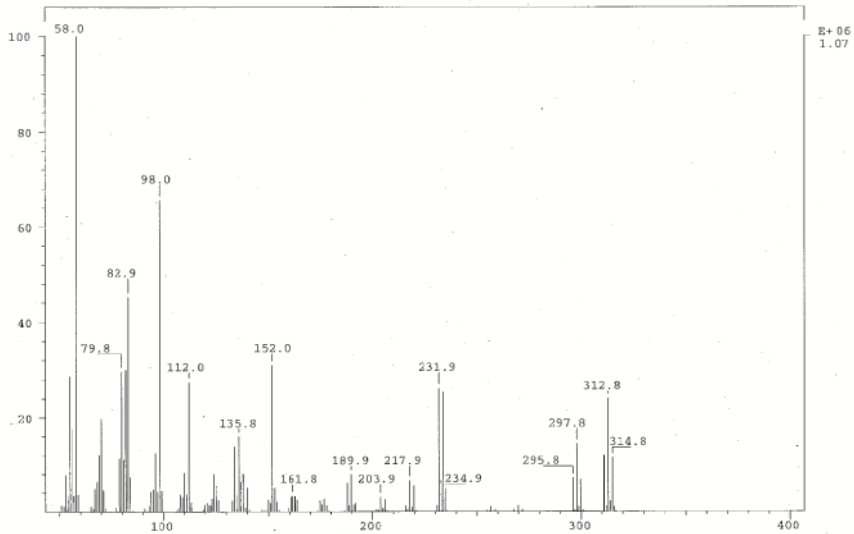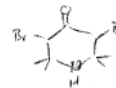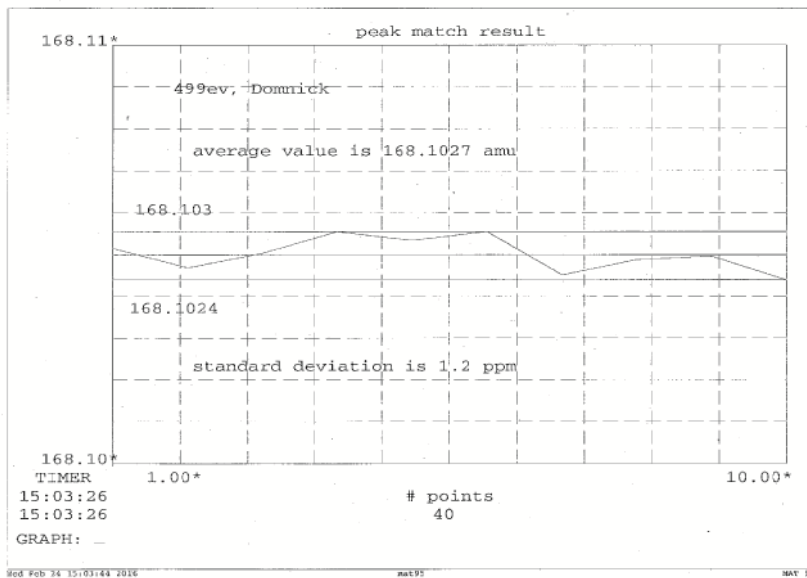
EI spectrum of **109**.

HR-MS (EI) of **112**.
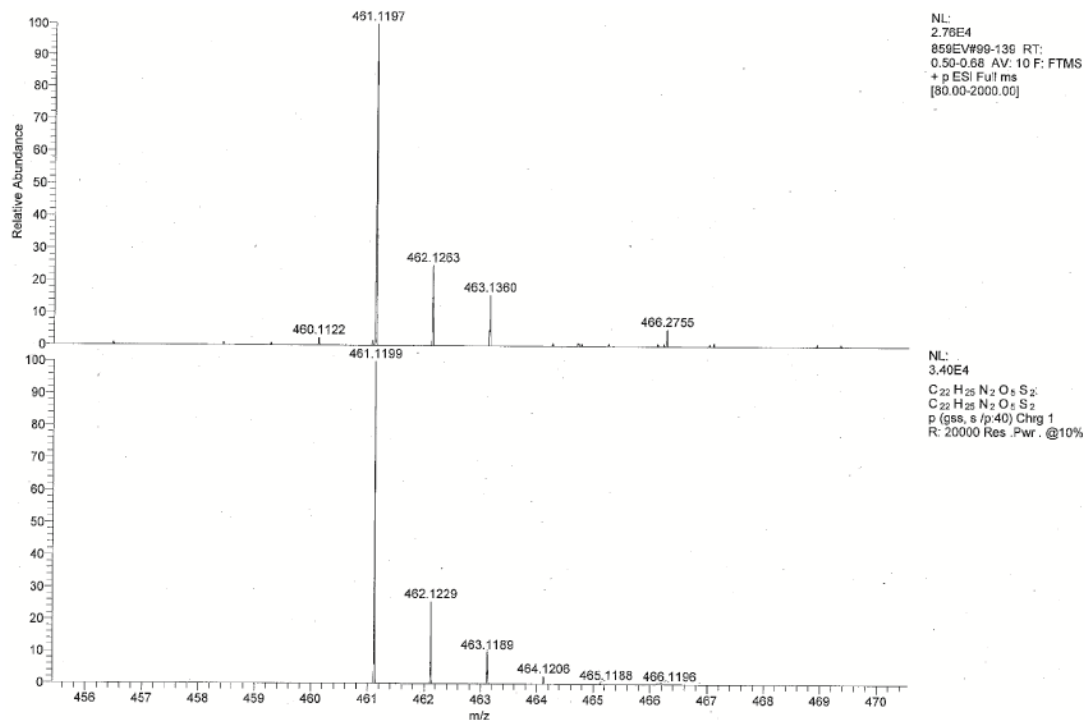
HR-MS (ESI$^+$) of **117**.
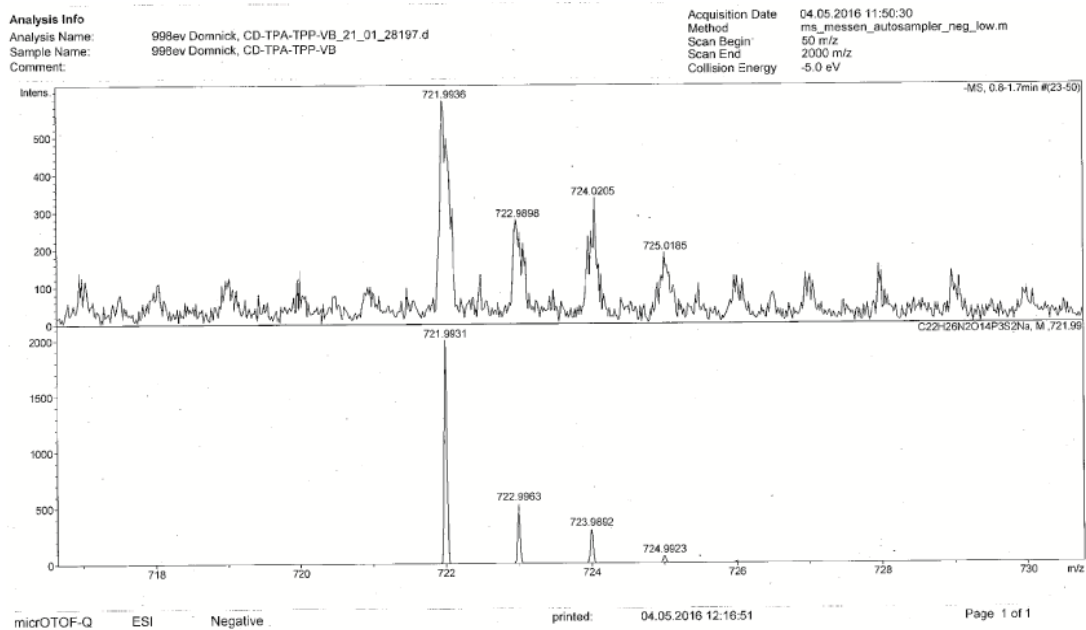
HR-MS (ESI$^-$) of **119**.
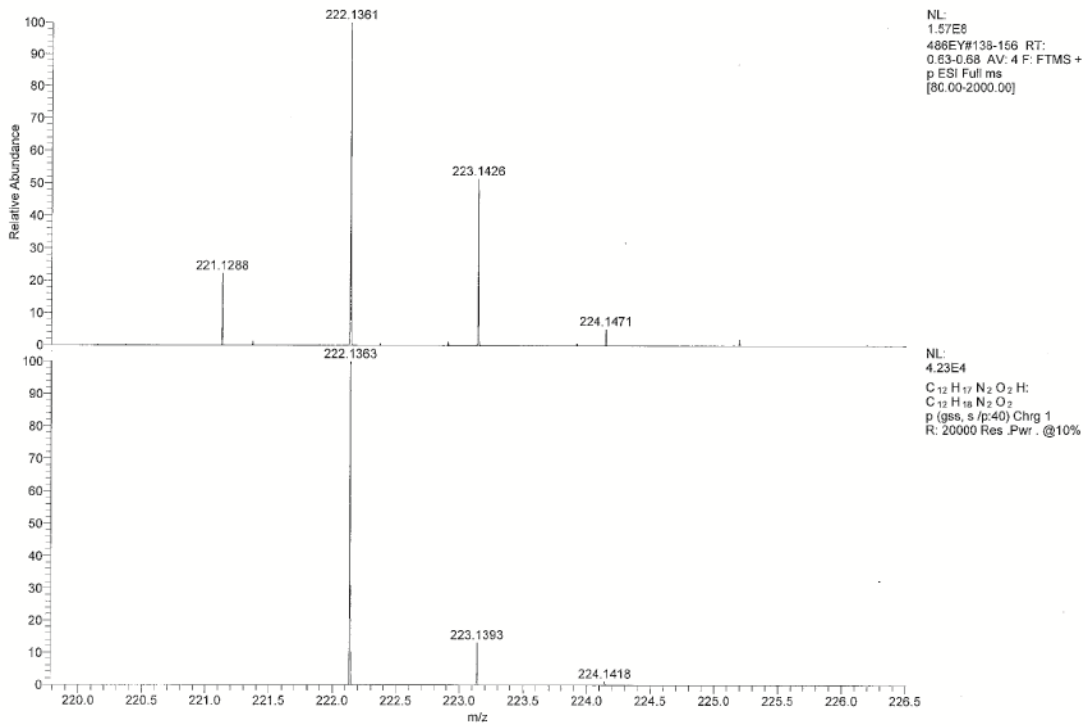
HR-MS (ESI⁺) of **124**.
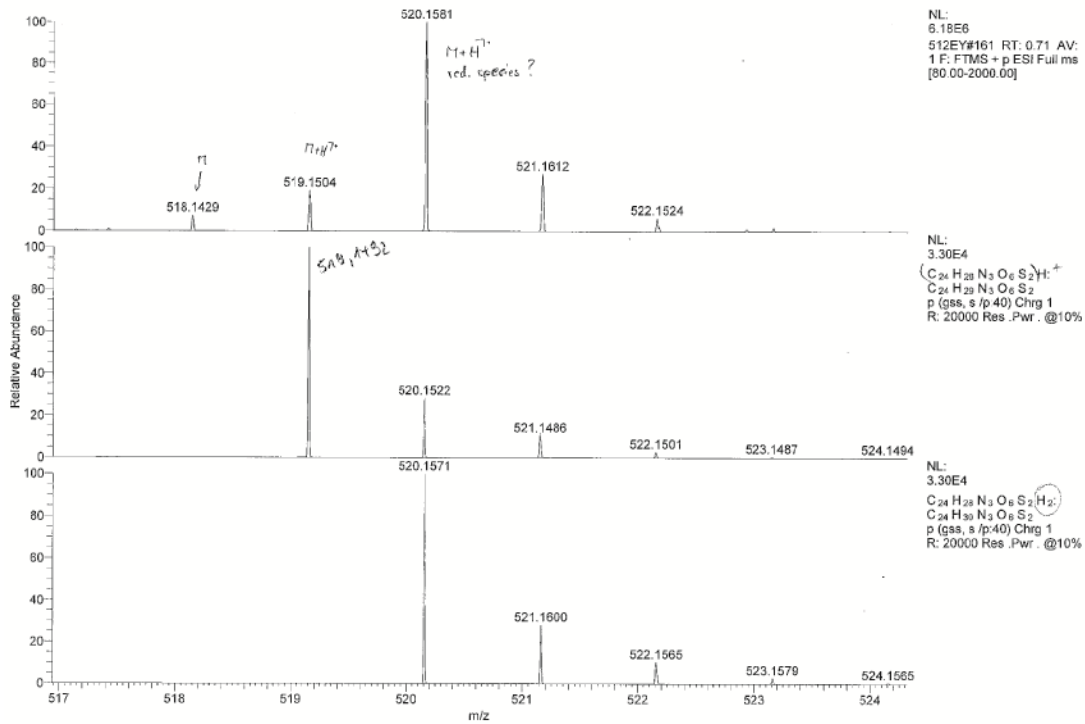
HR-MS (ESI⁺) of **125**.
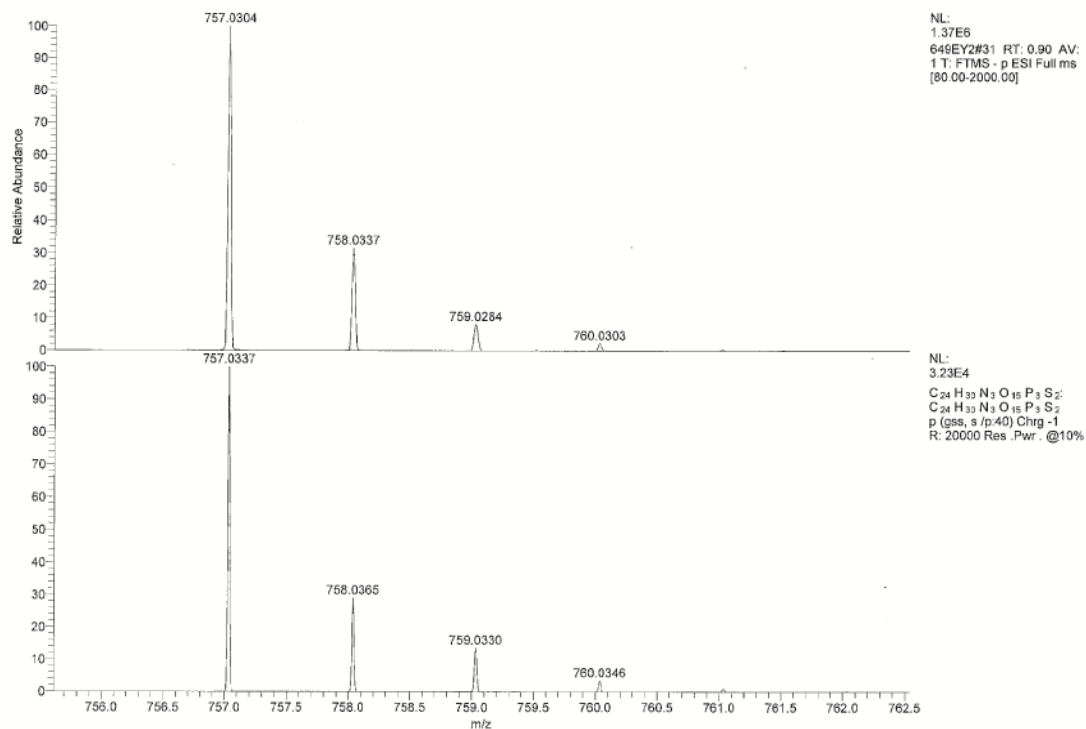
HR-MS (ESI⁻) of **126**.
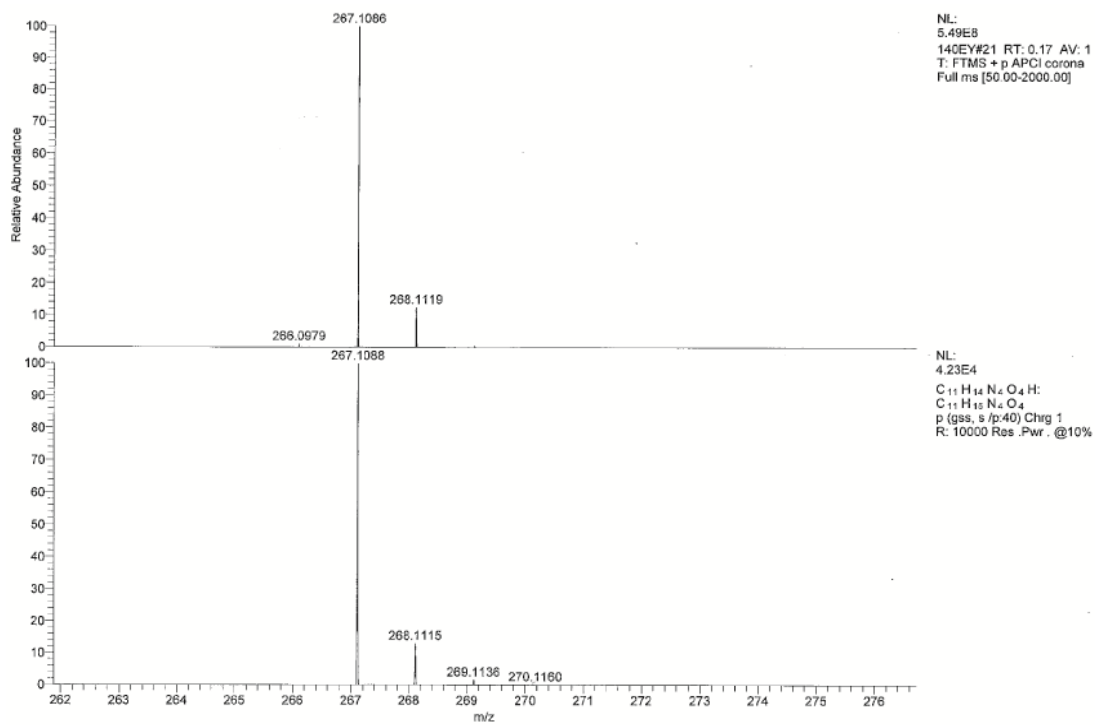
HR-MS (ESI⁺) spectrum of **39**.
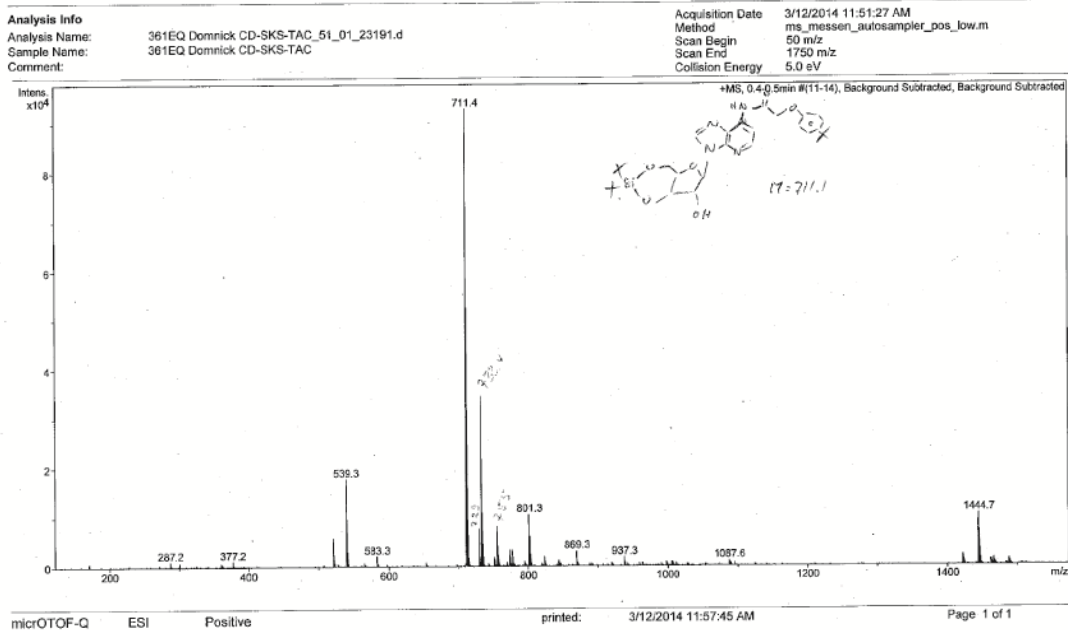
ESI⁺ spectrum of **41**.
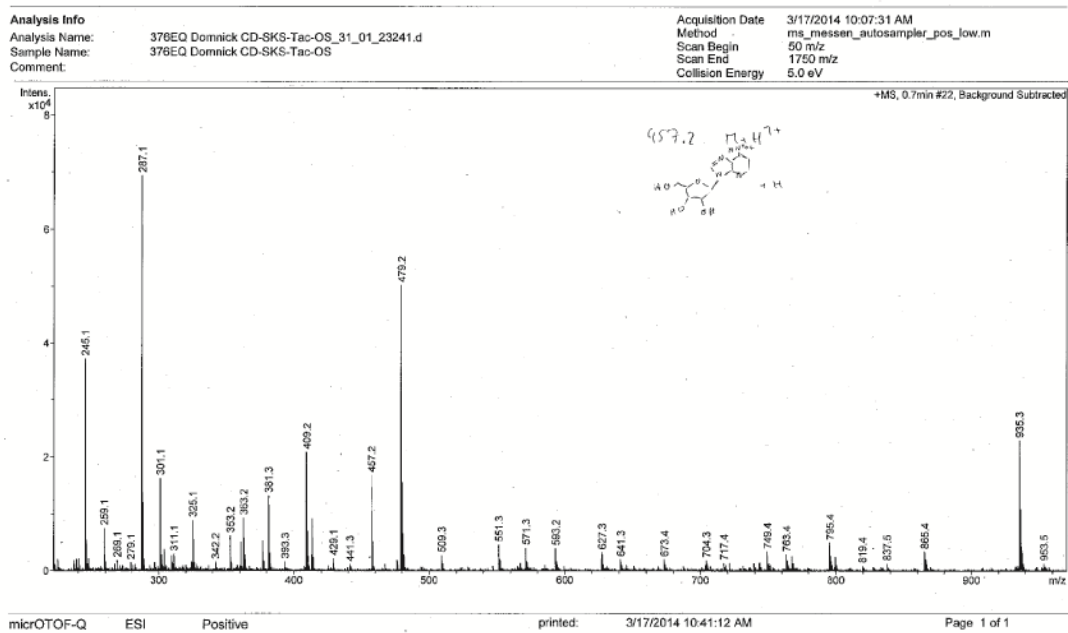
ESI⁺ spectrum of failed deprotection from **41** to **132**.
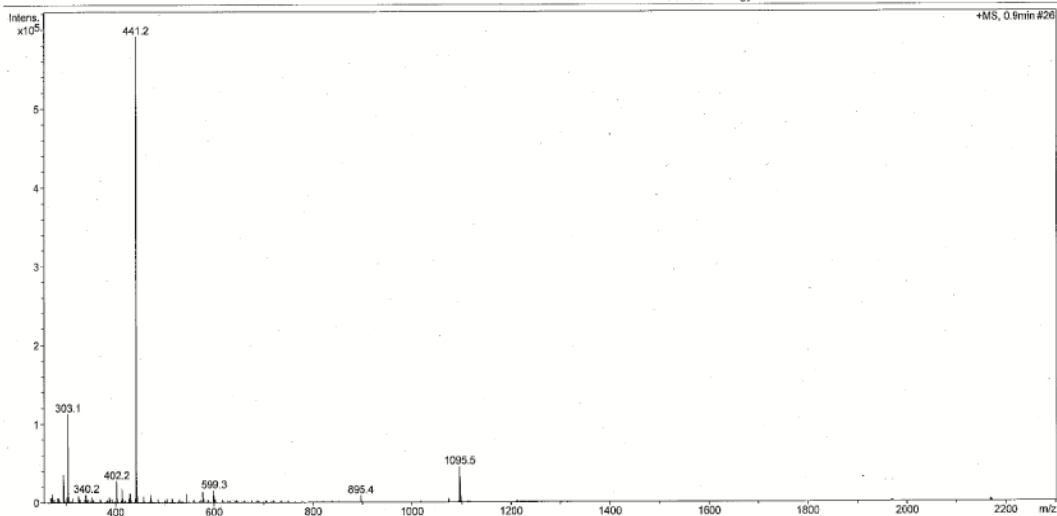
EI spectrum of **44**.

7.4 HPLC spectra:
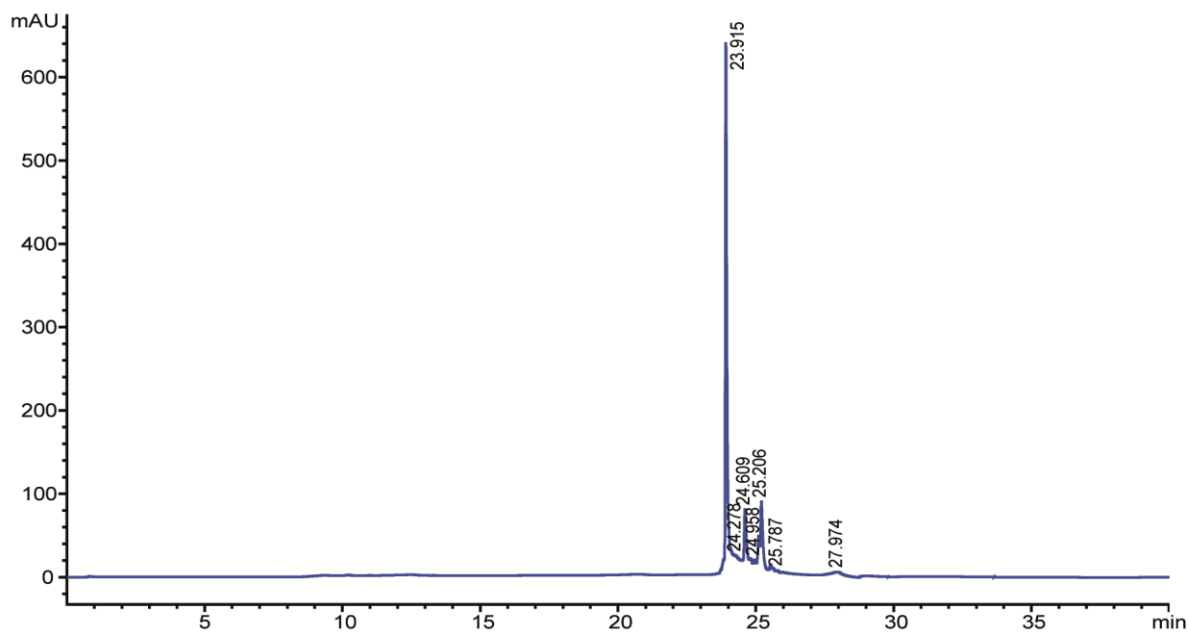
HPLC UV-trace (λ = 260 nm) of **103**.
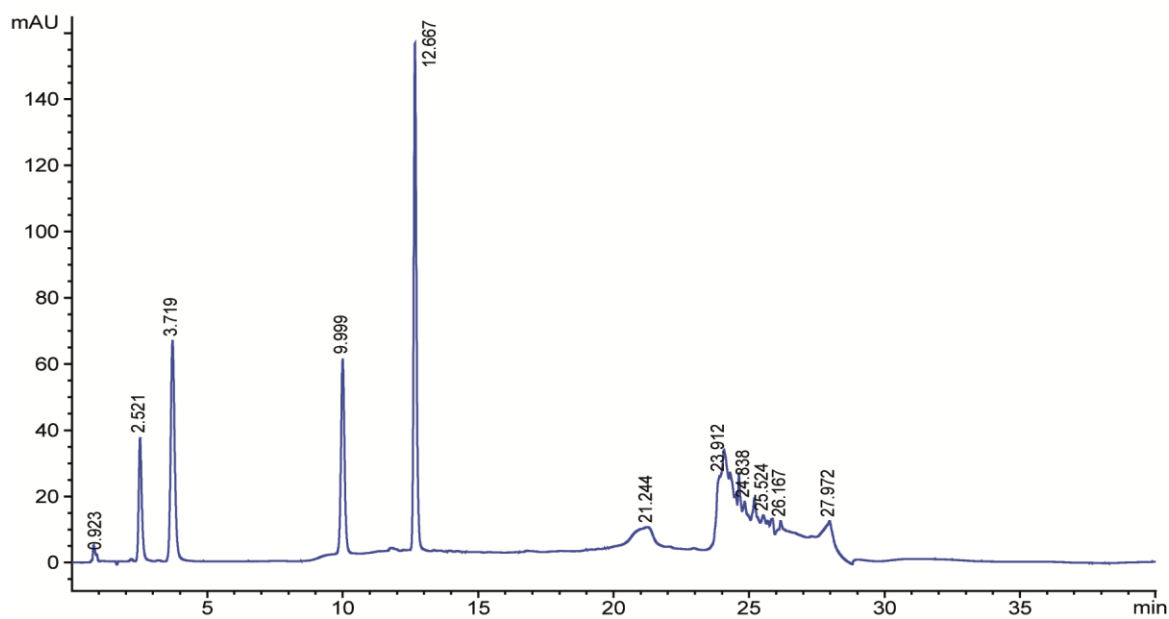
HPLC UV-trave (λ = 260 nm) of ribonucleosides (adenosine, cytidine, guanosine, and uridine) to receive corresponding retention times.
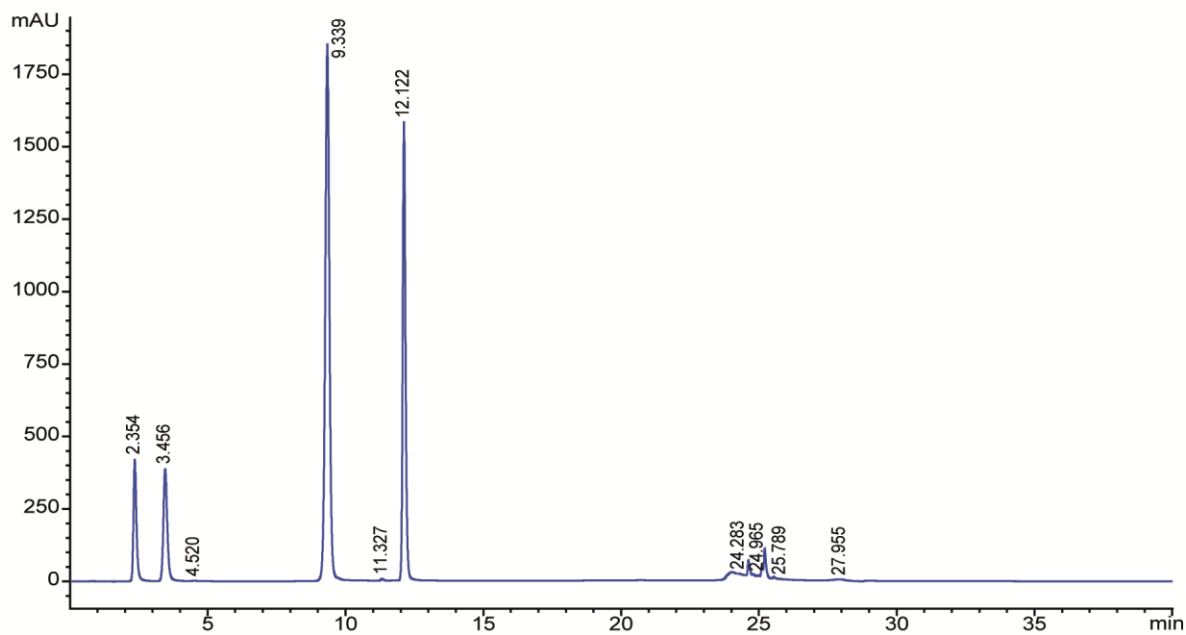
HPLC UV-trave (λ = 260 nm) of enzymatic digestion to the nucleosides of **RNA 5**
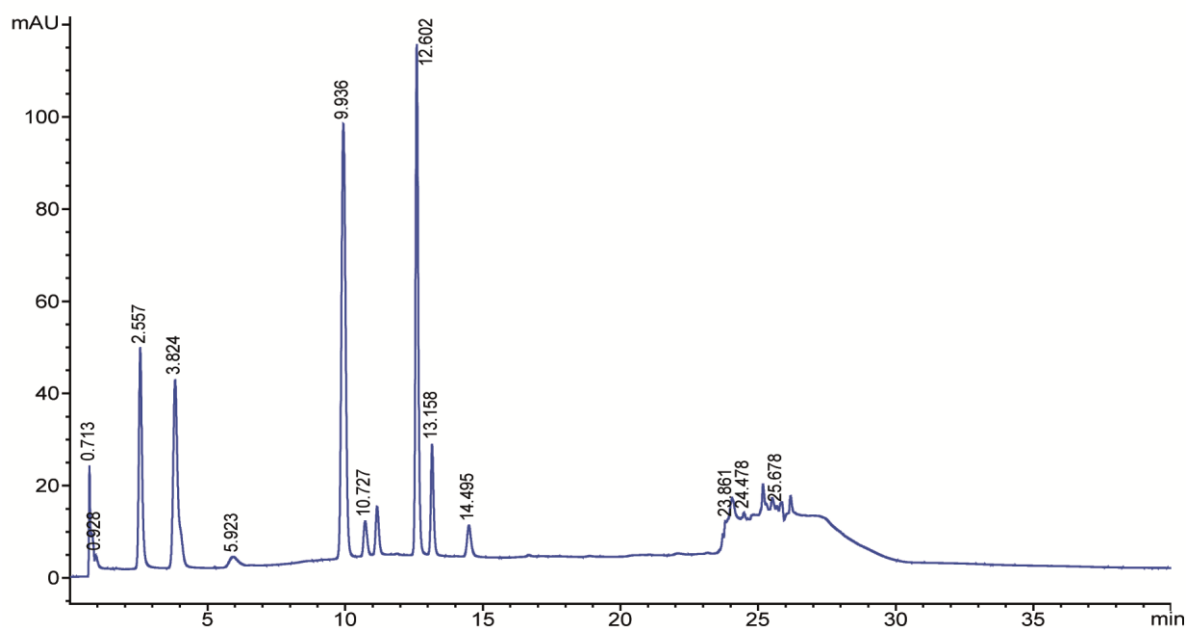
HPLC UV-trave (λ = 260 nm) of enzymatic digestion to the nucleosides of **RNA 3^G**.
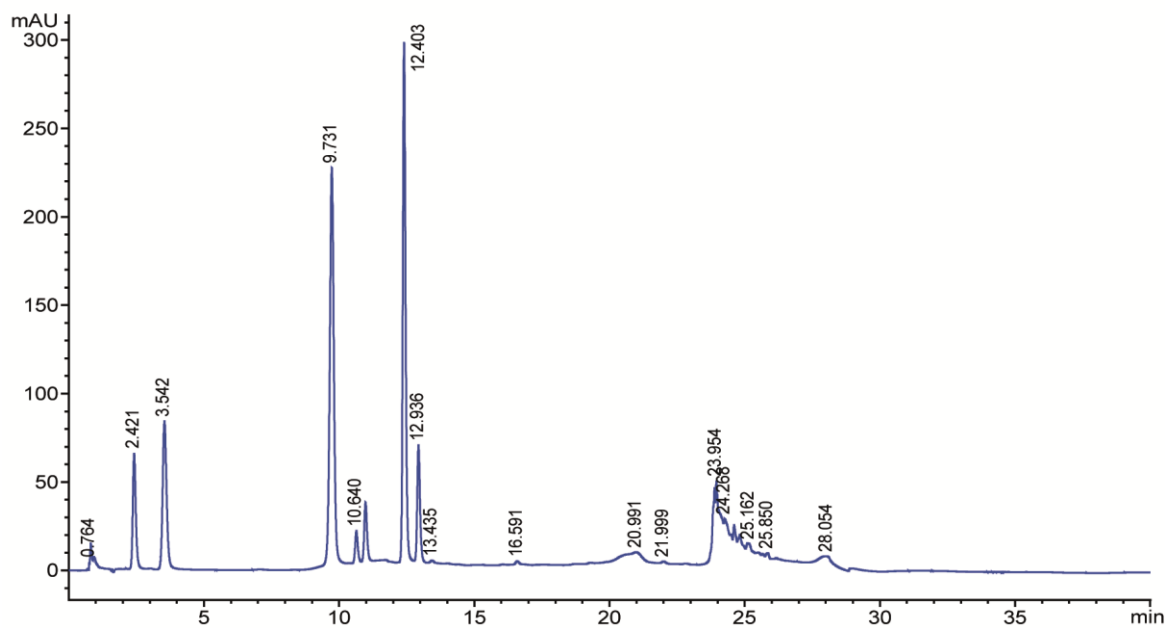
HPLC UV-trave (λ = 260 nm) of enzymatic digestion to the nucleosides of **RNA 3**[53].

7.5 EPR spectra:
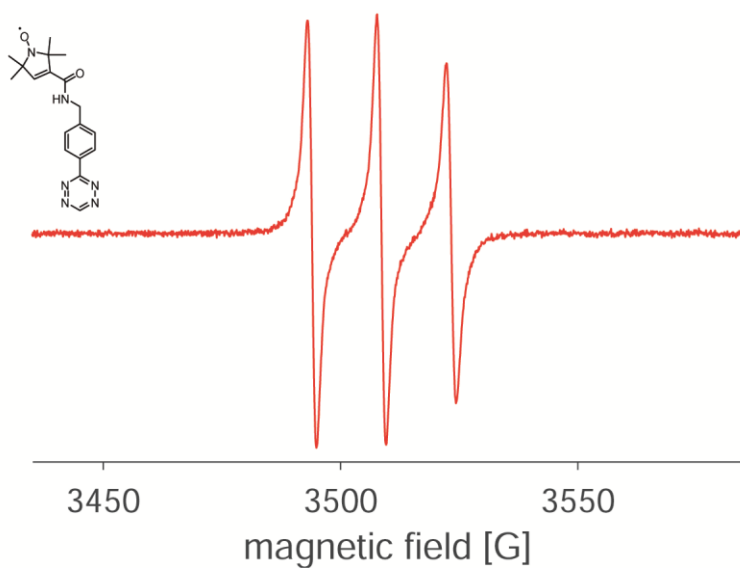
Cw X-band EPR of **107** measured in MeCN
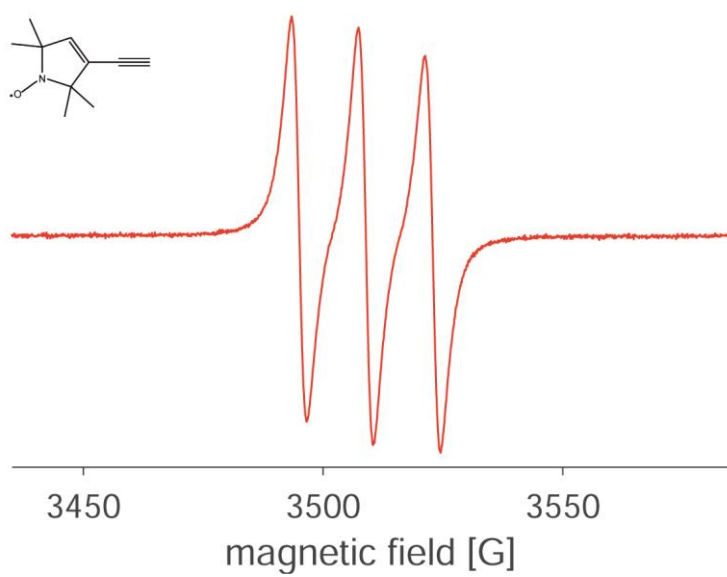
Cw X-band EPR of **114** measured in Cy
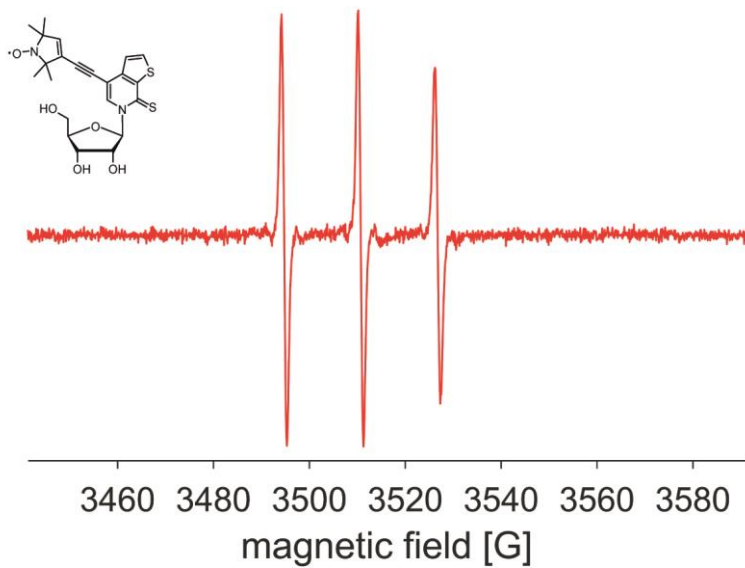
Cw X-band EPR of **117** measured in H_2O
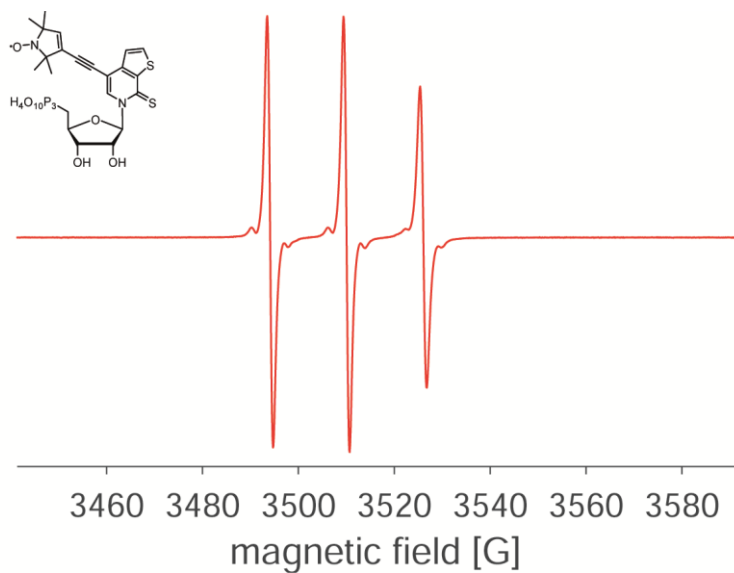
Cw X-band EPR of **119** measured in H_2O synthesized according to Kovács and Ötvös.[321]
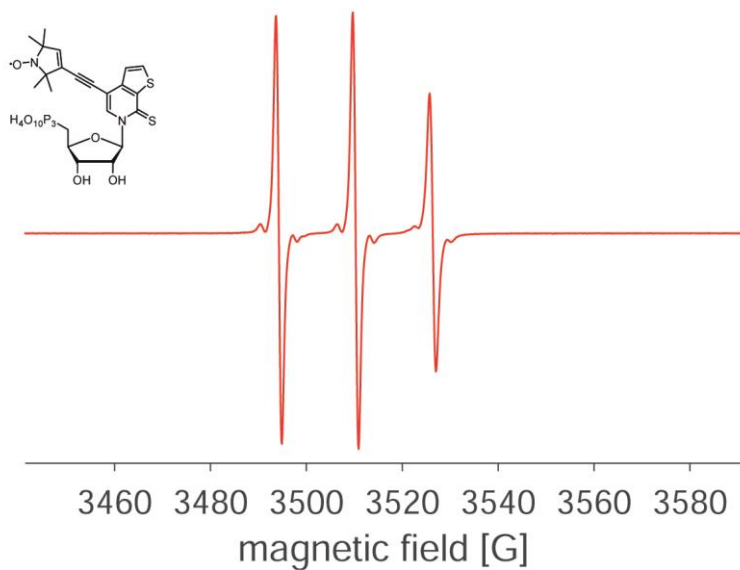
Cw X-band EPR of **119** measured in H_2O according to Ludwig and Eckstein.[354]
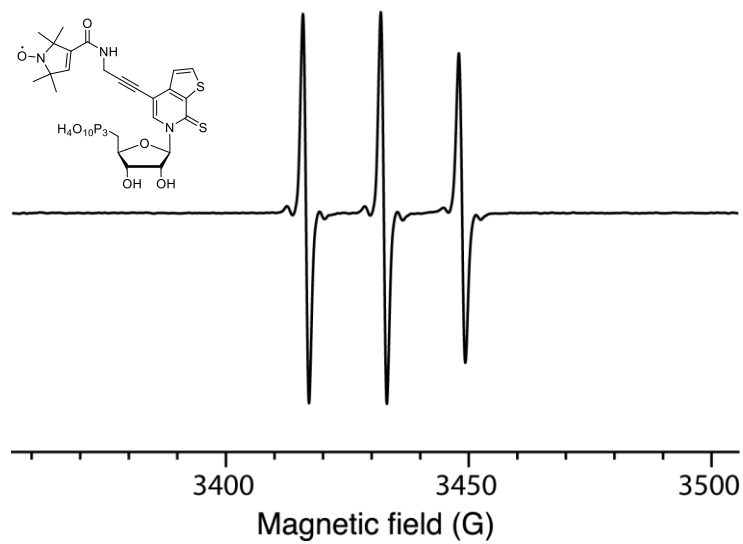
Cw X-band EPR of **126** measured in H_2O.
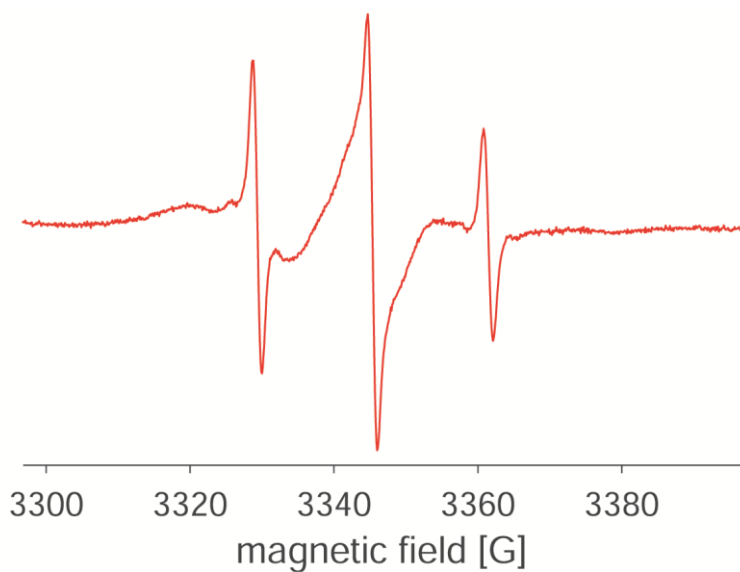
Cw X-band EPR of **RNA 7** bearing **119** measured in H_2O.
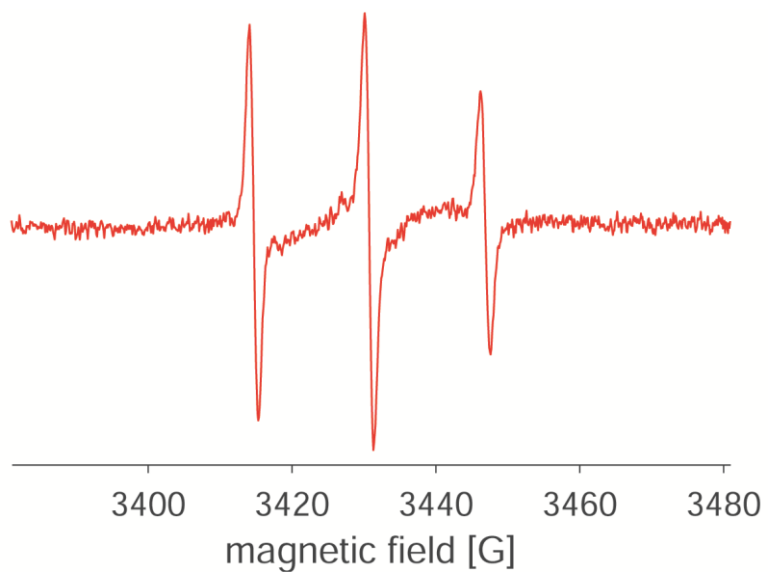
Cw X-band EPR of **RNA 8** bearing **119** measured in H_2O.
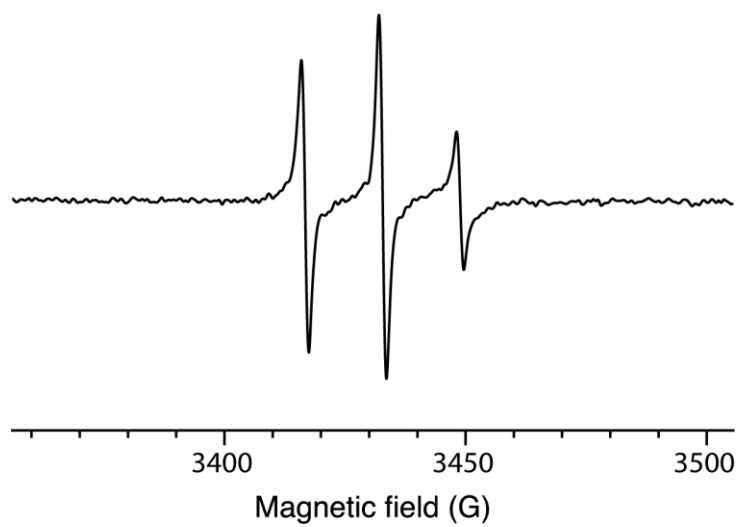
Cw X-band EPR of **RNA 8** bearing **126** measured in H_2O.

7.6 PAGE

PAGE 1:

20% denat. *PAGE* of **RNA-U^{NOR}-24** after click reaction on conjugates 57, 22, 58, 23. Data of SYBR safe stain (left) and fluorescent readout (right) is shown in Fig. 55
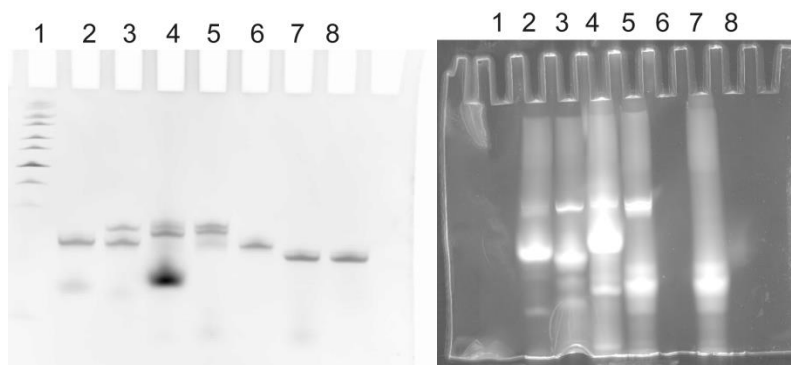
Lane 1: ULR, Lane 2: **RNA-U^{NOR}-24** w/ **23**, Lane 3: **RNA-U^{NOR}-24** w/ **58**, Lane 4: **RNA-U^{NOR}-24** w/ **22**, Lane 5: **RNA-U^{NOR}-24** w/ **57**, Lane 6: **RNA-U^{NOR}-24** w/o 57, Lane 7: **RNA-U-24** w/ **57**, Lane 8: **RNA-U-24** w/o conjugate

PAGE 2:

Full gel of 20% denat. *PAGE* shown in Fig. 63
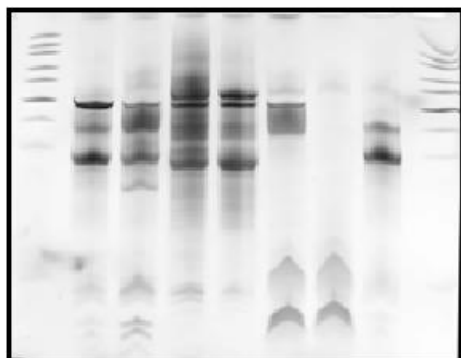
PAGE 3:

Full gel of 20% denat. *PAGE* shown in Fig. 63 and Fig. 65
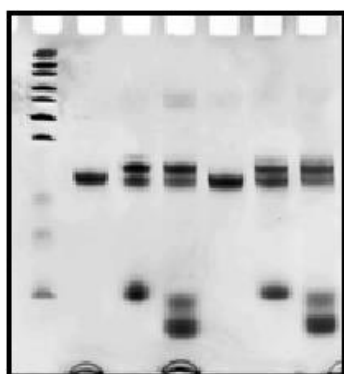
PAGE 3:

Full gel of 20% denat. *PAGE* shown in Fig. 64
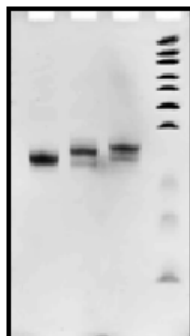
PAGE 4:

20% denat. *PAGE* of radioactive labeled reverse transcriptions of RNA 3 using **34** as specifically recognized unnatural DNA building block. Details are shown in Fig. 69
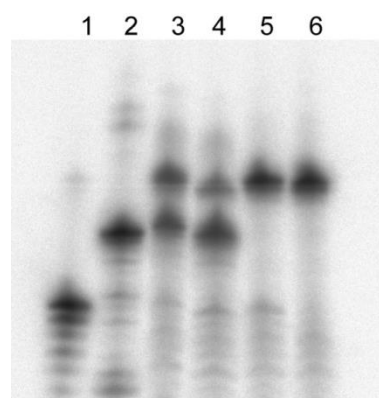
Lane 1: 15 nt long ^{32}P-labelled **RNA 11**, Lane 2: 22 nt long ^{32}P labelled **RNA 12**, Lane 3: crude reverse transcription of **RNA 3** w/ **34**, Lane 4: crude reverse transcription of **RNA 3** w/o **34**, Lane 5: crude reverse transcription of **RNA 3^{U}** w/ **34**, Lane 6: crude reverse transcription of **RNA 3^{U}** w/o **34**.

PAGE 5:

15% denat. *PAGE* of **RNA 7** using **42** as unnatural nucleotide. Details are shown in Fig. 97.
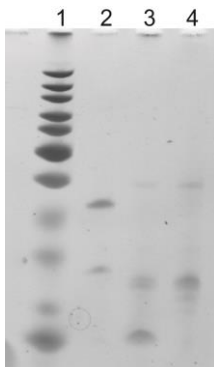
Lane 1: ULR, Lane 2: crude transcription of CXT DNA template, Lane 3: DNase digested transcription of CXT transcription, Lane 3: purified RNA of CXT transcriptions after DNase digestion

PAGE 6:

15% denat. PAGE of **RNA 8** using **42** as unnatural nucleotide yielding **RNA 8**. Details are not shown in this work.
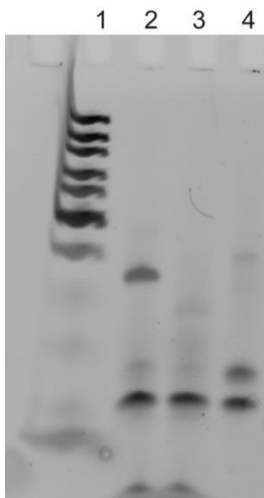
Lane 1: ULR, Lane 2: crude transcription of **DNA 8** as template yielding **RNA 8**, Lane 3: DNase digested transcription of template **DNA 8** yielding **RNA 8** shown in lane 1, Lane 3: purified **RNA 8** after DNase digestion. Clearly visible is truncation at position 15.

***PAGE* 7:**

20% denat. *PAGE* of **DNA 8** using **45** as unnatural nucleotide yielding **RNA 8**. Details are shown Fig. 104.
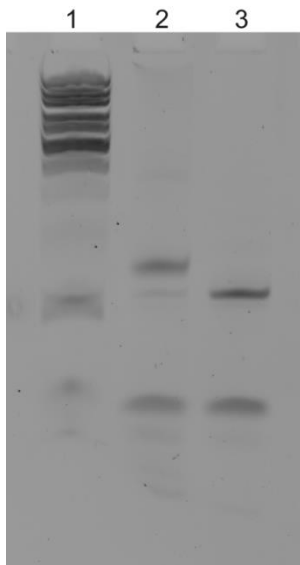
Lane 1: ULR, Lane 2: crude transcription of **DNA 8** using **45**, Lane 3: crude transcription of **DNA 8** w/o unnatural nucleotide **45**.

***PAGE* 8:**

20% denat. *PAGE* of transcriptions yielding **RNA 8** to compare the incorporation and truncation ratios of different unnatural nucleotides. Details are shown in Fig. 106
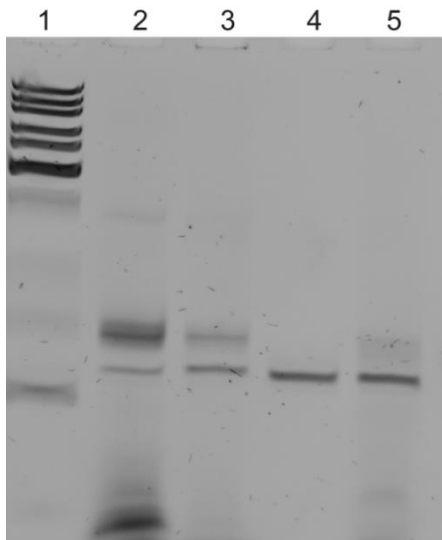
Lane 1: ULR, Lane 2: transcription yielding **RNA 8** bearing **45** as unnatural nucleotide, Lane 3: transcription yielding **RNA 8** bearing **TPT3^{CP}-TP**, Lane 4: transcription yielding truncated **RNA 8** w/o unnatural nucleotide, Lane 5: transcription yielding **RNA 8** bearing **42** as unnatural nucleotide.

20% denat. *PAGE* of **DNA 7** transcripts yielding **RNA 7** to compare the incorporation of synthesized 53. Details are shown in Fig. 77.
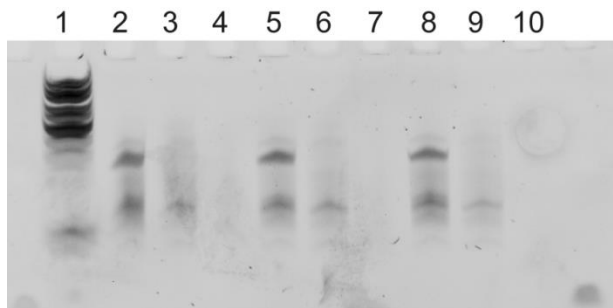
Lane 1: ULR, Lane 2: *in vitro* transcription of **DNA 7** yielding **RNA 7** transcript w/o unnatural nucleotide, Lane 3: *in vitro* transcription of **DNA 7** yielding **RNA 7** transcript w/o unnatural nucleotide after Dnase digest, Lane 4: *in vitro* transcription of **DNA 7** yielding **RNA 7** transcript w/o unnatural nucleotide after Dnase digest and G-25 purification, Lane 5: *in vitro* transcription of **DNA 7** yielding **RNA 7** transcript w/ **53**, Lane 6: *in vitro* transcription of **DNA 7** yielding **RNA 7** transcript w/ **53** (1st approach) after Dnase digest, Lane 7: *in vitro* transcription of **DNA 7** yielding **RNA 7** transcript w/ **53** (1st approach) after Dnase digest and G-25 purification, Lane 8: *in vitro* transcription of **DNA 7** yielding **RNA 7** transcript w/ **53** (2nd approach), Lane 9: *in vitro* transcription of **DNA 7** yielding **RNA 7** transcript w/ **53** (2nd approach) after Dnase digest, Lane 10: *in vitro* transcription of **DNA 7** yielding **RNA 7** transcript w/ **53** (2nd approach) after Dnase digest and G-25 purification. Details are shown in Fig. 77.
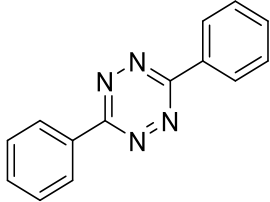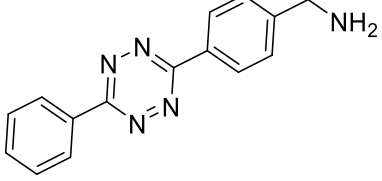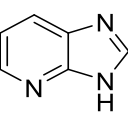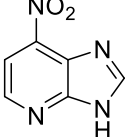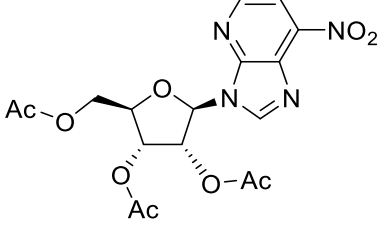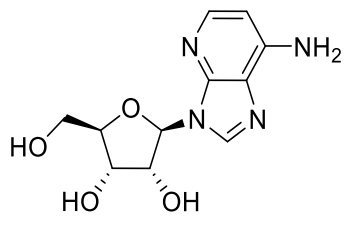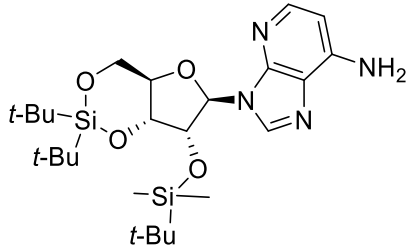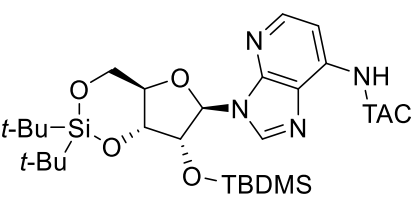
7.7 List of abbreviations

Abbreviation	Full form
Abs.	Absolute
Ac	Acetyl
AcOH	Glacial acetic acid
AIBN	Azobisisobutyronitrile
anhydr.	Anhydrous
APCI$^+$	Atmopheric pressure chemical ionization (positive mode)
APS	Ammonium persulfate
aq.	Aqueous
Ar - atm	Argon atmosphere
ATP	Adenosine triphosphate
BF$_3$*Et$_2$O	Boron trifluoride diethyl etherate
Bn	Benzyl
BSA	Bis(trimethylsilyl)acetamide
CD	Circular dichroism
CEP	Cyanoethyldiiopropylphosphoramidite
CO	Cyclooctyne
CPN	Cyclopentene
CTP	Cytosine triphosphate
Cy	Cyclohexane
DCM	Dichloromethane
dd	Double distilled
DDQ	2,3-Dichloro-5,6-dicyano-1,4-benzoquinone
DIBAL	Diisobutylaluminium hydride
DiPEA	*N,N*-Diisopropylethylamine
dist.	Distilled
DMAP	4-(Dimethylamino)-pyridin
DMF	Dimethylformamide
DMSO	Dimethyl sulfoxide
DMT	Dimethoxytrityl
DMT-Cl	4,4′-Dimethoxytrityl chloride
DNA	Deoxyribonucleic acid
dNTP	Deoxyribonucleoside triphosphate
E. Coli	*Eschericia coli*
EDG	Electron donating group
EDTA	Ethylenediaminetetraacetic acid
EE	Ethyl acetate
EI	Electron ionization
EPR	Electron paramagnetic resonance
eq.	Equivalent(s)
ESI$^{+/-}$	Electro spray ionization (positive/negative mode)
Et$_2$O	Diethylether
Et$_3$SiH	Triethylsilane
EtOH	Ethanol
eV	Electron volt

EWG	Electron withdrawing group
GFP	Green fluorescent protein
GTP	Guanosine triphosphate
HFIP	Hexafluoroisopropanol
HNO_3 (fum.)	Fuming nitric acid
HOMO	Highest occupied molecular orbital
HPLC	High-performance liquid chromatography
HR-MS	High-resolution mass spectrometry
Hz	Hertz
IEDDA	Inverse electron-demand Diels-Alder
iPP	Inorganic Pyrophosphatase
iPr	Isopropyl
KO^{t}Bu	Potassium *tert*-butoxide
LC-MS	Liquid chromatography mass spectrometry
lnc	Long non-coding
LUMO	Lowest unoccupied molecular orbital
M	Molar
m-	Meta
m/z	Mass-to-charge ratio
mCPBA	*Meta*-chlorperoxybenzoic acid
MeCN	Acetonitrile
MeOH	Methanol
MHz	Megahertz
mmol	Millimol
MS	Mass spectrometry
MW	Molecular weight
NBS	N-bromosuccinimide
NBu_3	Tributylamine
n-BuLi	*n*-Butyl lithium
NEt_3	Triethylamine
NH_4OAc	Ammonium acetate
nmol	Nanomol
NMR	Nuclear magnetic resonance
NOR	Norbornene
NTP	Ribonucleoside triphosphate
o-	Ortho
p-	Para
PAGE	Polyacrylamide gel electrophoresis
PCR	Polymerase chain reaction
Pd/C	Palladium on carbon
PELDOR	Pulsed electron-electron double resonance
pmol	Picomol
ppm	Parts per million
Proton sponge	1,8-Bis(dimethylamino)naphthalene
Py	Pyridine
r.t.	Room temperature
R_f	Retention factor

RNA	Ribonucleic acid
RNAP	Ribonucleic acid polymerase
sat.	Saturated
t-	*Tertial*
TAC	(4-*tert*-butylphenoxy)-acetyl
TBAF	Tetra-*n*-butylammonium fluoride
TBS	*Tert*-butyldimethylsilyl
TBS-Cl	*Tert*-butyldimethylsilylchloride
TBDPS	*Tert*-butyldiphenylsilyl
TBE	Tris/Borate/EDTA
TCO	Trans-cyclooctene
TEAB	Triethylammonium bicarbonate
TEMED	N,N,N',N-Tetramethylethylenediamine
TEMPYO	1-Oxyl-2,2,5,5-tetramethylpyrroline-3-carboxylate
TFA	Trifluoroacetic acid
THF	Tetrahydrofurane
TIDPSi-Cl$_2$	1,3-Dichloro-1,1,3,3-tetraisopropyldisiloxane
TLC	Thin-layer chromatography
TMAD	Tetramethylazodicarboxamide
TMS	Trimethylsilan (-yl)
Tol	Toluene
Tris	Tris(hydroxymethyl)aminomethane
U	Unit(s)
UTP	Uridine triphosphate
UV	Ultraviolet
UV-Vis	Ultraviolet-visible
v/v	Volume fraction
w/	with
w/o	without
w/v	Mass concentration

7.8 List of synthesized compounds

Number of compound	Chemical structure
7	
20a	
36	
37	
38	
39	
40	
41	
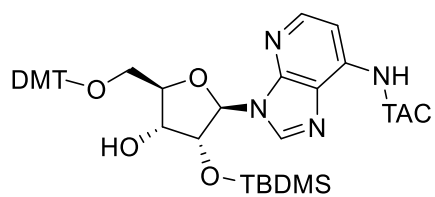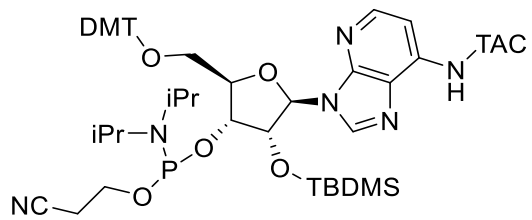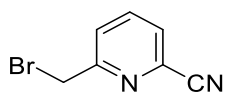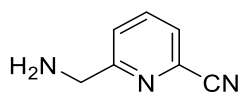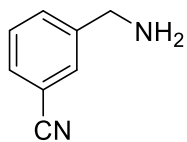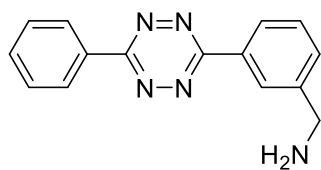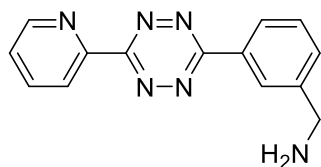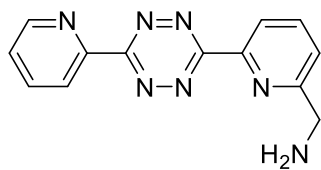
43	
44	
46	
47	
49	
51	
53	
54	
62	
63	
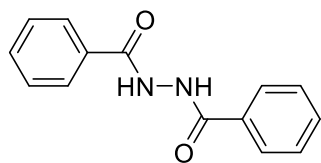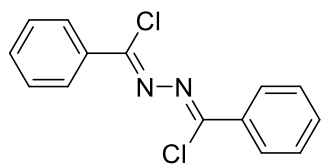
66
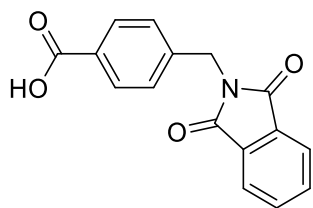
66
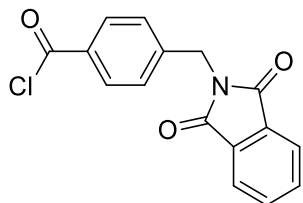
67
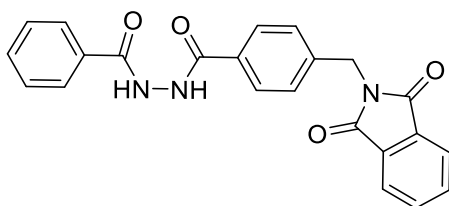
68
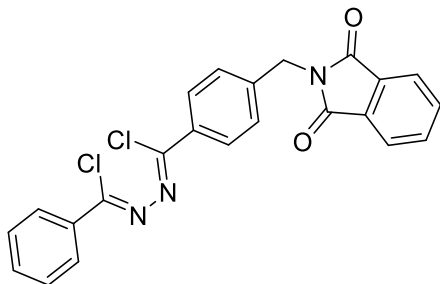
70
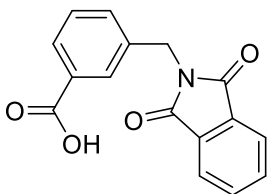
70
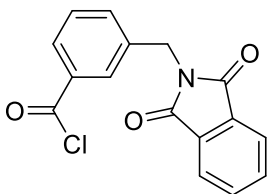
71
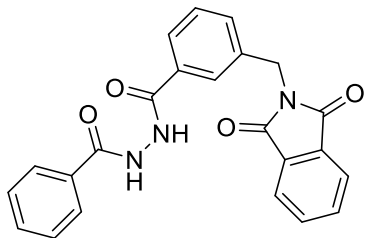
76
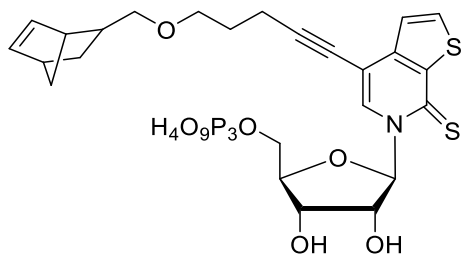
78
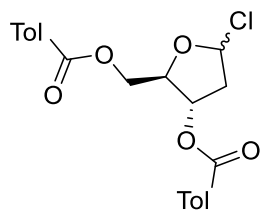
80
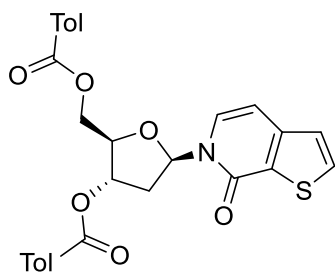
81
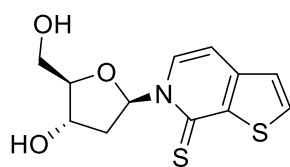
82
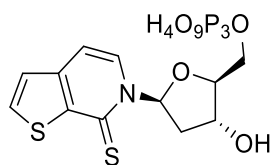
84
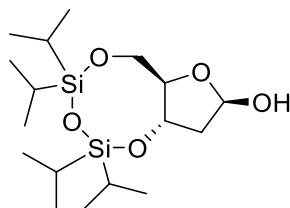
86
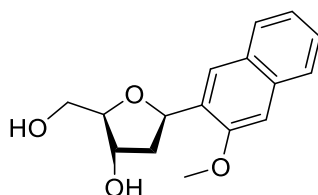
87
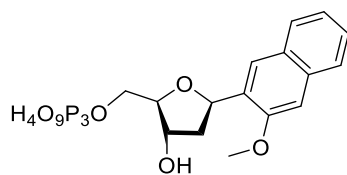
89
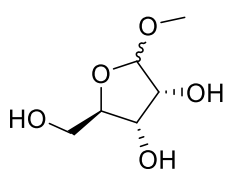
90
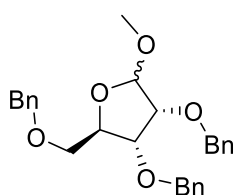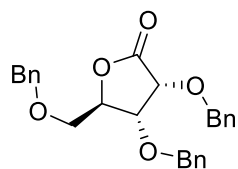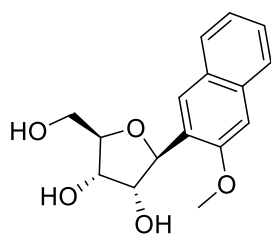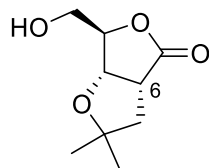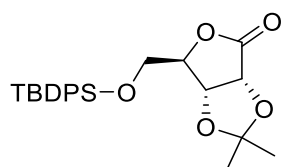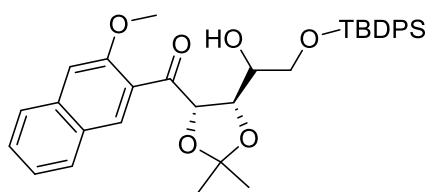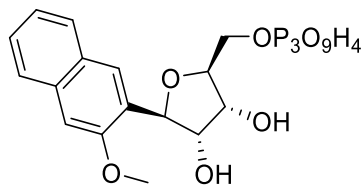
92	
96	
101	
101	
102	
103	
107	
109	
110	
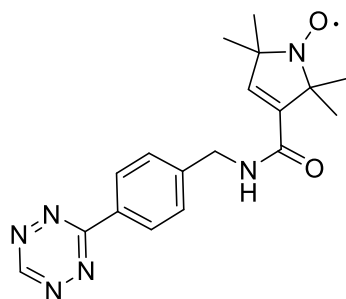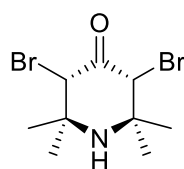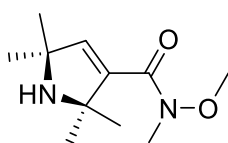
111
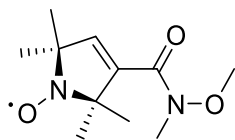
112
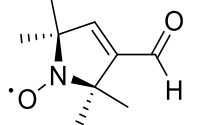
113
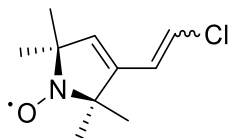
114
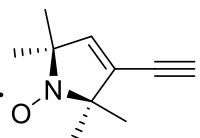
117
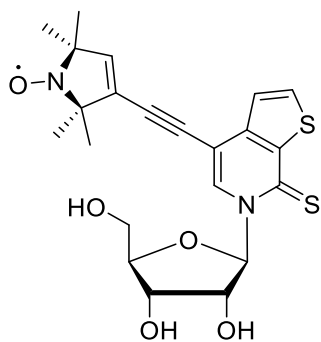
119
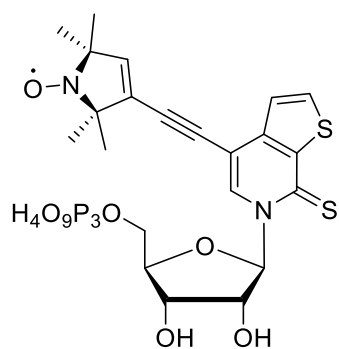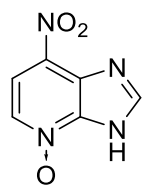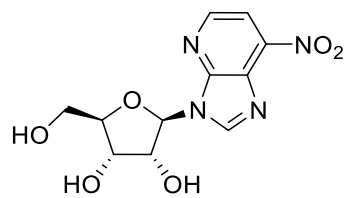
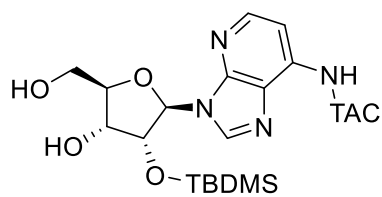**124**
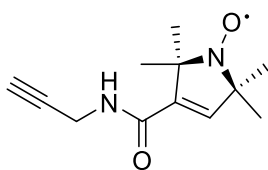
125
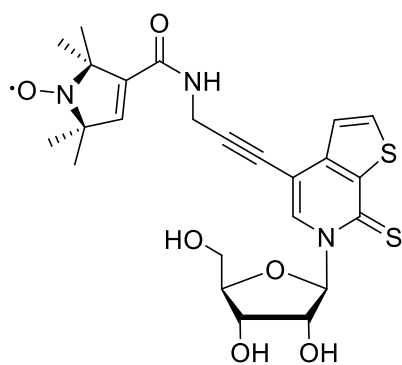
126
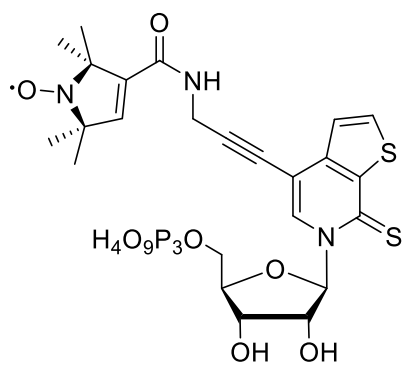
128
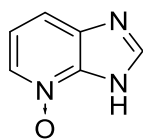
129

131

132

8 Selbstständigkeitserklärung

Hiermit erkläre ich, dass die vorliegende Arbeit sowohl ohne die unerlaubte Hilfe Dritter als auch ohne die Benutzung anderer als der angegebenen Hilfsmittel angefertigt wurde.

Daten, Konzepte und Ideen, die direkt oder indirekt aus Quellen übernommen wurden, sind entsprechend gekennzeichnet. Diese Arbeit ist werde identisch noch teilidentisch mit einer Arbeit, die an der Rheinischen Friedrich-Wilhelms-Universität Bonn oder einer anderen Hochschule zur Erlangung eines akademischen Grades oder als Prüfungsleistung vorgelegt worden ist.

Die Promotionsordnung der Mathematisch-Naturwissenschaftlichen Fakultät der Rheinischen Friedrich-Wilhelms-Universität Bonn ist mir bekannt.

Christof Domnick

Bonn, den

9 Liste der Veröffentlichungen

C. Domnick, G. Hagelueken, F. Eggert, O. Schiemann and S. Kath-Schorr
"Posttranscriptional spin labeling of RNA by tetrazine-based cycloaddition" *Org. Biomol. Chem.*, **2019**, Advance article, DOI: 10.1039/C8OB02597E.

F. Eggert, K. Kulikov, C. Domnick, P. Leifels and S. Kath-Schorr*
"Iluminated by foreign letters - strategies for site-specific cyclopropene modification of large functional RNAs via in vitro transcription" *Methods* **2017**, *120*, 17 – 27.

C. T. Wilson, Y. Liu, C. Domnick, S. Kath-Schorr* and D. M. J. Lilley*
"The Novel Chemical Mechanism of the Twister Ribozyme" *J. Amer. Chem. Soc.* **2016**, *138*, 6151 – 6162.

C. Domnick[‡], F. Eggert[‡] and S. Kath-Schorr*
"Site-specific enzymatic introduction of a norbornene modified unnatural base into RNA and application in posttranscriptional labeling" *Chem. Commun.* **2015**, *51*, 8253 – 8256.

A. M. Pyka, C. Domnick, F. Braun and S. Kath-Schorr*
"Diels-Alder Cycloadditions on Synthetic RNA in Mammalian Cells" *Bioconjugate Chem.* **2014**, *25*, 1438 – 1443.

Submitted articles:
F. Eggert[‡], C. Domnick[‡], G. Hagelueken, O. Schiemann and S. Kath-Schorr
"Spin labeling of RNA by genetic alphabet expansion transcription" *Angew. Chem. Int. Ed.*, in revision.

‡ Authors contributed equally